NORTH ATLANTIC TREATY ORGANIZATION

SCIENCE AND TECHNOLOGY ORGANIZATION

AC/323(AVT-248)TP/891

www.sto.nato.int

STO TECHNICAL REPORT **TR-AVT-248**

Next-Generation NATO Reference Mobility Model (NG-NRMM) Development

(Développement du modèle de mobilité de référence de l'OTAN (NG-NRMM) de nouvelle génération)

Final Report of AVT-248.

Published April 2020

Distribution and Availability on Back Cover



NORTH ATLANTIC TREATY ORGANIZATION

SCIENCE AND TECHNOLOGY ORGANIZATION

AC/323(AVT-248)TP/891

www.sto.nato.int

STO TECHNICAL REPORT **TR-AVT-248**

Next-Generation NATO Reference Mobility Model (NG-NRMM) Development

(Développement du modèle de mobilité de référence de l'OTAN (NG-NRMM) de nouvelle génération)

Final report of AVT-248.

Edited by

Jean Dasch and Paramsothy Jayakumar

Authors

Ole Balling, Michael Bradbury, Jonathan Bruce, Mark Cammarere, KK Choi, Jean Dasch, Craig Foster, Matthew Funk, Nicholas Gaul, Henry Hodges, Abhinandan Jain, Paramsothy Jayakumar, Michael McCullough, Jeffrey Niemann, Elham Ramyar, Joseph Scalia, Tamer Wasfy, Brian Wojtysiak

The NATO Science and Technology Organization

Science & Technology (S&T) in the NATO context is defined as the selective and rigorous generation and application of state-of-the-art, validated knowledge for defence and security purposes. S&T activities embrace scientific research, technology development, transition, application and field-testing, experimentation and a range of related scientific activities that include systems engineering, operational research and analysis, synthesis, integration and validation of knowledge derived through the scientific method.

In NATO, S&T is addressed using different business models, namely a collaborative business model where NATO provides a forum where NATO Nations and partner Nations elect to use their national resources to define, conduct and promote cooperative research and information exchange, and secondly an in-house delivery business model where S&T activities are conducted in a NATO dedicated executive body, having its own personnel, capabilities and infrastructure.

The mission of the NATO Science & Technology Organization (STO) is to help position the Nations' and NATO's S&T investments as a strategic enabler of the knowledge and technology advantage for the defence and security posture of NATO Nations and partner Nations, by conducting and promoting S&T activities that augment and leverage the capabilities and programmes of the Alliance, of the NATO Nations and the partner Nations, in support of NATO's objectives, and contributing to NATO's ability to enable and influence security and defence related capability development and threat mitigation in NATO Nations and partner Nations, in accordance with NATO policies.

The total spectrum of this collaborative effort is addressed by six Technical Panels who manage a wide range of scientific research activities, a Group specialising in modelling and simulation, plus a Committee dedicated to supporting the information management needs of the organization.

- AVT Applied Vehicle Technology Panel
- HFM Human Factors and Medicine Panel
- IST Information Systems Technology Panel
- NMSG NATO Modelling and Simulation Group
- SAS System Analysis and Studies Panel
- SCI Systems Concepts and Integration Panel
- SET Sensors and Electronics Technology Panel

These Panels and Group are the power-house of the collaborative model and are made up of national representatives as well as recognised world-class scientists, engineers and information specialists. In addition to providing critical technical oversight, they also provide a communication link to military users and other NATO bodies.

The scientific and technological work is carried out by Technical Teams, created under one or more of these eight bodies, for specific research activities which have a defined duration. These research activities can take a variety of forms, including Task Groups, Workshops, Symposia, Specialists' Meetings, Lecture Series and Technical Courses.

The content of this publication has been reproduced directly from material supplied by STO or the authors.

Published April 2020

Copyright © STO/NATO 2020
All Rights Reserved

ISBN 978-92-837-2215-1

Single copies of this publication or of a part of it may be made for individual use only by those organisations or individuals in NATO Nations defined by the limitation notice printed on the front cover. The approval of the STO Information Management Systems Branch is required for more than one copy to be made or an extract included in another publication. Requests to do so should be sent to the address on the back cover.

Table of Contents

	Page
List of Figures	**xv**
List of Tables	**xxx**
List of Acronyms	**xxxii**
AVT-248 Membership List	**xxxvi**
Executive Summary and Synthèse	**ES-1**
Chapter 1 – Introduction	**1-1**
1.1 Background	1-1
1.2 NRMM History	1-1
1.3 Objectives	1-2
1.4 References	1-3
Chapter 2 – Approach	**2-1**
2.1 AVT-248 Organization	2-1
2.2 AVT-248 Deliverables	2-2
2.2.1 Prototype Demonstrations	2-2
2.2.2 Verification and Validation (V&V)	2-3
2.2.3 STANREC	2-3
2.3 Final Report Overview	2-3
Chapter 3 – TA1: Geographical Information Systems (GIS) Terrain and Mobility Mapping	**3-1**
3.1 Goals and Deliverables	3-1
3.1.1 GIS Terrain and Mobility Mapping Goals	3-1
3.1.2 GIS Terrain and Mobility Mapping Deliverables	3-1
3.2 GIS Terrain and Mobility Mapping Team Membership	3-2
3.3 Introduction	3-2
3.3.1 Output Metrics	3-2
3.3.2 Terminology	3-3
3.4 Process / Methodology for Translation of GIS Data into NG-NRMM Compliant Terrain Data	3-5
3.4.1 Minimum Geospatial Soil Data Requirements to Support Simulation	3-7
3.4.2 Building an Example Geospatial Dataset and Prototype Tools	3-8
3.4.2.1 Elevation and Derivatives	3-9
3.4.2.2 Soil Type and Bulk Density Parameters	3-11
3.4.2.3 Soil Moisture Parameter	3-12

3.4.2.4 Land Use Parameter 3-12
3.4.2.5 Process to Combine Each "Intermediate" Property Dataset into One NG-NRMM Terrain File 3-14
3.4.3 Additional Requirements – Metadata for Data Sources 3-15
3.5 Geodatabase Description and Data Models 3-15
3.5.1 Geodatabase Description and Population of an Example Geodatabase 3-15
3.5.2 NG-NRMM Terrain Data Models 3-16
3.5.3 NRMM Terrain Parameters (Version 2.8.2) 3-17
3.5.4 NRMM Terrain Parameters (Version 3.0 Beta) 3-21
3.5.5 Unique NG-NRMM Terrain Parameters 3-22
3.6 Interchange Formats 3-22
3.6.1 NRMM MAPTBL (Code 11) 3-23
3.6.2 GeoTIFF 3-24
3.7 NG-NRMM Output Products: Visualizing Mobility Results 3-25
3.7.1 GO/NOGO Maps and NOGO Reason Code Maps 3-25
3.7.2 Speed-Made-Good Maps 3-26
3.7.3 Additional Output Map Products 3-28
3.7.4 Least Cost Path 3-28
3.8 Gaps, Challenges, and Future Work 3-28
3.8.1 Resolution of Data Sources 3-28
3.8.2 Data Availability to Field User 3-29
3.8.3 Limitations of MAPTBL Format with NG-NRMM Resolution / Data Requirements 3-29
3.9 NATO Standard Recommendation (STANREC) 3-30
3.9.1 Geographic Terrain Data Provided as Input to Off-Road Mobility M&S 3-31
3.9.1.1 Input Data Schema 3-31
3.9.1.2 Input Data Formats 3-31
3.9.1.3 Input Environment Scenario Data 3-32
3.9.2 Mobility M&S Output to Geographic Map Overlays 3-32
3.9.2.1 Formats 3-32
3.9.2.2 Trafficability NOGO 3-32
3.9.2.3 Speed-Made-Good 3-32
3.10 Summary 3-33
3.11 Standards 3-33
3.12 References 3-34

Chapter 4 – TA2: Simple Terramechanics 4-1

4.1 Goals and Team Members 4-1
4.2 Introduction 4-2
4.3 Process/Methodology 4-5
4.3.1 Vehicle-as-a-Sensor 4-8
4.3.2 Database Development 4-12
4.4 Prototype Demonstration 4-14
4.4.1 University of Wisconsin-Madison (UW-M) 4-14

4.4.2 Nevada Automotive Test Center (NATC) 4-18
4.4.3 Jet Propulsion Laboratory (JPL) 4-18
4.4.4 Vehicle Systems Development Corporation (VSDC), National Research Council (NRC) Canada 4-18
4.4.5 South African Council for Scientific and Industrial Research (CSIR) 4-19
4.4.6 Germany 4-19
4.5 STANREC 4-19
4.5.1 Simple Terramechanics for Soft Soil 4-20
4.6 Gaps and Path Forward 4-22
4.7 Summary 4-23
4.8 References 4-23

Chapter 5A – TA3: Complex Terramechanics Requirements 5A-1
5A.1 Goals and Team Members 5A-1
5A.2 Introduction 5A-2
5A.2.1 Motivation 5A-2
5A.2.2 Model Types 5A-3
5A.2.2.1 Micro-Scale Soil Model 5A-3
5A.2.2.2 Macro-Scale Soil Model 5A-8
5A.2.2.3 Height Field and Height Soil Models 5A-9
5A.2.2.4 Empirical Equation Soil Models 5A-10
5A.3 Review of Macro-Scale Soil Models 5A-10
5A.3.1 Mesh-Based Finite Element Soil Models 5A-10
5A.3.2 Mesh-Free Particle-Based Soil Models 5A-13
5A.3.2.1 Discrete Element Method 5A-13
5A.3.2.2 Smoothed Particle Hydrodynamics 5A-15
5A.3.2.3 Material Point Method 5A-16
5A.3.3 Technology Readiness of the Macro-Scale Terramechanics Modeling Techniques 5A-17
5A.4 Complex Terramechanics Software Tools Requirements 5A-18
5A.4.1 Ability to Predict the Vehicle Mobility Measures 5A-18
5A.4.2 Ability to Predict Terrain Deformation/Damage Caused by the Vehicle 5A-20
5A.4.3 Ability to Accurately Predict Soil Mechanical Response for Small-Scale Terramechanics Experiments 5A-21
5A.4.4 Ability to Reproduce the Mechanical Response of Worldwide Soils/Terrains 5A-26
5A.4.5 Ability to Provide the Mapping Function that Maps the Physical Soil Properties into the Soil Mechanical Properties 5A-27
5A.4.6 Ability to Represent Heterogeneous Terrains 5A-29
5A.4.7 Ability to Represent Multiple Layers of Soil 5A-29
5A.4.8 Ability to Represent Water Covered Terrains 5A-29
5A.4.9 Ability to Model Long Complex Topography Terrains 5A-31
5A.4.10 Ability to Represent All Types and Sizes of Vegetation Identified in USNVC 5A-31
5A.4.11 Ability to Represent Natural and Urban Obstacles 5A-32

5A.4.12 Ability to Read the Terrain Input Data from GIS Software Tools 5A-32
5A.4.13 Ability to Generate Terrain Mobility Maps and Display the Maps in GIS Software Tools 5A-34
5A.4.14 Ability to Conduct Coupled Simulations with Multibody Dynamics Software for Modeling the Vehicle 5A-34
5A.5 References 5A-36

Chapter 5B – TA3: DIS/GroundVehicle: Complex Terramechanics Prototype 5B-1

5B.1 Introduction 5B-1
5B.2 Key Features of DIS/IVRESS 5B-1
5B.2.1 Multibody Dynamics/Finite Element Method 5B-4
5B.2.2 Discrete Element Method 5B-7
5B.2.3 Smoothed Particle Hydrodynamics 5B-14
5B.2.4 IVRESS Virtual Reality Visualization Engine 5B-16
5B.3 Prototype Capabilities 5B-17
5B.3.1 Ability to Predict the Vehicle Mobility Measures of Interest to the End Users 5B-17
5B.3.2 Ability to Predict the Terrain Damage Caused by the Vehicle 5B-21
5B.3.3 Ability to Accurately Predict Soil Mechanical Response for Small-Scale Terramechanics Experiments 5B-23
5B.3.4 Ability to Accurately Represent the Mechanical Response of Worldwide Soils 5B-24
5B.3.5 Ability to Provide the Mapping Function Which Maps the Physical Soil Properties into the Mechanical Soil Properties 5B-25
5B.3.6 Ability to Represent Heterogeneous Terrains 5B-26
5B.3.7 Ability to Represent Multiple Layers of Soil 5B-27
5B.3.8 Ability to Represent Water Covered Terrains 5B-27
5B.3.9 Ability to Model Long Complex Topography Terrains 5B-27
5B.3.10 Ability to Represent All Types and Sizes of Vegetation Identified in USNVC 5B-32
5B.3.11 Ability to Represent Urban Obstacles 5B-33
5B.3.12 Ability to Read the Terrain Input Data from GIS Software Tools 5B-33
5B.3.13 Ability to Generate Terrain Mobility Maps and Display the Maps in GIS Software Tools 5B-34
5B.3.14 Ability to Conduct Coupled Simulations with MBD Software for Modeling the Vehicle 5B-34
5B.3.14.1 Ability to Model Pneumatic Tires 5B-35
5B.3.14.2 Ability to Model Segmented Tracks 5B-45
5B.3.14.3 Ability to Model Continuous Belt-Type Tracks 5B-46
5B.3.14.4 Ability to Model the Interaction of Any Vehicle Part with the Terrain 5B-47
5B.3.14.5 Ability to Model the Vehicle Systems Necessary for Mobility 5B-47
5B.3.14.6 Ability to Model Payloads and Occupants 5B-49
5B.3.14.7 Ability to Model the Various Types of Vehicle Maneuvers on Any Terrain 5B-49

5B.4 Procedure to Produce a Mobility Terrain Map 5B-53
5B.4.1 Prototype Demonstration of the Monterey Bay Region 5B-55
5B.5 References 5B-57

Chapter 5C – TA3: Other Complex Terramechanics Software Tools 5C-1

5C.1 Introduction 5C-1
5C.2 Chrono 5C-1
5C.2.1 Multibody System Dynamics and Frictional Contact 5C-1
5C.2.2 Vehicle Modeling 5C-2
5C.2.3 Soft Soil Modeling and Complex Terramechanics 5C-3
5C.2.4 Parallelization 5C-4
5C.3 MSC/ADAMS 5C-5
5C.4 RecurDyn 5C-8
5C.4.1 Soft Soil DEM Model/Formulation Provided in the EDEM Software 5C-9
5C.4.2 RecurDyn Multibody Dynamics Formulation 5C-10
5C.4.3 Co-Simulation of RecurDyn Multibody Dynamics and EDEM Discrete Element Capabilities 5C-10
5C.4.4 Example of a RecurDyn – EDEM Soft Soil Vehicle Mobility Co-Simulation 5C-12
5C.5 EDEM 5C-12
5C.5.1 EDEM UI and Solver 5C-13
5C.5.2 CAE Integration 5C-14
5C.5.3 Material Modeling 5C-14
5C.5.4 Modeling Soils in EDEM 5C-15
5C.5.5 Advanced Customization 5C-15
5C.6 References 5C-16
5C.6.1 Chrono References 5C-16
5C.6.2 Adams References 5C-16
5C.6.3 RecurDyn References 5C-16
5C.6.4 EDEM Contact Model References 5C-17

Chapter 6 – TA5: Uncertainty Treatment 6-1

6.1 Goals and Team Members 6-1
6.2 Introduction 6-1
6.3 Framework/Methodology 6-4
6.3.1 Elevation and Soil Property Data Including Variability 6-4
6.3.2 Advanced Kriging for Terrain Modeling 6-6
6.3.3 Propagation of Uncertainty for Reliability Assessment of Mobility 6-8
6.4 Prototype Demonstration 6-10
6.4.1 Complex Terramechanics Prototype 6-10
6.4.2 Simple Terramechanics Prototype 6-17

6.5 Standard 6-19
6.5.1 Variability Versus Uncertainty in NG-NRMM 6-20
6.5.2 GIS Data and Higher Resolution of Terrain Variables 6-21
6.5.3 Variability Models of Terrain Variables 6-21
6.5.4 Propagation of Uncertainty 6-22
6.5.5 Output Mobility Map 6-23
6.6 Results 6-23
6.7 Gaps and Path Forward 6-23
6.7.1 Raster Data 6-23
6.7.2 Terramechanics Simulation Model 6-23
6.7.3 Soil Parameter Data 6-24
6.8 Summary 6-24
6.9 References 6-25

Chapter 7 – TA4: Intelligent Vehicles 7-1
7.1 Introduction 7-1
7.1.1 Intelligent Vehicles 7-1
7.1.2 Mobility 7-1
7.1.3 Operational Environments 7-3
7.1.4 Intelligent Vehicle Operation 7-3
7.2 Process and Methodology 7-5
7.2.1 Autonomy Levels 7-5
7.2.2 Autonomy Map 7-5
7.2.3 Intelligent Vehicle Performance Modeling 7-7
7.3 Prototype Demonstration 7-7
7.3.1 Pilot Project 7-8
7.3.2 Pilot Project Approach 7-8
7.3.2.1 NG-NRMM via M&S 7-8
7.3.2.2 Sampling Approach 7-9
7.3.2.3 ROAMS UGV Mobility Simulator 7-9
7.3.3 Pilot Project Reference Problem 7-9
7.3.3.1 Prototype Intelligent Vehicle 7-10
7.3.3.2 Autonomy Modes 7-10
7.3.3.3 Prototype Terrain Environment 7-12
7.3.4 Obstacles and Hazards 7-13
7.3.5 Simulation Experiments 7-14
7.4 Results 7-16
7.4.1 Traverse Performance Results 7-17
7.4.1.1 Performance with Decreased Slope Threshold for Obstacles 7-18
7.4.2 Qualitative Validation 7-19
7.4.2.1 Effect of Changing Obstacle Detection Field of View 7-20
7.4.2.2 Effect of Changing Camera Depth 7-20
7.4.2.3 Effect of Low vs. High Speed Limits 7-21
7.4.3 Autonomy Maps 7-21

7.5 Standards 7-22
7.5.1 NG-NRMM(I) Challenges 7-23
7.5.2 NG-NRMM(I) Inputs 7-24
7.5.3 NG-NRMM(I) Outputs 7-26
7.5.4 NG-NRMM(I) Process 7-26
7.6 Gaps and Path Forward 7-27
7.6.1 Extending the Prototype Demonstration 7-27
7.6.1.1 Vehicle Platform 7-27
7.6.1.2 Intelligent Mobility 7-28
7.6.1.3 Terrain Environment 7-28
7.6.1.4 M&S Process 7-28
7.6.1.5 GO/NOGO Map Generation 7-28
7.6.1.6 Autonomy Map Generation 7-28
7.6.2 Longer Term Challenges 7-29
7.6.2.1 Open Issues with M&S Based Sampling 7-29
7.7 Acknowledgements 7-31
7.8 References 7-31

Chapter 8A – TA6: Tracked Vehicle Verification and Validation 8A-1

8A.1 Goals and Team Members 8A-1
8A.2 Introduction 8A-1
8A.3 Process/Methodology 8A-1
8A.4 Tracked Vehicle Benchmark Events 8A-3
8A.4.1 Steering Performance 8A-3
8A.4.2 Side Slope Stability (SSS) 8A-3
8A.4.3 Grade Climbing 8A-4
8A.4.4 Ride Quality 8A-4
8A.4.5 Obstacle Crossing 8A-4
8A.4.6 Off-Road Trafficability 8A-5
8A.4.7 Fuel Economy 8A-5
8A.4.8 Amphibious Operations 8A-5
8A.4.9 Intelligent Vehicle 8A-6
8A.5 Benchmark Entries and Data Sources 8A-6
8A.5.1 Tracked Vehicle Data 8A-6
8A.5.2 NRMM 8A-6
8A.5.2.1 VehDyn Model Overview 8A-6
8A.5.2.2 Ride Quality 8A-7
8A.5.2.3 Shock Quality 8A-7
8A.5.2.4 Obstacle Crossing 8A-8
8A.5.2.5 NRMM Mobility Prediction Overview 8A-8
8A.5.3 NG-NRMM Benchmark Participants 8A-8
8A.5.3.1 Advanced Science and Automation Corporation 8A-8
8A.5.3.2 MotionPort 8A-10
8A.5.3.3 MSC Software Corporation 8A-12

8A.5.3.4 University of Wisconsin 8A-14
8A.5.3.5 Vehicle Systems Development Corporation (VSDC), Toronto, Ontario, Canada 8A-16
8A.6 Benchmark Results 8A-17
8A.6.1 Wall-To-Wall Turn Radius 8A-17
8A.6.2 Steady-State Cornering 8A-18
8A.6.3 Double Lane Change 8A-19
8A.6.4 Side Slope Stability 8A-21
8A.6.5 Grade Climbing 8A-22
8A.6.6 Random Terrain Ride 8A-25
8A.6.7 Half Round Obstacle 8A-26
8A.6.8 Step and Gap Obstacle Negotiation 8A-27
8A.6.9 Trapezoidal Obstacle Negotiation 8A-28
8A.6.10 Off-Road Trafficability 8A-29
8A.6.11 Drawbar Pull 8A-30
8A.6.12 Motion Resistance 8A-31
8A.6.13 Closed-Loop Traverse/Fuel Economy 8A-32
8A.7 Summary and Conclusions 8A-33
8A.8 References 8A-37

Chapter 8B – TA6: Wheeled Vehicle Platform Verification and Validation 8B-1

8B.1 Goals and Team Members 8B-1
8B.2 Introduction 8B-1
8B.3 Process/Methodology 8B-1
8B.4 Wheeled Vehicle Benchmark Events 8B-2
8B.4.1 Paved Straight Line Acceleration (SLA) 8B-2
8B.4.2 Wall-to-Wall Turn Radius (WTW) 8B-2
8B.4.3 Steady-State Cornering (SSC) 8B-2
8B.4.4 Paved Double Lane Change (DLC) 8B-2
8B.4.5 Gravel Double Lane Change (DLC) 8B-3
8B.4.6 Side Slope Stability (SSS) 8B-3
8B.4.7 Sand Slope Gradeability (SSG) 8B-3
8B.4.8 Ride Quality 8B-3
8B.4.9 Drawbar Pull 8B-3
8B.5 Benchmark Entries 8B-3
8B.5.1 Vehicle and Test Data 8B-3
8B.5.2 NRMM 8B-4
8B.5.3 Benchmark Participants 8B-4
8B.5.3.1 CM Labs Organization 8B-4
8B.6 Benchmark Results 8B-5
8B.6.1 Paved Straight Line Acceleration 8B-5
8B.6.2 Wall-to-Wall Turn Radius 8B-6
8B.6.3 Steady-State Cornering 200 ft. Radius 8B-7
8B.6.4 Paved Double Lane Change 8B-9

8B.6.5 Gravel Double Lane Change 8B-12
8B.6.6 Side Slope Stability 8B-16
8B.6.7 Sand Slope Gradeability 8B-19
8B.6.8 Ride Quality 8B-22
8B.6.9 Drawbar Pull 8B-25
8B.7 Benchmark Updated Results 8B-26
8B.7.1 Wall-to-Wall Turn Radius 8B-26
8B.7.2 Steady-State Cornering 8B-27
8B.7.3 Paved Double Lane Change 8B-27
8B.7.4 Side Slope Stability 8B-27
8B.7.5 Sand Slope Gradeability 8B-28
8B.8 Summary and Conclusions 8B-28
8B.9 References 8B-31

Chapter 9 – TA7: Data Gaps; Operational Readiness 9-1
9.1 Goals and Team Members 9-1
9.2 Introduction 9-1
9.3 Capability Gaps Methodology 9-2
9.3.1 Introduction 9-2
9.3.2 Methodology 9-3
9.4 Identification 9-5
9.4.1 Introduction 9-5
9.4.2 Layers 9-5
9.4.3 Levels 9-8
9.4.4 Summary 9-10
9.5 NG-NRMM Use/User Profile 9-10
9.5.1 NG-NRMM Use/User Profile Observations 9-16
9.6 Capability Gaps and Challenges 9-17
9.6.1 NG-NRMM Input 9-17
9.6.2 NG-NRMM Modeling 9-21
9.6.3 NG-NRMM Output 9-28
9.7 Summary 9-30
9.8 References 9-31

Chapter 10 – Summary and Conclusions 10-1
10.1 TA1 GIS Terrain and Mobility Map 10-1
10.2 TA2 Simple Terramechanics (ST) 10-2
10.3 TA3 Complex Terramechanics (CT) 10-2
10.4 TA5 Uncertainty Treatment 10-2
10.5 TA6 Intelligent Vehicles 10-3
10.6 TA6 Vehicle Verification and Validation 10-3
10.7 TA7 Data Gaps and Operational Readiness 10-3

Chapter 11 – ADDITIONAL REFERENCES 11-1

Annex A – Technical Activity Proposal (TAP) and Terms of Reference (TOR) A-1

A.1 Technical Activity Proposal (TAP) A-1
I. Background and Justification (Relevance to NATO) A-1
II. Objective(s) A-2
III. Topics to be Covered A-2
IV. Deliverables (e.g., S/W Engage Model, Database, etc.) and/or End Product (e.g., Final Report) A-3
V. Technical Team Leader and Lead Nation A-3
VI. Nations Willing/Invited to Participate A-3
VII. National and/or NATO Resources Needed (Physical and Non-physical Assets) A-4
VIII. STO/CSO Resources Needed A-4
A.2 Terms of Reference (TOR) A-4
I. Origin A-4
A. Background A-4
B. Justification (Relevance for NATO) A-5
II. Objectives A-5
III. Resources A-6
A. Membership A-6
B. National and/or NATO Resources Needed A-7
C. STO/CSO Resources Needed A-7
IV. Security Classification Level A-7
V. Participation by Partner Nations PfP Nations (Excluding Russia) Listed Above A-7
VI. Liaison A-7

Annex B – Modified NRMM Code 11 "MAPTBL" Terrain Data Interchange Format B-1

B.1 *.ASC ASCII Raster Format B-1
B.2 *.PRJ ASCII Raster Spatial Reference Support File B-2
B.3 *.TER Terrain File B-5
B.3.1 First Record B-5
B.3.2 General Comments B-6
B.3.3 Field Header Metadata B-6
B.3.4 Field Header B-15
B.3.5 Data Section B-15
B.4 References B-16

Annex C – Fine Resolution Soil Moisture Estimation C-1

C.1 Goals and Team Members C-1
C.1.1 Goal of Fine Resolution Soil Moisture Estimation C-1
C.1.2 Team Members C-1
C.2 Introduction C-1
C.3 Fine Resolution Soil Moisture – Mean C-2

C.4 Fine Resolution Soil Moisture – Stochastic Variations C-6
C.5 Fine Resolution Soil Moisture – Map-Based Application C-8
C.6 References C-10

Annex D – Soil Strength Estimation Overview D-1
D.1 Goals and Team Members D-1
D.1.1 Goal of Soil Strength Estimation D-1
D.1.2 Team Members D-1
D.2 Introduction D-1
D.3 Soil Strength Estimation Framework – Inputs D-3
D.4 Soil Strength Estimation Framework – Sample Outputs D-5
D.5 References D-8

Annex E – Terramechanics Database E-1
E.1 Background E-1

Annex F – Measurement and Analysis of Geotechnical Properties F-1
F.1 Goals and Team Members F-1
F.1.1 Goal of Measurement and Analysis of Geotechnical Properties F-1
F.1.2 Team Members F-1
F.2 Introduction F-1
F.3 Continuum Soil Models F-2
F.3.1 Common Parameters and Properties F-3
F.3.1.1 Common Tests F-3
F.3.2 Mohr-Coulomb Model F-4
F.3.2.1 Parameters F-4
F.3.2.2 Tests F-4
F.3.3 Approximations to the Mohr-Coulomb Model F-5
F.3.3.1 The Drucker-Prager Model F-5
F.3.3.2 The Lade-Duncan Model F-6
F.3.3.3 The Matsuoka-Nakai Model F-7
F.3.4 Linear Hardening Models F-8
F.3.5 Cam-Clay Model F-9
F.3.5.1 Parameters F-9
F.3.5.2 Tests F-9
F.3.6 The Sandia GeoModel F-10
F.3.6.1 Parameters F-10
F.3.6.2 Tests and Fitting Procedure F-12
F.3.7 Viscoplasticity F-14
F.3.7.1 Parameters F-14
F.3.7.2 Tests F-15
F.4 Semi-Empirical Terramechanics Models F-15
F.4.1 Parameters F-15

F.4.2 Tests F-16
F.5 Discrete Element Models F-17
F.5.1 Parameters F-18
F.5.2 Tests F-21
F.5.2.1 Particle-Scale Approach F-21
F.5.2.2 Bulk Fitting Approach F-22
F.6 Summary F-23
F.7 References F-24

Annex G – TA6: Tracked Vehicle Test Data G-1
G.1 Introduction G-1
G1.1 Disclaimer G-1
G.2 Tracked Vehicle Data G-2
G.3 Supplementary Vehicle Data G-5
G.4 Tracked Vehicle-Terrain Data G-6
G.4.1 Terrain Parameters for LETE Sand G-6
G.4.2 Terrain Parameters for Petawawa Muskeg B G-7
G.4.3 Terrain Parameters for Petawawa Snow A G-8
G.5 Tracked Vehicle Test Data G-10
G.5.1 Random Terrain Ride G-10
G.5.2 Half Round Obstacles G-10
G.5.3 Trapezoidal Obstacles G-11
G.6 References G-11

Annex H – TA6: Wheeled Vehicle Platform Test Data H-1
H.1 WVP Vehicle Data H-1
H.2 Soft Soil Data H-3
H.3 Test Data H-4

Annex I – TA7: Questionnaire Comments and Obstacle Analysis I-1
I.1 Questionnaire 1 Comments I-1
I.1.1 Question 1 I-1
I.1.2 Question 2 I-2
I.1.2 Question 3 I-3
I.2 Obstacle I-3
I.3 Vegetation I-10

List of Figures

Figure		Page
Figure 3-1	Example of Cartographic Rut Depth Prediction	3-3
Figure 3-2	General Data Flow	3-7
Figure 3-3	Sample Dataset – Monterey Bay, California	3-8
Figure 3-4	Processing Workflow to Generate Elevation, Slope and Aspect Terrain Properties	3-10
Figure 3-5	Resulting Sample Elevation (Meters) and Slope (%)	3-10
Figure 3-6	USDA Web Soil Survey Interface	3-11
Figure 3-7	Processing Workflow to Generate Soil Terrain Properties	3-12
Figure 3-8	Sample USCS Soil Types and Bulk Density	3-12
Figure 3-9	Sample Soil Moisture	3-13
Figure 3-10	Processing Workflow to Generate Land Use Terrain Properties	3-13
Figure 3-11	Sample NLCD Land Cover / Land Use	3-14
Figure 3-12	Process to Combine “Intermediate” Datasets into One NG-NRMM Terrain File	3-15
Figure 3-13	Sample NRMM ASC Terrain File	3-23
Figure 3-14	Sample NRMM TER Terrain File	3-24
Figure 3-15	Example GO/NOGO Map (with Urban Areas)	3-25
Figure 3-16	GO/NOGO Reason Code Map Example	3-26
Figure 3-17	Speed-Made-Good Map Example	3-26
Figure 3-18	Two Examples of Speed-Made-Good Maps for Different Vehicles	3-27
Figure 3-19	Least Cost Path Over Speed-Made-Good	3-27
Figure 3-20	Notional Example of Speed-Made-Good at 20%, 50% and 80% Confidence Levels	3-28
Figure 4-1	Full Featured NG-NRMM Simulation Begins with GIS-Based Data,Predicts Mobility and Maps it Back Onto the Terrain as an Additional GIS Parameter	4-2
Figure 4-2	Replacing the Cone Index Methods Used in the Current NRMM,Simple Terramechanics Models will Bring the Full 3D Mechanics of Vehicles Together with Existing Terramechanics	4-3
Figure 4-3	The Bekker-Wong Model Includes Procedures for Parameter Identification from Test Data and, Most Importantly, Recognition of the Elastic Unload/Reload Portions of the Response, D and D’	4-7

Figure 4-4	The Classic Bekker-Wong-Janosi (BWJ) Terramechanics Models (e.g., Pressure-Sinkage (p-z), Shear Stress-Shear Displacement (τ-j))	4-8
Figure 4-5	"Running Gear Level" Terramechanics Model	4-9
Figure 4-6	Pressure-Sinkage and Soil Work Curves, Normalized to Equilibrium Wheel Load and Rut Depth	4-11
Figure 4-7	Pressure-Sinkage Data from a Soil with an Apparently Weak Top Layer and Loose Deep Second Layer	4-11
Figure 4-8	Two Examples of the Slope Climbing Speed Performance vs Moisture Content Response – Surface Surrogate Models for Two USCS Unique BWJ Model Soil Parameter Data Sets from the Notional Data in Table 4-2 (Slope Scale: 1 = 40% Slope)	4-15
Figure 4-9	UW-M Utilized their Tracked Vehicle (TV) Benchmark Model to Generate a Prototype NG-NRMM Speed-Made-Good Map on the Monterey Terrain Data Set Based on Grade Climbing Performance	4-16
Figure 4-10	UW-M Simple Terramechanics Modeling Prototype NG-NRMM Speed-Made-Good Performance Results Over the Monterey Terrain	4-17
Figure 4-11	Sample Results of the NATC NG-NRMM Prototype Modeling Effort Utilizing Running Gear Level Simple Terramechanics Methods in their Vehicle Models	4-17
Figure 5A-1	Spectrum of Soil Models Based on Model Fidelity and Scale	5A-3
Figure 5A-2	USDA Soil Triangle Based on Percent Clay, Silt, and Sand	5A-4
Figure 5A-3	Typical Particle Size Distribution Curve	5A-4
Figure 5A-4	Classification of Soil Particle Shapes	5A-5
Figure 5A-5	Soil Atterberg Limits Based on Water Content	5A-6
Figure 5A-6	Soil Adhesion to a Tire Caused by the Soil Particles-Rubber Forces	5A-7
Figure 5A-7	Abaqus Finite Element Vehicle Mobility Soil Models	5A-11
Figure 5A-8	Adaptation of Finite Element Size Near the Surface	5A-12
Figure 5A-9	Simulation of Wheeled and Tracked Multibody Dynamics Vehicle Models over Long and Side Sloped DEM Soft Terrains	5A-14
Figure 5A-10	PAM-SHOCK and LS-DYNA Coupled SPH Soil-Tire Models	5A-16
Figure 5A-11	Computer Graphics Model of a Snow Plow and a Snow Ball	5A-17
Figure 5A-12	Terrain Damage Caused by a Vehicle Measured by the Rut Depth, Width, Shape and Side Wall Height	5A-20
Figure 5A-13	Simulation of a Uniaxial Piston-Cylinder Soil Compression Test	5A-21

Figure 5A-14	Bulk Density Versus Hydrostatic Pressure Obtained Using a Hydrostatic Compression Test or a Uniaxial Piston-Cylinder Test	5A-22
Figure 5A-15	Simulation of Cylindrical and Cubical Shear Cells	5A-22
Figure 5A-16	Triaxial Cell	5A-23
Figure 5A-17	Bevameter	5A-23
Figure 5A-18	Translational Shear Plate	5A-23
Figure 5A-19	Maximum Shear Stress Versus Current Normal Stress and Previously Applied Normal Stress Obtained Using a Shear Cell or a Triaxial Cell	5A-24
Figure 5A-20	Penetration Pressure Versus Time for 30° Angle Cone Penetrometer	5A-24
Figure 5A-21	Penetration Pressure Versus Sinkage for a Rectangular Penetroplate	5A-25
Figure 5A-22	DEM Model of a Rigid Wheel Moving on Soil	5A-25
Figure 5A-23	Wheel Torque and Drawbar Pull versus Slip for a Rigid Wheel Moving on Soil	5A-25
Figure 5A-24	Adhesion of Organic Soil to a Tire	5A-27
Figure 5A-25	Mapping of Soil Physical Properties to Soil Mechanical Properties Required by the Complex Terramechanics Software Tool	5A-28
Figure 5A-26	Mapping of Soil Physical Properties and Vehicle Surface Material Type to Soil – Vehicle Surface Material Mechanical Properties Required by the Complex Terramechanics Software Tool	5A-28
Figure 5A-27	Soil Embedded Rocks, Stones, and Boulders	5A-29
Figure 5A-28	Terrain with a Top Layer of (a) Tilled Soil; (b) Organic Muskeg Soil; (c) Snow	5A-30
Figure 5A-29	Water Fording and Swimming	5A-30
Figure 5A-30	Soil Embedded Large Tree Stem or Pole Interacting with the Vehicle and the Soil	5A-32
Figure 5A-31	Terrain Map Colored by the Speed-Made-Good	5A-34
Figure 5B-1	IVRESS Model Tree Editor and Graphical Display Window for Creating Multibody Dynamics Vehicle Models and Simulation Scenarios	5B-2
Figure 5B-2	DIS/Groundvehicle Spreadsheet Template for the Main Vehicle Frame	5B-3
Figure 5B-3	DIS/GroundVehicle Spreadsheet Template for the Double-Wish-Bone Suspension System	5B-3
Figure 5B-4	DEM Particle Density Iso-Surface Showing the Surface of the Soil and DEM Soil Particles Colored using Height	5B-4
Figure 5B-5	DIS Simulation of a Humanoid Robot Arm Catching a Ball	5B-6
Figure 5B-6	DIS Simulation of a 2-Legged Humanoid Robot and a 4-Legged Walking Vehicle on Soft DEM Soil	5B-6

Figure 5B-7	DIS DEM Rigid Body Particle Shapes	5B-7
Figure 5B-8	Sand Flow from a Hopper with the Sand Modeled using Cubical Particles	5B-8
Figure 5B-9	Contact Surface and Contact Point, and Particle-to-Particle Contact	5B-9
Figure 5B-10	Particle Adhesion and Repulsion Forces as a Function of Inter-Particle Penetration Distance (D)	5B-9
Figure 5B-11	Typical Curve of Particle Plastic Strain as a Function of Compressive Stress	5B-10
Figure 5B-12	Typical Maximum Adhesive Stress Versus Plastic Strain Curve	5B-10
Figure 5B-13	Asperity-Based Physical Interpretation of Friction	5B-11
Figure 5B-14	Asperity-Spring Friction Model	5B-12
Figure 5B-15	Angle of Repose of a Material Pile: Gravel and Mud	5B-13
Figure 5B-16	Simulation of Sand Flow Rate from a Hopper using Cubical DEM Particles	5B-13
Figure 5B-17	Simulation of Water Fording	5B-15
Figure 5B-18	Simulation of Liquid Sloshing for a Tanker Truck	5B-15
Figure 5B-19	Effect of Soil Cohesion on Rut Depth for a Tracked Vehicle Moving at its Maximum Possible Speed on a Level Terrain Using the Moving Soil Patch Technique	5B-18
Figure 5B-20	Effect of Soil Friction on Rut Depth and Shape for a Tracked Vehicle Moving at its Maximum Possible Speed on a Level Terrain Using the Moving Soil Patch Technique	5B-19
Figure 5B-21	Snapshots of a Bulldozer Digging through Cohesive Mud	5B-19
Figure 5B-22	Time-History of the Bulldozer Speed, Rear-Wheel Angular Velocity and Rear-Wheel Torque	5B-20
Figure 5B-23	Rut Shape for Cohesive Soil Non-Cohesive Soil of Comparable Shear Strength Measured by the Cone Index for a Wheeled Vehicle Traveling at 5 mph	5B-21
Figure 5B-24	Effect of Soil Cohesion on Rut Depth at 10 mph	5B-21
Figure 5B-25	Effect of Soil Cohesion on Rut Depth for a Wheeled Vehicle Moving at its Maximum Possible Speed on the Terrain Using the Moving Soil Patch Technique	5B-22
Figure 5B-26	Effect of Soil Cohesion on Rut Depth for a Walking Legged Vehicle Using the Moving Soil Patch Technique	5B-22
Figure 5B-27	Wall Shear Experiment	5B-23
Figure 5B-28	Variation of a Wheeled Vehicle Speed	5B-25
Figure 5B-29	Segment of the Churchville-B High Resolution 2D Profiled Polygonal Terrain with a Segmented Track Vehicle Going over a Prescribed Steering Path on the Terrain Track	5B-28
Figure 5B-30	RMS Courses Created Using a Polygonal Terrain	5B-29
Figure 5B-31	Trapezoidal and Semi-Circular Bump Courses Created Using a Polygonal Terrain	5B-29

Figure 5B-32	Moving DEM Complex Topography Terrain Patch Modeled Using an I-J Ordered Quadrilateral Grid Representing the Terrain's Surface, an Emitter Surface, a Leveling Surface, and a Sink Surface	5B-30
Figure 5B-33	Snapshots of the Moving DEM Complex Topography Terrain Patch in Typical Vehicle Mobility Simulations: 90° Turn and Going Down a Slope on Rough Soft Soil Terrains	5B-30
Figure 5B-34	Terrain Roughness Input Interface in DIS/Ground Vehicle Using a Harmonic Function Object that Allows Specifying Wave Length Versus Amplitude	5B-31
Figure 5B-35	IVRESS/DIS Harmonic Function Object that Allows Specifying Wave Length Versus Amplitude	5B-31
Figure 5B-36	Snapshot of a Tracked Vehicle Going over a Rough Soft Soil Terrain with the Terrain Roughness Generated Using a Vertically Moving Surface and a Harmonic function Object that Allows Specifying Road Roughness Wave Length vs. Height	5B-32
Figure 5B-37	Snapshots of a Tracked Vehicle (M113) Pushing a Rigid Cylinder Embedded in the Soft Soil	5B-32
Figure 5B-38	Utility for Reading the Map 11 Raster Ascii Input File	5B-34
Figure 5B-39	Diagram Showing the Tire Forces, Moments, and Angles	5B-36
Figure 5B-40	Polygonal Tread Surface of the Simple Tire Model	5B-37
Figure 5B-41	NATC Wheeled Vehicle Platform Undergoing a Double Lane Change at 48 mph and a 200 ft Constant Radius Turn on Pavement with the Tire Forces/ Moments Calculated Using the Simple Tire Model	5B-37
Figure 5B-42	Tire Cross-Section Components	5B-38
Figure 5B-43	Finite Element Tire Reinforcements, Rubber Brick Elements, and Tread Proxy Contact Surface	5B-38
Figure 5B-44	Snapshots of the Multibody Vehicle Model with Finite Element Flexible Tires Displayed using the Tread Proxy Contact Surface	5B-39
Figure 5B-45	Snapshots of the Multibody Vehicle Model with Finite Element Flexible Tires Displayed using the Original Finite Element Tire Surface	5B-39
Figure 5B-46	Snapshot of the Multibody Vehicle Model with Finite Element Flexible Tires Colored Using the Lateral Shear Stress	5B-40
Figure 5B-47	Snapshots of a Vehicle Simulation with a Flexible Tire having a Complex Tread Pattern Running on DEM Soft Soil	5B-40
Figure 5B-48	Top View of the Soil, Vehicle and Finite Element Tire	5B-41
Figure 5B-49	DIS/GroundVehicle User Input Spreadsheet for the Main Tire Parameters	5B-42

Figure 5B-50	Model of a 4-DOF (Longitudinal, Vertical, Camber and Steering) Tire Test Rig	5B-43
Figure 5B-51	Tire Deflection Versus Normal Load on Pavement Obtained Using the Single Wheel Test Rig Model	5B-43
Figure 5B-52	Rolling Resistance: Longitudinal Force Versus Speed and Normal Load on Pavement Obtained Using the Single Wheel Test Rig Model	5B-43
Figure 5B-53	Longitudinal Force Versus Slip and Normal Load on Pavement: Comparison of Single Wheel Test Rig Simple Tire Model and Pacejka89 Experimental Tire Data (Vehicle Speed = 50 Km/Hr, Nominal Normal Load = x = 34.814 kN)	5B-44
Figure 5B-54	Lateral Force vs. Slip Angle on Pavement: Comparison of Single Wheel Test Rig Simple Tire Model and Pacejka89 Experimental Tire Data (Vehicle Speed = 50 Km/Hr Nominal Normal Load = X = 34.814 kN)	5B-44
Figure 5B-55	Self-Aligning Torque vs. Slip Angle on Pavement: Comparison of Single Wheel Test Rig Simple Tire Model and Pacejka89 Experimental Tire Data (Vehicle Speed = 50 Km/Hr, Nominal Normal Load = X = 34.814 kN)	5B-45
Figure 5B-56	Typical Single Pin Segmented Track: One Revolute Joint in Each Sprocket Groove	5B-45
Figure 5B-57	Typical Double-Pin Track Segmented Track: Two Revolute Joints in Each Sprocket Groove	5B-46
Figure 5B-58	Continuous Belt-Type Track Modeled using Brick Elements, and Longitudinal Beam Elements and Lateral Beam Elements Representing the Belt Reinforcements	5B-46
Figure 5B-59	Snapshots of Typical Simulations of a Continuous Belt Tracked Vehicle Over a Complex Topography Polygonal Terrain	5B-47
Figure 5B-60	Snapshot of a Backhoe Digging through Non-Cohesive Sand Type Soil Modeled Using Cubical Rigid Body DEM Particles	5B-48
Figure 5B-61	Snapshot of a Military Tanker Truck-Trailer Vehicle Carrying a Water Tank with the Water Modeled Using SPH	5B-49
Figure 5B-62	Gradeability on Positive Slopes of the NATC Wheeled Vehicle Platform on LETE Sand	5B-50
Figure 5B-63	Gradeability on Positive and Negative Slopes of the M113 Benchmark Tracked Vehicle on LETE Sand	5B-51
Figure 5B-64	Snapshots of the M113 Tracked Vehicle Braking over a 0° and -10°Long Slope after the Vehicle Comes to a Stop on Soft Soil Terrain with a Cone Index of 30	5B-51
Figure 5B-65	Time-History of Vehicle Speed While Braking on 0°, -5°, -10° and -15°Long Slope Soil Terrain with a Cone Index of 30 Starting from the Maximum Speed Achievable on that Slope	5B-52
Figure 5B-66	Snapshots of the NATC Wheeled Vehicle Platform Going Over a 3.6” RMS Terrain at 15 and 35 mph	5B-52

Figure 5B-67	Snapshots from the Drawbar Pull Simulations of the NATC Wheeled Vehicle Platform and the M113 Track Vehicle on LETE Sand	5B-53
Figure 5B-68	Terrain Map Colored by the Speed-Made-Good	5B-54
Figure 5B-69	Physics-Based Model's Steady-State Vehicle Speed (Speed-Made-Good) vs. CI and Terrain Slope	5B-54
Figure 5B-70	Snapshots of a HMMWV-Type Vehicle Going Over Terrains of Various Slopes and Cone Indices	5B-55
Figure 5B-71	DIS/GroundVehicle Model of NATC Wheeled Vehicle Platform on a Soft Soil Terrain	5B-56
Figure 5B-72	Monterey, California Terrain Map Colored by The Speed-Made-Good Generated Using the DIS/ GroundVehicle Complex Terramechanics Prototype	5B-56
Figure 5C-1	Snapshots from Various Chrono::Vehicle-Enabled Simulations	5C-2
Figure 5C-2	Snapshot from a Chrono Simulation of a Vehicle with Flexible Tires on Deformable Granular Terrain (DEM-P Formulation) Negotiating a Cylindrical Obstacle	5C-5
Figure 5C-3	Typical Adams-EDEM Workflow	5C-6
Figure 5C-4	Adams-EDEM Typical Information Exchange	5C-7
Figure 5C-5	FED Vehicle Model Turning in Fine-Grain Sand Pit	5C-8
Figure 5C-6	Range of EDEM Soil Materials	5C-9
Figure 5C-7	Simulation of a Bulk Material Bucket Elevator Using Recurdyn and EDEM	5C-11
Figure 5C-8	RecurDyn Particle Solver and Post-Processing Objects Used in Conjunction with an EDEM Co-Simulation	5C-12
Figure 5C-9	Snapshots of a Typical RecurDyn Soft Soil Vehicle Simulation	5C-12
Figure 5C-10	EDEM Software is Used to Solve Design Challenges Involving Bulk and Granular Materials Across a Variety of Different Industries	5C-13
Figure 5C-11	A Schematic Overview of a Typical DEM Material Model	5C-14
Figure 5C-12	EDEM Soil Modeling for Terramechanical Applications	5C-15
Figure 6-1	NG-NRMM Mobility Map Generation	6-2
Figure 6-2	Elevation Variability and Distribution	6-4
Figure 6-3	ArcGIS Slope Calculation Toolbox	6-5
Figure 6-4	Variability of Soil Properties	6-6
Figure 6-5	Generation of Reliability-Based Stochastic Mobility Map	6-8
Figure 6-6	Complex Terramechanics Model of NATC Wheeled Vehicle Platform	6-10
Figure 6-7	Propagation of Variability to Generate Reliability-Based Stochastic Mobility Maps for Terramechanics	6-11

Figure 6-8	Distribution of Speed-Made-Good for Each Cell of Raster for Complex Terramechanics	6-12
Figure 6-9	Reliability-Based Stochastic and Deterministic Speed-Made-Good Mobility Maps for Complex Terramechanics	6-12
Figure 6-10	Reliability of Deterministic Speed-Made-Good Mobility Maps for Complex Terramechanics	6-13
Figure 6-11	Reliability-Based GO/NOGO Mobility Maps for Complex Terramechanics	6-14
Figure 6-12	Deterministic Friction Angle in Degrees	6-15
Figure 6-13	Cohesion Maps in Dry Season	6-15
Figure 6-14	Cohesion Maps in Wet Season	6-16
Figure 6-15	Reliability-Based Stochastic Speed-Made-Good Mobility Maps in Dry Season	6-16
Figure 6-16	Reliability-Based Stochastic Speed-Made-Good Mobility Maps in Wet Season	6-17
Figure 6-17	Reliability-Based Stochastic and Deterministic Speed-Made-Good Mobility Maps for Simple Terramechanics	6-19
Figure 6-18	Reliability-Based GO/NOGO Mobility Maps for Simple Terramechanics	6-20
Figure 6-19	Framework for Developing Reliability-Based Stochastic Mobility Map	6-22
Figure 7-1	Closed-Loop Interaction Between the Onboard Intelligent Control and Autonomy Software, the Environment, and the Vehicle	7-2
Figure 7-2	Building NG-NRMM(I) Off Of, or In Parallel with, NG-NRMM	7-4
Figure 7-3	Different Autonomous Mobility Level Knob Settings are Required for Different Terrains and Scenarios	7-6
Figure 7-4	Inputs to and Outputs from a Sample Autonomy Map	7-7
Figure 7-5	Model for Developing Performance Metrics and Autonomy Levels from Available Data; Currently Lacks Established Capability Across All of the Pipeline Elements	7-8
Figure 7-6	Simplified Approach to Obstacle Avoidance and Motion Planning	7-10
Figure 7-7	HMMWV Autonomous Drive to Goal (No Obstacles)	7-11
Figure 7-8	Autonomous Obstacle Avoidance Algorithm in ROAMS	7-11
Figure 7-9	Autonomous Waypoint Following in ROAMS	7-12
Figure 7-10	California GIS Data Imported into Simscape; Topography Tiles in Simscape	7-13
Figure 7-11	ROAMS HMMWV on the GIS Terrain	7-13
Figure 7-12	Selected 2 Km Square Region; Slope Map for Chosen Region; Accentuated Slope Map with 22.5° Slope Threshold	7-14

Figure 7-13	Traverse Paths in the Presence of Obstacles	7-14
Figure 7-14	Multiple Prototype Experiment	7-15
Figure 7-15	Simulation Setup	7-15
Figure 7-16	Data Analysis Pipeline	7-16
Figure 7-17	Sampling Coverage	7-16
Figure 7-18	Traverse Success and Failure Rates	7-17
Figure 7-19	Low Maximum Speed; High Maximum Speed	7-18
Figure 7-20	Blind Drives with Obstacle Detection and Avoidance Disabled	7-18
Figure 7-21	Occupancy Maps with a Lower Slope Threshold	7-19
Figure 7-22	Blind Drives with Obstacle Detection and Avoidance Disabled	7-19
Figure 7-23	Small Camera FOV; Large Camera FOV	7-20
Figure 7-24	Small Camera Depth; Large Camera Depth	7-20
Figure 7-25	Low Maximum Speed; High Maximum Speed	7-21
Figure 7-26	Autonomy and Speed Maps Over the 2 Km Area	7-21
Figure 7-27	Balancing Criteria: Safety and Speed; Safety Only	7-22
Figure 7-28	Balancing Criteria; Aggressive Slope Threshold Of 22°; Conservative Slope Threshold of 10°	7-23
Figure 7-29	Multi-Resolution Modeling Strategy	7-30
Figure 7-30	Examples of Multi-Resolution Models in Specific Areas	7-30
Figure 8A-1	Fuel Economy Loop Course	8A-5
Figure 8A-2	VehDyn Model Overview	8A-7
Figure 8A-3	Snapshots of Typical DIS Soft Soil Vehicle Mobility Simulations of Wheeled and Tracked Vehicles With the Soil Modeled Using DEM	8A-9
Figure 8A-4	RecurDyn Icons	8A-11
Figure 8A-5	Track Assembly Modeling	8A-11
Figure 8A-6	Computational Effort for a Double Lane Change Event on a Hard Surface	8A-12
Figure 8A-7	Wall-To-Wall Clockwise and Counterclockwise: Diameter	8A-18
Figure 8A-8	Wall-To-Wall Maturity Level Achieved by Vendors	8A-18
Figure 8A-9	Steady-State Cornering Limited Power and Unlimited Power:Maximum Speed	8A-19
Figure 8A-10	Steady-State Cornering Maturity Level Achieved by Vendors	8A-19
Figure 8A-11	Double Lane Change Paved and Gravel: Maximum Speed	8A-20
Figure 8A-12	Double Lane Change Maturity Level Achieved by Vendors	8A-20
Figure 8A-13	Side Slope Stability Paved and Deformable Terrain: Maximum Speed	8A-21

Figure 8A-14	Side Slope Stability Maturity Level Achieved by Vendors	8A-21
Figure 8A-15	Maximum Steerable Up Slope Paved and Deformable Terrain: Maximum Slope	8A-22
Figure 8A-16	Grade Climbing Up Slope Maturity Level Achieved by Vendors	8A-22
Figure 8A-17	Maximum Steerable Down Slope Paved and Deformable Terrain: Maximum Slope	8A-23
Figure 8A-18	Maximum Steerable Down Slope Paved and Deformable Terrain: Maximum Slope	8A-23
Figure 8A-19	Straight Maximum Speed from Up Slope Paved: Maximum Speed	8A-24
Figure 8A-20	Straight Maximum Speed from Up Slope Deformable Terrain:Maximum Speed	8A-24
Figure 8A-21	Maximum Speed on Grades Maturity Level Achieved by Vendors	8A-24
Figure 8A-22	Random Terrain Ride 3 cm RMS and 6 cm RMS: Limiting Speed	8A-25
Figure 8A-23	Random Terrain 9 cm RMS: Limiting Speed	8A-25
Figure 8A-24	Ride Quality on Random Terrain Maturity Level Achieved by Vendors	8A-25
Figure 8A-25	Half Round Obstacle 4 Inch and 6 Inch: Limiting Speed	8A-26
Figure 8A-26	Half Round Obstacle 8 Inch and 10 Inch: Limiting Speed	8A-26
Figure 8A-27	Half Round Obstacle 12 Inch: Limiting Speed	8A-27
Figure 8A-28	Half Round Obstacles Maturity Level Achieved by Vendors	8A-27
Figure 8A-29	Step Climb Height Limit and Gap Crossing Limits: Height/Gap Limit	8A-27
Figure 8A-30	Step and Gap Obstacle Negotiation Maturity Level Achieved by Vendors	8A-28
Figure 8A-31	Trapezoidal Obstacles Maturity Level Achieved by Vendors	8A-29
Figure 8A-32	Single and Multi Pass: Soil Strength Limit	8A-30
Figure 8A-33	Off-Road Trafficability Maturity Level Achieved by Vendors	8A-30
Figure 8A-34	Drawbar Pull 2 Mph: Drawbar Pull Coefficient	8A-31
Figure 8A-35	Drawbar Pull Maturity Level Achieved by Vendors	8A-31
Figure 8A-36	Motion Resistance Powered and Towed: Motion Resistance Coefficient	8A-31
Figure 8A-37	Motion Resistance Maturity Level Achieved by Vendors	8A-32
Figure 8A-38	Fuel Economy On-Road and Off-Road: Motion Resistance Coefficient	8A-32

Figure 8A-39	Fuel Economy Maturity Level Achieved by Vendors	8A-33
Figure 8A-40	Scoring based on Maturity Scale	8A-33
Figure 8A-41	Tracked Vehicle Maturity Level	8A-34
Figure 8A-42	Participant Simulation Maturity Level	8A-35
Figure 8B-1	Straight Line Acceleration Speed	8B-5
Figure 8B-2	Paved Straight Line Acceleration: Maximum Speed	8B-6
Figure 8B-3	Paved Straight Line Acceleration Maturity Level Achieved by Vendors	8B-6
Figure 8B-4	Wall-To-Wall Clockwise and Counterclockwise: Diameter	8B-6
Figure 8B-5	Wall-To-Wall Maturity Level Achieved by Vendors	8B-7
Figure 8B-6	Steady-State Cornering 200 ft. Radius: Steering Angle vs. Lateral Acceleration	8B-7
Figure 8B-7	Steady-State Cornering Clockwise and Counterclockwise: Maximum Speed	8B-8
Figure 8B-8	Steady-State Cornering Clockwise and Counterclockwise: Maximum Lateral Acceleration	8B-8
Figure 8B-9	Steady-State Cornering Maturity Level Achieved by Vendors	8B-9
Figure 8B-10	Paved Double Lane Change LTF: Roll Rate	8B-9
Figure 8B-11	Paved Double Lane Change LTF: Yaw Rate	8B-10
Figure 8B-12	Paved Double Lane Change LTF: Lateral Acceleration	8B-10
Figure 8B-13	Paved Double Lane Change LTF: Steering Angle	8B-11
Figure 8B-14	Paved Double Lane Change Steering Open Loop, Left Turn First and Right Turn First: Maximum Speed	8B-11
Figure 8B-15	Paved Double Lane Change Steering Closed Loop, Left Turn First and Right Turn First: Maximum Speed	8B-12
Figure 8B-16	Gravel Double Lane Change LTF: Roll Rate	8B-12
Figure 8B-17	Gravel Double Lane Change LTF: Yaw Rate	8B-13
Figure 8B-18	Gravel Double Lane Change LTF: Lateral Acceleration	8B-13
Figure 8B-19	Gravel Double Lane Change LTF: Steering Angle	8B-14
Figure 8B-20	Gravel Double Lane Change Steering Open Loop, Left Turn First and Right Turn First: Maximum Speed	8B-14
Figure 8B-21	Gravel Double Lane Change Steering Closed Loop, Left Turn First and Right Turn First: Maximum Speed	8B-15
Figure 8B-22	Double Lane Change Left Turn First Maturity Level Achieved by Vendors	8B-15

Figure 8B-23	Double Lane Change Right Turn First Maturity Level Achieved by Vendors	8B-16
Figure 8B-24	Side Slope Stability: Lateral Acceleration	8B-16
Figure 8B-25	Side Slope Stability: Roll Rate	8B-17
Figure 8B-26	Side Slope Stability: Yaw Rate	8B-17
Figure 8B-27	Side Slope Stability: Steering Angle	8B-18
Figure 8B-28	Side Slope Stability Steering Open Loop, Left Side Down and Right Side Down: Maximum Speed	8B-18
Figure 8B-29	Side Slope Stability Maturity Level Achieved by Vendors	8B-19
Figure 8B-30	30% Sand Gradeability: Engine RPM	8B-19
Figure 8B-31	30% Sand Gradeability: Engine Torque	8B-20
Figure 8B-32	30% Sand Gradeability: Vehicle Speed	8B-20
Figure 8B-33	Sand Slope Gradeability Open Differentials and Full Locked Driveline: Maximum Slope	8B-21
Figure 8B-34	Sand Slope Gradeability Maturity Level Achieved by Vendors	8B-21
Figure 8B-35	Ride Quality: 1.0 RMS	8B-22
Figure 8B-36	Ride Quality: 1.2 RMS	8B-22
Figure 8B-37	Ride Quality: 2.4 RMS	8B-23
Figure 8B-38	Ride Quality: 3.6 RMS	8B-23
Figure 8B-39	Ride Quality: 6-Watt Absorbed Power Curve	8B-24
Figure 8B-40	Random Terrain Ride 1 Inch RMS and 1.2 Inch RMS: Limiting Speed	8B-24
Figure 8B-41	Random Terrain Ride 2.4 Inch RMS and 3.6 Inch RMS: Limiting Speed	8B-25
Figure 8B-42	RMS Maturity Level Achieved by Vendors	8B-25
Figure 8B-43	Drawbar Pull Open Differential and Locked Differentials: Drawbar Pull Coefficient at 20% Slip	8B-26
Figure 8B-44	Drawbar Open Differential and Locked Differentials: Drawbar Pull Coefficient at Peak Slip	8B-26
Figure 8B-45	Sand Traction Maturity Level Achieved by Vendors	8B-27
Figure 8B-46	Side Slope Stability Steering Closed Loop, Left Side Down and Right Side Down: Maximum Speed	8B-27
Figure 8B-47	Sand Slope Gradeability Open Differentials and Full Locked Driveline: Maximum Slope	8B-28
Figure 8B-48	Wheeled Vehicle Maturity Level	8B-30
Figure 9-1	Legacy NRMM2 Cross-Country Methodology	9-3
Figure 9-2	Assessment of Areas Addressed in NG-NRMM Compared to Legacy NRMM2 Cross-Country Methodology	9-4
Figure 9-3	Key New Requirements as Determined by ET-148	9-4

Figure 9-4	Generic NG-NRMM Methodology	9-7
Figure 9-5	NRMM2 vs. Long-Term NG-NRMM Using Approach 1	9-9
Figure 9-6	Example of Tool Comparisons Using Approach 1	9-9
Figure 9-7	Questions 1 and 2 Paired Response Summary from Ten Respondents	9-12
Figure 9-8	Questions 2 and 3 Paired Response Summary from Ten Respondents	9-15
Figure 9-9	Scope of Section 'Input'	9-17
Figure 9-10	Scope of Section 'Modeling'	9-21
Figure 9-11	Scope of Section 'Output'	9-28
Figure B-1	Example *.ASC File.	B-1
Figure C-1	Four Hydrologic Processes Considered in EMT+VS Model	C-2
Figure C-2	Relative Importance of the Four Hydrologic Processes with Spatial-Average Soil Moisture	C-5
Figure C-3	Sample 30 m EMT+VS Output for Monterey Bay, CA Sample Area	C-5
Figure C-4	Test Catchments for Soil Moisture Stochastic Variations Models	C-6
Figure C-5	Soil Moisture Maps (Observed Soil Moisture; Deterministic EMT+VS;Generalized EMT+VS, Indirect; and Generalized EMT+VS, Direct)	C-7
Figure C-6	EMT+VS Model Process Chain	C-8
Figure C-7	EMT+VS Soil Moisture Estimator Map-Centric Application Interface	C-9
Figure C-8	Sample Intermediate EMT+VS Model Results for Fort Pickett	C-9
Figure C-9	Sample EMT+VS Model Outputs for Fort Pickett	C-10
Figure D-1	Soil Strength Estimation Framework	D-2
Figure D-2	Generalized EMT+VS Soil Moisture Estimates for Monterey Bay (Nov 2015)	D-3
Figure D-3	USDA Soil Classes for the Monterey Bay Test Area	D-4
Figure D-4	Soil Strength Parameters for Monterey Bay Test Area	D-7
Figure D-5	Soil Strength Parameters for Monterey Bay Test Area (Nov. 2015)	D-7
Figure D-6	Moisture-Variable Cohesion (kPa) for the Monterey Bay Test Area (Nov. 2015)	D-8
Figure E-1	Current Bekker-Wong Model Parameter Sets	E-2

Figure F-1	Fitting the Secant Modulus E50 and Linear Hardening Tangent Modulus to a Uniaxial (or Shearing Phase of a Triaxial) Compression Test	F-3
Figure F-2	Yield Surfaces for Mohr-Coulomb, Drucker-Prager, Lade-Duncan,and Matsuoka-Nakai Models Fit to the Triaxial Compression Corners	F-6
Figure F-3	Cam-Clay Volumetric Deformation	F-10
Figure F-4	Shear Failure Surface Plotted Using Series of Triaxial Compression (TXC) Tests Conducted to Failure	F-12
Figure F-5	Illustration of Offset Parameter, N	F-13
Figure F-6	Effect of Kinematic Hardening Parameter, cα	F-13
Figure F-7	Pressure-Sinkage Relationship and Parameters for Empirical Terramechanics Models	F-16
Figure F-8	Particle-To-Particle Contact Model for Hertz-Mindlin Contact	F-19
Figure F-9	Particle-to-Wall Contact Model for Hertz-Mindlin Contact	F-20
Figure H-1	Top View of Vehicle	H-1
Figure H-2	Front View of Vehicle	H-2
Figure H-3	Side View of Vehicle	H-2
Figure H-4	Straight Line Acceleration	H-4
Figure H-5	Steady-State Cornering: Steering Angle vs. Lateral Acceleration	H-4
Figure H-6	Paved Double Lane Change Left Turn First: Yaw Rate	H-5
Figure H-7	Paved Double Lane Change Left Turn First: Roll Rate	H-5
Figure H-8	Paved Double Lane Change Left Turn First: Lateral Acceleration	H-6
Figure H-9	Paved Double Lane Change Left Turn First: Steering Angle	H-6
Figure H-10	Paved Double Lane Change Right Turn First: Yaw Rate	H-7
Figure H-11	Paved Double Lane Change Right Turn First: Roll Rate	H-7
Figure H-12	Paved Double Lane Change Right Turn First: Lateral Acceleration	H-8
Figure H-13	Paved Double Lane Change Right Turn First: Steering Angle	H-8
Figure H-14	Paved Double Lane Change Right Turn First: Yaw Rate	H-9
Figure H-15	Gravel Double Lane Change Left Turn First: Roll Rate	H-9
Figure H-16	Gravel Double Lane Change Left Turn First: Lateral Acceleration	H-10
Figure H-17	Gravel Double Lane Change Left Turn First: Steering Angle	H-10
Figure H-18	Gravel Double Lane Change Right Turn First: Yaw Rate	H-11
Figure H-19	Gravel Double Lane Change Right Turn First: Roll Rate	H-11

Figure H-20	Gravel Double Lane Change Right Turn First: Lateral Accleration	H-12
Figure H-21	Gravel Double Lane Change Right Turn First: Steering Angle	H-12
Figure H-22	Side Slope Stability Right Side Down: Yaw Rate	H-13
Figure H-23	Side Slope Stability Right Side Down: Roll Rate	H-13
Figure H-24	Side Slope Stability Right Side Down: Lateral Acceleration	H-14
Figure H-25	Side Slope Stability Right Side Down: Steering Angle	H-14
Figure H-26	30% Sand Gradeability: Engine RPM	H-15
Figure H-27	30% Sand Gradeability: Engine Torque	H-15
Figure H-28	30% Sand Gradeability: Vehicle Speed	H-16
Figure H-29	1.0 RMS	H-16
Figure H-30	1.2 RMS	H-17
Figure H-31	2.4 RMS	H-17
Figure H-32	3.6 RMS	H-18
Figure I-1	Comparison of Obstacle Height Distribution in the Two Terrain Files	I-4
Figure I-2	Comparison of All9 Approach Angle Distribution in Terrain Files	I-5
Figure I-3	Comparison of Approach Angle Distribution in Terrain Files	I-5
Figure I-4	Comparison of Obstacle Height vs Approach Angle for the Two Maps	I-6
Figure I-5	Example Cumulative Speed Curve Chart	I-7
Figure I-6	Example NRMM2 Predictions for Three Generic Vehicles, Dry/Normal Scenario	I-8
Figure I-7	Example NRMM2 Predictions for 3 Generic Vehicles, Wet/Slippery Scenario	I-9

List of Tables

Table		Page
Table 3-1	Terrain Parameters Present in the Latest NRMM Release (Version 2.8.2)	3-17
Table 3-2	Terrain Parameters Present in NRMM 3.0 Beta	3-22
Table 3-3	Terrain Parameters Added to Support Unique NG-NRMM Requirements	3-22
Table 4-1	Expected Simple Terramechanics (ST) Model Impacts on Legacy NRMM Mobility Factors and Their Inclusion in the Current NG-NRMM Benchmarks	4-4
Table 4-2	Notional Simple Terramechanics (ST) Model Parameters Assumed for the UW-M Prototype Demonstration of Speed-Made-Good Slope Climbing Performance on the Monterey GIS Data Set	4-16
Table 5A-1	Estimate of the Technology Readiness Levels of Macro-Scale Terramechanics Modeling Techniques	5A-17
Table 5C-1	Industries Using EDEM	5C-13
Table 5C-2	Physical Models of Soil Representations	5C-15
Table 6-1	Eight Bekker-Wong-Janosi Parameters	6-18
Table 6-2	Nine Unique Soil Type List	6-18
Table 6-3	Two Parameters for the DKG Surrogate Models	6-18
Table 8A-1	Tracked Vehicle Events Categories	8A-2
Table 8A-2	NG-NRMM Benchmark Modeling and Simulation Predictive Capability Maturity Levels	8A-2
Table 8A-3	Sample List of Vehicle Properties Required to Model the Vehicle in VehDyn	8A-6
Table 8A-4	Courses Used to Test Ride Quality, Shock Quality, and its Obstacle Crossing Ability	8A-7
Table 8A-5	Tracked Vehicle Benchmark Participants Listed by Software Developer Organization	8A-8
Table 8A-6	Computational Effort	8A-14
Table 8A-7	Trapezoidal Fixed Barrier Limits	8A-28
Table 8A-8	Trapezoidal Ditch Crossing Limits	8A-29
Table 8A-9	Tracked Vehicle Benchmark Maturity Levels	8A-36
Table 8B-1	NG-NRMM Benchmark Modeling and Simulation Predictive Capability Maturity Levels	8B-2

Table 8B-2	Wheeled Vehicle Benchmark Maturity Levels	8B-29
Table 9-1	Levels Definition Example	9-10
Table 9-2	Definitions of User Types	9-11
Table B-1	ASCII Raster Format Identifiers	B-2
Table B-2	PROJECTION Options	B-3
Table B-3	UNITS Options	B-3
Table B-4	PARAMETERS	B-4
Table B-5	Terrain Data Input Items	B-7
Table D-1	Comparison of Particle Size Classifications	D-4
Table D-2	Binned Unsaturated Soil Parameter Estimates	D-5
Table D-3	Binned Soil Strength Parameter Estimates	D-6
Table G-1	Pressure-Sinkage and Repetitive Loading Parameters for LETE Sand	G-6
Table G-2	Parameters for Internal and Rubber-Terrain Shearing for LETE Sand	G-7
Table G-3	Pressure-Sinkage Parameter Km for Petawawa Muskeg B, Obtained with the Surface Mat Being Cut	G-7
Table G-4	Shear Parameters for the Peat of Petawawa Muskeg B	G-8
Table G-5	Pressure-Sinkage and Repetitive Loading Parameters for Petawawa Snow A	G-9
Table G-6	Internal Shear Parameters for Petawawa Snow A	G-9
Table G-7	Parameters for Rubber-Snow Shearing for Petawawa Snow A	G-10
Table H-1	General Vehicle Data	H-3

List of Acronyms

2D	Two-Dimensional
3D	Three-Dimensional
AASHTO	American Association of State Highway and Transportation Officials
ABS	Anti-lock Braking System
ACSI	Adams Co-Simulation Interface
ALE	Arbitrary Lagrangian-Eulerian
AMC	Army Materiel Command
AMSAA	US Army Materiel Systems Analysis Activity
ANCF	Absolute Nodal Coordinate Formulation
AOI	Area of Interest
API	Application Programming Interface
ARL	Army Research Laboratory
ASA	Advanced Science and Automation Corp.
ASME	American Society of Mechanical Engineers
ASTM	American Society for Testing and Materials
ATV	Adams Tracked Vehicle
AVT	Applied Vehicle Technology
AVTP	Allied Vehicle Testing Publication
BSD	Berkeley Source Distribution
BWJ	Bekker-Wong-Janosi
CAE	Computer Aided Engineering
CCDC	Combat Capabilities Development Command
CCW	Counter Clockwise
CDT	Cooperative Demonstration of Technology
CFD	Computational Fluid Dynamics
CG	Center of Gravity
CI	Cone Index
COTS	Commercial Off-the-Shelf
CRREL	Cold Regions Research and Engineering Laboratory
CSIR	South African Council for Scientific and Industrial Research
CSO	NATO Collaboration Support Office
CTIS	Central Tire Inflation System
CTS	Combinatorial Trade Study
CV	Constant Velocity
CVT	Continuously Variable Transmission
CW	Clockwise
DAE	Differential Algebraic Equations
DARTS	Dynamics Algorithms for Real-Time Simulation
DDI	Deep Drainage Index
DEM	Digital Elevation Model
DEM	Discrete Element Method
DEM-C	DEM Penalty-Based
DEM-P	DEM Complementarity-Based
DFDD	DGIWG Feature Data Dictionary
DGIWG	Defence Geospatial Information Working Group

DIGEST	Digital Geographic Information Exchange Standard
DIS	Dynamic Interactions Simulator
DKG	Dynamic Kriging
DLC	Double Lane Change
DMT	Derjaguin-Muller-Toporov
DoD	US Department of Defense
DOE	Design of Experiments
DOF	Degree of Freedom
DTED	Digital Terrain Elevation Data
DVI	Differential Variational Inequality
EDEM	Edinburgh Discrete Element Modeling Software
EEPA	Edinburgh Elasto-Plastic Adhesion Model
EMT+VS	Equilibrium Moisture from Topography, Vegetation, and Soil
ERDC	Engineer Research and Development Center
ESC	Electronic Stability Control
ET	Evapotranspiration
ET	Exploratory Team
FACC	Feature Attribute Coding Catalogue
FEM	Finite Element Model
FOV	Field of View
GDG	Geospatial Data Gateway
GEMM	Generic EDEM Material Model
GIS	Geographical Information System
GPS	Global Positioning System
GPU	Graphics Processing Unit
GVSC	Ground Vehicle Systems Center
GUI	Graphical User Interface
HDF	Hierarchical Data Format
HGTM	High-Resolution Ground Vehicle and Terrain Mechanics
HMMWV	High Mobility Multipurpose Wheeled Vehicle
HPC	High-Performance Computing
IMU	Inertial Measurement Unit
ISO	International Organization for Standardization
ISRIC-WISE	International Soil Reference and Information Centre-World Inventory of Soil Emission Potentials
ISTVS	International Society for Terrain-Vehicle Systems
IVRESS	Integrated Virtual Reality Environment for Synthesis and Simulation
JKR	Johnson-Kendall-Roberts
JPL	Jet Propulsion Lab
LFI	Lateral Flow Index
LIDAR	Light Detection and Ranging
LL	Liquid Limit
LSD	Left Side Down
LTF	Left Turn First
M&S	Modeling and Simulation
MBD	Multibody Dynamics

MC	Moisture Content
MCS	Monte Carlo Simulation
MDO	Multi-discipline Optimization
MGCP	Multinational Geospatial Co-Production
MMP	Mean Maximum Pressure
mph	Miles per Hour
MPI	Message Passing Interface
MPM	Material Point Method
MSE	Mean Square Error
MSIE	Modeling & Simulation Integrating Environment
MSL	Mars Science Lab
NAAG	NARO Army Armament Group
NATC	Nevada Automotive Test Center
NATC	Nevada Automotive Test Center
NATO	North American Treaty Organization
NED	National Elevation Dataset
NetCDF	Network Common Data Format
NG-NRMM	Next Generation NATO Reference Mobility Model
NLCD	National Land Cover Dataset
NRC	National Research Council
NRCS	National Resources Conservation Service
NRMM	NATO Reference Mobility Model
NRMM(I)	NG-NRMM for Intelligent Vehicles
NSC	Non-Smooth Contact
NTU	Number of Terrain Units
NWTVM	Nepean Tracked Vehicle Performance Model
NWVPM	Nepean Wheeled Vehicle Performance Model
OBAA	Obstacle Approach Angle
OBH	Obstacle Height
OBW	Obstacle Width
ODE	Ordinary Differential Equations
OGC	Open Geospatial Consortium
PC	Personal Computer
PDE	Partial Differential Equations
PID	Proportional–integral–derivative
POMC	Proctor Optimal Moisture Content
RCI	Rating Cone Index
REI	Radiation Evapotranspiration Index
RMS	Root Mean Square
RMSE	Root Mean Square Error
ROAMS	Rover Analysis, Modeling and Simulator
RPM`	Revolutions per Minute
RSD	Right Side Down
RTF	Right Turn First
RTG	Research Task Group
RTO	NATO Research and Technology Organization
RVD	Relative Velocity Dependent
SAE	Society of Automotive Engineers
SAVI	Soil Adjusted Vegetation Index

SBIR	Small Business Innovation Research
SCM	Soil Contact Model
SLA	Straight Line Acceleration
SLAM	Simultaneous Localization and Mapping
SMAP	Soil Moisture Active Passive
SMC	Smooth Contact
SPH	Smoothed Particle Hydrodynamics
SPI	Standard Particle Interface
SPI	Standard Particles Interface
SRTM	Shuttle Radar Topography Mission
SRTM	Shuttle Radar Topography Mission
SSC	Steady State Cornering
SSG	Sand Slope Gradeability
SSS	Side Slope Stability
SSURGO	Soil Survey Geographic Database
ST	Simple Terramechanics
STANREC	Standard Recommendation
STO	NATO Science and Technology Organization
TA	AVT-248 Thrust Area
TAP	Technical Activity Proposal
TARDEC	Tank Automotive Research, Development and Engineering Center (changed in FEB 2019 to CCDC Ground Vehicle Systems Center)
TCS	Traction Control System
TIFF	Tagged Image File Format
TIN	Triangulated Irregular Network
TOR	Terms of Reference
TRL	Technology Readiness Level
TSC	Technology Service Corporation
TV	Tracked Vehicle
UAV	Unmanned Aerial Vehicle
UGV	Unmanned Ground Vehicle
UQ	Uncertainty Quantification
USACE	United States Army Corps of Engineers
USCS	Unified Soil Classification System
USDA	United States Department of Agriculture
USGS	United States Geological Survey
UTM	Universal Transverse Mercator
UW-M	University of Wisconsin - Madison
V&V	Verification and Validation
VCI	Vehicle Cone Index
VEHDYN	Vehicle Dynamics part of NRMM code
VI	Vehicle Intelligence
VSDC	Vehicle Systems Development Corporation
VTI	Vehicle Terrain Interface; Vehicle Terrain Interaction
WD	Wheel Drive
WES	Waterways Experimental Station
WNS	Wave Number Spectra
WTW	Wall to Wall
WVP	Wheeled Vehicle Prototype

AVT-248 Membership List

CO-CHAIRS

Dr.-Ing. Michael HÖNLINGER
Krauss-Maffei Wegmann GmbH & Co. KG
GERMANY
Email: michael.hoenlinger@kmweg.de

Dr. Paramsothy JAYAKUMAR*
US Army CCDC Ground Vehicle Systems Center
UNITED STATES
Email: paramsothy.jayakumar.civ@mail.mil

MEMBERS

Dr. Ozgen AKALIN
Istanbul Technical University
TURKEY
Email: akalin@itu.edu.tr

Mr. Russell ALGER
Michigan Technological University / Keweenaw Research Center
UNITED STATES
Email: rgalger@mtu.edu

Dr. Ole BALLING*
Aarhus University
DENMARK
Email: oba@eng.au.dk

Dr.-Ing. habil. Andreas BECKER
Technical University of Kaiserslautern
GERMANY
Email: becker@rhrk.uni-kl.de

Mr. Michael BRADBURY*
Defence Science & Technology Laboratory (Dstl)
UNITED KINGDOM
Email: mbradbury@dstl.gov.uk

Mr. Jonathan BRUCE*
Defence Science & Technology Laboratory (Dstl)
UNITED KINGDOM
Email: jlbruce@dstl.gov.uk

Mr. Mark CAMMARERE*
Technology Service Corporation
UNITED STATES
Email: mcammarere@tsc.com

Dr. Kyung K. CHOI*
University of Iowa
UNITED STATES
Email: kkchoi@engineering.uiowa.edu

Capt. Francesco CORSO
Secretariat General of Defence and National Armaments Directorate 5th Department
ITALY
Email: r5u2s1add1@sgd.difesa.it

Dr. Jean DASCH*
Alion Science & Technology
UNITED STATES
Email: jean.m.dasch.ctr@mail.mil

Mr. Wim DE KLERK
Netherlands Organisation for Applied Scientific Research (TNO)
NETHERLANDS
Email: wim.deklerk@tno.nl

Dr. Susan FRANKENSTEIN
US Army ERDC CRREL
UNITED STATES
Email: Susan.Frankenstein@usace.army.mil

Mr. Matthew FUNK*
Esri, Inc.
UNITED STATES
Email: mfunk@esri.com

Dr. Nicholas GAUL*
RAMDO Solutions, LLC
UNITED STATES
Email: nicholas-gaul@ramdosolutions.com

Mr. Rainer GERICKE (ret.)
Bundeswehr
GERMANY
Email: rainergericke@bundeswehr.org

* Author

Prof. Amer HAMEED
Cranfield University
UNITED KINGDOM
Email: a.hameed@cranfield.ac.uk

Captain Hrvoje HEŠTERA
Croatian Defence Academy
CROATIA
Email: hrvoje.hestera@morh.hr

Mr. Henry HODGES*
Hodges Transportation, Inc.
UNITED STATES
Email: hhodgesJr@natc-ht.com

Dr. Abhinandan JAIN*
Jet Propulsion Laboratory
UNITED STATES
Email: jain@jpl.nasa.gov

Col (ret.) Eugeniusz JENDRASZCZAK
War Studies University
POLAND
Email: e.jendraszczak@akademia.mil.pl

Dr. Andrew JONES
Colorado State University
UNITED STATES
Email: Andrew.S.Jones@ColoState.edu

Mr. Michael LETHERWOOD
US Army CCDC Ground Vehicle Systems Center
UNITED STATES
Email: michael.d.letherwood.ctr@mail.mil

Mr. William MAYDA
National Research Council
CANADA
Email: william.mayda@nrc-cnrc.gc.ca

Dr. Michael McCULLOUGH*
BAE Systems Inc.
UNITED STATES
Email: michael.mccullough@baesystems.com

Mr. Dean MENGEL
Lockheed Martin Missiles and Fire Control
UNITED STATES
Email: dean.mengel@lmco.com

Dr. Vlastimil NEUMANN
University of Defence
CZECH REPUBLIC
Email: vlastimil.neumann@unob.cz

Dr. Jeffrey NIEMANN*
Colorado State University
UNITED STATES
Email: jniemann@engr.colostate.edu

Mr. Phumlane NKOSI
Armaments Corporation of South Africa (Armscor)
SOUTH AFRICA
Email: phumlanen@armscor.co.za

Mr. Kevin PERRY
Lockheed Martin Missiles and Fire Control
UNITED STATES
Email: kevin.a.perry@lmco.com

Mr. Jon PRESTON-THOMAS
National Research Council Canada (NRC)
CANADA
Email: jon.preston-thomas@nrc-cnrc.gc.ca

Mr. Johann David REINECKE
Council for Scientific and Industrial Research (CSIR)
SOUTH AFRICA
Email: dreinecke@csir.co.za

Maj. Petru ROSCA
Military Equipment and Technologies Research Agency
ROMANIA
Email: prosca@acttm.ro

Assoc. Prof. Marian RYBANSKY
University of Defence in Brno
CZECH REPUBLIC
Email: marian.rybansky@unob.cz

Dr. Gregory SCHULTZ
US Army Aberdeen Test Center
UNITED STATES
Email: gregory.a.schultz.civ@mail.mil

Dr. Radu SERBAN
University of Wisconsin-Madison
UNITED STATES
Email: serban@wisc.edu

Dr. Sally SHOOP
US Army ERDC CRREL
UNITED STATES
Email: sally.a.shoop@usace.army.mil

* Author

Dr. Ravi THYAGARAJAN
US Army CCDC Ground Vehicle Systems Center
UNITED STATES
Email: ravi.thyagarajan@mail.mil

Prof. Vladimir VANTSEVICH
University of Alabama at Birmingham
UNITED STATES
Email: vantsevi@uab.edu

Captain Kersti VENNIK
Estonian National Defence College
ESTONIA
Email: kersti.vennik@mil.ee

Mr. Tom VON STURM ZU VEHLINGEN
Wehrtechnische Dienststelle fuer Kraftfahrzeuge und Panzer (WTD 41)
GERMANY
Email: tomvonsturmzuvehlingen@bundeswehr.org

Dr. Tamer WASFY*
Advanced Science and Automation Corp.
UNITED STATES
Email: tamerwasfy@ascience.com

Mr. Brian WOJTYSIAK*
US Army Material Systems Analysis Activity (AMSAA)
UNITED STATES
Email: brian.l.wojtysiak.civ@mail.mil

Dr. Jozef WRONA
Military University of Technology
POLAND
Email: Jozef.wrona@wat.edu.pl

Dr. Marko Zecevic
Croation Military Academy
CROATIA
Email: marko.zecevic@morh.hr

Ms. Petra ZIEGER
BGIC Bundeswehr Geoinformation Centre
GERMANY
Email: petrazieger@bundeswehr.org

ADDITIONAL CONTRIBUTORS

Mr. David AGUILAR
SmartUQ
UNITED STATES
Email: david.aguilar@smartuq.com

Mr. Jim AJLOUNY
Alion Science & Technology
UNITED STATES
Email: jajlouny@alionscience.com

Mr. Mark ANDREWS
SmartUQ
UNITED STATES
Email: mark.andrews@smartuq.com

Mr. Scott BRADLEY
Michigan Technological University / Keweenaw Research Center
UNITED STATES
Email: sabradle@mtu.edu

Dr. Craig FOSTER*
University of Illinois at Chicago
UNITED STATES
Email: fosterc@uic.edu

Mr. Bernard FROMAN
Ricardo Defense
UNITED STATES
Email: befroman@ricardodefense.com

Dr. Richard GERTH
US Army CCDC Ground Vehicle Systems Center
UNITED STATES
Email: richard.j.gerth.civ@mail.mil

Mr. Jakub GLOWKA
Industrial Research Institute for Automation and Measurements
POLAND
Email: jglowka@piap.pl

* Author

Mr. David GUNTER
US Army CCDC Ground Vehicle Systems Center
UNITED STATES
Email: david.d.gunter2.civ@mail.mil

Dr. Eric McDONALD
Desert Research Institute (DRI)
UNITED STATES
Email: Eric.Mcdonald@dri.edu

Dr. Dithoto MODUNGWA
CSIR
SOUTH AFRICA
Email: Dmodungwa@csir.co.za

Ms. Melissa MORGAN
US Army CCDC Ground Vehicle Systems Center
UNITED STATES
Email: melissa.b.morgan3.civ@mail.mil

Prof. Dan NEGRUT
University of Wisconsin-Madison
UNITED STATES
Email: negrut@wisc.edu

Mr. Brian ORTEGA
Army Materiel Systems Analysis Activity
UNITED STATES
Email: brian.k.ortega.civ@mail.mil

Mr. Mark OSBORNE
Michigan Technological University / Keweenaw Research Center
UNITED STATES
Email: mosborne@mtu.edu

Mr. Reid PULLEY*
Nevada Automotive Test Center
UNITED STATES
Email: rpulley@natc-ht.com

Ms. Lorraine RAGALAVHANDA
Armaments Corporation of South Africa (Armscor)
SOUTH AFRICA
Email: lorraineg@armscor.co.za

Dr. Elham RAMYAR*
Northwestern University
UNITED STATES
Email: Elhamramyar2022@u.northwestern.edu

Dr. Joseph SCALIA*
Colorado State University
UNITED STATES
Email: joseph.scalia@colostate.edu

Mr. Wesley SCHARMEN
Ricardo Defense Systems LLC
UNITED STATES
Email: wesley.scharmen@ricardo.com

Mr. Albert SHYU
BAE Systems Land and Armaments
UNITED STATES
Email: albert.shyu@baesystems.com

Dr. Amandeep SINGH
US Army CCDC Ground Vehicle Systems Center
UNITED STATES
Email: amandeep.singh2.civ@mail.mil

Dr. James WEAKLAND
Environmental Systems Research Institute, Inc.
UNITED STATES
Email: jweakland@esri.com

Dr. Xiaobo YANG
Oshkosh Corporation
UNITED STATES
Email: xyang@oshkoshcorp.com

* Author

PANEL/GROUP MENTOR

Dr.-Ing. Michael HÖNLINGER
Krauss-Maffei Wegmann GmbH & Co. KG
GERMANY
Email: michael.hoenlinger@kmweg.de

Next-Generation NATO Reference Mobility Model (NG-NRMM) Development

(STO-TR-AVT-248)

Executive Summary

The NATO Reference Mobility Model (NRMM) is a simulation tool aimed at predicting the capability of a vehicle to move over specified terrains. NRMM was developed and validated by the US Army Tank Automotive Research, Development, and Engineering Center (TARDEC: Changed in FEB 2019 to CCDC Ground Vehicle Systems Center) and Engineer Research and Development Center (ERDC) in the 1960s and '70s, and has been revised and updated through the years, resulting in the most recent version, NRMM II. NRMM is traditionally used to facilitate comparisons between vehicle design candidates and to assess the mobility of existing vehicles under specific scenarios.

Although NRMM has proven to be of great practical utility to the NATO forces, it exhibits several inherent limitations. It is based on empirical observations, and therefore extrapolation outside of test conditions is difficult or impossible. It cannot simulate contemporary vehicle designs and technologies, nor does it benefit from advances in simulation and computational capabilities. This led to the formation of Exploratory Team 148 followed by Research Task Group AVT-248 to develop a Next-Generation NATO Reference Mobility Model (NG-NRMM).

Seven Thrust Areas were formed within AVT-248, including GIS Terrain and Mobility Map; Simple Terramechanics; Complex Terramechanics; Intelligent Vehicles; Uncertainty Treatment;Verification and Validation (V&V); Data Gaps and Operational Readiness. As part of the V&V Thrust Area, software developers were invited to compare their state-of-the-art, physics-based mobility models against actual test data for a tracked vehicle and a wheeled vehicle on both paved surfaces and soft soil. The developers were able to evaluate the strengths and weaknesses of their models and enhance their models to meet the goals of NG-NRMM.

The deliverables from AVT-248 included a simple terramechanics prototype demonstration, a complex terramechanics prototype demonstration, the V&V benchmarking exercise mentioned above, and the initial release of a STANREC documenting the requirements for an NG-NRMM. All of these are covered in this Final Report. In addition, two complementary Research Task Groups were spun off as new activities: – a Cooperative Demonstration of Technology (AVT-308); and a STANREC RTG to continue to upgrade and manage the initial STANREC release (AVT-327).

NG-NRMM is vital to NATO's mission as it will add new capabilities in the design, modeling, and simulation of a broad class of vehicles, with the potential to reduce costs and improve performance. This could yield a new paradigm for ground vehicle mobility with the possibility to model complex vehicle maneuvers in high fidelity. AVT-248 was initiated in January 2016 and concluded in December 2018. At the conclusion of AVT-248, the committee included 70 appointed members and contributors representing 15 nations in all.

Développement du modèle de mobilité de référence de l'OTAN (NRMM) de nouvelle génération

(STO-TM-AVT-248)

Synthèse

Le modèle de mobilité de référence de l'OTAN (NRMM) est un outil de simulation visant à prédire la capacité d'un véhicule à se déplacer sur des terrains spécifiés. Le NRMM a été développé et validé par le Tank Automotive Research, Development and Engineering Center (TARDEC, qui a pris le nom de CCDC Ground Vehicle Systems Center en février 2019) et l'Engineer Research and Development Center (ERDC) de l'armée des États-Unis dans les années 1960 et 1970 et a été révisé et mis à jour au fil du temps, pour donner naissance à sa version la plus récente, le NRMM II. Le NRMM sert habituellement à faciliter la comparaison entre les projets de conception de véhicule et à évaluer la mobilité des véhicules existants dans des scénarios particuliers.

Bien que le NRMM ait démontré sa grande utilité pratique pour les forces de l'OTAN, il présente des limites intrinsèques. Il repose sur des observations empiriques, ce qui rend difficile, voire impossible, l'extrapolation en dehors des conditions d'essai. Il ne peut pas simuler les conceptions et technologies des véhicules contemporains et ne bénéficie pas des progrès des capacités de simulation et de calcul. Cet état de fait a entraîné la formation de l'équipe exploratoire 148, suivie du groupe de recherche AVT-248, afin de développer un modèle de mobilité de référence de l'OTAN de nouvelle génération (NG-NRMM).

Sept domaines d'intervention ont été établis au sein de l'AVT-248 : carte morphographique et de mobilité pour SIG, mécanique des sols simple, mécanique des sols complexe, véhicules intelligents, traitement de l'incertitude, vérification et validation (V&V), lacunes en matière de données et état de préparation opérationnelle. Dans le cadre du domaine d'intervention V&V, les développeurs de logiciels ont été invités à comparer leurs modèles de mobilité de pointe basés sur la physique avec les données d'essai réelles, concernant un véhicule chenillé et un véhicule à roues, sur des surfaces revêtues et sur un sol souple. Les développeurs ont été en mesure d'évaluer les forces et faiblesses de leurs modèles et d'améliorer ces derniers pour répondre aux objectifs du NG-NRMM.

Les éléments livrables de l'AVT-248 incluaient une démonstration de prototype de mécanique des sols simple, une démonstration de prototype de mécanique des sols complexe, l'exercice d'analyse comparative de V&V mentionné plus haut et la publication initiale d'un STANREC documentant les besoins d'un NG-NRMM. Tous ces éléments sont traités dans le présent rapport final. De plus, deux groupes de recherche complémentaires ont été créés en tant que nouvelles activités : une démonstration en coopération des technologies (AVT-308) et un RTG STANREC pour continuer à actualiser et gérer la publication initiale du STANREC (AVT-327).

Le NG-NRMM est vital pour la mission de l'OTAN, car il ajoutera de nouvelles capacités à la conception, modélisation et simulation d'une large catégorie de véhicules, en ayant le potentiel de réduire les coûts et améliorer les performances. Cela pourrait donner lieu à un nouveau paradigme de mobilité des véhicules terrestres, laissant la possibilité de modéliser des manœuvres complexes de véhicules avec une fidélité élevée. L'AVT-248 a été lancé en janvier 2016 et clos en décembre 2018. Lors de la conclusion de l'AVT-248, le comité comptait 70 membres et contributeurs désignés représentant 15 pays.

Chapter 1 – INTRODUCTION

Jean Dasch
Alion Science and Technology
UNITED STATES

1.1 BACKGROUND

The NATO Reference Mobility Model (NRMM) is the accepted international standard for modeling the mobility of ground combat and tactical vehicles. It is a simulation tool aimed at predicting the comparative capability of a vehicle to move over specified terrain. NRMM can be used for on-road and cross-country scenarios, and it can account for several parameters such as terrain type, moisture content, terrain roughness, and vehicle geometry.

NRMM has proven to be of great practical value to the NATO nations since its development in the 1960s and '70s. Although it has been revised over the years, the basis of NRMM is over 50 years old. When compared to modern modeling tools, it exhibits inherent limitations; primarily:

- It is heavily dependent on empirical observations such as in-situ soil measurements so that extrapolation outside of test conditions is difficult.
- Only two-dimensional analysis is possible.
- It does not account for vehicle dynamic effects; rather it only considers steady-state conditions for cross-country mobility.
- It is not easily implemented with modern vehicle dynamics simulations or other terramechanics models.
- It does not address uncertainty.
- It does not account for the different drivers and constraints associated with unmanned ground vehicles or alternate vehicle control strategies.

Due to the recognition of the need for an updated model, a NATO Exploratory Team was proposed during the spring 2014 NATO AVT meeting in Copenhagen, Denmark by Panel Member Dr. David Gorsich, Chief Scientist of GVSC. The scope of Exploratory Team 148 (ET-148) was to investigate an efficient simulation-based Next-Generation NRMM. ET-148 concluded in December 2015 with a total of 39 members from 13 nations. The final report was issued in 2017 [1] and a descriptive journal paper was published in 2017 [2]. Based on the results of the Exploratory Team, a Research Task Group AVT-248 was approved to develop a Next-Generation NRMM. See Technical Activity Proposal (TAP) and Terms Of Reference (TOR) in Annex A and Ref. [3]. AVT-248 was initiated in January 2016 and concluded in December 2018 and included 66 appointed members and contributors from 15 nations.

1.2 NRMM HISTORY

Mobility modeling began in the U.S. to address vehicle shortcomings recognized during World War II. Vehicle-terrain testing labs were set up with extensive test facilities at the United States Army laboratories, WES [4] and the TARDEC Land Locomotion Laboratory [5]. Following decades of research, the Army Materiel Command requested that the two Army Labs (TARDEC, WES) work together on a mobility model. The two labs in coordination with Stevens Institute of Technology issued the AMC-71 Mobility Model in 1971 [6].

As described in the Foreword to the report on the model, "mathematical modeling allows for the evaluation of the entire vehicle system (engine, transmission, suspension, weight, geometry, inertia, winching capacity, and so on) as it interacts with soil, vegetation, slopes, ditches, mounds and other features in a synergistic fashion."

Meanwhile in 1976, NATO AC/225 Panel II, which was part of the NATO Army Armament Group (NAAG), recognized the need for standardized techniques to compare vehicle performance and the U.S. offered to help initiate this effort [7]. This was accepted by Panel II and AC 225/Working Group I (WGI) was established with membership from six countries (Canada, France, Germany, the Netherlands, the United Kingdom, and the United States) and the first meeting was held at TARDEC in 1977.

Research and development continued and the second version of the model, NRMM II, was issued in 1992 incorporating many of the changes that were made in the interim [8]. The new algorithms were mainly due to the mobility tests conducted by WES since 1979 including the wheeled vs. tracked test program and included new equations in the area of soil traction, soil resistance, and surface slipperiness [9]. In addition, special software was included to encompass radial tires and Central Tire Inflation Systems (CTIS).

There was a need to reassemble the international community to consolidate various independent and often duplicative efforts into a collection of tools that would be considered a new version of NRMM and, subsequently to validate, standardize and maintain the resulting package as a shared NATO resource. Dr. Richard McClelland, TARDEC Director, proposed the idea to the NATO Applied Vehicle Technology (AVT) panel in the fall of 2002 [10]. The NATO AVT-107 – Mobility Modeling Working Group was set up to coordinate and conduct this task. AVT-107 first met in October 2002 and concluded in 2006, with eight meetings held in the interim. The primary countries involved were Canada, France, Romania, the United Kingdom and the United States with lesser involvement by the Netherlands and Germany.

The results from AVT-107 were presented to the AVT Panel on 6 October 2006 and the final report was published in 2011 [4]. The committee's work and the final report are valuable in several respects in that the following areas are extensively discussed:

- A history of the development of the NRMM model from the 1960s;
- A detailed status of the model;
- Identified limitations; and
- Communication of NRMM usage and upgrades by various nations.

Despite the successes of AVT-107, many of the NRMM tool limitations were eventually not addressed. As a result, NRMM is less effectively used by the NATO nations. One significant concern is that if the current tool is not enhanced with higher fidelity and efficiency, it will leave the NATO nations with a subpar mobility tool that is neither capable of accurately differentiating competing designs nor capable of accurately predicting mobility performance of a specific design in various operational scenarios. A more complete history of NRMM can be found in Ref. [1].

1.3 OBJECTIVES

Four objectives were envisioned for AVT-248:

1) The first objective of AVT-248 was to implement the development of a prototype Next-Generation NATO Reference Mobility Model (NG-NRMM) involving several areas of effort:

- Integration of GIS-based terrain data and implementation of mobility mapping metric into mobility simulation software.
- Identification of vehicle-terrain interaction models, i.e., terramechanics models, that balance fidelity with computational efficiency. These models may be semi-empirical, or fully analytical such as those based on discrete elements.
- Development of in-situ and real-time measurement tools to identify required terrain parameters.
- Integration of terramechanics models into modern vehicle dynamic simulation software, and development of efficient, automated tools that will enable the use of high-performance computational techniques.
- Identification of the type and form of desired responses, to yield rich mobility predictions and useful auxiliary outputs.
- Development of stochastic mobility output by embedding stochastic terrain and vehicle data.
- Since the Next-Generation NRMM can be computationally intensive, there exists a need to investigate numerical algorithms to improve computational efficiency.

2) The second objective was to develop two prototype demonstrations, one in the area of Simple Terramechanics and the second in the area of Complex Terramechanics. Both are physics-based, but the Complex model provides a vision of the future possibilities to produce real-time mobility simulations possible with high performance computing.

3) The third objective was to conduct a Verification and Validation Exercise using both a tracked and wheeled vehicle. Software developers were invited to participate and were provided with vehicle data and tasked with modeling the vehicle as it engaged in a variety of events over different terrains. Their results were compared to actual test results to evaluate the state of modern terramechanical models and move them toward the goals of the NG-NRMM.

4) The final objective was to write a Recommended Standard (STANREC) to provide guidance for M&S standards that are applicable to the development of an NG-NRMM.

The realization of these objectives is captured in this Final Report. In addition, two complementary Research Task Groups were spun off as new activities: A Cooperative Demonstration of Technology (AVT-308); and STANREC RTG to continue to upgrade and manage the initial STANREC release (AVT-327).

1.4 REFERENCES

[1] Dasch, J.M. and Jayakumar, P. (Ed). 2018. Next-Generation NATO Reference Mobility Model Development, NATO STO-AVT-ET-148 Report, AC/323(AVT-ET-148)TP/728.

[2] McCullough, M., Jayakumar, P., Dasch, J. and Gorsich, D. 2017. The Next-Generation NATO Reference Mobility Model Development, Journal of Terramechanics, 73:49-60.

[3] AVT-248, RTG-085. 2016. Technical Activity Proposal, Next-Generation NATO Reference Mobility Model (NRMM) Development. Endorsed by NATO AVT Panel in Brussels, Belgium.

[4] Jones, R., Ciobotaru, T. and Galway, M. (Eds). 2011. NATO Reference Mobility Modeling, NATO RTO Technical Report TR-AVT-107.

[5] Liston, R.A. 1965. The Land Locomotion Laboratory. Journal of Terramechanics, 2(4).

[6] AMC ‘71 Mobility Model. 1973. AMC ‘71 Mobility Model. Technical Report No. 11789 (LL 143).

[7] Haley, P.W., Jurkat, M.P. and Brady, P.M. 1979. NATO Reference Mobility Model, Edition I. Users Guide, Vol. 1 (ADB047979) and Vol. II (ADB047980).

[8] Ahlvin, R.B. and Haley, P.W. 1992. NATO Reference Mobility Model, Edition II. NRMM II Users Guide, Technical Report Gl-92-19, US Army Corps of Engineers Geotechnical Laboratory, Vicksburg, MS.

[9] Willoughby, W.E., Jones, R.A., Cothren, C.D., Moore, D.W. and Rogillio, D.M. 1991. US Army Wheeled Versus Tracked Vehicle Mobility Performance Test Program, Report 1. Mobility in Slippery Soils and Across Gaps, Vol. 1, Program Summary, ADB152890 (restricted to U.S. Government only).

[10] McClelland, R. 2002. A Proposed NATO Study Group on Ground Vehicle Mobility Modeling. Presentation to NATO AVT Panel.

Chapter 2 – APPROACH

Jean Dasch
Alion Science and Technology
UNITED STATES

2.1 AVT-248 ORGANIZATION

The formation of Research Technical Group AVT-248 was approved in the fall 2014 NATO meeting in Brussels, Belgium. Dr. Paramsothy Jayakumar of the United States and Dr. Michael Hoenlinger of Germany serve as Co-Chairs. The project ran from January 2016 to December 2018. By the conclusion membership had grown to 70 members and participants. Membership included 15 nations (Canada, Croatia, Czech Republic, Denmark, Estonia, Germany, Italy, Netherlands, Poland, Romania, Slovakia, South Africa, Turkey, the United Kingdom, and the United States). Teleconferences were held on a monthly basis and the group met face-to-face six times at NATO AVT Panel Business Meetings in Tallinn, Estonia April 2016, in Avila, Spain September 2016, in Vilnius, Lithuania May 2017, in Utrecht, The Netherlands October 2017, in Torino, Italy April 2018 and in Athens, Greece December 2018. All meetings were attended by 25 to 30 persons.

The overall project was divided into seven Thrust Areas, each with a lead or leads. Members of AVT-248 selected one or more Thrust Areas to join, depending on their interest and area of expertise. The seven Thrust Areas and their leads were:

- Thrust Area 1: GIS Terrain and Mobility Map — Matt Funk, Brian Wojtysiak.
- Thrust Area 2: Simple Terramechanics — Mike McCullough
- Thrust Area 3: Complex Terramechanics — Tamer Wasfy.
- Thrust Area 4: Intelligent Vehicle — Abhi Jain.
- Thrust Area 5: Uncertainty Treatment — K.K. Choi, Nick Gaul.
- Thrust Area 6: Verification and Validation — Ole Balling.
- Thrust Area 7: Data Gaps; Operational Readiness — Mike Bradbury, Jonathan Bruce.

A very brief description of the primary objective of each Thrust Area is shown below:

TA-1. GIS Terrain and Mobility Mapping: Identify a GIS-based mapping tool that implements and integrates existing valid mobility metrics (%NOGO and Speed-Made-Good) in an open architected environment.

TA-2. Simple Terramechanics: Identify most promising existing terramechanics methods supporting NG-NRMM requirements that provide a means of correlating the requisite terrain characteristics to remotely sensed GIS data.

TA-3. Complex Terramechanics: Establish a vision for the long-term terramechanics approaches that overcome the limitations of existing models.

TA-4. Intelligent Vehicle. Identify unique mobility metrics and M&S methods necessary for mobility assessments of intelligent vehicles over a sliding scale of data and control system resolutions.

TA-5. Uncertainty Treatment: Identify the practical steps required to embed stochastic characteristics of vehicle and terrain data to extend and refine the current deterministic mobility metrics.

TA-6. Verification & Validation (V&V). Implement near-term vehicle-terrain interaction benchmarks for verification of candidate NG-NRMM M&S software solutions and lay the groundwork for long-term validation data through cooperative development with test organizations standards committees.

TA-7. Data Gaps and Operational Readiness. Identify gaps that have not been addressed in AVT-248. Determine the path forward to attain operational readiness.

In the following Final Report, a chapter or chapters will be devoted to the work of each Thrust Area.

2.2 AVT-248 DELIVERABLES

Five deliverables were envisioned for AVT-248:

- Prototype Demonstrations;
- Verification and Validation;
- STANREC – initial release;
- Cooperative Demonstration of Technology (CDT); and
- Final Report.

The Prototype Demonstration, the V&V and the STANREC will be covered extensively in this, the Final Report. The CDT effort became a new Research Task Group (AVT-308) and will be covered separately in a later final report. The initial release of the Standard Recommendation (STANREC) is covered in this report; however, a new RTG was also formed (AVT-327) to improve and manage the STANREC.

2.2.1 Prototype Demonstrations

The prototype demonstrations are meant to provide the reader with an example of how a portion of the NG-NRMM would work. For instance, TA-1 will provide a suite of geospatial terrain construction tools to create a terrain profile for use by the other Thrust Areas. TA-2 and TA-3 will take this profile and demonstrate the mobility of a vehicle across this terrain using Simple Terramechanics tools or Complex Terramechanics tools. TA-4 will consider the ramifications of an intelligent unmanned vehicle. TA-5 will calculate the uncertainty for the Simple and Complex Terramechanics approaches.

All of these efforts are based on the same location for mobility calculations, the Monterey Bay area of California, USA. Chapter 3 will describe the site and the sources of information used to describe the terrain, such as elevation and soil type. Annex C and D will also describe the methodology to determine soil moisture content and soil strength, respectively, for the Monterey Bay area. Based on the terrain information, Chapters 4 and 5 describe calculations to determine the mobility of a prototype vehicle across the Monterey Bay terrain using Simple or Complex Terramechanics methods. Chapters 6 will examine the uncertainty of the mobility calculations from the Simple and Complex approaches (Chapters 4 and 5). Chapter 7 will consider intelligent vehicle mobility, again in the Monterey Bay region.

2.2.2 Verification and Validation (V&V)

An extensive V&V or Benchmarking effort was mounted in which software developers were invited to demonstrate the maturity level of their mobility software against a series of driving events on hard surfaces and deformable soft-soil terrains. Event definitions were provided to the developers and vehicle data for a military tracked vehicle and a prototype military wheeled vehicle. Actual test data was available for both vehicles to allow a comparison with modeled results. In addition to demonstrating the maturity of their software, the software developers were able to improve their models based on the comparison with the results of others and especially the actual test data.

2.2.3 STANREC

A Standardization Proposal was made to the NATO Modeling and Simulation Group. The purpose was to define the NG-NRMM to be any mobility M&S capability that facilitates interoperation with current and evolving M&S tools including: Geographic Information Systems (GIS) software, physics-based vehicle dynamic, terramechanical, and autonomous control M&S software, as well as uncertainty quantification software supporting probabilistic M&S. These tools have already been adopted by the combat vehicle and automotive industries, as well as the NATO nations' national labs. Through development of this STANREC, NG-NRMM will become more than a specific computer code. Rather, it will be a ground vehicle mobility modeling and simulation architectural specification.

2.3 FINAL REPORT OVERVIEW

The final report will be broken down in chapters as follows:

- Chapter 1 Introduction
- Chapter 2 Approach
- Chapter 3 TA1: GIS Terrain and Mobility Map
- Chapter 4 TA2: Simple Terramechanics
- Chapter 5A TA3: Complex Terramechanics
- Chapter 5B TA3: DIS/GROUNDVEHICLE: Complex Terramechanics Prototype
- Chapter 5C TA3: Other Complex Terramechanics Software Tools
- Chapter 6 TA5: Uncertainty Treatment
- Chapter 7 TA4: Intelligent Vehicle
- Chapter 8A TA6: Tracked Vehicle Verification and Validation
- Chapter 8B TA6: Wheeled Vehicle Platform Verification and Validation
- Chapter 9 TA7: Data Gaps; Operational Readiness
- Chapter 10 Summary and Conclusions
- Chapter 11 Supporting Material
- Annex A Technical Activity Proposal (TAP) and Terms of Reference (TOR)
- Annex B Modified NRMM Code 11 "MAPTBL" Terrain Data Interchange Format

- Annex C Fine Resolution Soil Moisture Estimation
- Annex D Soil Strength Estimation Overview
- Annex E Terramechanics Database
- Annex F Measurement and Analysis of Geotechnical Properties
- Annex G TA6: Tracked Vehicle Test Data
- Annex H TA6: Wheeled Vehicle Platform Test Data
- Annex I TA7: Questionnaire Comments and Obstacle Analysis

Chapters 3 – 7 will include the prototype demonstrations that will help guide the reader through the methodology. Chapters 3 – 8 will include a STANREC description for that area. Chapter 9 will show the areas that have not been fully developed in AVT-248 and a path forward.

Chapter 3 – TA1: GEOGRAPHICAL INFORMATION SYSTEMS (GIS) TERRAIN AND MOBILITY MAPPING

Matthew Funk
Esri, Inc.
UNITED STATES

Brian Wojtysiak
U.S. Army Materiel Systems Analysis Activity (AMSAA)
UNITED STATES

3.1 GOALS AND DELIVERABLES

3.1.1 GIS Terrain and Mobility Mapping Goals

The goals of the GIS Terrain and Mobility Mapping Thrust Area are:

1) Develop improved, standardized methodologies to transform high resolution satellite imagery / remotely sensed GIS data into accurate NRMM terrain representations; and
2) Develop an example suite of geospatial terrain construction tools to demonstrate capabilities required by the Next-Generation NATO Reference Mobility Model (NG-NRMM).

To achieve the first goal, the Thrust Area will contribute to the development of a NATO Standard Recommendation (STANREC) that will guide development of future NG-NRMM terrain generation tools and enable cartographic visualization of NG-NRMM output products.

To achieve the second goal, an example suite of geospatial terrain construction tools will be constructed to demonstrate the capabilities required by NG-NRMM. Geoprocessing tools will ingest terrain data from various sources and resolutions and create a "standard" terrain file that can be utilized within NG-NRMM.

3.1.2 GIS Terrain and Mobility Mapping Deliverables

Thrust Area 1 deliverables include:

1) A chapter in this report and related annexes detailing the Thrust Area's work and findings.
2) A section in the corresponding STANREC defining the recommendations needed to ensure interoperability between geospatial software and multibody, physics-based vehicle dynamic models.
3) A set of prototype GIS tools created in Esri's ArcGIS software.
4) A collection of sample GIS data representing Monterey, California (to be utilized by all Thrust Areas to demonstrate the "end-to-end" process to generate NG-NRMM results).

Although the tools were developed within Esri's ArcGIS software, the proposed recommendations are agnostic of any commercial software vendor. The prototype tools will generate the geodatabase schema and convert data from the prescribed geodatabase to interchange formats, and back as needed.

3.2 GIS TERRAIN AND MOBILITY MAPPING TEAM MEMBERSHIP

The team members are noted below:

- Marko Zecevic, Croatia;
- Marian Rybansky, Czech Republic;
- Kersti Vennik, Estonia;
- Petra Zieger, Germany;
- Phumlane Nkosi, South Africa;
- David Reinecke, South Africa;
- Mark Cammarere, USA;
- Susan Frankenstein, USA;
- **Matthew Funk (Leader)**, USA;
- Andy Jones, USA;
- Jeffrey Niemann, USA;
- Joseph Scalia, USA;
- Sally Shoop, USA; and
- **Brian Wojtysiak (Leader)**, USA.

3.3 INTRODUCTION

A Next-Generation NATO Reference Mobility Model (NG-NRMM) is defined to be any Modeling and Simulation (M&S) capability that predicts land and amphibious vehicle mobility through coordinated interoperation of Geographic Information Systems (GIS) software and multibody, physics-based vehicle dynamic modeling and simulation software. The multibody, physics-based vehicle dynamic modeling and simulation software must be capable of utilizing Terramechanics to properly assess vehicle / terrain soft-soil interactions, incorporate capabilities to portray autonomous control systems, and include uncertainty quantification to enable probabilistic M&S.

The current version of NRMM contains a library of standard terrain locations; however, the process to build / update these terrain files can be cumbersome and time-consuming. As a result, the standard NRMM terrains have not been updated in nearly 40 years. Due to the proliferation of high resolution satellite imagery and remotely sensed GIS terrain data, NG-NRMM must enable users to leverage these data to quickly and efficiently create new operationally-relevant terrain files. Following generation of NG-NRMM results in the multibody, physics-based vehicle dynamic modeling and simulation software, the results must be able to be visualized cartographically.

3.3.1 Output Metrics

At a minimum, NG-NRMM must be capable of replicating the existing NRMM output products. These include:

- Primary mobility metrics: GO/NOGO trafficability and Speed-Made-Good.
- Secondary mobility metrics: GO/NOGO trafficability / speed limiting reason codes and single pass / multi-pass results.

Newly desired output metric capabilities include generating for:

1) Vehicle stability / handling;
2) Urban maneuverability;
3) Path modeling;
4) Fuel consumption / range estimation; and
5) Rut depths created (as shown in Figure 3-1).

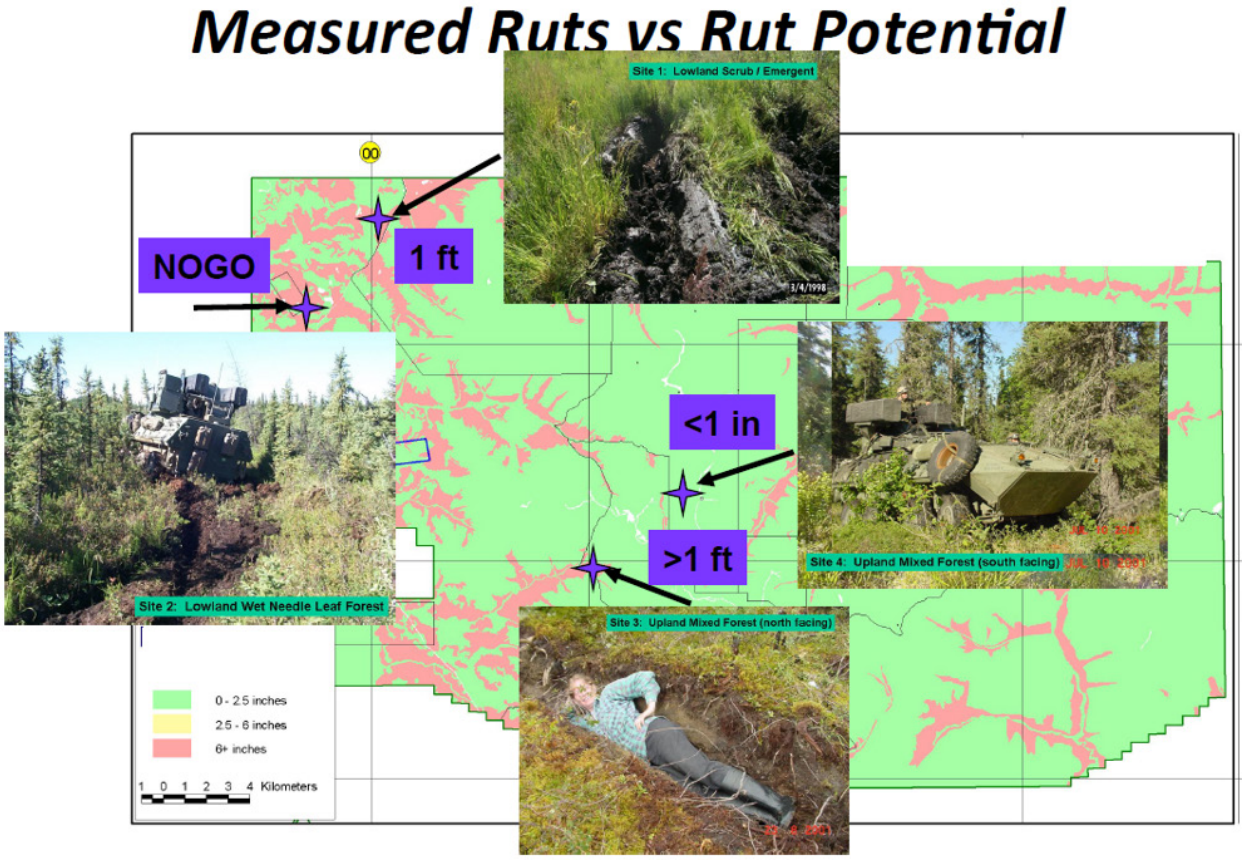


Figure 3-1: Example of Cartographic Rut Depth Prediction.

NG-NRMM software tools must be capable of predicting a real vehicle mobility results on any given terrain map to support operational analysis and mission planning purposes, to include selecting the optimum vehicle path on a terrain map based on the mission requirements.

3.3.2 Terminology

In order to promote a common understanding of the geospatial requirements, the section below will identify important GIS terminology and define the context in which these terms will be used throughout this chapter. Additional information regarding GIS terminology can be found using the reference below.

As defined in GIS.com's GIS Glossary [1]:

- **Cartesian Coordinate System** – A two-dimensional, planar coordinate system in which horizontal distance is measured along an x-axis and vertical distance is measured along a y-axis. Each point on the plane is defined by an x,y coordinate. Relative measures of distance, area, and direction are constant throughout the Cartesian coordinate plane. The Cartesian coordinate system is named for the French mathematician and philosopher René Descartes.
- **Coordinate System** – A reference framework consisting of a set of points, lines, and/or surfaces, and a set of rules, used to define the positions of points in space in either two or three dimensions. The Cartesian coordinate system and the geographic coordinate system used on the earth's surface are common examples of coordinate systems.
- **Delaunay Triangulation** – A technique for creating a mesh of contiguous, non-overlapping triangles from a dataset of points. Each triangle's circumscribing circle contains no points from the dataset in its interior. Delaunay triangulation is named for the Russian mathematician Boris Nikolaevich Delaunay.
- **File Geodatabase** – A geodatabase stored as a folder of files. A File Geodatabase can be used simultaneously by several users, but only one user at a time can edit the same data.
- **Geodatabase** – A database or file structure used primarily to store, query, and manipulate spatial data. Geodatabases store geometry, a spatial reference system, attributes, and behavioral rules for data. Various types of geographic datasets can be collected within a geodatabase, including feature classes, attribute tables, raster datasets, network datasets, topologies, and many others. Geodatabases can be stored in IBM DB2, IBM Informix, Oracle, Microsoft Access, Microsoft SQL Server, and PostgreSQL relational database management systems, or in a system of files, such as a File Geodatabase.
- **Projection** – A method by which the curved surface of the earth is portrayed on a flat surface. This generally requires a systematic mathematical transformation of the earth's graticule of lines of longitude and latitude onto a plane. Some projections can be visualized as a transparent globe with a light bulb at its center (though not all projections emanate from the globe's center) casting lines of latitude and longitude onto a sheet of paper. Generally, the paper is either flat and placed tangential to the globe (a planar or azimuthal projection) or formed into a cone or cylinder and placed over the globe (cylindrical and conical projections). Every map projection distorts distance, area, shape, direction, or some combination thereof.
- **Raster** – A spatial data model that defines space as an array of equally sized cells arranged in rows and columns, and composed of single or multiple bands. Each cell contains an attribute value and location coordinates. Unlike a vector structure, which stores coordinates explicitly, raster coordinates are contained in the ordering of the matrix. Groups of cells that share the same value represent the same type of geographic feature.
- **Spatial Reference System** – A reference framework consisting of a set of points, lines, and/or surfaces, and a set of rules, used to define the positions of points in space in either two or three dimensions. The Cartesian coordinate system and the geographic coordinate system used on the earth's surface are common examples of coordinate systems.
- **Triangulated Irregular Network (TIN)** – A vector data structure that partitions geographic space into contiguous, non-overlapping triangles. The vertices of each triangle are sample data points with x-, y-, and z-values. These sample points are connected by lines to form Delaunay triangles. TINs are used to store and display surface models.

- **Vector (Dataset)** – A coordinate-based data model that represents geographic features as points, lines, and polygons. Each point feature is represented as a single coordinate pair, while line and polygon features are represented as ordered lists of vertices. Attributes are associated with each vector feature, as opposed to a raster data model, which associates attributes with grid cells.

3.4 PROCESS / METHODOLOGY FOR TRANSLATION OF GIS DATA INTO NG-NRMM COMPLIANT TERRAIN DATA

In order to build prototype tools and draft requirements needed to ensure GIS software and multibody, physics-based vehicle dynamic model interoperability, it is necessary to define the process / workflow required to convert high resolution satellite imagery / remotely sensed GIS data into NG-NRMM compliant terrain files. This section of the report will identify the data required by the multibody, physics-based vehicle dynamic models and simulations; and, illustrate the step-by-step process utilized to translate GIS data into NG-NRMM compliant terrain.

The first step in the process is to identify all of the terrain / environmental parameters needed to build an NG-NRMM terrain file. Following this step, it is necessary to determine the availability of geospatial and remotely sensed data (raster and vector datasets) for each of these parameters for the location of interest. It is important to understand that these data files most likely were not originally built for the purpose of ground vehicle mobility characterization; therefore, the production quality, spatial resolution, temporal resolution, level of attribution, quantity of features attributed, etc. will vary greatly and potentially impact NG-NRMM end-use feasibility. For example, these data can vary greatly from production agency to production agency, from project to project, and collection source to collection source; therefore, it is imperative that the end user:

1) Review the data;
2) Determine if the data are viable for use as an input to build NG-NRMM terrain;
3) Address any data voids (due to terrain generation limitations listed above); and
4) Prepare the data for translation into an NG-NRMM compliant dataset.

Standard GIS tools and processes will be used to organize data into a File Geodatabase schema (see File Geodatabase and Geodatabase description in Section 3.4 for additional information). A File Geodatabase "defines and describes a fundamental model for computer representations of geometry and topology that is referenced to reality by coordinates systems" [2].

The File Geodatabase schema was selected as the standard for the following reasons:

1) File Geodatabases maintain the spatial integrity of each terrain parameter layer.
2) File Geodatabases provide a flexible framework to analyze and aggregate terrain properties across multiple layers.
3) File Geodatabases are a widely accepted standard for storing / manipulating spatially-oriented data; thereby, providing maximum breadth for all analytic requirements. Despite this flexibility, not all schema properties may be used (as the properties will be limited to the availability of the input data).
4) The File Geodatabase schema aligns with historical terrain generation approaches used by the GIS / M&S communities while providing flexibility to incorporate new data elements.

5) File Geodatabases provide an open source, software agnostic file format.
6) File Geodatabases comply with ISO TC/211 and more specifically ISO 19107 – standards which have been universally accepted by the international defence community – to include the Digital Geographic Information Working Group (DGIWG) which is comprised of many NATO member nations.

The DGIWG "is the multinational body responsible for geospatial standardization for the defence organizations of member nations. [The] DGIWG has been established under a memorandum of understanding between member nations, and addresses the requirements for these nations to have access to compatible geospatial information for joint operations. It supports the requirements of NATO and the other alliances that its member nations participate in, including UN sanctioned peace keeping, etc. The DGIWG geospatial standards are built upon the generic and abstract standards for geographic information defined by the International Organization for Standardization (ISO TC/211)" [3], [4].

In addition, "DGIWG defines information components for use in the development of product specifications and application schemas for military geospatial data. DGIWG also establishes service specifications, encoding formats and testing methodologies to meet military geospatial intelligence requirements" [3]. To promote maximum interoperability, DGIWG and ISO TC/211 compliant data schemas were selected for use.

The previous DGIWG standard was known as the Digital Geographic Information Exchange Standard (DIGEST). The DGIWG is "preparing to retire the DIGEST standard and is working to develop a suite of more flexible geographic information standards for military applications based on the suite of ISO/TC 211 19100 series standards" [5]. File Geodatabases comply with DGIWG requirements.

The next step in the process is to export the data from the File Geodatabase to an NG-NRMM "interchange" terrain file format. Currently, two formats are being generated: 1) A NRMM Code 11 / Map 11 (also known as MAPTBL) format; or 2) A GeoTIFF, raster dataset [6], [7]. The MAPTBL format for NG-NRMM is described in Annex B (and provides terrain generation capability for the current version of NRMM). Each interchange terrain file will contain all the important environmental characteristic data needed to assess vehicle mobility. All terrain feature data will incorporate and preserve all relevant spatial information to provide cartographic visualization and route analysis capabilities.

The last step in the process is to load the terrain data into NG-NRMM and verify the data has been properly processed for the selected vignettes. Benchmark "historic" NRMM vehicles should be run over the new terrains to identify any potential problems with the terrain data (e.g., attribution, resolution, data voids, etc.). Finally, results from the multibody, physics-based vehicle dynamic modeling and simulation software should be visualized using GIS software to ensure end-to-end interoperability – verifying that the spatial orientation of the data has been preserved throughout the vehicle analysis process.

Figure 3-2 depicts the flow of data through the NG-NRMM analysis process. First GIS data is collected and aggregated into a File Geodatabase using standard GIS tools and processes. The data in the File Geodatabase are processed to generate the terrain properties needed by the multibody, physics-based vehicle dynamic modeling and simulation software. Once all the required properties have been populated, the File Geodatabase is converted into a raster-based NG-NRMM compliant data format ("interchange" format) – either NRMM Code 11 / Map 11 or GeoTIFF. The Multibody Dynamic (MBD) vehicle modeling software executes vehicle runs using the NRMM Code 11 / Map 11 or GeoTIFF terrain files and generates results for each terrain unit. NG-NRMM compliant software preserves the spatial orientation of the data by linking the results (e.g., Raster Output) to the original terrain file (as shown in the Results Raster). Using GIS software, the data in the Results Raster can now be visualized to produce spatially-oriented, map products.

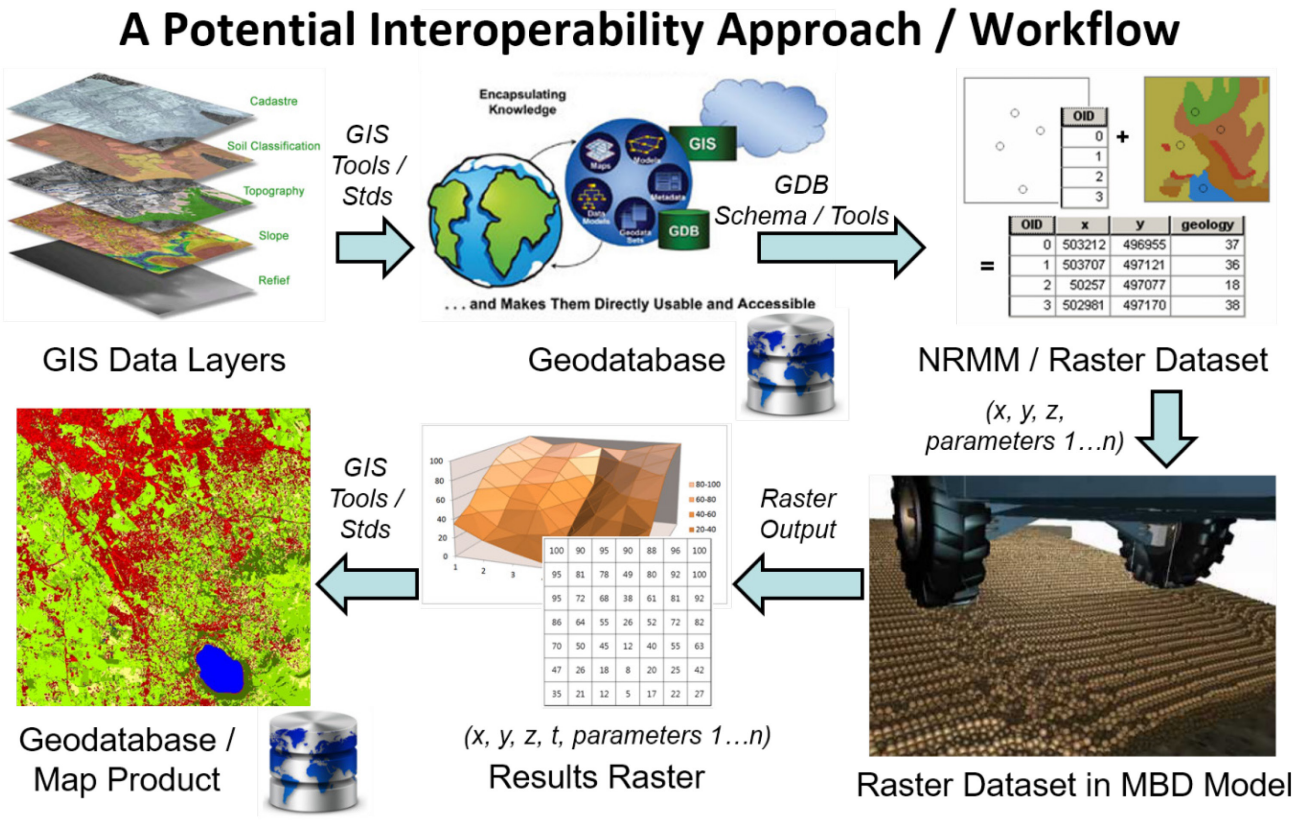


Figure 3-2: General Data Flow.

3.4.1 Minimum Geospatial Soil Data Requirements to Support Simulation

To properly describe the effects of soil mechanics on vehicle systems a minimum set of usable data was requested from the other Thrust Areas.

- **Soil type** as defined by the Unified Soil Classification System (USCS) ASTM D2487-11 at first and second significant strength layer depths.
- **Soil moisture** as a percentage of soil volume content at first and second significant strength layer depths.[1]
- **Soil temperature** in degrees Kelvin at the first and second significant strength layer depths.
- **Land use**, as a substitute for soil compaction, using the Multinational Geospatial Co-production Program (MGCP) Land Use Classification type VEG.

[1] Other than direct measurement, at resolutions approaching those necessary for use with NG-NRMM, fine resolution soil moisture can be derived from combining: 1) remotely sensed coarse soil moisture measurements or estimates; 2) local terrain elevation; 3) local vegetation; and 4) soil type. A technique for generating improved resolution soil moisture data is described in Annex C, and is being applied to provide soil moisture at the first significant strength layer depth.

- **First and Second Significant Strength Layer Depth** from surface or first layer, with soil type, soil moisture, and soil temperature at each. [2]

Although not requested by the other Thrust Areas (since the data requirements listed above are exclusively related to vehicle / soil interactions), terrain data is also required for items like surface roughness, slopes, obstacles, and vegetation to properly characterize vehicle mobility.

3.4.2 Building an Example Geospatial Dataset and Prototype Tools

To promote maximum collaboration on NG-NRMM (e.g., military, commercial, academic, etc.) without restrictions on data sharing, a location of interest had to be selected where a complete set of high resolution GIS terrain data was available in the public domain. After a thorough search of available GIS datasets, a four-county area in coastal central California in the United States, roughly inland of the Monterey Bay, between 122 and 121.5 degrees West and 36.5 and 37 degrees North was selected (as depicted in Figure 3-3). The sample area is 2490 square kilometers in size.

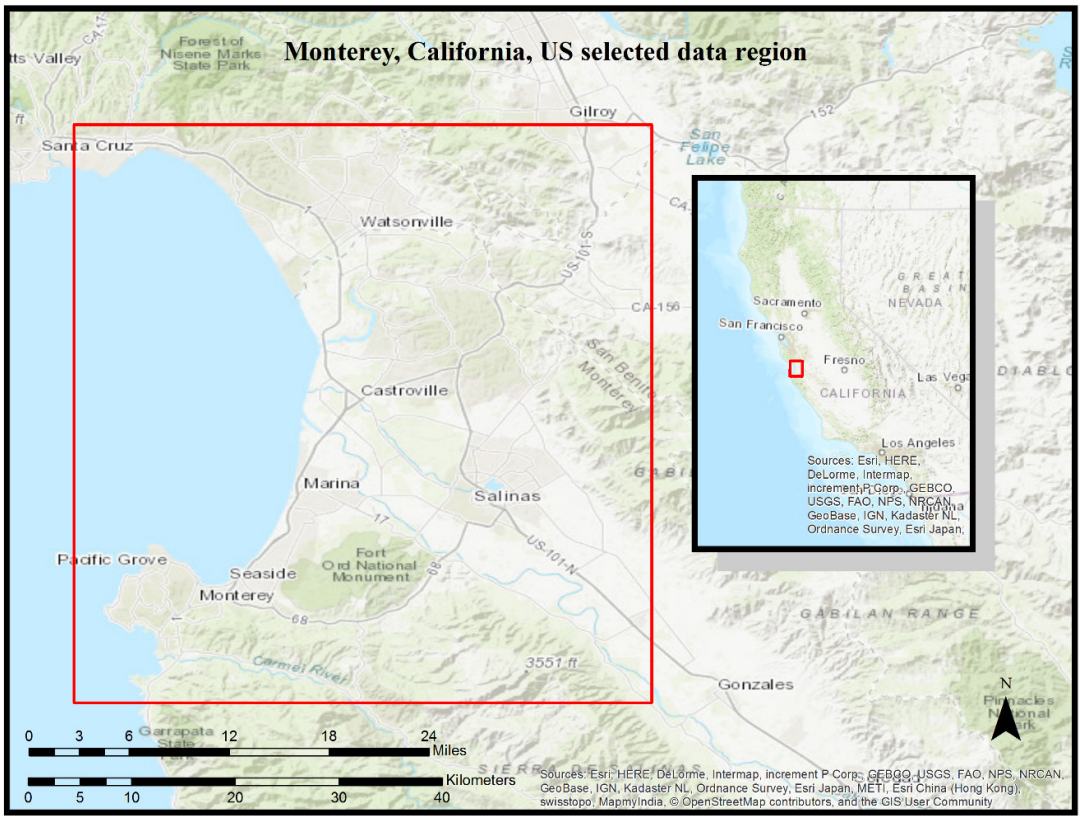


Figure 3-3: Sample Dataset – Monterey Bay, California.

[2] Research in characterizing the strength of unsaturated soils is in its infancy. Effective Friction Angle (the component of soil strength resulting from inter-particle friction) and Effective Cohesion (the component of soil strength resulting primarily from electrostatic inter-particle forces) have been suggested (by the TA2 and TA3 leads) to date. A potential technique for estimating both of these parameters is discussed in Annex D.

This section of the report will utilize the sample Monterey Bay data to describe:

1) The "raw" GIS for each NG-NRMM terrain parameter;
2) The processes used to enrich / convert / manipulate the data to produce NG-NRMM model-ready terrain data; and
3) The process used to build the final NG-NRMM compliant terrain file (either NRMM Code 11 / Map 11 or GeoTIFF).

This section of the report will also describe the prototype tools built to demonstrate the feasibility to construct NG-NRMM terrain generation tools.

3.4.2.1 Elevation and Derivatives

In addition to the soil properties listed previously, elevation data (and its derivatives) are also needed to properly characterize vehicle / terrain interactions in NG-NRMM.

Elevation data, measured as a relative height above a known datum (sea level), is used to describe the terrain for an area. Data of this type are measured from aerial platforms and stored as either raster or Light Detection and Ranging (LIDAR) data.

Additional terrain properties needed for NG-NRMM can be derived from elevation data, specifically the slope (change in elevation) and aspect (direction of change). For the Monterey dataset, two types of source elevation data of varying resolutions were used: Shuttle Radar Topography Mission (SRTM) at 1 arc second and 3 arc seconds, and National Elevation Dataset (NED) at 1/3rd arc seconds. The relevant files were downloaded from United States Geological Survey (USGS) EarthExplorer[3] and USGS National Map viewer [8]. [4]

To begin, an end user would select a source elevation dataset to use (from the sources mentioned above): lower resolution / smaller data size (3 arc second), medium resolution / data size (1 arc second) or highest resolution / largest data size (1/3rd arc second). Figure 3-4 depicts the workflow to generate the slope (e.g., percentage slope and degrees slope) and aspect properties from the elevation data. The elevation data is imported and clipped to the Monterey Bay "area of interest". In the next step, individual elevation files are merged together to produce a single elevation dataset. The elevation data is then projected into the Universal Transverse Mercator (UTM) zone 10 North coordinate system (in meters) to ensure spatial accuracy [9]. The projected elevation dataset is then analyzed using ArcGIS 10.3's Spatial Analyst functions to generate percentage slope, degrees slope, and aspect results.

The results from each of these processes (e.g., percentage slope, degrees slope, and aspect) are then converted from raster format to vector "polygon" format. Conversion to polygons dramatically reduces the size of the data, since a single polygon can be used to represent multiple terrain areas that contain same value. In raster format, the value associated with each cell must be stored (and subsequently manipulated). As a result, generating polygons will also reduce the number of subsequent terrain processing transactions.

[3] USGS EarthExplorer: Data available from the U.S. Geological Survey. Questions concerning the use or redistribution of USGS data should be directed to: ask@usgs.gov or 1-888-ASK-USGS (1-888-275-8747).

[4] USGS The National Map: Data available from the U.S. Geological Survey. Questions concerning the use or redistribution of USGS data should be directed to: ask@usgs.gov or 1-888-ASK-USGS (1-888-275-8747).

Each of the individual polygon layers, (percentage slope, degrees slope, and aspect) are then combined using the Union function to generate a single "new" elevation file. This new elevation file, called intermediate elevation polygon in the diagram below, will now contain the NG-NRMM properties for ELEV, GRADE, and ASPECT. Figure 3-5 shows the results generated using the medium resolution / data size (1 arc second) data.

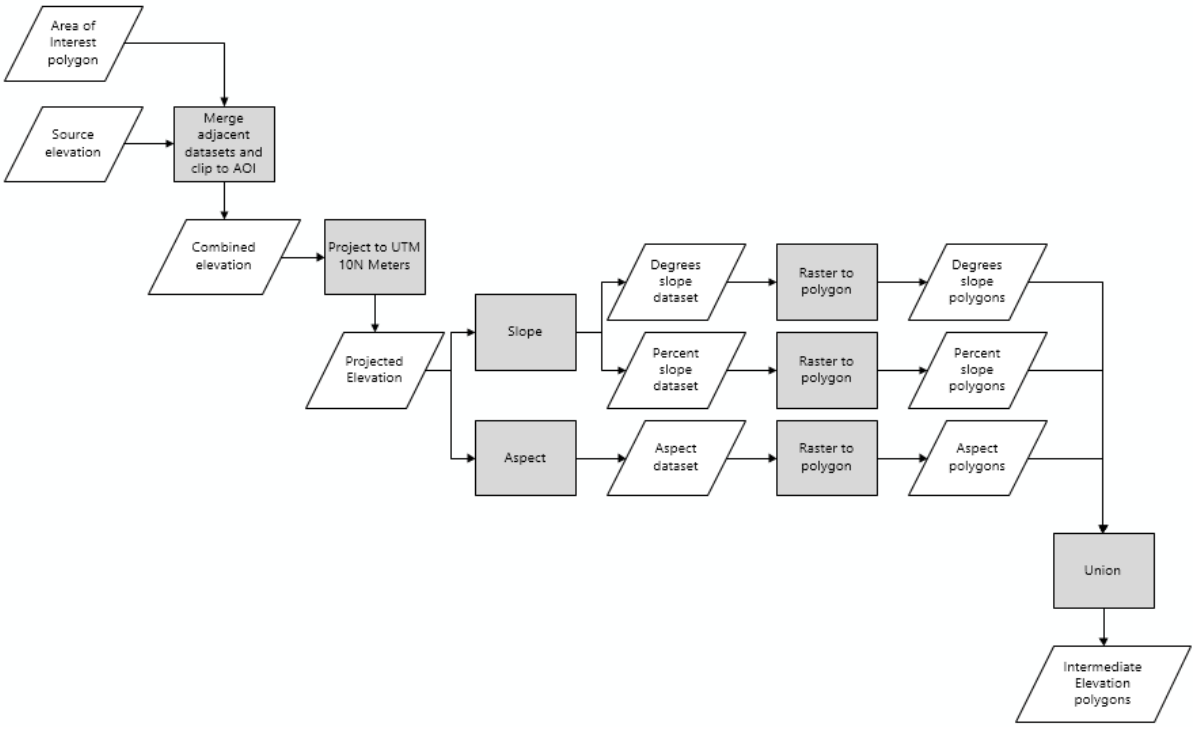


Figure 3-4: Processing Workflow to Generate Elevation, Slope and Aspect Terrain Properties.

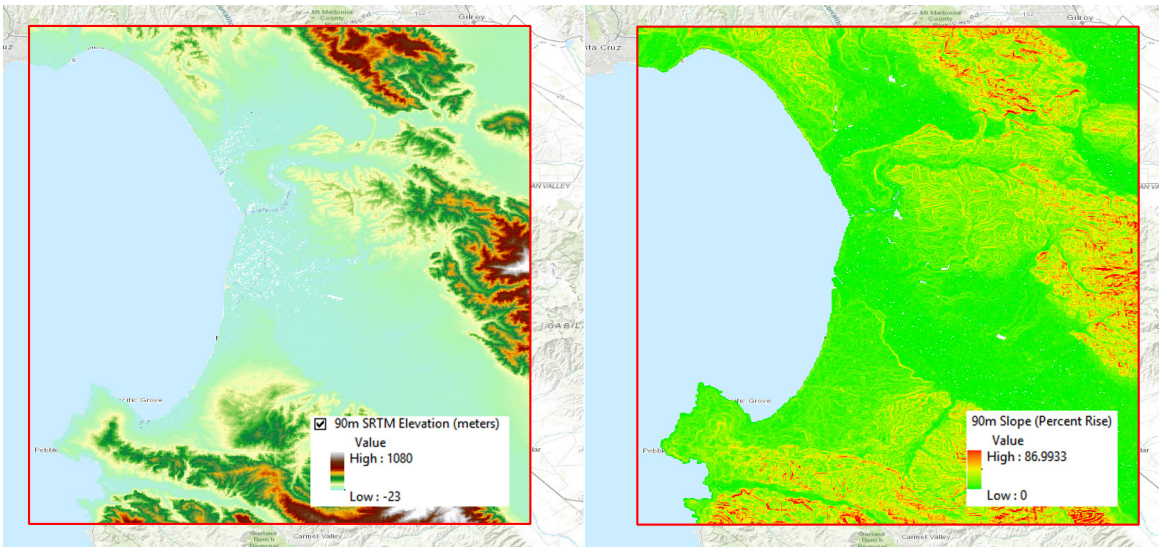


Figure 3-5: Resulting Sample Elevation (Meters) and Slope (%).

3.4.2.2 Soil Type and Bulk Density Parameters

Soil data was obtained from the United States Natural Resources Conservation Service's Web Soil Survey [10], as a Soil Survey Geographic Database (SSURGO) [11]. The SSURGO datasets required additional processing as it is distributed as a series of flat files and must be imported into a SSURGO schema. The additional processing was done using ArcGIS 10.3 and the Web Soil Survey's Soil Data Viewer v6.2 Rev 1046 [12]. Soil Data Viewer allows the extraction of geospatial soil property datasets from the SSURGO database as polygon features. Figure 3-6 depicts the Soil Data Viewer interface in ArcMap and illustrates the extraction of the Unified Soil Classification System (USCS) soil types as a new map layer. Soil properties extracted from this tool as polygons include USCS soil types and bulk density (g/cm^3 @ 1/3 bar water tension). The extracted soil property polygons were then combined from multiple adjacent datasets, merged to create a single soil dataset and clipped to the Monterey Bay "area of interest" to generate the intermediate soil polygon dataset (as shown in Figure 3-7). Figure 3-8 shows the USCS soil types and bulk density results generated for the area of interest.

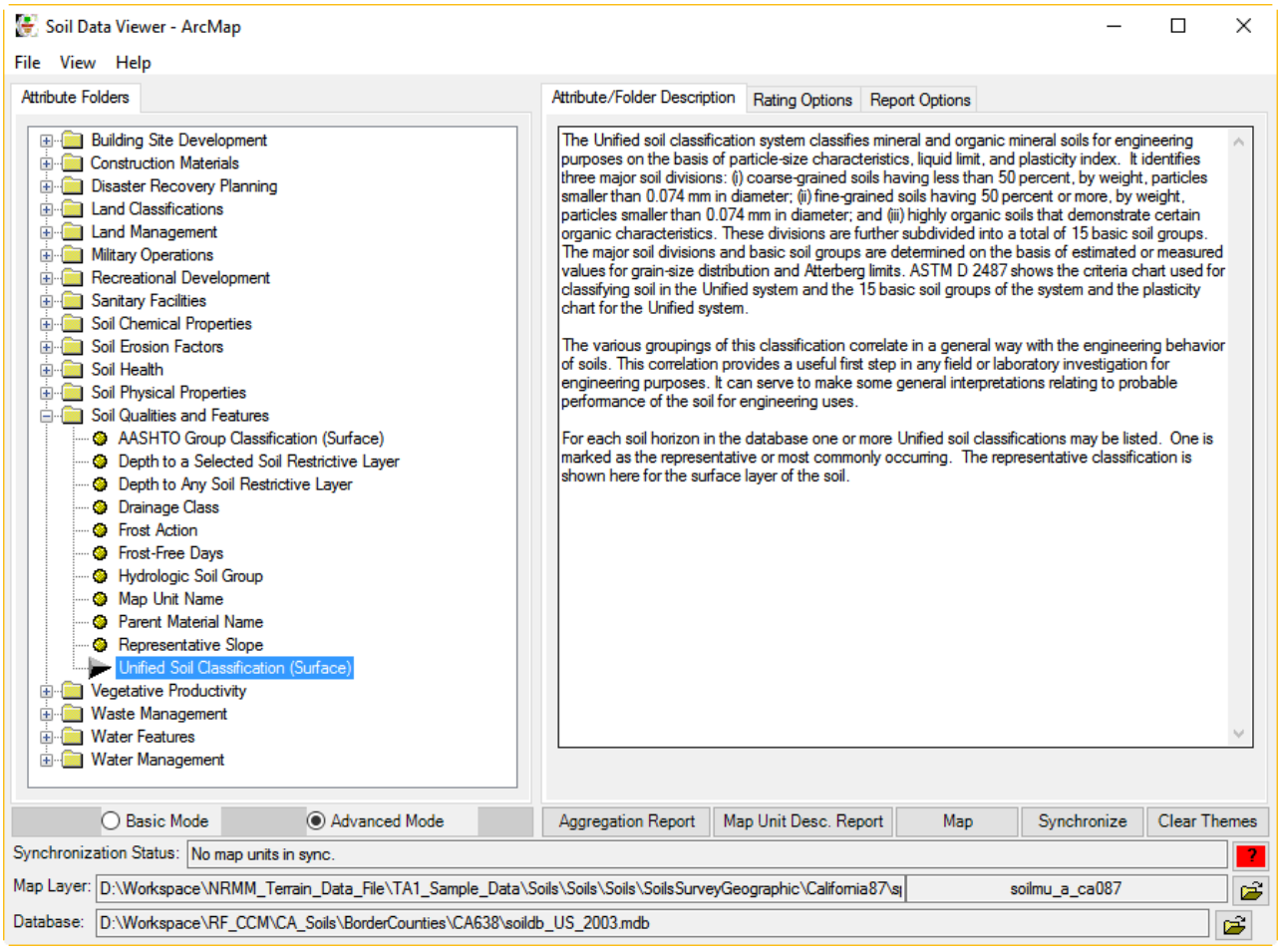


Figure 3-6: USDA Web Soil Survey Interface.

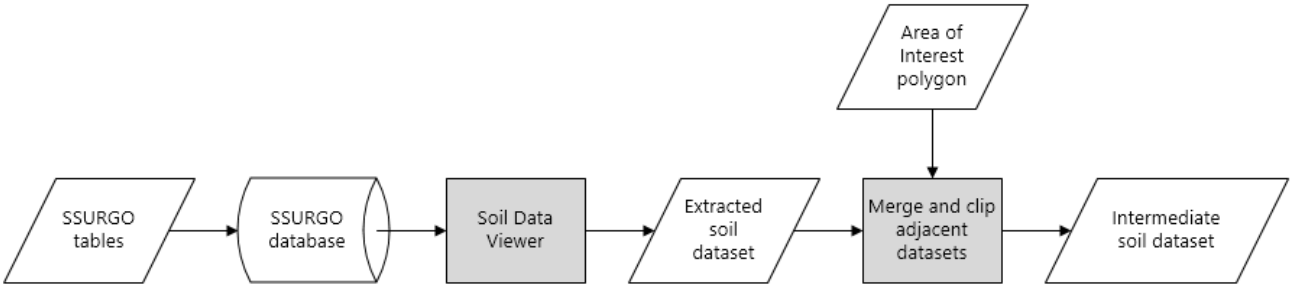


Figure 3-7: Processing Workflow to Generate Soil Terrain Properties.

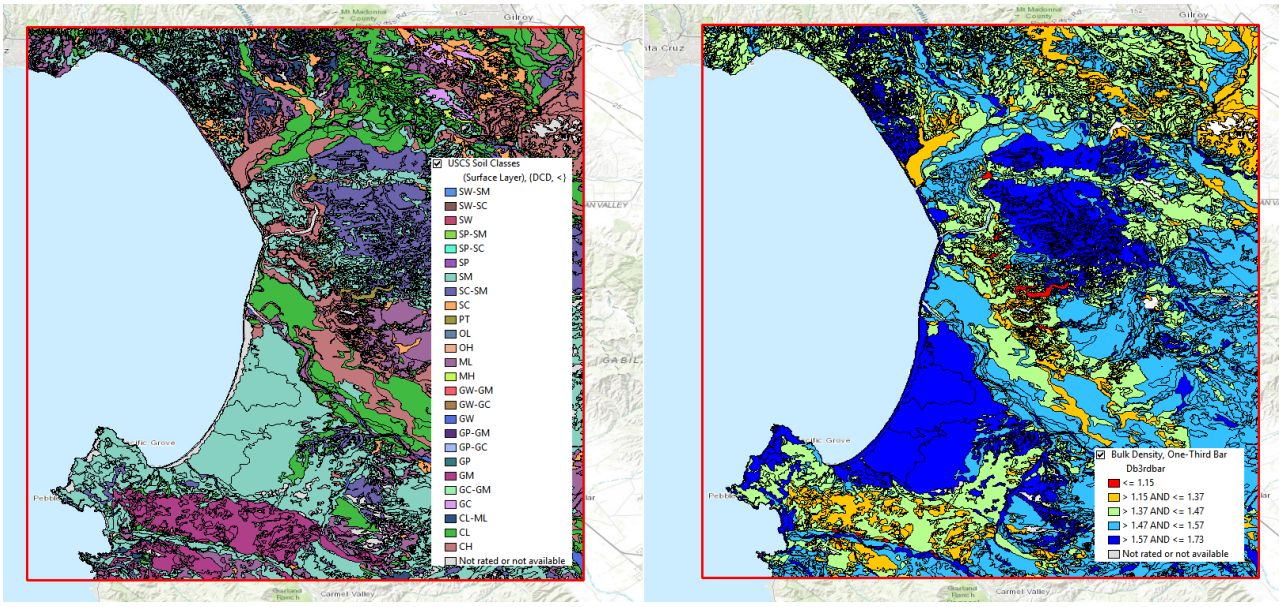


Figure 3-8: Sample USCS Soil Types and Bulk Density.

3.4.2.3 Soil Moisture Parameter

The soil moisture parameter, TMOIST, is calculated from coarse resolution soil moisture, and higher resolution elevation and soil properties. This process is discussed in detail in Annex C and its related Annex D. Like the previous data types, soil moisture must be categorized and then converted from raster cells into vector polygons. The sample volumetric soil moisture data for Monterey (as shown in Figure 3-9) was provided by Colorado State University and Technology Service Corporation (TSC) as part of research produced for AVT-248.

3.4.2.4 Land Use Parameter

Although land use is not directly used in the multibody dynamic models, it can be used to estimate certain soil mechanical properties, such as compaction, along with soil parameters described in Section 3.4.2.2 above. Land use has also been used (with some additional information) to infer additional terrain properties (e.g., surface roughness) used by NRMM. These inference routines are documented in the “Methodology for the Development

of Inference Algorithms for Worldwide Application of Interim Terrain Data to the NATO Reference Mobility Model", Technical Report GL-94-37 from September 1994 [13].

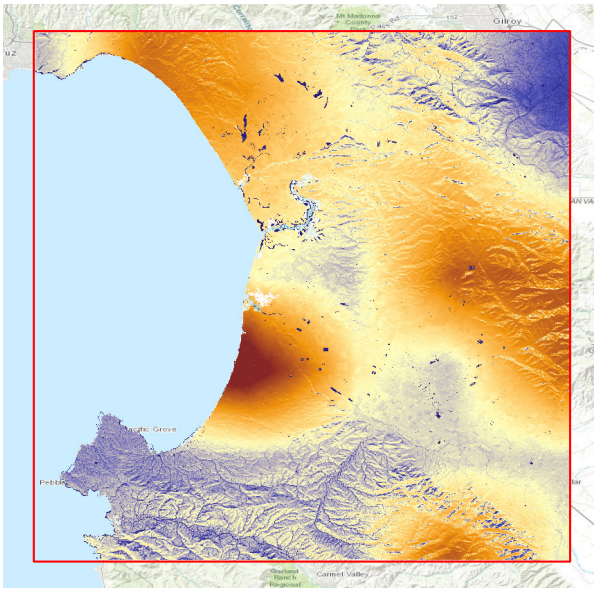


Figure 3-9: Sample Soil Moisture.

While land use can be categorized by different methods for varying purposes, the most widely distributed content is produced by the U.S. Department of Agriculture (USDA). The 2011 National Land Cover Dataset (NLCD) data was obtained from the United States Natural Resources Conservation Service (NRCS) in TIFF format [14]. It was downloaded from the USDA Geospatial Data Gateway (GDG). Similar to the previous processes, the NLCD data was clipped to the "area of interest" and converted into polygon features (as shown in Figure 3-10 below). This dataset is categorized into 16 USGS land use classes, which will populate the LUSE field for the sample Monterey, CA dataset (see Figure 3-11). However, moving forward it is recommended that the land use categorizations be mapped to Multinational Geospatial Co-Production (MGCP) land use classes to promote better interoperability with internationally-generated datasets [15].

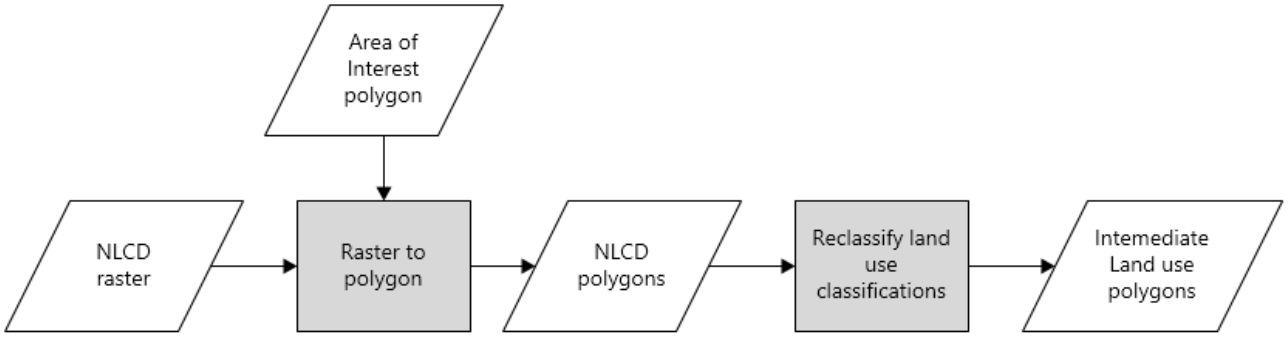


Figure 3-10: Processing Workflow to Generate Land Use Terrain Properties.

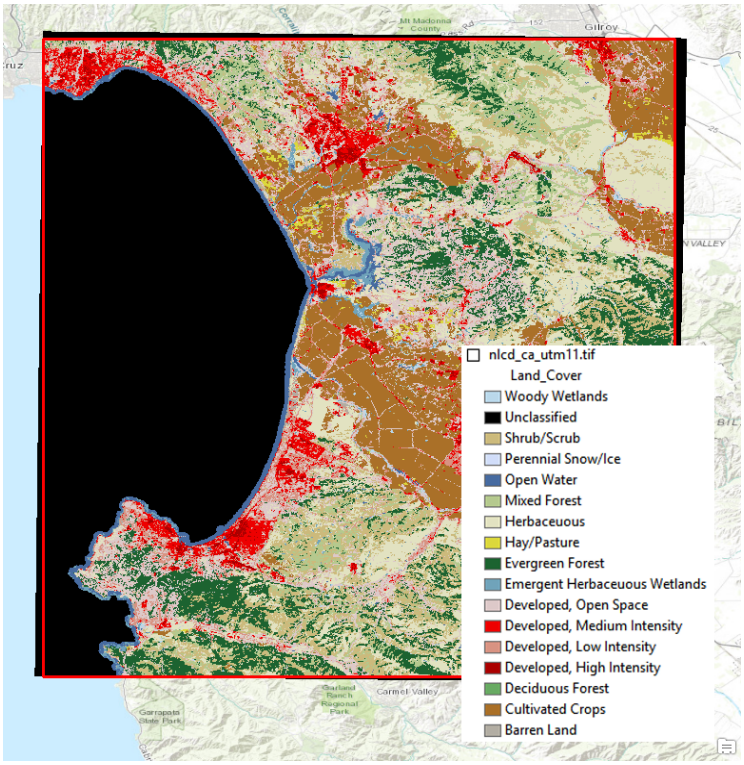


Figure 3-11: Sample NLCD Land Cover / Land Use.

3.4.2.5 Process to Combine Each "Intermediate" Property Dataset into One NG-NRMM Terrain File

As discussed in Sections 3.4.2.1 through 3.4.2.5, each process generated an "intermediate" dataset that contained a subset of the terrain properties needed for NG-NRMM. For example, the intermediate elevation dataset contained the terrain properties: ELEV, GRADE, and ASPECT while the intermediate soil dataset contained the properties for BULKDNS and KUSCS (soil type).

The final step to build the NG-NRMM File Geodatabase is to combine each of these individual "intermediate" datasets into one aggregated dataset (as shown in the process depicted in Figure 3-12 below). The process involves a series of sequential unions which combine two intermediate datasets (described in Sections 3.4.2.1 through 3.4.2.5 above). After this initial union is completed, a new intermediate dataset is generated – containing both the soil and elevation terrain properties. The process is repeated to incorporate the land use polygons; and subsequently, the soil moisture polygons.

After each union step, the process also involves dissolving boundaries between adjacent polygons if they contain the same attribute values. This step is utilized to minimize the total number of polygons generated. At the end of this process, a single File Geodatabase exists containing all the final polygons with accompanying terrain properties. The process was accomplished with ArcGIS 10.3's Union and Dissolve tools; however, other commercial and open source GIS software could be employed.

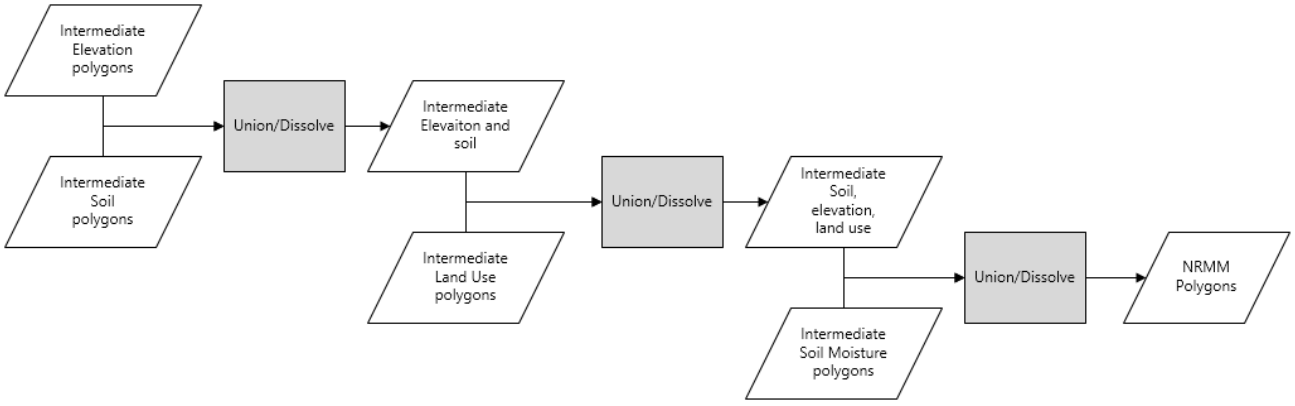


Figure 3-12: Process to Combine "Intermediate" Datasets into One NG-NRMM Terrain File.

3.4.3 Additional Requirements – Metadata for Data Sources

Additional NG-NRMM requirements included:

1) Providing terrain generation support for "legacy" NRMM software; and
2) Enabling NG-NRMM to run "legacy" terrain files. Therefore future NG-NRMM data must be backwards compatible to support older terrain interchange files and new terrain files must be capable of running in legacy NRMM.

Throughout the terrain generation process, significant data voids were often encountered. To overcome some of these data challenges, terrain properties were often inferred. As a result, NG-NRMM terrain files could contain terrain properties generated using four different measures:

1) Measured / tested;
2) Inferred;
3) Legacy; and
4) Notional.

To ensure that the pedigree of every terrain property was accurately tracked, a "data source type header tag" was created with values of "c" for legacy, "i" for inferred, "m" for measured and "n" for notional. If the data source is unknown, the header tag should contain the tag "unknown".

3.5 GEODATABASE DESCRIPTION AND DATA MODELS

3.5.1 Geodatabase Description and Population of an Example Geodatabase

After initial geospatial data collection, all NG-NRMM geospatial data should be stored and organized within a File Geodatabase [16], [17]. To build new terrains for the current version of NRMM, the U.S. Army Materiel Systems Analysis Activity (AMSAA) collected most of the geospatial data required to build a new NRMM terrain file. This collection of data was stored in a File Geodatabase and processed using Esri ArcGIS 10.3.1 software using the processing workflows described in the preceding section.

To fill data voids where data were unavailable / not measured, the U.S. Army Materiel Systems Analysis Activity (AMSAA) filled the voids in the NRMM terrain File Geodatabase using methodologies spelled out in Bullock [13].

GIS vector data using the Feature Attribute Coding Catalogue (FACC) data model schema was used as a base, and the feature data was initially mapped to NRMM MAP89 Code 4 file format. The input data used the FACC data model, which matched the data used in TR GL-94-37. Terrain files were initially built to the Map 4 file format specifications since MAP89 Code 4 closely aligned to the outputs of the inference routines used in TR GL-94-37. The terrain files were then migrated to MAPTBL Code 11 file formats to take advantage of the flexibility provided with this format.[5] The geodatabase spatial reference should use the Universal Transverse Mercator (UTM) coordinate system with linear units of Meters.

3.5.2 NG-NRMM Terrain Data Models

The FACC was developed by the DGIWG as part of the Digital Geographic Information Exchange Standard (DIGEST). DIGEST is broken into four parts:

Part 1: General Description;

Part 2: Theoretical Model, Exchange Structure, Encapsulation Specifications (Annexes A through D) and a Standard ASCII Table of Contents (Annex E);

Part 3: Codes and Parameters; and

Part 4: Feature Attribute Coding Catalogue (FACC) Data Dictionary.

The entire DIGEST set of standards is covered by NATO Standardization Agreement 7074 [18].

> "The DGIWG FACC is a comprehensive dictionary and coding scheme for feature types, feature attributes (properties or characteristics associated with features), and attribute values (domain of feature attributes). A standardized dictionary is required to support encoding in order to maximize interoperability and to understand the production, exchange, distribution, and exploitation of digital geographic data. The DGIWG FACC has not been developed to satisfy the requirements of any single application, product, or database. It is intended to be independent from level of resolution (scale), representation, and portrayal. The appropriate selection of DGIWG FACC feature types and feature attributes are intended to be implemented as part of the overall solution for an application, by means of a database (supported by a data schema or model), a product, or dataset (defined according to a format specification and a data model). The DGIWG FACC allows for individual nations to define "national" feature types and feature attributes for cases where such feature types and feature attributes are not readily defined in the normative DGIWG FACC. National extensions are not specified within the normative DGIWG FACC, and may not support interoperability. National extensions may, if proposed and approved, be incorporated into future editions of the normative DGIWG FACC [19]."

Data parameters not included within the normative DGIWG FACC data dictionary can be added as "national" features to supplement FACC datasets. These datasets allow use of non-standard data features to fulfil specialized requirements not envisioned by the DGIWG. Datasets which include additional "national" feature data are referred to as FACC+. As identified in the last sentence in the previous paragraph, the DGIWG DIGEST

[5] Code 11 or Map 11 NRMM terrain files provide more flexibility throughout the terrain generation due to the unstructured nature of the terrain data. In Code 4 and Code 5 NRMM terrain files, the terrain properties must be organized in a prescribed sequence; however, the data in Code 11 NRMM terrain files can be in any order. NRMM is able to determine the contents of the column by interpreting the information contained in the column header.

framework has defined processes to review and approve changes to the FACC data dictionary, thereby providing a mechanism to incorporate future data elements required by NATO members. As a NATO STANAG, FACC and FACC+ align with much of the vector datasets built for the U.S. Military and are used by the U.S. Modeling and Simulation community.

However, the DGIWG "is preparing to retire the DIGEST standard and is working to develop a suite of more flexible geographic information standards for military applications based on the suite of ISO/TC 211 19100 series standards. Although DIGEST remains a valid standard, Part 4 (FACC) has been sunsetted by DGIWG. Sunset standards are those that have been identified and approved for retirement… In addition, a replacement standard is frequently identified. For FACC the DGIWG Feature Data Dictionary (DFDD) is the replacement standard. Backward compatibility is supported since the final version of FACC was the basis for the initial contents of the DFDD register. Feature catalogues based on the DFDD will also be registered to facilitate interoperability between data products based on the DFDD. Users of FACC are advised to use the DFDD in lieu of FACC for future implementations" [5].

Due to the impending retirement of FACC and DIGEST, all NG-NRMM terrain data should be encoded using the DFDD model. The DFDD is backward compliant with FACC standards and will ensure interoperability with future implementations. Non-standard data parameters missing from the DFDD should also be included as "national" features to create a DFDD+ dataset.

In the next three sections, the list of NRMM terrain parameters will be defined.

3.5.3 NRMM Terrain Parameters (Version 2.8.2)

Table 3-1 provides the terrain parameters required to maintain the present level of NRMM analysis capability and support backward compatibility.

Table 3-1: Terrain Parameters Present in the Latest NRMM Release (Version 2.8.2).

Field	Data Type	Description/Alias	Default Value
ACTRMS	DOUBLE	"Surface Roughness"	NULL
BRDGMLC1	DOUBLE	"Bridge Military Load Class, One-way Wheeled"	0
BRDGMLC2	DOUBLE	"Bridge Military load Class, Two-way Wheeled"	0
BRDGMLC3	DOUBLE	"Bridge Military Load Class, One-way Tracked"	0
BRDGMLC4	DOUBLE	"Bridge Military Load Class, Two-way Tracked"	0
CI1	DOUBLE	"Cone Index 0 – 6 inches (psi)"	NULL
CI2	DOUBLE	"Cone Index 6 – 12 inches (psi)"	NULL
CLUTTER	LONG	"Road Segment Restricted Width Due to Clutter"	0
CRVSPD	DOUBLE	"Curve Speed Limit"	NULL
DBROCK	DOUBLE	"Depth to Bedrock (inches)"	99
DFREEZ	DOUBLE	"Freeze Depth (inches)"	0

Field	Data Type	Description/Alias	Default Value
DIST	DOUBLE	“On-Road Distance Patch (km)”	0
DSNOW	DOUBLE	“Snow Depth (inches)”	0
DTHAW	DOUBLE	“Thaw Depth (inches)”	0
EANG	DOUBLE	“Road Super-Elevation Angle (radians)”	0
ELEV	Double	“Surface Elevation”	NULL
GRADE	DOUBLE	“Slope (%)”	0
IOST	LONG	“Obstacle Avoidability”	1
IROAD	LONG	“Road Type”	0
ISCOND	LONG	“Surface Condition”	0
IST	LONG	“NRMM Soil Model Code”	NULL
ITURNLR	LONG	“Curve Turn Direction”	0
IURB	LONG	“Urban Code”	4
KUSCS	LONG	“Soil Type (coded)”	5
KWI	LONG	“Wetness Index”	NULL
LOCHARD	LONG	“Hard Overhead Clearance”	NULL
LTRAFFIC	LONG	“Direction of Each Road Lane”	0
LUSE	LONG	“Land Use Classification”	NULL
NLANES	LONG	“Number of Road Travel Lanes”	1
NTU	LONG	“NRMM Terrain Unit”	NULL
OBAA	DOUBLE	“Obstacle Approach Angle (degrees)”	math.pi
OBH	DOUBLE	“Obstacle Height (inches)”	0
OBL	DOUBLE	“Obstacle Length (inches)”	0
OBS	DOUBLE	“Obstacle Spacing (inches)”	999
OBW	DOUBLE	“Obstacle Width (inches)”	0
OHCLEAR	DOUBLE	“Minimum Overhead Clearance (inches)”	0
RADC	DOUBLE	“Road Radius of Curvature (inches)”	68760
RCIC11	LONG	“Soil Strength – Dry (psi), 0 – 6 inches”	NULL
RCIC12	LONG	“Soil Strength – Dry (psi), 6 – 12 inches”	NULL
RCIC21	LONG	“Soil Strength – Average (psi), 0 – 6 inches”	NULL

Field	Data Type	Description/Alias	Default Value
RCIC22	LONG	"Soil Strength – Average (psi), 6 – 12 inches"	NULL
RCIC31	LONG	"Soil Strength – Wet (psi), 0 – 6 inches"	NULL
RCIC32	LONG	"Soil Strength – Wet (psi), 6 – 12 inches"	NULL
RCIC41	LONG	"Soil Strength – Wet-Wet (psi), 0 – 6 inches"	NULL
RCIC42	LONG	"Soil Strength – Wet-Wet (psi), 6 – 12 inches"	NULL
RDA1	DOUBLE	"Recognition Distance – January (feet)"	3600
RDA2	DOUBLE	"Recognition Distance – February (feet)"	3600
RDA3	DOUBLE	"Recognition Distance – March (feet)"	3600
RDA4	DOUBLE	"Recognition Distance – April (feet)"	3600
RDA5	DOUBLE	"Recognition Distance – May (feet)"	3600
RDA6	DOUBLE	"Recognition Distance – June (feet)"	3600
RDA7	DOUBLE	"Recognition Distance – July (feet)"	3600
RDA8	DOUBLE	"Recognition Distance - August (feet)"	3600
RDA9	DOUBLE	"Recognition Distance – September (feet)"	3600
RDA10	DOUBLE	"Recognition Distance – October (feet)"	3600
RDA11	DOUBLE	"Recognition Distance – November (feet)"	3600
RDA12	DOUBLE	"Recognition Distance – December (feet)"	3600
RDBDANG1	DOUBLE	"Road Bed Left Side Angle (radians)"	0
RDBDANG2	DOUBLE	"Road Bed Right Side Angle (radians)"	0
RDBDWID1	DOUBLE	"Road Bed Left Side Width (inches)"	0
RDBDWID2	DOUBLE	"Road Bed Right Side Width (inches)"	0
RDBHGT1	DOUBLE	"Road Bed Left Side Height (inches)"	0
RDBHGT2	DOUBLE	"Road Bed Right Side Height (inches)"	0
RDSHWID1	DOUBLE	"Road Shoulder Left Width (inches)"	0
RDSHWID2	DOUBLE	"Road Shoulder Right Width (inches)"	0
RDSTRNGS111	DOUBLE	"Soil Strength Roadway, Left Side, 0 – 6 inches"	0
RDSTRNGS112	DOUBLE	"Soil Strength Roadway, Left Side, 6 – 12 inches"	0
RDSTRNGS121	DOUBLE	"Soil Strength Roadway, Right Side, 0 – 6 inches"	0
RDSTRNGS122	DOUBLE	"Soil Strength Roadway, Right Side, 6 – 12 inches"	0

Field	Data Type	Description/Alias	Default Value
RDSTRNGS211	DOUBLE	“Soil Strength Shoulder, Left Side, 0 – 6 inches”	0
RDSTRNGS212	DOUBLE	“Soil Strength Shoulder, Left Side, 6 – 12 inches”	0
RDSTRNGS221	DOUBLE	“Soil Strength Shoulder, Right Side, 0 – 6 inches”	0
RDSTRNGS222	DOUBLE	“Soil Strength Shoulder, Right Side, 6 – 12 inches”	0
RDSTRNGS311	DOUBLE	“Soil Strength Road Bed, Left Side, 0 – 6 inches”	0
RDSTRNGS312	DOUBLE	“Soil Strength Road Bed, Left Side, 6 – 12 inches”	0
RDSTRNGS321	DOUBLE	“Soil Strength Road Bed, Right Side, 0 – 6 inches”	0
RDSTRNGS322	DOUBLE	“Soil Strength Road Bed, Right Side, 6 – 12 inches”	0
RDSTYPS11	DOUBLE	“Soil Type Roadway, Left Side”	0
RDSTYPS12	DOUBLE	“Soil Type Roadway, Right Side”	0
RDSTYPS21	DOUBLE	“Soil Type Shoulder, Left Side”	0
RDSTYPS22	DOUBLE	“Soil Type Shoulder, Right Side”	0
RDSTYPS31	DOUBLE	“Soil Type Road Bed, Left Side”	0
RDSTYPS32	DOUBLE	“Soil Type Road Bed, Right Side”	0
RECD	DOUBLE	“Recognition Distance (inches)”	NULL
S	LONG	“Scenario Number”	NULL
S1	LONG	“Stem Spacing (feet) of Stem Diameter > (0 cm)”	3936
S2	LONG	“Stem Spacing (feet) of Stem Diameter > (2.5 cm)”	3936
S3	LONG	“Stem Spacing (feet) of Stem Diameter > (6 cm)”	3936
S4	LONG	“Stem Spacing (feet) of Stem Diameter > (10 cm)”	3936
S5	LONG	“Stem Spacing (feet) of Stem Diameter > (14 cm)”	3936
S6	LONG	“Stem Spacing (feet) of Stem Diameter > (18 cm)”	3936
S7	LONG	“Stem Spacing (feet) of Stem Diameter > (22 cm)”	3936
S8	LONG	“Stem Spacing (feet) of Stem Diameter > (25 cm)”	3936
S9	LONG	“Stem Spacing (feet) of Stem Diameter > (cm)”	
SD1	DOUBLE	“Average Stem Diameter (0.49)”	0.49
SD2	DOUBLE	“Average Stem Diameter (1.67)”	1.67
SD3	DOUBLE	“Average Stem Diameter (3.15)”	3.15
SD4	DOUBLE	“Average Stem Diameter (4.73)”	4.73

Field	Data Type	Description/Alias	Default Value
SD5	DOUBLE	“Average Stem Diameter (6.30)”	6.3
SD6	DOUBLE	“Average Stem Diameter (7.88)”	7.88
SD7	DOUBLE	“Average Stem Diameter (9.25)”	9.25
SD8	DOUBLE	“Average Stem Diameter (12.42)”	12.42
SD9	DOUBLE	“Average Stem Diameter (99.0)”	99
SDL1	DOUBLE	“Maximum Stem Diameter (0.98)”	0.98
SDL2	DOUBLE	“Maximum Stem Diameter (2.36)”	2.36
SDL3	DOUBLE	“Maximum Stem Diameter (3.94)”	3.94
SDL4	DOUBLE	“Maximum Stem Diameter (5.51)”	5.51
SDL5	DOUBLE	“Maximum Stem Diameter (7.09)”	7.09
SDL6	DOUBLE	“Maximum Stem Diameter (8.66)”	8.66
SDL7	DOUBLE	“Maximum Stem Diameter (9.84)”	9.84
SDL8	DOUBLE	“Maximum Stem Diameter (15.0)”	15
SDL9	DOUBLE	“Maximum Stem Diameter (99.0)”	99
SIGMA	DOUBLE	“Snow Density (g/cm^3)”	0.3
SNOMCH	LONG	“Used to Change Roughness”	0
T	LONG	“Terrain Number”	NULL
TMOIST	DOUBLE	“Soil Moisture Content by Volume (%)”	0
TPSDMAX1	DOUBLE	“Bridge/Tunnel/Roadway Speed Limit (inches/second)”	1760
TPSDMAX2	DOUBLE	“VHGTMAX Interference Speed Limit (inches/second)”	1760
TUID	LONG	“NTU Map 11 Format”	NULL
TWIDMIN	DOUBLE	“Bridge/Tunnel/Roadway Minimum Width (inches)”	0
USCS	TEXT	“Soil Type (text)”	“SM-SC”
V	LONG	“Vehicle Number”	NULL
WD	DOUBLE	“Standing Water Depth (inches)”	0
WLANES	DOUBLE	“Travel Lane Width (inches)”	0

3.5.4 NRMM Terrain Parameters (Version 3.0 Beta)

The U.S. Army Corps of Engineers Engineer Research and Development Center Cold Regions Research and Engineering Laboratory (USACE ERDC CRREL) and the U.S. Army Materiel Systems Analysis Activity

(AMSAA) are working to release a new version of NRMM known as NRMM 3.0 Beta. New terrain properties required for NRMM 3.0 Beta are listed in Table 3-2.

Table 3-2: Terrain Parameters Present in NRMM 3.0 Beta.

Field	Data Type	Description/Alias	Default Value
CPRIS	DOUBLE	"Soil Prism Cohesion (psi)"	0
DELTAPRIS	DOUBLE	"Soil Prism External Friction Angle (degrees)"	0
ENG_C	DOUBLE	"Soil Cohesive Strength (psi)"	0
ENG_G	DOUBLE	"Elastic Shear Modulus (psi)"	0
ENG_GAMMA	DOUBLE	"Total Unit Weight (lb/ft^3)"	0
ENG_PHI	DOUBLE	"Soil Friction Angle (degrees)"	0
EXTFRICT	DOUBLE	"External Friction Angle (degrees)"	0
GAMMAPRIS	DOUBLE	"Soil Prism Unit Weight (lb/ft^3)"	0
PHIPRIS	DOUBLE	"Soil Prism Friction Angle (degrees)"	0

3.5.5 Unique NG-NRMM Terrain Parameters

To address the unique vehicle / soft-soil modeling data needs for NG-NRMM identified in Section 3.4.1, the four terrain parameters (shown in Table 3-3) were added to the data dictionary.

Table 3-3: Terrain Parameters Added to Support Unique NG-NRMM Requirements.

Field	Data Type	Description/Alias	Default Value
BULKDNS	DOUBLE	"Bulk Density (g/cm^3)"	NULL
KUSCS2	LONG	"USCS Soil Code for SSL2"	5
TEMP2	DOUBLE	"Soil Temperature (K) for SSL2"	295
TMOIST2	DOUBLE	"Soil Moisture Content by Volume (%) for SSL2"	0

3.6 INTERCHANGE FORMATS

Once all the geospatial terrain data is aggregated and organized in a single File Geodatabase, the data will be exported to one of two interchange formats – either NRMM MAPTBL "Code 11" format (Annex B) or a GeoTIFF. Both offer advantages and disadvantages in representing geospatial data.

Prototype tools, developed by Thrust Area 1, demonstrate examples exporting the File Geodatabase into both the MAPTBL and GeoTIFF formats. The tools include options to choose which terrain properties will be included in the interchange file giving the user some control over the size of the output dataset.

3.6.1 NRMM MAPTBL (Code 11)

The MAPTBL format is a legacy ASCII format that stores geospatial data and attribution in three different files:

- .ASC file – an ASCII Raster format of Numbered Terrain Units (NTUs) and their spatial location (see Figure 3-13 below for an example).
- .PRJ file – stores the geospatial coordinate system description of the .ASC file.
- .TER file – stores the attribution data for each NTU (see Figure 3-14 for an example).

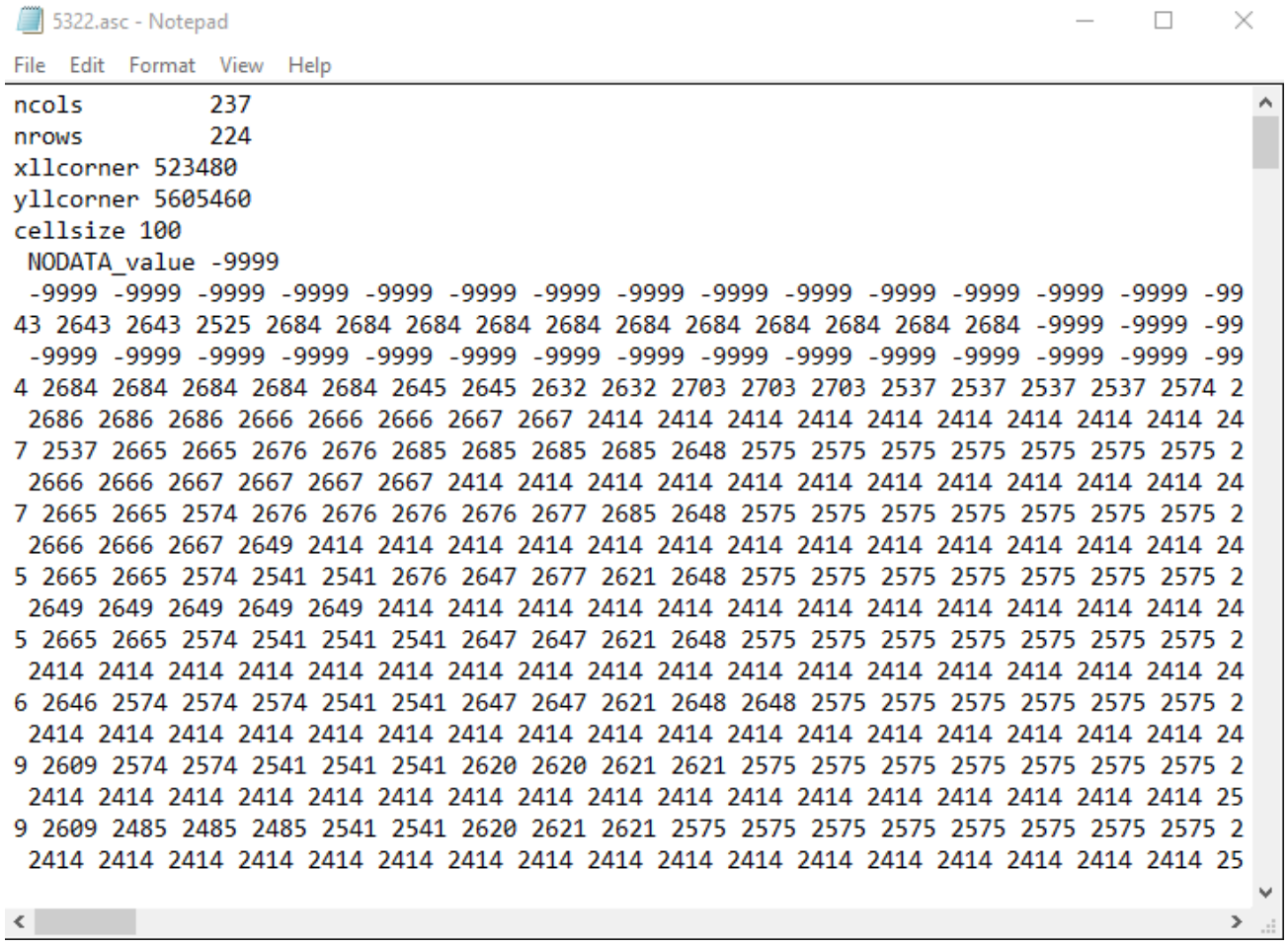


Figure 3-13: Sample NRMM ASC Terrain File.

One of the advantages of this format is its simplicity. Files in this format can be readily opened in many different text reader software packages. Changes to the file can be made easily without specialized software. The ASCII format is one of the most basic formats for data interchange. This format also provides backward compatibility to support the current version of NRMM.

The disadvantages associated with ASCII are its scalability and format support. For small areas with few NTUs and attributes, the size of the files is minimal. However with larger and more complex arrangements, the file size

can grow to be unwieldy, difficult to move, and easy to corrupt. While the format can be opened in any text reader, special libraries must be written to read the file and extract the necessary data. This is not a common or standardized data interchange format.

The MAPTBL Code 11 format is discussed in further detail in Annex B.

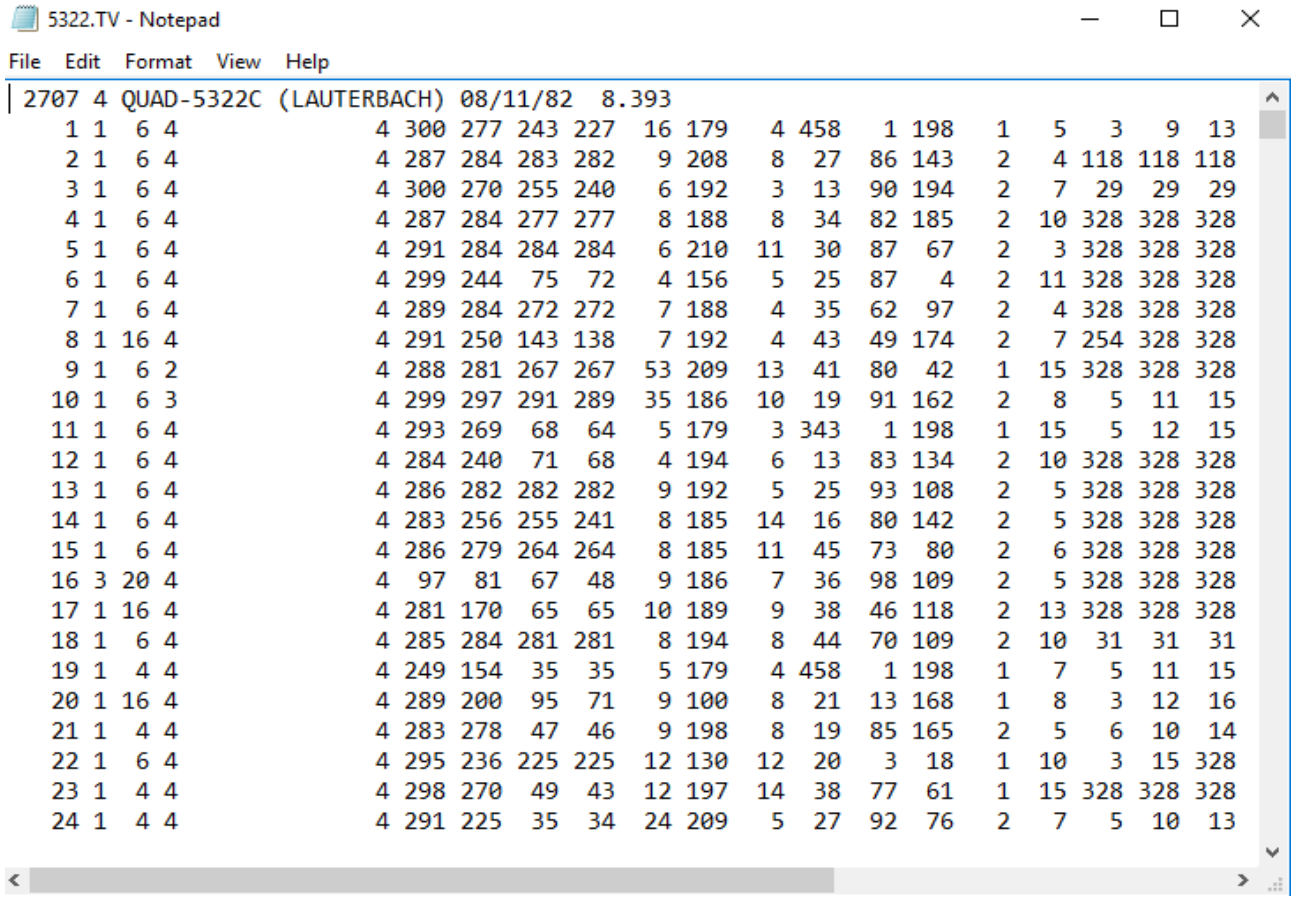


Figure 3-14: Sample NRMM TER Terrain File.

3.6.2 GeoTIFF

GeoTIFF is an alternative raster-based data interchange format that works well for geospatial data [6], [7]. The base Tagged Image File Format (TIFF) is a well-known standard for raster (imagery) interchange. The addition of geospatial tags (including the internal file header), makes it a common format for geospatial data. Data stored in a GeoTIFF can be arranged as individual single-band datasets representing each of the terrain / mechanical properties.

Though better than an ASCII format, the GeoTIFF can still grow to be a very large file, even after it's compressed. Any metadata must be stored in separate, but associated files.

3.7 NG-NRMM OUTPUT PRODUCTS: VISUALIZING MOBILITY RESULTS

After the Multibody Dynamics (MBD) modeling and Uncertainty Quantification (UQ) runs are completed, the results must be visualized to depict the mobility performance of the vehicle for the area of analysis. These visualizations must meet all end user needs (e.g., Vehicle Designers, Acquisition Community, Operational Units – Mission Planning, etc.). The general approach is to ingest resulting outputs from MBD / UQ models, convert these outputs to appropriate geospatial data formats (as necessary), and visualize the various outputs for the area of interest as individual maps or sets of maps. The following sections describe a few of the common visualizations; however, the list is not exhaustive and is not intended to identify every cartographic product needed. It also should be noted that new visualization techniques are continuously emerging; and, therefore, may not represent all the visualization products required by NG-NRMM. In order to leverage this visualization approach, it is critical to understand that the MBD / UQ models must preserve the spatial location and orientation of all the original terrain units so that these models can append their results to the list of terrain units.

3.7.1 GO/NOGO Maps and NOGO Reason Code Maps

Given a set of input parameters (e.g., vehicle, terrain, scenario), GO/NOGO maps identify areas where the modeled vehicle can and cannot go. The binary output results in two categories – Go areas and NOGO areas. The Go areas are usually portrayed as "green" areas on the map, while NOGO areas are normally portrayed as either "red" or "black" (as seen in Figure 3-15 below). In this example, the "urban areas" are also identified since the cross-country prediction modules for NRMM ignore urban areas.

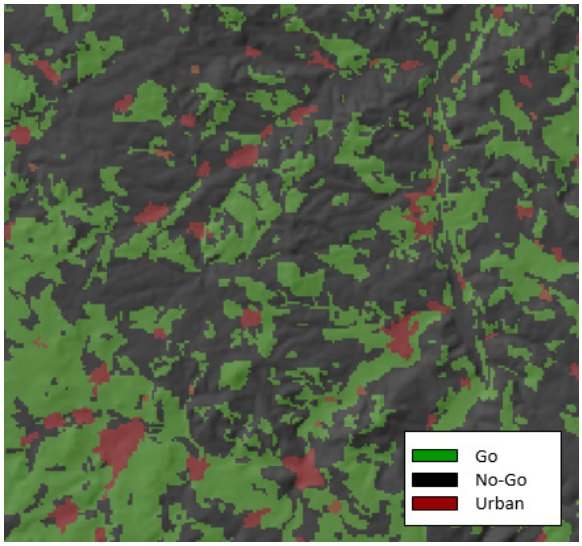


Figure 3-15: Example GO/NOGO Map (with Urban Areas).

In addition to generating the GO/NOGO condition for each terrain unit, NRMM also generates a list of "reason codes" that provide further insight into the causes behind a vehicle's immobilization. These additional insights can shape route planning, choice of a vehicle for a selected mission, and inform vehicle acquisition / modernization decisions. Example reason codes include: inability to negotiate/overcome obstacles; inability to negotiate vegetation; and inability to overcome soft soil/slope resistances. Figure 3-16 portrays a sample color-coded map indicating the NOGO Reason Codes (for an area other than the Monterey sample data).

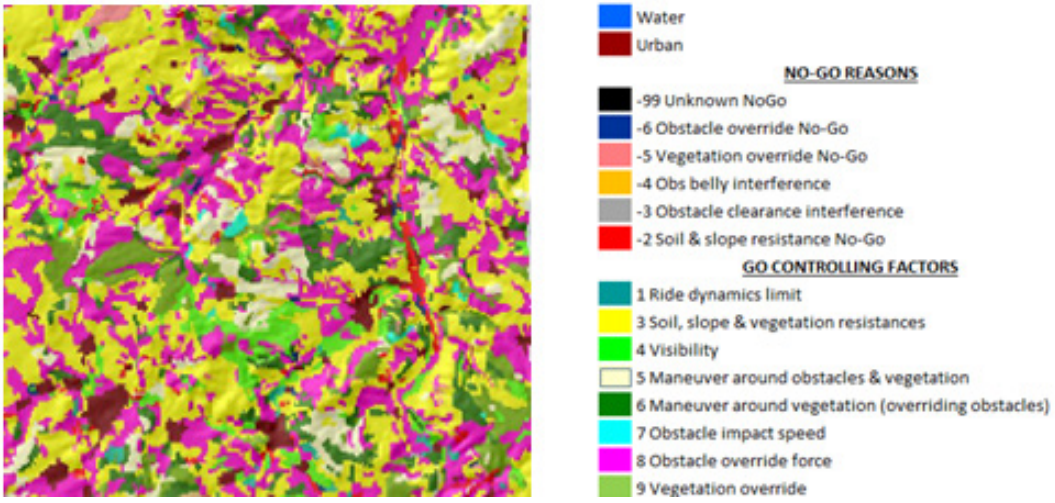


Figure 3-16: GO/NOGO Reason Code Map Example.

3.7.2 Speed-Made-Good Maps

Given a set of input parameters (e.g., vehicle, terrain, scenario), NRMM generates a predicted maximum safe speed for each terrain unit. "Speed-Made-Good" maps enable users to quickly and easily determine the best areas to conduct operations. The speed results from NRMM are normally binned into categories with each speed category being assigned a unique color. In Figure 3-17 below, six (6) colors were used to classify the vehicle speed over the terrain. NOGO areas, with a speed of 0 mph, were colored "black" and urban areas, ignored by the cross-country module, were colored "maroon". The remaining areas where the vehicle could operate were colored as follows: up to 10 mph – "dark brown"; > 10 to < = 20 mph – "orange"; > 20 to < = 30 mph – "yellow"; and > 30 mph – "green". Speed-Made-Good maps can also be visualized as a "stoplight chart". With the stoplight approach, the speeds are classified into three bins: green = unrestricted terrain, yellow = restricted terrain, and red = severely restricted terrain. NOGO areas are represented in "black".

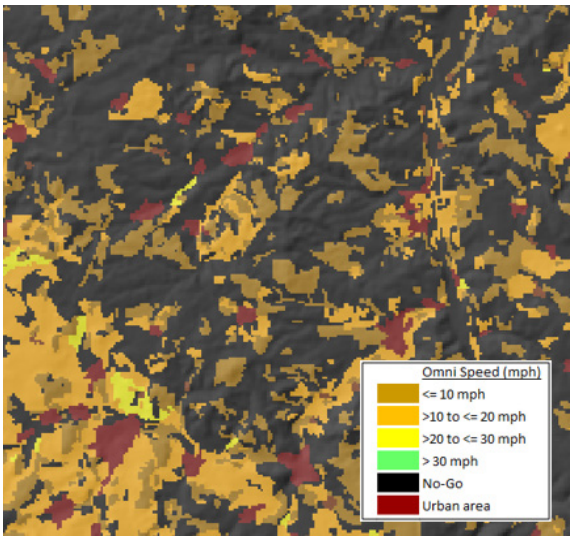


Figure 3-17: Speed-Made-Good Map Example.

Figure 3-18 shows two example Speed-Made-Good maps for different vehicles (for an area other than the Monterey sample data). In these examples, the unrestricted bin was set at > = 45mph, the restricted bin was set at > = 20 to < 45 mph, and the severely restricted bin was set at < 20 mph; however, the end user usually defines what thresholds to use for the speed classification. As seen in Figure 3-19, the bins were set at: 0 – 8 mph, 8 – 20 mph, and 20 – 30 mph.

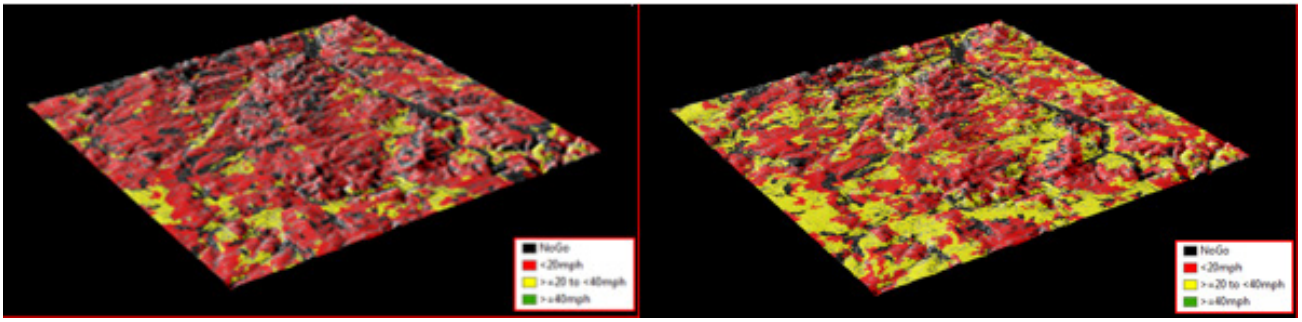


Figure 3-18: Two Examples of Speed-Made-Good Maps for Different Vehicles.

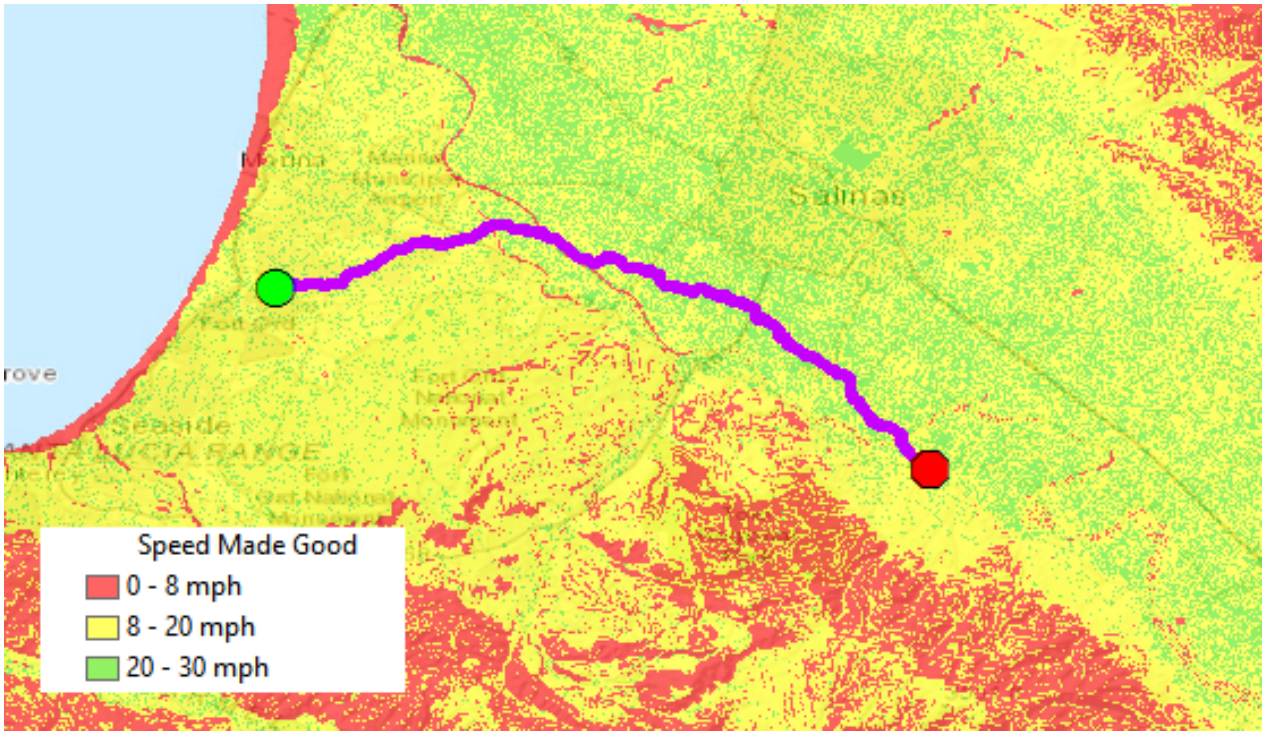


Figure 3-19: Least Cost Path Over Speed-Made-Good.

With the addition of uncertainty quantification in NG-NRMM, a series of speed maps can be created to show the vehicle speed at different confidence levels (as shown in Figure 3-20). Commanders may require a certain confidence level of data be used to inform mission planning purposes or they may be willing to accept some risk to gain a maneuver advantage.

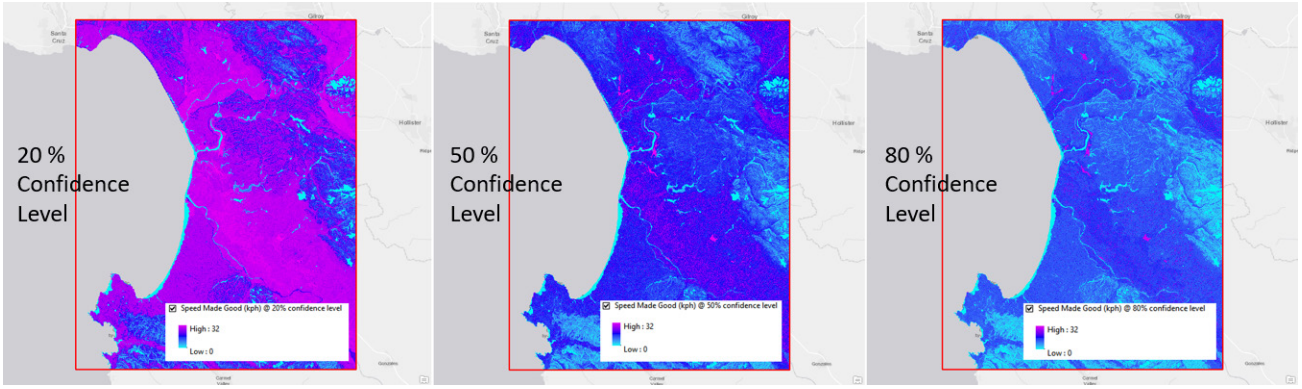


Figure 3-20: Notional Example of Speed-Made-Good at 20%, 50% and 80% Confidence Levels.

3.7.3 Additional Output Map Products

Additional results generated by the multibody dynamics models or uncertainty quantification processes can be represented as a map or map series. Since each output can be mapped to a Numbered Terrain Unit (NTU), the property can be symbolized on a map. For example, Figure 3-1 illustrates the estimated rut depth created by the vehicle traversing the soil. Oftentimes, maps are created to compare two vehicles – e.g., where can vehicle A go that vehicle B cannot, where can vehicle B go that vehicle A cannot, where is one vehicle faster than the other, etc. Additional products include fuel consumption / fuel economy; vehicle range; and single vehicle pass vs. multiple vehicle passes (e.g., convoy operations).

3.7.4 Least Cost Path

By spatially visualizing the results, additional analysis of the simulation results can yield critical insights (e.g., optimized route planning). For example, Least Cost Path is the analysis of terrain and other factors to reduce to find the "easiest" or most efficient path through the terrain from a starting location to a desired destination [20]. The "ease" of movement is based on a cost surface that is a combination of one or more factors, including terrain, vegetation, soil composition, etc. As each pixel from the source starting point is considered, its associated cost to traverse that pixel is calculated. Between the starting point and ending point these costs are accumulated to be the minimum possible. An example Least Cost Path (i.e., optimized path) analysis result is shown in Figure 3-19 using Speed-Made-Good prediction results for the Monterey Bay, CA area.

3.8 GAPS, CHALLENGES, AND FUTURE WORK

The processes presented here are neither exhaustive nor complete. During the work of AVT-248 several issues were identified as gaps in knowledge, challenges to using the proscribed processes, and potential ideas for progressing the work of NG-NRMM for the future. This section describes the most prominent gaps, challenges, and future work.

3.8.1 Resolution of Data Sources

Most geospatial data is collected remotely for vastly different purposes using a wide array of sensors and techniques. The data are also distributed by many different methods. Therefore, it is not unexpected that the various required inputs to NRMM have different resolutions. For example, large area (small-scale) elevation

data are widely available at 90 meters, 30 meters, and 10 meters. However, these resolutions are still too large to be useful to properly characterize surface roughness. Surface roughness parameters (e.g., RMS / WNS) require extremely high-resolution measurement (~1 m and less) that is not universally available and can be costly to collect or purchase, especially for large areas. Data of this nature is not collected by satellite or other earth-orbiting platforms like the SRTM datasets mentioned earlier. High resolution LIDAR and high-resolution imagery are collected from terrestrial or low-altitude platforms such as Unmanned Aerial Vehicles (UAVs) or ground vehicle-mounted scanners. These can be costly to collect, and usually require local "boots-on-the-ground" collection. Depending on the size of the area, it may take several weeks or months to produce a single dataset. Due to the high resolution of measurement, datasets of this type will also increase the amount of data to store, manage, and process.

3.8.2 Data Availability to Field User

What data are available to the general NG-NRMM user? What data would be available to a field based NG-NRMM user in an operational planning role? Will the same data be available to the various international members?

Data availability is another challenge that end users may contend with. While elevation data at low resolution (90 meters) may be available globally, acquiring high resolution soil property data may severely limit the usefulness of NG-NRMM, especially to operational personnel in the field with limited network connectivity. Many of the traditional soil mechanical inputs have little or no data availability, or are derived from other quantities. For example, very little Bekker-Wong bevameter data exists at the global scale; and, are linked to vehicle weight / contact patch area (and not collected for other purposes) thus further limiting data availability. Former RCI soil strength data were vehicle agnostic measurements and data of this type were often collected for other purposes (e.g., road / building construction). In the absence of necessary data, higher fidelity MBD methodologies will not generate more accurate results if users must guess at terrain/soil/land use input values. Likewise, investments in ultrahigh fidelity physics-based models will not generate more accurate results if coarse resolution and/or ill-defined terrain parameters are used as model inputs.

3.8.3 Limitations of MAPTBL Format with NG-NRMM Resolution / Data Requirements

The NRMM MAPTBL Code 11 format is an ASCII-based interchange format introduced for the NRMM II software and was used as the basis for interchange in NG-NRMM for legacy support. As described earlier, it is a simple, easy-to-use format. However, there are many conditions that will severely limit the MAPTBL usefulness. One of the main restrictions is the amount and complexity of data that can be transferred with this format. MAPTBL terrain files use unique combinations of map units, which can be combinatorically complex. That is, the number of unique combinations of all input variables, e.g., elevation, slope, aspect, bulk density, etc. can increase the number of possible records in the MAPTBL interchange file. Due to the additional terrain attribution and resolution needed to support high-fidelity physics-based modeling, the number of unique terrain units (and resulting terrain file size) can become extremely large.

For example, in the Monterey, CA area of interest, a 90 meter SRTM elevation dataset (for an area encompassing 90 km x 110 km) contained 3601 rows x 3601 columns of data, with 1826 possible elevation values. For this same area, there were 218 unique slope percentage values and 361 unique Aspect (azimuth) values. Considering that each combination of elevation, slope, and aspect could be unique: 1836 * 218 * 361 ~ 144,489,528 possible combinations could exist. Fortunately, the overall sample data contained similar values yielding only 10,251,513 actual combinations (79.0% unique).

A second dataset was built using the same Monterey, CA, sample data; however, the area of interest was reduced to 55 km x 45 km (2490 km^2). All required NG-NRMM input data were generated (GRADE, ASPECT, BULKDNS, KUSCS, KUSCS2 and default values used for: LUSE, SSL, SSL2, TMOIST, TMOIST2, TEMP, TEMP2). For this second dataset, increased resolution elevation data was also utilized (SRTM 30 m instead of 90 m). The resulting terrain file only contained 2,577,172 unique records in the output MAPTBL format. While 2.5 million records is an improvement over the initial estimate of 144 million, the resulting data files are approximately 2 gigabytes in size when stored on disk.

One approach to minimizing the combinatorial complexity would be to bin the data into classes (e.g., slope classes – 5%, 10%, 15%, etc.). Rather than storing the unique value of each slope, a slope class could encompass a range of slope values. This strategy could be utilized for many of the terrain parameters to reduce the number of unique combinations of terrain parameters; however, classifying the data into bins will reduce terrain resolution and affect the accuracy of NG-NRMM results. As covered in the preceding section, investments in ultrahigh fidelity physics-based models will not generate more accurate results if coarse resolution and/or ill-defined terrain parameters are used as model inputs.

For the future other geospatially-enabled scientific data formats, such as Network Common Data Format (NetCDF) [21] and Hierarchical Data Format (HDF) [22], should be reviewed and considered as a more acceptable interchange format. Scientific formats can support multiple resolutions of data of various types, are compressible, and have wide support in their respective communities. If these formats are pursued, interoperability with uncertainty quantification and multibody physics-based vehicle models must be considered. These models would need to be capable of importing NetCDF / HDF data, preserving the spatial orientation and location of the terrain units while running the vehicle-soil interaction modules, and be capable of exporting results generated by NG-NRMM to these data formats. Since NetCDF / HDF are considered "scientific" formats, ease of use for all end users must also be considered.

3.9 NATO STANDARD RECOMMENDATION (STANREC)

Properly characterizing terrain is critical to generate accurate, operationally relevant ground vehicle performance results using NG-NRMM. To build the required terrains needed to support coalition mission planning and operational effectiveness analyses, NG-NRMM must be able to import and aggregate remotely sensed Geographic Information Systems (GIS) data and generate terrains that can be analyzed in the NG-NRMM vehicle / terramechanical analysis software.

To ensure that both the terrain data and NG-NRMM can be used by all NATO members, a STANREC was constructed to describe the architecture and provide terrain data development guidance to ensure that terrain data products are interoperable between NATO and other alliance members. The recommendations provided align with the Defence Geospatial Information Working Group (DGIWG) – the multinational body responsible for geospatial standardization for the defence organizations of member nations, to provide compatible geospatial information for joint operations.

The STANREC defines the product specifications, encoding formats and application schemas for military geospatial data; and is built upon generic and abstract standards for geographic information defined by the International Organization for Standardization (ISO TC/211) and the Open Geospatial Consortium (OGC).

3.9.1 Geographic Terrain Data Provided as Input to Off-Road Mobility M&S

From a broad array of GIS data, NG-NRMM terrain data input files shall be specifically constructed and formatted to support probabilistic mobility predictions. For each individual off-road Numbered Terrain Unit (NTU), at the lowest level of digital elevation map resolution, the following minimum of 32 characterizing data fields shall be included in the NG-NRMM terrain data:

1) USCS soil type;
2) Bulk density (g/cm^3);
3) Moisture content (% volume);
4) Temperature (° K);
5) Land use (coded value);
6) Top layer depth (inches);
7) – 10) Items 1 to 4 repeated, for the 2^{nd} substrate layer;
11) Surface roughness measure as Root Mean Square (RMS) measure in inches;
12) Surface downhill slope in percent rise;
13) Vegetation, recommending Multinational Geospatial Co-Production (MGCP) classification schema for vegetation. Classification schema must also include attribution of vegetation properties that influence off-road mobility, such as: stem spacing, stem diameter, vegetation height, and vegetation type) [23] [24], [25];
14) Obstacle length (inches);
15) Obstacle height (inches);
16) Obstacle width (inches); and
17) – 32) Uncertainty Quantification values of 1) to 16) above.

- Tags will also be included identifying the source of the data as: measured/“m”, inferred/“i”, legacy/“c”, or notional/“n”. Inferred data shall provide the inference algorithm.

3.9.1.1 Input Data Schema

The following will be supported:

1) FACC+ (with eventual migration to DFDD+); and
2) Legacy NRMM Code 11 MAPTBL format.

3.9.1.2 Input Data Formats

File Geodatabase, MAPTBL via ASCII (“flat file”), GeoTIFF, xml (metadata) – ISO 19139 – Geographic Information – Metadata (templates exist in ArcGIS).

3.9.1.2.1 Geospatial Data Storage Formats

File Geodatabase.

3.9.1.3 Input Environment Scenario Data

An optional environment-defining scenario data input file (i.e., such as non-permanent weather-related conditions that modify terrain responses) shall have the same format as the terrain data file. Data fields that are customizable to the scenario conditions shall comply with input data schema and be labelled to reflect their transient nature (e.g., fields flooded for rice cultivation, areas inundated during a "rainy season", frozen water bodies, etc.). Environment-defining scenario files also provide an opportunity to partition scenario-specific terrain parameters outside the base NG-NRMM terrain file; thereby, significantly reducing the number of terrain parameters, the number of unique terrain combinations, and the size of the base NG-NRMM terrain file. For example, parameters that are unique to an urban environment could be captured while less relevant terrain parameters like soft-soil properties may be able to be excluded.

3.9.2 Mobility M&S Output to Geographic Map Overlays

Mobility metrics shall be computed by the NG-NRMM mobility M&S capability for each NTU. These metrics are, at a minimum, trafficability (single pass GO/NOGO), Speed-Made-Good and speed / trafficability limiting reason codes, including probabilistic measurement. Detailed definition of the algorithmic basis for each mobility metrics should be clearly defined. The legacy NRMM definitions are accepted as a minimum baseline, but probabilistic mobility and terrain property related metrics for map plotting from a NG-NRMM capability shall be defined by each end use.

3.9.2.1 Formats

In addition to the integer valued GO/NOGO (1 = GO, 0 = NOGO), and three (3) Speed-Made-Good data fields (upslope, downslope, across slope), there shall be four (4) data fields for the variance of each of the standard mobility metrics, twenty-two (22) speed and/or trafficability reason code fields (to preserve existing NRMM capability) and fifteen (15) additional real valued customizable mobility-related parameters fields per NTU in raster format.

3.9.2.2 Trafficability NOGO

Trafficability is the ability of a vehicle to traverse a given area of terrain. It shall be expressed as a binary result indicating success (GO) or failure (NOGO). Using available data that quantify variability of terrain properties, probabilistic trafficability metrics shall be developed. The subordinate reasons for results and their respective limits shall be made available in the GIS output file. The algorithms supporting the results shall be fully documented.

3.9.2.3 Speed-Made-Good

Speed-Made-Good is the maximum safe speed a given vehicle can traverse an NTU. Slope dependence can be averaged out to yield a single performance metric, omni-directional (i.e., "omni-speed"), or the results can be provided as a triplet including upslope, cross slope, and downslope speed limits. When using omni-speed, all three data fields will be equal, having the omni-speed average value. Using available data that quantify variability of terrain properties, probabilistic Speed-Made-Good metrics shall be developed. The subordinate reasons for results and their respective limits shall be made available in the GIS output file. The algorithms supporting the results shall be fully documented.

3.10 SUMMARY

In this chapter, the Geographical Information Systems (GIS) Terrain and Mobility Mapping Thrust Area team constructed a list of recommendations to support and shape the development of the Next-Generation NATO Reference Mobility Model (NG-NRMM) STANREC and included appropriate justifications to underpin the recommendations made. The team demonstrated the feasibility of building new NG-NRMM terrain by constructing a sample dataset and developing a set of prototype tools. These prototype tools were used to generate new terrain files that were interoperable with Uncertainty Quantification (UQ) and vehicle Multibody Dynamic (MBD) modeling software. The UQ and MBD tools were then asked to deliver results that could be visualized using GIS software to demonstrate an end-to-end NG-NRMM solution. The requirements for the minimum set of terrain data needed to produce NG-NRMM results were established. Data schemas and models were defined to ensure interoperability. Relevant references, standards and specifications were identified to inform the recommendations and documented to support future efforts to improve the initial NG-NRMM STANREC. Examples of geospatial visualization products were provided to illustrate potential usage applications for NG-NRMM results. Finally, potential data gaps and challenges were captured to inform future investment / development efforts and recommendations for additional future GIS terrain work provided.

3.11 STANDARDS

The following is a list of prescribed international standards for working with geospatial data that should be followed:

- STANAG 2592 – “NATO Geospatial Information Framework (NGIF)”.
- STANAG 7074 – “Digital Information Exchange Standard (DIGEST)”.
- ISO/TC 211 – “Geographic Information / Geomatics”.
- ISO 19107:2003 – “Geographic Information – Spatial Schema”.
- ISO 19117:2005 – “Geographic Information – Portrayal”.
- ISO 19103:2005 – “Conceptual schema language”.
- ISO 19109:2005 – “Rules for application schema”.
- ISO 19115:2003 – “Metadata”.
- ISO 19126:2009 – “Profile – FACC Data Dictionary”.
- ISO 19135:2005 – “Procedures for registration of geographical information items”.
- ASTM D2487-11 “Standard Practice for Classification of Soils for Engineering Purposes (Unified Soil Classification System)”.
- Tagged Image File Format (TIFF) [26].
- GeoTIFF Format Specification, GeoTIFF Revision 1.0 [27].

3.12 REFERENCES

[1] GIS Glossary, Wiki.GIS: http://wiki.gis.com/wiki/index.php/GIS_Glossary [accessed May 25, 2018].

[2] Esri Support pfor Geospatial Standards, OGC and ISO TC/211 page: http://www.esri.com/library/whitepapers/pdfs/supported-ogc-iso-standards.pdf [accessed July 05, 2018].

[3] Digital Geographic Information Working Group page: https://www.dgiwg.org/dgiwg/ [accessed July 05, 2018].

[4] International Organization for Standardization (ISO) TC/211 page: http://www.isotc211.org/ [accessed July 05, 2018]

[5] Digital Geographic Information Working Group, Digital Geographic Information Exchange Standard (DIGEST) page: https://www.dgiwg.org/digest/ [accessed July 05, 2018].

[6] GeoTIFF Format Specification, GeoTIFF Revision 1.0 page: http://web.archive.org/web/20160403164508/http://www.remotesensing.org/geotiff/spec/geotiffhome.html [accessed Nov 27,2017].

[7] U.S. Department of the Interior | U.S. Geological Survey, USGS EarthExplorer page: https://earthexplorer.usgs.gov/ [accessed February 23, 2018].

[8] U.S. Department of the Interior | U.S. Geological Survey, The National Map URL: https://viewer.nationalmap.gov/advanced-viewer/ Page Contact Information: The National Map [accessed February 23, 2018].

[9] World Geodetic Service. 1984. http://earth-info.nga.mil/GandG/update/index.php?action=home#tab_wgs84-data. [accessed February 23, 2018].

[10] U.S. National Resources Conservation Service (NRCS) Web Soil Survey home page: https://websoilsurvey.sc.egov.usda.gov/App/HomePage.htm [accessed February 9, 2018].

[11] Description of SSURGO Database, U.S. Natural Resources Conservation Service page: https://www.nrcs.usda.gov/wps/portal/nrcs/detail/soils/survey/geo/?cid=nrcs142p2_053627 [accessed February 9, 2018].

[12] U.S. National Resources Conservation Service (NRCS) Soil Data Viewer extension to ArcMap page: https://www.nrcs.usda.gov/wps/portal/nrcs/detail/soils/home/?cid=nrcs142p2_053620 [accessed February 9, 2018].

[13] Bullock, C.D. 1994. Methodology for the Development of Inference Algorithms for Worldwide Application of Interim Terrain Data to the NATO Reference Mobility Model. United States. U.S. Army Engineer Waterways Experiment Station and Geotechnical Laboratory (U.S.). Vicksburg, Miss.: U.S. Army Engineer Waterways Experiment Station.

[14] Homer, C.G., Dewitz, J.A., Yang, L., Jin, S., Danielson, P., Xian, G., Coulston, J., Herold, N.D., Wickham, J.D. and Megown, K. 2015. Completion of the 2011 National Land Cover Database for the Conterminous United States – Representing a decade of land cover change information. Photogrammetric Engineering and Remote Sensing, 81(5):345-354.

[15] MGCP LandCover features, Esri, Inc. page: http://desktop.arcgis.com/en/arcmap/latest/extensions/defense-mapping/mgcp-landcover-features.htm [accessed May 25, 2018].

[16] GeoDB, Esri Geodatabase (File-based), U.S. Library of Congress page: https://www.loc.gov/preservation/digital/formats/fdd/fdd000294.shtml [accessed Nov 27, 2017].

[17] Esri/file-geodatabase-api, GitHub.com page: https://github.com/Esri/file-geodatabase-api [accessed Nov 27, 2017].

[18] Digital Geographic Information Working Group, DIGEST Overview page: https://www.dgiwg.org/digest/Overview2.htm#TOP [accessed July 06, 2018].

[19] DGIWG FACC, About This Standard page: http://www.gwg.nga.mil/documents/asfe/DGIWG_FACC.htm [accessed July 06, 2018].

[20] Briney, A. 2014. Overview of Least Cost Path Analysis, GIS Lounge page: https://www.gislounge.com/overview-least-cost-path-analysis/ [accessed December 11, 2017].

[21] Network Common Data Format (NetCDF), UCAR/Unidata page: https://www.unidata.ucar.edu/software/netcdf/ (http://doi.org/10.5065/D6H70CW6) [accessed May 25, 2018].

[22] The Hierarchical Data Format (HDF) Group, Welcome to the HDF5 Support Page: http://www.hdfgroup.org/HDF5/ [accessed May 25, 2018].

[23] Rybansky, M. 2009. Modelling and Cartographic Visualisation of Transport During Crisis Situations and Military Operations, page: https://icaci.org/files/documents/ICC_proceedings/ICC2009/html/refer/4_3.pdf [accessed July 21, 2018].

[24] Messmore, J., Vogel, T., and Pearson, A. 1979. Terrain Analysis Procedural Guide for Vegetation. Fort Belvoir, Virginia: Army Corps of Engineers Engineer Topographic Laboratories. United States, Army Corps of Engineers Engineer Topographic Laboratories (U.S.). Accessed from: http://acwc.sdp.sirsi.net/client/en_US/default/index.assetbox.assetactionicon.view/1045814?rm=SPECIAL+REPORTS8%7C%7C%7C1%7C%7C%7C0%7C%7C%7Ctrue&lm=WES [accessed July 21, 2018].

[25] US Army Field Manual (FM) 5-33: Terrain Analysis. 1990. Accessed from: http://www.enlistment.us/field-manuals/fm-5-33-terrain-analysis.shtml [accessed July 21, 2018].

[26] Tagged Image File Format (TIFF), FAQ page: https://www.awaresystems.be/imaging/tiff/faq.html [accessed Nov 27, 2017].

[27] GeoTIFF Format Specification, GeoTIFF Revision 1.0 page: http://web.archive.org/web/20160403164508/http:/www.remotesensing.org/geotiff/spec/geotiffhome.html [accessed Nov 27, 2017].



Chapter 4 – TA2: SIMPLE TERRAMECHANICS

Michael McCullough
BAE Systems Inc.
UNITED STATES

4.1 GOALS AND TEAM MEMBERS

Thrust Area 2 (TA2), Simple Terramechanics (ST), seeks to collect, describe, and codify existing deformable soil Modeling and Simulation (M&S) approaches, along with their complementary supporting experimental methods that are based on pressure-sinkage formulations of soft soil bearing pressure upon vehicle running gear along with their complementary traction-slip equations for traction stress response. Terramechanics effects are one of the primary attributes affecting vehicle mobility and have been judged by ATV-248 to be a foundational capability required in both the current NRMM and the NG-NRMM, and therefore one of the primary focus areas of the RTG [1]. Specific derived goals include:

1) Defining the input and output parameters required for ST models to interact with GIS-based input and output processes from Thrust Area 1 (TA1);
2) Identifying and promoting prototypical demonstrations of GIS-based end-to-end ST models and simulations;
3) Developing initial release standards describing NG-NRMM ST models;
4) Establishing a NG-NRMM ST database of valid ST parameter data sets, along with estimates of uncertainty, for soft soils at varying moisture contents, including the supporting raw data from the terrain characterization experiments, when available; and
5) Developing and implementing M&S Verification and Validation (V&V) benchmarks for NG-NRMM ST models.

The team members comprise those AVT-248 members and guests who have expressed interest in participating in TA2 specific activities and contributing to the ongoing goals of the ST models and simulations in the context of the NG-NRMM. These members are as follows:

- Jon Preston-Thomas, Canada;
- Marian Rybansky, Czech Republic;
- Ole Balling, Denmark;
- Kersti Vennik, Estonia;
- Andreas Becker, Germany;
- Tom von Sturm zu Vehlingen, Germany;
- Phumlane Nkosi, South Africa;
- David Reinecke, South Africa;
- Susan Frankenstein, USA;
- Henry Hodges, USA;
- **Mike McCullough: Leader**, USA;

- Radu Serban, USA;
- Sally Shoop, USA;
- Vladimir Vantsevich, USA; and
- Tamer Wasfy, USA.

4.2 INTRODUCTION

Terramechanics modeling is focused on vehicle terrain interaction that accounts for soft soil (i.e., deformable soil) effects on mobility. The end-to-end NG-NRMM simulation capability, under the broad scope of its requirements, is depicted in Figure 4-1, wherein terrain mechanical (i.e., terramechanics) properties are one of many overlaid geographically distributed attributes and features that affect vehicle mobility. Based on the terrain properties, mobility will be computed and displayed as a map of GO/NOGO capability and/or maximum speeds attainable (i.e., Speed-Made-Good) across a given region of interest. While terramechanics is a very active and prolific research domain, TA2 is specifically focused on the immediately applicable terramechanics models that have direct impacts to military vehicle mobility predictions.

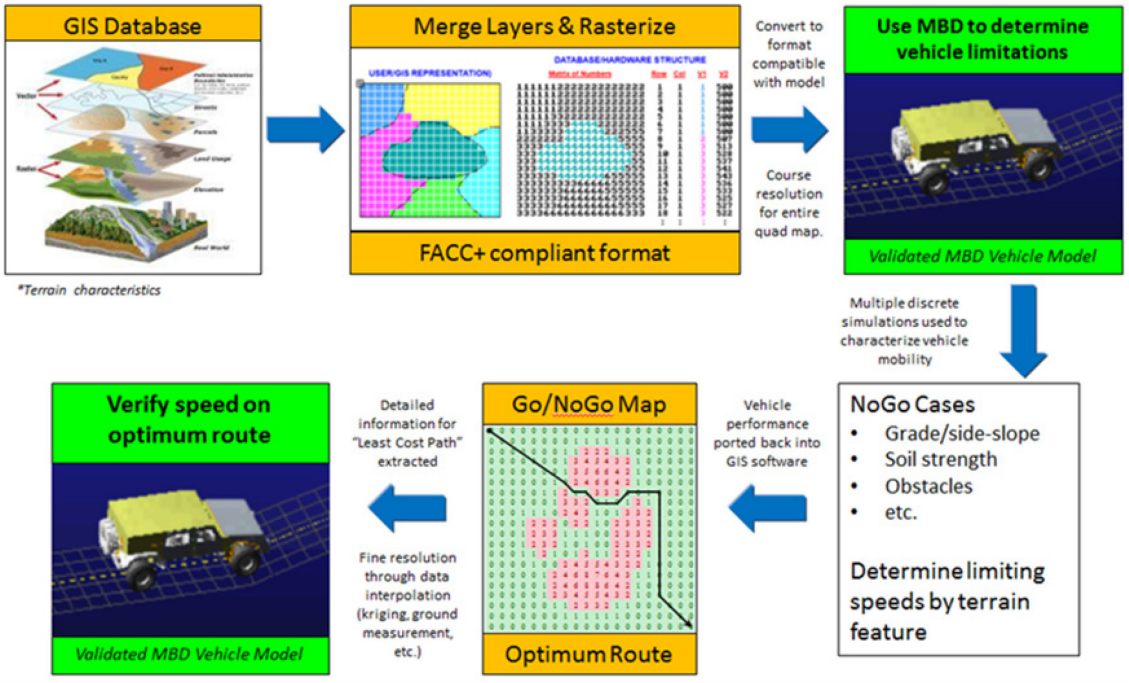


Figure 4-1: Full Featured NG-NRMM Simulation Begins with GIS-Based Data, Predicts Mobility and Maps it Back Onto the Terrain as an Additional GIS Parameter [2].

The NRMM approach to soft soil strength measurement and modeling is the cone penetrometer and the Cone Index (CI) metric. It holds a practical appeal for linking terrain strength to vehicle performance because CI is so easy to measure for most soft soils and the penetrometer is compact and portable. Unfortunately, a cone penetrometer is not a very close physical analog to vehicle running gear bearing and tractive interactions with soil. And, it is dimensionally insufficient to characterize the independent development of tractive and bearing

loads as well as the fundamental soil properties and processes involved in the development of soil strength. NG-NRMM employs a dual development path focusing on more theoretically correct soft soil models. Models based on the use of pressure-sinkage and traction-slip data developed from platens and shear rings that more closely resemble vehicle running gear interaction with the soil are covered under the title "Simple Terramechanics" (TA2). The platens and shear ring load-displacement equipment and instrumentation for acquiring these semi-empirical data are typically referred to as a "bevameter" , which is a contraction of "Bekker Value Meter", referring to its original developer [3]. The bevameter measurements for soil strength parameters require significantly more effort than a cone penetrometer. The longer-term higher fidelity objective approach entitled "Complex Terramechanics" (covered by TA3 in Chapter 5) allows for inclusion of theoretical and numerical approaches that are still under development, but show great promise to overcome theoretical and practical limitations of Simple Terramechanics models using fully 3D continuum failure and flow models. Figure 4-2 depicts the spectrum of soft soil terramechanics models beginning with the incumbent NRMM Cone Index (CI) empirically based method, extending through the semi-empirical Simple Terramechanics models, and ranging up to the Complex Terramechanics models. Simple Terramechanics models provide an immediate practical approach that, to a very large degree, has already been developed and applied to several specific mobility problems.

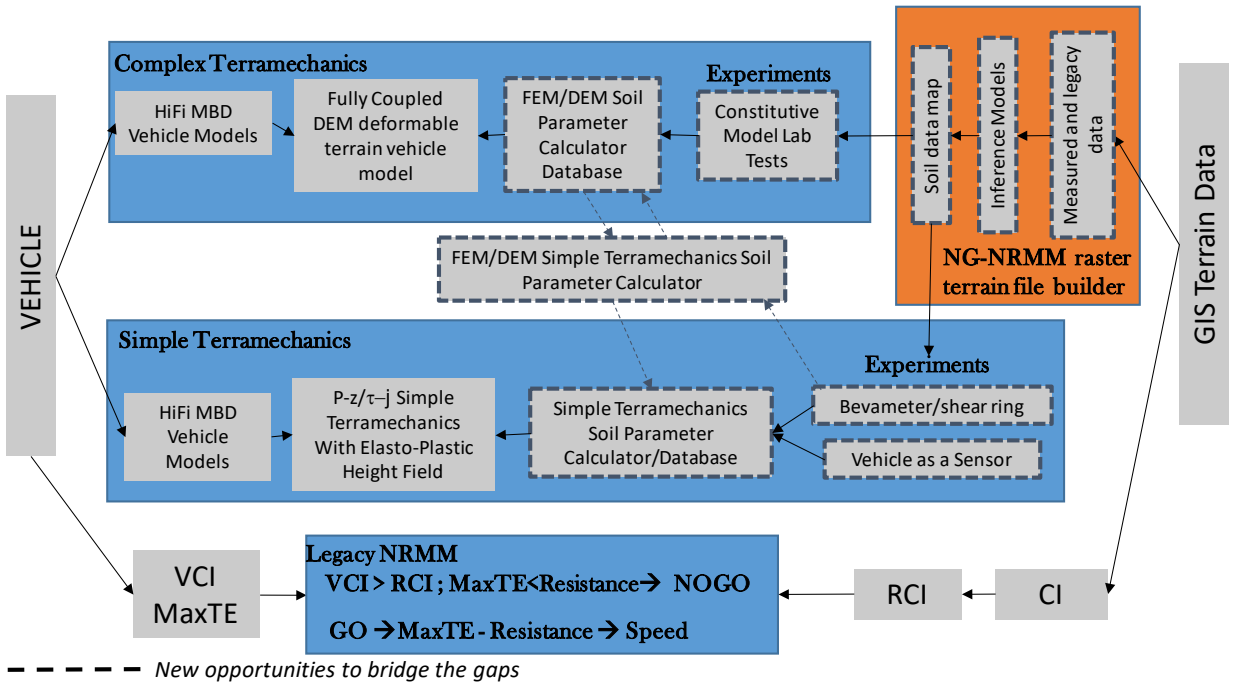


Figure 4-2: Replacing the Cone Index Methods Used in the Current NRMM, Simple Terramechanics Models will Bring the Full 3D Mechanics of Vehicles Together with Existing Terramechanics.Replacing the Cone Index (CI) Methods Used in the Current NRMM, Simple Terramechanics models will bring the full 3D mechanics of vehicles together with existing terramechanics to provide a means for calculating critical mobility metrics on soft soil that are foundational components in the higher level mobility aggregated predictions of feasible trafficability (GO/NOGO regions) and maximum speed attainable.

Within the broader scope of all the factors affecting trafficability and limiting speeds over off-road terrains, the operational module of current NRMM breaks the mobility prediction task into a series of "reason codes". These reason codes are the high level taxonomy of the prediction algorithms that must be upgraded in NG-NRMM to include soft soil effects. A summary of the areas and impacts that ST models will have on mobility predictions in NG-NRMM is summarized in Table 4-1 below.

The NG-NRMM initial Tracked and Wheeled Vehicle benchmark events (see Chapter 8) were defined and selected to highlight the demonstrated improvements that terramechanics models have on the mobility factors summarized by these legacy NRMM reason codes.

Table 4-1: Expected Simple Terramechanics (ST) Model Impacts on Legacy NRMM Mobility Factors and Their Inclusion in the Current NG-NRMM Benchmarks (See Chapter 8).

GO Ride Limiting Speed Controlling Factors		2D ST Soft Soil Model Impact	3D ST Soft Soil Model Impact	Current NG-NRMM Benchmark?
1	Ride dynamics (vride) limit	1st order is geometric RMS, 2nd order is 3D, soft soil is distant 3rd order effect.	3D geometry is a close 2nd order effect, soft soil is distant 3rd order.	Yes, 3D RMS method demo'ed at CDT.
2	Tire speed limit	None	None	None
3	Soil, slope and vegetation resistances	Primary	Primary	Soil and slope only
4	Visibility	None	None	None
5	Maneuver around vegetation and obstacles	None	Primary	None
6	Maneuver around vegetation only	None	Primary	None
7	Obstacle impact (VOOB) speed (half rounds)	Performance is significantly degraded by soft soil.	Significantly altered by 3D and degraded by soft soil.	Yes, 2D paved only
8	Obstacle override force	Performance is significantly degraded by soft soil.	Significantly altered by 3D and degraded by soft soil.	Yes, 2D paved only
9	Driver prudence overriding vegetation	None	None	None
10	External (scenario) limit	Primarily for weather	Primarily for weather	None
11	AASHTO curvature speed limit	None	None	None

GO Ride Limiting Speed Controlling Factors		2D ST Soft Soil Model Impact	3D ST Soft Soil Model Impact	Current NG-NRMM Benchmark?
12	Sliding on curves	None	Primary	Yes
13	Tipping on curves	None	Primary	Yes
	NOGO Reasons			
1	Inability to brake (visibility)	None	None	None
2	Soil and slope resistance	Primary	Primary	Yes
3	Obstacle clearance interference	Primary	Primary	Yes
4	Obstacle belly interference	Primary	Primary	Yes
5	Vegetation override	None	None	None
6	Obstacle override	Performance is significantly degraded by soft soil.	Significantly altered by 3D and degraded by soft soil.	Yes, 2D paved only
7	VCI (Soil no-go on level)	Primary	Primary	Yes
8	Sliding on side slope	Performance is significantly degraded by soft soil.	Significantly altered by 3D and degraded by soft soil.	Yes
9	Tipping on side slope	Performance is significantly degraded by soft soil.	Significantly altered by 3D and degraded by soft soil.	Yes

4.3 PROCESS/METHODOLOGY

The bevameter measurements for Simple Terramechanics models soil strength parameters require significantly more effort than a cone penetrometer. Nevertheless, bevameter measurements consisting of pressure-sinkage testing using bearing stress platens, combined with grouser enhanced shear rings for tractive stress (both assumed to be geometric analogs of the vehicle running gear) are the most widely used improvement to the CI methods for characterizing soil strength [3], [4]. Dimensionally, there are at least five independent parameters determined by the calibrating experiments. For bearing pressure, these are commonly represented as "**p-z**" equations where **p** is the bearing pressure under the platen that is pushed into the soil, **z** is the platen sinkage, and **k** and **n** are the best fit parameters in the equations that have taken several forms over the years. Originally, Bernstein [5] proposed the following power law form of the plastic limit pressure:

$$p = kz^n \tag{4-1}$$

Bekker [3], added the effects of a primary running gear dimension, **b**, typically the width or smaller dimension of the contact patch, or radius of a circular contact area:

$$p = \left(\frac{k_c}{b} + k_\varphi\right) z^n \tag{4-2}$$

where $\mathbf{k_c}$ and $\mathbf{k_\phi}$ are intended to capture the cohesive and frictional soil strength effects, and developed the first bevameter data acquisition system. Later, Reece proposed the Bekker-Wong-Reece form [6] of the plastic limiting bearing envelope:

$$p = \left(k'_c + bk'_\varphi\right)\left(\frac{z}{b}\right)^n \tag{4-3}$$

where the coefficients have slightly different units and meaning with the potential to account for geometric scale more effectively. Wong [4] developed the bevameter experimental data reduction methodology for parameter identification to identify Bekker (or Reece) parameters from pressure-sinkage experiments. He also developed the elasto-plastic model of repetitive unload reload cycles augmenting the Bekker model (see regime D in Figure 4-3). In combination, these are dubbed herein the "Bekker-Wong" model and must include the parameters associated with the slope $\mathbf{k_{unload}}$ of the elastic unload/load in regime D:

$$k_{unload} = k_0 + A_{unload}\, z_{unload} \tag{4-4}$$

where $\mathbf{k_0}$ and $\mathbf{A_{unload}}$ are developed from multiple repetitive load experiments.

When combined with a shear response model developed from measurements using an annular ring shear device [7], they form the basis of most modern Simple Terramechanics models. The traction equations (shear stress vs shear displacement, or **"τ-j")** were proposed and demonstrated by Hanamoto and Janosi [7] in the following simplest form:

$$\tau = [c + p\tan\varphi]\left(1 - e^{\left(-j/k_s\right)}\right) \tag{4-5}$$

where τ is the tractive or shear stress, j is shear-slip, $\mathbf{k_s}$ is an exponential function constant describing initial rise rate from zero slip, **c** is cohesion and ϕ is the soil internal friction angle. This is the "plastic" soil response. Brittle soils exhibit a more complex shear behavior in which a maximum shear is achieved at a particular slip displacement value (usually in the range of 5 – 20 %) and then degrades upon further shear displacement. The most convenient mathematical form describing this brittle tractive response behavior has been proposed and used to fit experimental data by Wong in Ref. [8]. It takes the following mathematical form:

$$\tau = \tau_{max}\left\{K_r + \left[\left(\frac{1}{1-\frac{1}{e}}\right) - K_r\right] e^{\left(1-\frac{j}{K_w}\right)}\right\}\left\{1 - e^{\left(\frac{-j}{K_w}\right)}\right\} \tag{4-6}$$

where:

$$\tau_{max} = c + p\tan\varphi \tag{4-7}$$

and $\mathbf{K_r}$ is the ratio of the large shear displacement residual shear stress to the $\boldsymbol{\tau_{max}}$, and $\mathbf{K_w}$ is the shear displacement at the point that $\boldsymbol{\tau_{max}}$ occurs. They have been validated at the vehicle level for both tracked vehicles [4] and wheeled vehicles [7], and can take other more complex mathematical forms when necessary.

For deformable soils, all Simple Terramechanics models must include some means of tracking permanent deformation (i.e., the sinkage at d1 in Figure 4-3 following the passage of an individual wheel or a running gear system) and modifying the soil response due to the effects of compaction and flow as well as sheared soil layers (i.e., slip-sinkage). This typically requires a discretization of the soil substrate into cells for which the sinkage and shear states are numerically computed and tracked. This general construct has been described in Refs. [8] and [10] in the context of Vehicle-Terrain Interface (VTI) real-time models for simulators, but is commonly known in recent engineering analysis implementations as a "height field" local terrain model [11], discussed later and shown in Figure 4-4.

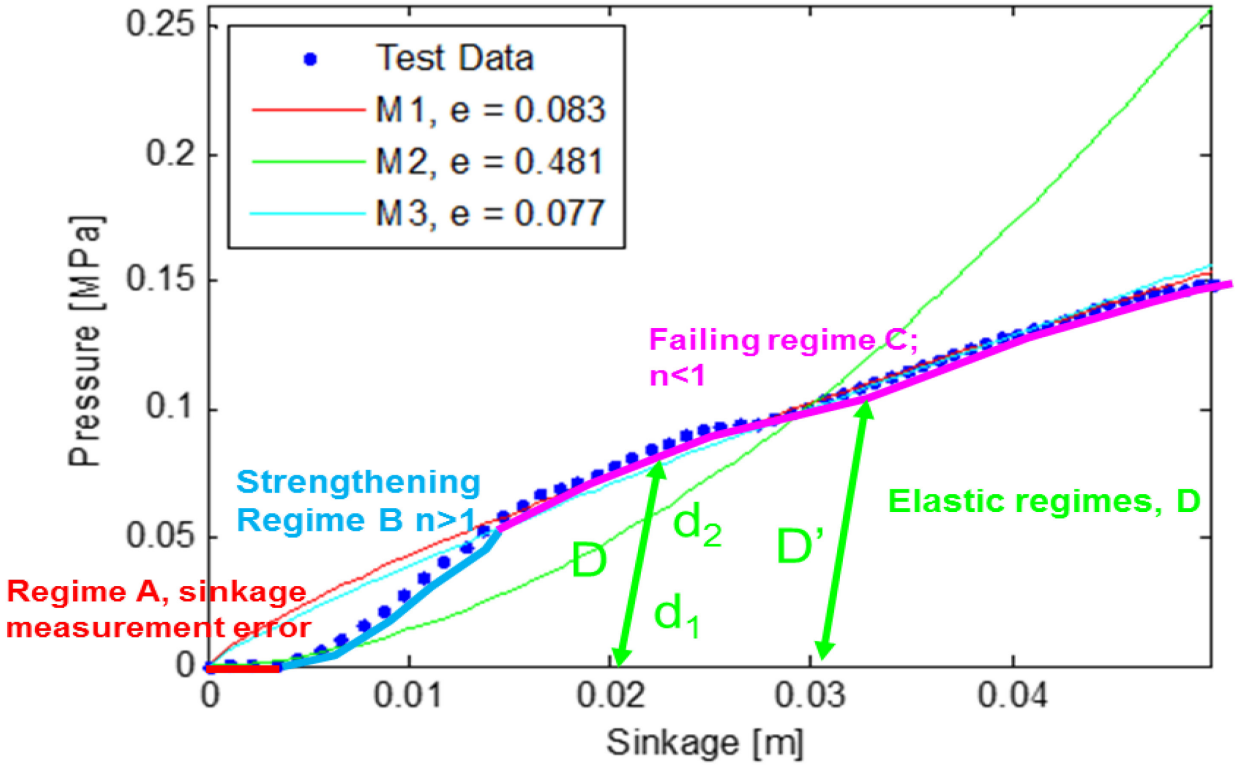


Figure 4-3: Data From Ref. [8] Shows That the Bekker-Wong Model Includes Procedures for Parameter Identification From Test Data and, Most Importantly, Recognition of the Elastic Unload/Reload Portions of the Response, D and D' [4], [12]. Regime A is sinkage measurement error offset to the onset of actual soil loading; regime B is the compacting of loose soil so the soil is strengthening and n > 1; the transition to regime C is an inflection point with changing exponent, toward n < 1 in regime C, which is soil bearing failure controlled by the growth of shear-slip line fields in the far field. Thus, the model parameter identification is dependent upon peak pressure regime in the specific vehicle application for which it will be used.

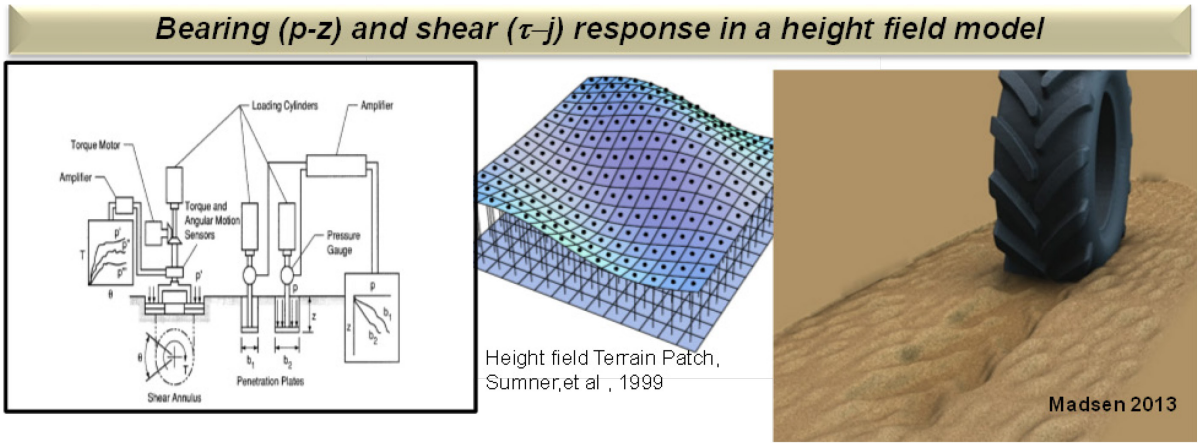


Figure 4-4: The Classic Bekker-Wong-Janosi (BWJ) Terramechanics Models (e.g., Pressure-Sinkage (p-z), Shear Stress-Shear Displacement (τ-j)). Note: Along with associated bevameter [3] experimental methods, these are the most widely developed model suites that improve upon the Cone Index approach and are ready for immediate application in NG-NRMM when implemented in the context of a terrain height field model [10], [11], [12], [13], [14].

All of the analytical methods that apply **p-z** and **τ-j** equations are based on integrations of the normal and shear stress distributions over the geometric soil-running gear contact areas. These methods are ubiquitous in multibody vehicle dynamics with off-road terramechanics models.

The fundamental assumptions and limitations of Simple Terramechanics experimental methods and their associated analytical constructs are:

1) Bevameter platens and shear rings are good stress state surrogates for the vehicle tires and tracks (bevameter method only).
2) In-situ bevameter measurements are geospatial point estimates that are very sensitive to soil substrate heterogeneities such as rocks and roots.
3) The soil is unconfined, homogeneous and deep enough to be unaffected by boundary effects.
4) Coupling between the bearing and traction strength components is either negligible, or explicitly accounted for using a slip-sinkage model [12].
5) Vertical height field discretization models can be used to account for plastic deformation and flow.
6) They are not true continuum models and do not scale down to smaller terrain profile geometric features below the geometric scale of the platen or characteristic wheel footprint length [15].
7) Due to effects of gravity on soil strength and increased coupling of shear and bearing capacity, accuracy progressively degrades with increasing slope [16].

4.3.1 Vehicle-as-a-Sensor

Experimental methods based on wheel load sensing technology have been proposed and implemented that reduce the experimental measurement effort and geometric similarity gap of the standard bevameter [16], [17]. They directly measure load and wheel center in-soil deflection **Δ** for a given terrain condition. As shown in Figure 4-5, the

empirical **F-Δ** relationship (normal force versus normal wheel center displacement) is then derived from known tire force-deflection relationships (**F-δ)** by decoupling the curve to identify only the soil force-sinkage curve (**F-z**) and finally the soil pressure-sinkage curve (**p-z**). Using tire contact patch models, these relationships are directly used in the vehicle dynamic model. The model must have a separate tire ring body defined to enable tire and soil deflection decoupling. The traction relationship (thrust vs. wheel slip) is also directly measured and ported to the vehicle model. Shown in Figure 4-5, the proposed method is called a "running gear level" terrimechanics model [16], [17].

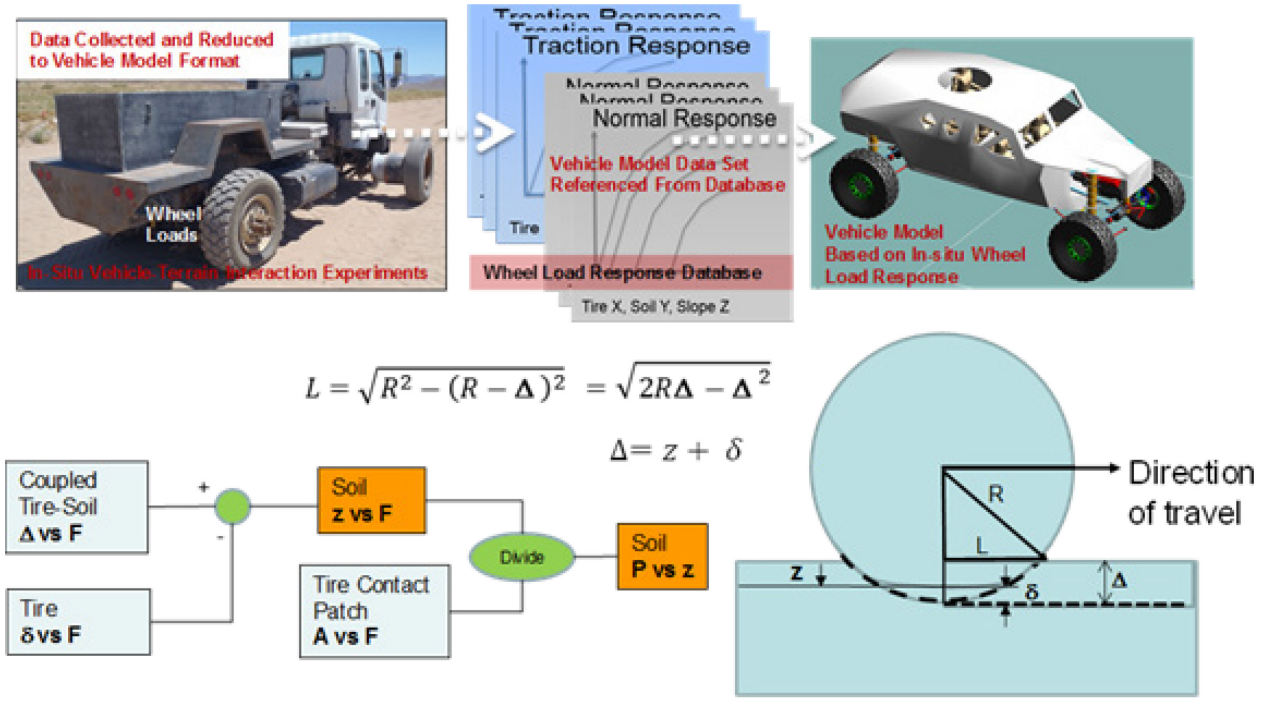


Figure 4-5: "Running Gear Level" Terramechanics Model. The advent of low cost onboard sensor suites such as 6-DOF wheel load sensors has been proposed as the basis for empirical on-vehicle real-time collection and characterization of bearing load and traction load responses to terrain that takes advantage of superior repeatability, automated data collection, data reduction, and database development to build running gear level models of terramechanical response based on lookup tables directly from the response measurement database [16], [17].

The running gear level models and methods of parameter identification are derived from observations indicating that the most accurate method for modeling the strength of terrain in response to vehicle forces is to measure the loading of a vehicle of similar nominal ground pressure. For example, surrogate or scout vehicles can be helpful for predicting vehicle performance of even much larger vehicles, if they have similar ground pressures [16]. While onboard sensors to measure wheel loads for traction and resistance are the most obvious approach [16], [17], vehicle sensors have been also used as indicators of weather or road conditions [18], for classifying terrain types for planetary rovers [15], [19], and recently, cameras and digital image correlation have been used for rut depth, tire slip and profiling [20], [21], [22], [23] in all types of terrain [24].

Using rut depth and motion resistance on-vehicle sensors, there is an untapped and unique opportunity to develop an alternative to the bevameter for soil characterization support of Simple Terramechanics models. This opportunity derives from the fact that vehicle running gear bearing strength obeys

a mathematical form described by the Bernstein power law. First, notice that these can be used to derive a simple approach to a bearing strength model parameter identification, provided that measurements of rolling resistance, $\mathbf{R_C}$ and rut depth, $\mathbf{z_s}$, can be made by the vehicle's onboard sensors, or other means.

By integrating the bearing force through the process of compaction to the equilibrium sinkage, a direct equation for the compaction work done can be derived:

$$Compaction\ Rolling\ Resistance\ Work = R_C l = \mu_{soil} W l = \int_0^{z_s} 2blkz^n dz = 2blk\left[\frac{z_s^{n+1}}{n+1}\right] \tag{4-8}$$

If the work due to vehicle powertrain and running gear internal resistance is known and all other soil related losses such as bulldozing can be assumed negligible, this equation can be combined with the original pressure-sinkage relationship applied to all vehicle wheels for the gross weight of the vehicle:

$$W = 2NbLkz^n \tag{4-9}$$

where **N** is the number of axles, **b** is running gear width and **L** is the contact patch length over which the compaction occurs. Substitution of this equation into the work equations yields an equation for the soil compaction work motion resistance coefficient:

$$\mu_{soil} = \left[\frac{z_s}{NL(n+1)}\right] \tag{4-10}$$

Solving for the bearing strength exponent, **n**:

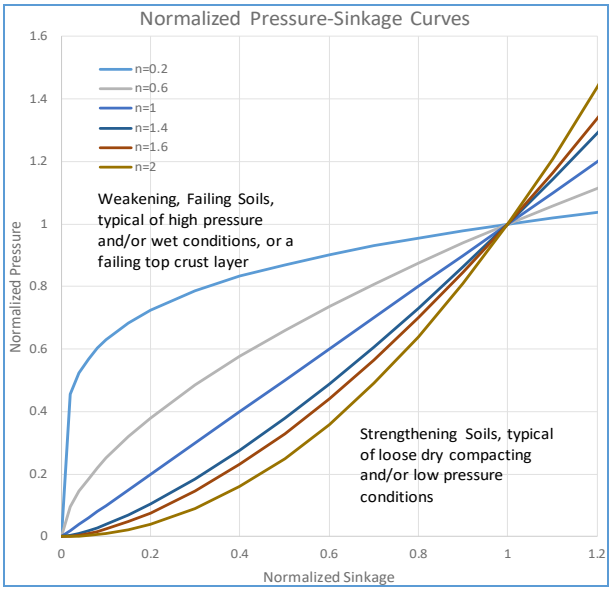
$$n = \left[\frac{z_s}{NL\mu_{soil}}\right] - 1 \tag{4-11}$$

A coast down experiment on any soil of interest can be used to determine μ_{soil}:

$$\mu_{soil} = \left(\frac{V^2}{2gd} - \mu_{vehicle}\right) \tag{4-12}$$

where **V** is the initial velocity, **d** is the coast down distance, **g** is gravitational constant and $\mu_{vehicle}$ is the vehicle powertrain internal rolling resistance, determined by coast down experiments on pavement. It should also be noted that load sensors on the front axle wheels could be used to directly measure the resistance load and the equations adjusted for a single axle load. In this latter mode of operation, the vehicle could stream soil parameters continuously to a live route database. In either mode, the **p-z** equation parameters become averages over a large path length rather than single geospatial point estimates.

The soil work is the integral under the pressure load (assuming constant area) curves shown in the left plot of Figure 4-6. Consistent with intuition, values of $n > 1$ are typical of loose dry soils undergoing compaction, and "$n < 1$" soils are descriptive of soils that have reached compaction limits and are failing due to internal shearing in their far field. It should be noted that a thin hard top crust will also behave like a "$n < 1$" soil, but then subsequently under further sinkage, transition to a "$n > 1$" behavior as the deeper lower layer is loose and not compacted (see Figure 4-7).



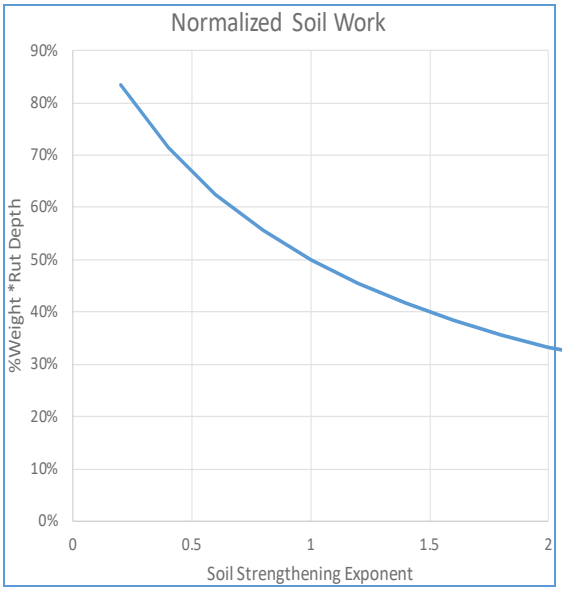


Figure 4-6: Pressure-Sinkage and Soil Work Curves, Normalized to Equilibrium Wheel Load and Rut Depth. These show how the exponent n can have a qualitative correlation to soil natural density and moisture content states. The conclusions are an aggregation of qualitative descriptions accompanying the actual bevameter data published in various sources [3], [4], [12], [25].

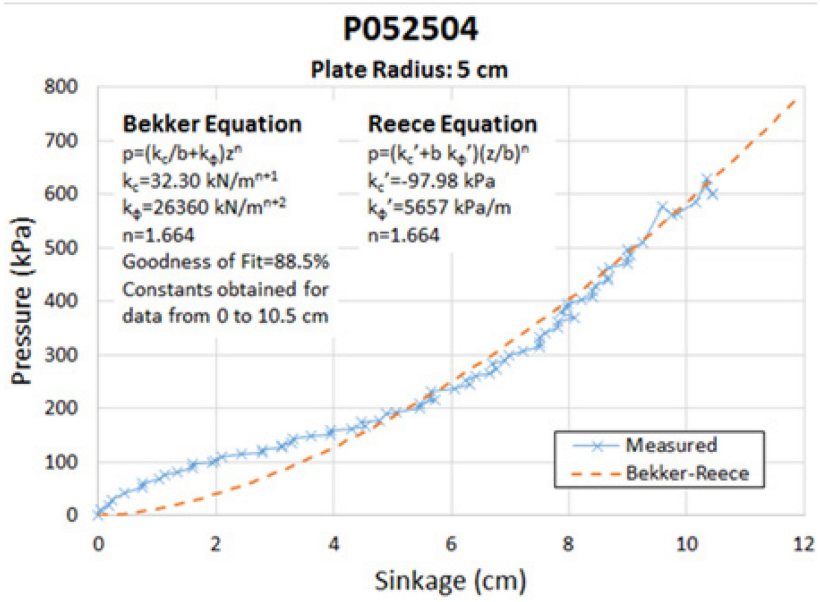


Figure 4-7: Pressure-Sinkage Data from a Soil with an Apparently Weak Top Layer and Loose Deep Second Layer [25].

Next, having determined the bearing strength exponent, **n**, the bearing strength coefficient **k**, can be determined using the rut depth, z_s, the nominal wheel load, and Bernstein's equation, multiplied by the contact patch area.

Note that the assumption that bulldozing is negligible is a progressively invalid assumption with higher sinkage. However, the assumption does capture the first order primary source of rolling resistance and the method described here can be extended to include bulldozing losses provided that those losses are described analytically as a function of sinkage.

The second useful implication that can be derived from observations of the parametric behavior of the Bernstein power law as it applies to particular soil types and states is illustrated in Figure 4-6 (plot on right), where typical exponent values associated with their soil strength trends are shown. Note that soil work gets smaller for larger values of **n**. This is typical of a loose dry soil that strengthens progressively with higher bearing loads, primarily due to compaction.

However, as ***n*** gets smaller, it becomes more characteristic of a weaker soil, or weak crust layer, for which the bearing strength is almost asymptotically limited. These observations are consistent with the equations describing soil motion resistance due to compaction, which is only dependent upon the strength exponent, **n**, the rut depth, $\mathbf{z_s}$, and the characteristic contact patch length, **L**.

Given the correlations between exponent **n** and soil states shown in Figure 4-6, to be conservative for motion resistance estimates, it is best to underestimate **n**. Thus, given the dependence upon contact patch length, **L**, it is therefore important that this parameter be conservatively estimated so that **n** is not overestimated. As previously shown in Figure 4-5, a conservative estimate for **L** based on wheel radius and sinkage is:

$$L = \sqrt{R^2 - (R - z)^2} = \sqrt{2Rz - z^2} \tag{4-13}$$

For tracked vehicles, track pad length is usually not a good nominal estimate for **L** for increasing rut depths, so the method of Figure 4-5 is suggested where the road wheel radius augmented by the track thickness, is a simple effective compaction radius.

The importance of properly computing the compaction exponent, n, leads to important observations and guidance when interpreting and reducing bevameter pressure-sinkage data. When the pressure-sinkage response has the "snaking" behavior shown in Figure 4-7, it becomes clear that there are at least two load regimes that will lead to very different values for the exponent, **n**. The initial portion of the curve seems to represent a brittle crust layer with crushing stress ~ 100 KPa and $\mathbf{n} < 1$. For higher pressures, the soil exhibits "$\mathbf{n} > 1$ behavior" typical of a compacting loose soil. Thus, Simple Terramechanics **p-z** relationships cannot be extrapolated to pressure loading regimes beyond the range for which the model parameters were computed. And, maximal pressures should be used in bevameter experiments that closely match the model applications. If maximal bevameter pressures match the maximal vehicle running gear nominal pressures and the data exhibit transitions such as that shown in Figure 4-7 the lower pressure-sinkage magnitude regime is ignored because it is least important for parameter identification. Models that separately account for multiple layers have not been developed so the single most influential layer must be used. However, second layer effects are an open area of research and development and the NG-NRMM standard terrain file format has established place-holders to account for parameters describing a second layer.

4.3.2 Database Development

A key initiative of AVT-248 to enable the success of the NG-NRMM is the development of a database of ST soil parameter data sets for as many representative soils and moisture content states as possible. The ST database of model parameter data sets has been established from a collection of known sources [3], [4], [6], [8], [26]. Initially this database will be realized as an Excel spreadsheet and assigned as Attachment 4 of

the STANREC [27].

Going forward, development and expanded collection of these ST parameter data sets will be essential to the success of the ST models for predicting operational speeds, mobility limit analysis (GO/NOGO) as well as performance for specific mobility events used in acquisition processes.

A common minimal set of soil properties have been defined as part of the standard GIS-based terrain file format. Place holder data fields for these have been defined in the NG-NRMM GIS terrain file. Methods to derive or infer additional data will have to be developed to meet the needs for current Simple Terramechanics models and the ST database fulfills this requirement without burdening the GIS terrain files.

However, for any soil and moisture content, there are unique derived or inferred data requirements for the ST models and it is the purpose of the ST database to provide the best known estimates. And, as noted in the discussion of the pressure-sinkage data in Figure 4-7, most data and research to date focus on homogeneous, deep, single-layer soil response characterization even though two-layer effects are frequently encountered. Second layer data characterization is an open research and development topic. Second layer data place-holders foresee the eventual development and availability of data and models that address layers of significantly different strengths, where both are influential on mobility.

The following are a list of essential measurements required for a unique entry in the ST database:

$\mathbf{p_{max}}$ applicable max pressure range;

$\mathbf{R_{elax}}$ 2-second normal stress relaxation of bevameter platen at $\mathbf{p_{max}}$ (%);

MC applicable moisture content (dry weight basis);

$\mathbf{K_{USCS}}$ soil type;

γ_s specific gravity of solids;

$\mathbf{G_s}$ maximum dry (or wet) density (must specify) [also known as max bulk density];

$\mathbf{D_r}$ relative density of natural in-situ sample [or natural bulk density];

c surface layer cohesion;

ϕ surface layer internal friction angle;

k surface layer shear strength modulus;

n bearing strength exponent;

$\mathbf{k_\phi}$ bearing strength frictional constant;

$\mathbf{k_c}$ bearing strength cohesive constant;

$\mathbf{K_0}$ bearing elastic reload stiffness;

$\mathbf{A_u}$ bearing elastic progressive stiffening;

$\mathbf{k_{\phi 2}}$ 2nd layer frictional bearing strength;

$\mathbf{k_{c2}}$ 2nd layer cohesive bearing strength;

$\mathbf{n_2}$ 2nd layer bearing strength exponent;

$\mathbf{K_{02}}$ bearing elastic reload stiffness;

$\mathbf{A_{u2}}$ bearing elastic progressive stiffening; and

$\mathbf{p_{max2}}$ applicable max pressure range.

These data will populate a specific Simple Terramechanics database separate from standard terrain files coming from GIS. At the higher level, the NG-NRMM STANREC will require expandable open interfaces to permit additional GIS interoperable data fields to account for future development.

These key input/output relationships and parameters have been defined to help drive the software interface and database requirements, as well as future development opportunities in terrain strength characterization from GIS-based data. Fundamental to this effort are the several competing methods whereby the Simple Terramechanics model parameters (or the running gear model databases) are to be inferred, derived or developed from the available GIS remotely sensed data, or other augmenting GIS data. In addition to the vehicle-as-a-sensor efforts already described, these methods include large-scale cooperative efforts to collect broad spectrum field test traditional single point bevameter data [25], as well as analytical methods leveraging Complex Terramechanics models and their relationships to GIS-mapped soil types and moisture contents. As was depicted in the dashed boxes connecting the Complex and Simple Terramechanics approaches shown in Figure 4-2, the latter include the development of fundamental soil strength numerical models (e.g., Finite or Discrete Element Models (FEM/DEM)), that can successfully predict running gear, bevameter and shear ring response across the necessary spectrum of soils and environmental conditions [28], [29], [30], [31].

4.4 PROTOTYPE DEMONSTRATION

The tracked and wheeled vehicle benchmarks described in detail in Chapter 8 provide explicit examples of results from several M&S software developers relative to the important mobility metrics that are affected by ST. All of the results, except one, were generated using ST models. While the purpose of these benchmarks was not the end-to-end GIS interfaces, they do provide a thorough demonstration of the application of ST as the current state-of-the-art for 3D multibody dynamics applications to the detailed off-road mobility metrics that were enumerated in Table 4-1.

However, at the higher level of aggregation, demonstrations of GIS end-to-end simulations based on embedded ST models have been accomplished and/or planned by the following groups that are members of AVT-248. The first group conducted a ST prototype demonstration of a vehicle in the Monterey Bay area as described in Chapter 3.

4.4.1 University of Wisconsin-Madison (UW-M)

UW-M (AVT-248 Members Radu Serban and Dan Negrut) has developed significant vehicle dynamic modeling capabilities using the open source multibody dynamics code found in the Chrono suite of tools [32], [33], which provides extensive support for both simple and Complex Terramechanics. For the former, they have implemented vehicle-terrain interaction using the Soil Contact Model (SCM) [34]. The version of SCM implemented in Chrono includes several enhancements for generality, flexibility, and efficiency. In particular, it can work with an arbitrary terrain triangular mesh representation with an option for adaptive mesh refinement around contact patches (as depicted in Figure 4-8). For computational efficiency considerations, the Chrono SCM implementation also provides an option for a moving patch approach suitable for simulations on very large

terrain domains. Finally, for generality, the parameter "b" in the Bekker formula is calculated automatically for any arbitrary object interacting with the SCM terrain patch by monitoring each individual contact patch and computing its perimeter and area.

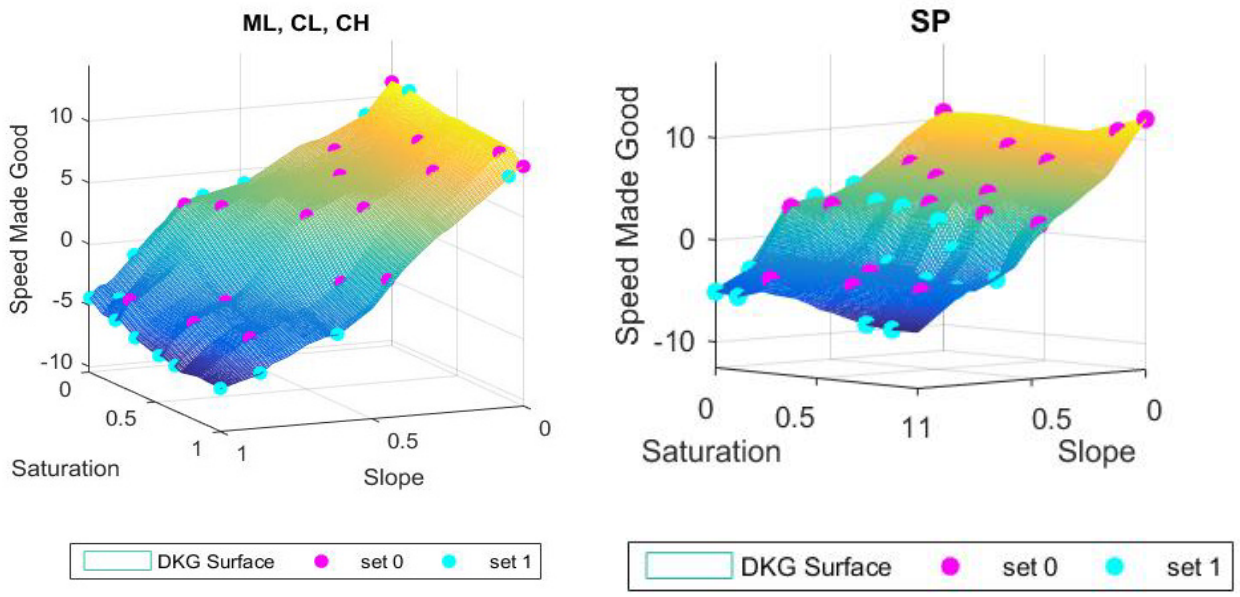


Figure 4-8: Two Examples of the Slope Climbing Speed Performance vs Moisture Content Response – Surface Surrogate Models for Two USCS unique BWJ model soil parameter data sets from the notional data in Table 4-2 (Slope Scale: 1 = 40% Slope).

Note: Sequential DOE simulation run sets (Set 0, Set 1) using normalized slope and saturation level were used to progressively converge to these results.

The Chrono::Vehicle generic modeling capability was used to develop NG-NRMM event level results for both the Tracked Vehicle (TV) and Wheeled Vehicle Prototype (WVP) benchmarks described in Chapter 8. To develop a GIS end-to-end prototype, the TA1 standard Monterey dataset was assumed along with a notional Bekker-Wong-Janosi (BWJ) model parameterization spanning the USCS soil types and Moisture Content (MC) ranging from dry (MC = 0) to saturation (MC = 1.0). The UW-M team used the Tracked Vehicle (TV) benchmark model (see Figure 4-9, Chapter 8 and Attachment 5 of the STANREC [27]) to compute grade climbing performance up to 40 degrees across the full soil type and moisture content BWJ model parameter space as shown in Table 4-2.

The approach took advantage of sequential Design of Experiment (DOE) series of simulations to construct a surrogate model. This was necessary due to the large number of simulations required to span this parameter space as well as the desire to perform an Uncertainty Quantification (UQ) prototype demonstration. A separate surrogate model of slope climbing performance vs slope and MC was developed for each of nine different soil parameter data sets describing a nominal USCS soil type. The USCS soil types were identified as a typical set for which SURGO data were available from public domain sources.

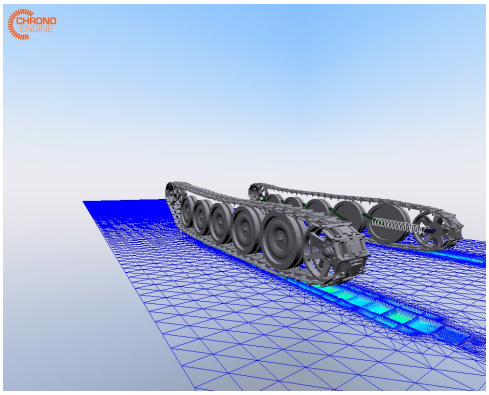


Figure 4-9: UW-M Utilized their Tracked Vehicle (TV) Benchmark Model to Generate a Prototype NG-NRMM Speed-Made-Good Map on the Monterey Terrain Data Set Based on Grade Climbing Performance.

Table 4-2: Notional Simple Terramechanics (ST) Model Parameters Assumed for the UW-M Prototype Demonstration of Speed-Made-Good Slope Climbing Performance on the Monterey GIS Data Set.

		From Karafiath[34] Eq1.2.7 and table 1.13		Bearing (Bekker-Wong)					Shear (Janosi - ductile)			
USCS		Moisture Content (dry weight basis)	Saturation Level	n	Kf	Kc	k0	Aunload	c (kPa)	ϕ (deg)	k (cm)	
Grain Size Rank	Type	Raw MC (%)										Database Ref
1	GW	0	Dry (0)	1.00	10000	100	0	2012000	1	40.0	0.50	
		17%	Saturated (1)	1.00	10000	100	0	2012000	1	40.0	0.50	
2	GW-GM	0	Dry (0)	1.00	10000	100	0	1006000	1	40.0	0.50	
		17%	Saturated (1)	1.00	10000	100	0	1006000	1	40.0	0.50	
3	GM	0	Dry (0)	1.00	10000	100	0	1006000	1	40.0	0.50	
		10%	Saturated (1)	1.00	10000	100	0	1006000	1	40.0	0.50	
4	GC-GM	0	Dry (0)	1.00	10000	100	0	1006000	1	40.0	0.50	
		14%	Saturated (1)	1.00	10000	100	0	1006000	10	40.0	0.10	
5	GC	0	Dry (0)	1.00	10000	100	0	1006000	1	40.0	0.50	
		14%	Saturated (1)	1.00	10000	100	0	1006000	20	40.0	0.05	
6	SP	0	Dry (0)	0.79	5301	102	0	503000	1	31.6	1.60	1
		27%	Saturated (1)	0.20	2000	200	0	503000	7	18.0	0.20	
7	SM	0	Dry (0)	0.79	5301	102	0	503000	1	31.6	1.60	1
		36%	Saturated (1)	0.20	2000	200	0	503000	7	18.0	0.10	
8	SC-SM	0	Dry (0)	0.79	5301	102	0	503000	1	31.6	1.60	1
		22%	Saturated (1)	0.20	2000	200	0	503000	7	18.0	0.05	
9	SC	0	Dry (0)	0.79	5301	102	0	503000	1	31.6	1.60	1
		22%	Saturated (1)	0.20	2000	200	0	503000	20	18.0	0.05	
10	ML	0	Dry (0)	0.70	10000	1	0	503000	2	34.0	1.60	13-16
		46%	Saturated (1)	0.13	100	13	0	503000	35	10.0	0.05	
11	CL-ML	0	Dry (0)	0.70	10000	1	0	503000	2	34.0	1.60	13-16
		25%	Saturated (1)	0.13	100	13	0	503000	35	10.0	0.05	
12	CL	0	Dry (0)	0.70	10000	1	0	503000	2	34.0	1.60	13-16
		25%	Saturated (1)	0.13	100	13	0	503000	35	10.0	0.05	
13	MH	0	Dry (0)	0.70	2000	120	0	503000	2	30.0	1.60	17,18
		79%	Saturated (1)	0.15	25	2	0	503000	35	11.0	0.05	
14	CH	0	Dry (0)	0.70	10000	1	0	503000	2	34.0	1.60	13-16
		53%	Saturated (1)	0.13	100	13	0	503000	35	10.0	0.05	
15	PT	100%	Saturated	0	424			50300 *	5	37.7	3.29	2

Figure 4-10 shows the slope climbing speed performance response surface surrogate models for two unique soil parameter sets. Based on these DOE-based surrogate models, the GIS-mapped Speed-Made-Good performance results over the millions of Monterey terrain units were generated and mapped as shown in Figure 4-11. The UQ results for this demonstration are provided in Chapter 6.

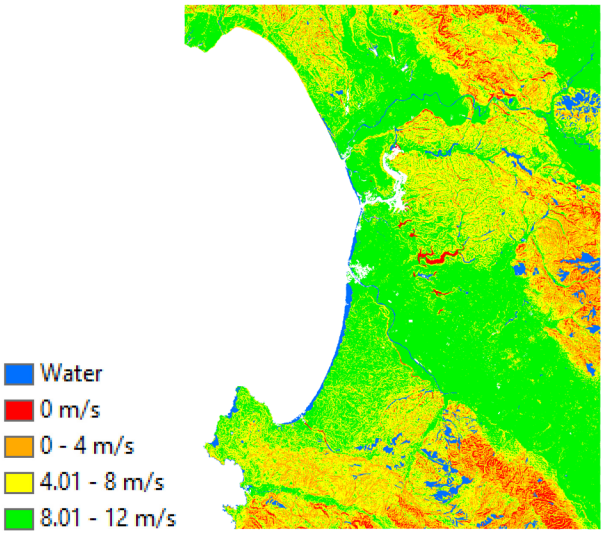


Figure 4-10: UW-M Simple Terramechanics Modeling Prototype NG-NRMM Speed-Made-Good Performance Results Over the Monterey Terrain.

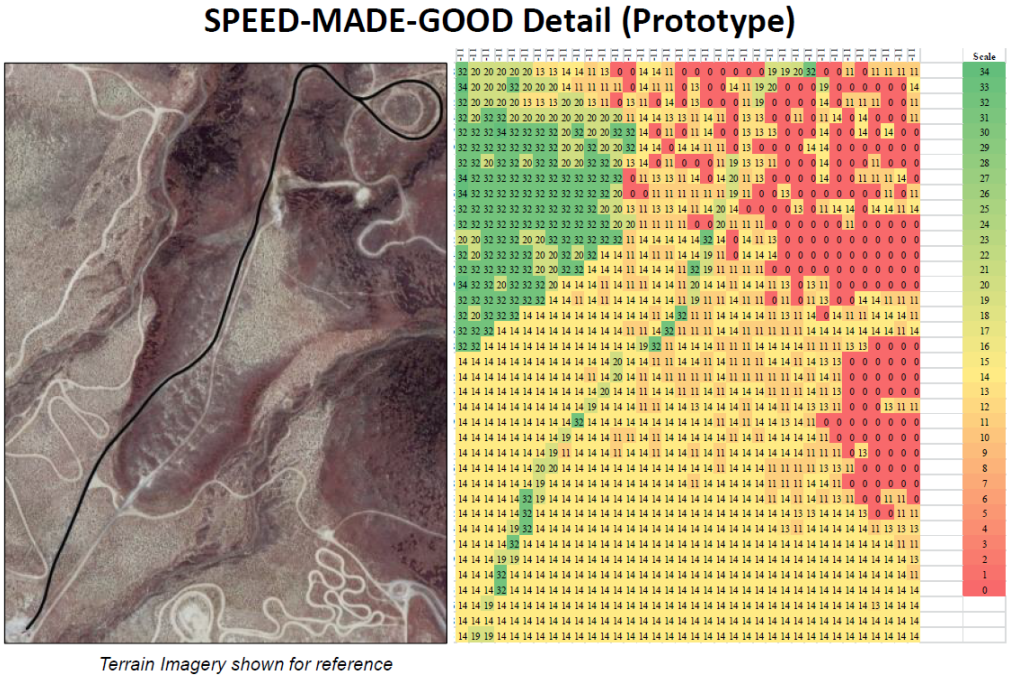


Figure 4-11: Sample Results of the NATC NG-NRMM Prototype Modeling Effort Utilizing Running Gear Level Simple Terramechanics Methods in their Vehicle Models.

4.4.2 Nevada Automotive Test Center (NATC)

Over the past two decades, NATC (AVT-248 Member Henry Hodges) has engaged in several different efforts that comprise most of the essential elements required for a GIS-based end-to-end demonstration of a NG-NRMM capability. Pulling results from all of these separate efforts together, Figure 4-1 showed NATC's overall approach. For Terramechanics, NATC has been a strong proponent of the vehicle-as-a-sensor approach and has described, at a general level in Figure 4-5 their approach toward measurement and identification of Bernstein power law parameters and the Janosi traction-slip equation parameters as applied to a single wheel in dry sand. This soil covers a broad area of the terrain at their test center. Additionally, they have constructed a NG-NRMM operational module that does the aggregated mobility predictions. They also conducted high resolution terrain elevation mapping, as well as detailed local roughness measurements. These support the end-to-end GIS-based demonstration as well as the Wheeled Vehicle Prototype (WVP) benchmark defined in the STANREC, Attachment 6 [27]. Presentations of their terramechanics modeling approach and the results were presented at the two AVT-248 meetings [2], [35], and also at a meeting held at the NATC facility that included actual ride-along vehicle demonstrations and experimental methods used in the derivation of the Simple Terramechanics model WVP Verification and Validation benchmark [36]. Figure 4-1 and Figure 4-5 above summarize the modeling methods while Figure 4-11 provides an example of mapped Speed-Made-Good results on a representative terrain. More detailed WVP benchmark and model descriptions are found in Chapter 8 and STANREC, Attachment 6 [27].

4.4.3 Jet Propulsion Laboratory (JPL)

JPL's Rover Analysis, Modeling and Simulation (ROAMS) ground vehicle simulator [37] used for TA4 Intelligent Vehicle prototype development includes Simple Terramechanics models and is another example of the current state-of-the-art for mobility simulations wherein soft soil models are used to describe a non-linear elastic surface medium with rigid wheels (see Chapter 7) and tire models for mobility on paved roads. Extensions for tracking of plastic (permanent) deformation of the soil media are planned for the future. ROAMS uses a minimal coordinates recursive dynamics formulation for fast computational performance needed for closed-loop real-time simulations. ROAMS includes special modules for handling GIS and large terrain datasets, and for hi-res visualizations. ROAMS is also actively used for autonomy in the loop (with cameras, etc. sensors) simulations. The TA4 prototype demonstration results show the successful integration of the GIS data sources using the GeoTIFF file format for input and output. See Chapter 7 for example applications and visualizations.

4.4.4 Vehicle Systems Development Corporation (VSDC), National Research Council (NRC) Canada

VSDC and NRC Canada (AVT-248 Member Jon Preston-Thomas) are developing a Supplementary Module for the Nepean Wheeled Vehicle Performance Model (NWVPM), a Simple Terramechanics software package developed by Wong [8], [26] to model the interaction of wheeled vehicles on soft soil. The new Supplementary Module will adapt NWVPM to provide predictions of wheeled vehicle performance on deformable terrain in place of the existing NRMM module. This includes adding powertrain capabilities and calculating the Speed-Made-Good due to deformability of the terrain. The Supplementary Module will provide the Speed-Made-Good due to operation on deformable terrain directly to the GIS database, as part of a complete end-to-end mobility prediction. The capabilities of the Supplementary Module may be extended to include the prediction of vehicle operating fuel economy and other performance metrics, if needed. The methodology will be applicable to the Nepean Tracked Vehicle Performance Model (NTVPM), a Simple Terramechanics software package also developed by Wong [8], [26] to model the interaction of tracked vehicles on deformable terrain, thus extending its capabilities in the same way. The development of the Supplementary Module for

NWVPM and NTVPM is currently in its initial stage, and no results on its applications to predicting vehicle Speed-Made-Good or operating fuel economy have been obtained so far [38].

4.4.5 South African Council for Scientific and Industrial Research (CSIR)

South Africa CSIR (AVT-248 Member David Reinecke) have a capability that includes experimental equipment and Mobility Modeling and Simulation Software (MOBSIM) with plans of developing an end-to-end modeling demonstration as well as V&V benchmark predictions from their test capabilities. No results have been developed so far [39].

4.4.6 Germany

Terramechanics and tire measurements progress including new bevameter plans were shared by AVT-248 Member Tom von Sturm zu Vehlingen [40]. Much of the German modeling capabilities are based on ST models and have been documented in Ref. [12]. GIS-based applications, interfaces and issues are being addressed most recently by AVT-248 Member Petra Zieger [41].

4.5 STANREC

NG-NRMM must utilize vehicle-terrain interaction models, also known as terramechanics models that are geometrically and mechanically consistent with their end-use application and are theoretically extensible across a range of vehicle and terrain environment scales and morphologies. NG-NRMM Terramechanics models must include the soil elasto-plastic response to bearing and tractive repetitive loads using models that can be correlated to available in-situ geospatially mapped and remotely sensed soil characteristics. Soil properties for each unique soil type that should be collected in a complete characterization suite to include:

1) USCS or other soil type (ASTM D2487 and ASTM C 136 sieve testing).
2) Moisture Content (MC) by weight (measured by ASTM D4643).
3) Sample as-tested total (wet) bulk density (or dry density with MC, sand cone (ASTM D1556-07), drive cylinder (ASTM D2937-17e1), or nuclear densometer (ASTM D6938)).
4) Maximum total bulk density (derived from a Standard Proctor compaction test, ASTM D698).
5) Liquid and Plastic limits (ASTM D422) for plastic soils.
6) Saturation Test for non-plastic soils.
7) Specific Gravity test.
8) Soil strengths expressed as cohesion and internal friction angle using triaxial shear testing (consolidated drained ASTM D7181-11 for sand and ASTM D4767-11 for consolidated undrained triaxial compression test for cohesive soils.) for the dilatancy (volumetric) response and deviatoric (shear) response Mohr-Coulomb failure theory parameters at 4 moisture levels:
    a) Near dry [~half of Proctor Optimal MC (POMC)];
    b) At POMC;
    c) At 0.95 times Liquid Limit (LL), or saturation at field density (SatMC) for non-plastic soils;
    d) 0.5*(LL + POMC) for plastic soils; or
    e) 0.5*(SatMC + POMC) for non-plastic soils.

9) Top two strength determining layer depths.
10) Temperature of layers.
11) Cone Index at the 0 – 6 ” and 6 – 12 ” layer depths.
12) Land Use (MGCP land cover descriptors).
13) Rock and vegetative/organic material (i.e., roots, grass mats, etc) content.
14) Confining and drainage conditions.

Other effects which the terramechanics model must address are:

1) Hard surface and urban terrains and obstacles;
2) Heterogeneous (multi-component, such as rocks, roots, etc) soil;
3) Multilayered soil;
4) Snow and ice;
5) Bodies of water and water covered terrains;
6) Vegetation covered terrains; and
7) Complex terrain topography.

4.5.1 Simple Terramechanics for Soft Soil

NG-NRMM Simple Terramechanics (ST) models are those that depend upon complementary calibrating experimental methods that are geometrically similar and physically analogous to vehicle running gear interaction with soft soil terrain. The nominal approach utilizes a bearing load or stress response model consisting of at least two parameters and a separate complementary tractive load or stress response model that includes dependence on bearing stress, soil cohesion (or adhesion), and running gear slip.

1) The nominal ST analytical model must predict both bearing and tractive performance of vehicles on deformable terrain:
   a) Elasto-plastic repetitive load response model tracks permanent soil substrate normal and tractive/shear deformations via some means such as a height field model.
   b) Height field model: a discretized terrain model that tracks deformation by using a vertical height and/or shear-slip dynamic state variables at each discrete terrain point or cell.
2) For hard surfaces and hard off-road terrain where terrain-vehicle response is dominated by the vehicle running gear, no terrain discretization and permanent terrain deformation tracking is required, but surface-specific traction response characteristics (friction ellipse, friction vs slip curve) must be provided.
3) The complementary experimental method must have demonstrated repeatability with associated statistical uncertainty characteristics to support probabilistic M&S.
4) An evolving database of ST modeling parameters is provided in Attachment 4 of the STANREC [27] for NG-NRMM with soft soil modeling parameters supporting:
   a) Pressure-sinkage relationships consisting of at least two scaling parameters and a power law exponent as well as at least two parameters describing and characterizing the repetitive

load-deformation characteristics such as a linear stiffness and stiffness progression parameter, plus the applicable maximum bearing pressure loading in the data set from which the model parameters are derived [3], [4], [5], [6].

b) Shear-slip relationships characterizing the interface between the soil and the vehicle running gear (e.g., wheel, tire, track pad, rubber, etc.) consisting of a cohesion (or adhesion constant), friction angle, and at least two exponential shear-slip law parameters, plus the applicable maximum bearing pressure loading in the data set from which the model parameters are derived [7], [16].

c) Shear-slip relationships characterizing the soil substrate internal failure limits characterized with a Coulomb-Mohr criteria, i.e., a soil cohesion parameter and a soil friction angle, and at least two exponential shear-slip law moduli parameters plus the applicable maximum bearing pressure loading in the data set from which the model parameters are derived [7], [16].

d) Customizable expansion to be inclusive of multiple soil layer characterization and also any unknown future model innovation and development such as slip-sinkage model parameters.

5) When a bevameter process is being planned for use to acquire ST soil response data:

a) The suite of geotechnical soil properties listed in paragraph 4.5 shall also be measured to characterize the soil.

b) For pressure-sinkage bearing capacity there should be a minimum of two different platen sizes with areas that differ by a factor of two such that they allow for peak pressures equal to the maximum vehicle localized running gear element (wheel, track pad) static ground pressure, and another at twice that value.

c) The rate of application of the pressure load shall be documented as well as the pressure relaxation or sinkage creep at the maximum pressure level.

d) Pressure-sinkage power law parameters shall be developed using the weighted least squares data fitting methods. An example is described in Ref. [42].

e) For shear ring measurements to get running gear to soil interface friction angle, cohesion/adhesion, and initial load development exponential parameters:

i) At least three normal loads shall be used including the nominal local running gear (wheel or track pad) static bearing load, plus two more: one at 50% of nominal bearing load and a second at 150% of nominal bearing load.

ii) The exponential shear development shape function parameters shall be based on this shear ring data using least squares fitting as described in Ref. [43].

6) When a wheel load sensor test vehicle is being planned for use to acquire running gear level ST soil response data [16]:

a) The suite of geotechnical soil properties listed in paragraph 4.5 shall also be measured to characterize the soil.

b) Vehicle primary physical characteristics shall be reported.

c) Instrumentation shall be fully described for both bearing/normal load response as well as traction/shear response.

d) Pavement tests shall be performed to demonstrate sensor calibration.

e) Tire-soil response decoupling methods or assumptions shall be fully described.

f) Correlation of single wheel response to full-vehicle response shall be developed when possible.

g) Data should be collected for at least three different normal bearing loads.

7) When ST models are developed by inference from ST running gear data or from closed form soil mechanics footing bearing equations and/or other fundamental geotechnical tests and properties [44]:

a) The suite of geotechnical soil properties listed in paragraph 4.5 shall also be measured (or developed from references) to the greatest extent possible to characterize the soil.

b) Analytical assumptions and background theory shall be cited for each bounding property or characteristic.

c) Numerical assumptions and background theory shall be cited for all interpolations and extrapolations.

d) A notional model for inferring ST parameters for any soil type and moisture content using linear interpolation of consistent, but notional, ST parameter sets for a range of soil types and moisture content values is provided as an example of the eventual goal of the ST database development. See Attachment 4 of the STANREC [27].

8) To facilitate the transition from past measurements of mobility, whenever possible, NG-NRMM predictions of GO/NOGO soft soil performance should be compared to predictions using legacy metrics of performance such as Vehicle Cone Index (VCI) or Mean Maximum Pressure (MMP) [45].

The reader is also referred to Annex F on the Measurement and Analysis of Geotechnical Properties.

4.6 GAPS AND PATH FORWARD

To complete the inauguration of Simple Terramechanics models as the default method of computing GO/NOGO and Speed-Made-Good mobility predictions in NG-NRMM models and simulations, a more complete database of model parameters is needed covering the range of soils and moisture contents for soils that are relevant to operational and acquisition analysis needs. This challenge can be readily met through a strong commitment from the NATO countries to this common approach and a sharing of available data. Additionally, the vehicle-as-a-sensor approach provides a means by which relevant data sets can be quickly collected and compiled.

Additional challenges that should be addressed are as follows:

1) Specific V&V efforts for whole-vehicle predictions for more rigorous benchmarks;

2) A long-term configuration management approach to the database;

3) A long-term configuration management approach to the STANREC;

4) Advancement of the vehicle-as-a-sensor method;

5) M&S methods addressing the slope limitations;

6) M&S and parameter ID methods addressing slip-sinkage;

7) M&S methods addressing longitudinal bulldozing;
8) M&S methods addressing lateral bulldozing;
9) M&S along with experimental methods that address layer effects;
10) M&S along with experimental methods that address load rate effects;
11) Leverage Complex Terramechanics developments to extend the Simple Terramechanics database; and
12) Investigations correlating simpler closed form soil strength metrics, such as Terzaghi and Meyerhof methods [44], to first order vehicle trafficability prediction will facilitate real-time operational assessments of remotely sensed terrain, soil and moisture content data.

4.7 SUMMARY

Terramechanics effects are one of the primary attributes affecting vehicle mobility and have been judged by ATV-248 to be a foundational capability required in both the current NRMM and the NG-NRMM, and therefore one of the primary focus areas of the RTG [1]. TA2 efforts have produced GIS end-to-end demonstration simulations, a draft STANREC covering NG-NRMM Simple Terramechanics, V&V benchmarks and results demonstrating numerous available multibody codes that utilize Simple Terramechanics models, a draft database of model parameters, and described a feasible practical approach to immediately improve upon the legacy Cone Index approach to soft soil modeling for mobility predictions. While there remain limitations and challenges, Simple Terramechanics models provide an immediate improvement upon the Cone Index methods for predicting soft soil impacts upon mobility.

4.8 REFERENCES

[1] Dasch, J. and, Jayakumar, P. (Eds). 2016. Final Report ET-148 Next-Generation NATO Reference Mobility Model (NRMM). NATO-AVT.

[2] Hodges, H. 2017. Simple Terramechanics Running Gear Models. NATO AVT248 Panel Meeting, May 2017, Vilnius, Lithuania.

[3] Bekker, M. G. 1969. Introduction to Terrain-Vehicle Systems. University of Michigan Press, Ann Arbor, MI.

[4] Wong, J.Y., Garber, M. and Preston-Thomas, J. 1984. Theoretical Prediction and Experimental Substantiation of the Ground Pressure Distribution and Tractive Performance of Tracked Vehicles. Proceedings of the Institution of Mechanical Engineers, 198D(15):265-285.

[5] Bernstein, R. 1913. Probleme zur Experimentellen Motorpflugmechanik. Der Motorwagen, Vol 13.

[6] Reece, A.R. 1965. Principles of Soil-Vehicle Mechanics. Proceedings of the Institution of Mechanical Engineers, 180(Part 2A 2):45-47.

[7] Hanamoto, B. and Janosi, Z. 1961. The Analytical Determination of Drawbar Pull as a Function of Slip for Tracked Vehicles in Deformable Soils. Proceedings of the 1st International Conference on Mechanics of Soil-Vehicle Systems, Turin, Italy.

[8] Wong, J.Y. 2010. Terramechanics and Off-Road Vehicle Engineering, 2nd Edition. Elsevier, Oxford, England.

[9] Jayakumar, P., Melanz, D., MacLennan, J., Gorsich, D., Senatore, C. and Iagnemma, K. 2014. Scalability of Classical Terramechanics Models for Lightweight Vehicle Applications Incorporating Stochastic Modeling and Uncertainty Propagation. Journal of Terramechanics 54:37-57.

[10] Sumner, R.W., et al. 1999. Animating Sand, Mud, and Snow. Computer Graphics Forum, 18(1):17-26.

[11] Lamb, D., Reid A., Truong, N. and Wellor, J. 2003. Terrain Validation and Enhancements for a Virtual Proving Ground. Proceedings of the Driving Simulation Conference.

[12] Schmid, I.C. 1995. Interaction of Terrain and Vehicle Results from 10 Years of Research at IKK. Journal of Terramechanics, 2(1):3-26.

[13] Reid, A., et al. 2007. High-Fidelity Ground Platform and Terrain Mechanics Modeling for Military Applications Involving Vehicle Dynamics and Mobility Analysis. Proceedings of the Joint North America, Asia-Pacific ISTVS Conference and Annual Meeting of Japanese Society for Terramechanics, Fairbanks, Alaska, USA.

[14] Madsen, J. 2014. Mobility Prediction of Multibody Vehicle Dynamics Handling Simulations on Deformable Terrain. PhD Thesis, University of Wisconsin.

[15] Richter, L, et al. 2014. Development of the FASTER Wheeled Bevameter. European Planetary Science Congress 2014, EPSC Abstracts, Vol. 9. ID: EPSC2014-818.

[16] Shoop, S. 1993. Terrain Characterization for Trafficability. CRREL Report 93-6, US Army Corps of Engineers Cold Regions Research & Engineering Laboratory.

[17] Hodges, H. 2015. Benchmarking Approaches Presentation for ET-148 Next-Generation NATO Reference Mobility Model. NATO STO Prague Meeting.

[18] Shoop, S. and Coutermarsh, B. 2007. Vehicles as Weather and Road Condition Sensors. International Symposium on Cold Regions Development, Tempere, Finland, September 2007, 117-118.

[19] Iagnemma K., Kang S., Brooks C. and Dubowsky, S. 2003. Multi-Sensor Terrain Estimation for Planetary Rovers. Proceedings of the Seventh International Symposium On Artificial Intelligence. Robotics and Automation in Space, i-SAIRAS.

[20] Botha, T.R. and Els, P.S. 2015. Rough Terrain Profiling Using Digital Image Correlation. Journal of Terramechanics, 59:1-17.

[21] Botha, T.R. and Els, P.S. 2015. Digital Image Correlation Techniques For Measuring Tyre-Road Interface Parameters: Part 1 – Side-slip angle measurement on rough terrain. Journal of Terramechanics, 61:87-100.

[22] Botha, T.R. and Els, P.S. 2015. Digital Image Correlation Techniques for Measuring Tyre-Road Interface Parameters: Part 2 – Longitudinal tyre slip ratio measurement. Journal of Terramechanics, 61:101-112.

[23] Botha, T.R. and Els, P.S. 2015. Rut Measurement Of Soft-Soil Terrain Using Digital Image Correlation. Proceedings 13th European Conference of the ISTVS, Rome, Italy.

[24] Shoop, S., Sopher, A., Stanley, J., Botha, T., Becker, C. and Els, S. 2016. Digital Image Correlation for Off-Road Mobility. GVSETS, Novi, Michigan.

[25] Preston-Thomas, J. 2016. Presentation of Near-Term NextGen NRMM Solution Part II – Addressing the Challenges of Getting Terrain Parameter Data. NATO AVT248 Meeting in Tallin, Estonia.

[26] Wong, J.Y. 2008. Theory of Ground Vehicles, 4th Edition. John Wiley: New Jersey.

[27] AMSP-06, Standardization Recommendation (STANREC) Development for Next-Generation NATO Reference Mobility Models, AMSP-06, version 1, September 2019.

[28] Reeves, T. 2013. Prediction of Discrete Element Parameters for Modeling the Strength of Sandy Soils in Wheel/Soil Traction Applications. PhD Dissertation, Clemson University.

[29] Fleischmann, J. 2016. Determination of Continuum Properties for Geomaterials Using the Discrete Element Method. 1st CFDEM® project user meeting & workshop, Linz, Austria.

[30] Melanz, D., Jayakumar, P. and Negrut, D. 2016. Experimental Validation of a Differential Variational Inequality-Based Approach for Handling Friction and Contact in Vehicle/Granular-Terrain Interaction. Journal of Terramechanics, 65:1-13.

[31] Foster, C. 2017. Draft Measurement and Analysis of Geotechnical Properties for Deformable Terrain Dynamics. Final Project Report, University of Illinois, Chicago.

[32] Tasora, A., Serban, R., Mazhar, H., Pazouki, A., Melanz, D., Fleischmann, J., Taylor, M., Sugiyama, H., Negrut, H. and Chrono, D. 2016. An Open Source Multi-Physics Dynamics Engine. T. Kozubek (Ed.), High Performance Computing in Science and Engineering – Lecture Notes in Computer Science, Springer, pp. 19-49. Project Chrono, http://projectchrono.org/.

[33] Serban, R., Negrut, D. and Tasora, A. 2018. Chrono: Vehicle – Template-based Ground Vehicle Modeling and Simulation. International Journal of Vehicle Performance, 2018.

[34] Tasora, A., Magnoni, D., Negrut, D., Serban, R. and Jayakumar, P. 2018. Deformable Soil with Adaptive Level of Detail for Tracked and Wheeled Vehicles. International Journal of Vehicle Performance, 2018.

[35] Hodges, H. 2017. Presentation of NG-NRMM Demonstration at Nevada Automotive Test Center, Simplified Terramechanics Validation and Verification to Predicted Values. NATO 40th AVT Panel Business Meeting, Utrecht, Netherlands. p. 94.

[36] Hodges, H. 2017. NG-NRMM Wheeled Vehicle Benchmark Demonstration to Software Developers. NATO AVT248 Special Meeting, Silver Springs Nevada.

[37] Jain, A., Calvin K., Paramsothy J. and Cameraon, J. 2016. Constraint Embedding for Vehicle Suspension Dynamics. Archive of Mechanical Engineering, 63(2):193-213.

[38] Preston-Thomas, J. 2017. Status Update on VSDC-NRC Prototype Demonstration Model for Tracked Vehicle Mobility. NATO 40th AVT Panel Business Meeting, Utrecht, Netherlands.

[39] Reinecke, D. 2017. Mobility Modelling and Simulation (MOBSIM) 2017/18. NATO 40th AVT Panel Business Meeting, Utrecht, Netherlands.

[40] Von Sturm zu Vehlingen, T. 2017. Germany Capabilities and Challenges. NATO 40th AVT Panel Business Meeting, Utrecht, Netherlands.

[41] Zieger, P. 2017. Germany's Cross Country Model Focusing on Soil Moisture Prediction. NATO 40th AVT Panel Business Meeting, Utrecht, Netherlands.

[42] Wong, J.Y. 1980. Data Processsing Methodology in the Characterization of the Mechanical Properties of Terrain. Journal of Terramechanics, 17(1): 13-41.

[43] Senatore, C. and Iagnemma, K.D. 2011. Direct Shear Behaviour of Dry, Granular Soils for Low Normal Stress With Application to Lightweight Robotic Vehicle Modelling. 17th International Conference on Terrain-Vehicle Systems ISTVS, Blacksburg, Virginia, USA, ed, 2011.

[44] Karafiath, L.L. and Nowatzki, E.A. 1978. Soil Mechanics for Off-Road Engineering, TransTech Publications.

[45] Priddy, J.D. and Willoughby, W.E. 2006. Clarification of Vehicle Cone Index with Reference to Mean Maximum Pressure. Journal of Terramechanics, 43:85-96.

Chapter 5A – TA3: COMPLEX TERRAMECHANICS REQUIREMENTS

Tamer M. Wasfy
Advanced Science and Automation Corp.
UNITED STATES

5A.1 GOALS AND TEAM MEMBERS

Soil affects vehicle mobility through:

- Contact with vehicle surfaces (such as tires, tracks, skis, legs, underbody, blades, tines, etc.).
- Contact with soil embedded obstacles (e.g., tree stems, poles, rocks, etc.) which in turn can contact the vehicle.

Thus, developing an accurate mechanics model of soil is essential for accurate prediction of vehicle mobility. NG-NRMM Complex Terramechanics models are those that utilize full three-dimensional (3D) soil models capable of accounting for the 3D flow/deformation of the soil including both elastic and plastic (permanent) deformation under any 3D loading condition of a vehicle running gear/surface such as tires, tracks, or legs; or in general any vehicle component such as underbody, bucket, blade, tines, etc. Accounting for 3D soil deformation includes prediction of:

- Rut depth/width/shape;
- Rut side wall height;
- Bulldozing of the soil; and
- Soil separation/reattachment from the terrain.

Typical complex terramechanics models include continuum models such as the Finite Element Method (FEM); and particle models such as the Discrete Element Method (DEM); and Smoothed Particle Hydrodynamics (SPH), or Material Point Method (MPM). Those complex terramechanics models must be fully coupled to high-fidelity Multibody Dynamics (MBD) vehicle models capable of accurately representing the main vehicle systems involved in locomotion including: chassis, engine, driveline, suspension system, steering system, and running gear.

The two main goals of Thrust Area 3 “Complex Terramechanics” are:

1) Provide a set of requirements which will guide development of complex terramechanics software tools and associated calibration and validation experiments for the Next-Generation NATO Reference Mobility Model (NG-NRMM). Those software tools will be used to accurately predict the vehicle mobility measures on various worldwide terrains that are encountered in ground vehicle military applications, especially off-road soft-soil terrains. Those recommendations include recommendations for: terramechanics models, experimental calibration of the terramechanics models, mechanics models of the interface between the soil and the vehicle surface (including tire models), and required complex terramechanics data in GIS software tools.
2) Present complex terramechanics prototype software tools that attempt to satisfy the requirements. The complex terramechanics prototypes can be used as examples for other complex terramechanics software tools and to demonstrate that the requirements are achievable in a relatively short term.

The team members for Thrust Area 3 are:

- Jon Preston-Thomas, Canada;
- Ole Balling, Denmark;
- Andreas Becker, Germany;
- Tom von Sturm zu Vehlingen, Germany;
- Phumlane Nkosi, South Africa;
- David Reinecke, South Africa;
- Russ Alger, USA;
- Scott Bradley, USA;
- Craig Foster, USA;
- Susan Frankenstein, USA;
- Michael McCullough, USA;
- Dan Negrut, USA;
- Sally Shoop, USA;
- Radu Serban, USA;
- **Tamer Wasfy: Leader**, USA; and
- Xiaobo Yang, USA.

5A.2 INTRODUCTION

5A.2.1 Motivation

Accurate complex terramechanics models coupled with high-fidelity multibody vehicle models can be used in the following military related tasks:

1) Predicting vehicle mobility for military operational analysis/mission planning purposes (evaluating vehicle mobility over the operating scenario of a specific mission and ground vehicle route planning). This includes generating mobility maps with the terrain colored using the mobility measure such as Speed-Made-Good.
2) Improving the design process of new and existing vehicles. Software tools that can accurately predict vehicle mobility will enable:
   - Reducing design cost and time by resolving design problems prior to fabrication and in general reducing dependence on physical prototypes.
   - Achieving more optimized vehicles which have higher performance (especially off-road) than traditionally designed systems. Vehicle designs can be virtually tested. The design optimization process can be performed on virtual vehicles. This will reduce design cost; speed-up the design process; and allow exploration of a larger design space in order to achieve a more optimum design.
3) Allowing more accurate and faster assessment and evaluation of alternative vehicle systems/designs during sourcing, acquisition, and procurement.

4) Establishing a high-fidelity virtual model (digital thread/digital twin) of DoD vehicles which includes: geometry, parts, joints/connections, materials, and physical characteristics of the vehicle that can be used in support of decisions throughout the vehicle's life including: inception, design, evaluation, production, deployment, operation, sustainment, and disposal/recycling.
5) Planning and rehearsing physical tests to ensure that the tests can best evaluate the vehicle's performance.
6) Accident reconstruction.
7) Predicting damage due to rutting on off-road and on-road surfaces after single/multiple vehicle passes.

5A.2.2 Model Types

Figure 5A-1 shows the spectrum of soil models from the highest fidelity (sub-atomic quantum mechanics models) to the lowest fidelity (one equation empirical models). The two highest fidelity models, namely, sub-atomic (quantum) and molecular scale models are not currently computationally feasible since they will require at least 10^{18} soil Degrees of Freedom (DOFs) for a typical ground vehicle mobility application. Those models are only shown in Figure 5A-1 for comparison purposes. The rest of the models are discussed below.

	Quantum Mechanics	Molecular Dynamics	Micro-scale Model	Macro-Scale Model	Height Field Model	Height Model	Empirical Steady-State model
Fidelity	Very high →						Very low
Description	Sub-atomic to atomic scale models	Molecular scale model	Soil particles individually modeled	Soil particles lumped to form a virtual particle or a finite element (e.g. DEM or FEM)	Terrain is divided into vertical cells. For each cell height and state of stress is stored. A Bekker-Wong-Janosi type pressure-sinkage-traction-slip model is used for each cell.	Normal stress and slip are used to calculate sinkage and tractive force using a Bekker-Wong-Janosi type model.	NRMM / NRMM-II
Number of Soil DOFs for vehicle mobility applications	$>10^{20}$	10^{18}	$10^{14} – 10^{11}$	$10^{7} – 10^{6}$	$10^{4} – 10^{3}$	1	0
Current Computational Cost	Prohibitive	Prohibitive	Years of HPC time.	6 hours to 1 week	Minutes/ real time	Faster than real time	Faster than real time
Our current state of knowledge	Unknown how to take the model to the macro-scale	Taking the model to the macro-scale requires more research because the soil consists of many materials	More research is needed to understand the micro-mechanical soil interaction forces	More research is needed to improve, calibrate, and validate the soil models	More research is needed to improve, calibrate, and validate the soil models	More research is needed to improve, calibrate, and validate the soil models	Implemented in NRMM/NRMM-II

Figure 5A-1: Spectrum of Soil Models Based on Model Fidelity and Scale. Complex Terramechanics is Focused on the Macro-Scale Model.

5A.2.2.1 Micro-Scale Soil Model

In micro-scale models **each soil particle (with the actual particles' geometries and scales) is modeled along with the interaction forces between the particles**. On the micro-scale, soil is composed of particles/grains of varying:

- **Particle sizes** (Figure 5A-2): Clay < 0.002 mm; Silt 0.002 to 0.05 mm; Sand 0.05 to 2 mm; Gravel 2 to 75 mm; Cobbles 75 to 250 mm; Stones 250 to 600 mm; Boulders > 600 mm.

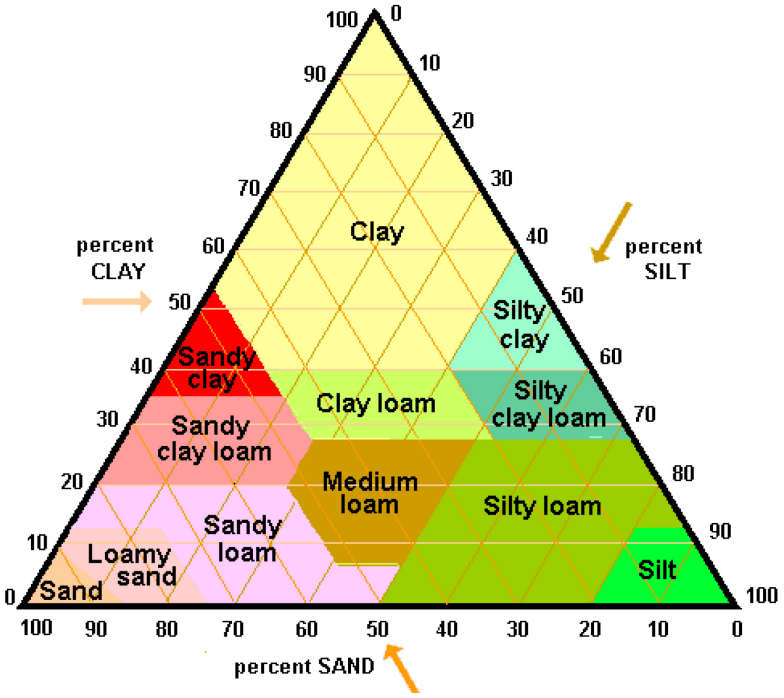


Figure 5A-2: USDA Soil Triangle Based on Percent Clay, Silt, and Sand.

- **Particle size distribution** (or soil grading) is measured using the particle diameter/size versus percentage of the total soil weight passing through a sieve of mesh spacing equal to the particle diameter (Figure 5A-3). Well graded soils have a nearly continuous smooth particle size distribution curve. This means that all particle sizes across the soil particle size range are equally present in the soil. Poorly graded soil has a non-smooth particle size distribution curve. This means that some particles sizes are not well represented in the soil.

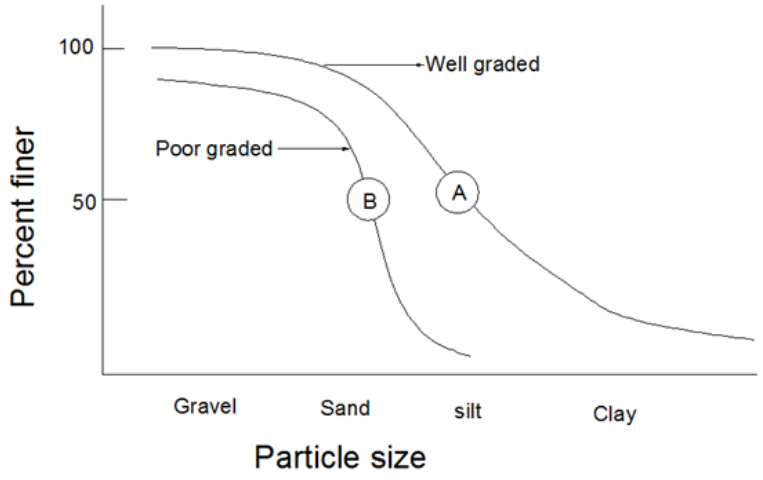


Figure 5A-3: Typical Particle Size Distribution Curve.

- **Chemical composition**, including:
  - Inorganic compounds (crystalline/amorphous): Sand SiO_2, Calcite $CaCO_3$, Feldspar, Mica, etc.; and
  - Organic COHN compounds.
- **Particle shapes** (Figure 5A-4), including:
  - Round/angular;
  - Spherical, elliptical;
  - Cylindrical;
  - Rectangular;
  - Prismatic;
  - Cubical;
  - Wedge; and
  - Flake/plate.

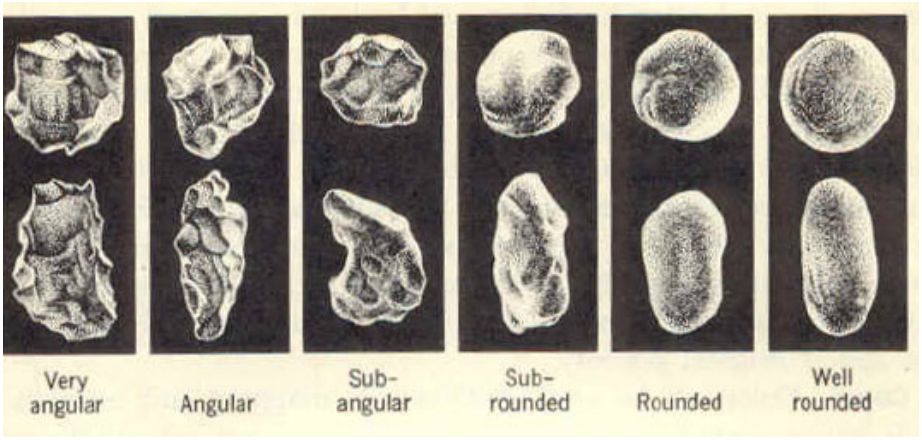






Figure 5A-4: Classification of Soil Particle Shapes.

- **Particle surface roughness**: smooth to rough.
- **Soil moisture content** can vary between the following Atterberg limits [1] (Figure 5A-5):
  - Dry; shrinkage limit;
  - Plastic limit;
  - Liquid limit; and
  - Above the liquid limit.

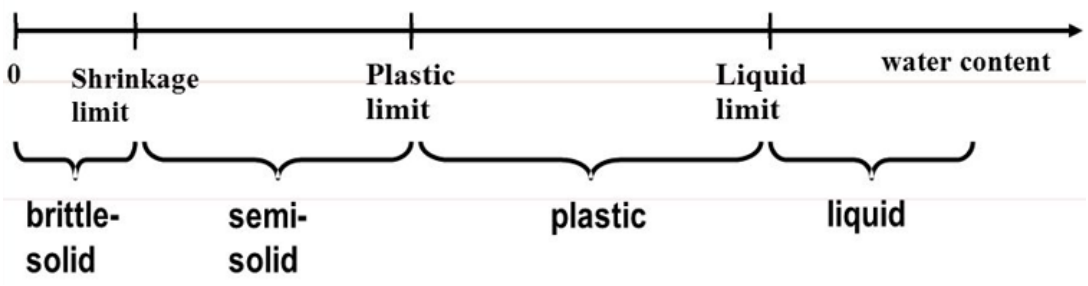


Figure 5A-5: Soil Atterberg Limits Based on Water Content.

- **Compaction state**. Soil shear strength generally increases as the soil compaction increases. Soil compaction can be increased for well graded soil by subjecting the soil to hydrostatic pressure which reduces the size of the voids between particles. Poorly graded soils, such as gravel or sand with no fines, can be compacted by vibration (e.g., using vibratory plates and rollers) which can reorient the particles in such a way to reduce the void volume. Compaction can be reduced for well graded soils by tilling and for poorly graded non-cohesive soils by vibration.
- **Temperature**: mainly affects soil due to variation of water properties with temperature especially around the water freezing temperature. For example the strength of frozen peat is 300 – 400 times that of unfrozen peat [2]. In addition, water viscosity and surface tension are a function of temperature. At 4° C water viscosity is 1.6 mPa.s and surface tension is 0.08 N/m. At 40° C water viscosity is 0.6 mPa.s and surface tension is 0.07 N/m. Thus, temperature is expected to affect moist soil viscosity and cohesive strength. Note that a principle component of soil cohesive strength is the capillary liquid-bridging force due to water surface tension.

The micro-mechanical soil inter-particles forces, soil particles-to-vehicle surface forces (Figure 5A-6), and soil particle properties are all a function of the aforementioned soil physical conditions. Micro-mechanical forces between soil particles and the vehicle surface materials are also a function of the solid surface roughness and material type. The micro-mechanical soil inter-particle and soil particles-to-vehicle surface forces include:

- Normal contact forces: elastic (repulsive) and damping (repulsive).
- Tangential forces: friction and viscosity (oppose relative tangential velocity).
- Capillary liquid-bridging forces (repulsive when particles are very close and attractive/cohesive when the particles move further apart).
- Van der Waals forces (attractive/cohesive).

- Chemical bonding forces (attractive).
- Electrostatic forces (attractive/cohesive if the particles are oppositely charged and repulsive if the particles are similarly charged).

The micro-mechanical soil particles properties include:

- Particle mass density.
- Soil particle compliance including particle elastic stiffness (Young's modulus, Poisson ratio) and damping.
- Soil particle fracture strength.



Figure 5A-6: Soil Adhesion to a Tire Caused by the Soil Particles-Rubber Forces.

The main challenges in using a micro-mechanical soil model are:

- Large number of soil particles. Using a particle size of 2 cm, a typical DEM code running on one 32-core computer can simulate about 106 spherical point particles for 5 sec in 1 day or 105 complex shape rigid body particles for 5 sec in 1 day. In order to model a soil patch that is 10 m × 4 m × 0.5 m, with an average particle size of 0.1 mm, 25 × 1012 rigid body particles of complex shape are needed. Assuming the time step reduces with the cube of particle size and assuming we can divide the problem to HPC nodes and get a linear speed-up, then we need 0.5 × 1015 HPC nodes to complete a 5 sec simulation in 1 day. Thus simulating a soil patch using the actual soil particle size is not currently feasible using existing computer technology. Furthermore, actual soil particle sizes in many actual soils can be smaller than 1 μm. Therefore, lumping many soil particles is necessary for practical soft-soil vehicle mobility applications.

- The model must reflect the actual distribution of varying particle materials, shapes, sizes, and surface roughness as the actual soil. Those soil parameters are all difficult to experimentally measure. In addition, the number and variability of the soil particle parameters make the task of measuring those parameters even more daunting.
- Inter-particle interactions on the micro-scale are still not well understood especially between complex shape, rough surface, and multimaterial (including mineral and organic materials) soil particles. Those interactions forces include:
  - Capillary liquid-bridging forces.
  - Van der Waals, chemical bonding, and electrostatic forces.
  - Micro-scale viscous and damping forces.
- The phenomenon of particle fracture/merger at high-stresses and high slip rates is not well understood.
- Single particle stress-strain and stress-strain rate relations need to be experimentally measured and calibrated.

Examples of research studies where micro-mechanical DEM soil models are investigated include:

- DEM along with computed tomography [3] and imaging [4] were used to model non-cohesive granular soil in a triaxial test. Individual soil particles are modeled along with their accurate shape and orientation. Only friction and normal inter-particle elastic forces are considered. The soil box is small (a few cm cubed) and the number of soil particles is also relatively small (on the order of 10^5). In addition, the motion of the particles was very small since only a triaxial quasi-static type loading is considered.
- DEM simulation of non-cohesive soil (sand) flow from a hopper using polyhedral [5] and poly-spherical [5], [6] cubical particles. Actual particle sizes and hopper orifice diameter are used. An average cubical particle shape is assumed. A high normal contact stiffness is used to ensure that the material is nearly incompressible. Inter-particle and particle-hopper friction are the main physical effects included in the model. The models can accurately predict the material flow rate given by the Beverloo equation [7]. The models were also used to predict the angle of repose of the resulting soil material pile [6].

5A.2.2.2 Macro-Scale Soil Model

The next-highest fidelity soil models are macro-scale models where many soil particles are lumped using either a Lagrangian, an Eulerian, or an Arbitrary Lagrangian-Eulerian (ALE) description. The complex terramechanics Thrust Area is focused on macro-scale soil models. Those models include the Finite Element Method (FEM) along with an Eulerian and ALE formulation; and Lagrangian particle methods such as the Discrete Element Method (DEM), Smoothed Particle Hydrodynamics (SPH), and Material Point Method (MPM). Those types of models currently require on the order of 106 to 107 particles/elements and hours to days of HPC time for practical vehicle mobility applications. The main current limitation of those models is mapping the physical soil parameters such as soil type (based on the soil chemical composition), moisture content, and temperature, to the material model parameters required by those models. Currently, the main method to obtain this mapping is to perform physical terramechanics experiments, then model the experiment using the complex terramechanics software tool and calibrate the material model parameters such that the model and experiment responses match. Another method is to use a higher fidelity model such as a micro-scale soil model to calibrate the macro-scale model. However, this is not currently possible due to the fact that micro-scale soil models are not well developed.

It was agreed in the NG-NRMM committee to use the Unified Soil Classification System (USCS) to identify the soil type for macro-mechanical soil models based on committee members experience and the fact that USCS is the classification system currently used in NRMM [8]. Other potential soil classification systems which can be used in the NG-NRMM include AASHTO [9] and USDA [10]. All current soil classification systems suffer from the following deficiencies:

1) **Nonuniqueness**. Soils with different mechanical properties may map to the same soil type.
2) **Difficulty to remotely determine the soil type** using remote sensing such as multi-spectral imaging and ultrasound. In order to "accurately" determine the soil type a physical soil sample needs to be analyzed in the lab.
3) **They don't fully consider the detailed chemical composition of the different soil grains**. They just consider mineral and organic content.

There are at least twenty different USCS soil types [11]. At least seven moisture contents need to be tested for each soil type (see Figure 5A-5 on Atterberg limits). This is due to the fact that soil mechanical properties can vary dramatically and non-linearly with moisture content. Also, at least five temperatures (below freezing -10°, at freezing 0°, slightly above freezing 4°, 20° and 35°) need to be tested. Soil temperature affects mechanical properties especially around the water freezing point where soil strength can vary from very soft to very hard. Thus a total of at least $20 \times 7 \times 5 = 700$ terramechanics experiments may be needed to calibrate the macro-mechanical soil model for all soil types, moisture contents, and temperatures.

Also, note that since there are many types of macro-mechanical models (e.g., FEM, DEM, SPH, and MPM), the complex terramechanics software tool requirements should not depend on the choice of modeling technique. In order to achieve this, the model will be defined by its ability to predict soil mechanical response in terramechanics experiments (e.g., piston-cylinder, shear cell, triaxial cell, penetrometer, bevameter, wheel on soil, etc.). Those experiments will be modeled using high-fidelity complex terramechanics/MBD modeling techniques and the chosen high-fidelity soil model (FEM, SPH, DEM, etc.) parameters can be fitted to the experimental data. A review of the various macro-scale soil model types in ground vehicle mobility applications is presented in Section 5A.3.

5A.2.2.3 Height Field and Height Soil Models

The next type of models based on fidelity are height field models which use the vertical soil deformation (wheel sinkage) normal to the terrain, wheel slip, and the normal and shear stresses as a function of the two planar horizontal directions as the main terrain response variables. Thus only 2D space subdivision is needed rather than a full 3D space subdivision as in the case of the macro-scale models. Those models require on the order of 10^3 to 10^4 planar cells and minutes to near real-time of computer time for practical vehicle mobility applications. Those types of models are the ones used in the Simple Terramechanics Thrust Area.

The next type of models are the height models where sinkage is calculated based on ground pressure and tractive/resistance forces are calculated based on sinkage and wheel slip with no spatial tracking/history of terrain deformation. Those models run faster than real-time since no spatial subdivision is needed for the terrain.

Both height field and height models currently have the same limitation as macro-scale soil models, namely that fully mapping the physical soil parameters to the material model parameters requires performing terramechanics experiments. In addition, another calibration step using macro-scale models may be needed for height field and height models since the terramechanics experiments such as shear cell, triaxial cell, or bevameter cannot be accurately modeled using those simple models.

5A.2.2.4 Empirical Equation Soil Models

The final type of soil models are the ones currently used in the NRMM based on steady-state empirical equations using the Cone Index. Those models have the lowest fidelity and suffer from following disadvantages:

- They only work at steady-state. Higher fidelity models can be used to predict vehicle mobility during both steady and unsteady state operation.
- They only work well for vehicles and soil conditions that were used to calibrate the models. They are difficult to extrapolate to new vehicle designs such as lightweight vehicles, small robotic vehicles, autonomous vehicles, and new running gear (tire and track) designs, since new calibration experiments will be needed. In fact the main advantage of using higher fidelity complex terramechanics models over simple models such as empirical equations models is that once the terramechanics model is calibrated they, in theory, should produce accurate mobility predictions for any type of vehicle and running gear.

The reader is also referred to Annex F on the Measurement and Analysis of Geotechnical Properties.

5A.3 REVIEW OF MACRO-SCALE SOIL MODELS

Macro-scale soil models used in vehicle mobility applications can be divided into two main types:

1) Mesh-based finite element models; and

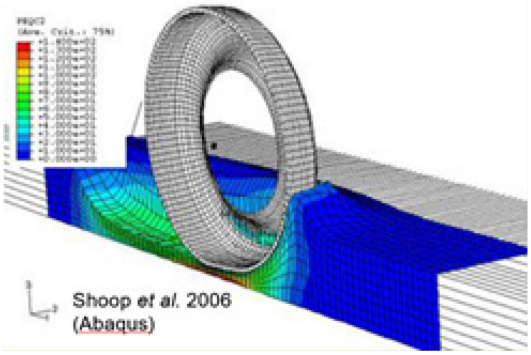
2) Mesh-free particle-based models.

5A.3.1 Mesh-Based Finite Element Soil Models

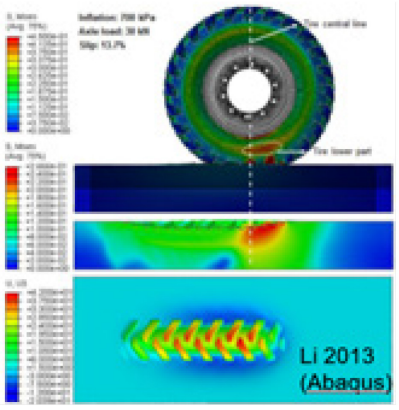
In mesh-based Finite Element (FE) soil models [12], [13], [14], [15], [16], [17], [18], [19] the soil is discretized into an FE mesh and an elasto-visco-plastic continuum mechanics constitutive material model [20] such as the Drucker-Prager/Cap [21], [22] model, which is used to approximate the Mohr-Coulomb yield behavior of the soil (soil plastic yielding, internal friction, cohesion, and flow). Several commercial FE codes such as Abaqus [23], PAM-CRASH [24], and LS-DYNA [25] include various soil constitutive material models such as the Drucker-Prager/Cap model and have been used to simulate soil-wheel interaction. For example, Abaqus was used to study tire and wheel soft soil interaction in Refs. [12], [13], [14], [15], [16], [26], [27] and full-vehicle soft soil interaction in Ref. [14] (Figure 5A-7). PAM-CRASH was used in Ref. [17] to study single tire and multi-tire soft soil interaction. Wright [19] used LS-DYNA along with an Eulerian FE soil model to study a single tire rolling resistance, drawbar pull, and tractive efficiency.

Most FE soil models use a Lagrangian formulation where the soil deformation is modeled using the motion of the FE nodes. The main disadvantage of a Lagrangian formulation is that if soil deformation is not relatively small, then remeshing is needed in order to avoid excessive element distortion. The remeshing step is computationally expensive and degrades solution accuracy since the solution fields (including plastic and elastic deformations) need to be re-interpolated to the new mesh. Some FE studies use the Arbitrary Lagrangian-Eulerian (ALE) formulation which allows mass transfer between elements to extend the range of soil deformation [12], [13]. However, even with ALE, effects such as soil bulldozing and separation/reattachment still require remeshing. In addition, a cohesive soil continuum mechanics constitutive material model which accounts for the combined effects of material flow/fracture, plasticity, friction, and cohesion and the dependence of those properties on current stress and consolidation stress (or stress history) is still an open research problem. Wright [19], used the Eulerian formulation of LS-DYNA to model tire interaction with non-cohesive soil. In Eulerian formulations a fixed mesh (typically a Cartesian grid) is used.

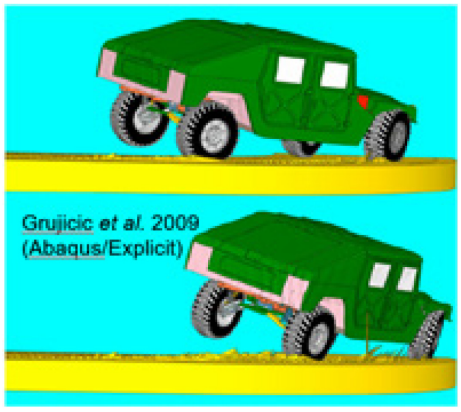
Cut-cell boundary conditions are used to model solid surfaces, and the free surface of the soil can be modeled using the Volume-Of-Fluid (VOF) or level-set methods [28]. The Eulerian formulation can handle soil flow and separation/reattachment with no need for remeshing. In Ref. [19] a non-cohesive soil material model was used since a Drucker-Prager cohesive type material model was not available in LS-DYNA using the Eulerian formulation. In general, a cohesive soil material model which includes the combined mechanical behaviors of plasticity, friction, and cohesion is more difficult to implement within an Eulerian formulation than a Lagrangian formulation.



(a)



(b)



(c)

Figure 5A-7: Abaqus Finite Element Vehicle Mobility Soil Models [12], [13], [14], [15], [16], [26], [27].

The main advantages of mesh-based FE soil models are:

- Element size can be adapted. Small elements can be used in areas of high deformation gradients near the surface and near the tire, and large elements can be used in areas of low deformation gradients deep in the soil and far away from the tire (Figure 5A-8). Thus, the number of DOFs is in general smaller than particle-based methods.
- The Lagrangian FE formulation with no remeshing is suitable for moderate soil deformation with no soil flow.
- ALE can extend the soil deformation range and include the effects of material flow.
- The Eulerian formulation can be used in case large soil deformations and material flow effects are present.

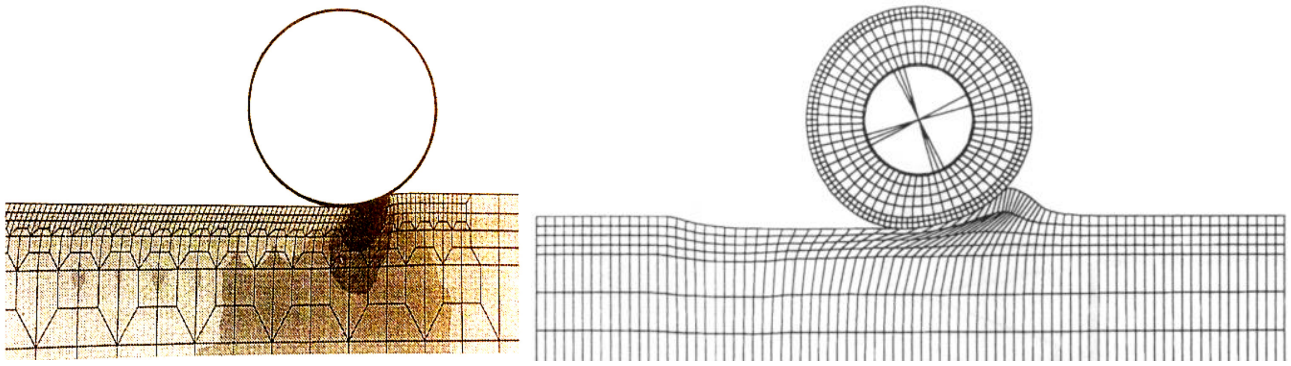


Figure 5A-8: Adaptation of Finite Element Size Near the Surface [29].

The main disadvantages of mesh-based FE soil models are:

- Large soil deformation requires remeshing which is computationally expensive and reduces solution accuracy in Lagrangian and ALE FE models.
- It is difficult to capture soil separation and reattachment even with remeshing.
- A Lagrangian finite formulation is inherently incapable of modeling material flow between elements. This is due to the fact that material which is inside one element remains inside that element since the mass of the element nodes is constant.
- When an ALE formulation is used a model of material flow between elements which conserves mass needs to be added. In addition nodal masses are not constant which makes the problems difficult to solve when nodal masses become small. Also, in Eulerian formulations, it is difficult to maintain mass conservation especially with solid boundaries (such as tires and tracks) moving at high speed using the cut-cell boundary conditions.
- FEM relies on a continuum mechanics formulation (i.e., assumes the soil is a continuum). Drucker-Prager type constitutive material models are typically used for soils, but they are generally limited to moderate strains. Currently, there is no constitutive material model which accounts for the combined effects of material large strain/flow, plasticity, elasticity, fracture, friction, viscosity, damping, compressibility, and cohesion. Implementing this material model within an Eulerian formulation is even more challenging.
- For moderate soil deformation with negligible soil flow effects height field-based models (simple terramechanics models) may provide comparable accuracy as FE methods, but are much faster (can run in real-time).
- Mesh generation step can be complex in case element size is varied across the soil height and/or soil embedded obstacles are present.
- In Eulerian formulations, it is difficult to accurately account for friction and viscous forces at the solid boundaries using the cut-cell boundary conditions.

Areas where further research is needed for finite element soil models to be used in practical ground vehicle mobility simulations include:

- Cohesive soil and non-cohesive continuum mechanics soil constitutive material models which account for material flow, friction, plasticity/compaction, and shear strength variation due to compaction and normal stress.

- Accounting for particle size and shape effects in non-cohesive soils. According to the Beverloo equation, soil flowability depends on particle size and shape [7]. Techniques to include particle size effects in FE formulations need further investigation.
- Algorithms for remeshing and reinterpolation of the solution field which conserve mass and energy and at the same time can capture soil bulldozing, ruts, and soil separation/reattachment.
- Parallel solution: including GPUs and distributed memory HPCs.
- Modeling multi-soil layer terrains including snow and water layers.
- Modeling obstacles embedded in the soil.
- Calibration of the constitutive material models for: different types of soils, moisture content, and temperature using physical experiments.
- Validation of the coupled FE soil models and vehicle models using full-vehicle experiments.

5A.3.2 Mesh-Free Particle-Based Soil Models

In particle-based models discrete particles are used to model the soil with inter-particle forces used to model the soil mechanical behavior. Particle models are the closest models to the actual physics of the soil. The main advantage of particle-based methods is their ability to naturally model material flow and separation/reattachment. Their main disadvantage is the large number of particles and high computational cost needed to accurately model the soil. There are many particle-based formulations that have been used to model soils in vehicle mobility simulations, including: DEM, SPH and MPM.

5A.3.2.1 Discrete Element Method

In the DEM material behavior is modeled using inter-particle forces which include: normal contact forces (which can be deflection and/or velocity-dependent) which prevent the particles from penetrating each other, attraction forces, tangential contact forces (including friction and viscous forces) and distance dependent forces (gravity, electrostatic and magnetic forces) [30], [31]. DEM particles can have: only translational DOFs (i.e., point particles); or both translational and rotational DOFs (i.e., rigid body particles). Point particles are spherical, while rigid body particles can have arbitrary shapes (e.g., spherical, elliptical, cubical, or polyhedral). In Refs. [32], [33] spherical DEM particles were used to model soils in vehicle mobility applications. The inter-particle force model included particle stiffness and friction but did not include cohesive forces and plasticity. In Ref. [34], the DEM technique developed in Refs. [32], [33] was extended to non-spherical ellipsoid particles. In Ref. [35] a 2D DEM model that includes a tensile spring for accounting for soil cohesion was developed and used in soil-tire interaction simulations. In Ref. [36] the particle force model developed in Ref. [35] was implemented in a 3D DEM model and used to model a rigid wheel interaction with a cohesive soil. In Refs. [37], [38], [39] an implicit Differential Variational Inequality (DVI) solver was developed and used in ground vehicle mobility simulations. The model included the effects of soil cohesion, friction, viscosity, and elasticity, but did not include plastic deformation and consolidation effects. In Ref. [40] a DEM cohesive soil material model was presented that can account for soil plasticity/bulk density, and cohesion including their dependence on normal stress and consolidating stress. In addition, the inter-particle force model also includes normal elastic and damping forces, and tangential friction and viscous forces. The model was demonstrated in typical ground vehicle mobility [40] and earth moving [41] applications. In Ref. [42] the model presented in Ref. [40] was extended to allow loss of cohesive strength due to tension using a time relaxation model of the soil plastic deformation. In Ref. [43] a moving soil patch technique was added to allow simulating the vehicle

operation on an arbitrarily long soft-soil terrain. The DEM soil model developed in Refs. [40], [41], [42], [43] was integrated into the DIS [44] explicit multibody dynamics code and was demonstrated in full-vehicle mobility simulations over long soft-soil terrains with various longitudinal and side slopes (Figure 5A-9).

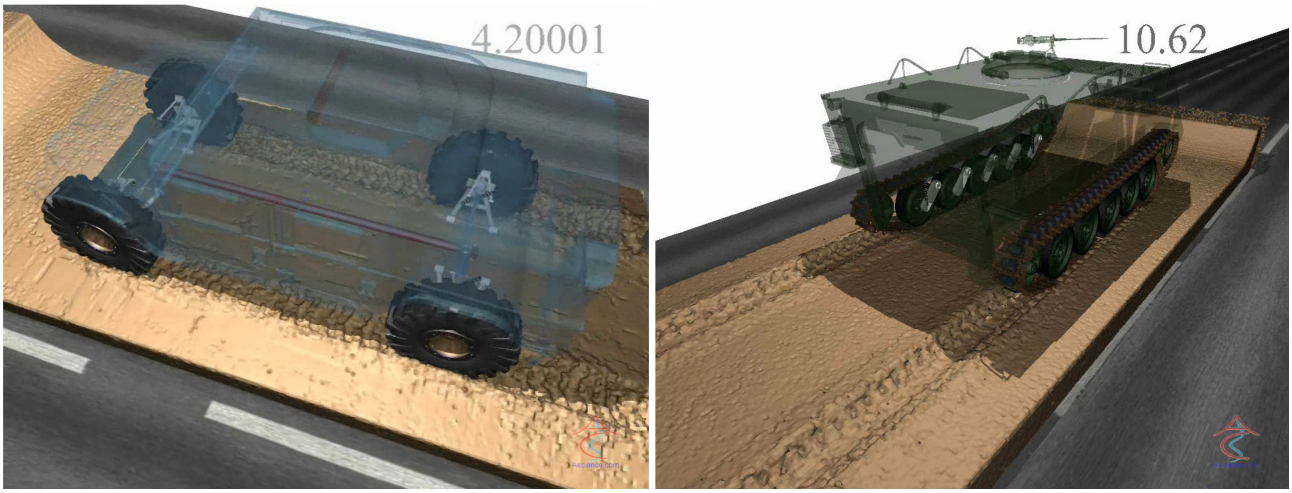


Figure 5A-9: Simulation of Wheeled and Tracked Multibody Dynamics Vehicle Models over Long and Side Sloped DEM Soft Terrains.

The main advantages of DEM soft-soil models in ground vehicle mobility simulations include:

- DEM can be used for large soil deformation including soil flow, separation/reattachment, and adhesion with vehicle components.
- A DEM inter-particle force model which can account for the combined effects of plasticity, elasticity, damping, viscosity, fracture, friction, compressibility, and cohesion has been developed by many groups and used in practical applications.

The weaknesses of DEM soft-soil models in ground vehicle mobility applications include:

- A large number of particles is needed since the smallest needed particle size must be used throughout the soil domain since any particle can move/flow near the tires or any other vehicle contact surface.
- Particle size affects the soil model parameters because mechanical properties such as friction, cohesion, and plasticity scale differently with particle size. For example, non-cohesive soil (such as sand) flows more easily as the average particle size decreases according to Beverloo equation [7] which give the granular flow rate (W) through an orifice of diameter D_0:

$$W = C\,\rho_B \sqrt{g}\,(D_0 - kd)^{2.5} \tag{5-1}$$

C, k are material constants, ρ_B is the material bulk density, d is the particle diameter. Thus, more research is needed to effectively calibrate the DEM model parameters such that they are independent of particle size. Also, note that when the particle size becomes much smaller than the orifice diameter, flow rate is no longer dependent on particle size.

Areas where further research is needed in soft soil DEM models for vehicle mobility applications include:

- Create a robust method to automatically set the DEM material model parameters based on the chosen DEM particle size.
- Improving the inter-particle force model:
  - Based on physical calibration experiments.
  - Based on micro-mechanical inter-particle forces including: capillary liquid-bridging (including water flow under loading effects) and van der Waals forces.
- Parallel solution: including GPUs and distributed memory HPCs.
- Modeling multi-soil layer terrains including snow and water layers.
- Calibration of the inter-particle force model for: different types of soils, moisture content, and temperature using many types of physical experiments.
- Validation of coupled DEM soil models and vehicle models using full-vehicle experiments.

5A.3.2.2 Smoothed Particle Hydrodynamics

SPH is a mesh-free method where the particles are used as interpolation points for solving the continuum mechanics governing equations (Cauchy equation of motion in the case of soils) [45], [46]. The continuum equations are discretized for each particle using a kernel smoothing function that is used to evaluate each particle's properties and fluxes/forces acting on a particle using neighboring particles. Lescoe et al. [47], [48] and Dhillon et al. [49] created a coupled FE tire and SPH soil model using PAM-CRASH [24] (Figure 5A-10). This model was used to simulate the rolling of rigid and flexible tires on soft soil. A hydrodynamic elastic-plastic material was used for the soil. The SPH model showed promise but it was concluded that the material models need to be further refined since it either showed excessive viscosity or incorrect material compressibility. Shokouhfar [50] created a coupled FE tire and SPH soil model using LS-DYNA [25] (Figure 5A-10). The model was used to simulate the rolling of rigid and flexible tires on soft soil. A pressure dependent soil material model was used which includes friction and cohesive effects. The SPH model again showed promise, but the material model had artificial cohesion so it could not account for the zero soil cohesion case. Also, the model did not include the effect of compaction/plasticity on the soil strength. Similar, to other particle techniques such as DEM, the main advantage of SPH is it can be used in large soil deformation including soil flow, separation/reattachment and soil adhesion to solid surfaces. The main weaknesses of SPH soil models in vehicle mobility applications include:

- Large number of particles is needed since the smallest needed particle size must be used throughout the soil domain since any particle can move/flow near the tires or any other vehicle contact surface.
- Computational speed is slower than DEM since a particle not only interacts with its immediate neighbors but with all the particles within the kernel radius which, for accuracy, has to be in the range of 20 to 50 particles (or more).
- SPH relies on a continuum mechanics formulation (i.e., assumes the soil is a continuum). Currently, no constitutive soil material model can accurately account for the combined effects of large strain/flow, plasticity, elasticity, fracture, friction, compressibility, and cohesion. It was noted in previous SPH soil models (see Refs. [47], [48], [49], [50]) that one of the main areas of needed improvement are the soil material models, where problems with excessive viscosity and cohesion were noted, and effects of compaction/plasticity on shear strength were not included.

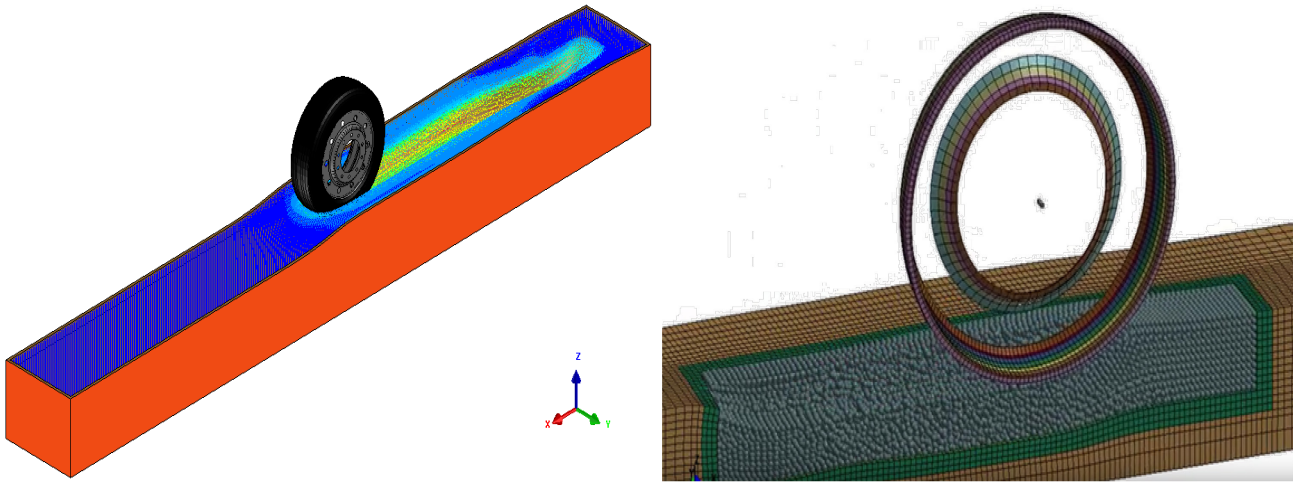


Figure 5A-10: PAM-SHOCK (Left) [47] and LS-DYNA (Right) [50] Coupled SPH Soil-Tire Models.

In addition to improving the soil material models, areas where further research is needed in soft soil SPH models for vehicle mobility applications include:

- Parallel solution: including GPUs and distributed memory HPCs.
- Modeling multi-soil layer terrains including snow and water layers.
- Calibration of the constitutive material models for: different types of soils, moisture content, and temperature using physical experiments.
- Validation of the coupled FE soil models and vehicle models using full-vehicle experiments.

5A.3.2.3 Material Point Method

In the MPM [51] a Cartesian grid is used along with the particles to find neighboring particles as well as to discretize and solve the continuum mechanics governing equations. In Ref. [52] the MPM was used to model snow for computer graphics applications, including rigid body interaction, using a snow material model that includes stiffness, plasticity and fracture (Figure 5A-11) In Ref. [53] MPM was used to model soil-structure interaction including pile driving and land-slides. A non-linear hypo-elastic sand material model was developed. Similar to other particle techniques such as DEM and SPH, the main advantage of MPM is it can be used in large soil deformation including soil flow, separation/reattachment and soil adhesion to solid surfaces. The main weaknesses of MPM soil models in vehicle mobility applications include:

- Large number of particles is needed because the smallest needed particle size must be used for all the particles since the particles can flow.
- MPM relies on a continuum mechanics formulation (i.e., assumes the soil is a continuum). Currently, no constitutive soil material model can accurately account for the combined effects of large strain/flow, plasticity, elasticity, fracture, friction, compressibility, and cohesion.
- MPM has not been demonstrated with a full multibody vehicle model in a soft-soil vehicle mobility simulation.

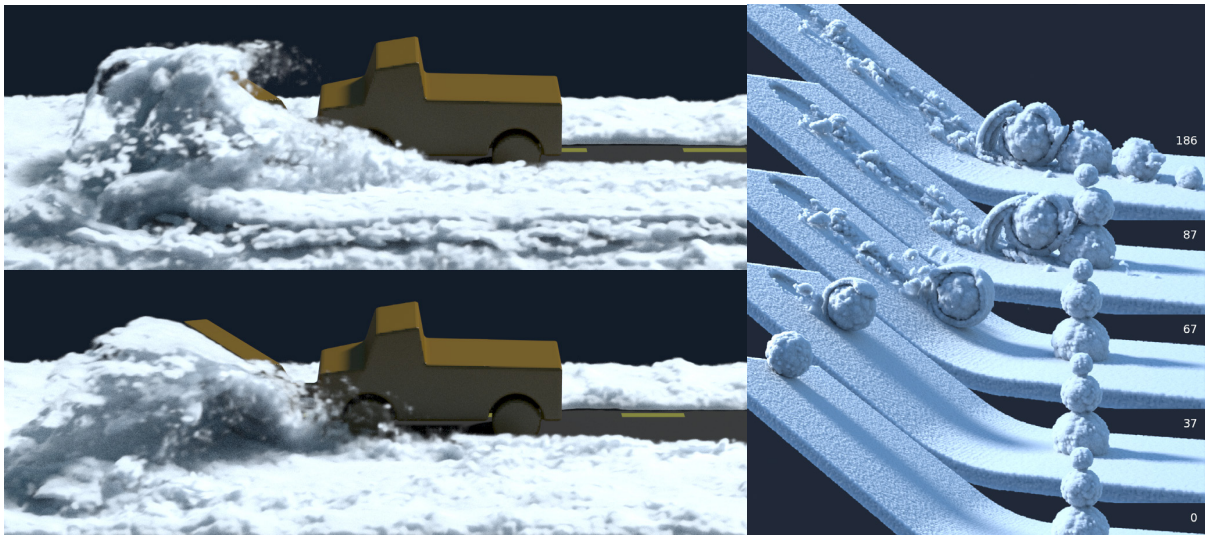


Figure 5A-11: Computer Graphics Model of a Snow Plow and a Snow Ball [52].

5A.3.3 Technology Readiness of the Macro-Scale Terramechanics Modeling Techniques

Table 5A-1 shows our estimate of the Technology Readiness Level (TRL) of the currently available macro-scale terramechanics modeling techniques. The TRL scale is from 1 to 9 with 9 being the most mature technologies. From the table and the discussion in this section, it can be concluded that DEM is the most mature soil modeling technique followed by SPH and MPM. Eulerian FEM needs a lot of development to bring it to the maturity level of particle-based methods. Lagrangian/ALE FEM is only recommended for modeling soil in vehicle mobility applications when soil deformation is small to moderate and soil flow is negligible. Lagrangian/ALE FEM is not recommended in case of large soil deformation and flow.

Table 5A-1: Estimate of the Technology Readiness Levels of Macro-Scale Terramechanics Modeling Techniques.

Measure	Lagrangian /ALE FEM	Eulerian FEM	DEM	SPH	MPM
Accuracy/generality of soil material models	5	3	8	6	6
Range of soil deformation	4	9	9	9	9
Ability to include embedded obstacles	3	7	9	9	9
Fidelity of the soil-vehicle interface	5	7	8	8	8
Computational speed	5	7	6	5	6
Experimental validation	4	4	6	5	4
Current use in vehicle mobility	5	4	8	6	5
Total	**31**	**41**	**54**	**48**	**47**

5A.4 COMPLEX TERRAMECHANICS SOFTWARE TOOLS REQUIREMENTS

In this section we list and describe the main requirements (needed capabilities) for NG-NRMM complex terramechanics physics-based software tools. The main function of those tools is to accurately predict the mobility of manned, unmanned, and autonomous ground vehicles of various sizes that are supported by wheels (including pneumatic tires and airless tires), tracks (including segmented tracks and continuous belt-type tracks), skis and/or legs while operating on the various types of worldwide terrains, especially soft soil terrains, that are encountered in military applications while carrying any variation allowable of payloads/occupants. The following simplifying assumptions can be used in the complex terramechanics models:

- Soil is isotropic (same response in any direction).
- Soil is homogeneous/uniform (same properties in any location) under the running gear.
- Vehicle loading to the soil is fast so that soil type does not change during the vehicle loading. This includes:
  - Moisture content. Soil mechanical properties dramatically vary with soil water content. Water takes time to drain out or to evaporate from the soil. In general, change in water content in the soil occurs at a much longer time scale than the vehicle loading. Therefore we will assume that water content is constant during vehicle loading.
  - Temperature: soil temperature remains constant during loading (except when modeling snow/ice when melting at the interface can significantly affect vehicle mobility).

The combined MBD and complex terramechanics models must have the 14 capabilities described in the following subsections. Those capabilities can be categorized as follows:

- Capability 1 consists of the required vehicle response quantities to be predicted and their accuracy bounds.
- Capability 2 consists of the required soil response quantities to be predicted and their accuracy bounds.
- Capabilities 3 to 6 are the requirements for the complex terramechanics soil material models.
- Capabilities 7 to 11 list the requirements for complex terramechanics models to be able to handle the various terrain conditions such as obstacles and vegetation.
- Capabilities 12 and 13 include the requirements for interfacing the complex terramechanics models with GIS software and generating the vehicle mobility maps.
- Capability 14 includes the requirements for interfacing with MBD software for modeling the vehicle.

5A.4.1 Ability to Predict the Vehicle Mobility Measures

The combined complex terramechanics and vehicle models must be able to predict the following vehicle mobility measures which are of interest to the end users:

1) GO/NOGO.
2) Speed. Of special interest is the Speed-Made-Good which is the maximum speed of the vehicle in the desired direction while the vehicle is stable and under control, i.e., can be stopped and steered by the driver.

3) Rate of fuel/energy consumption and total fuel/energy consumption along the vehicle's path.
4) Engine torque/power.
5) Wheel/track sinkage.
6) Wheel/track slip.
7) Tire deflection.
8) Suspension system deflection.
9) Available drawbar pull.
10) Transmitted vibration power to the vehicle's occupants/payloads.
11) Vehicle component's dynamic stresses and fatigue life.
12) Braking distance.
13) Stability: rollover along any axis on side/long slopes and during turning, lane change or obstacle avoidance maneuvers.
14) Stability: loss of speed control, including acceleration and/or braking control.
15) Stability: loss of directional control including under- and over-steering.
16) Vehicle control activity.
17) Factors which limit performance.
18) 3D interaction forces exerted by the soil on any vehicle component (e.g., tires, track, underbody, tines, etc.). The forces include tractive (tangential) and bearing (normal) forces. The vehicle component can be spatially moving/rotating in any arbitrary 3D path with respect to the soil within the component's allowable speed range.

This includes ability to predict the above quantities along any direction, including:

1) Omni value: worst possible value in any direction.
2) Uphill value.
3) Downhill value.
4) Side-hill value.
5) Along a specified direction.
6) Along the traverse direction.

This also includes the ability to predict instantaneous, maximum, minimum, and average value of the above quantities over each terrain cell. The ability to predict each mobility measure can be validated using a full-scale instrumented vehicle. The maximum error between the actual value of each of the above variables and the value predicted using the complex terramechanics model depends on the variable and the application. But as a guideline the required maximum error is ±10%. The error percentage (E) is calculated using:

$$E = 100(v_{exp} - v_{model})/v_{max} \quad (5\text{-}2)$$

where v_{exp} is the experimental value of the variable, v_{model} is the model value, and v_{max} is the maximum practical absolute value of the variable. Some examples of v_{max} are:

- For wheel sinkage v_{max} is the tire radius.
- For engine torque v_{max} is the maximum engine torque.
- For vehicle speed $v_{max}$is the maximum operational vehicle speed.

Note that E is not normalized using v_{exp} because if v_{exp} is relatively small, it may result in artificially large error values.

5A.4.2 Ability to Predict Terrain Deformation/Damage Caused by the Vehicle

This includes the instantaneous (transient) 3D soil deformation/flow including soil bulldozing in front of the running gear, side rut formation, and separation/reattachment of the soil. It also includes the final resulting terrain deformation Figure 5A-12), including:

1) Rut depth below the undisturbed soil level.
2) Rut width.
3) Rut shape.
4) Rut side wall height above the undisturbed soil level.
5) Effect of vehicle operation on roads and other relatively hard surfaces. This includes:
   a) Terrain elastic deformation.
   b) Road/terrain damage. For example, a tank may severely damage urban hard surfaces so that they become a rougher terrain for subsequent vehicles.



Figure 5A-12: Terrain Damage Caused by a Vehicle Measured by the Rut Depth, Width, Shape and Side Wall Height.

This includes the ability to predict the above quantities along any direction, including:

1) Omni value: worst possible value in any direction;
2) Uphill value;
3) Downhill value;
4) Side-hill value;
5) Along a specified direction; and
6) Along the traverse direction.

As a guideline, the maximum error between the actual terrain deformation and that predicted by the complex terramechanics model is ±10% and is given by Equation (5-1).

5A.4.3 Ability to Accurately Predict Soil Mechanical Response for Small-Scale Terramechanics Experiments

Those include:

1) Quasi-static hydrostatic compression using a hydrostatic compression/triaxial cell or a piston-cylinder uniaxial compression test (Figure 5A-13). The model must be able to reproduce the bulk density versus currently applied hydrostatic pressure (e.g., Figure 5A-14). In addition, the model must be able to reproduce the bulk density versus previously applied hydrostatic pressure curve (i.e., the hydrostatic pressure is applied to compact the soil, then removed and the soil bulk density is measured).

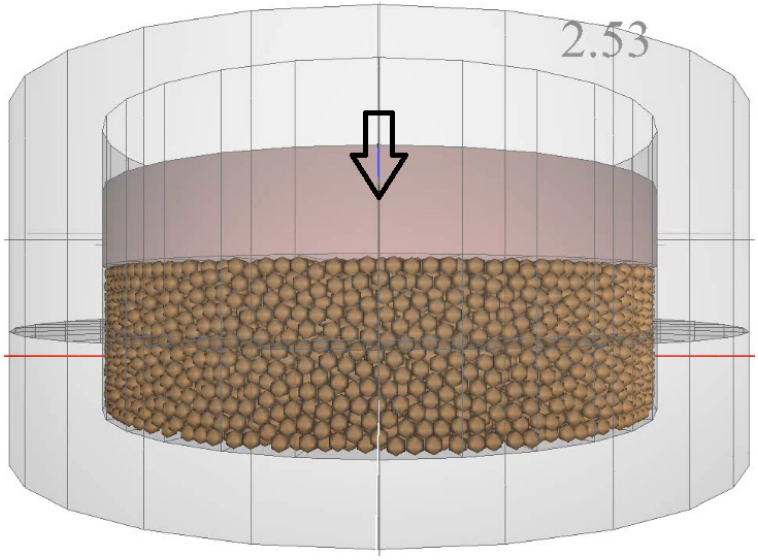


Figure 5A-13: Simulation of a Uniaxial Piston-Cylinder Soil Compression Test.

2) Shear using a shear cell (Figure 5A-15) [54], a triaxial cell (Figure 5A-16) [55], [56], a rotational bevameter (Figure 5A-17) [29], [57], [58], [59], or a translational shear plate (Figure 5A-18) [59]. The model must be able to reproduce the raw experiment results of shear stress versus shear displacement for varying current normal stress and previously applied normal stress when a quasi-static

shear displacement is applied. In addition, the model must be able to reproduce the end experiment results of current normal stress and previously applied normal stress versus maximum shear strength (e.g., Figure 5A-19). The angle that each line in Figure 5A-19 makes with the horizontal axis is the friction angle and the intercept with the vertical axis is the cohesion stress. Note that both the friction angle and the cohesion vary with previously applied normal stress, which determines the compaction state of the soil. It is also desirable that the model can predict the above instantaneous and maximum shear stress at high shear speeds in order to ensure that the model can capture viscous effects in the soil.

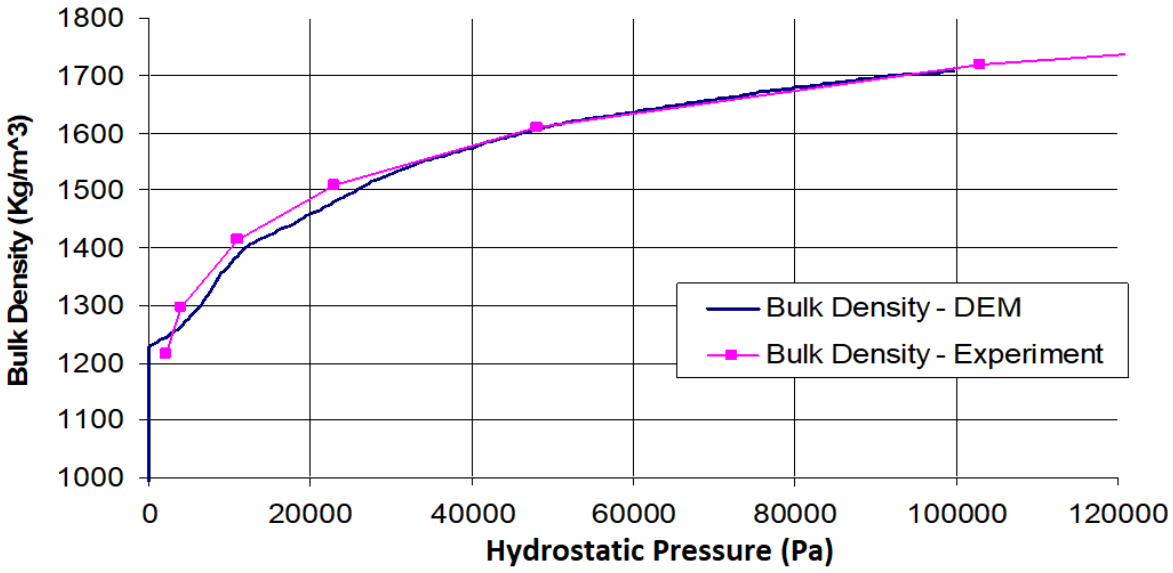


Figure 5A-14: Bulk Density Versus Hydrostatic Pressure Obtained Using a Hydrostatic Compression Test or a Uniaxial Piston-Cylinder Test.

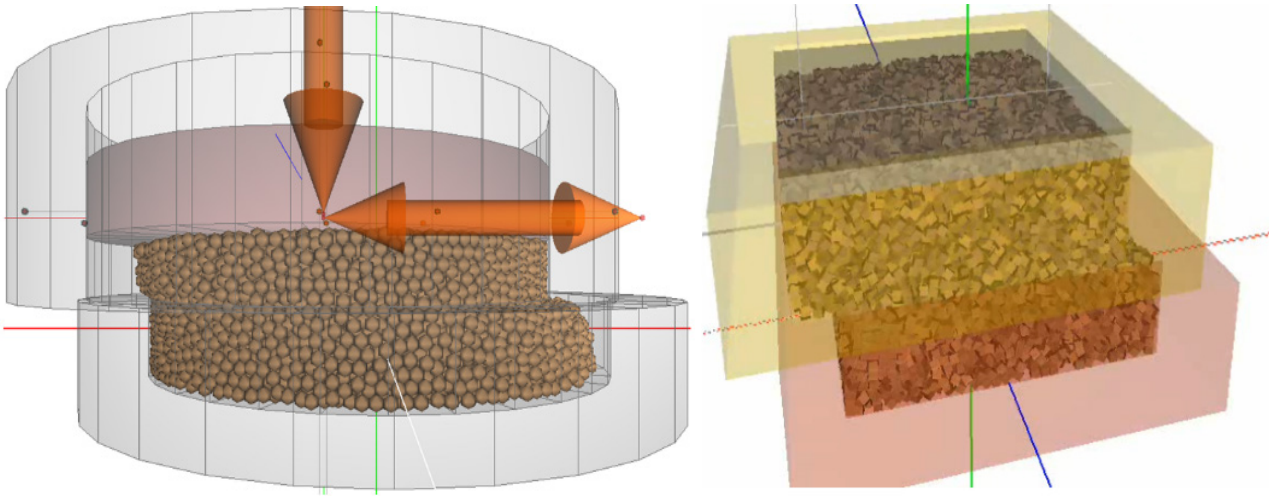


Figure 5A-15: Simulation of Cylindrical [3] and Cubical Shear Cells.

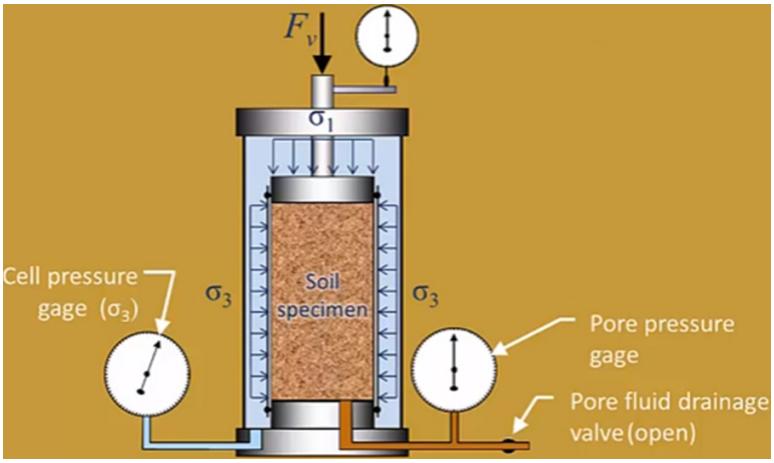


Figure 5A-16: Triaxial Cell [4], [5].

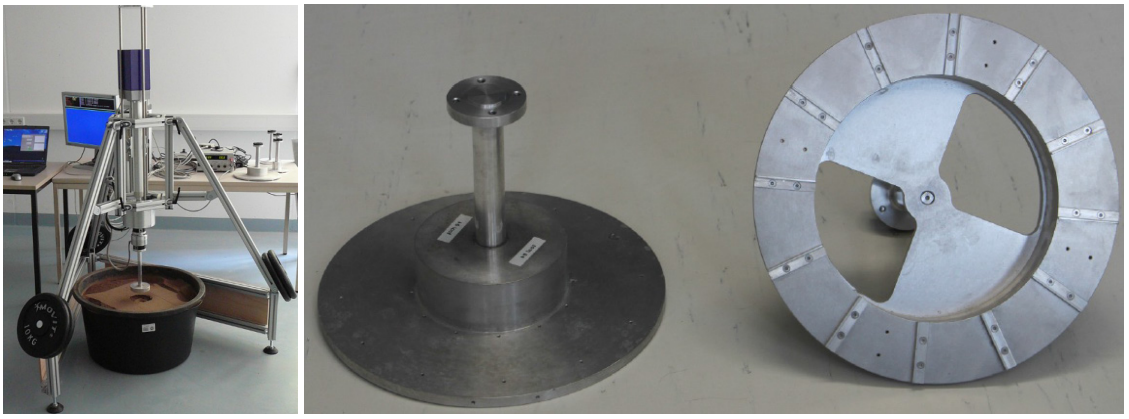


Figure 5A-17: Bevameter [6], [7], [8], [9].

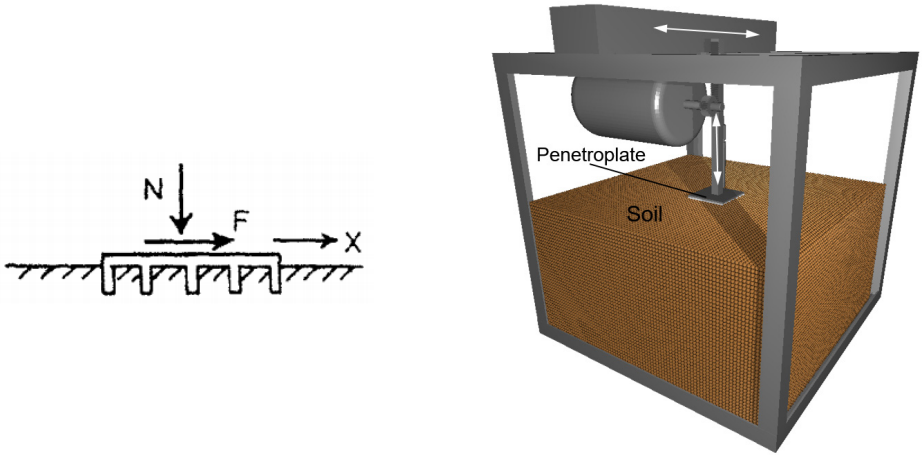


Figure 5A-18: Translational Shear Plate [9].

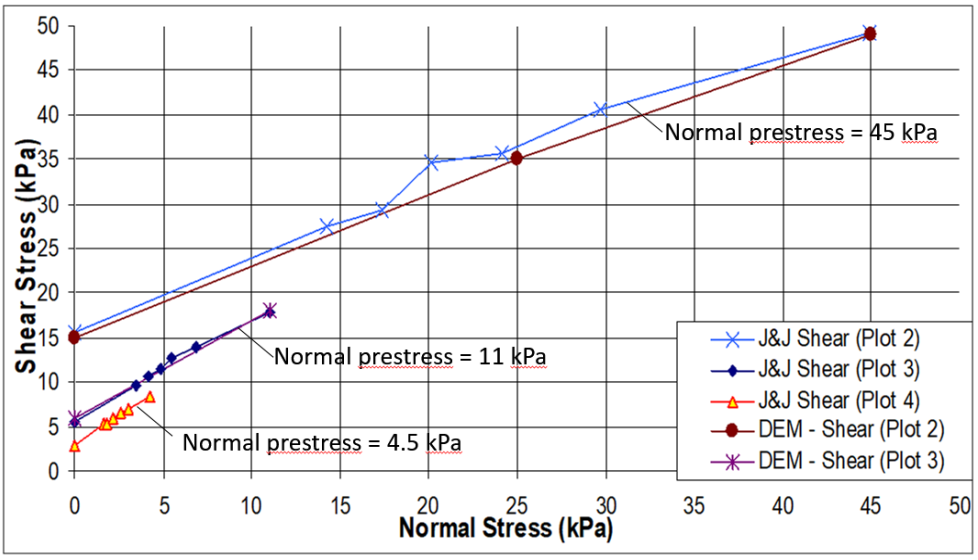


Figure 5A-19: Maximum Shear Stress Versus Current Normal Stress and Previously Applied Normal Stress Obtained Using a Shear Cell or a Triaxial Cell.

Note: Comparison of experiment and DEM simulation of shear stress vs. normal stress for different pre-shear normal stress levels. The angle between the X-axis and each curve is the soil friction angle and the intersection point of the curve with the Y-axis is the soil cohesive shear strength.

3) Penetrometer. The model must be able to reproduce the maximum normal pressure during the penetration into the soil at a prescribed slow speed (quasi-static load) as well the normal force versus penetration distance or time (Figure 5A-20 and Figure 5A-21). The penetrometer can be a standard 30° cone penetrometer [60], [61] (Figure 5A-22) or any other type such as a plate (Figure 5A-23) [59]. Also, it is desirable that the model can also predict the normal force versus penetration distance or time for different values of penetration speeds up to 10 m/s. This is needed in order to make sure that the soil model can accurately capture rate effects of the soil including damping and viscous effects.

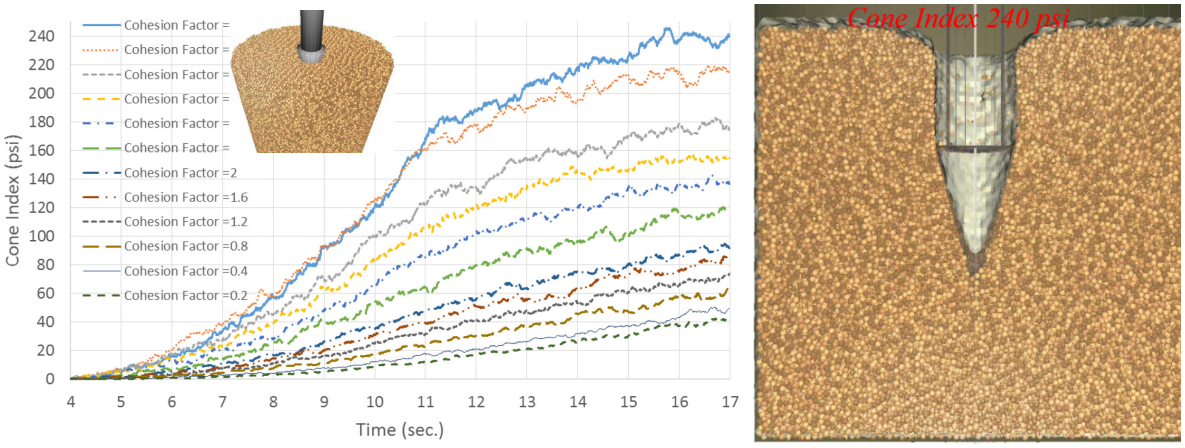


Figure 5A-20: Penetration Pressure Versus Time for 30° Angle Cone Penetrometer. (Right) Snapshot of the Cone during Penetration in a 240 Psi (Cohesion Factor = 12) Soil.

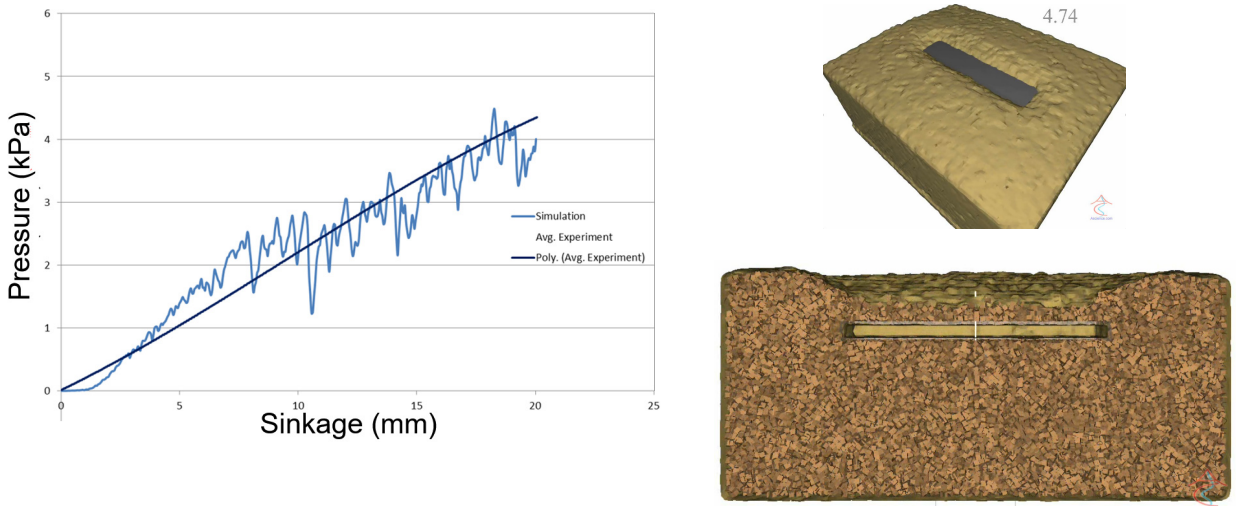


Figure 5A-21: Penetration Pressure Versus Sinkage for a Rectangular Penetroplate.

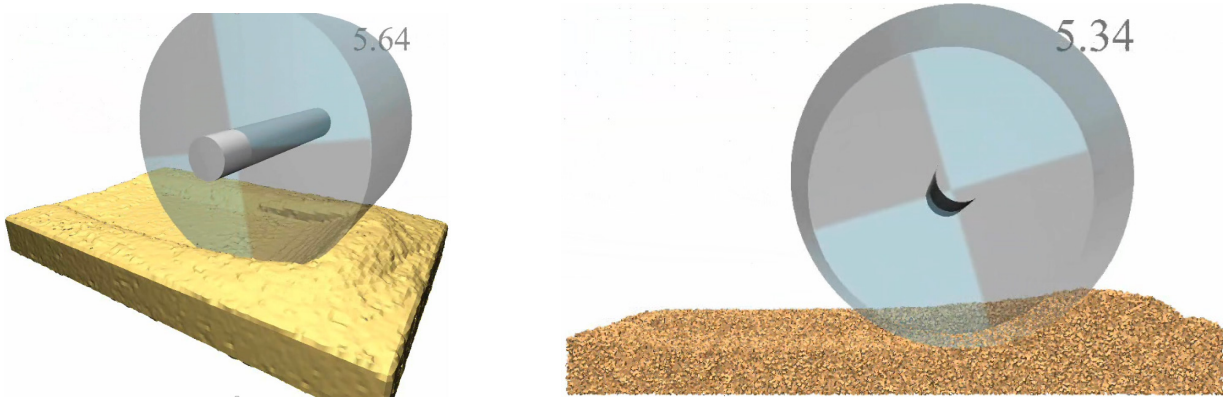


Figure 5A-22: DEM Model of a Rigid Wheel Moving on Soil.

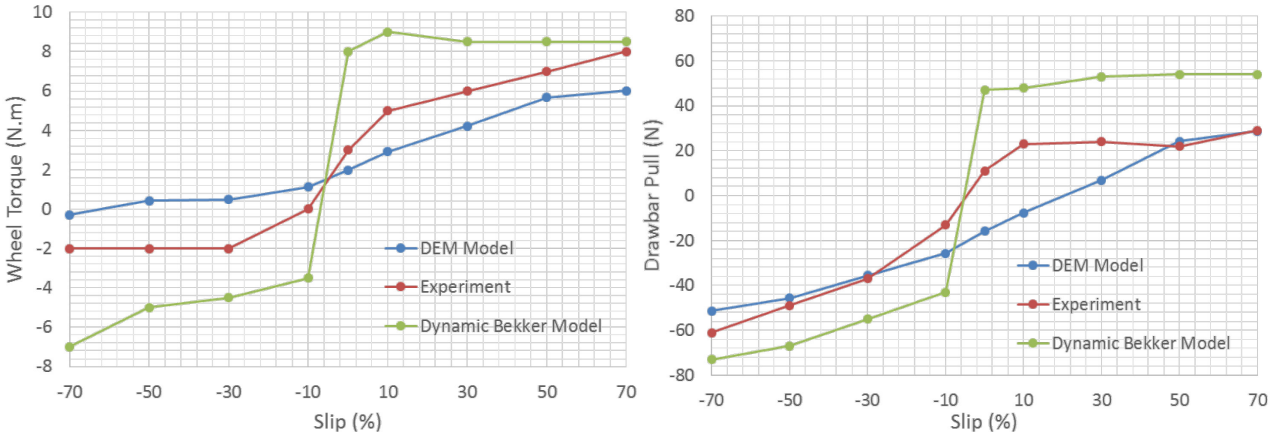


Figure 5A-23: Wheel Torque and Drawbar Pull versus Slip for a Rigid Wheel Moving on Soil.

4) Single rigid wheel (with or without grousers) on soil Figure 5A-22). The model must be able to reproduce the normal load, slip percentage, and linear speed versus drawbar force and wheel torque (Figure 5A-23).

Those experiments can be modeled using the complex terramechanics software tool (high-fidelity soil coupled with MBD) and the complex terramechanics model parameters can be fitted to the experimental data in order to calibrate the complex terramechanics models.

This also includes the ability to accurately predict small-scale terramechanics experiments for soil – wall surface material mechanical response, including:

1) Shear using a wall shear cell or a rotational bevameter [29], [57], [58], [59] or a translational shear plate [59] without grousers. The shearing surface is made out of the vehicle surface material such as rubber or steel. The model must be able to reproduce the end experiment results of current normal stress and previously applied normal stress versus maximum soil – wall shear strength (e.g., Figure 5A-19).
2) Soil adhesion to a plate as a function of applied normal stress. The plate is pressed against the soil using a certain normal stress, then the plate is lifted up. The amount of soil which adhered to the plate can be used to estimate the adhesion force between the plate material and the soil.

As a guideline, the maximum error between the small-scale terramechanics experiments and the complex terramechanics model is ±10% and is given by Equation (5-1).

5A.4.4 Ability to Reproduce the Mechanical Response of Worldwide Soils/Terrains

Worldwide soils/terrains include:

1) Natural worldwide soils including all USCS soil types [8] including the influence of the following physical conditions on the soil mechanical properties:
    a) Moisture at and between all Atterberg limits (Figure 5A-5) [1].
    b) Compaction state.
    c) Temperature including: freezing effects near the water freezing temperature; and effects of high temperatures (> 40°) on soil mechanical response especially in dry desert areas.
2) Roads and other hard surfaces including:
    a) Paved roads with any given 3D geometry, including asphalt, concrete, brick, and Belgian block. This also includes the ability to represent roads of various decaying conditions.
    b) Compacted dirt roads including gravel, sand, and clay roads.
    c) Hard urban surfaces including sidewalks made of brick, rock, or marble.

The mechanical soil response includes the following effects:

1) Traction of the vehicle running gear. This includes friction between the terrain and the running gear and shear strength of the terrain.
2) Change in soil bulk density as a function of soil compaction state (Figure 5A-14). Many soil types including moist soils and soil with organic material content are compressible. This means that the soil bulk density decreases with an applied compressive hydrostatic pressure. After removal of the hydrostatic stress,

the soil retains a part of the deformation (i.e., the residual bulk density is higher than the original uncompressed bulk density) which means the soil has undergone plastic deformation. The currently applied hydrostatic stress and previously applied hydrostatic stress define the soil compaction state.

3) Change in shear strength as a function of soil compaction state (Figure 5A-19). The soil shear strength is a function of the cohesion and internal friction. The currently applied hydrostatic stress and previously applied hydrostatic stress define the soil compaction state. When soil compaction increases, the soil cohesion increases and the internal friction also generally slightly increases. Hence soil shear strength increases with soil compaction.

4) Soil dilation. This includes reduction of bulk density and shear strength after tilling type loading (shearing and tension).

5) Velocity-dependent soil forces. It is desirable to have the ability to account for the velocity-dependent soil forces**.** Those can also be measured using the small-scale terramechanics tests listed above by applying the normal or shear displacement at a controlled speed:

   a) Soil normal stress as a function of normal strain rate (soil damping effects).

   b) Soil shear stress as a function of shear strain rate (soil viscosity effects).

6) Ability to account for adhesion of the soil to the vehicle surfaces. Figure 5A-24 shows a typical tire with moist organic soil stuck to it. Typically adhesion between the soil and vehicle surfaces increases with the increase in soil moisture below the soil liquid limit.



Figure 5A-24: Adhesion of Organic Soil to a Tire.

5A.4.5 Ability to Provide the Mapping Function that Maps the Physical Soil Properties into the Soil Mechanical Properties

Physical soil properties include USCS soil type, moisture content and temperature. The soil mechanical model properties are the properties required by the complex terramechanics software such as elasticity (Young's modulus), cohesive strength, friction angle, bulk density, etc. A database or mapping function *f* in Figure 5A-25, which gives the soil mechanical model properties in terms of the physical soil properties needs to be developed. This database/mapping can be experimentally developed using the small-scale terramechanics experiments in Section 5A.4.3 by performing the terramechanics experiments for all USCS soil types at different soil moisture contents and temperatures.

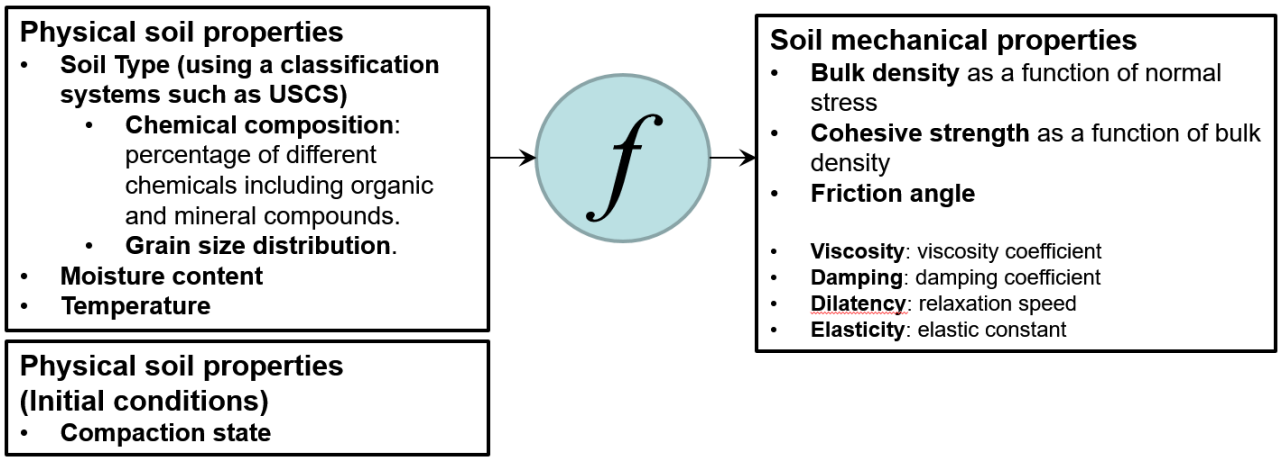


Figure 5A-25: Mapping of Soil Physical Properties to Soil Mechanical Properties Required by the Complex Terramechanics Software Tool.

In addition, another database/mapping is needed for the soil-vehicle surface model mechanical properties in terms of the physical soil properties and vehicle surface material type (Figure 5A-26). The soil-vehicle surface model mechanical properties required by the complex terramechanics software include adhesive strength and friction coefficient between the soil and the surface material. Again, this mapping can be experimentally developed using the small-scale terramechanics experiments in Section 5A.4.3 by performing the terramechanics experiments for all USCS soil types and vehicle surface material types at different soil moisture contents and temperatures.

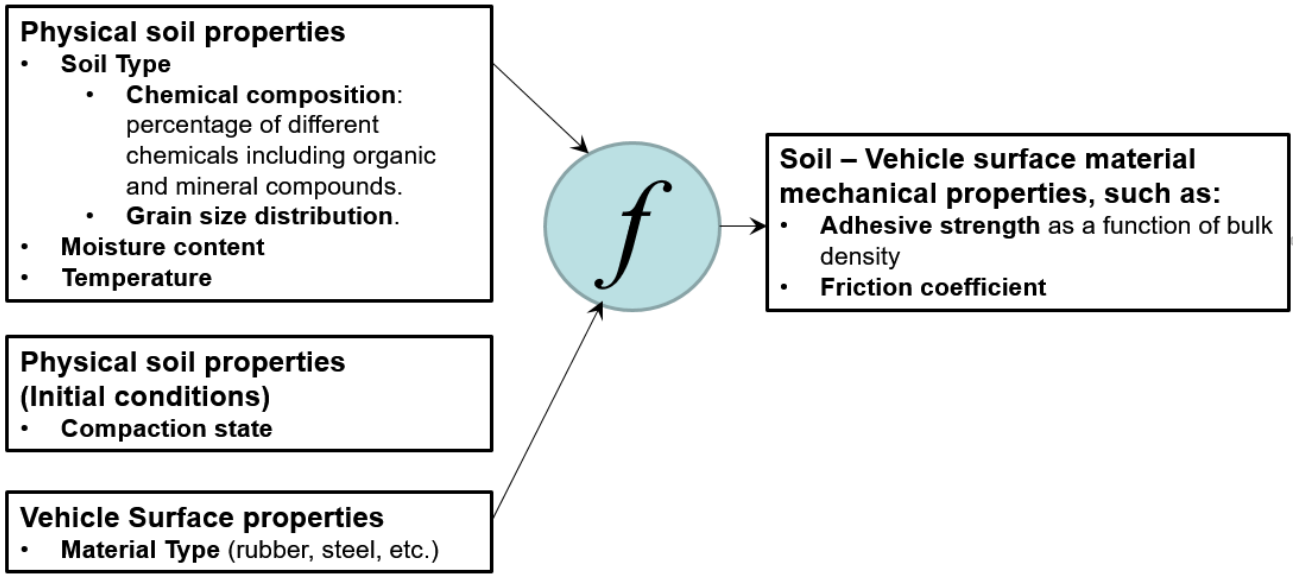


Figure 5A-26: Mapping of Soil Physical Properties and Vehicle Surface Material Type to Soil – Vehicle Surface Material Mechanical Properties Required by the Complex Terramechanics Software Tool.

5A.4.6 Ability to Represent Heterogeneous Terrains

Heterogeneous terrains are multi-component terrains which include:

1) Terrains which have discrete patches of different soil type.
2) Terrains with embedded boulders, rocks, stones, and/or gravel (e.g., Figure 5A-27). This includes modeling the mechanical properties at the interface between the soil and discrete terrain component including adhesion and friction.

The discrete terrain component can be specified by its size, shape, and spacing distributions as well as its mechanical properties.



Figure 5A-27: Soil Embedded Rocks, Stones, and Boulders.

5A.4.7 Ability to Represent Multiple Layers of Soil

Each layer can have different mechanical properties and each layer can have a different thickness. It is required that the complex terramechanics software tool support at least two soil layers. The layers can include:

1) Tilled soil (Figure 5A-28a).
2) Organic muskeg layer on compacted soil (Figure 5A-28b).
3) Snow and ice covered terrains (Figure 5A-28c). This includes the ability to model transition from snow to ice to water as vehicle passes over snow (melting effects).

5A.4.8 Ability to Represent Water Covered Terrains

This includes modeling the following effects for fording and swimming vehicles (Figure 5A-29):

1) Representing water resistance to the vehicle motion due to viscosity and inertia.
2) Representing soil entrainment/suspension in the water.
3) Including the effects of air bubble entrainment (that can affect vehicle buoyancy) due to rotation/motion of propellers, tires, and vehicle body.

4) Representing the soft soil water bottom which can include soft organic soil, sand, gravel, etc.
5) Modeling water currents including current speed and direction.
6) Modeling water waves direction and amplitude.
7) Ability to deal with multiple solid bodies moving and deforming arbitrarily in the flow field, and a liquid free surface with surface breakup and reattachment.
8) Ability to model the response/mobility of the vehicle during fording (when the vehicle is propelled by the wheels in contact with bottom soil) and swimming (when the vehicle is fully floating in the water).
9) Modeling propellers and water jets for swimming.
10) Transition of the vehicle from solid terrain to flooded terrain and vice versa.
11) Modeling different types of water bodies including swamps, rivers/streams, lakes, and seas/oceans.



(a) (b) (c)

Figure 5A-28: Terrain with a Top Layer of (a) Tilled Soil; (b) Organic Muskeg Soil; (c) Snow.



Figure 5A-29: Water Fording (Left) and Swimming (Right).

5A.4.9 Ability to Model Long Complex Topography Terrains

Support of arbitrarily long terrain is needed in order to allow the vehicle to accelerate until it reaches its maximum steady-state speed on the terrain. Complex terrain topography includes:

1) Discrete ditches specified by depth, width, and spacing distribution.
2) Discrete bumps specified by depth, width, and spacing distribution.
3) Sloped terrains: positive and negative long slopes and side slopes.
4) Roughness specified by the distribution (spectrum) of wave height versus wave length in two directions. The smallest wave length must be about $1/10^{th}$ of the smallest dimension of the running gear.
5) Terrain vertical height as a function of the X and Y horizontal terrain coordinates. The resolution should be about the same size as the smallest dimension of the vehicle running gear (such as tire or track segment).

5A.4.10 Ability to Represent All Types and Sizes of Vegetation Identified in USNVC

U.S. National Vegetation Classification (USNVC) is a scheme for classification of natural and cultural vegetation in the United States [62]. Vegetation can be further categorized into:

- Compliant vegetation including grasses, shrubs, bushes, crops, and small trees.
- Stiff vegetation (Figure 5A-30) including standing and fallen medium and large tree stems and branches.
- Fallen leaves.

Vegetation models entail the following:

1) Modeling the vegetation roots (including depth and size) and how they affect the soil mechanical response.
2) Modeling the frictional contact between the vegetation and vehicle, and the vegetation and the soil.
3) Accounting for the elastic axial, bending, and torsional stiffness/damping of the vegetation.
4) Accounting for breaking of the vegetation under axial, bending or torsional loads.
5) Accounting for the mechanical properties at the interface between the soil and the vegetation, including adhesion and friction.

The response quantities of interest include:

1) 3D motion/deflection/breakage of the vegetation.
2) 3D interaction forces between the vegetation and the vehicle.
3) GO/NOGO. Can the vehicle override the vegetation given the available engine power and the maximum traction the soil can support?
4) Override force at any vehicle speed and impact direction. The override force must be smaller than the force which will cause permanent deformation to the vehicle body.
5) Resistance force at any vehicle speed and impact direction.
6) Soil rut depth and width created by the vegetation.



Figure 5A-30: Soil Embedded Large Tree Stem or Pole Interacting with the Vehicle and the Soil.

5A.4.11 Ability to Represent Natural and Urban Obstacles

Natural obstacles (excluding vegetation) include rocks. Urban obstacles include poles (Figure 5A-30), walls (including brick, concrete, and sheet metal), fences (including metal wire, metal bars, and wood), bridges, tunnels, other vehicles, debris, and small structures. This includes:

1) Mechanical compliance and strength of the obstacle.
2) Interaction of the obstacle with the soil. The obstacle can be embedded/buried in the soil.
3) Obstacle parameters include type, geometry, and mechanical properties.
4) Mechanical properties at the interface between the soil and the obstacle, including adhesion and friction.

The response quantities of interest include:

1) 3D motion/deflection/breakage of the obstacle.
2) 3D interaction forces between the obstacle and the vehicle.
3) GO/NOGO. Can the vehicle override the obstacle given the available engine power and the maximum traction the soil can support?
4) Override force at any vehicle speed and impact direction. The override force must be smaller than the force which will cause permanent deformation to the vehicle body.
5) Resistance force at any vehicle speed and impact direction.
6) Soil rut depth and width created by the obstacle.

5A.4.12 Ability to Read the Terrain Input Data from GIS Software Tools

The terrain map is rasterized into cells of nearly the size of the vehicle (e.g., 10 m x 10 m). For each terrain cell, the following complex terramechanics input parameters need to be specified:

- Terrain topography:
  - Elevation above a known reference (such as sea level).
  - Slope/grade and slope/grade direction.
  - Roughness measure by spectrum of wave length versus roughness/height amplitude in two directions.
  - Maximum trench (negative obstacle) width, depth, and spacing.
  - Maximum bump (positive obstacle) width, depth, and spacing.
- Soil: Two to three layers each having:
  - Soil type (USCS), moisture, and temperature (those will map to the soil complex terramechanics model material parameters such as cohesion, friction, density, damping, and viscosity).
  - Layer thickness.
- Heterogeneous terrain:
  - Type: Embedded rocks, embedded debris, soil patches.
  - Shape distribution.
  - Size distribution.
  - Spacing distribution.
- Land use.
- Vegetation:
  - Vegetation type.
  - Root sizes and spacing distributions.
  - Stem sizes and spacing distributions.
- Urban obstacles, including:
  - Roads (different classes).
  - Ditches.
  - Buildings.
  - Poles.
  - Walls (brick, concrete, etc.).
  - Fences.
  - Structures.
  - Bridges.
  - Tunnels.
  - Vehicles.
  - Debris.

5A.4.13 Ability to Generate Terrain Mobility Maps and Display the Maps in GIS Software Tools

One of the main requirements of the integrated NG-NRMM software tool is to enable predicting the vehicle mobility measures on any given terrain map for operational analysis and mission planning purposes. Specifically, NG-NRMM will enable selecting the optimum vehicle path on a terrain map based on the mission requirements.

The complex terramechanics software tool must be able to read each terrain cell properties (Section 5A.4.12) and write the response quantities in Sections 5A.4.1 and 5A.4.2 for each terrain cell such that the terrain map can be colored using a desired response quantity. For example, in Figure 5A-31 a rectangular terrain map is colored using the Speed-Made-Good, which is one of the main output quantities of the integrated complex terramechanics and vehicle dynamics NG-NRMM software tool.

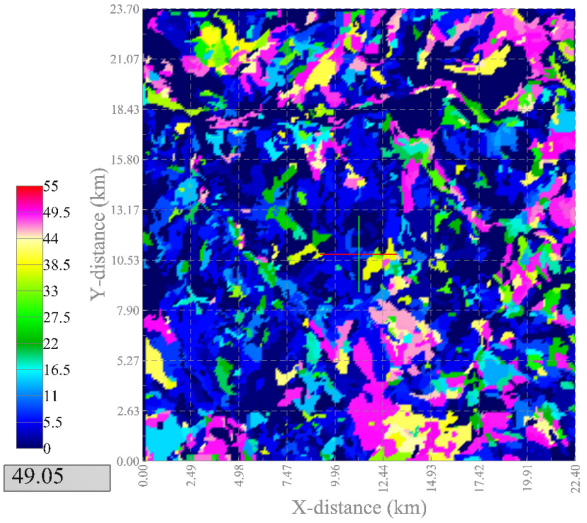


Figure 5A-31: Terrain Map Colored by the Speed-Made-Good.

Each of the above quantities can also have a probability distribution. Also each response quantity can be predicted at a desired confidence level from 0 to 100 %, where the confidence level indicates the probability that the actual response quantity will be at or better (above or below depending on the variable) than the predicted value (see Chapter 6).

5A.4.14 Ability to Conduct Coupled Simulations with Multibody Dynamics Software for Modeling the Vehicle

This includes the following capabilities:

1) Ability to model pneumatic tires. The tire model must have the following capabilities.
   a) Tire inflation pressure. Under-inflated tires typically yield high vehicle mobility on soft soil and low mobility on hard terrains, while the reverse is true for tire inflated to the nominal pressure. Those effects must be captured by the coupled complex terramechanics and flexible multibody dynamics tire/vehicle models.

b) Tire construction including layout and material properties of the ply, belt, and bead reinforcements and the rubber matrix.

c) Tire tread pattern.

2) Ability to model segmented tracks. This includes the effects of shoe grouser pattern and pad material on the vehicle mobility.

3) Ability to model continuous belt-type tracks. This includes:

a) Track construction including layout and material properties of the longitudinal and lateral track reinforcements and the rubber matrix.

b) Track tread pattern and track back (wheel) side pattern.

4) Ability to model the interaction of any vehicle part with the terrain. Those include:

a) Underbody.

b) Legs.

c) Blades and buckets.

d) Tines for tilling the soil and for mine sweeping.

5) Ability to model the vehicle systems necessary for mobility, including:

a) Suspension system.

b) Steering system.

c) Driveline.

d) Axles.

e) Engine.

f) Brakes.

g) Vehicle controls such as: Electronic Stability Control (ESC), Anti-lock Braking System (ABS), and Vehicle Intelligence (VI).

6) Ability to model vehicle payloads and occupants. Those include:

a) Military equipment including other vehicles.

b) Containers.

c) Liquid filled tanks.

d) Human occupants.

e) Trailers.

7) Ability to model the various types of vehicle maneuvers on any terrain in the full-vehicle speed range. Those include:

a) Steering: Single and double lane changes, and obstacle avoidance maneuvers.

b) Constant radius turning/cornering.

c) Neutral axis spin for tracked and legged vehicles.

d) Traveling in a prescribed path and speed on any given terrain (including side slopes, long slopes, and complex topography terrains).

e) Braking. This includes predicting the stopping distance from any initial speed.

5A.5 REFERENCES

[1] ASTM, ASTM D4318-10. 2010. Standard Test Methods for Liquid Limit, Plastic Limit, and Plasticity Index of Soils. ASTM International, West Conshohocken, PA.

[2] McFarlane, L.C. 1968. Strength and Deformation Tests on Frozen Peat, in Third International Peat Congress. Quebec, Canada. pp. 143-149.

[3] Vlahinić, I., Kawamoto, R., Andò, E., Viggiani, G. and Andrade, J.E. 2017. From Computed Tomography to Mechanics of Granular Materials via Level Set Bridge. Acta Geotechnica, 12(1):85-95.

[4] Tahmasebi, P., Sahimi, M. and Andrade, J.E.D. 2017. Image-Based Modeling of Granular Porous Media. Geophysical Ressearch Letters, 44(10):4738-4746.

[5] Höhner, D., Wirtz, S. and Scherer, V. 2012. A Numerical Study on the Influence of Particle Shape on Hopper Discharge Within the Polyhedral and Multi-Sphere Discrete Element Method. Powder Technology, 226:16-28.

[6] Wasfy, T.M., Ahmadi, S., Wasfy, H.M. and Peters, J.M. 2013. Multibody Dynamics Modeling of Sand Flow from a Hopper and Sand Angle of Repose. 2013 International Design Engineering Technical Conference, 9th International Conference on Multibody Systems, Nonlinear Dynamics, and Control (MSNDC).

[7] Beverloo, W.A., Leniger, H.A. and Velde. J.V.D. 1960. The Flow of Granular Solids Through Orifices. Chemical Engineering Science, 15(3-4):260-269.

[8] ASTM, ASTM Standard D2487. 2000. Standard Practice for Classification of Soils for Engineering Purposes (Unified Soil Classification System). ASTM International, West Conshohocken, PA.

[9] ASTM, ASTM D3282-15. 2015. Standard Practice for Classification of Soils and Soil-Aggregate Mixtures for Highway Construction Purposes. ASTM International, West Conshohocken, PA.

[10] Staff, S.S. 1999. Soil Taxonomy: A Basic System of Soil Classification for Making and Interpreting Soil Surveys. United States Department of Agriculture, Natural Resources Conservation Service, Washington, DC.

[11] Ahlvin, R. and Haley, P. 1992. NATO Reference Mobility Model Edition II, User's Guide, in Technical Report Number GL-92-19. U.S. Army Waterways Experiment Station, Corps of Engineers, Vicksburg, MS.

[12] Shoop, S.A. 2001. Finite Element Modeling of Tire – Terrain Interaction. US Army Corps of Engineers, Engineer Research and Development Center, Cold Regions Research and Engineering Laboratory, Hanover, NH.

[13] Shoop, S.A., Richmond, P.W. and Lacombe, J. 2006. Overview of Cold Regions Mobility Modeling at CRREL. Journal of Terramechanics, 43(1):1-26.

[14] Grujicic, M., Bell, W.C., Arakere, G. and Haque, I. 2009. Finite Element Analysis of the Effect of Up-Armouring on the Off-Road Braking and Sharp-Turn Performance of a High-Mobility Multi-Purpose Wheeled Vehicle. Proceedings of the Institution of Mechanical Engineers, Part D. Journal of Automobile Engineering, 223(11):1419-1434.

[15] Xia, K.M. 2011. Finite Element Modeling of Tire/Terrain Interaction: Application to Predicting Soil Compaction and Tire Mobility. Journal of Terramechanics, 48(2):113-123.

[16] Li, H. 2013. Analysis of Off-Road Tire-Soil Interaction Through Analytical and Finite Element Methods. University of Kaiserslautern, Department of Mechanical Engineering, Germany.

[17] Ragheb, H., El-Gindy, M. and Kishawy, H.A. 2013. Multi-Wheeled Combat Vehicle Modeling on Rigid and Soft Terrain. 2013 NDIA Ground Vehicle Systems Engineering and Technology Symposium, Modeling & Simulation, Testing and Validation (MSTV) mini-symposium, Troy, MI.

[18] Jafari, H. 2015. 3D Finite Element Model to Simulate the Rolling Resistance of a Radial Ply Tire Validated by Experiments in Soil Bin Testing Facility. Journal of Advances in Vehicle Engineering, 1(2):37-45.

[19] Wright, A. 2012. Tyre / Soil Interaction Modelling Within a Virtual Proving Ground Environment. Cranfield University, School of Applied Sciences.

[20] Ti, K.S., Huat, B.B.K., Noorzaei, J., Jaafar, M.D.S. and Sew, G.S. 2009. A Review of Basic Soil Constitutive Models for Geotechnical Application. Electronic Journal of Geotechnical Engineering, 14:1-18.

[21] Drucker, D.C. and Prager, W. 1952. Soil Mechanics and Plastic Analysis for Limit Design. Quarterly of Applied Mathematics, 10(2):157-165.

[22] Sandler, I.S. and Rubin, D. 1973. An Algorithm and a Modular Subroutine for the Cap Model. International Journal for Numerical and Analytical Methods in Geomechanics, 3:173-186.

[23] Dassault Systemes, 2016. Simulia, Abaqus Unified FEA, cited 2016; Available from: http://www.3ds.com/products-services/simulia/products/abaqus/.

[24] ESI-Group, Visual-Crash PAM, cited 2016; Available from: http://www.esi-group.com.

[25] Livermore Software Technology Corporation. LS-DYNA, cited 2016; Available from: http://www.lstc.com/products/ls-dyna.

[26] Chiroux, R.C., Foster, J., W.A., Johnson, C.E., Shoop, S.A. and Raper, R.L. 2005. Three Dimensional Finite Element Analysis of Soil Interaction with a Rigid Wheel. Applied Mathematics and Computation, 162:707-722.

[27] Shoop, S.A., Haehnel, R., Kestler, K., Stebbings, K. and Alger, R. 1999. Finite Element Analysis of a Wheel Rolling in Snow. 10th International Conference on Cold Regions Engineering, Lincoln, NH. pp. 519-530.

[28] Gornak, T. 2013. A Goal Oriented Survey on Immersed Boundary Methods. Berichte des Fraunhofer ITWM.

[29] Wong, J.Y. 2009. Terranechanics and Off-Road Vehicles (Second Edition). Elsevier, New York.

[30] Cundall, P.A. and Strack, O.D.L. 1979. A Discrete Numerical Model for Granular Assemblies. Geotechnique, 29(1):47-65.

[31] Cundall, P.A. 1971. A Computer Model for Simulating Progressive Large-Scale Movements In Block Rock Mechanics. Proc. Symp. Int. Soc. Rock Mech. Nancy.

[32] Carrillo, A., Horner, D., Peters, J. and West, J. 1996. Design of a Large Scale Discrete Element Soil Model for High Performance Computing Systems. Proceedings of the 1996 ACM/IEEE conference on Supercomputing.

[33] Horner, D., Peters, J. and Carrillo, A. 2001. Large Scale Discrete Element Modeling of Vehicle-Soil Interaction. Journal of Engineering Mechanics, 127:1027-1032.

[34] Peters, J.F., Hopkins, M.A., Kala, R. and Wahl, R.E. 2009. A Poly-Ellipsoid Particle for Non-Spherical Discrete Element Method. Engineering Computations, 26(6).

[35] Nakashima, H. and Oida, A. 2004. Algorithm and Implementation of Soil-Tire Contact Analysis Code Based on Dynamic FE-DE Method. Journal of Terramechanics, 41(2/3):127-137.

[36] Smith, W. and Peng, H. 2013. Modeling of Wheel – Soil Interaction Over Rough Terrain Using the Discrete Element Method. Journal of Terramechanics, 50(5-6):277-287.

[37] Negrut, D., Mazhar, H., Melanz, D., Lamb, D., Jayakumar, P., Letherwood, M., Jain, A. and Quadrelli, M. 2012. Investigating the Mobility of Light Autonomous Tracked Vehicles Using a High Performance Computing Simulation Capability. 2012 NDIA Ground Vehicle Systems Engineering and Technology Symposium, MSTV Mini-symposium, Troy, MI.

[38] Negrut, D., Melanz, D., Mazhar, H., Lamb, D., Jayakumar, P. and Letherwood, M. 2013. Investigating Through Simulation the Mobility of Light Tracked Vehicles Operating on Discrete Granular Terrain. SAE World Congress, SAE: Detroit, MI.

[39] Tasora, A., Anitescu, M., Negrini, S. and Negrut, D. 2013. A Compliant Visco-Plastic Particle Contact Model Based on Differential Variational Inequalities. International Journal of Non-Linear Mechanics.

[40] Wasfy, T.M., Wasfy, H.M. and Peters, J.M. 2014. Coupled Multibody Dynamics and Discrete Element Modeling of Vehicle Mobility on Cohesive Granular Terrains. 10th International Conference on Multibody Systems, Nonlinear Dynamics, and Control, ASME, Buffalo, NY.

[41] Sane, A., Wasfy, T.M., Wasfy, H.M. and Peters, J.M. 2015. Coupled Multibody Dynamics and Discrete Element Modeling of Bulldozers Cohesive Soil Moving Operation. 11th International Conference on Multibody Systems, Nonlinear Dynamics, and Control, ASME, Boston, MA.

[42] Wasfy, T.M., Wasfy, H.M. and Peters, J.M. 2015. High-Fidelity Multibody Dynamics Vehicle Model Coupled with a Cohesive Soil Discrete Element Model for Predicting Vehicle Mobility. 11th International Conference on Multibody Systems, Nonlinear Dynamics, and Control, ASME, Boston, MA.

[43] Wasfy, T.M., Jayakumar, P., Mechergui, D. and Sanikommu. S. 2016. Prediction of Vehicle Mobility on Large-Scale Soft-Soil Terrain Maps Using Physics-Based Simulation. 2016 NDIA Ground Vehicle Systems Engineering and Technology Symposium, Modeling & Simulation, Testing and Validation (MSTV) Technical Session, Novi, MI.

[44] Advanced Science and Automation Core, Dynamic Interactions Simulator (DIS). 2016. [cited 2016]; Available from: http://www.ascience.com/ScProducts.htm.

[45] Monaghan, J. 2005. Smoothed Particle Hydrodynamics. Rep. Prog. Phys., 68:1703-1759.

[46] Monaghan, J. and Gingold, R.J. 1977. Smoothed Particle Hydrodynamics. Mon. Not. Roy. Astr. Soc., 181:375-389.

[47] Lescoe, R., El-Gindy, M., Koudela, K., Öijer, F., Trivedi, M. and Johansson, I. 2010. Tire-Soil Modeling Using Finite Element Analysis and Smooth Particle Hydrodynamics Techniques. 2010 ASME International Design Engineering Technical Conferences and Computers and Information in Engineering Conference.

[48] Lescoe, R. 2010. Improvement of Soil Modeling in a Tire-Soil Interaction Using Finite Element Analysis and Smoothed Particle Hydrodynamics. Mechanical Engineering, Pennsylvania State University.

[49] Dhillon, R., Ali, R., El-Gindy, M., Philipps, D., Öijer, F. and Johansson, I. 2013. Development of Truck Tire-Soil Interaction Model using FEA and SPH. Proceedings of SAE 2013 World Congress, SAE, Detroit, MI, USA.

[50] Shokouhfar, S. 2017. A Virtual Test Platform for Analyses of Rolling Tyres on Rigid and Deformable Terrains. The Department of Mechanical and Industrial Engineering, Concordia University, Montréal, Québec, Canada.

[51] Sulsky, D., Zhou, S.-J. and Schreyer, H. 1995. Application of Particle-in-Cell Method to Solid Mechanics. Comp. Phys. Comm., 87:236-252.

[52] Stomakhin, A., Schroedery, C., Chai, L., Teran, J. and Selle, A. 2013. A Material Point Method for Snow Simulation. ACM Transactions on Graphics, 32(4):Article 102.

[53] Al-Kafaji, I.K.J. 2103. Formulation of a Dynamic Material Point Method (MPM) for Geomechanical Problems. Universität Stuttgart.

[54] ASTM Standard D6128-16. 2016. Standard Test Method for Shear Testing of Bulk Solids Using the Jenike Shear Cell. ASTM International, West Conshohocken, PA, USA.

[55] ASTM D4767-11. 2011. Standard Test Method for Consolidated Undrained Triaxial Compression Test for Cohesive Soils. ASTM International, West Conshohocken, PA, USA.

[56] ASTM D2850-15. 2015. Standard Test Method for Unconsolidated-Undrained Triaxial Compression Test on Cohesive Soils. ASTM International, West Conshohocken, PA, USA.

[57] Apfelbeck, M., Kuß, S., Rebele, B. and Schäfer, B. 2011. A Systematic Approach to Reliably Characterize Soils Based on Bevameter Testing. Journal of Terramechanics, 48(5):360-371.

[58] Bilanski, W.K. and Esperance, A.L.L. 1990. An Investigation of the Bevameter Soil Physical Measurements in the Prediction Of Soil Tool Draft. Journal of Terramechanics, 27(1):41-50.

[59] Shoop, S. 1993. Terrain Characterization for Trafficability. US Army Corps of Engineers, Cold Regions Research & Engineering Laboratory (CRREL).

[60] ASAE. 1985. Soil Cone Penetrometer, in Standard ASAE S3 13.2. American Society of Agricultural Engineers.

[61] SAE. 1967. Off-Road Vehicle Mobility Evaluation. SAE Recommended Practice Handbook Supplement. Society of Automotive Engineers (SAE), Warrendale, PA.

[62] Federal Geographic Data Committee – FGDC 2008 National Vegetation Classification Standard. FGDC-STD-005-2008 (Version 2). 2017. http://www.fgdc.gov/standards/projects/FGDC-standards-projects/vegetation/NVCS_V2_FINAL_2008-02.pdf.

Chapter 5B – TA3: DIS/GROUNDVEHICLE: COMPLEX TERRAMECHANICS PROTOTYPE

Tamer M. Wasfy
Advanced Science and Automation Corp.
UNITED STATES

5B.1 INTRODUCTION

The purpose of an NG-NRMM Complex Terramechanics compliant software tool is to predict the mobility measures listed in Section 5A.4.1 for any given ground vehicle, and terrain damage measures listed in Section 5A.4.2 on any given terrain map which can include the various terrain conditions identified in Sections 5A.4.4 to 5A.4.11. Thus, the final output of an NG-NRMM Complex Terramechanics software tool is a terrain mobility map of a vehicle mobility measure, such as Speed-Made-Good. In order to achieve this goal the Complex Terramechanics software tool must include high-fidelity coupled models of the vehicle and the terrain. This chapter will describe Advanced Science and Automation Corps (ASA) DIS/GroundVehicle complex terramechanics prototype software tool. Other Complex Terramechanics software tools will be described in Chapter 5C. The chapter will include the following sections:

- Key features of DIS/GroundVehicle related to ground vehicle mobility.

The capabilities of DIS/GroundVehicle corresponding to the fourteen requirements described in Section 5A.4.

- Procedure and demonstration for producing typical mobility terrain maps using DIS/GroundVehicle. This includes the Prototype Demonstration mobility terrain map of the Monterey Bay area.

5B.2 KEY FEATURES OF DIS/IVRESS

DIS/GroundVehicle can be used to predict the dynamic response of ground vehicles, including wheeled vehicles, tracked vehicles, small robotic vehicles, legged vehicles, tanker trucks with sloshing payloads, and amphibious vehicles, while rolling/sledding/walking on the hard and soft soil terrains, or fording/swimming in water. DIS/GroundVehicle is a user-friendly template-based interface to the DIS (Dynamic Interactions Simulator) solver [1], which is a general purpose computational mechanics code. DIS includes a virtual reality near-photorealistic visualization engine called IVRESS (Integrated Virtual Reality Environment for Synthesis and Simulation) which is used as a graphical pre- and post-processor [1]. DIS and IVRESS are both developed by ASA. Key features of **DIS/IVRESS** include:

1) Seamlessly integrating and coupling the following computational techniques into **One Solver**:
   a) **Multibody Dynamics (MBD)** for modeling rigid bodies, joints, frictional contact between bodies, rotary/linear actuators, and control algorithms.
   b) **Finite Element Method (FEM)** for modeling flexible bodies such as tires, flexible belt-type tracks, and suspension components such as leaf-springs.
   c) **Discrete Element Method (DEM)** for modeling granular non-cohesive soils (such as dry sand, gravel and rubble piles) and cohesive soils (such as wet sand/clay/silt, peat, muskeg or snow).
   d) **Smoothed Particle Hydrodynamics (SPH)** for modeling fluid interaction with rigid and flexible bodies including water (for fording and swimming) and air (for modeling vehicle aerodynamics).

The implementation and features of those computational techniques in DIS are described in the subsections below.

2) **Parallel Solver**. The DIS solver uses an explicit time integration solution methodology that is theoretically "embarrassingly" parallel and runs simultaneously on both distributed memory and/or shared memory Windows and Linux High Performance Computers (HPCs). In other words, the problem can be divided among many compute nodes as well as compute cores within one node. The actual parallel speed-up depends on the network bus bandwidth/speed and latency for distributed memory parallel processing, and shared memory bandwidth/speed and latency for shared memory parallel processing.

3) **Hierarchical Model Tree Editor and Graphical Scene Display/Editor**. Users can use IVRESS graphical pre-processor and model tree editor (Figure 5B-1) to graphically create the vehicle model and the mobility scenarios by creating the model objects, arranging them in a tree structure, then connecting the objects to each other using joints and contact surfaces (similar to how an actual vehicle is constructed). This includes a high-fidelity MBD/FEM model of the full vehicle(s), a DEM model of the soil, an SPH model of water pools, polygonal model of firm roads, desired vehicle(s) speed, and desired vehicle steering path.

4) **DIS/Ground Vehicle Template-Based Interface** for creating a high-fidelity vehicle model, terrain model, and mobility scenario. The template-based interface allows creating those models using spreadsheet tabular templates where the user can enter the parameters for each vehicle subsystem including: chassis (Figure 5B-2); suspension system, including double-wish-bone (Figure 5B-3), McPherson strut, leaf-spring, and walking beam; engine; steering system; gear box; differential; axles (solid-axle and independent suspension); tires; and tracks.

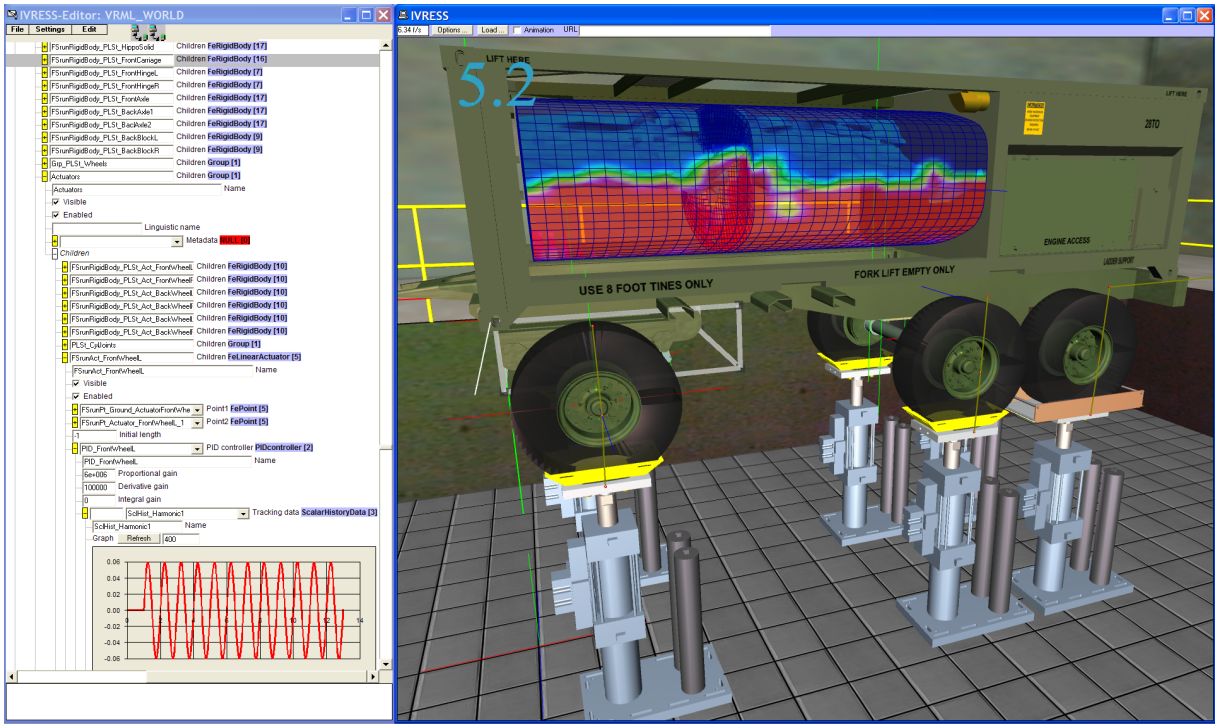


Figure 5B-1: IVRESS Model Tree Editor (Left) and Graphical Display Window (Right) for Creating Multibody Dynamics Vehicle Models and Simulation Scenarios.

Vehicle1	Comment:	This is a comment			
Parameter Description	**Symbol**	**Value1**	**Value2**	**Value3**	**Units**
Enable vehicle	*Enabled*	Yes			
Vehicle global position (ground point at center of front axle)	*GlobalPos*	0	0	0	
CG position (X, Y, Z) relative to center of front axle	*CG*	-1.2	0	0.5	m
Mass of frame/body	*M*	4000			kg
Inertia of frame/body around (length, width, height) direction	*I*	2160	8640	10000	kg.m^2
Off-diagonal Inertia of frame/body around (Ixy, Ixz, Iyz)	*Ioff*	0	0	0	kg.m^2
Frame icon file name	*File*	hummer_prt.wrl			
Frame icon translation (*X*, *Y*, *Z*)	*Trans*	-1.94	0	0.1	m
Frame icon scale (*X*, *Y*, *Z*)	*Scale*	1	1	1	
Euler Angles	*Angles*	90	90	0	degree
Initial icon visibility	*IconVisible*	No			
Front Axle	*FrontAxle*	Axle1			
Back Axle 1	*BackAxle1*	Axle2			
Back Axle 2	*BackAxle2*	None			
Steering	*Steering*	SteeringRackPinion1			
Motor	*Motor*	Motor1			
Vehicle Steering and Speed	*SteerAndSpeed*	SteeringAndSpeed1			
Air density	Ro_{Air}	1.225			kg/m^3
Vehicle frontal area	$Area_{Front}$	2			m^2
Vehicle side area	$Area_{Side}$	3.5			m^2
Vehicle top area	$Area_{Top}$	5			m^2
Characteristic lift length	L_{Lift}	2.8			m
Aerodynamic frontal drag coefficient	$C_{DragFront}$	0			
Aerodynamic side drag coefficient	$C_{DragSide}$	0			
Aerodynamic top drag coefficient	$C_{DragTop}$	0			
Aerodynamic lift coefficient	C_{Lift}	0			
Aerodynamic lift moment coefficient	$C_{MomLift}$	0			
Wind velocity	v_{wind}	0	0	0	m/s
Slave contact geometry file	*SlaveContFile*				
Slave contact geometry translation (*X*, *Y*, *Z*)	*TransSlave*	0	0	0	m

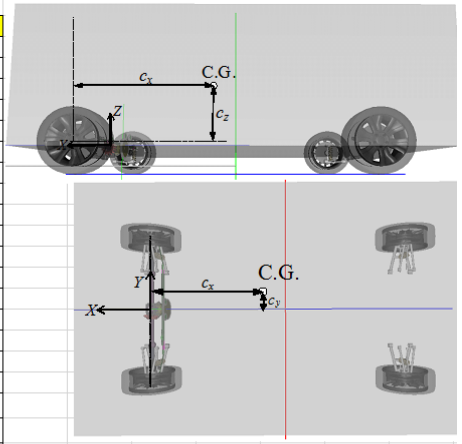


Figure 5B-2: DIS/Groundvehicle Spreadsheet Template for the Main Vehicle Frame.

SuspDBW1	Comment:	This is a comment ...			
Parameter Description	**Symbol**	**Value1**	**Value2**	**Value3**	**Units**
Hard points reference frame origin	*Origin*	*Axle Center*			
Upper control arm point P_1 (*X*, *Y*, *Z*)	p_1	0.15	0.43	0.068	m
Upper control arm point P_2 (*X*, *Y*, *Z*)	p_2	-0.15	0.43	0.068	m
Lower control arm point P_3 (*X*, *Y*, *Z*)	p_3	0.15	0.428	-0.137	m
Lower control arm point P_4 (*X*, *Y*, *Z*)	p_4	-0.15	0.428	-0.137	m
Upper knuckle point P_5 (*X*, *Y*, *Z*)	p_5	0	0.718	0.103	m
Lower knuckle point P_6 (*X*, *Y*, *Z*)	p_6	0	0.718	-0.137	m
Lower suspension strut point P_7 (*X*, *Y*, *Z*)	p_7	0.06	0.573	-0.11	m
Upper suspension strut point P_8 (*X*, *Y*, *Z*)	p_8	0.03	0.573	0.063	m
Lower Suspension Strut P_7 is connected to:	*StrutConn*	*Lower control arm*			
Strut Data	*Strut*	*Spring1*			
Mass of upper control arm	M_U	3			kg
Mass of lower control arm	M_L	3			kg
Mass of knuckle	M_K	3			kg
Moment of inertia of upper control arm	I_U	0.03	0.03	0.03	kg.m^2
Moment of inertia of lower control arm	I_L	0.03	0.03	0.03	kg.m^2
Moment of inertia of knuckle	I_K	0.03	0.03	0.03	kg.m^2
Upper control arm icon	$File_U$				
Upper control arm icon translation (*X*, *Y*, *Z*)	$Trans_U$	0	0	0	m
Upper control arm icon scale (*X*, *Y*, *Z*)	$Scale_U$	1	1	1	
Lower control arm icon	$File_L$				
Lower control arm icon translation (*X*, *Y*, *Z*)	$Trans_L$	0	0	0	m
Lower control arm icon scale (*X*, *Y*, *Z*)	$Scale_L$	1	1	1	
Knuckle icon	$File_K$				
Knuckle icon translation (*X*, *Y*, *Z*)	$Trans_K$	0	0	0	m
Knuckle icon scale (*X*, *Y*, *Z*)	$Scale_K$	1	1	1	
Automatically set joint stiffnees and damping	*AutoStiff*	AutoStiff			

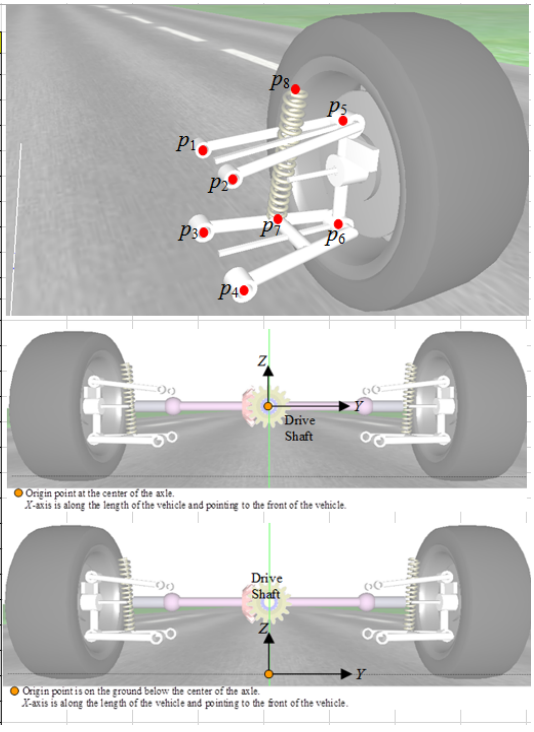


Figure 5B-3: DIS/GroundVehicle Spreadsheet Template for the Double-Wish-Bone Suspension System.

5) **Scientific Visualization Objects.** IVRESS post-processor can display colored/contoured surfaces, streamlines, iso-surfaces, cutting planes, and animated arrows/particles. For example, Figure 5B-4 shows a DEM particle density iso-surface representing the soil surface and DEM soil particles colored using height.

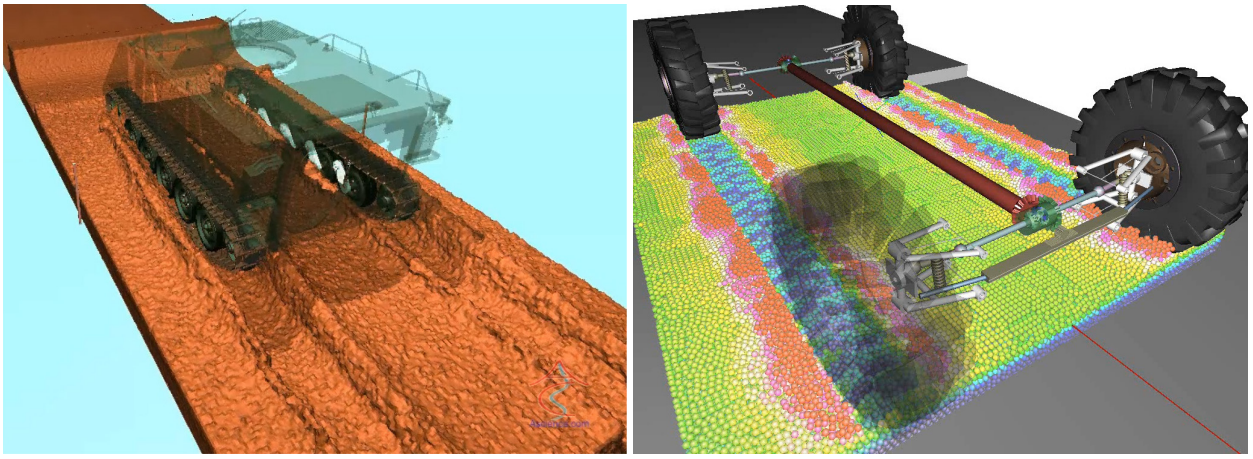


Figure 5B-4: DEM Particle Density Iso-Surface Showing the Surface of the Soil (Left) and DEM Soil Particles Colored using Height (Right).

6) **Network Socket Interface** for co-simulation with other software. This can be used to co-simulate with control software for: active suspension systems, steering/driver models, traction control, anti-lock braking, stability control, transmission/engine control, and navigation control (for autonomous and semi-autonomous vehicles).

7) **Integrated JAVAscript and Python Interpreters.** The scripts can also be used to model custom vehicle controls.

8) **Ability to Simulate and Visualize Any Number of Vehicles on the Same Terrain**. IVRESS/DIS is a general purpose computational mechanics code which uses an object-oriented hierarchical modeling framework. The framework can be used to create complex systems including multiple complex vehicle models with no limit to the complexity or size of the model except available computer memory.

9) **Real-time Simulation for Simple Models.** Simulations involving mechanical systems/vehicles with up to about 100 rigid bodies, can run in real-time. The real-time model can be used for driver training and virtual vehicle drivability/handling testing.

5B.2.1 Multibody Dynamics/Finite Element Method

Flexible multibody systems (MBD/FEM systems) which were modeled using DIS include: tracked vehicles, trucks, cars, bulldozers, backhoes, space telescopes, spacecraft, tires, automotive/industrial belt-drives, conveyor belts, timing belts, elevators, chain-drives, gear-boxes, toroidal Continuous Variable Transmission Systems (CVTs), brakes, robot arms, robotic manipulators, and walking robots/animals. The flexible multibody dynamics formulations/techniques used in **DIS** were presented in many publications.

Those techniques include:

- A semi-explicit time-integration solution procedure with a lumped mass and a lumped inertia tensor [2], [3]. The solution cost per time step is linearly proportional to the number of elements. Also, the solution procedure is embarrassingly parallel, i.e., the elements can be divided on available compute nodes and processor cores on each compute node, with a linear parallel speed-up.
- An algorithm for accurate accounting of rigid body rotational motion [4]. In this algorithm, the rotational equations of motion are written in a body fixed frame. Thus the body inertia tensor is constant. The total rotation matrix relative to the inertial frame is used to measure the rotation of the rigid bodies. Then, the total body rotation matrix is updated every time step using an incremental rotation matrix corresponding to incremental rotations angles, which are obtained by integrating the rotational equations of motion.
- The penalty technique is used for modeling joint constraints including spherical, revolute, cylindrical, prismatic, and Constant Velocity (CV) joints [4], [5].
- Master/slave contact model where contact is detected between discrete points on a master contact surface and a polygonal slave contact surface [6], [7], [8], [9], [10].
- General fast binary-tree hierarchical bounding box/sphere contact search algorithm for finding the contact penetration between points on the master contact surfaces and polygons on slave contact surfaces [9], [10].
- Penalty technique for imposing the normal contact constraints [6], [7], [8], [9], [10].
- Friction (for joints, contact surfaces, and DEM/SPH particles) is modeled using an accurate and efficient asperity-based friction model [7], [11].
- Total-Lagrangian lumped parameters 3D large rotation and deformation finite elements including spring/truss, thin beam [12], thin shell [2], thick beam [13], and solid brick finite elements [14], [15]. The elements can be used to model flexible components undergoing large rotations and large deflections such as tires [7] and belt-type tracks [9].
- Ability to model stiff bodies using the component mode synthesis technique. First, the finite element model of the body is used to calculate the stiffness, damping and mass matrix of the body. Then the body vibration mode shapes are extracted. Then, the component mode synthesis [16], [17], [18], [19] approach is used to predict the dynamic response of the stiff body coupled with the rest of the multibody system. Note that the component mode synthesis method is only valid for relatively stiff bodies which can only undergo small deflections.
- Hierarchical object-oriented framework which enables creating large complex vehicle models [20], [21], [22], [23]. The modeling objects include rigid body; flexible bodies (thick beam, shell, general solid, and belt); joints (spherical, revolute, cylindrical, and prismatic); rigid and flexible contact surfaces; linear and rotary actuators; PID controller; and user-defined scripts (in JAVAscript or Python Script). Using those basic objects the user can create any hierarchical flexible multibody system using the model tree editor and the graphical on-screen model editor.
- Inverse kinematics/dynamics for automatically calculating joint angles/torques for kinematic chains consisting of any number of bodies connected using revolute or prismatic joints given the desired end-effector motion. The inverse kinematics problem is solved using Newton's method, a numerically calculated Jacobian, along with a Moore-Penrose pseudoinverse of the Jacobian [24]. Figure 5B-5 shows a DIS simulation of a humanoid robot arm catching a ball that uses inverse kinematics along

with rotary actuators and PID control at each joint. DIS also includes a walking controller that uses inverse kinematics for the legs. The walking controller can be used to simulate stable natural walking motion on two or more legs (Figure 5B-6).

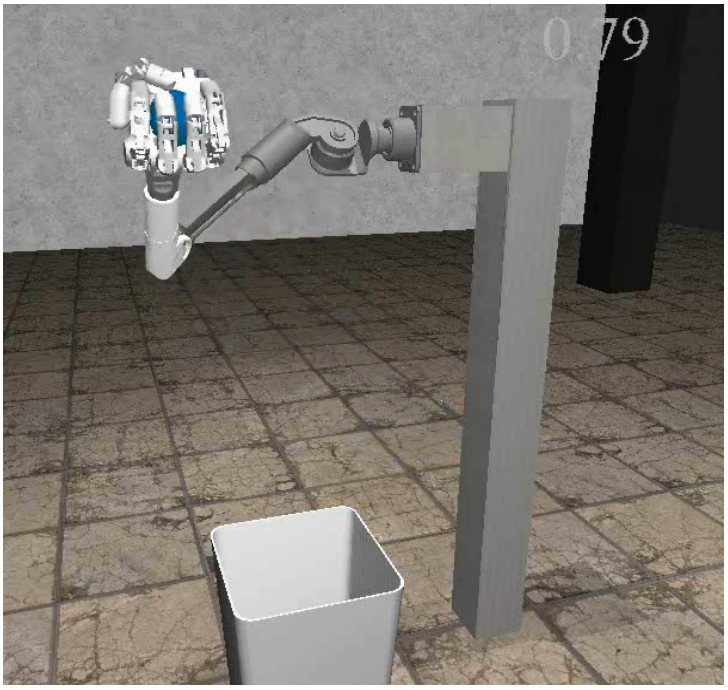


Figure 5B-5: DIS Simulation of a Humanoid Robot Arm Catching a Ball.

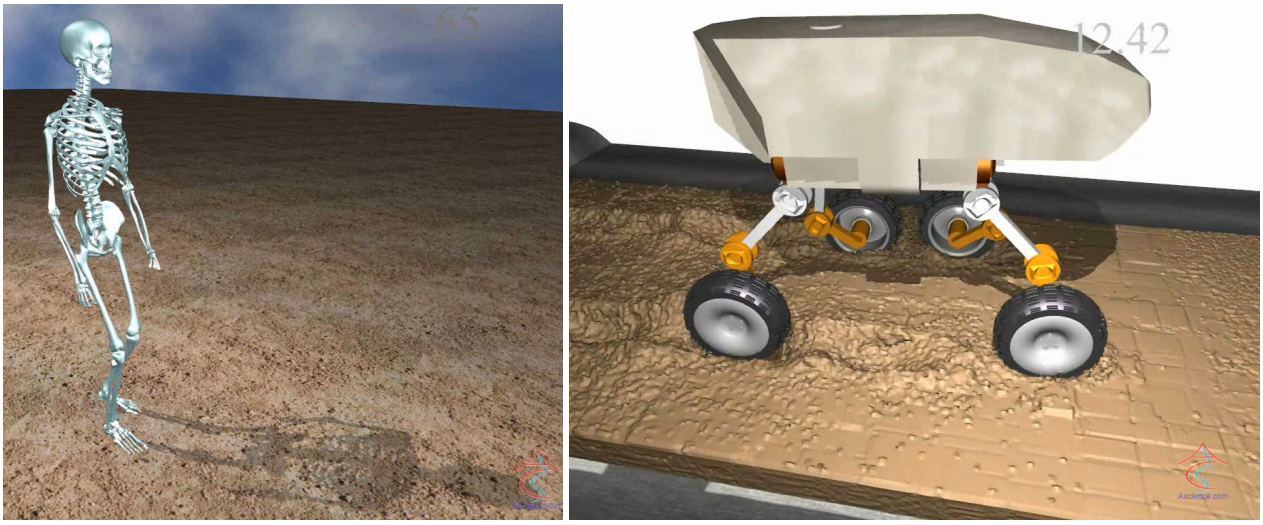


Figure 5B-6: DIS Simulation of a 2-Legged Humanoid Robot and a 4-Legged Walking Vehicle on Soft DEM Soil.

5B.2.2 Discrete Element Method

DIS's DEM capabilities were used to model many types of cohesive and non-cohesive bulk and granular materials interacting with various mechanical systems. Those include:

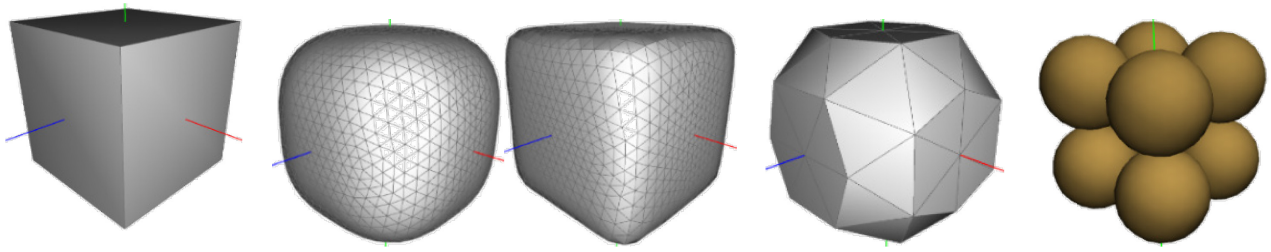
- Wheeled, tracked and legged ground vehicle (soft soil interactions in off-road vehicle mobility simulations).
- Earth moving equipment simulations, including bulldozers and backhoes.
- Bulk material conveyor belts and handling equipment.

The DEM formulation used in the DIS code was presented in Refs. [25], [26], [27], [28], [29], [30]. DEM particles can be either point particles which have only translational Degrees Of Freedom (DOFs) and no rotational DOFs or rigid body type particles with both translational and rotational DOFs. Point particles can only have a spherical shape since their orientation is not tracked. Point particles are suitable for modeling isotropic soil materials for which the continuum assumption is a good approximation such as fine grained cohesive and non-cohesive soils and snow. Point particles are about 3 to 5 times faster computationally than rigid body type particles. Figure 5B-7 shows examples of soils modeled using point particles. Rigid body particles are suitable for modeling granular materials with relatively large grains such as sand and gravel. For rigid body particles, the particle shape (and consequently contact penetration) can be defined using the following shapes (Figure 5B-7):

- Simple primitives including sphere, rectangular cube, ellipsoid, elliptical cylinder, cone, or torus.
- Superquadric surface defined by the equation:

$$\left(\frac{x_1}{r_1}\right)^{p_1} + \left(\frac{x_2}{r_2}\right)^{p_2} + \left(\frac{x_3}{r_3}\right)^{p_3} = 1 \qquad \text{(5B-1)}$$

  where x_i are the spatial coordinates on the surface of the particles, r_i and p_i (i = 1, 2, 3) are adjustable constants which are used to define the particle shape.
- Polygonal surface.
- Glued primitive shapes. Any of the above shapes can be "glued" together to form one particle.



(a) (b) (c) (d)

Figure 5B-7: DIS DEM Rigid Body Particle Shapes. (a) Simple Primitives Such as a Rectangular Cube; (b) Superquadric; (c) Polygonal; (d) Glued Primitive Shapes Such as Eight Glued Spheres.

In general any particle shape geometric description which allows determining the signed distance and normal vector between any point and the surface of the particle can be used to define the shape of a rigid

body particle. Figure 5B-8 shows an example of sand flow from a hopper with the sand modeled using rigid body cubical particles.

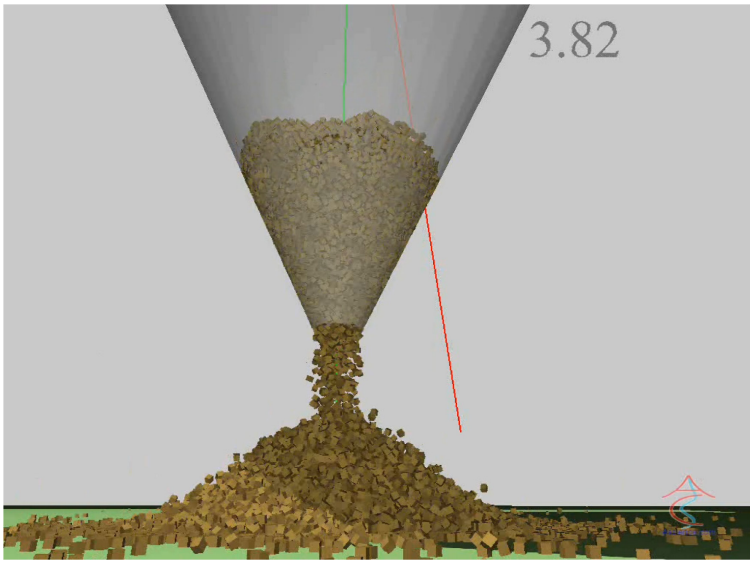


Figure 5B-8: Sand Flow from a Hopper with the Sand Modeled using Cubical Particles. Master Surface is Modeled using Eight Glued Spheres and Slave Surface Modeled Using a Primitive Cube.

The inter-particle and particle-to-vehicle surface (such as tires, wheels and track segments) contact force (F_{ci}) is given by:

$$F_{c_i} = F_{n_i} + F_{t_i} \tag{5B-2}$$

where i = 1, 2, 3. The contact force vector is divided into a normal force (F_{n_i}) and a tangential force (F_{t_i}) vectors given by (Figure 5B-9):

$$F_{n_i} = n_i \left|F_n\right| \tag{5B-3}$$

$$F_{t_i} = t_i \left|F_t\right| \tag{5B-4}$$

where n_i is the surface normal unit vector, t_i is a unit vector along the tangential velocity direction, and $\left|F_n\right|$ and $\left|F_t\right|$ are the magnitudes of the normal and tangential forces, respectively. $\left|F_n\right|$ is calculated using:

$$\left|F_n\right| = F_{adhesion} + F_{repulsion} + F_{damping} \tag{5B-5}$$

where:

$$F_{damping} = c_n \dot{d} \tag{5B-6}$$

where $F_{adhesion}$ is the adhesion (cohesive) force, $F_{repulsion}$ is the repulsive force, $F_{damping}$ is the damping force, d is the penetration, $\dot{d}$ is the penetration rate, and c_n is the penalty damping coefficient. Note that c_n can be specified as a function of d and $\dot{d}$.

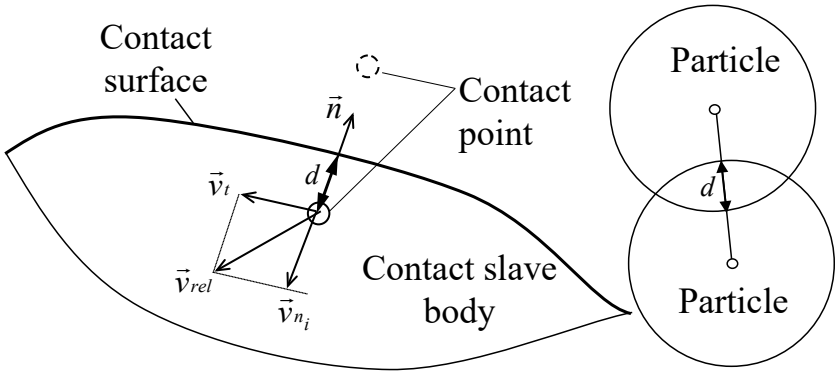


Figure 5B-9: Contact Surface and Contact Point, and Particle-to-Particle Contact. D is The Penetration.

$F_{adhesion}$ and $F_{repulsion}$ are both specified as a function of penetration d (Figure 5B-10). Up to a penetration distance d_0 the contact forces are adhesive (attractive). A force greater than $F_{adhesion,max}$ is needed to separate the two bodies. If the penetration exceeds d_0 then the contact force becomes repulsive thus opposing further penetration. The adhesive force along with the friction force contribute to the shear strength of the soil. Note that the adhesive and the repulsive force can be a non-linear function of d. The actual shape of the curve in Figure 5B-10 can be tuned using experimental data or an analytical contact model such as Hertzian contact. Also note that $F_{repulsion}$ versus d defines the elastic behavior of the DEM particle.

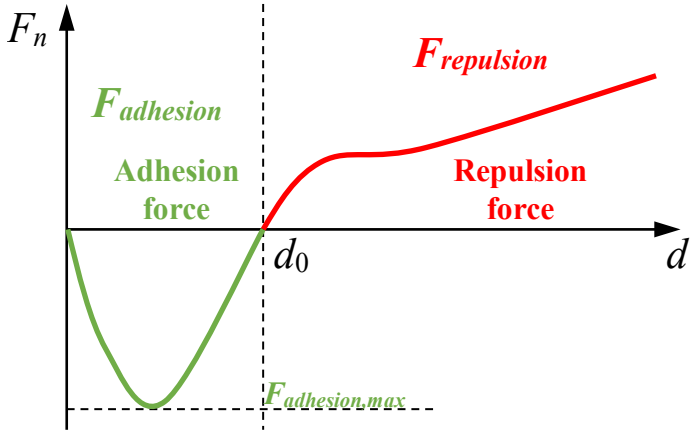


Figure 5B-10: Particle Adhesion and Repulsion Forces as a Function of Inter-Particle Penetration Distance (D).

In order to model soil plasticity which is also the permanent change of bulk density with soil compaction state, the plastic deformation ($\delta_{plastic}$) of a DEM particle is specified as a function of repulsive (compression) force ($F_{repulsion}$). The radius of a particle's contact surface is reduced by an amount equal to $\delta_{plastic}$. Figure 5B-11 shows a

typical particle plastic strain curve versus compressive stress. The $\delta_{plastic}$ versus $F_{repulsion}$ curve can be tuned to match the bulk density versus hydrostatic pressure curve for the soil (Figure A-14) obtained using a piston-cylinder soil uniaxial compression experiment (Figure A-13) or a hydrostatic compression test. The elastic behavior of the DEM particle defined using $F_{repulsion}$ versus d, can be tuned using the recoil of the soil bulk density when the normal hydrostatic stress is removed.

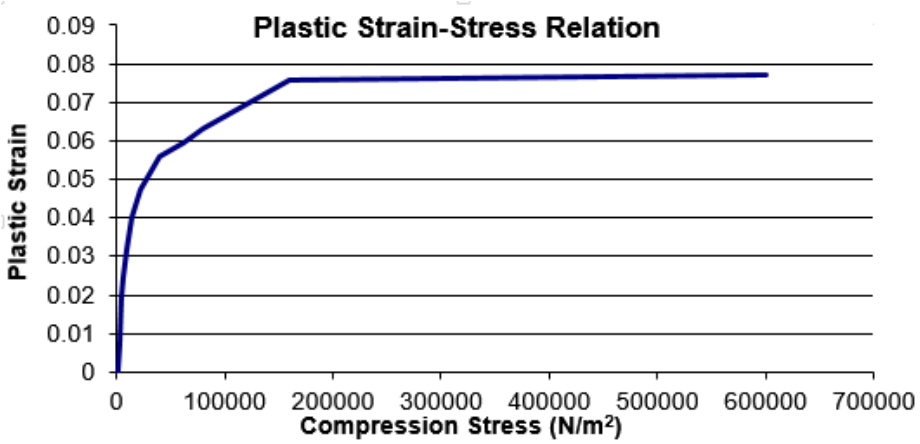


Figure 5B-11: Typical Curve of Particle Plastic Strain as a Function of Compressive Stress.

In order to account for the increase in soil cohesive strength of compacted soil, the maximum adhesive force ($F_{adhesion,max}$) in Figure 5B-10 is specified as a function of the plastic deformation. For example, Figure 5B-12 shows a typical maximum adhesion stress versus plastic strain for a DEM particle. Also note that the friction coefficient (μ), viscosity coefficient (c_n) and damping coefficient (c_t) can also be specified as a function of the plastic deformation ($\delta_{plastic}$). The curve in Figure 5B-12 along with the friction coefficient can be tuned to match the shear stress versus normal stress for different consolidation normal stress values obtained using a shear cell [31] (e.g., Figure 5A-19). In Figure 5A-19 the angle between the x-axis and each curve is the soil friction angle and the intersection point with the y-axis is the soil cohesive strength. This figure can be obtained using a simulation of shear cell (Figure 5A-15) or a triaxial cell (Figure 5A-16).

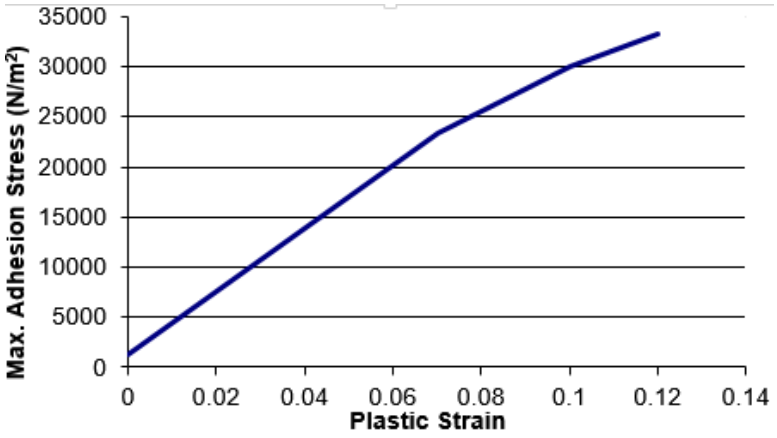


Figure 5B-12: Typical Maximum Adhesive Stress Versus Plastic Strain Curve.

In order to account for soil dilation which is the reduction of soil bulk density and soil cohesive strength due to shear/tension (removal of compression), a time relaxation is applied to the soil plastic deformation at each time step:

$$\delta_{plastic} = \delta_{plastic} - \begin{cases} 0 & F_{repulsion} \geq F_{adhesion,\max} \\ V_{relax} \times \Delta t & F_{repulsion} < F_{adhesion,\max} \end{cases} \quad \text{(5B-7)}$$

where V_{relax} is the speed of plastic relaxation (in distance/time) and Δt is the explicit solution time step. If the particle's repulsive (compressive) force (maximum force value over all adjacent particles) is larger than the maximum adhesive (tensile) force then the particle plastic deformation is left unchanged. If the particle repulsive force is smaller than the maximum adhesion force, then the particle plastic deformation is reduced at a speed of V_{relax}. The smallest allowable plastic deformation value is zero. The value of V_{relax} is experimentally tuned.

The tangential force $|F_t|$ is calculated using:

$$|F_t| = F_{viscous} + F_{friction} \quad \text{(5B-8)}$$

$$F_{viscous} = c_t |v_t| \quad \text{(5B-9)}$$

where:

$$|v_t| = \sqrt{{v_{t_1}}^2 + {v_{t_2}}^2 + {v_{t_3}}^2} \quad \text{(5B-10)}$$

c_t is the viscosity coefficient and $|v_t|$ is the tangential velocity magnitude Figure 5B-11). An asperity friction model is used along with the normal repulsion ($F_{repulsion}$) force to calculate the tangential friction force ($F_{friction}$) [11]. In this model, friction is modeled using a piece-wise linear velocity-dependent approximate Coulomb friction element in parallel with a variable anchor point spring. The model approximates asperity friction where friction forces between two rough surfaces in contact arise due to the interaction of the surface asperities (Figure 5B-13).

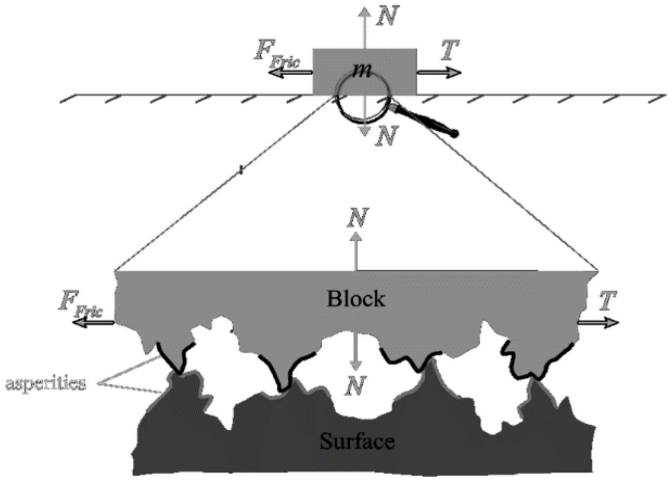


Figure 5B-13: Asperity-Based Physical Interpretation of Friction.

When two surfaces are in static (stick) contact, the surface asperities act like tangential springs. When a tangential force is applied, the springs elastically deform and pull the surfaces to their original position. If the tangential force is large enough, the surface asperities yield (i.e., the springs break) allowing sliding to occur between the two surfaces. The breakaway force is proportional to the normal repulsion contact force ($F_{repulsion}$). In addition, when the two surfaces are sliding past each other, the asperities provide resistance to the motion that is a function of the sliding velocity and acceleration, and the normal repulsion contact force. Figure 5B-14 shows a schematic diagram of the asperity friction model. It is composed of a simple piece-wise linear velocity-dependent approximate Coulomb friction element in parallel with a variable anchor point spring.

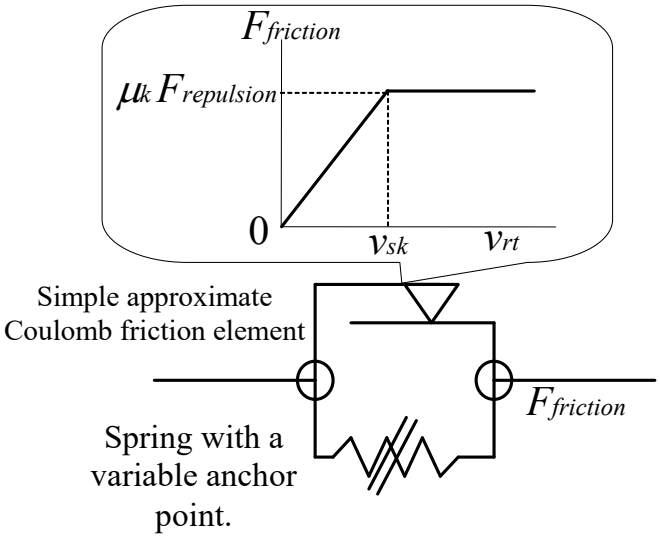


Figure 5B-14: Asperity-Spring Friction Model. $F_{friction}$ is the Tangential Friction Force, $F_{repulsion}$ is the Normal Repulsion Force, μ_k is the Kinetic Friction Coefficient, and v_{rt} is the Relative Tangential Velocity between the two Points in Contact.

Note that in order to connect two points on two bodies using an asperity spring, the model must keep track of which rigid bodies are in contact and of the local position vectors of the asperity-spring anchor points on the two contacting bodies. Also, note that the two rigid bodies can be in contact at more than one point, therefore the model must keep track of the corresponding contact points on the two contact bodies. The force model can be tuned/calibrated to a particular soil material using the following experiments:

- Piston-cylinder uniaxial compression apparatus for measuring the soil bulk density versus consolidating pressure (Figure 5A-13).
- Shear apparatus [31] for measuring the soil cohesive strength and internal friction as a function of consolidation pressure and applied normal pressure (Figure 5A-15).
- Cone (Figure 5A-20) and plate penetrometers (Figure 5A-21) can also be used to measure the soil shear strength and tune the DEM model cohesive strength and inter-particle friction coefficient.
- Angle of repose of a material pile (Figure 5B-15) can be used to tune the unconsolidated (loose) soil cohesive strength and inter-particle friction coefficient.
- Flow rate from hoppers (Figure 5B-16) can be used to tune the soil cohesive strength, inter-particle friction coefficient, and wall adhesion/friction.

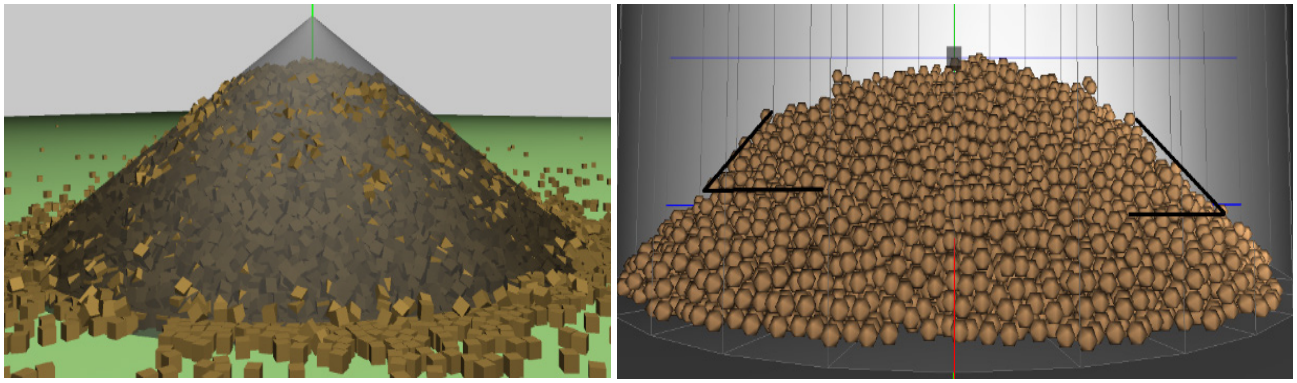


Figure 5B-15: Angle of Repose of a Material Pile: Gravel (Left) and Mud (Right).

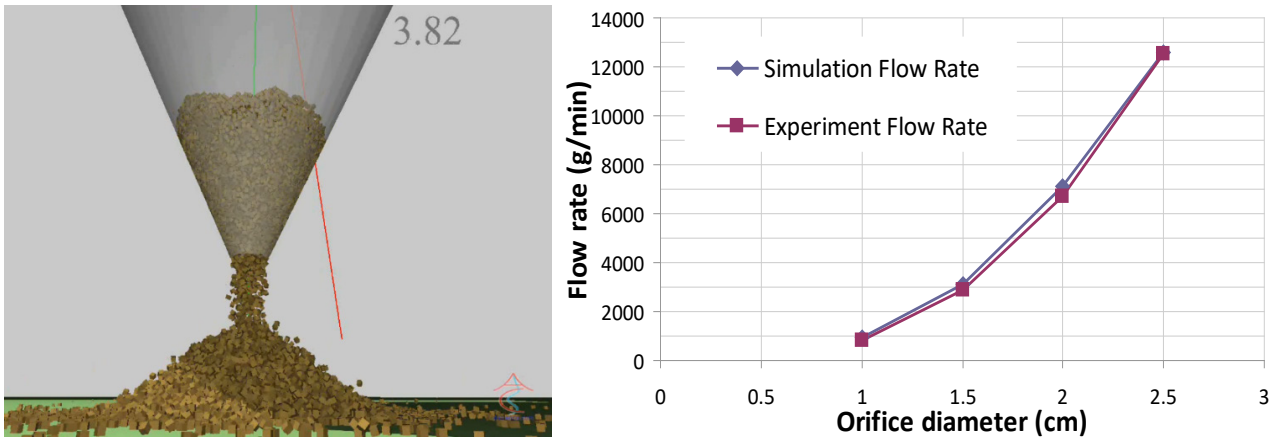


Figure 5B-16: Simulation of Sand Flow Rate from a Hopper using Cubical DEM Particles.

- Wall material shear apparatus can be used to tune the friction and adhesion to wall materials.
- Bevameter experiments (Figure 5A-17 and Figure 5A-18) measuring the current normal pressure versus maximum shear stress. This experiment can be used to tune/verify the soil cohesive strength, inter-particle friction coefficient and plastic relaxation speed.
- Wheel–soil experiments (Figure 5A-22) measuring torque, angular velocity, speed, drawbar force, normal force and sinkage. This experiment can be used to verify/tune the soil cohesive strength and inter-particle friction coefficient.

The force model can also be used as the soil-wall force model to model the contact between soil and other solid bodies (such as tires, tracks, skis, etc.). The force model can be tuned to particular soil and wall materials using a shear apparatus for measuring wall friction.

In summary, the soil model can include the following effects:

1) **Normal contact forces**: elastic forces; damping forces; and cohesive (adhesion) forces.
2) **Tangential contact forces**: viscous forces; and friction forces using the asperity-spring model [11].

3) **Shear strength** including cohesive strength as a function of bulk density; and friction angle.
4) **Increase of cohesion (shear strength) due to consolidation/compaction** (increase of plastic deformation).
5) **Plasticity:** Hydrostatic stress versus bulk density.
6) **Dilation**: Volume increase due to relaxation of soil plastic deformation (and also cohesion) due to tension/shear.
7) **Elasticity**: Recovered part of strain after a normal stress.
8) **Damping:** Hydrostatic stress versus normal strain rate.
9) **Viscosity:** shear stress versus shear strain rate.
10) **Effect of particle shapes** including multiple particle shapes.
11) **Soil – vehicle surface mechanical properties** including friction coefficient, viscosity, damping, elasticity, and adhesion as a function of bulk density.

This DEM material model can be used for cohesive soils such as mud and snow [5], [29]. Also, by turning off cohesive forces and plastic deformation the DEM model can be used for non-cohesive soils such as sand and gravel [25], [26]. Finally the DEM model in DIS includes the following additional features:

- Fast Cartesian grid based $O(n)$ parallel particle neighbor search algorithm [26].
- The master-slave multibody dynamics contact model used in DIS is used to couple the DEM particles with the rest of the multibody system. Particles are typically defined as master surfaces with the vehicle components such as tires, wheels and tracks defined as a polygonal slave contact surfaces. The hierarchical bounding box contact search algorithm is used to allow fast detection of the slave surface contact polygon with the master contact point(s) on a particle. The aforementioned general particle contact force is used between the particles and the multibody system contact surface, thus allowing wall friction, viscous forces and adhesion forces.
- Multiple DEM particle shapes, sizes and inter-particle force models can be used in the same model. This allows modeling mixed terrains such as gravel mixed with sand and hybrid terrains such as snow over mud.

5B.2.3 Smoothed Particle Hydrodynamics

SPH is a meshless particle-based method for modeling fluids and semi-fluids [32], [33]. The SPH formulation used in the DIS code was presented in Refs. [34], [35] and follows the formulation presented in Ref. [32]. It uses the same Cartesian grid based $O(n)$ parallel particle neighbor search algorithm [26] as the DEM. It can be used to model both compressible and incompressible fluids. Incompressible fluids are modeled as slightly compressible using the artificial compressibility technique. Turbulence is modeled using a Smagorinsky zero-equation large eddy-viscosity model. SPH particles in DIS are point particles. Interaction forces (including skin friction and viscous forces) between the SPH particles and the rest of the flexible multibody system (including rigid and flexible bodies) are calculated using the techniques described in Section 5B.2.2. The DIS code does not distinguish between DEM or SPH particles in their interaction with the rest of the multibody system, it only distinguishes between them in their interaction with each other. Another feature of the DIS code is that SPH particles can interact with DEM particles using the DEM formulation. This allows modeling the interaction of the soil with a fluid. For ground vehicles, this allows modeling vehicle mobility over mud covered with water, such as fording in shallow water. SPH particles representing one fluid can also interact with other SPH particles representing another fluid. This allows modeling multiple fluids such as oil,

water and air in the same simulation. SPH can be used to simulate the splashing, floating, swimming and fording of vehicles in water pools (Figure 5B-17). SPH can also be used to simulate sloshing inside fluid filled tanks including water/petroleum payloads tanks and fuel tanks (Figure 5B-18). In summary the key features of DIS SPH modeling capability are:

1) Modeling fully coupled fluid-flexible multibody dynamics systems including moving/rotating rigid and flexible objects (such as vehicle body, tires, propellers, etc.).
2) Capturing free surfaces including surface breakup and reattachment.
3) Including turbulence effects.
4) Mixed soil-fluid flow.

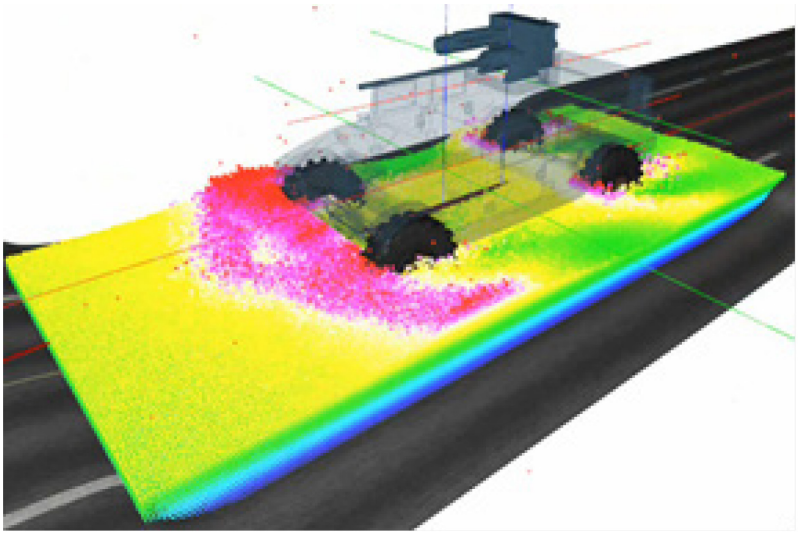


Figure 5B-17: Simulation of Water Fording.



Figure 5B-18: Simulation of Liquid Sloshing for a Tanker Truck.

5B.2.4 IVRESS Virtual Reality Visualization Engine

ASA develops IVRESS [1] which is an object-oriented event-driven software system for constructing virtual models of engineering systems (for visualization and trasining applications) and real-time interactive viewing of scientific datasets [21], [36], [37], [38], [39]. IVRESS interfaces with the following output devices: immersive stereoscopic displays and speakers; and a variety of input devices including head/hand tracking devices, joystick, mouse, microphone, and keyboard. IVRESS incorporates the following types of primitive software objects:

- **Container objects** are grouping objects that can contain "children" objects. They also can include a geometric transformation (translation, rotation, scale) for their children objects.
- **User-interface objects** include buttons, check boxes, slider bars, text boxes, labels, graphs, tables, light sources, and selection tools.
- **Support objects** contain information that can be referenced by other objects such as material colors, image textures, and constitutive material model for flexible bodies.
- **Geometric entities** represent the geometry of the physical components. They include box, sphere, cylinder, cone, torus, NURBS surface and general polygonal surface.
- **Computational mechanics objects** include rigid bodies, flexible bodies (grouping of truss, thin beam, thick beam, shell, or brick elements), DEM/SPH particles, joints (spherical, revolute, cylindrical, prismatic, and CV), actuators (linear and rotary), and contact surfaces. They represent the physics model of mechanical systems.

Each object encapsulates a set of properties, methods, and events that define its behavior, appearance, and functions. IVRESS includes two scripting languages: JAVAscript and Python script. IVRESS supports multiple concurrent users simultaneously collaborating on the editing and viewing of the visualization scene. A description of the main features of IVRESS which are relevant to the current proposal is given below:

- **Model tree editor** (Figure 5B-1). It is used to create and edit IVRESS models (pre-processing) and visualize (post-processing) scientific datasets. The hierarchical model tree editor can be used to create a scene that has any number of complex mechanical systems, to define the connections between the components of mechanical systems within the scene (spherical joints, cylindrical joints, revolute joints, …), to texture the scene's objects, to set up the scene's lighting and environmental effects, and to setup the simulations that will run inside the scene.
- **On-screen editing**. The editor allows on-screen selection and placement of the model objects.
- **Template menus**. The model tree editor can be used to create and simulate any complex mechanical system model, yet creating the mechanical systems such as ground vehicles and robotic vehicles using the model tree editor can be time-consuming. The template-based interface allows users to create a complex mechanical system such as a tracked vehicle by entering the main vehicle and appendages parameters in intuitive tables. Many of the table fields can be left to their default values. ASA created a template for modeling wheeled and tracked ground vehicles.
- **Scientific visualization objects**. IVRESS has a wide range of data visualization capabilities which include:
    - Streamlines, stream ribbons or stream volumes that can be colored using any primitive or derived scalar response quantity and displayed statically or using animated arrows or particles. For unsteady flows particle path-lines and streak-lines can also be displayed.

- Coloring and/or contouring any surface using any scalar response quantity.
- Cutting planes.
- Volume and surface arrows.
- Iso-surfaces and elevation surfaces.
- Flow feature extraction including vortex cores and surface separation/attachment lines.
- Any of the above visualization objects can be used as an interactive probe.
- 2D Graphing: Can be used in conjunction with other visualization objects including probes.

- IVRESS can be used to visualize multiple scientific datasets of any arbitrary size simultaneously within a Virtual Reality (VR) visualization scene. This is useful for comparing the simulation results of several designs side by side, or for displaying several coupled analyses of the same system simultaneously, such as the CFD and stress analyses of a fluid-structure interaction simulation.
- **Scene Publishing**. Users can publish their visualization scenes using:
  - **Movies** can be generated using built-in ray tracer and written as avi files. Users are also able to specify the video file's resolution and frame rate. The ray tracer includes complex shadows, reflections, refractions, and transparency.
  - **VR animation**: A single user or multiple concurrent users can view the visualization scene. In this case, the users viewing the scene are not bound by a given preset camera position, angle and zoom as in a movie. Each user can fly through the scene, look in any direction and focus on any scene object while the animation is running. Alternatively, a user can choose to link his/her viewpoint to any given scene object as it moves within the scene, such as following behind a vehicle. The VR visualization mode also allows the users to interactively adjust the visualization parameters within a collaborative visualization session, such as changing the scalar response quantity that a surface is colored by.

5B.3 PROTOTYPE CAPABILITIES

In this section we will describe how the complex terramechanics prototype presented in this section satisfies each of the complex terramechanics software tools requirements listed in Section 5A.4 as well as areas where more development is needed for the prototype to satisfy the requirements.

5B.3.1 Ability to Predict the Vehicle Mobility Measures of Interest to the End Users

Figure 5B-19 to Figure 5B-22 show snapshots from typical tracked and wheeled vehicles operating on soft DEM soil. By default all DIS/GroundVehicle models include, as standard vehicle output data, the following output quantities as a function of time:

- Engine: RPM, output torque (Figure 5B-19 and Figure 5B-20), torque after losses, available torque.
- Gear box: current gear.
- Position, velocity and acceleration vectors of key vehicle points: CG, vehicle center, vehicle corners, and driver seat.
- Pitch, yaw and roll angles, angular velocities, and angular accelerations of the vehicle frame.
- Aerodynamic vehicle forces and moments including frontal and side drag and lift.
- Struts deflection, length, velocity, and force.

- Vehicle position, actual speed (Figure 5B-18 and Figure 5B-20), desired speed, and acceleration along the steering path.
- Wheels steering angle.
- Wheels angular velocity (Figure 5B-21 and Figure 5B-22).
- Tire slip.
- Tire slip angle.
- Wheels center point position.
- Vehicle distance error to steering path and angle error to steering heading.
- Pitman arm angle or steering rack position.
- Steering wheel angle.
- Steering wheel torque.
- Any control system activity such as traction control and steering control.
- 3D soil forces and moments on any vehicle component in contact with the soil such as underbody, wheels hubs, tires, sprockets, or any vehicle appendages. Figure 5B-19 and Figure 5B-20 show the torque at the driving sprocket for a tracked vehicle necessary to drive the vehicle at its maximum speed on the soil. Figure 5B-21 shows snapshots from a simulation of a bulldozer digging through a layer of cohesive mud. Figure 5B-22 show the time-histories of the bulldozer speed, rear-wheel angular velocity, and rear-wheel torque. At steady-state, the sum of all the soil tangential resistance forces is equal to the tractive forces generated by the driving sprocket or wheels. The figures demonstrate that the DIS prototype can predict the interaction with soil with both the vehicle wheels as well as any other vehicle part such as a blade (Figure 5B-21).

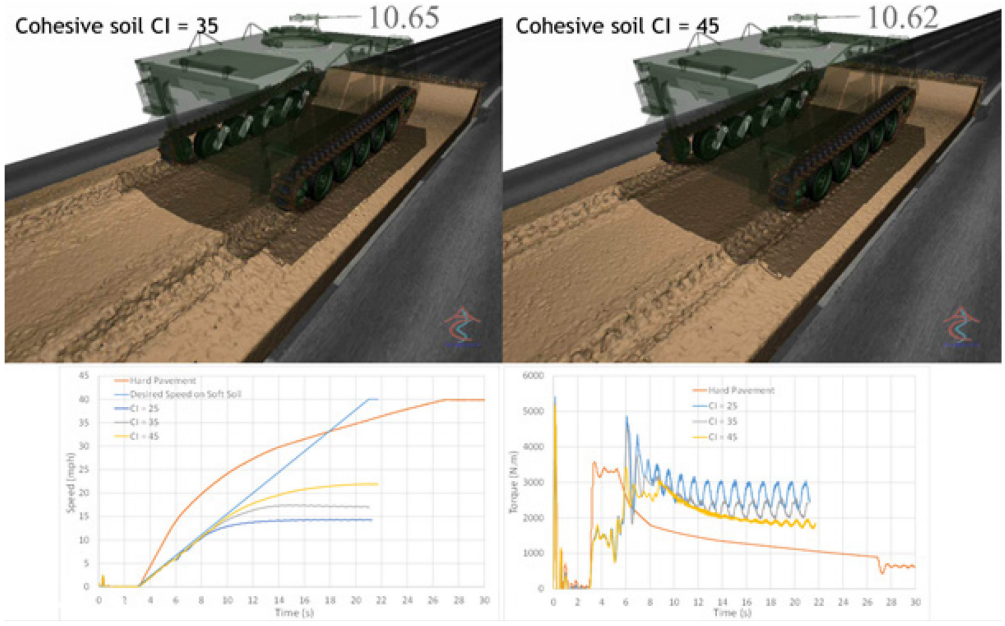


Figure 5B-19: Effect of Soil Cohesion on Rut Depth for a Tracked Vehicle Moving at its Maximum Possible Speed on a Level Terrain Using the Moving Soil Patch Technique. The graphs show the speed and torque time-histories of the vehicle as a function of soil cone index.

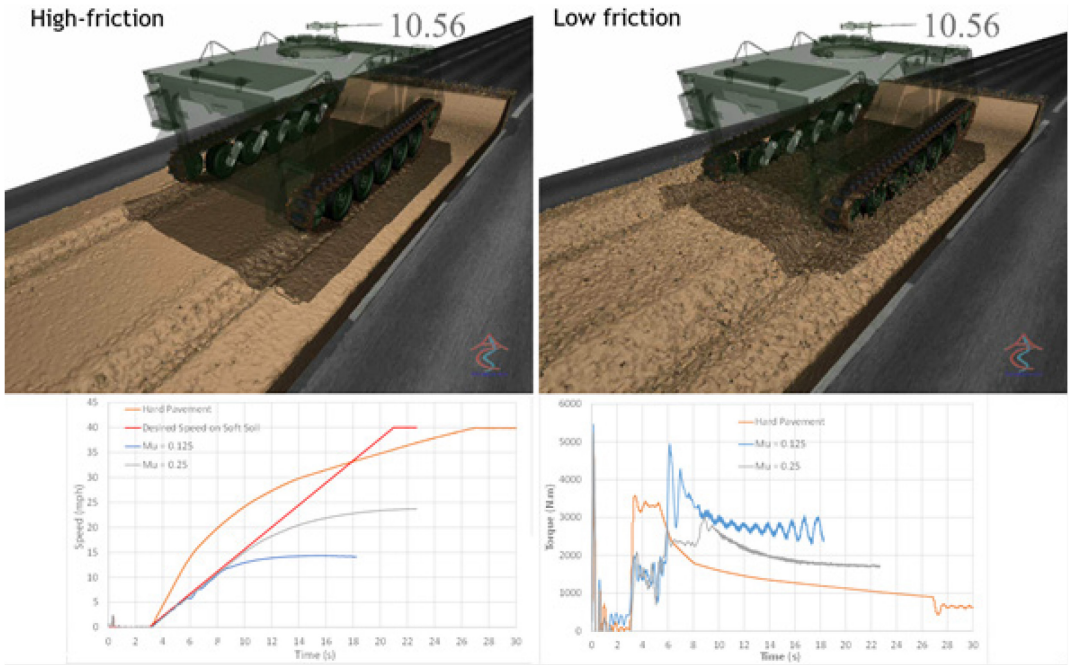


Figure 5B-20: Effect of Soil Friction on Rut Depth and Shape for a Tracked Vehicle Moving at its Maximum Possible Speed on a Level Terrain Using the Moving Soil Patch Technique. The graphs show the speed and sprocket torque time-histories of the vehicle as a function of inter-particle friction coefficient.

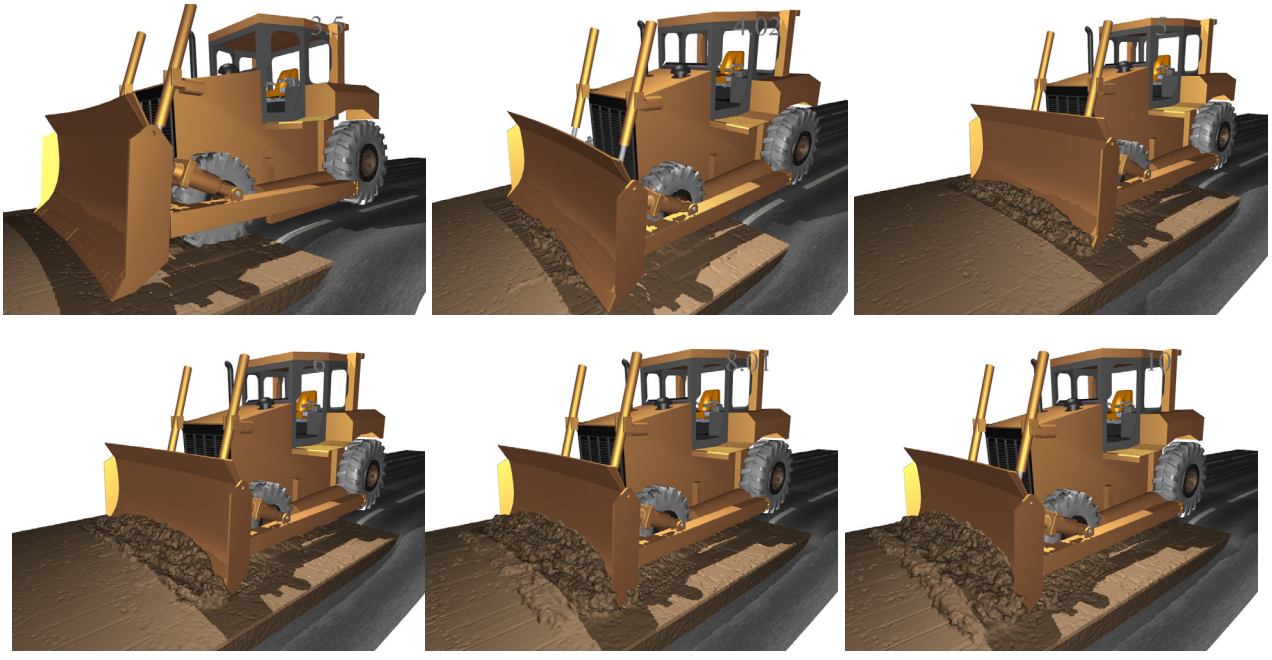


Figure 5B-21: Snapshots of a Bulldozer Digging through Cohesive Mud.

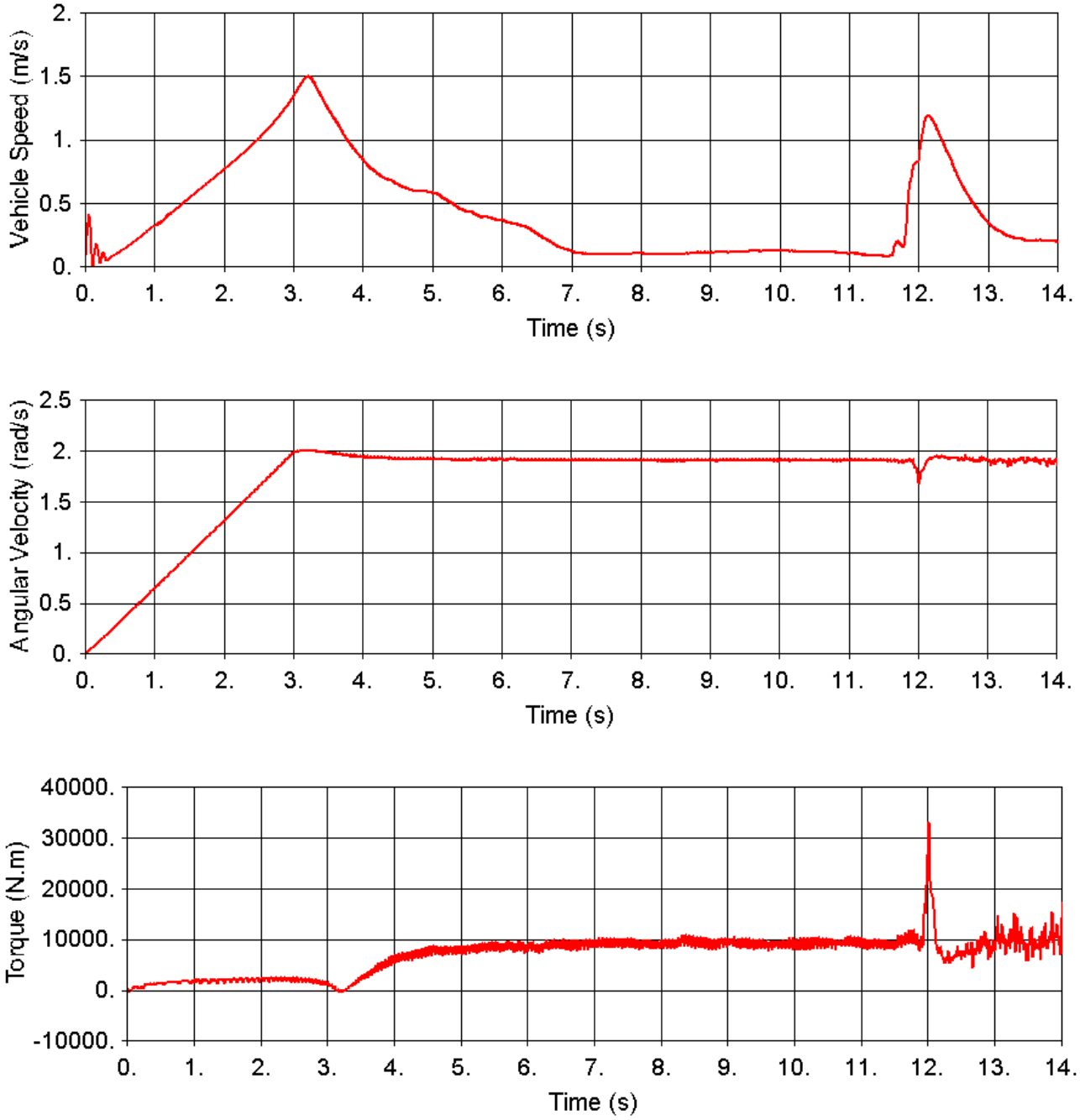


Figure 5B-22: Time-History of the Bulldozer Speed (Top), Rear-Wheel Angular Velocity (Center), and Rear-Wheel Torque (Bottom). The speed decreases and the wheel torque increases when the bulldozer starts digging in the soil.

The vehicle response quantities listed in the requirements are either one of the above output quantities or can be easily calculated using one or more of the above output quantities. For example, the transmitted vibration power can be computed using the acceleration vector at the driver seat along with the 6-watt absorbed vibration power

algorithm. Also, note that from the time-histories, the maximum, minimum, and average values of each response quantity can be calculated.

5B.3.2 Ability to Predict the Terrain Damage Caused by the Vehicle

Figure 5B-19 to Figure 5B-26 show examples of ruts (terrain damage) caused by wheeled, tracked and legged vehicles on various cohesive soils and non-cohesive soils with varying cohesive strength and internal friction values. The rut depth, width, shape and side wall height can all be measured from DEM terrain deformation and they all vary with soil material parameters (soil type) and vehicle parameters such as weight, running gear type (tire/track/leg), and speed.

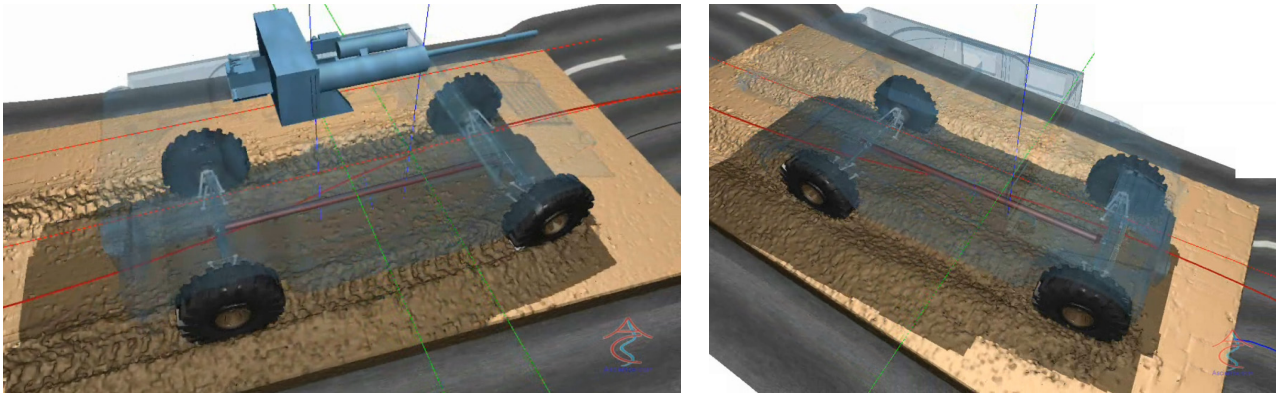


Figure 5B-23: Rut Shape for Cohesive Soil (Left) and Non-Cohesive Soil (Right) of Comparable Shear Strength Measured by the Cone Index for a Wheeled Vehicle Traveling at 5 mph. For cohesive soil the ruts side walls are nearly vertical. for non-cohesive soil the ruts are V-shaped.

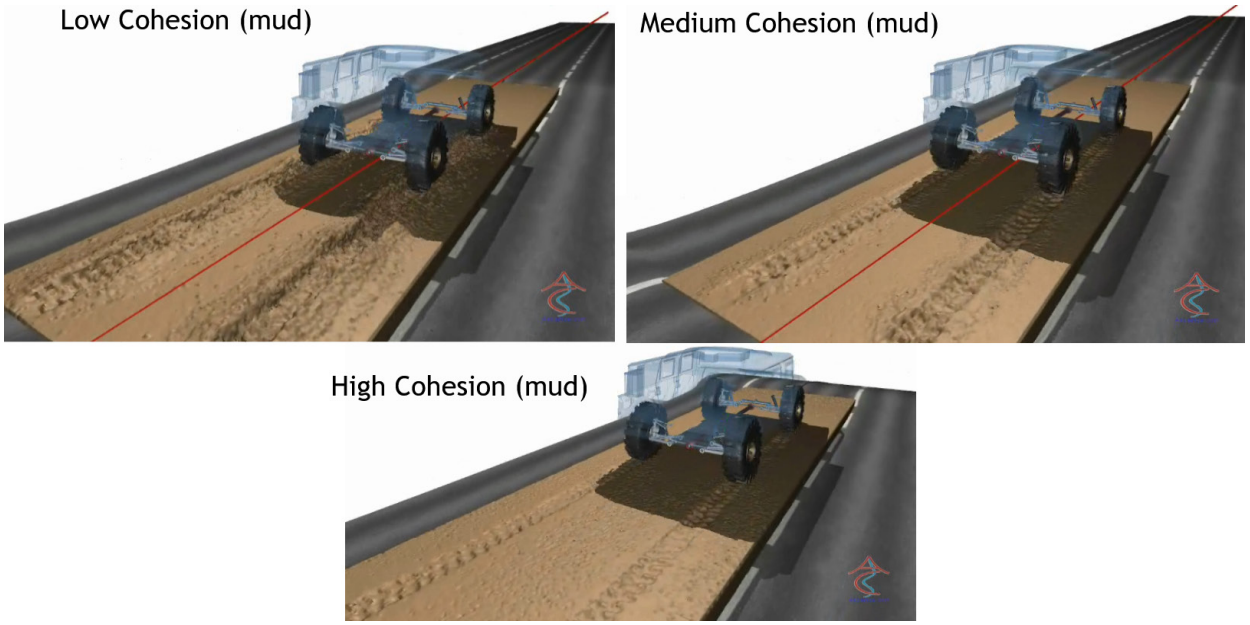


Figure 5B-24: Effect of Soil Cohesion on Rut Depth at 10 mph.

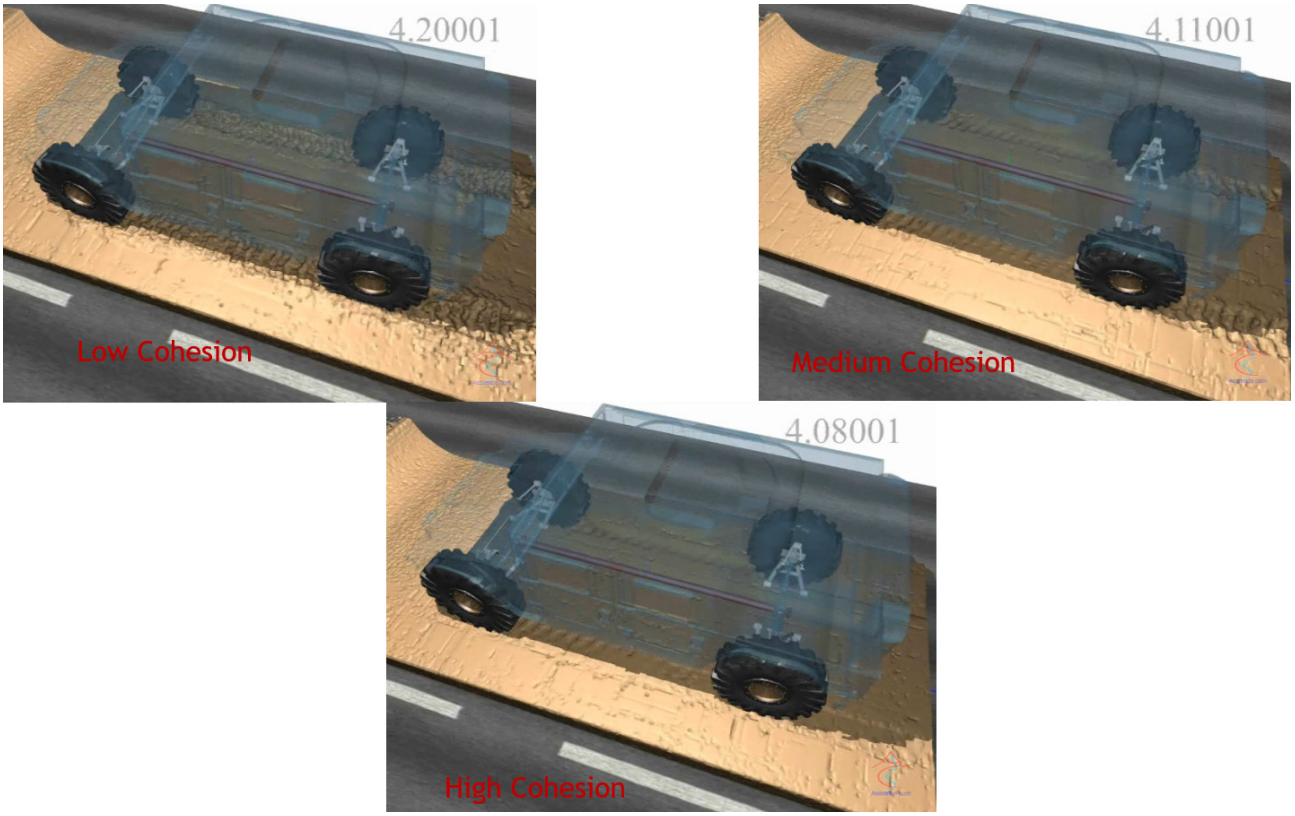


Figure 5B-25: Effect of Soil Cohesion on Rut Depth for a Wheeled Vehicle Moving at its Maximum Possible Speed on the Terrain Using the Moving Soil Patch Technique.

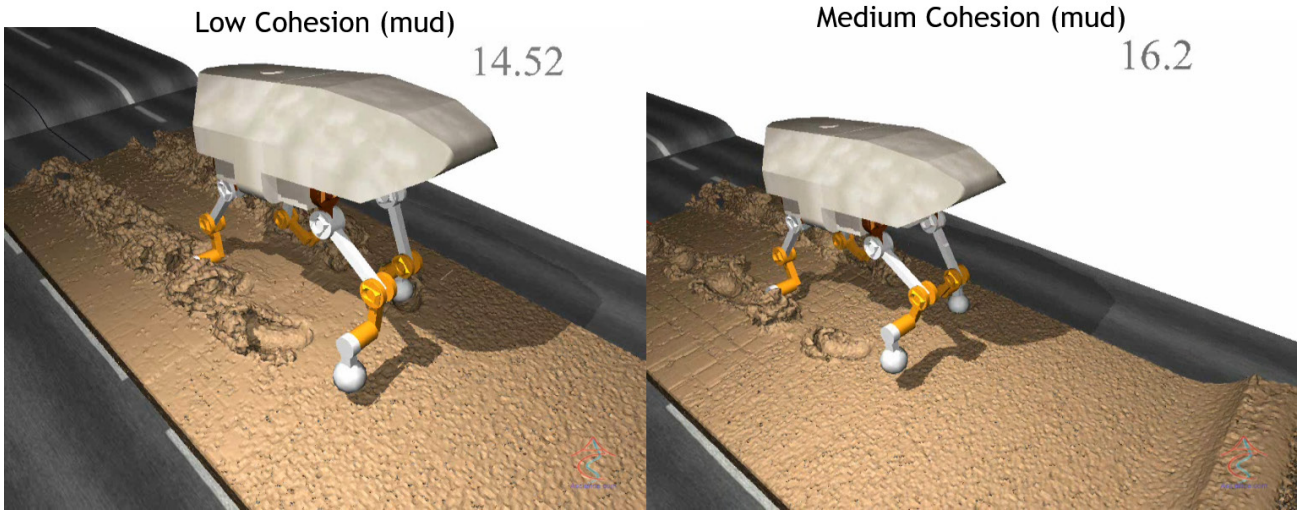


Figure 5B-26: Effect of Soil Cohesion on Rut Depth for a Walking Legged Vehicle Using the Moving Soil Patch Technique.

5B.3.3 Ability to Accurately Predict Soil Mechanical Response for Small-Scale Terramechanics Experiments

Models of the following small-scale terramechanics experiments were created using DIS and used to tune the DEM inter-particle force models to specific soils:

1) Piston-cylinder uniaxial compression test (Figure 5A-13). This experiment is used to tune the $\delta_{plastic}$ versus $F_{repulsion}$ curve (Figure 5B-11) to match the bulk density versus hydrostatic pressure curve for the soil (Figure 5A-14) obtained using the experiment. It can also be used to estimate the elastic constant of the soil by measuring the amount of rebound after the normal load is removed.
2) Shear cell (Figure 5A-15) [40]. This experiment is used to tune the maximum adhesive force ($F_{adhesion,max}$) in (Figure 5B-10) as a function of the plastic deformation ($\delta_{plastic}$) (Figure 5B-12) along with the DEM inter-particle friction coefficient to match the shear stress versus normal stress for different hydrostatic normal stress values (Figure 5A-19) obtained using the shear cell. In this figure, the angle between the x-axis and each curve is the soil friction angle and the intersection point with the y-axis is the soil cohesive strength.
3) Penetrometer. This experiment is used to tune the combined effects of adhesion ($F_{adhesion,max}$) and DEM inter-particle friction coefficient on the soil shear strength. Those two parameters are used to match the maximum normal pressure during the penetration into the soil at a prescribed slow speed (quasi-static load) (Figure 5A-20). Note that the effect of adhesion and friction cannot be separated using this experiment. The penetrometer can be of various shapes such as a 30^{o} cone (Figure 5A-20) or a plate (Figure 5A-21).
4) Single rigid wheel (with or without grousers) on soil (Figure 5A-22). The model can be used to tune the DEM shear strength parameters including $F_{adhesion,max}$ and DEM inter-particle friction coefficient to reproduce the normal load, slip percentage and linear speed versus drawbar force and wheel torque.

Also, the following small-scale soil – vehicle material surface experiments where created using DIS and used to tune the DEM to vehicle material surface force models. Those include:

1) Quasi-static wall shear using a wall shear cell (Figure 5B-27). In this experiment the soil is compressed using a known normal load, then the soil is sheared against the wall material in order to measure the soil-wall material friction coefficient and adhesion.

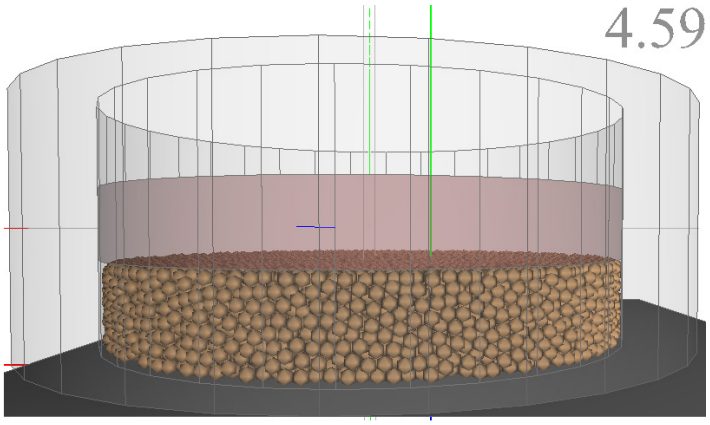


Figure 5B-27: Wall Shear Experiment.

2) The single rigid wheel without grousers on soil (Figure 5A-22) can be used to tune the DEM soil-wheel material friction coefficient and adhesion.

5B.3.4 Ability to Accurately Represent the Mechanical Response of Worldwide Soils

This includes cohesive soils such as mud, clay and snow, and non-cohesive soils such as sand and gravel. Figure 5B-23 shows a comparison between the rut shape for a cohesive and non-cohesive (sand) soils for a wheeled vehicle. For cohesive soil the ruts side walls are nearly vertical and the tread patterns are clearly imprinted in the soil. For non-cohesive soil the ruts are V-shaped and the tread pattern imprinted in the soil quickly collapses after the vehicle passes over the soil. Figure 5B-24 and Figure 5B-25 show that, for a wheeled vehicle, as soil cohesion increases, rut depth decreases for both slow and fast moving vehicles. The ruts are somewhat shallower as vehicle speed increases due to increased inertia and viscosity resistance of the soil. Similarly Figure 5B-19 shows that, for a tracked vehicle, as soil cohesion increases rut depth decreases. Figure 5B-20 shows the effect of soil internal friction on rut depth and shape for a tracked vehicle. The figure shows that as internal friction decreases the ruts become deeper and more V-shaped and the tread pattern does not clearly imprint in the soil. In all those figures as soil cohesion decreases and/or as internal friction decreases, the maximum vehicle speed on the soil decreases, wheel slip increases, and the torque required to drive the vehicle at its maximum speed increases. Figure 5B-26 shows that for a legged vehicle rut depth increases as soil cohesion decreases. Figure 5B-28 shows the effect of soil density on vehicle speed, rut depth, wheel slip, and driving torque (tractive effort) for a wheeled vehicle going at its maximum possible speed on the terrain. The figure shows that as soil density increases, rut depth, wheel slip, and driving torque decrease while vehicle speed increases. This is due to the increased inertia of the soil which makes the soil more resistant to motion. Note that the vehicle is moving at high speeds, thus the soil inertia forces are not zero and increase with soil density. The aforementioned figures show that the DIS code can represent a wide variation of soils by just varying three parameters of soil, namely cohesion, internal friction, and density. In addition, the DEM model has three other soil parameters that affect mobility on soft soil to a lesser degree, namely viscosity, damping, and dilation (see Section 5B.2.2).

Furthermore, as described in Section 5B.2.2, the DEM model used in DIS can reproduce the following soil mechanical behaviors:

1) Traction of the vehicle running gear. This includes friction between the terrain and the running gear and shear strength of the terrain.
2) Change in soil bulk density as a function of soil compaction state (Figure 5A-14).
3) Change in shear strength, including cohesive strength and internal friction, as a function of soil compaction state (Figure 5A-19).
4) Soil dilation.
5) Velocity-dependent soil forces including damping and viscous forces.
6) Adhesion of the soil to the vehicle surfaces. The DEM inter-particle contact model in Section 5B.2.2, can be used between a DEM particle and a vehicle surface. In that case the $F_{adhesion,max}$ in Figure 5B-10 defines the maximum adhesion force of a particle to the vehicle surface.

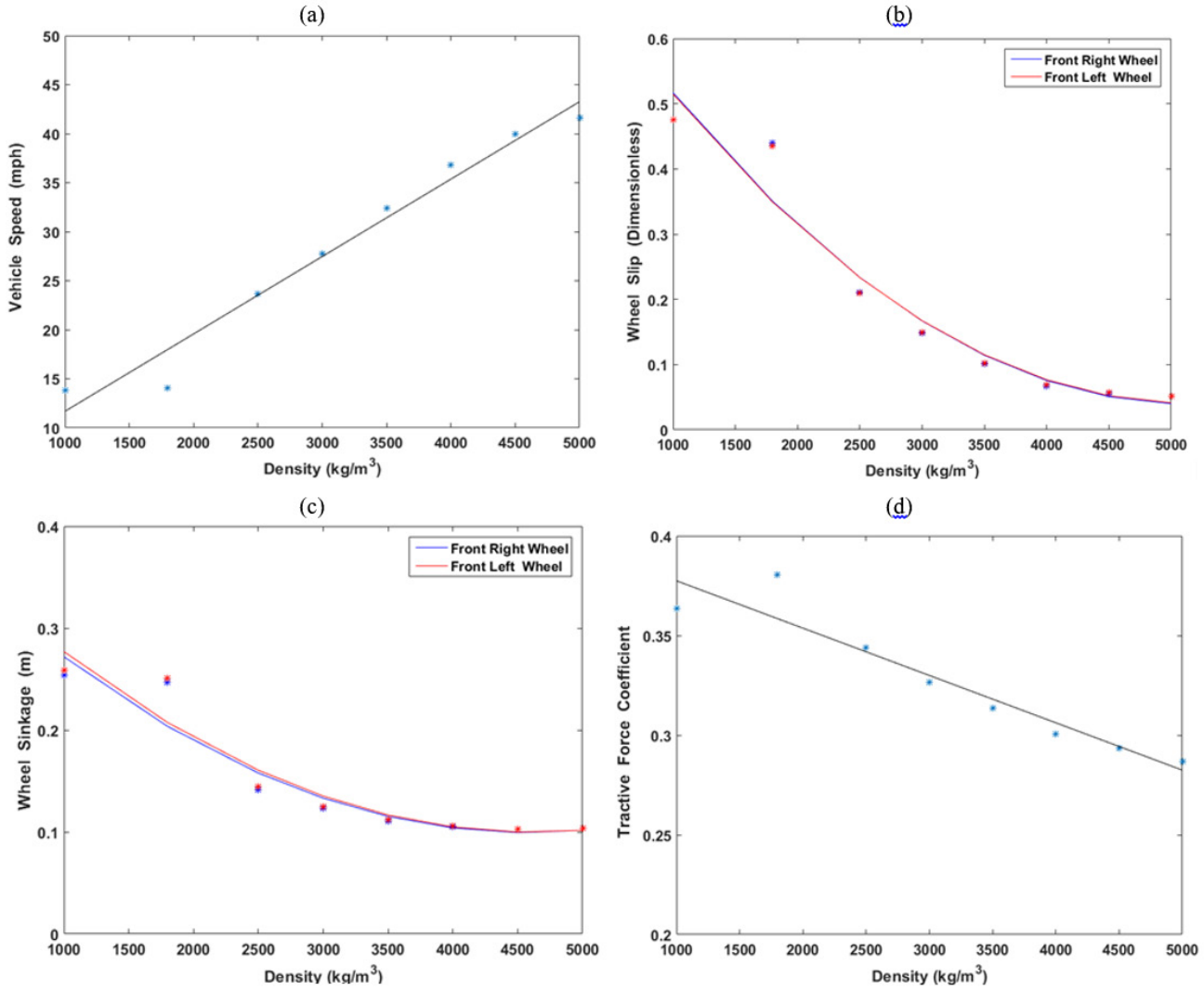


Figure 5B-28: Variation of a Wheeled Vehicle Speed. (a) Wheel Slip; (b) Wheel Sinkage; (c) Tractive Force Coefficient; (d) as a Function of DEM Particle Density.

5B.3.5 Ability to Provide the Mapping Function Which Maps the Physical Soil Properties into the Mechanical Soil Properties

This mapping is the functions *f* in Figure 5B-25 and Figure 5B-26 which map the physical soil properties into the DEM model soil parameters. Physical soil properties include USCS soil type, moisture content and temperature. The DEM material model parameters in DIS are:

1) Particles mass.
2) Particle shape.
3) Inter-particle friction coefficient. Note that this friction coefficient can also be a function of the particle plastic deformation.

4) Inter-particle repulsion force as a function of inter-particle penetration (Figure 5B-10).
5) Inter-particle adhesion force as a function of inter-particle penetration (Figure 5B-10).
6) Particle plastic strain as a function of compressive stress (Figure 5B-11).
7) Particle maximum adhesive stress versus plastic strain curve (Figure 5B-12).
8) Inter-particle damping coefficient.
9) Inter-particle viscosity.
10) Particle plastic relaxation speed.

In addition, the DEM to particle surface material model parameters in DIS are:

1) Particle-to-vehicle material friction coefficient.
2) Particle-to-vehicle material repulsion force as a function of penetration (Figure 5B-10).
3) Particle-to-vehicle material adhesion force as a function of penetration (Figure 5B-10).
4) Particle-to-vehicle material maximum adhesive stress versus plastic strain curve (Figure 5B-12).
5) Particle-to-vehicle material damping coefficient.
6) Particle-to-vehicle material viscosity.

This mapping can be experimentally developed using the small-scale terramechanics experiments described in Section 5B.3.3 above by performing the terramechanics experiments for all USCS soil types at different soil moisture contents and temperatures.

As mentioned in Section 5A.2.2.2, there are at least twenty USCS soil types. At least seven moisture contents need to be tested for each soil type. Also, at least five temperatures need to be tested. Thus a total of $20 \times 7 \times 5 = 700$ experiments are needed to develop the mapping function f for all soil types, moisture contents, and temperatures. In addition, there are at least two vehicle surface interface materials: vulcanized rubber and steel. Thus a total of $2 \times 700 = 1400$ experiments are needed to develop the mapping function for vehicle surface interface materials and all soil types, moisture contents, and temperatures.

DOE and interpolation techniques can be used to considerably reduce the required number of physical experiments. However, more research is needed into developing, improving and validating those techniques.

5B.3.6 Ability to Represent Heterogeneous Terrains

Heterogeneous terrains include:

1) Terrains which have discrete patches of different soil types.
2) Terrains with embedded boulders, rocks, stones, and/or gravel. This includes modeling the mechanical properties at the interface between the soil and discrete terrain components including adhesion and friction.

The DEM capability in DIS supports multiple DEM particle types, including both point and rigid body particles, in one simulation. However, this capability has not yet been demonstrated in a vehicle mobility simulation. Future developments will attempt to:

1) Develop the capability to represent various rock geometric shapes by varying parameters for: ellipticity and angularity. Each rock surface can then be tessellated into a general polygonal surface.
2) Develop the capability to model the rocks as rigid body DEM particles with random geometric shapes represented using polygonal surfaces.
3) Develop the capability to combine a DEM model of soil modeled using point particles and rocks modeled using rigid body particles into one model and to use the DEM contact force model including friction and adhesion between the rocks and the soil.
4) Develop the capability to disperse the rocks in the DEM soil using a given inter-rock spacing distribution.
5) Develop the capability to disperse soil patches with varying material properties.
6) Test the combined soil-rock model using typical vehicle simulations over long complex topography terrains.

5B.3.7 Ability to Represent Multiple Layers of Soil

The DEM capability in DIS supports multiple soil layers with each layer having different DEM material parameters. However, this capability has not yet been demonstrated in a vehicle mobility simulation. Future developments will include:

1) Modifying the moving soil patch to allow laying out multiple soil layers on a complex topography terrain. Each layer can have different mechanical properties and each layer can have a specified thickness.
2) Testing the multi-layer soil model using typical vehicle simulations over long complex topography terrains with two or more soil layers (e.g., snow-soil; and tilled soil-compacted soil).

5B.3.8 Ability to Represent Water Covered Terrains

A DIS demonstration of vehicle water fording over a hard terrain water bottom was presented in Ref. [30] (Figure 5B-17). The water was modeled using SPH. The wheels and the vehicle body were used as contact surfaces for the SPH particles. Future developments will include:

1) Modifying the DEM model to allow modeling both SPH and DEM particles in the same simulation. This will allow modeling water fording with a soft soil water bottom.
2) Modifying the moving soil patch to allow modeling flooded terrains.
3) Demonstrate the flooded terrain model using a typical vehicle fording simulation over long complex topography terrains (see Section 5B.3.9 below).

5B.3.9 Ability to Model Long Complex Topography Terrains

Complex topography includes:

1) Sloped terrains: positive and negative long slopes and side slopes.
2) Roughness which can be modeled using wave length versus amplitude.
3) Discrete ditches and bumps specified by depth, width, and spacing distribution.

4) Turns.

5) Variable soil/terrain conditions along the terrain.

DIS includes the ability to model both hard and soft soil long arbitrary topology terrains. Support of arbitrarily long terrain is needed in order to allow the vehicle to accelerate until it reaches its maximum steady-state speed on the terrain. Hard terrains long arbitrary topology are represented using polygonal surfaces (consisting of triangles and/or quadrilateral faces) of the following types:

- A 2D digitized surface (Figure 5B-29).
- A 1D distance versus height list (Figure 5B-30). This surface can be used to model RMS courses. Left and right track surfaces can be different.
- A surface consisting of trapezoidal and/or semi-circular negative or positive obstacles (Figure 5B-31).

A master/slave contact model is used where contact is detected between discrete points on a master contact surface (such as tire or track) and a polygonal slave contact surface [6], [7], [8], [9], [10] (the terrain). A general fast binary-tree hierarchical bounding box/sphere contact search algorithm allows DIS to quickly find the contact penetration between points on a master contact point and the contact polygon on the slave contact surface [9], [10]. The penalty technique including both normal stiffness and damping is used for imposing the normal contact constraint [6], [7], [8], [9], [10] between the master and slave contact surfaces. The penalty stiffness and damping are set to the resultant stiffness and damping of the running gear (tire/track segment) and the terrain. Contact friction is modeled using an accurate and efficient asperity-based friction model [7], [11]. In addition, the coefficient of friction and road compliance between the running gear and the road can be set as a function of the distance along the vehicle steering path.

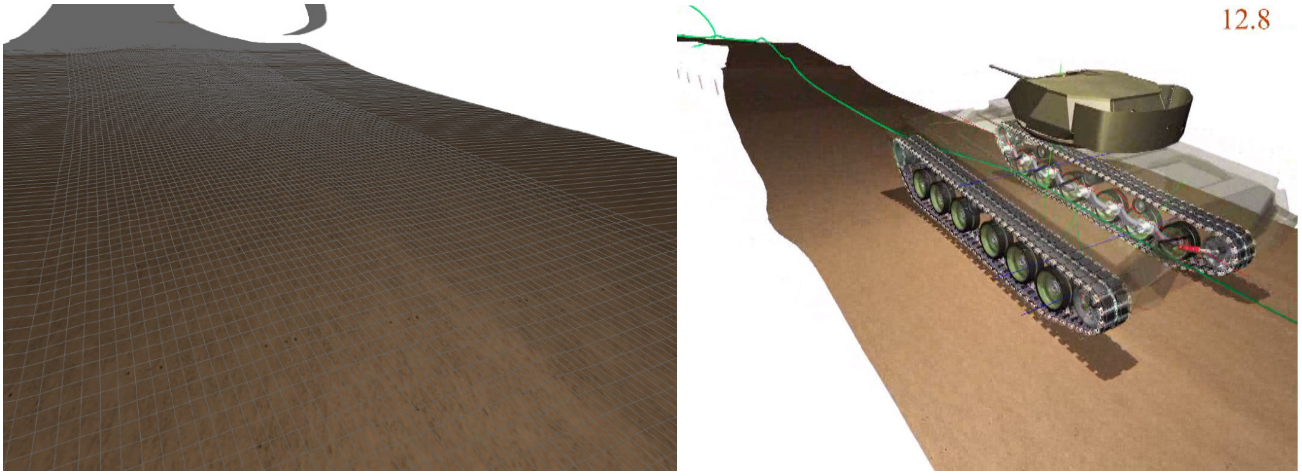


Figure 5B-29: Segment of the Churchville-B High Resolution 2D Profiled Polygonal Terrain (Left) with a Segmented Track Vehicle Going over a Prescribed Steering Path on the Terrain Track (Right).

DIS also includes the capability of modeling soft soil complex topography terrains of arbitrary length using a moving soil patch technique [28]. Using this technique particles which are far behind the vehicle are continuously eliminated and then reemitted as new particles in front of the vehicle. The terrain is defined using an *i-j* ordered quadrilateral grid along with an emitter surface, a leveling surface, and a sink surface

(Figure 5B-32). The simulation starts by filling a rectangular range, say from i_1 to i_2 and j_1 to j_2, where the i index is along the length of the soil patch and j is along the width, on the i-j terrain surface with DEM particles up to a desired depth. Side wall surface at $j = j_1$ and $j = j_2$ along with the sink and emitter surfaces keep the particles inside the soil box. Then, the initial particles are compressed and leveled from the top using the terrain surface such that the same terrain topography is impressed on the soft soil. Next, the sink, emitter, and leveling surfaces are enabled and moved along with the center of the vehicle. When a particle touches the sink surface behind the vehicle it is immediately disabled and then reemitted as a new particle from a random point on the emitter surface in front of the vehicle. The leveling surface levels and compresses the DEM particles that are emitted from the emitter surface. This effectively moves the soil patch along with the vehicle on the terrain. Since the sink, emitter and leveling surfaced all follow the underlying terrain's i-j surface, the topography of the soft soil patch follows the topography of the terrain's i-j surface. Figure 5B-33 shows snapshots of typical vehicle simulations on complex topography terrains with terrain roughness, turns, and variable long slopes.

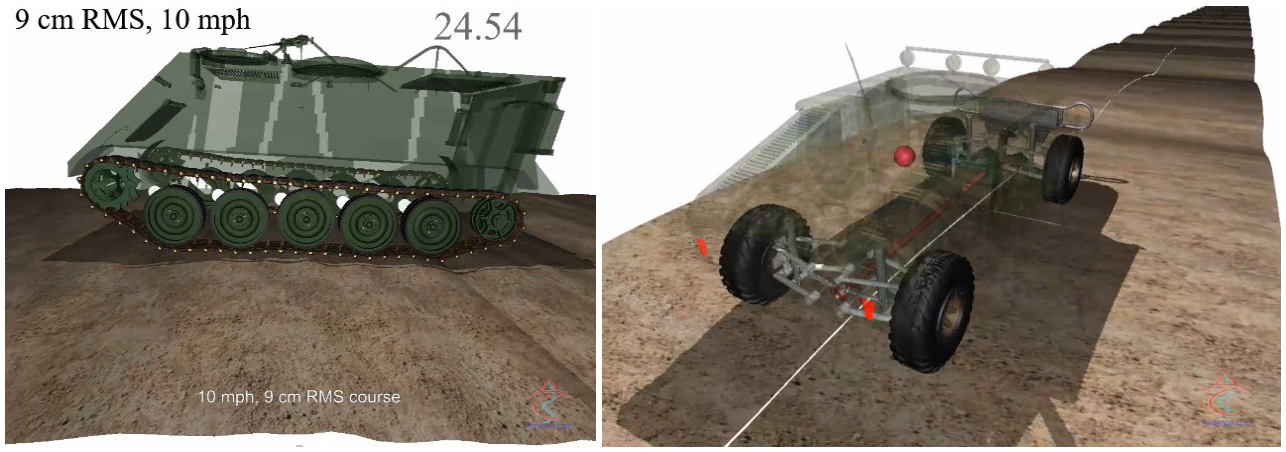


Figure 5B-30: RMS Courses Created Using a Polygonal Terrain.

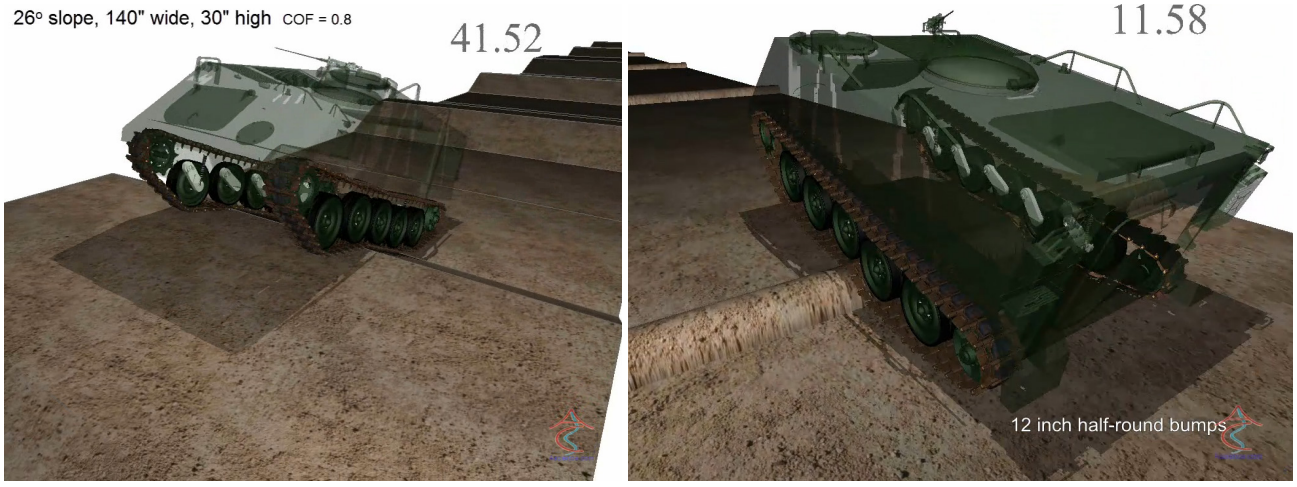


Figure 5B-31: Trapezoidal and Semi-Circular Bump Courses Created Using a Polygonal Terrain.

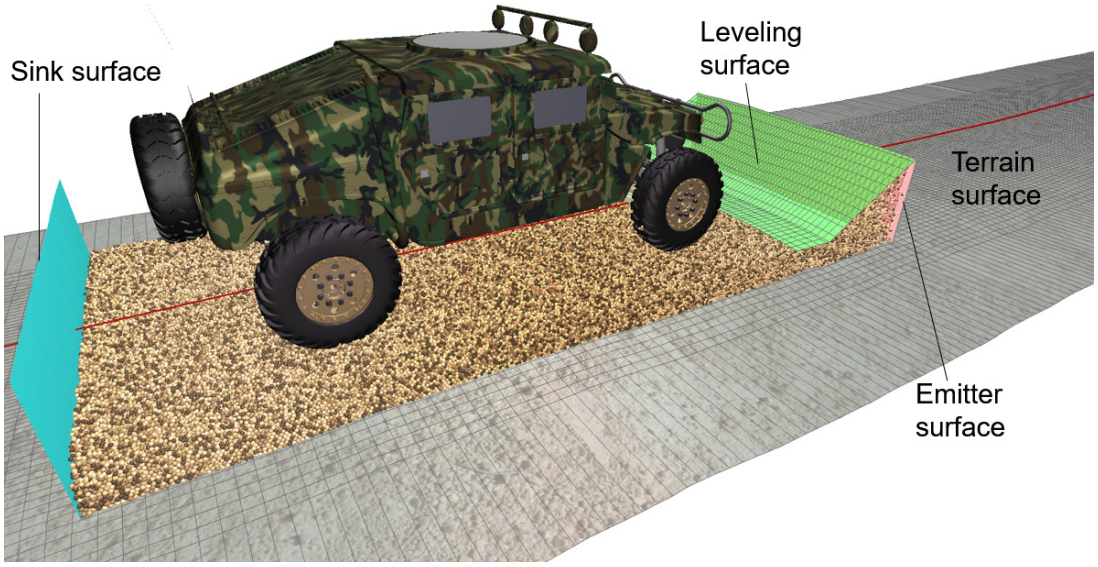


Figure 5B-32: Moving DEM Complex Topography Terrain Patch Modeled Using an I-J Ordered Quadrilateral Grid Representing the Terrain's Surface, an Emitter Surface, a Leveling Surface, and a Sink Surface.



Figure 5B-33: Snapshots of the Moving DEM Complex Topography Terrain Patch in Typical Vehicle Mobility Simulations: 90º Turn (Left) and Going Down a Slope (Right) on Rough Soft Soil Terrains.

The moving soil patch technique ensures that the number of DEM particles remains constant and relatively small for long vehicle travel distances, and that the simulation can complete in a reasonable amount of time. To reach its maximum speed of 60 mph from rest and run a few seconds at steady-state, the vehicle needs about a 400 m long terrain patch. If the patch width is 3.5 meters, consolidated soil depth is 0.4 meters, and consolidated particle diameter is 26.5 mm, then the required number of particles is about 67,000 particles per meter of terrain. So for a 400 m long terrain patch about 27 million particles are needed. At current simulation computational speeds, a 40 sec simulation with 27 million particles will take about 4.5 months to complete on five 32 core

HPC nodes. However, for typical DIS vehicle mobility simulations, the moving terrain patch is about 9 m to 11 m long and the number of particles is about 600 k to 1 M, a 40 sec vehicle simulation takes about 2.5 to 5 days on five 32 core HPC nodes.

Terrain roughness can be specified in the DIS/GroundVehicle using a HarmonicFunction object as horizontal wave lengths along the terrain versus vertical amplitudes of the terrain (Figure 5B-34). This HarmonicFunction object is translated to an equivalent DIS HarmonicFunction object shown in Figure 5B-35, with the actual resulting terrain height profile displayed in the shown graph. The terrain roughness can be introduced by moving the leveling surface in Figure 5B-32 vertically according to the graph shown in Figure 5B-35. A snapshot of a tracked vehicle going over a rough terrain with the roughness shown in Figure 5B-35 is shown in Figure 5B-36.

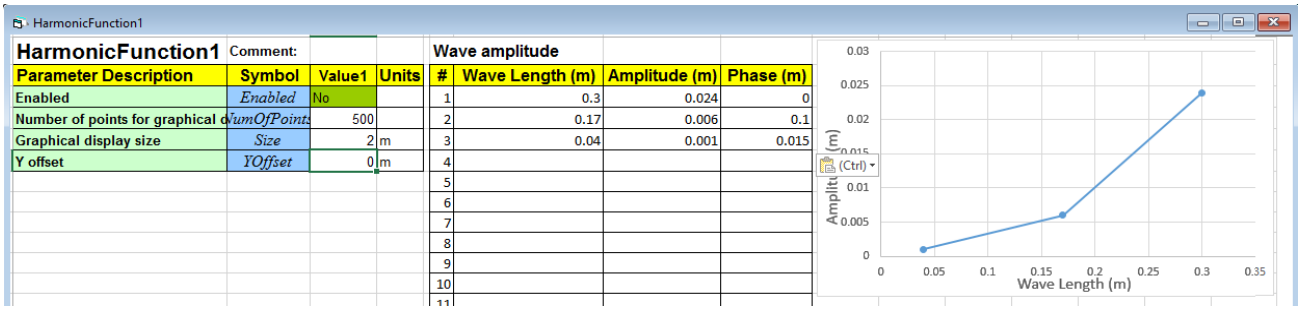


Figure 5B-34: Terrain Roughness Input Interface in DIS/Ground Vehicle Using a Harmonic Function Object that Allows Specifying Wave Length Versus Amplitude.

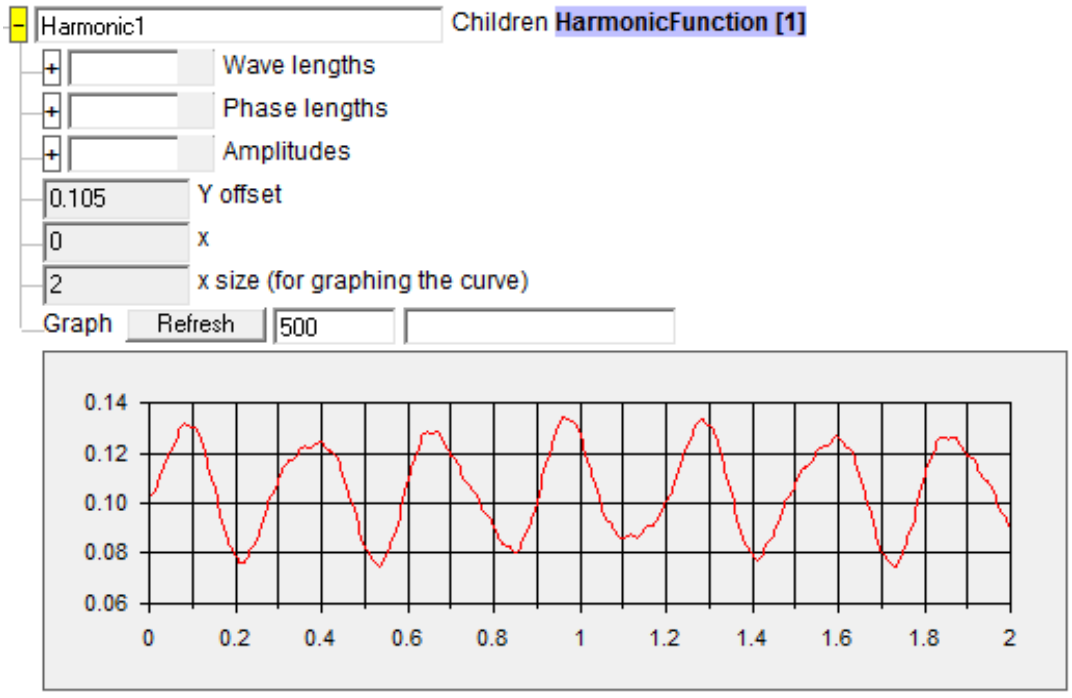


Figure 5B-35: IVRESS/DIS Harmonic Function Object that Allows Specifying Wave Length Versus Amplitude.

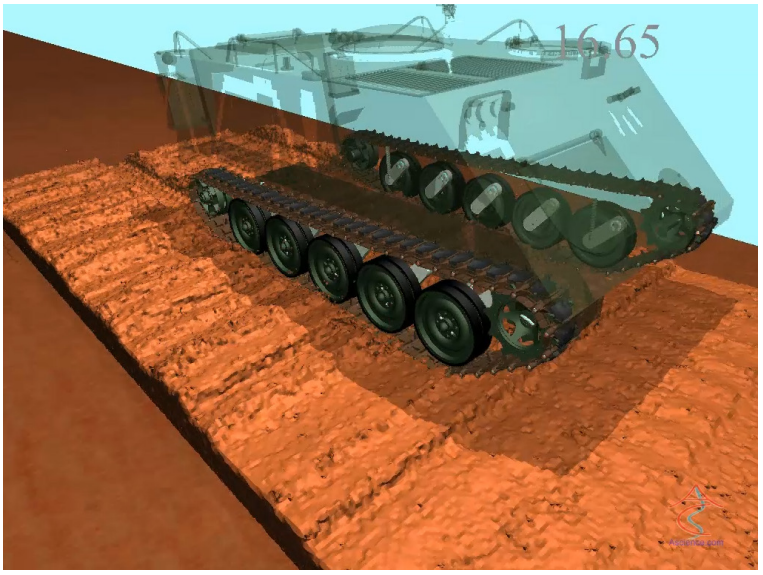


Figure 5B-36: Snapshot of a Tracked Vehicle Going over a Rough Soft Soil Terrain with the Terrain Roughness Generated Using a Vertically Moving Surface and A Harmonic Function Object that Allows Specifying Road Roughness Wave Length vs. Height.

5B.3.10 Ability to Represent All Types and Sizes of Vegetation Identified In USNVC

The capability is not yet fully developed in the DIS/GroundVehicle prototype. A demonstration of a tracked vehicle pushing a large tree stem/pole at 4 mph was created using DIS/GroundVehicle. The stem/pole is modeled as a rigid cylinder embedded in the DEM soil by first compressing a layer of soil on a rigid ground, then placing the cylinder on that soil layer. Then an additional soil layer of the desired stem depth in the soil is added and compressed around the pole. Then, a vehicle simulation with the cylinder and soil is performed. The maximum engine torque and initial vehicle speed (obstacle impact speed) required to override the obstacle (cylinder) is found. If the vehicle cannot override the obstacle then the terrain is considered as "No-Go". Figure 5B-37 shows snapshots of the motion of the vehicle, the obstacle, and the soil ruts caused by the pole and vehicle.

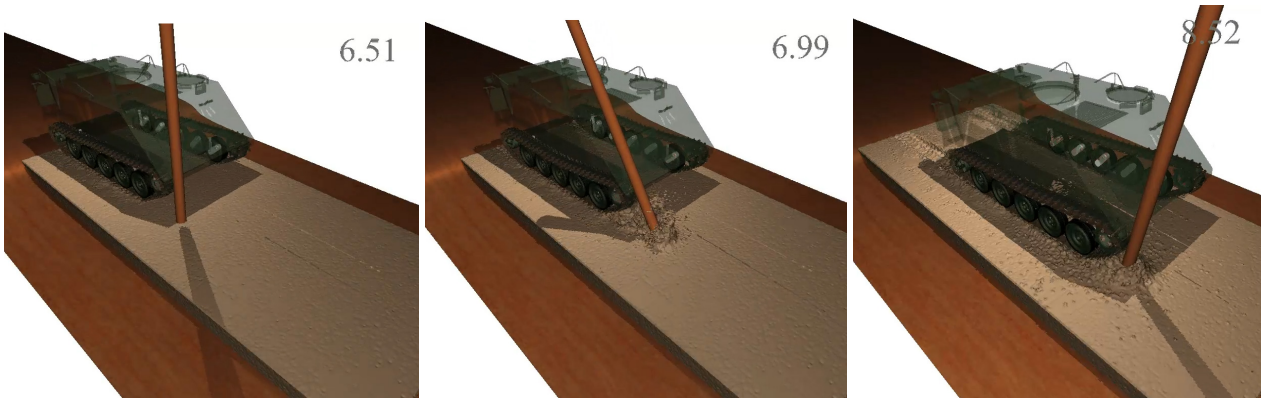


Figure 5B-37: Snapshots of a Tracked Vehicle (M113) Pushing a Rigid Cylinder Embedded in the Soft Soil.

Future developments will include:

- Adding an array of vegetation stems with a given spacing, size and embedding depth distribution.
- Using thick or thin beams to represent small tree stems and grass.
- Using a network of thick or thin beams to represent tree roots.

The model can be used to predict the response quantities of interest including:

1) 3D motion/deflection/breakage of the vegetation.
2) 3D interaction forces between the vegetation and the vehicle.
3) GO/NOGO. Can the vehicle override the vegetation given the available engine power and the maximum traction the soil can support?
4) Override force at any vehicle speed and impact direction. The override force must be smaller than the force which will cause permanent deformation to the vehicle body.
5) Resistance force at any vehicle speed and impact direction.
6) Soil rut depth and width created by the vegetation.

5B.3.11 Ability to Represent Urban Obstacles

This capability has not yet been demonstrated using the DIS/GroundVehicle prototype. As mentioned in Section 5B.3.10 above, a demonstration of a tracked vehicle pushing a large tree stem/pole at 4 mph was created using DIS/GroundVehicle. Future developments will include:

- Adding the capability to model urban obstacles as multibody systems composed of rigid and flexible bodies.
- Adding the capability to model urban obstacles using DEM particles connected using thin/thick beam, shell, or brick elements.
- Developing a library of standard urban obstacle models, including poles, walls (including brick, concrete, and sheet metal), fences (including metal wire, metal bars, and wood), bridges, tunnels, other vehicles, debris, and small structures.

5B.3.12 Ability to Read the Terrain Input Data from GIS Software Tools

A utility for reading the Map 11 raster ascii input files (both the .ter and the .asc files) (see the TA1 GIS Chapter) was developed and integrated into the DIS/GroundVehicle software tool (Figure 5B-38). A raster cell size in the Map 11 file can range from the size of a vehicle (e.g., 10 m × 10 m) to the size of the vehicle running gear (e.g., 0.1 m × 0.1 m). The Map 11 file contains the data listed in Section 5A.4.12 needed by the Complex Terramechanics prototype for each terrain cell.

The Map 11 reading utility can also be used to extract the ranges (minimum and maximum values) of the various terrain variables.

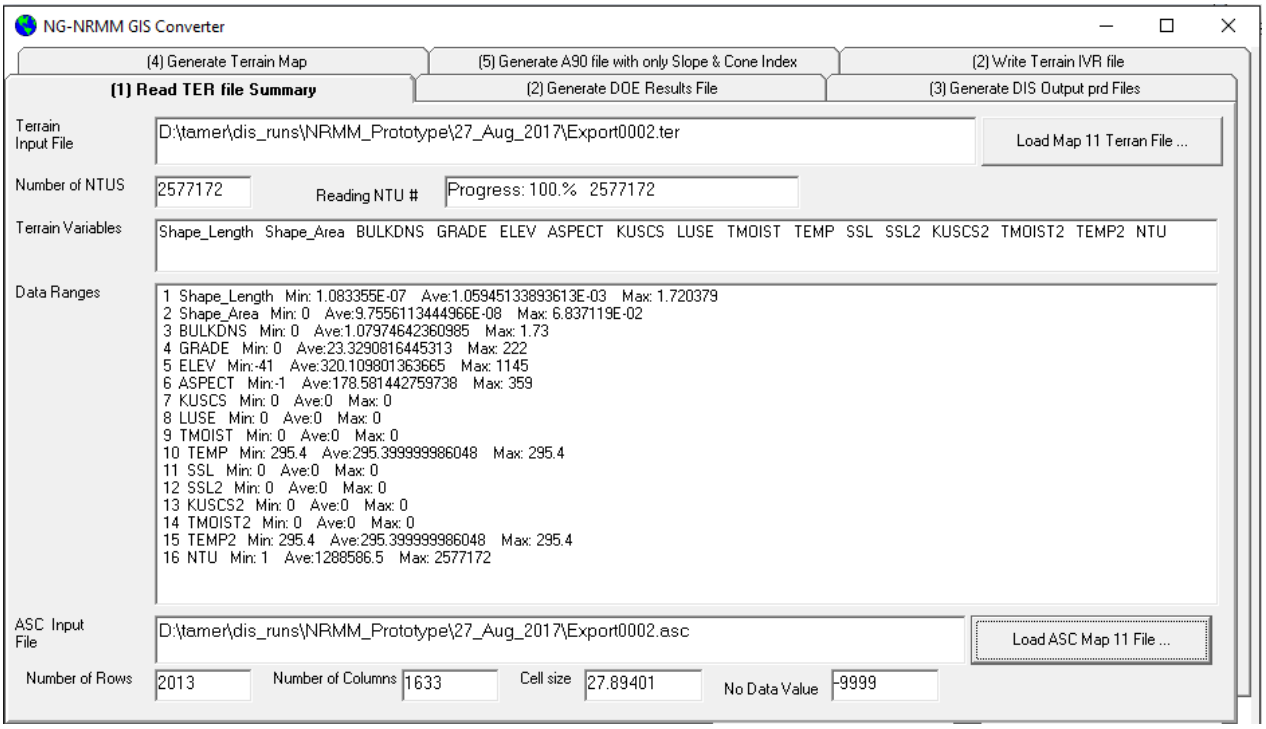


Figure 5B-38: Utility for Reading the Map 11 Raster Ascii Input File.

5B.3.13 Ability to Generate Terrain Mobility Maps and Display the Maps in GIS Software Tools

The complex terramechanics software tool must be able to read each terrain cell properties and write the response quantities in Sections 5A.4.1 and 5A.4.2 for each terrain cell such that the terrain map can be colored using a desired response quantity. The utility for reading the Map 11 terrain file (Figure 5B-38) can also be used to write a Map 11 file with those output response quantities. A procedure to generate the terrain mobility map using the DIS/GroundVehicle software tool is presented in Section 5B.4.

5B.3.14 Ability to Conduct Coupled Simulations with MBD Software for Modeling the Vehicle

DIS/GroundVehicle software system has the following MBD capabilities for modeling ground vehicles:

1) Ability to model pneumatic tires (Section 5B.3.14.1).
2) Ability to model segmented tracks (Section 5B.3.14.2).
3) Ability to model continuous belt-type tracks (Section 5B.3.14.3).
4) Ability to model the interaction of any vehicle part with the terrain (Section 5B.3.14.4).
5) Ability to model the vehicle systems necessary for mobility (Section 5B.3.14.5).
6) Ability to model vehicle payloads and occupants (Section 5B.3.14.6).
7) Ability to model the various types of vehicle maneuvers on any terrain (Section 5B.3.14.7).

5B.3.14.1 Ability to Model Pneumatic Tires

A diagram showing the various tire forces, moments, translational motions, and angles is shown in Figure 5B-39 [41]. They include:

1) Normal load.
2) Normal deflection and normal speed.
3) Longitudinal force including tractive and resistance force.
4) Linear speed.
5) Lateral force.
6) Lateral deflection and lateral slip.
7) Wheel torque (driving and braking).
8) Tire angular velocity or tire slip.
9) Slip angle.
10) Self-aligning moment.
11) Over-turning moment.
12) Camber angle.

The function of a tire model is to relate those variables. This includes:

1) Relating tire normal deflection and speed to normal force.
2) Relating normal load and linear speed to the resistance force.
3) Relating longitudinal force to tire slip, normal force, and linear speed.
4) Relating self-aligning torque to slip angle, normal load and linear speed.
5) Relating lateral force to slip angle, normal load and linear speed.
6) Relating over-turning moment to camber angle, normal load and linear speed.

DIS includes two types of tires models:

1) Simple one-body tire model; and
2) Finite Element (FE) tire model.

The simple tire model uses the experimental tire data to relate those variables. This experimental data includes normal load versus deflection, longitudinal force versus normal load and slip, lateral force versus normal load and slip angle, and self-aligning torque force versus normal load and slip angle. The FE tire model naturally couples all the tire variables. In that model, the tire rubber and reinforcements material and geometric parameters are set to match the actual tire construction and then further fine-tuned to match the tire's experimental data.

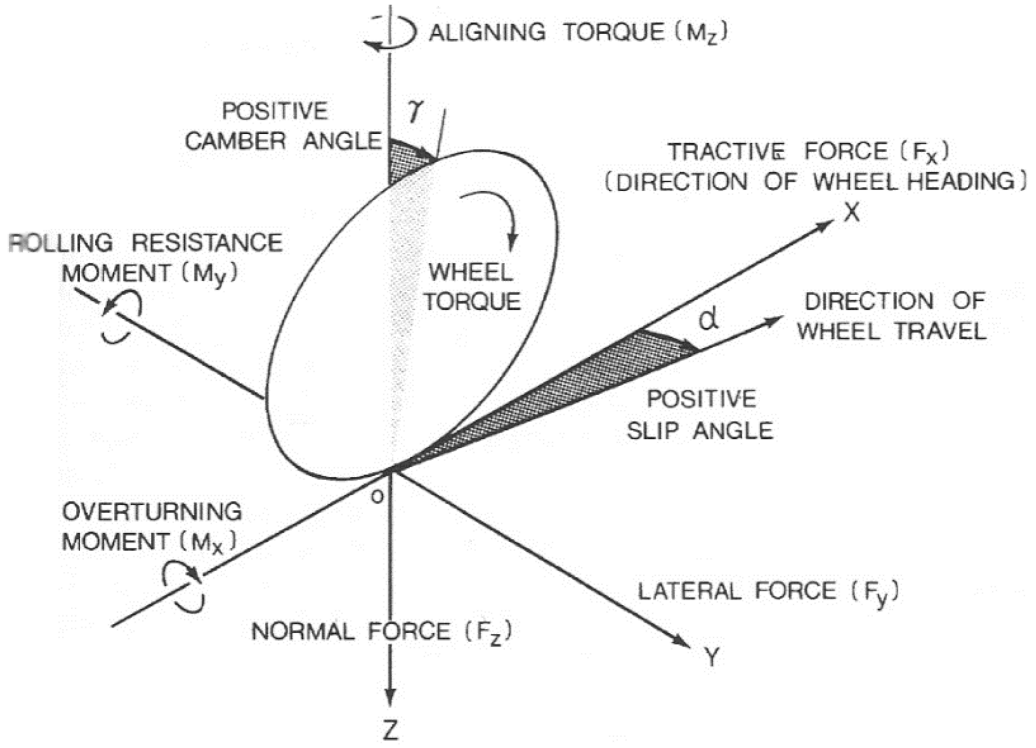


Figure 5B-39: Diagram Showing the Tire Forces, Moments, and Angles [41].

1) In the **simple tire model**, the tire surface is attached to the rigid body representing the wheel. Any polygonal surface can be used to represent the tire's tread surface (Figure 5B-40). Contact is distributed on the tire surface points with contact points position remaining fixed with respect to the wheel. The asperity-spring friction formulation is used to model friction and a normal force versus penetration is used to model normal contact. The simple tire model can be used with hard polygonal terrains as well as soft soil DEM terrains.

When used with hard terrains, the normal force versus penetration can be tuned to match the normal load versus deflection load of the tire at the given tire air pressure. Normal damping is used to match the tire rolling resistance moment. The tire-terrain friction model is tuned to match the longitudinal force versus slip and normal load experimental data (given by the Magic formula [42]). The experimental data of lateral force versus slip angle and normal force (given by the Magic formula) is directly used to calculate the lateral force. Similarly, the experimental data of self-aligning torque versus slip angle and normal force (given by the Magic formula) is directly used to calculate the lateral force. Finally, the over-turning moment can be tuned by adjusting the effective tire width (in conjunction with the normal load versus deflection curve). This model is computationally efficient and can be used in real-time vehicle simulation on hard terrains (such as driving simulators). Examples of simple tire model simulations on hard terrains are shown in Figure 5B-30, Figure 5B-31, and Figure 5B-41.

On DEM soft soil terrains the simple tire's tread polygonal surface is assumed to be rigid and is used as a slave contact surface for the DEM soil particles. The tire's forces and moments are the sum of all the forces from the DEM particles in contact with the tire. Examples of simple tire model simulations on various DEM soft soil terrains are shown in Figure 5B-4, Figure 5B-23, Figure 5B-24, Figure 5B-25, Figure 5B-69, and Figure 5B-70.



Figure 5B-40: Polygonal Tread Surface of the Simple Tire Model.

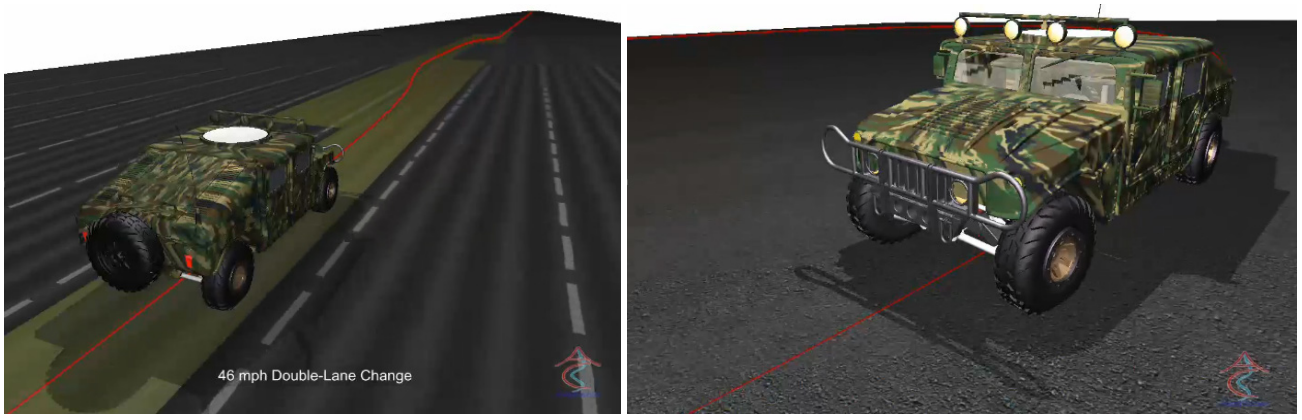


Figure 5B-41: NATC Wheeled Vehicle Platform Undergoing a Double Lane Change at 48 mph (Left) and a 200 ft Constant Radius Turn (Right) on Pavement with the Tire Forces/ Moments Calculated Using the Simple Tire Model.

2) **The FE tire model** can be used for simulating the vehicle on hard pavement as well as DEM soil. In this model, the tire rubber matrix is modeled using 8-node brick elements with a hyper-elastic material model. The tire reinforcements belt, ply, and bead along the circumference direction, and the ply along meridian direction Figure 5B-42) are modeled using thin beam elements which are embedded (share the same nodes) as the rubber brick elements (Figure 5B-43). A polygonal surface representing the tread is attached to the outer surface of the rubber brick elements as a proxy contact surface (Figure 5B-43). The positions of the points on the tread contact surface are calculated using the positions of the points on the finite element tire outer surface as follows:

   - Before the simulation starts, the closest surface element to each point on the tread surface is found by finding the distance between the center of the element and the point. The element with the shortest distance is the element associated with that tread surface point.
   - During the simulation, the positions of the tread surface points are dynamically updated such that the relative position between a point and the center of the associated element remains constant along the normal and two tangential directions to the element surface.

- During the element force evaluation step of the simulation the contact forces on a tread point are transferred to the nodes of the closest element by distributing the force based on the distance between the point and each of the element nodes.

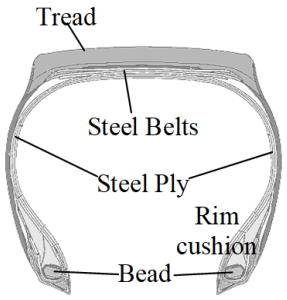


Figure 5B-42: Tire Cross-Section Components.

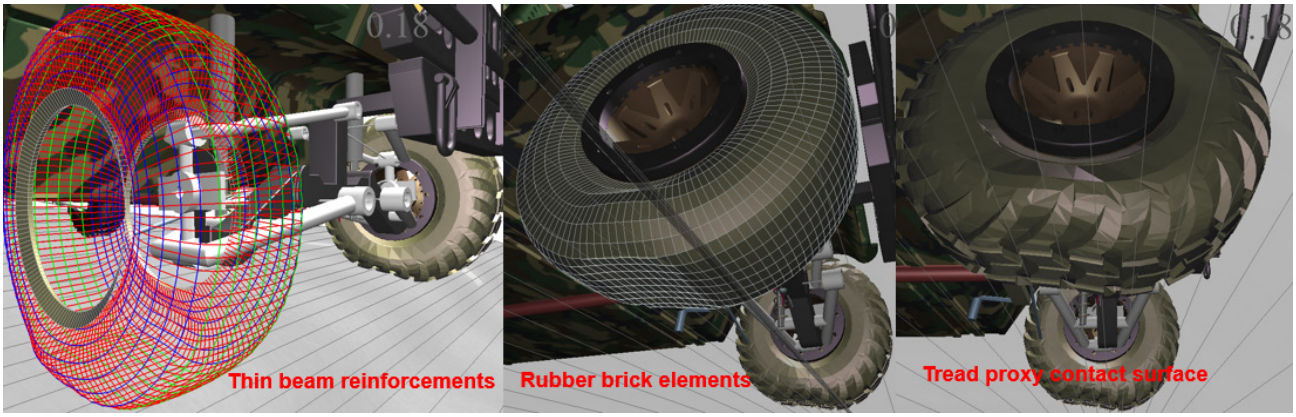


Figure 5B-43: Finite Element Tire Reinforcements (Left), Rubber Brick Elements (Center), and Tread Proxy Contact Surface (Right).

Finally, the tire uses a smaller time step than the time step used for the vehicle and soil. For each soil and vehicle time step, *n* tire time steps are performed. This is necessary because the time explicit time step needed for the tire is much smaller than that needed for the vehicle and soil. In summary, the pneumatic tire model in DIS can account for the following effects:

1) Tire inflation pressure. For example, under-inflated tires typically yield high vehicle mobility on soft soil and low mobility on hard terrains, while the reverse is true for tire inflated to the nominal pressure. Those effects must be captured by the coupled complex terramechanics and flexible multibody dynamics vehicle models.
2) Tire construction including layout and material properties of the ply, belt, and bead reinforcements and the rubber matrix.
3) Tire tread pattern.

The FE tire was tested with the tread on a rigid terrain. The tread proxy contact surface is used for contact calculation with the polygonal ground surface. The forces on the proxy surface contact points are then

interpolated to the finite element nodes. Figure 5B-44 shows snapshots from the simulation of a finite element tire with the proxy tread contact surface going over a polygonal terrain. Figure 5B-45 shows snapshots of the vehicle at the same time instants as Figure 5B-44 with the tire displayed using the finite element surface. Figure 5B-46 shows a snapshot of the multibody vehicle model with finite element tires colored using the lateral shear stress.



Figure 5B-44: Snapshots of the Multibody Vehicle Model with Finite Element Flexible Tires Displayed using the Tread Proxy Contact Surface. The Tire is Going over Hard Pavement.



Figure 5B-45: Snapshots of the Multibody Vehicle Model with Finite Element Flexible Tires Displayed using the Original Finite Element Tire Surface. The Tire is Going over Hard Pavement.

Figure 5B-47 and Figure 5B-48 show snapshots from a simulation of a multibody dynamics vehicle model with an FE tire with a complex tread surface modeled using the proxy contact surface technique going over a DEM soft soil terrain

A spreadsheet-based user interface is used for creating the FE tire model in DIS/GroundVehicle (Figure 5B-49). The user can define the following parameters through the interface:

- General tire parameters: wheel, internal pressure, circumference divisions, contact properties (stiffness, damping and friction), etc. (Figure 5B-49). Those also include the CAD model of the tread surface. The model is read in VRML 2.0 format.
- Tire cross-section coordinates and connectivity defining the tire cross-section discretization.
- Tire cross-section brick elements materials.
- Nodes along the tire cross-section which form the tire outer, inner, and rim surfaces.
- Nodes in the tire cross-section where circumference reinforcements are located and the reinforcements' mechanical properties (axial stiffness/damping, bending stiffness/damping and mass per unit length).
- Nodes in the tire cross-section where meridian rods reinforcements are located and the reinforcements' mechanical properties.
- Brick element material numbers.

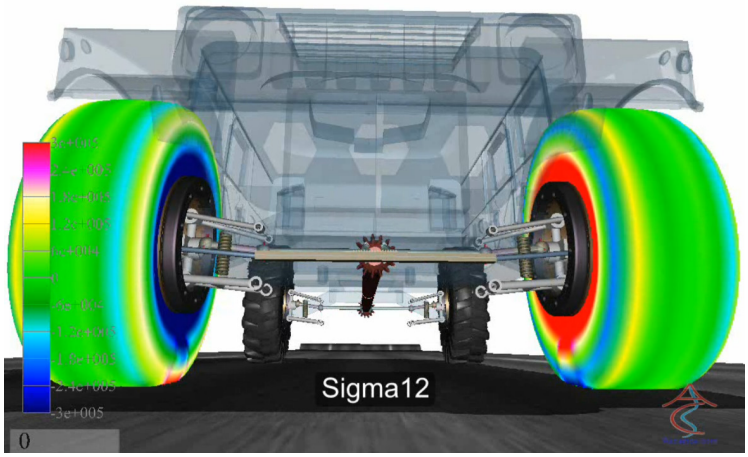


Figure 5B-46: Snapshot of the Multibody Vehicle Model with Finite Element Flexible Tires Colored Using the Lateral Shear Stress.

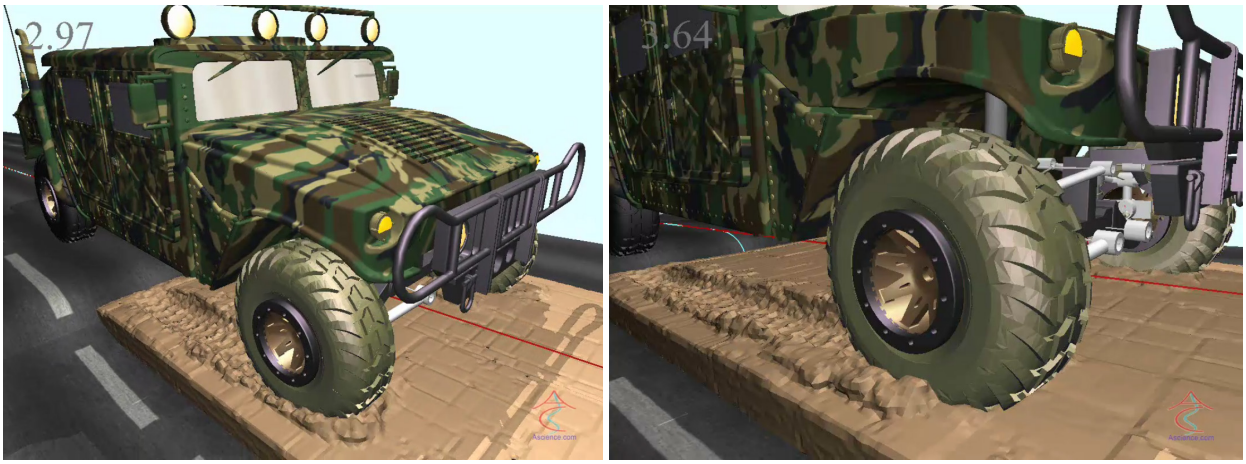


Figure 5B-47: Snapshots of a Vehicle Simulation with a Flexible Tire having a Complex Tread Pattern Running on DEM Soft Soil.

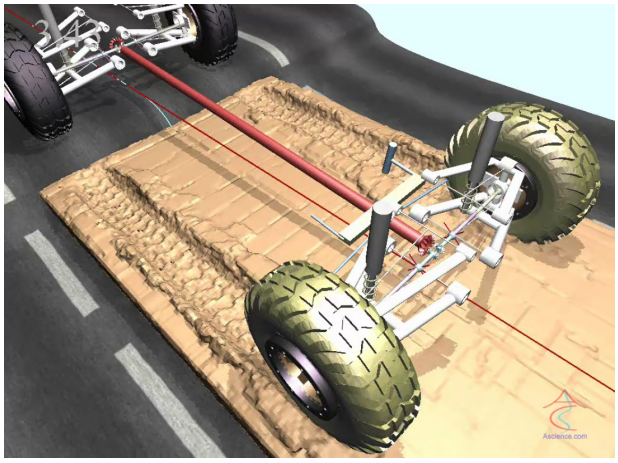


Figure 5B-48: Top View of the Soil, Vehicle and Finite Element Tire.

The single tire test rig shown in Figure 5B-50 can be used to experimentally calibrate the following tire response quantities on pavement and soft soil for both the simple tire and the FE tire models:

- Tire deflection versus normal load at a given internal air pressure (Figure 5B-51).
- Rolling Resistance: longitudinal force versus speed and normal load (Figure 5B-52).
- Longitudinal force versus slip, speed and normal load (Figure 5B-53).
- Lateral force versus slip angle and normal load (Figure 5B-54).
- Self-aligning torque versus slip angle and normal load (Figure 5B-55).

Areas where further research is needed to calibrate the FE tire include:

- Use an experimental tire test rig similar to the model in Figure 5B-50 which can control/measure the various tire loading variables and angles.
- Validation of the tire model on hard pavement using the tire test rig.
- Validation of the tire model on soft soil using the tire test rig.
- Validation of coupled tire - vehicle model on hard pavement.
- Validation of coupled tire - vehicle model on soft soil.

Some of the (steady-state and transient) quantities which need to be experimentally validated for the FE tire model using the single tire test rig include:

- Normal force versus deflection test (including footprint area).
- Vertical vibration test.
- Test for relation between drawbar force, torque, angular velocity, camber angle, and slip.
- Over-turning moment versus camber angle test.
- Cornering test: Self-aligning torque, lateral force, versus slip angle for different angular velocities.
- Normal contact force and tangential force distributions in the contact patch in the various tests.

TireDetailed1	Comment:				
Parameter Description	**Symbol**	**Value1**	**Value2**	**Value3**	**Units**
Wheel mass	M_{Wheel}	10			kg
Wheel rotational inertia	J_{Wheel}	0.4			$kg.m^2$
Wheel radial inertia	I_{Wheel}	0.4			$kg.m^2$
Wheel icon file name	$File_{Wheel}$				
Wheel icon translation (length, width, height)	$Trans_{Wheel}$	0	0	0	m
Wheel icon scale (radius, width)	$Scale_{Wheel}$	1	1		
Wheel icon Euler angles	$Angles_{Wheel}$	0	0	0	degree
Standard tire Wheel radius	$Radius_{Wheel}$	0.264			m
Standard tire Wheel width	$Width_{Wheel}$	0.351			m
Cross-section Translation	$Trans_{Cross}$	0	0		
Cross-section Scale	$Scale_{Cross}$	1	0.9		
Cross-section Post Scale Translation	$PostTrans_{Cross}$	0	0		
Axis rotation	$RotationAxis$	0	0	1	
Rotation angle around axis	$RotationAngle$	1.5708			rad
Circular divisions	$CircDivs$	128			
Tire pressure	$TirePressure$	2.60E+05			Pa
Pressure ramp time	$PressRampTime$	0.001			sec
Internal tire damping per unit area	$TireDamp$	80000			Pa/(m/s)
Search tolerance (Tire-Pavement)	$SearchTol_{Tire}$	0.02			m
Tire coefficient of friction	Mu_{Tire}	0.9			
Tire friction spring stiffness per unit area	$FricSpring_{Tire}$	4.00E+08			$N/m/m^2$
Tire velocity stiffness per unit area	$VelStiff_{Tire}$	1.70E+05			$N/(m/sec)/m^2$
Tire normal stiffness per unit area	$NorStiff_{Tire}$	4.00E+08			$N/m/m^2$
Tire normal damping per unit area	$NorDamp_{Tire}$	9.00E+04			$N/(m/sec)/m^2$
Tire separation damping factor	$SepDamp_{Tire}$	0.05			
Normal averaging	$NormalAve$	0.75			
Search tolerance (Tire-Rim)	$SearchTol_{Rim}$	0.015			m
Tire coefficient of friction	Mu_{Rim}	0.7			
Tire friction spring stiffness per unit area	$FricSpring_{Rim}$	3.00E+10			$N/m/m^2$
Tire velocity stiffness per unit area	$VelStiff_{Rim}$	1.70E+05			$N/(m/sec)/m^2$
Tire normal stiffness per unit area	$NorStiff_{Rim}$	3.00E+10			$N/m/m^2$
Tire normal damping per unit area	$NorDamp_{Rim}$	9.00E+04			$N/(m/sec)/m^2$
Rolling radius (with loaded vehicle)	$RollingRadius$	0.492063492			m
Number of time step subcylcles	$SubCycles$	6			
Tread surface	$TreadSurface$	..\tire2.wrl			
Tread surface translation (length, width, heigh	$Trans_{Tread}$	0	0	0	m
Tread surface scale (radius, width)	$Scale_{Tread}$	1	1		
Tread surface euler angles	$Angles_{Tread}$	0	0	0	degree

Figure 5B-49: DIS/GroundVehicle User Input Spreadsheet for the Main Tire Parameters.

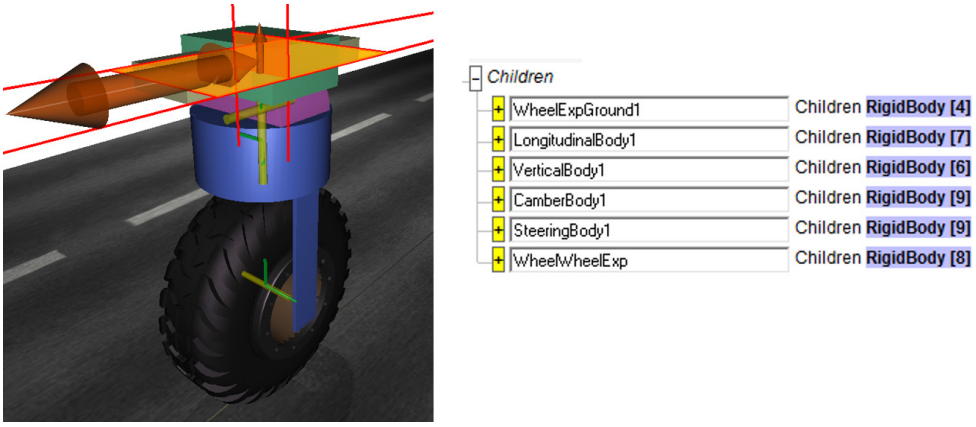


Figure 5B-50: Model of a 4-DOF (Longitudinal, Vertical, Camber and Steering) Tire Test Rig. The Rig consists of five Rigid Bodies: Longitudinal Body, Vertical Body, Camber Body, Steering Body, and Wheel.

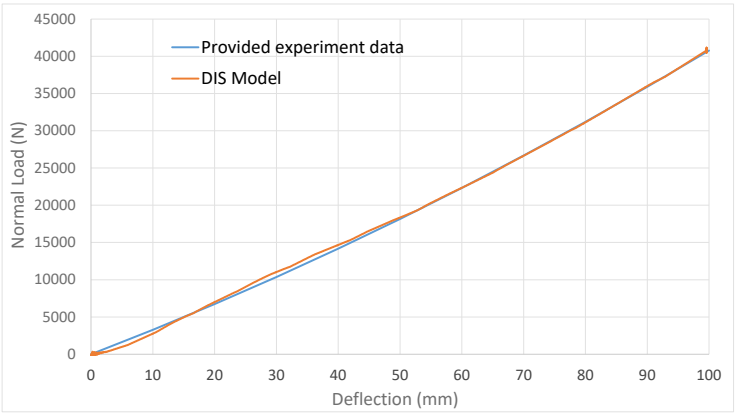


Figure 5B-51: Tire Deflection Versus Normal Load on Pavement Obtained Using the Single Wheel Test Rig Model.

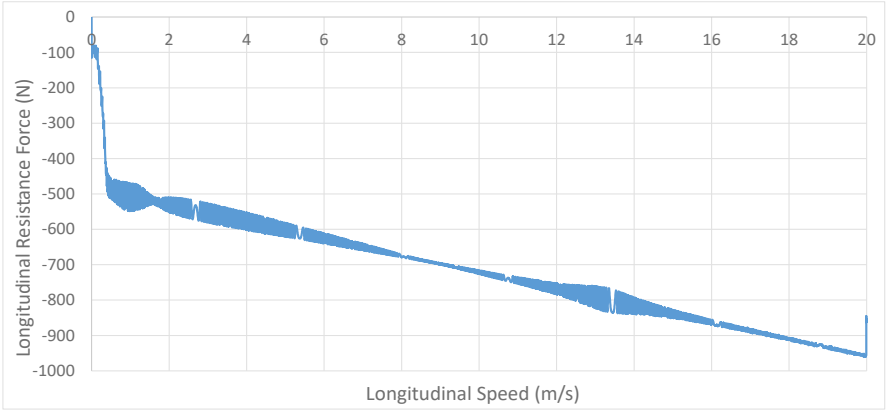


Figure 5B-52: Rolling Resistance: Longitudinal Force Versus Speed and Normal Load on Pavement Obtained Using the Single Wheel Test Rig Model.

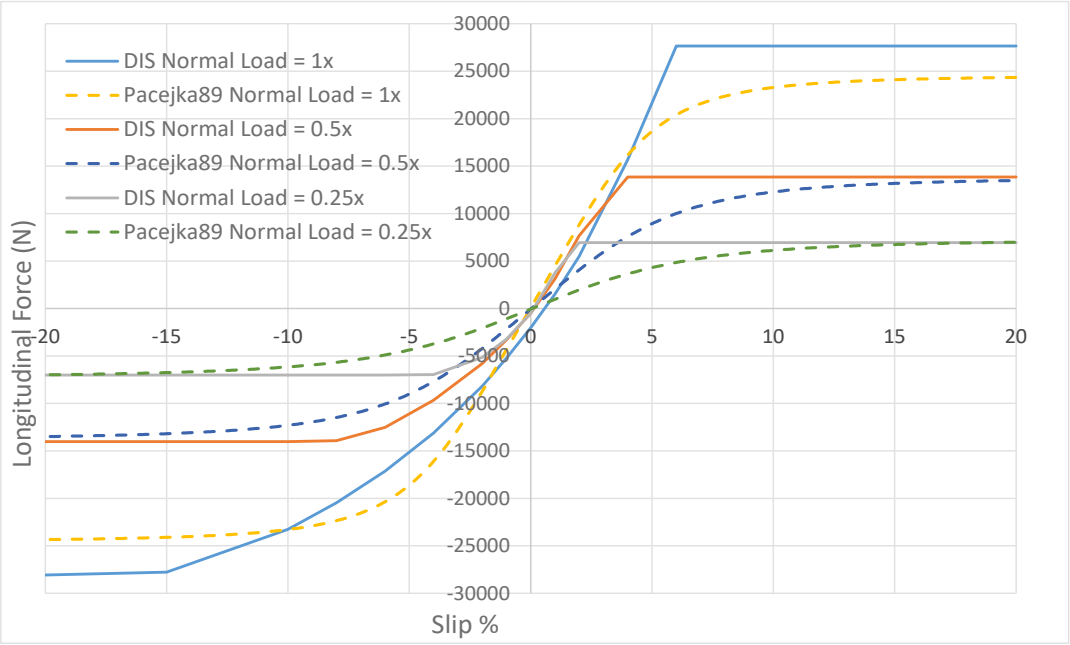


Figure 5B-53: Longitudinal Force Versus Slip and Normal Load on Pavement: Comparison of Single Wheel Test Rig Simple Tire Model And Pacejka89 Experimental Tire Data (Vehicle Speed = 50 Km/Hr, Nominal Normal Load = x = 34.814 kN).

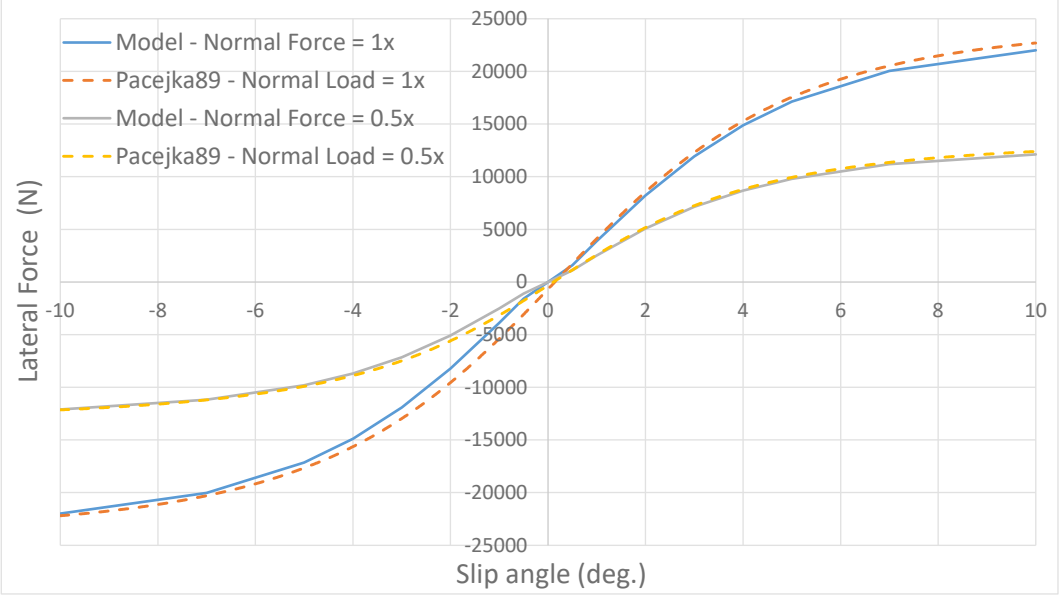


Figure 5B-54: Lateral Force Versus Slip Angle on Pavement: Comparison of Single Wheel Test Rig Simple Tire Model and Pacejka89 Experimental Tire Data (Vehicle Speed = 50 Km/Hr, Nominal Normal Load = X = 34.814 kN).

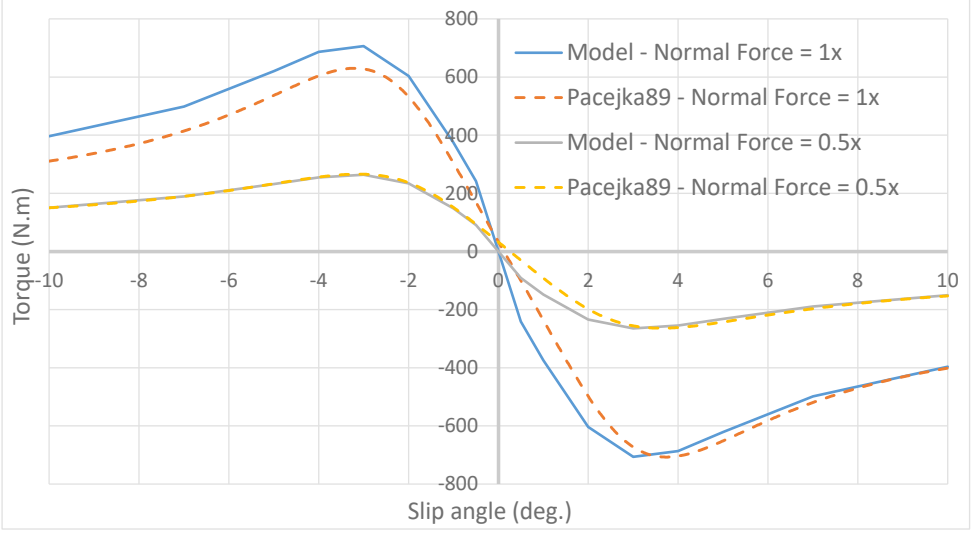


Figure 5B-55: Self-Aligning Torque Versus Slip Angle on Pavement: Comparison of Single Wheel Test Rig Simple Tire Model and Pacejka89 Experimental Tire Data (Vehicle Speed = 50 Km/Hr, Nominal Normal Load = X = 34.814 kN).

5B.3.14.2 Ability to Model Segmented Tracks

In the DIS segmented track model, each track segment, the road wheels, and the sprocket are modeled as rigid bodies. General polygonal contact surfaces can be defined for each track segments for sprocket-to-segment, road wheel-to-segment, and terrain-to-segment contact. For each contact surface the normal (penalty) and tangential (friction) contact parameters can be specified. This allows modeling compliance of the wheels and track shoes rubber layer. It also allows including friction between the track segments and the wheels/sprockets. General polygonal contact surfaces for the road wheels and the sprocket can also be specified. Thus, the effects of track segment, track shoe grouser pattern, and sprocket geometries on vehicle mobility and track vibrations are included in the model. The segmented track contact model works on both hard polygonal terrains (Figure 5B-30 and Figure 5B-31) and DEM soft soil terrains (Figure 5B-20, Figure 5B-36, and Figure 5B-37).

An automatic segmented track generator is included in DIS which allows specifying the routing of the track around the road wheels and sprocket. The automatic track generator supports single (Figure 5B-56) and double (Figure 5B-57) pin segmented tracks.

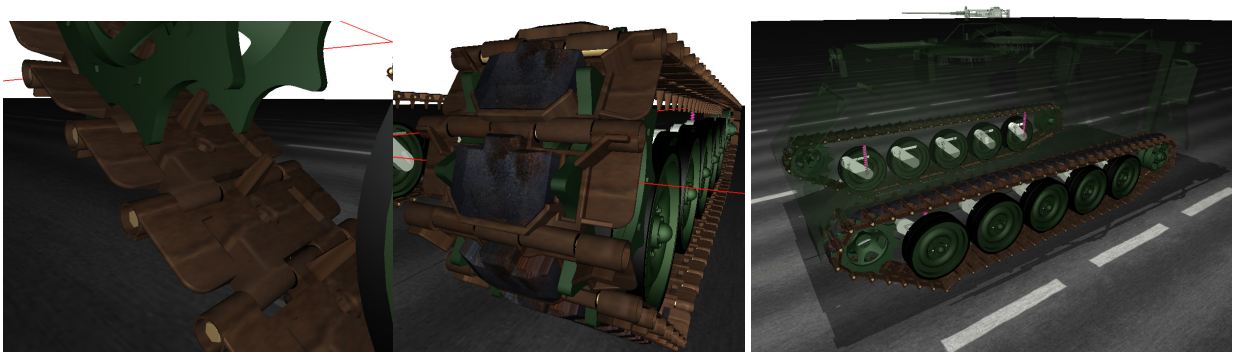


Figure 5B-56: Typical Single Pin Segmented Track: One Revolute Joint in Each Sprocket Groove.

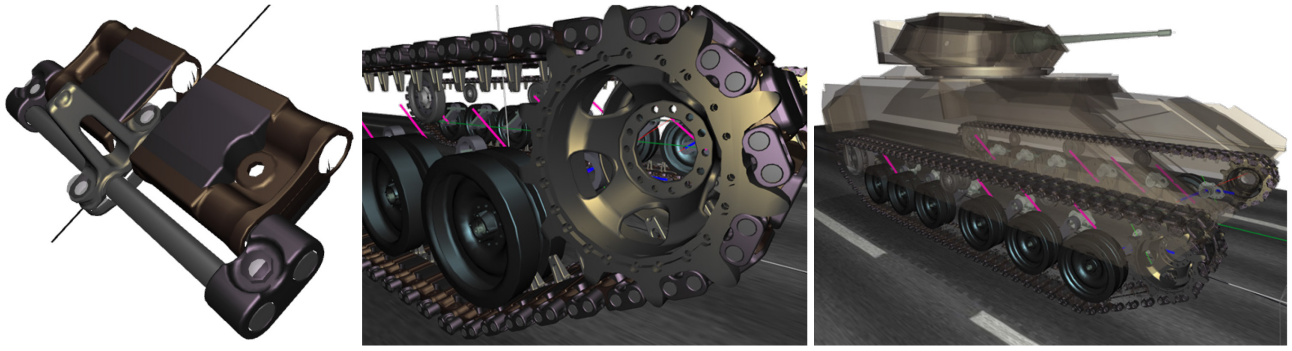


Figure 5B-57: Typical Double-Pin Track Segmented Track: Two Revolute Joints in Each Sprocket Groove.

5B.3.14.3 Ability to Model Continuous Belt-Type Tracks

Continuous belt-type tracks are modeled using an FE model similar to the tire FE model presented in Section 5B.3.14.1 [9], [43]. The belt rubber matrix is modeled using brick elements. The belt's longitudinal and lateral reinforcements are modeled using thin beam elements embedded in the brick elements along the length and width directions of the belt (Figure 5B-58). The track tread pattern and track wheel side (back) pattern are modeled using the proxy contract surface technique. Wheels and sprockets are modeled as rigid bodies. Any polygonal surface can be used to represent the wheels and sprockets. The penalty formulation is used for normal contact and the asperity-spring model is used to model friction. Snapshots of typical simulations of a continuous belt tracked vehicle over a complex topography polygonal terrain are shown in Figure 5B-59.

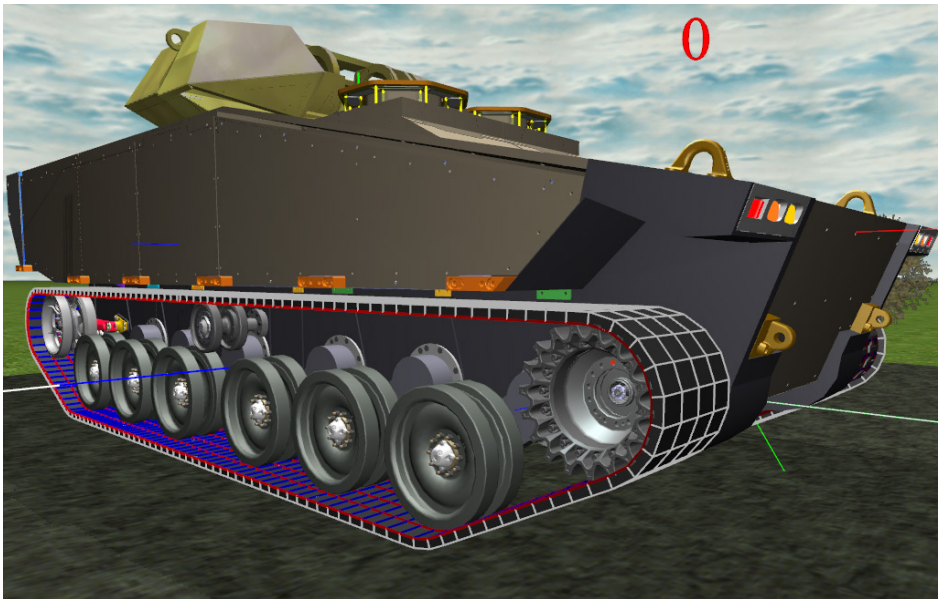


Figure 5B-58: Continuous Belt-Type Track Modeled using Brick Elements, and Longitudinal Beam Elements (Shown in Red) and Lateral Beam Elements (Shown in Blue) Representing the Belt Reinforcements.

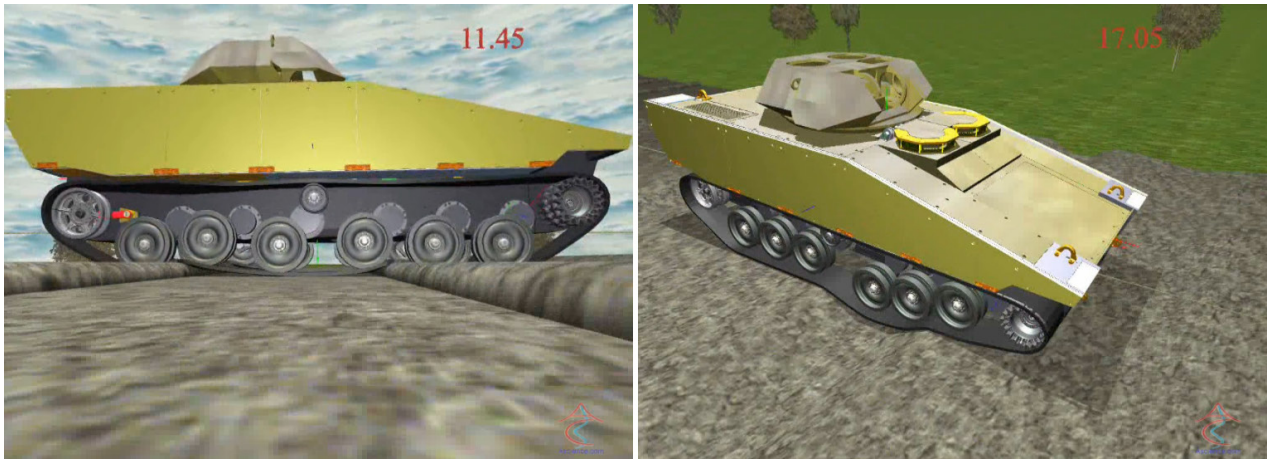


Figure 5B-59: Snapshots of Typical Simulations of a Continuous Belt Tracked Vehicle Over a Complex Topography Polygonal Terrain.

5B.3.14.4 Ability to Model the Interaction of Any Vehicle Part with the Terrain

Any vehicle part which comes into contact with the terrain can be modeled as either a rigid body with a polygonal contact surface or a finite element flexible body with a proxy contact surface (similar to the FE tire). The vehicle parts can include:

1) Vehicle body. For example, in Figure 5B-17 the vehicle body is used as a contact surface for the SPH water particles.
2) Legs (Figure 5B-6 and Figure 5B-26). Leg links are modeled as rigid bodies. Wheels/tires or feet can be attached to the legs. Inverse kinematics with a PID controller are used to control the foot position and orientation. Any number of legs can be used: 1, 2, 4, 6, etc. A balance controller is used to modify the legs and upper body joint angles to ensure stability. Penalty formulation is used for normal contact. Asperity-spring model is used to model friction.
3) Digging blades (Figure 5B-21) and buckets (Figure 5B-60).
4) Tines for tilling the soil (for mine sweeping).

5B.3.14.5 Ability to Model the Vehicle Systems Necessary for Mobility

A DIS vehicle model can include the following subsystems:

1) **Suspension system**. Any type of suspension system can be modeled. Bushings with prescribed radial and axial stiffness and damping curves can be included.
2) **Steering system** including rack and pinion and pitman arm steering systems.
3) **Driveline**. Fidelity of driveline model can be varied from high to low. Driveline model can include:
   - Gear box.
   - CVTs: Toroidal, Belt, and Chain types.
   - Differential.
   - Torque converter.

- Transfer cases.
- Geared hubs.
- Axle.
- CV-joints and/or U-joints.
- Axles including both rigid and independent suspension axles.

4) **Engine**. Fidelity of engine model can be varied from a full engine model to a lumped model. A lumped model consists of the engine's torque speed curve, the engine's rotating inertia, and a table of the gear box ratios and gear shifting speeds. The full engine model can include the following sub-models:
   a) Pistons and cylinders with tabular piston pressures (at various engine speeds and crank angles) [44].
   b) Crank shaft [44].
   c) Timing gear drive [44], [45].
   d) Timing chain-drives.
   e) Timing belt-drive [13], [46].
   f) Cams, tappets and valves.
   g) Accessory belt-drive [8], [47], [48].
   h) Accessory models.
   i) Gear box [44], [45].
5) **Brakes**. Brakes are modeled using the maximum braking torque versus speed curve of the brake.
6) **Vehicle controls** such as: ESC, ABS, and Vehicle Intelligence (VI). Custom vehicle controls can be modeled using the DIS built-in scripting languages which include JAVAscript and Python.

Spreadsheets are used for defining each vehicle subsystem including suspension system, steering system, axles, tires, tracks, engine, brakes, transfer cases, and differentials.



Figure 5B-60: Snapshot of a Backhoe Digging through Non-Cohesive Sand Type Soil Modeled Using Cubical Rigid Body DEM Particles.

5B.3.14.6 Ability to Model Payloads and Occupants

A DIS ground vehicle model can include the following:

- Other multibody systems models carried by the vehicle such as military equipment, machines, and other vehicles.
- Containers with solid payloads.
- Liquid filled tanks (Figure 5B-61).
- Trailers (Figure 5B-61).
- Human occupants.

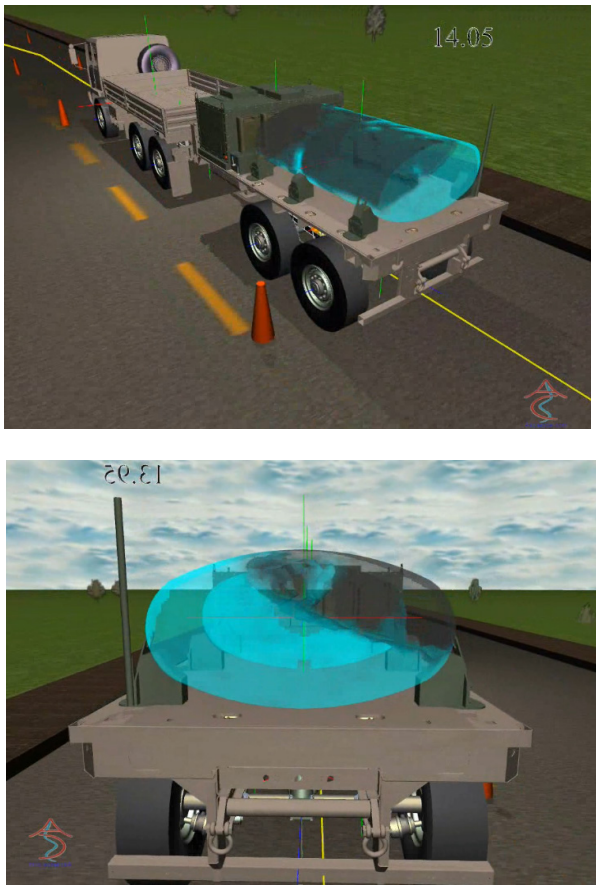


Figure 5B-61: Snapshot of a Military Tanker Truck-Trailer Vehicle Carrying a Water Tank with the Water Modeled Using SPH.

5B.3.14.7 Ability to Model the Various Types of Vehicle Maneuvers on Any Terrain

Typical vehicle maneuvers which were modeled using DIS include:

1) Gradeability:
   a) Long uphill slope (Figure 5B-70, Figure 5B-62 and Figure 5B-63).

b) Long negative slope.

c) Side slope.

2) Steering including predicting under-steering, over-steering, and rollovers:

a) Single and double lane changes (Figure 5B-41).

b) Obstacle avoidance maneuvers.

c) Constant radius turning/cornering (Figure 5B-41).

d) Neutral axis spin for tracked and legged vehicles.

3) Traveling in a prescribed path and speed on any given terrain, including side slopes, long slopes, and complex topography terrains (Figure 5B-29).

4) Braking (Figure 5B-64 and Figure 5B-65). This includes predicting the stopping distance as a function of initial speed, grade, and soil mechanical properties.

5) Rough terrain ride quality (Figure 5B-36 and Figure 5B-66).

6) Positive and negative obstacle crossing ability (Figure 5B-31 and Figure 5B-59).

7) Terrain embedded obstacle pushing ability (Figure 5B-37).

8) Drawbar pull (Figure 5B-67).

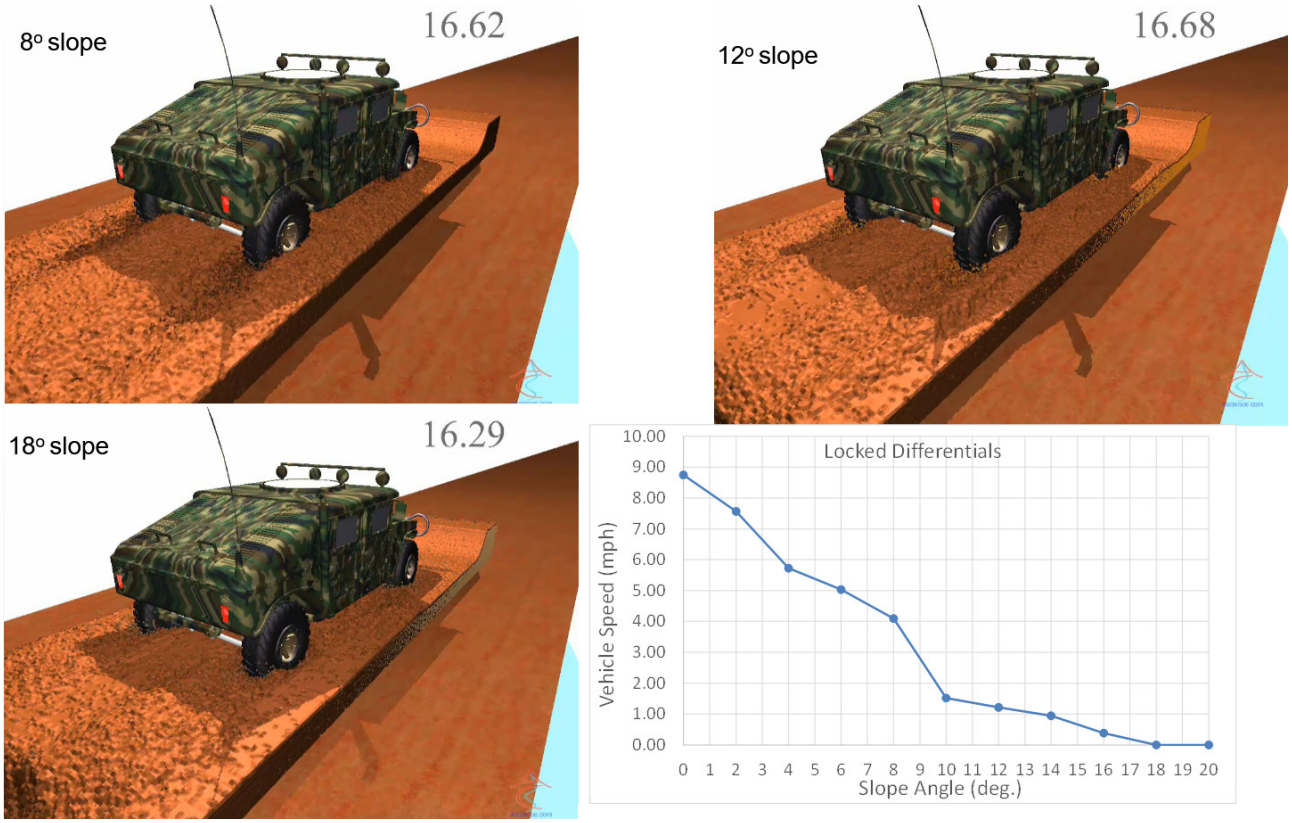


Figure 5B-62: Gradeability on Positive Slopes of the NATC Wheeled Vehicle Platform on LETE Sand.

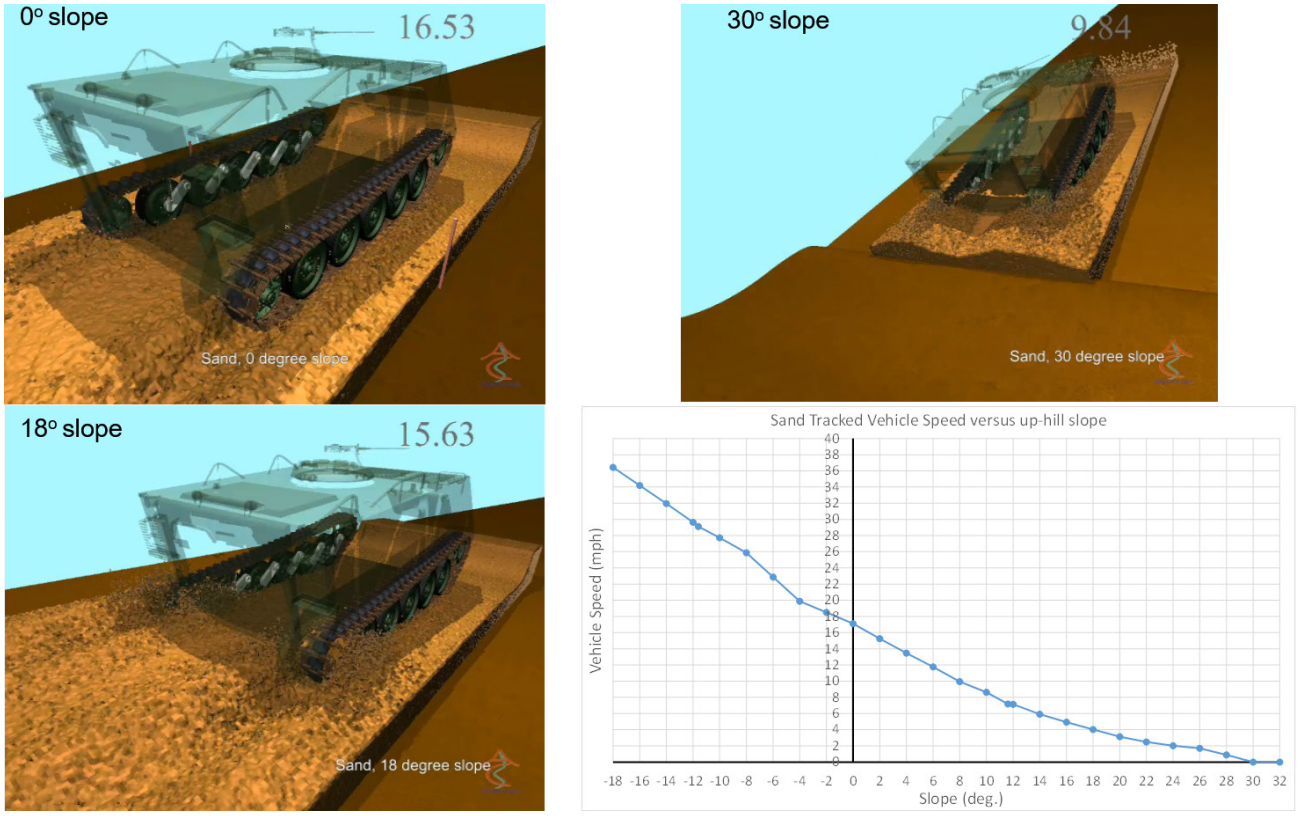


Figure 5B-63: Gradeability on Positive and Negative Slopes of the M113 Benchmark Tracked Vehicle on LETE Sand.

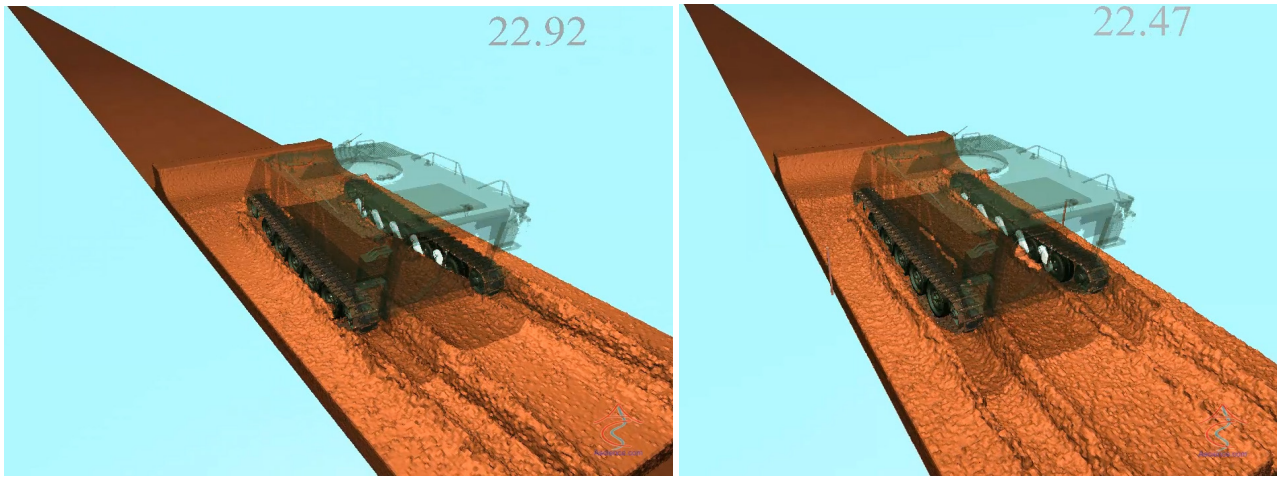


Figure 5B-64: Snapshots of the M113 Tracked Vehicle Braking over a 0° and -10° Long Slope after the Vehicle Comes to a Stop on Soft Soil Terrain with a Cone Index of 30.

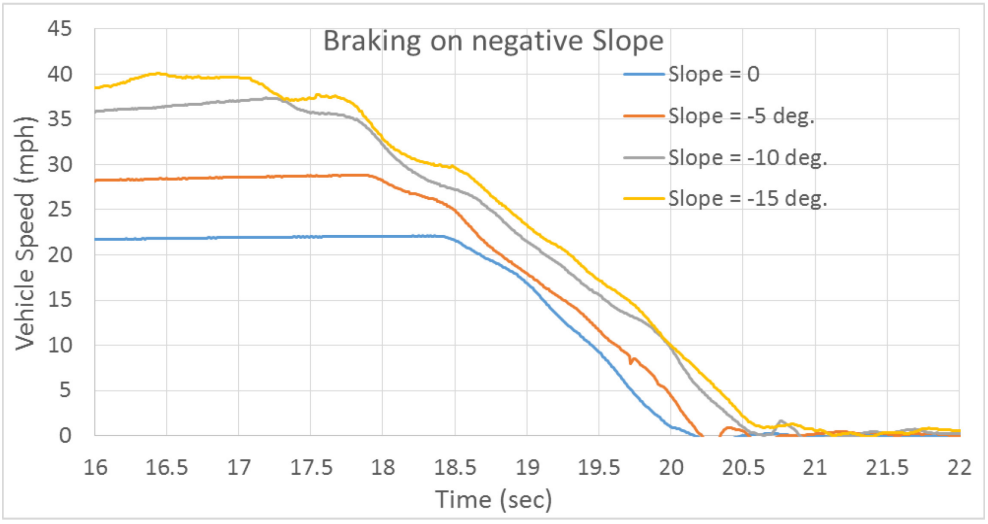


Figure 5B-65: Time-History of Vehicle Speed While Braking on 0°, -5°, -10° and -15° Long Slope Soil Terrain with a Cone Index of 30 Starting from the Maximum Speed Achievable on that Slope.

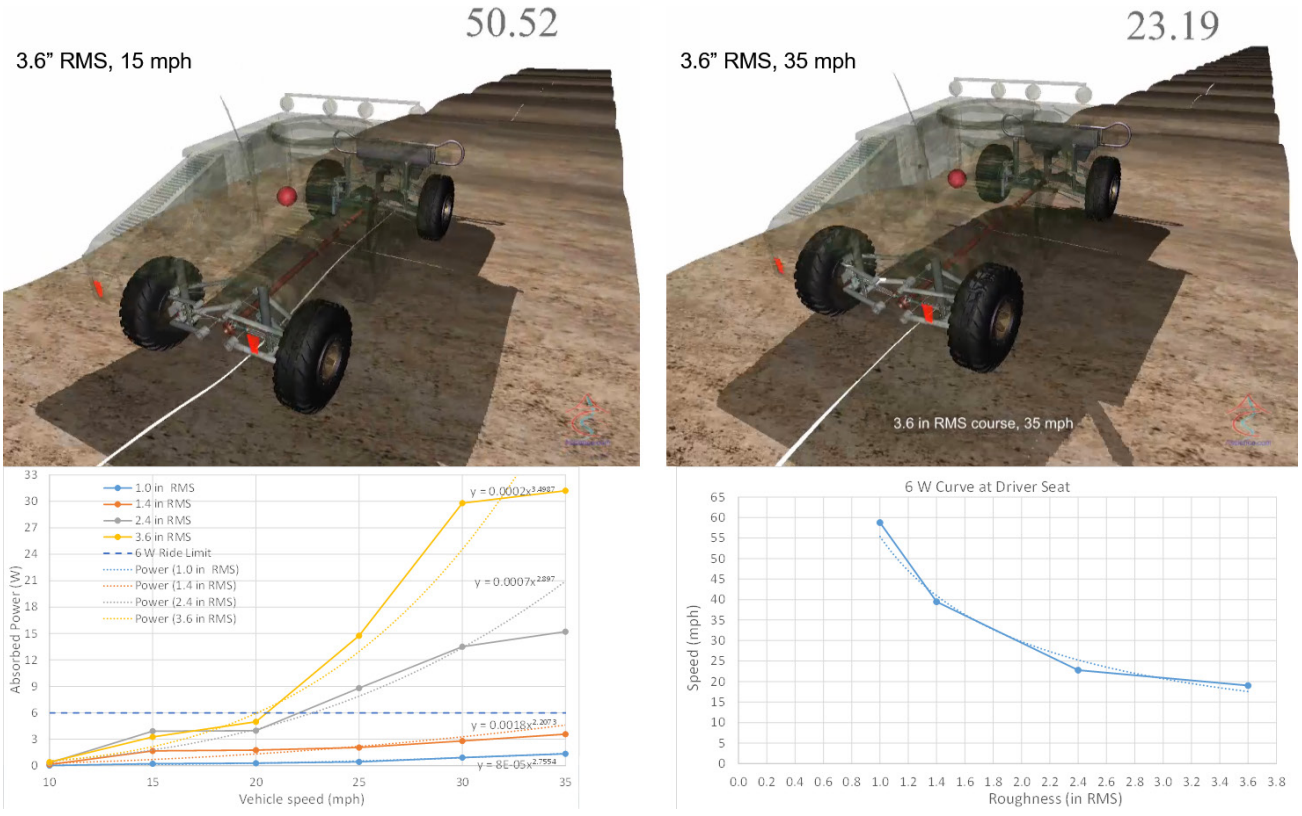


Figure 5B-66: Snapshots of the NATC Wheeled Vehicle Platform Going Over a 3.6” RMS Terrain at 15 and 35 mph. The Bottom Graphs Show the Vehicle Speed Versus Absorbed Power and the 6 W Absorbed Power Vehicle Speed Versus Terrain RMS Roughness.

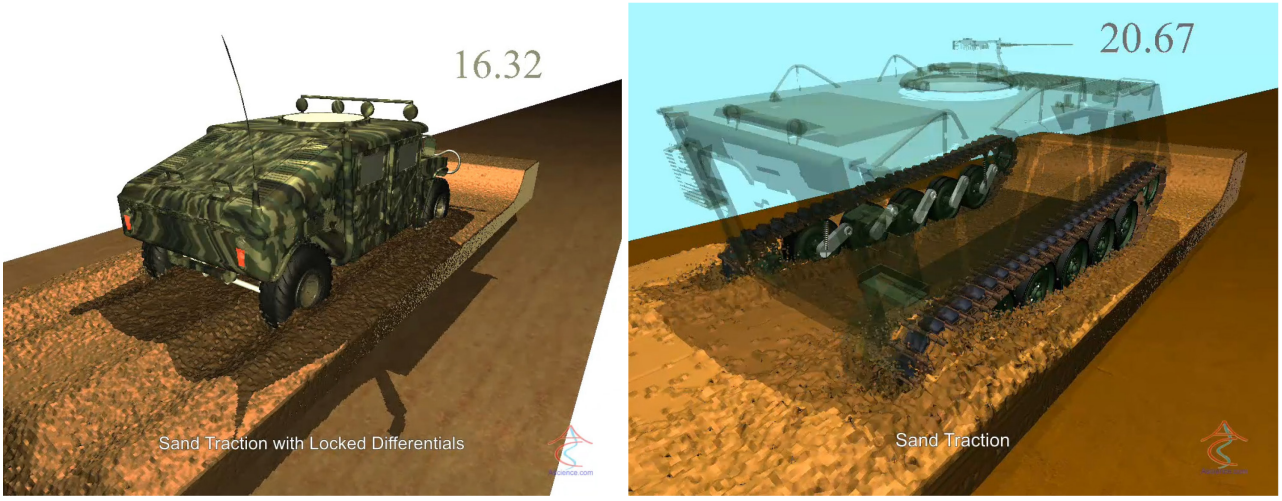


Figure 5B-67: Snapshots from the Drawbar Pull Simulations of the NATC Wheeled Vehicle Platform and the M113 Track Vehicle on LETE Sand.

5B.4 PROCEDURE TO PRODUCE A MOBILITY TERRAIN MAP

A demonstration of using the DIS/GroundVehicle complex terramechanics prototype in a Design Of Experiment (DOE) procedure to predict the "Speed-Made-Good" for a typical HMMWV-type military wheeled vehicle, over a large terrain map using two terrain variables was presented in Ref. [28]. The two terrain variables are: terrain long slope and soil Cone Index (CI) (based on varying the DEM inter-particle cohesion while keeping the DEM inter-particle coefficient of friction constant). The procedure consisted of the following steps:

1) A rectangular terrain map is divided into grid cells. For each grid cell, the value of the selected two terrain variables are extracted. Then, the ranges (minimum and maximum) of the two terrain variables over the entire terrain map are found.

2) The long slope range of the terrain map is discretized into a certain number of values (G). Also, the Cone Index range is discretized into a certain number of values (C). Then a vehicle mobility simulation is performed for each of the full-factorial $G \times C$ combinations of slope and cohesion values. All the combinations are run in parallel on individual HPC nodes. For each combination, the various steady-state vehicle mobility measures are calculated.

3) The mobility measures values are bi-linearly interpolated from the calculated values to the actual values for each terrain grid cell.

4) A map of the mobility measure over the entire terrain map is then generated by coloring each grid cell using the mobility measure, such as the Speed-Made-Good (Figure 5B-68).

The DOE procedure described above is used to generate a vehicle mobility map for a 22 km x 22 km rectangular terrain map in Figure 5B-68. The terrain map is divided into 20 m x 20 m rectangular cells. The ra\nge of slopes for the cells is from 0 to 39 degrees (80% grade). This range is discretized into 14 values 0, 3, 6, … 36, 39 °. The range of CI is 30 to 300 and is discretized using the 12 CI values. A vehicle simulation is performed for each combination of longitudinal slope and CI. Therefore, the mobility map in Figure 5B-68 required 14 × 12 = 168

vehicle simulation runs. Each run requires 2 to 7 days (depending on how many HPC nodes are used) to complete. However, all the runs can be performed at the same time on an HPC and therefore the total simulation times is 2 to 7 days. Note that without the DOE procedure, a separate run would be required for each terrain cell. The 22 km × 22 km would require 1100 × 1100 = 1.21 million runs instead of 168. Therefore, a DOE procedure along with a corresponding interpolation technique are needed to enable using a reduced set of runs. Also, note that for about half of the runs, the vehicle gets stuck (i.e., Speed-Made-Good is zero) after a few seconds of the simulation, due to the combined effect of high slope and low soil cohesion. Once the vehicle gets stuck then the run can be ended. A plot of the steady-state vehicle speed versus long slope and Cone Index (cohesion) is shown in Figure 5B-69. Snapshots of 4 combinations of soil CI and terrain slope simulations are shown in Figure 5B-70.

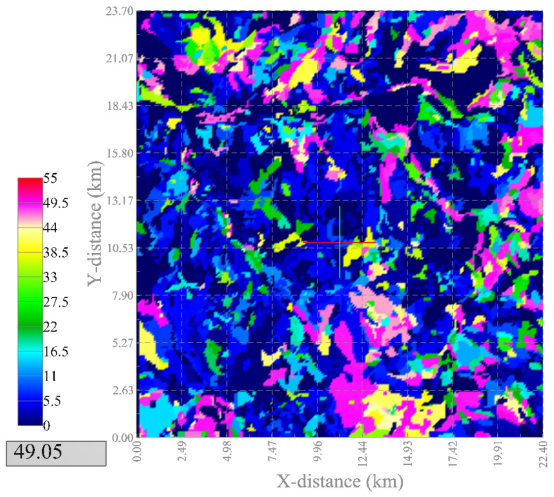


Figure 5B-68: Terrain Map Colored by the Speed-Made-Good [28].

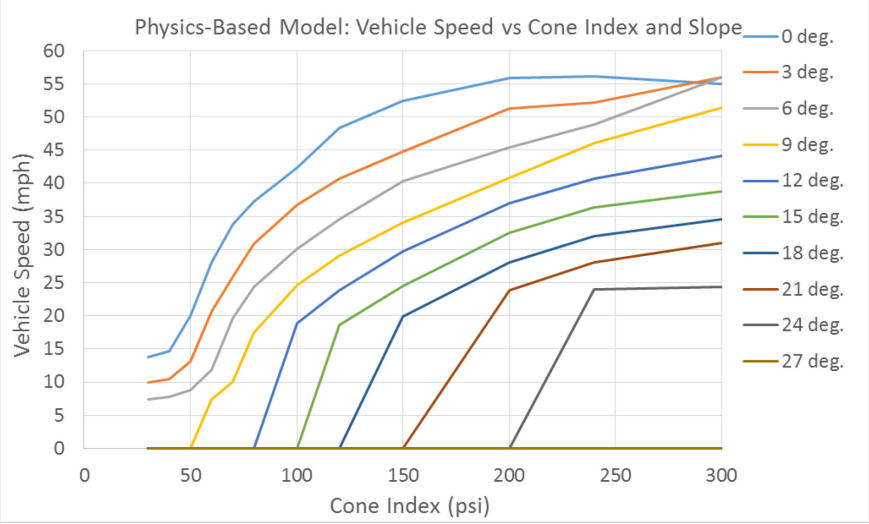


Figure 5B-69: Physics-Based Model's Steady-State Vehicle Speed (Speed-Made-Good) vs. CI and Terrain Slope.

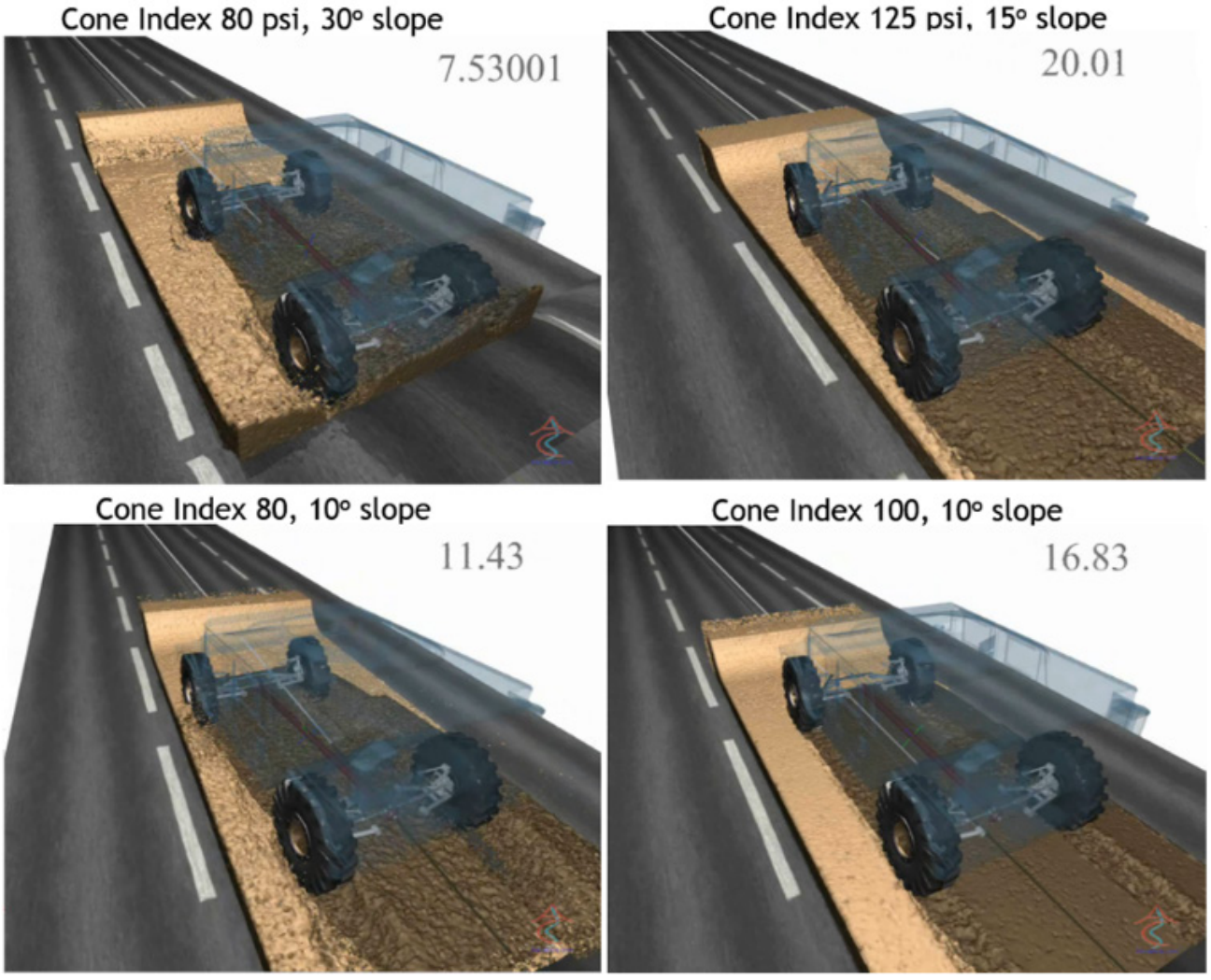


Figure 5B-70: Snapshots of a HMMWV-Type Vehicle Going Over Terrains of Various Slopes and Cone Indices.

5B.4.1 Prototype Demonstration of the Monterey Bay Region

Another demonstration of using the DIS/GroundVehicle Complex Terramechanics prototype along with using the RAMDO software system [49] as the DOE engine, to predict the "Speed-Made-Good" for the Nevada Automotive Test Center's (NATC) Wheeled Vehicle Platform is shown in Figure 5B-71, over a large terrain map, the Monterey Bay region. Four terrain variables are used, long slope, DEM inter-particle cohesion, DEM inter-particle friction coefficient, and DEM soil density; the methodology is presented in the TA5 Uncertainty Quantification (Chapter 6). The procedure consists of the following steps:

1) A rectangular terrain map is divided into grid cells. For each grid cell, the value of the selected four terrain variables are extracted. Then, the ranges (minimum and maximum) of the four terrain variables over the entire terrain map are found.

2) Using the ranges of terramechanics four input parameters, a reduced DOE set of runs with varying values of the four terrain variables based on a Dynamic Kriging (DKG) interpolation technique [49] is performed using DIS. For each run the steady-state vehicle speed is extracted. If necessary, sequential DOE samples are added where the DKG surrogate model has large amounts of Kriging variances.

3) A Dynamic Kriging (DKG) surrogate model [49] of the Speed-Made-Good is created using the DIS runs at the DOE points (see Chapter 6 for details on the DKG model).

4) The DKG surrogate model is used to calculate the Speed-Made-Good for each terrain grid cell.

5) A map of the mobility measure over the entire terrain map is then generated by coloring each grid cell using the mobility measure, such as the Speed-Made-Good (Figure 5B-72).

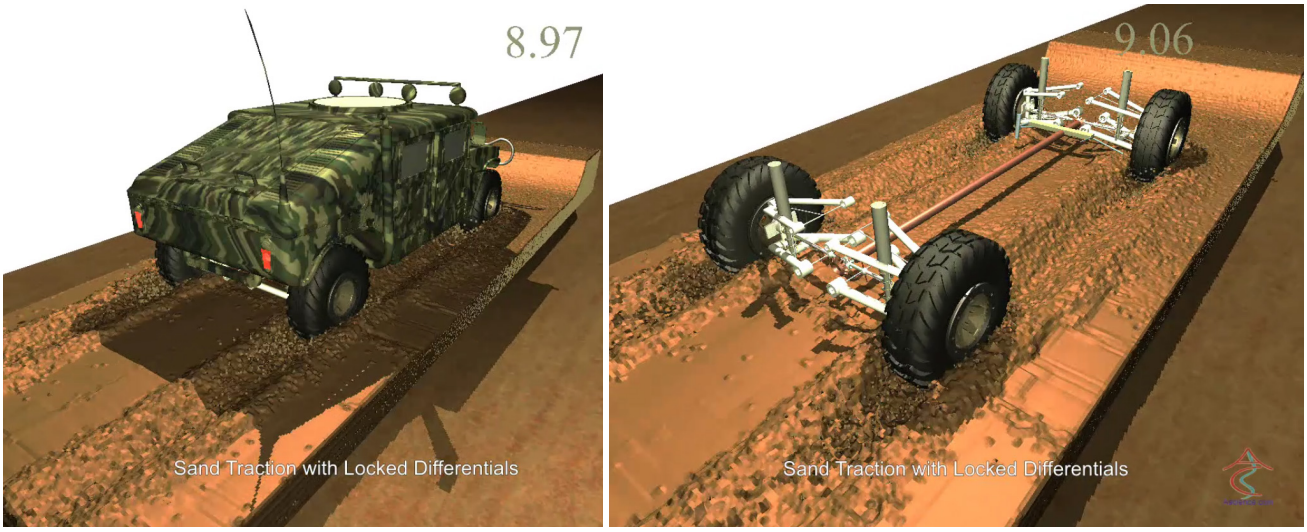


Figure 5B-71: DIS/GroundVehicle Model of NATC Wheeled Vehicle Platform on a Soft Soil Terrain.

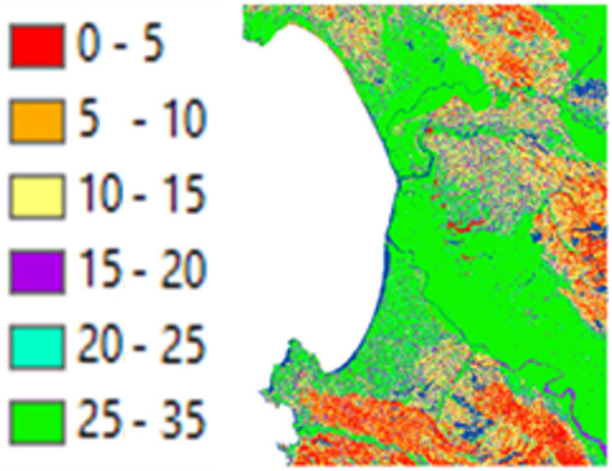


Figure 5B-72: Monterey, California Terrain Map Colored by The Speed-Made-Good Generated Using the DIS/GroundVehicle Complex Terramechanics Prototype.

Note that the simulations in two demonstrations are performed for the positive slope since this will typically result in the worst possible vehicle mobility while crossing a terrain, which is what mission planners are most interested in. Even if the actual vehicle motion direction is not along the maximum longitudinal slope direction, due to obstacles or mission uncertainties, it is possible that the vehicle may need to move along the maximum positive slope direction. Mission planners are also interested in the directional mobility maps (also called traverse map). Creating a DOE procedure to generate those mobility maps using the complex terramechanics prototype will be the subject of future research.

Future research will focus on creating a general expert system that uses a DOE procedure along with advanced interpolation techniques (including Kriging and Neural networks) to predict the vehicle mobility measures listed in Section 5A.4.1 and terrain damage measures listed in Section 5A.4.2, for any terrain with tens of terrain variables, such as those listed in Section 5A.4.12.

5B.5 REFERENCES

[1] Advanced Science and Automation Corp. Dynamic Interaction Simulator 2016, cited 2016; Available from: http://www.ascience.com.

[2] Wasfy, T.M. and Noor, A.K. 1996. Modeling and Sensitivity Analysis of Multibody Systems Using New Solid, Shell And Beam Elements. Computer Methods in Applied Mechanics and Engineering, 138(1-4):187-211.

[3] Wasfy, T.M., Wasfy, H.M. and Peters, J.M. 2014. Coupled Multibody Dynamics and Discrete Element Modeling of Vehicle Mobility on Cohesive Granular Terrains. 10th International Conference on Multibody Systems, Nonlinear Dynamics, and Control, ASME, Buffalo, NY, USA.

[4] Wasfy, T.M. 2004. Modeling Spatial Rigid Multibody Systems Using an Explicit-Time Integration Finite Element Solver and a Penalty Formulation. Proceeding of the DETC, 28th Biennial Mechanisms and Robotics Conference. ASME International, Salt Lake, UT, USA.

[5] Wasfy, T.M., Wasfy, H.M. and Peters, J.M. 2015. High-Fidelity Multibody Dynamics Vehicle Model Coupled with a Cohesive Soil Discrete Element Model for predicting Vehicle Mobility. 11th International Conference on Multibody Systems, Nonlinear Dynamics, and Control. ASME, Boston, MA, USA.

[6] Wasfy, T.M., Yildiz, C., Wasfy, H.M. and Peters, J.M. 2016. Effect of Flat Belt Thickness on Steady-State Belt Stresses and Slip. ASME Journal of Computational and Nonlinear Dynamics, 11(5).

[7] Wasfy, T.M.a.L., M.J. 2005. Modeling the Dynamic Frictional Contact of Tires Using an Explicit Finite Element Code. 5th International Conference on Multibody Systems, Nonlinear Dynamics, and Control. ASME, Long Beach, CA, USA.

[8] Leamy, M.J. and Wasfy, T.M. 2002. Transient and Steady-State Dynamic Finite Element Modeling of Belt-Drives. ASME Journal of Dynamics Systems, Measurement, and Control, 124(4):575-581.

[9] Wasfy, T.M. and O'Kins, J. 2009. Finite Element Modeling of the Dynamic Response of Tracked Vehicles. International Design Engineering Technical Conferences, 7th International Conference on Multibody Systems, Nonlinear Dynamics, and Control. ASME, San Diego, CA, USA.

[10] Yildiz, C. and Wasfy, T.M. 2011. Time-Accurate Multibody Dynamics Model for Toroidal Traction Drives. 2011 International Design Engineering Technical Conferences and Computers and Information in Engineering Conference (IDETC/CIE 2011), 8th International Conference on Multibody Systems, Nonlinear Dynamics, and Control. ASME, Washington, DC, USA.

[11] Wasfy, T.M. 2003. Asperity Spring Friction Model with Application to Belt-drives. 19th Biennial Conference on Mechanical Vibration and Noise. ASME International, Chicago, IL, USA.

[12] Wasfy, T.M. 1996. A Torsional Spring-Like Beam Element for the Dynamic Analysis of Flexible Multibody Systems. International Journal for Numerical Methods in Engineering, 39(7):1079-1096.

[13] Wasfy, T.M. 2011. High-Fidelity Modeling of Flexible Timing Belts Using an Explicit Finite Element Code. 8th International Conference on Multibody Systems, Nonlinear Dynamics, and Control. ASME, Washington, DC, USA.

[14] Wasfy, T.M. 2001. Lumped-Parameters Brick Element for Modeling Shell Flexible Multibody Systems. 18th Biennial Conference on Mechanical Vibration and Noise. ASME International, Pittsburgh, PA, USA.

[15] Wasfy, T.M. 2003. Edge Projected Planar Rectangular Element for Modeling Flexible Multibody Systems. 19th Biennial Conference on Mechanical Vibration and Noise. ASME International, Chicago, IL, USA.

[16] Wasfy, T.M. and Noor, A.K. 2003. Computational Strategies for Flexible Multibody Systems. ASME Applied Mechanics Reviews, 56(6):553-613.

[17] Shabana, A.A. 1997. Flexible Multibody Dynamics: Review of Past And Recent Developments. Multibody System Dynamics, 1:189-222.

[18] Shabana, A.A. 1996. Resonance Conditions and Deformable Body Co-Ordinate Systems. Journal of Sound and Vibration, 192:389-398.

[19] Bauchau, O.A. and Rodriguez, J. 2003. Formulation of Modal Based Elements in Nonlinear, Flexible Multibody Dynamics. Journal of Multiscale Computational Engineering, 1(2 and 3):161-180.

[20] Wasfy, T.M. and Leamy, M.J. 2002. An Object-Oriented Graphical Interface for Dynamic Finite Element Modeling of Belt-Drives. 27th Biennial Mechanisms and Robotics Conference. ASME International, Montreal, Canada.

[21] Wasfy, T.M. and Noor, A.K. 2001. Object-Oriented Virtual Reality Environment for Visualization of Flexible Multibody Systems. Advances in Engineering Software, 32(4):295-315.

[22] Wasfy, T.M. 2006. Object-Oriented Modeling Environment for Simulating Flexible Multibody Systems and Liquid-Sloshing. 26th Computers and Information in Engineering (CIE) Conference. ASME: Philadelphia, PA, USA.

[23] Wasfy, T.M. and Wasfy, H.M. 2006. Object-Oriented Environment for Dynamic Finite Element Modeling of Tires and Suspension Systems. Mechanical Engineering Congress and Exposition Conference. ASME: Chicago, IL, USA.

[24] Yesmunt, G.S. 2014. Design, Analysis, and Simulation of a Humanoid Robotic Arm Applied To Catching. Purdue University, IN, USA.

[25] Ahmadi, S., Wasfy, T.M., Wasfy, H.M. and Peters, J.M. 2013. High-Fidelity Modeling of a Backhoe Digging Operation Using an Explicit Multibody Dynamics Code with Integrated Discrete Particle Modeling Capability. 2013 International Design Engineering Technical Conference, 9th International Conference on Multibody Systems, Nonlinear Dynamics, and Control (MSNDC), ASME.

[26] Wasfy, T.M., Ahmadi, S., Wasfy, H.M. and Peters, J.M. 2013. Multibody Dynamics Modeling of Sand Flow from a Hopper and Sand Angle of Repose. 2013 International Design Engineering Technical Conference, 9th International Conference on Multibody Systems, Nonlinear Dynamics, and Control (MSNDC).

[27] Wasfy, T.M., Wasfy, H.M. and Peters, J.M. 2014. Coupled Multibody Dynamics and Discrete Element Modeling of Vehicle Mobility on Cohesive Granular Terrains. 10th International Conference on Multibody Systems, Nonlinear Dynamics, and Control (MSNDC), 2014 International Design Engineering Technical Conferences. ASME, Buffalo, NY, USA.

[28] Wasfy, T.M., Jayakumar, P., Mechergui, D. and Sanikommu, S. 2016. Prediction of Vehicle Mobility on Large-Scale Soft-Soil Terrain Maps Using Physics-Based Simulation. 2016 NDIA Ground Vehicle Systems Engineering and Technology Symposium, Modeling and Simulation, Testing and Validation (MSTV) Technical Session. Novi, MI, USA.

[29] Sane, A. and Wasfy, T.M., Coupled Multibody Dynamics and Discrete Element Modeling of Bulldozers Cohesive Soil Moving Operation, in 11th ASME International Conference on Multibody Systems, Nonlinear Dynamics, and Control (MSNDC). 2015, ASME: Boston, MA, USA.

[30] Wasfy, T.M., Wasfy, H.M. and Peters, J.M. 2015. High-Fidelity Multibody Dynamics Vehicle Model Coupled with a Cohesive Soil Discrete Element Model for predicting Vehicle Mobility. 11th International Conference on Multibody Systems, Nonlinear Dynamics, and Control. ASME, Boston, MA, USA.

[31] Standard Test Method for Shear Testing of Bulk Solids Using the Jenike Shear Cell. 2007, ASTM International: West Conshohocken, PA, USA.

[32] Monaghan, J. 2005. Smoothed Particle Hydrodynamics. Rep. Prog. Phys., 68:1703-1759.

[33] Monaghan, J. and Gingold, R.J. 1977. Smoothed Particle Hydrodynamics. Mon. Not. Roy. Astr. Soc., 181:375-389.

[34] Wasfy, T.M., Wasfy, H.M. and Peters, J.M. 2014. Coupled Multibody Dynamics and Smoothed Particle Hydrodynamics for Predicting Liquid Sloshing for Tanker Trucks. 10th International Conference on Multibody Systems, Nonlinear Dynamics, and Control. ASME, Buffalo, NY, USA.

[35] Wasfy, T.M., Wasfy, H.M. and Peters, J.M. 2015. Coupled Multibody Dynamics and Smoothed Particle Hydrodynamics for Modeling Vehicle Water Fording. 11th International Conference on Multibody Systems, Nonlinear Dynamics, and Control. ASME, Boston, MA, USA.

[36] Wasfy, T.M. and Wasfy, A.M. 2004. An Object-Oriented Graphical Interface for Dynamic Finite Element Modeling of Flexible Multibody Mechanical Systems. Proceeding of MDP-8, Cairo University Conference on Mechanical Design and Production. Cairo University, Cairo, Egypt.

[37] Wasfy, T.M. and Noor, A.K. 2001. Visualization of CFD results in immersive virtual environments. Advances in Engineering Software, 32:717-730.

[38] Noor, A.K. and Wasfy, T.M. 2001. Simulation of physical experiments in immersive virtual environments. Engineering Computations, 18(3-4):515-538.

[39] Wasfy, T.M. and Wasfy, A.M. 2003. Strategy for effective visualization of CFD datasets in virtual environments. 23rd Computers and Information in Engineering (CIE) Conference. ASME International, Chicago, IL.

[40] ASTM Standard D6128-16. 2016. Standard test method for shear testing of bulk solids using the Jenike shear cell. ASTM International, West Conshohocken, PA.

[41] Wong, J.Y. 2010. Terramechanics and Off-Road Vehicle Engineering (Second Edition). Elsevier, Oxford, UK.

[42] Pacejka, H.B. 2006. Tyre and vehicle dynamics (Second Edition). SAE International.

[43] Wasfy, T.M., O'Kins, J. and Ryan, D. 2011. Experimental validation of a multibody dynamics model of the suspension system of a tracked vehicle. 2011 NDIA Ground Vehicle Systems Engineering and Technology Symposium, Dearborn, MI.

[44] Foltz, A.D., Wasfy, T.M., Ostergaard, E., and Piraner, I., Multibody Dynamics Model of a Diesel Engine and Timing Gear Train with Experimental Validation, in ASME 2016 International Mechanical Engineering Congress and Exposition. 2016, ASME: Phoenix, Arizona.

[45] Wasfy, T.M. and Stark, M.L. 2011. Multibody dynamics model for predicting the vibration response and transient tooth loads for planetary gear systems. 11th ASME International Power Transmission and Gearing Conference, Washington, DC.

[46] Leamy, M.J. and Wasfy, T.M. 2005. Dynamic Modeling of Timing Belt Frictional Contact Using an Explicit Finite Element Formulation. SAE 2005 Transactions. Journal of Engines, pp. 605-610.

[47] Wasfy, T.M. and Leamy, M.J. 2002. Effect of Bending on the Dynamic and Steady-State Responses of Belt-Drives. 27th Biennial Mechanisms and Robotics Conference. ASME International, Montreal, Canada.

[48] Wasfy, T.M., Wasfy, H.M. and Peters, J.M. 2013. Prediction of the Normal and Tangential Friction forces for Thick Flat Belts Using an Explicit Finite Element Code. ASME 2013 International Design Engineering Technical Conference, 9th International Conference on Multibody Systems, Nonlinear Dynamics, and Control (MSNDC), Portland, OR.

[49] RAMDO Solutions, LLC. RAMDO Solutions. 2018. Available from: www.ramdosolutions.com.

Chapter 5C – TA3: OTHER COMPLEX TERRAMECHANICS SOFTWARE TOOLS

Tamer M. Wasfy
Advanced Science and Automation Corp.
UNITED STATES

5C.1 INTRODUCTION

In this chapter three software tools are presented which have Complex Terramechanics modeling capabilities, namely: Chrono, MSC/ADAMS, and RecurDyn. Similar to DIS/GroundVehicle, DEM is used in those tools for complex terramechanics modeling of the soil. In addition, the EDEM software tool is presented in the last section of this chapter. MSC/ADAMS and RecurDyn both use EDEM as the DEM engine for modeling the soil, along with a co-simulation framework.

5C.2 CHRONO

Author: Dr. Radu Serban, Research Scientist, Simulation-Based Engineering Lab, University of Wisconsin, Madison.

Distributed under a permissive BSD license, Chrono [1] is an open source multi-physics package used to model and simulate:

1) The dynamics of large systems of connected rigid bodies governed by Differential Algebraic Equations (DAE);
2) The dynamics of deformable bodies governed by Partial Differential Equations (PDE);
3) First order dynamic systems governed by Ordinary Differential Equations (ODE); and
4) Fluid-solid interaction problems whose dynamics is governed by coupled DAEs and PDEs.

Started almost 20 years ago, Chrono provides a mature and stable code base that continues to be augmented with new features and modules. The core functionality of Chrono provides support for the modeling, simulation, and visualization of rigid multibody systems with additional capabilities offered through optional modules. These modules provide support for additional classes of problems (e.g., deformable multibody systems through finite element analysis and fluid-solid interaction), for modeling and simulation of specialized systems (such as ground vehicles and granular dynamics problems), or for providing specialized parallel computing algorithms (multi-core, GPU, and distributed) for large-scale simulations [2].

Used in many different scientific and engineering problems by researchers from academia, industry, and government, Chrono has mature and sophisticated support for ground vehicle simulation and vehicle – terrain interaction. Some typical simulations, involving both wheeled and tracked vehicles and leveraging Chrono's multi-physics capabilities, are illustrated in Figure 5C-1.

5C.2.1 Multibody System Dynamics and Frictional Contact

While providing a full-fledged multibody simulation framework [2], a unique characteristic of Chrono lies with its support for large-scale granular dynamics, i.e., simulation problems with millions of bodies

interacting through contact and friction. For such problems, Chrono implements both Non-Smooth Contact (NSC) and Smooth Contact (SMC) approaches. These two approaches lead to different forms of the equations of motion – Differential Variational Inequalities (DVIs) and Differential Algebraic Equations (DAEs) for NSC, and exclusively DAEs for SMC. NSC and SMC also differ in terms of their modeling capabilities, parameterizations, as well as in their computational complexity and amenability to parallel computing. A salient feature of Chrono is that it provides full-fledged support for both, making it a valuable open platform for testing new methods and approaches that target either NSC or SMC. The two approaches to frictional contact implemented in Chrono have been compared and validated in Ref. [3].



Figure 5C-1: Snapshots from Various Chrono::Vehicle-Enabled Simulations.

Note: Clockwise from top left: a tracked vehicle obstacle climbing test, a simulation of a wheeled vehicle on granular terrain (dem-c formulation) modeled with more than 10 million particles, a fording maneuver in a coupled Chrono::Vehicle – Chrono::FSI simulation, and a simulation of a convoy of autonomous vehicles (using synchrono).

5C.2.2 Vehicle Modeling

Built as a Chrono extension module, Chrono::Vehicle is a C++ middleware library focused on the modeling, simulation, and visualization of ground vehicles [4]. Chrono::Vehicle provides a collection of templates for various topologies of both wheeled and tracked vehicle subsystems, as well as support for modeling of rigid, flexible, and granular terrain, support for closed-loop and interactive driver models, and run-time and off-line visualization of simulation results. Modeling of vehicle systems is done in a modular fashion, with a vehicle defined as an assembly of instances of various subsystems (suspension, steering, driveline, etc.). Flexibility in modeling is provided by adopting a template-based design. In Chrono::Vehicle, templates are parameterized models that define a particular implementation of a vehicle subsystem. As such, a template defines the basic modeling elements (bodies, joints, force elements), imposes the subsystem topology, prescribes the design

parameters, and implements the common functionality for a given type of subsystem (e.g., suspension) particularized to a specific template (e.g., double wishbone).

For wheeled vehicle systems, templates are provided for the following subsystems: suspension (double wishbone, reduced double wishbone using distance constraints, multilink, solid-axle, MacPherson strut, semi-trailing arm); steering (Pitman arm, rack-and pinion); driveline (2WD and 4WD shaft-based using specialized Chrono modeling elements, simplified kinematic driveline); wheel (simply a carrier for additional mass and inertia appended to the suspension's spindle body and, optionally, visualization information); brake (simple model using a constant torque modulated by the driver braking input).

Chrono::Vehicle offers a variety of tire models and associated templates, ranging from rigid tires (with either a cylindrical contact shape or given as a mesh), to empirical and semi-empirical models (such as Pacejka, Fiala, and TMeasy), to fully deformable tires modeled with finite elements (using either an ANCF formulation, or a co-rotational formulation). The latter FEA tire models allow for detailed specification of tire geometry and material properties, as well as specification of flexible 3D tire tread patterns.

For modeling tracked vehicles, templates are provided for suspension, road wheels, sprockets, track shoe assemblies, and idler with tensioner. Different suspension configurations are available, including torsion spring with linear or rotational dampers and a hydropneumatic suspension template, and both single- and double-pin track shoe models are supported. Sprocket profiles are defined as 2D curves (parameterized differently for sprockets engaging single- and double-pin track shoes) and the sprocket-track shoe contact is processed with a custom collision detection algorithm. Chrono::Vehicle provides functionality for automatic assembly of the track over the vehicle's wheels to eliminate the burden of consistent initialization of all track shoe bodies.

5C.2.3 Soft Soil Modeling and Complex Terramechanics

Various approaches for terrain modeling are supported in Chrono::Vehicle. The parameterized template for rigid terrain allows specification of a flat profile, arbitrary geometry specified as a mesh object, or else profiles constructed from height field information provided as gray images. Chrono provides support for deformable terrain at various degrees of accuracy and computational efficiency. An expeditious, but lower fidelity option is given by the Chrono::Vehicle extension of the Soil Contact Model (SCM) technique in which contact forces between the soil and the vehicle components (tires or track) are computed based on Bekker's formulation [5].

At the other extreme, Chrono::Vehicle can be easily interfaced to the granular dynamics support in Chrono to allow simulations of ground vehicles over granular terrain using either a compliant- or a rigid-body approach to the frictional contact problem [2]. An alternative high-fidelity approach to modeling deformable terrain is provided by templates for specifying FEA terrain patches, leveraging the support provided in the Chrono::FEA module.

Chrono provides mature support for fully resolved granular dynamics simulations, employing the so-called Discrete Element Method (DEM). Meaningful mobility simulations require large enough terrain patches and small enough particle dimensions that result in DEM problems involving frictional contact with millions of degrees of freedom. Broadly speaking, computational methods for DEM at this scale can be categorized into two classes: penalty-based (also known as a compliant-body approach; denoted here by DEM-P) and complementarity-based (also known as a rigid-body approach; denoted here by DEM-C). While differing in the underlying formulation employed for modeling and generating the normal and tangential forces at the contact interface, and thus leading to different mathematical models and different problem sizes, both methods rely crucially on efficient methods for proximity calculation. This common algorithmic step provides a complete

geometric characterization of the interaction between neighboring bodies, taking into account the current system state and specification of the contact shapes associated with all interacting bodies.

The DEM-P and DEM-C approaches are very unlike each other: a local vs. global view of the frictional contact interaction, compliant vs. rigid treatment of bodies for contact purposes, force-acceleration vs. impulse-momentum formulation of the resulting equations of motion. They each have their advantages, as well as shortcomings. Backed by a large body of literature and widely used in commercial DEM software packages, DEM-P has the attractive features of not requiring additional system states and allowing straightforward implementations that are easily scalable, as the numerical solution remains decoupled. However, they typically require small integration step-sizes, due to the resulting stiff differential equations and pose difficulties in identifying appropriate model parameters, especially for large heterogeneous systems, as well as in treating shapes with non-spherical geometry. On the other hand, DEM-C solutions permit integration with larger step-sizes, as they do not suffer from limitations due to numerical stability, rely on a small number of model parameters (effectively only the friction coefficient and cohesion properties), and have no underlying assumptions on shape geometry. But DEM-C requires a much more involved and expensive solution of an optimization problem at each step, increases the problem size by a significant factor, and, especially when friction is present, lack a unique solution (a direct consequence of the rigid-body assumption, see, for example Ref. [6]).

Chrono provides full support for both DEM approaches, through its Chrono::Granular module. Utilities in this module include:

- Samplers for initialization of granular material (uniform grid, hexagonal close packing, Poisson-disk sampling, etc.) allowing sampling of different domains (box, sphere, cylindrical) both in 2D and 3D;
- Generators for granular dynamics which permit creation of large number of particles randomly selected from mixtures of ingredients with prescribed expectations. Each mixture ingredient allows multivariate normal distributions for particle size and contact material properties; and
- Utilities for batch creation of particles, input/output, checkpointing, and validation.

The DEM-based granular terrain option in Chrono::Vehicle also includes options for using a moving patch feature, in which granular material is simulated only within a sliding window centered around and moving with the vehicle. Particles falling outside the moving patch behind the vehicle are reused by relocating them in front of the vehicle in chunks of spatial dimensions controlled by the user.

5C.2.4 Parallelization

One of Chrono's strengths is its reliance on advanced computing hardware at various stages of the solution process. Chrono embraces cache friendly data structures suitable for vectorization and algorithms that expose parallelism at data and task levels. The software infrastructure draws on three modules – Chrono::Cosimulation, Chrono::Distributed, and Chrono::Parallel – that enable Chrono to map for execution each of the many components of a complex model onto the appropriate parallel computing hardware architecture. This approach establishes a flexible, object-oriented infrastructure that:

1) Relies on co-simulation to handle in parallel and independently subsystems of a complex system;
2) Uses the MPI standard to further partition a large subsystem via Chrono::Distributed into parallel sub-groups; and

3) Invokes services provided by Chrono::Parallel to accelerate execution within each sub-group using two hardware platforms GPU computing or multi-core processors. Further details can be found in Refs. [7], [8].

Figure 5C-2 shows a snapshot from a simulation of a full-vehicle model with flexible ANCF-based tires driving on granular terrain and negotiating a large cylindrical obstacle.

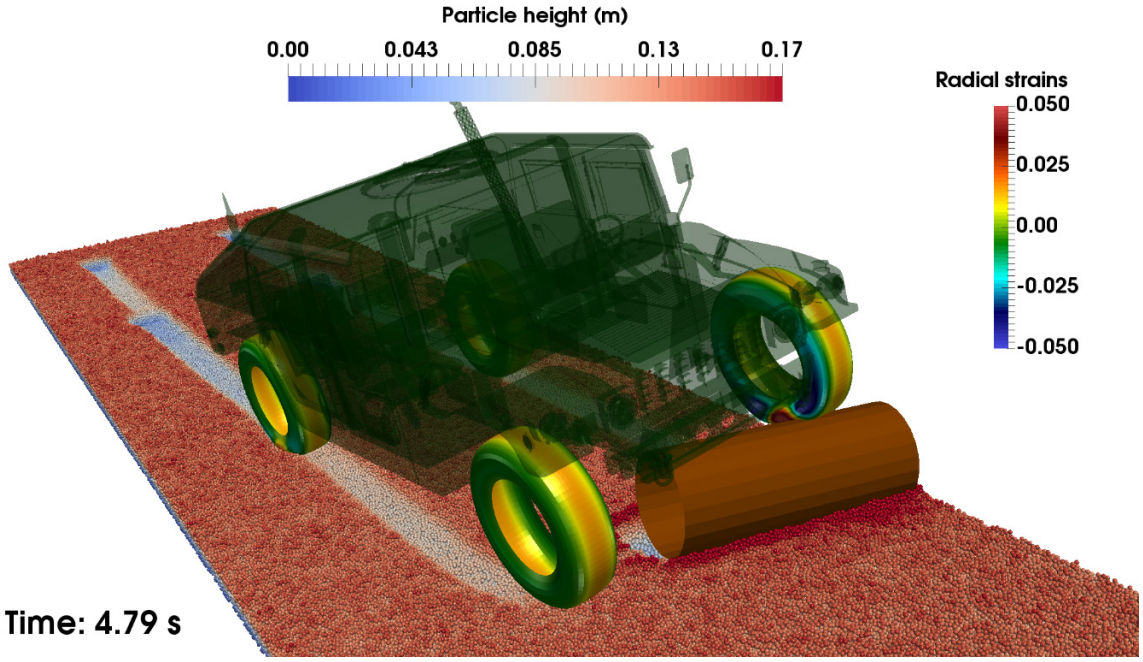


Figure 5C-2: Snapshot from a Chrono Simulation of a Vehicle with Flexible Tires on Deformable Granular Terrain (DEM-P Formulation) Negotiating a Cylindrical Obstacle.

5C.3 MSC/ADAMS

Submitted by: Dr. Eric Pesheck, Project Manager, Engineering Services, MSC Software

The Adams product suite is developed and sold by MSC Software. This toolset contains numerous products focused on the modeling and simulation of multibody dynamics systems. Originally, the software was developed at the University of Michigan in 1974. This was commercialized and expanded by Mechanical Dynamics, Inc., which was subsequently purchased by MSC Software in 2002. Today, MSC Adams is the world's most widely used software for analysis and simulation of multibody dynamic systems [9].

The Adams Solver lies at the core of the product line. It uses an Euler-Lagrange formulation for the system equations of motion, including all six rigid body displacements and velocities for each body, plus additional constraint equations for restricting relative motion between parts. In addition, the solver includes capabilities for incorporating Finite Element-based modal representations of flexible parts, and a diverse array of analytical elements including differential equations, transfer functions, sensors, and variables. Forces may be defined to act between the system parts in a wide variety of ways, including complex "pre-packaged" forces such as tires or CAD-geometry based contact, and open-ended force functions that allow user-defined function expressions or

even user-defined subroutines. The Adams Solver provides several integrator formulations, with numerous options to facilitate tailoring the underlying analytical approach to the user's specific modeling needs. In addition, the Solver supports multi-CPU computation options that can leverage modern multi-core processors for typical speed improvements of 2 x to 4 x (as of 2018).

Primarily, the Adams Solver inputs are defined by models built in the Adams View pre-processing interface or using vertical products such as Adams Car that are built on the Adams View framework. This framework enables model-building in a 3D CAD-like environment and supports significant scripting and customization capabilities, allowing users to adjust the modeling process to fit their needs. Adams View also includes an integrated post-processor that facilitates review of simulation results, including plots, animations, system modes, and comparison with test results.

The open architecture of the Adams Solver has facilitated interaction with numerous external simulation tools, allowing detailed interactions between Adams and other time-domain solutions such as aerodynamics, non-linear FEA, fluid dynamics, control systems, and Discrete Element soil Methods (DEM). Recently, MSC has implemented a more formal architecture to systematically support co-simulation with specific applications. The Adams Co-Simulation Interface (ACSI) currently supports co-simulations between Adams and either EDEM or Marc. The typical simulation process workflow is shown in Figure 5C-3.

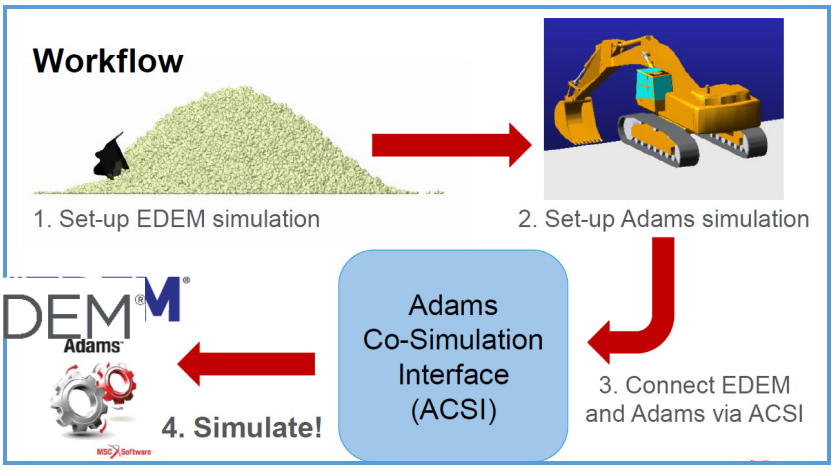


Figure 5C-3: Typical Adams-EDEM Workflow.

The EDEM software package is focused on the modeling and simulation of bulk materials such as loose rock, snow, grain, or soil. Its methods are tailored for defining and simulating large numbers of interacting particles. Given this, it is a suitable tool for complex terramechanics applications.

ACSI consists of two primary components: an interface that assists with the pre-processing and configuration of the co-simulation, and a "glue code" that manages the signal flow between solvers as the solution progresses. The interface allows users to specify which Adams parts will interact with EDEM, and configure the communication details. The glue code contains several different methods for managing the signals exchanged between the tools. The details of the analytical methods and associated options are covered in the Adams documentation [1]. Fundamentally, the approach is that Adams calculates system motions, passes these to EDEM, and EDEM generates resulting reaction forces which are passed back to Adams and applied to the Adams system model (Figure 5C-4).

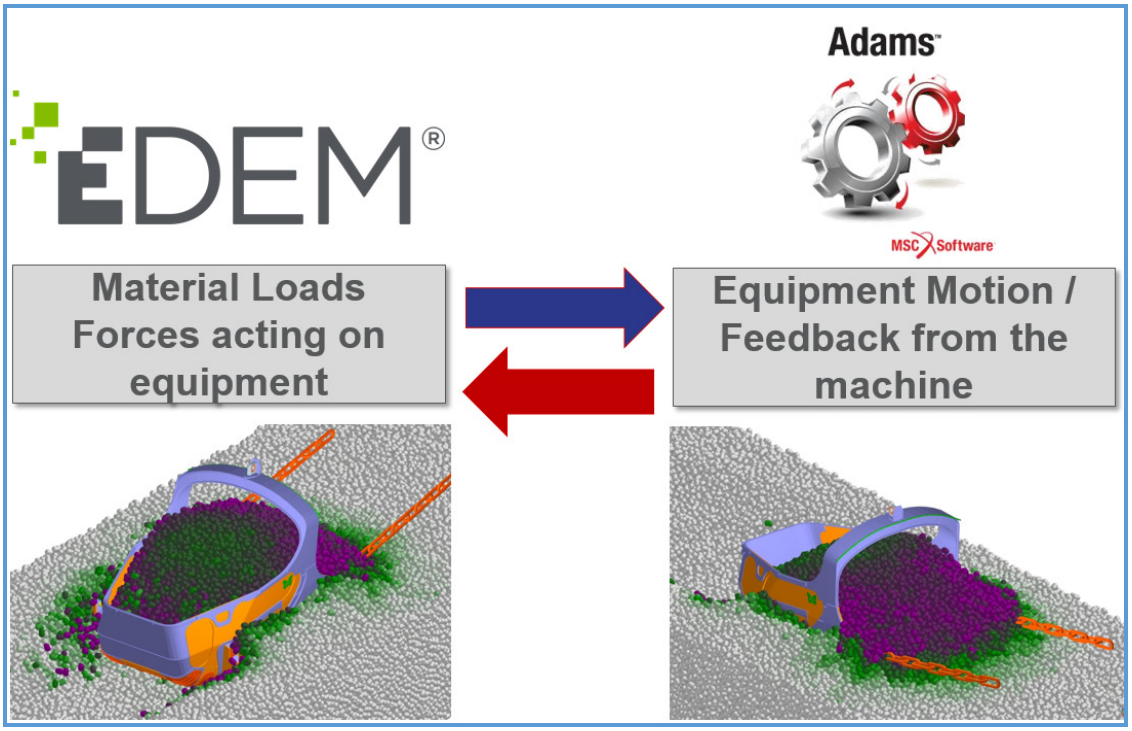


Figure 5C-4: Adams-EDEM Typical Information Exchange.

From a conceptual point of view, the standard EDEM approach currently employed by the ACSI glue code is to:

1) Use EDEM force history in glue code to extrapolate EDEM forces for the next Adams time step.
2) Use these predicted EDEM input forces within the Adams model via GFORCE element subroutines for a single time step.
3) Pass part motions back through the glue code to EDEM.
4) Continue the EDEM simulation using provided motion data to catch up with the Adams solution time.
5) Compare resultant EDEM forces with those predicted in Step 1 to monitor co-simulation error.
6) Return to Step 1 and predict new forces via extrapolation.

In the event that the co-simulation error is too large, or the process becomes unstable, the solution time steps can be reduced for improved accuracy. This approach sacrifices some simulation efficiency by alternating between the EDEM and Adams solvers. However, as the EDEM solution is typically much slower than Adams (by one to three orders of magnitude), the EDEM "turns" will take nearly all of the time and the net solution time is minimally increased by this sacrifice (Figure 5C-5).

This generalized approach allows any number of Adams parts to interact with arbitrary EDEM particle-system models covering a wide array of applications including, but not limited to, complex terramechanics. For complex terramechanics, this co-simulation approach allows users to leverage any pre-existing Adams vehicle models (with tracks or tires) for additional analysis of detailed system interaction with deformable terrain.

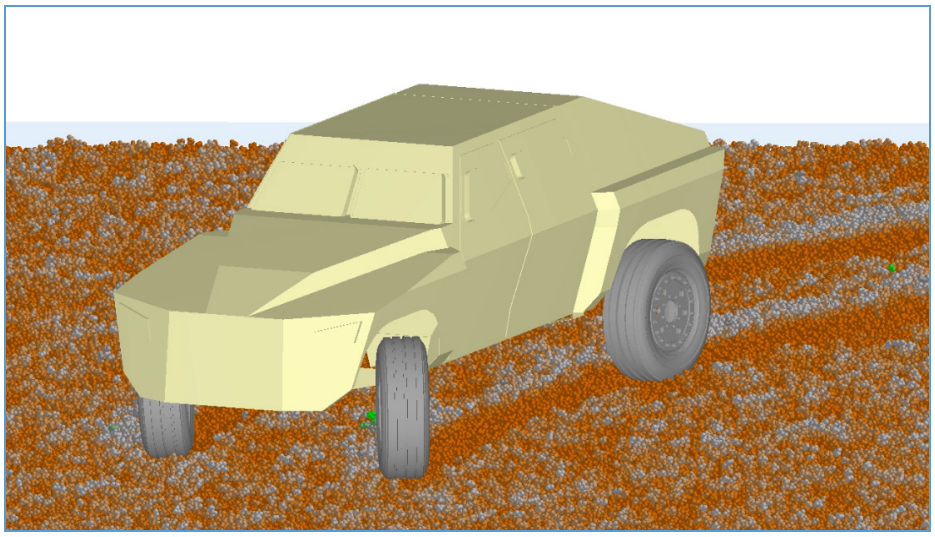


Figure 5C-5: FED Vehicle Model Turning in Fine-Grain Sand Pit.

While the numerical framework for successfully performing this co-simulation is now firmly in place, significant challenges remain for widespread use:

- **Usability.** It remains challenging to configure Adams and EDEM for robust successful communication and stable simulation performance.
- **Soil Characterization.** There are no pre-defined methods for aligning aggregate soil behavior with test results.
- **Scaling.** Soil tests are often performed at a scale that is inconvenient for system-level simulation. When particle size is changed, the properties must be adjusted to retain similar bulk behavior.
- **Terrain.** Preparing the EDEM model for general terrain geometries, especially at a large scale remains technically difficult.

These challenges do not represent any fundamental obstacles to effective implementation of these methods over time, but they do suggest areas where further investments may be necessary before widespread use is practical. As computational methods and efficiency continue to improve, these methods are likely to become increasingly attractive, as they are able to address fundamental behaviors that cannot be easily accounted for through other existing analytical approaches

5C.4 RECURDYN

Author: Dr. Brant A. Ross, President, MotionPort LLC

The RecurDyn software is a simulation platform that has a foundation of multibody dynamics and interfaces to a variety of other physics-based simulation capabilities to enable users to represent their systems with the appropriate fidelity. Of particular interest to the simulation of ground vehicles is RecurDyn's external Standard Particles Interface (SPI) which provides the ability to co-simulate with the well-known and market leading EDEM discrete element modeling software from DEM Solutions in Edinburgh, UK. The RecurDyn SPI, as described below, provides the ability for rigid bodies to move particles and for the particle to provide resistive

forces on contacting bodies. These features are sufficient to provide a high-fidelity simulation approach to allow tracked and wheeled vehicles to interact with particle-based soils [10], [11], [12].

5C.4.1 Soft Soil DEM Model/Formulation Provided in the EDEM Software

Included in the EDEM software installation is a starter pack of soils models. These models are representative of a range of different soils from hard gravel to compressible clay, as shown in Figure 5C-6. The simulation deck provided with each of the models can be run to view the characteristic described by the model's name. These material models may be used in a simulation by copying them into the material library or the simulation deck provided can be modified.



Figure 5C-6: Range of EDEM Soil Materials.

EDEM also supports a variety of contact models:

1) Edinburgh Elasto-Plastic Adhesion Model (EEPA).
2) Hertz-Mindlin (7 variations):
   a) No slip;
   b) No slip with RVD Rolling Friction;
   c) Archard Wear;
   d) Relative Wear;
   e) JKR Cohesion;
   f) Bonding; and
   g) Heat Conduction.
3) Hysteretic Spring.
4) Linear Cohesion:
   a) Linear Cohesion V1; and
   b) Linear Cohesion V2.
5) Linear Spring.

6) Moving Plane.

7) Particle to Geometry Rolling Friction.

Each contact has an associated parameters that describe its behavior. For example, consider the Edinburgh Elasto-Plastic Adhesion Model (EEPA). It captures the history dependence and the key characteristic behavior of cohesive solids. The model comprises a non-linear hysteretic spring model to account for the elastic-plastic contact deformation and an adhesive force component that is a function of the plastic contact deformation. The EEPA offers a versatility that allows it to be used in both linear and non-linear modes. The loading, unloading and adhesive conditions are described by the following six parameters:

- Constant Pull-Off Force, f0 (N): This defines ever-present forces that may occur, such as van der Waals type forces or electrostatic force.
- Meso-Contact Adhesion Energy, Δ_γ (J/m^2): This is the level of adhesion that is used in the calculation of the load dependent adhesive force in the contact.
- Contact Plasticity Ratio, λ_p: Defined as $(1-k_1/k_2)$, this is the level of contact plasticity used in the model.
- Power Value for k_1 and k_2 F-D Relationship, n: This is used to switch between linear and non-linear force-overlap relationships for the contact model.
- Power Value for Adhesion Branch, X: This defines the severity of the drop in the adhesion force following the peak tensile force being reached.
- Tangential Stiffness Multiplier, ζ_{tm}: This allows the tangential stiffness used in the model to be varied as a function of the loading stiffness.

5C.4.2 RecurDyn Multibody Dynamics Formulation

Constrained mechanical systems are represented by differential equations of motion and algebraic constraint equations (Differential Algebraic Equations, or DAEs). Several backwards difference formulation solutions methods have been proposed for DAEs. In particular, the parameterization method treated the DAEs as Ordinary Differential Equations (ODEs) on the kinematic constraint manifolds of the system. RecurDyn uses this method because its stability and convergence has been demonstrated. A recursive formulation is used to linearize the equations of motion, using state vector notation. The equations of motion are derived in a compact matrix form by using a velocity transformation method. The computational structure of the equations of motion in the joint space was carefully examined in order to classify all of the computation operations that can be done recursively. The generalized recursive formula for each category of the computational operations was developed and applied.

5C.4.3 Co-Simulation of RecurDyn Multibody Dynamics and EDEM Discrete Element Capabilities

RecurDyn has the ability to co-simulate with particle solvers using a Standard Particle Interface (SPI). Particle solvers simulate the motion of granular solid particles, such as EDEM from DEM Solutions. RecurDyn's capability to co-simulate with particle solvers allows for simulations that have a system of rigid and flexible bodies that interact with systems of granular particles and/or fluids, such as is shown in Figure 5C-7. For example, RecurDyn with EDEM can simulate the system of bodies in a full-vehicle model with particles that may represent a gravel, sandy or loam soil.

During a co-simulation the simulations are coupled through walls. The walls of the particle solver model are barriers that the particles cannot pass through. The particles apply forces to the walls either as contact forces or

pressures. Some or all of the walls of a particle model will be connected to bodies in the RecurDyn model. When a body that is connected to a wall moves in RecurDyn, the connected wall moves in the particle solver. When the particles apply a contact or pressure force to a wall in the particle solvers, the force is applied to the body in RecurDyn. This couples the dynamics of both the system of RecurDyn bodies and the system of particles in the particle solver to create an accurate multi-physics simulation. In the case of full-vehicle simulations, the tires are defined as walls.

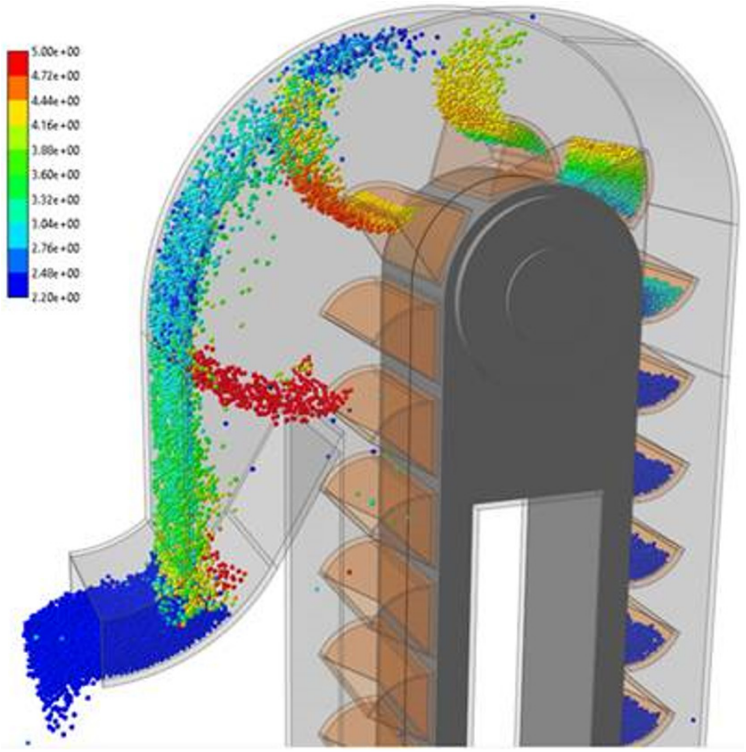


Figure 5C-7: Simulation of a Bulk Material Bucket Elevator Using Recurdyn and EDEM.

1) Create the **RecurDyn** full-vehicle model.
2) Create **walls** from the tire geometry in **RecurDyn** using the walls icon (see the image below).
3) Export the **walls** from **RecurDyn** (see icon in the Figure 5C-8).
4) Build the particle model of the terrain in the EDEM software. This involves selecting the material and the particle size.
5) Import the walls (tires) into the EDEM software.
6) Setup the **co-simulation** in the EDEM software.
7) Run the co-simulation from **RecurDyn**.
8) Use **Post-Processing** functions in **RecurDyn** and the EDEM software. After the simulation is finished, the simulation results can be viewed in **RecurDyn's GUI** and **RecurDyn** can be used for post-processing of both the rigid and flexible body model as well as certain aspects of the particle model. The animation can also be viewed in the EDEM software should be able to perform its normal post-processing of the particle model.



Figure 5C-8: RecurDyn Particle Solver and Post-Processing Objects Used in Conjunction with an EDEM Co-Simulation.

5C.4.4 Example of a RecurDyn – EDEM Soft Soil Vehicle Mobility Co-Simulation

The frames in the image below (Figure 5C-9) show various stages in a wheeled vehicle entering, traversing, and exited a soil pit, where the soil is represented by particles. The tires are pushing the particles down and to the side, while the particles are pushing back and providing sufficient force to support the vehicle.

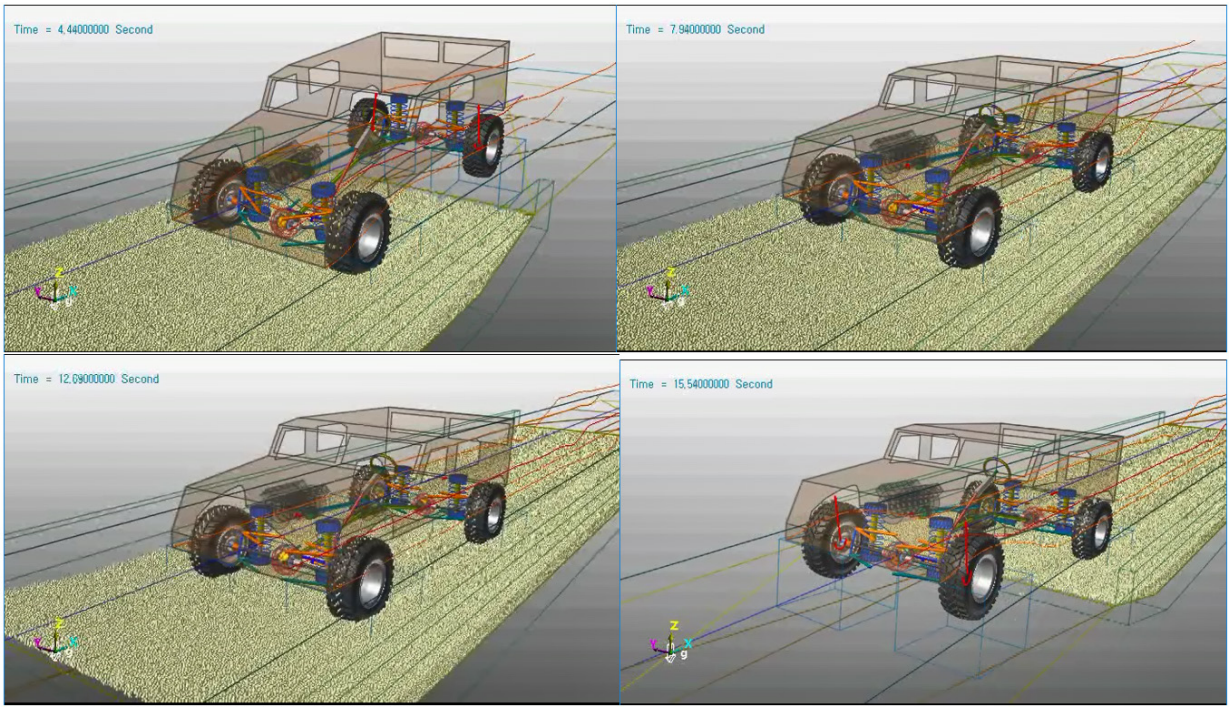


Figure 5C-9: Snapshots of a Typical RecurDyn Soft Soil Vehicle Simulation.

5C.5 EDEM

Submitted by: Dr. David Curry, Principal Engineer, Business Development, EDEM.

EDEM, launched in 2005, is the market-leading software for bulk and granular material simulation. Powered by Discrete Element Modeling (DEM) technology, EDEM quickly and accurately simulates and analyzes the behavior of bulk and granular materials such as coal, mined ores, soil, tablets, and powders (Figure 5C-10). EDEM software is used both in R&D and production design by its customers.

Historically, traditional prototyping methods are prohibitively expensive, and many companies can only test new products late in the design cycle. This has driven customers to rely heavily on simulation as a critical element of staying ahead and providing new products every year. EDEM provides engineers with crucial insight into how materials will interact with their equipment during a range of operation and process conditions.

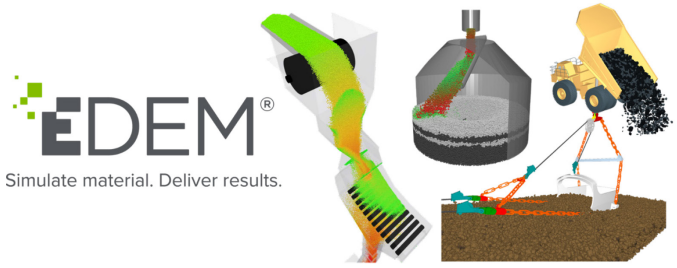


Figure 5C-10: EDEM Software is Used to Solve Design Challenges Involving Bulk and Granular Materials Across a Variety of Different Industries.

EDEM has been selected by over 200 companies in 30 countries around the world to design and optimize equipment that handles or processes granular materials. It is also the DEM software of choice for over 250 leading academic institutions worldwide. It is used in a variety of different industry areas to address challenges of bulk materials handling and processing (Table 5C-1).

Table 5C-1: Industries Using EDEM.

Industry Area	EDEM Uses
Process Manufacturing	• Optimize process configuration • Increase process efficiency • Drive product innovation
Heavy Equipment	• Fewer physical prototypes • Shorter design cycles • Optimized designs
Mining and Metals	• Verify design performance • Improve equipment reliability • Increase productivity
Automotive and Off-Road Vehicles	• Provide virtual proving and test ground for vehicles • Reduce prototyping • Improve accuracy of system dynamics simulations

5C.5.1 EDEM UI and Solver

EDEM is designed to be used by engineers on workstation machines. It offers an easy-to-use graphical user interface and has a self-contained pre- and post-processor, as well as the ability to export data for further

post-processing in 3rd party tools. EDEM will read a variety of CAD formats, allow definition of kinematics, and offers a variety of tools to help make set up and running of bulk materials simulations easy.

EDEM offers highly parallelized GPU, multi-GPU and Shared Memory Parallel CPU solver engines. DEM simulations are highly computationally demanding and EDEM's proprietary engines deliver high-levels of performance and scalability to allow large and complex particle systems to be investigated in time-frames suitable for industrial design.

5C.5.2 CAE Integration

In addition to running as a standalone software tool, EDEM is provides a variety to inter-CAE tool couplings. This includes one-way couples with Finite Element Analysis (FEA) tools to allow realistic structural analysis of assemblies that interact with bulk materials; and two-way couplings with Multibody Dynamics (MBD) and Computational Fluid Dynamics (CFD) tools. Solutions are available with a variety of leading CAE tools and this includes couplings with Adams (MSC Software) and RecurDyn (Function Bay).

5C.5.3 Material Modeling

At the center of any DEM simulation is the Material Model – a virtual representation of a real material. Material Models comprise of a variety of inputs from particle shape and size distribution, to the physics models and their inputs that describe the behavior of a material (Figure 5C-11).

EDEM offers a comprehensive range of validated physics models that can simulate a wide range of material types from large lumps to dry, fine sands, flexible stalks, and sticky/cohesive soils. Users can define their own material models or alternatively choose from extensive range of ready-defined materials models representing a variety of material types for different applications. This includes the GEMM Database (50,000 + materials) that users search with real-world values, to Powder and Soils Starter Packs.

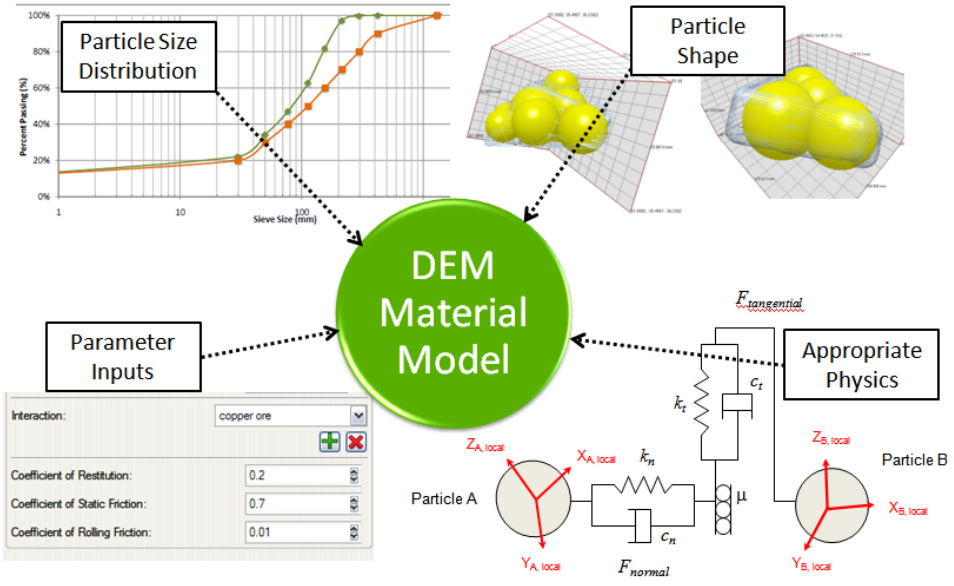


Figure 5C-11: A Schematic Overview of a Typical DEM Material Model. It Contains Choice of Particle Shape, Size, and Contact Physics Models.

5C.5.4 Modeling Soils in EDEM

The EDEM Soils Starter Pack provides users with access to a range of different example materials over two key soil behavioral ranges – dry vs sticky, and compressible vs incompressible. The soils representations are based on four physics models in Table 5C-2.

Table 5C-2: Physical Models of Soil Representations.

Physics Model	Behavioral Characteristics
Hertz-Mindlin [13]	Dry, free flowing Incompressible
Hertz-Mindlin with JKR Cohesion [14]	Sticky, resistance to motion Incompressible
Hysteretic Spring [15]	Dry, free flowing Compressible
Edinburgh Elasto-Plastic Adhesion Model (EEPA) [16]	Sticky, resistance to motion Compressible

The Soils Starter Pack contains 8 material models that have been designed for off-road vehicle modeling and provide a range of different soil behavior based on the behavioral characteristics of each physics model (see Figure 5C-12).

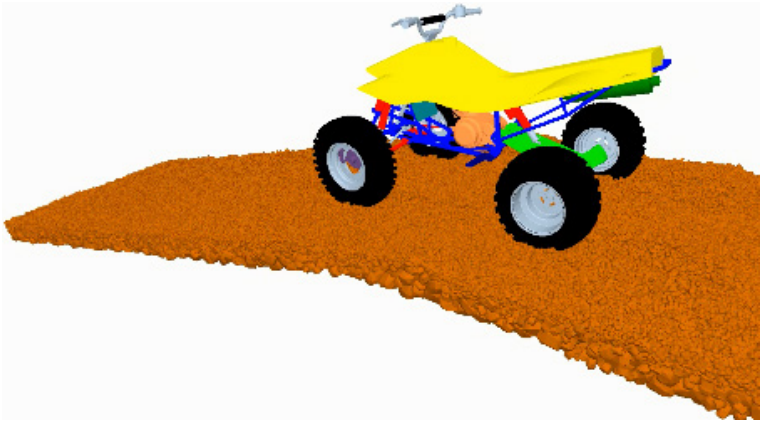


Figure 5C-12: EDEM Soil Modeling for Terramechanical Applications. Here an ATV travels down a slope comprised of sticky soil.

5C.5.5 Advanced Customization

In addition to the built-in physics models, EDEM also provides users with the tools to produce customized physics models using the EDEM Application Programming Interface (API). The EDEM API is highly versatile and enables complex simulations and advanced material behavior – such as breakage, flexible fibers, and more – to be simulated.

5C.6 REFERENCES

5C.6.1 Chrono References

[1] Project Chrono, Chrono: An Open Source Framework for the Physics-Based Simulation of Dynamics Systems, http://projectchrono.org. Accessed: 2018–06–06.

[2] Tasora, A., Serban, R., Mazhar, H., Pazouki, A., Melanz, D., Fleischmann, J., Taylor, M., Sugiyama, H. and Negrut, D. 2016. Chrono: An Open Source Multi-Physics Dynamics Engine, in High Performance Computing in Science and Engineering – Lecture Notes. Springer: Computer Science (T. Kozubek, Ed.), 19-49.

[3] Pazouki, A., Kwarta, M., Williams, K., Likos, W., Serban, R., Jayakumar, P. and Negrut, D. 2017. Compliant Versus Rigid Contact: A Comparison in the Context of Granular Dynamics. Phys. Rev. E, Vol. 96.

[4] Serban, R., Taylor, M., Negrut, D. and Tasora, A. 2018. Chrono: Vehicle Template-Based Ground Vehicle Modeling and Simulation. International Journal of Vehicle Performance. Jan 2019, (5) 18-39.

[5] Tasora, A., Magnoni, D., Negrut, D., Serban, R. and Jayakumar, P. 2018. Deformable Soil with Adaptive Level of Detail for Tracked and Wheeled Vehicles. International Journal of Vehicle Performance. Jan 2019 (5) 60-76.

[6] Anitescu, M. and Hart, G.D. 2004. A Constraint-Stabilized Time-Stepping Approach for Rigid Multibody Dynamics with Joints, Contact and Friction, International Journal for Numerical Methods in Engineering, 60(14):2335-2371.

[7] Serban, R., Recuero, A., Jayakumar, P., and Negrut. D. 2019. An Integrated Framework for High-Performance, High-Fidelity Simulation of Ground Vehicle-Tire-Terrain Interaction. International Journal on Vehicle Performance, 5(3) 233-259, doi: 10.1504/IJVP.2019.100698.

[8] Serban, R., Olsen, N. and Negrut, D. 2018. High Performance Computing Framework For Co-Simulation Of Ground Vehicle-Terrain Interaction. NDIA Ground Vehicle Systems Engineering and Technology Symposium, Novi, MI, USA, August 7-9, 2018.

5C.6.2 Adams References

[9] Adams. 2017. v2018 Help Documentation, Adams Co-Simulation Interface (ACSI). MSC Software, Newport Beach, CA, USA.

5C.6.3 RecurDyn References

[10] RecurDyn. 2017. V9R1 Help Documentation. FunctionBay, Seoul, Republic of Korea.

[11] EDEM .2018.1 Documentation. DEM Solutions, Edinburgh, UK.

[12] RecurDyn. 2017. V9R1 Theory Manual. FunctionBay, Seoul, Republic of Korea.

5C.6.4 EDEM Contact Model References

[13] Mindlin, R.D. and Deresiewicz, H. 1953. Elastic Spheres in Contact under Varying Oblique Force. ASME, Journal of Applied Mechanics, 20:327-344.

[14] Johnson, K.L., Kendall, K. and Roberts, A.D. 1971. Surface Energy and the Contact of Elastic Solids. In Proceedings of the Royal Society of London. Mathematical and Physical Sciences, 324(1558). 10.1098/rspa.1971.0141.

[15] Walton, O.R. 2006. (Linearized) Elastic-Plastic Contact Model. DEM Solutions Ltd., Edinburgh, UK.

[16] Thakur, S.C. et al. 2014. Micromechanical Analysis of Cohesive Granular Materials Using the Discrete Element Method with an Adhesive Elasto-Plastic Contact Model. Granular Matter, 16(3):383-400. 10.1007/s10035-014-0506-4.



Chapter 6 – TA5: UNCERTAINTY TREATMENT

K.K. Choi
University of Iowa
UNITED STATES

Nicholas Gaul
RAMDO Solutions, LLC
UNITED STATES

6.1 GOALS AND TEAM MEMBERS

The goal of Thrust Area 5 for the Next-Generation NATO Reference Mobility Model (NG-NRMM) is to develop a framework for a stochastic approach for vehicle mobility prediction over large regions using full stochastic knowledge of terrain properties and modern terramechanics Modeling and Simulation (M&S) capabilities and to demonstrate the generation of reliability-based stochastic mobility maps. The framework is for carrying out Uncertainty Quantification (UQ) and reliability assessment for Speed-Made-Good and GO/NOGO decisions for the ground vehicle based on the input variability models of the terrain elevation and soil property parameters. This framework is aimed to be part of a suite of NG-NRMM tools.

The team members are shown below:

- **K.K. Choi, Leader**, USA;
- Matt Funk, USA;
- Susan Frankenstein, USA;
- **Nicholas Gaul, Leader**, USA;
- Paramsothy Jayakuma, USA;
- Andrew Jones, USA;
- Michael McCullough, USA;
- Jeff Niemann, USA;
- Joseph Scalia IV, USA;
- Radu Serban, USA; and
- Tamer Wasfy, USA.

6.2 INTRODUCTION

For efficient coalition mission planning of NATO forces under different terrain scenarios and for selection of capable vehicles, reliability-based stochastic off-road mobility maps are developed. Traditionally, the analysis considers nominal deterministic values of key variables involved in the terrain properties and terramechanics simulation model. The generated deterministic mobility maps could be around 50% reliable and thus cannot be used effectively in mission planning of NATO forces under different terrain scenarios and for selection of capable next-generation combat vehicles. Thus, it is desirable to develop reliability-based stochastic mobility maps (i.e., Speed-Made-Good and GO/NOGO) that can provide desirable reliability levels in determining mobility of military vehicles across various terrains.

Key variables of off-road conditions include those related to terrain elevation data and soil property data as shown in Figure 6-1 [1]. The ground vehicle parameters and their variabilities could also be addressed for a full stochastics treatment, but were not considered in this study. The terrain elevation data are usually obtained using remote sensory techniques (i.e., radar technology, imagery methods, etc.). Those techniques lead to uncertainty in terrain data values as well as the spatial position of data points. Thus, any elevation model of the terrain includes uncertainty. Digital Elevation Models (DEMs) produced by the U.S. Geological Survey agency are a good example of this issue. Spatial variability of physical terrain properties (e.g., soil bulk density, cohesion, internal friction angle, Bekker-Wong parameters, etc.) also leads to uncertainty in vehicle-terrain interaction models. In addition, measurement methods of the soil properties are uncertain in nature.

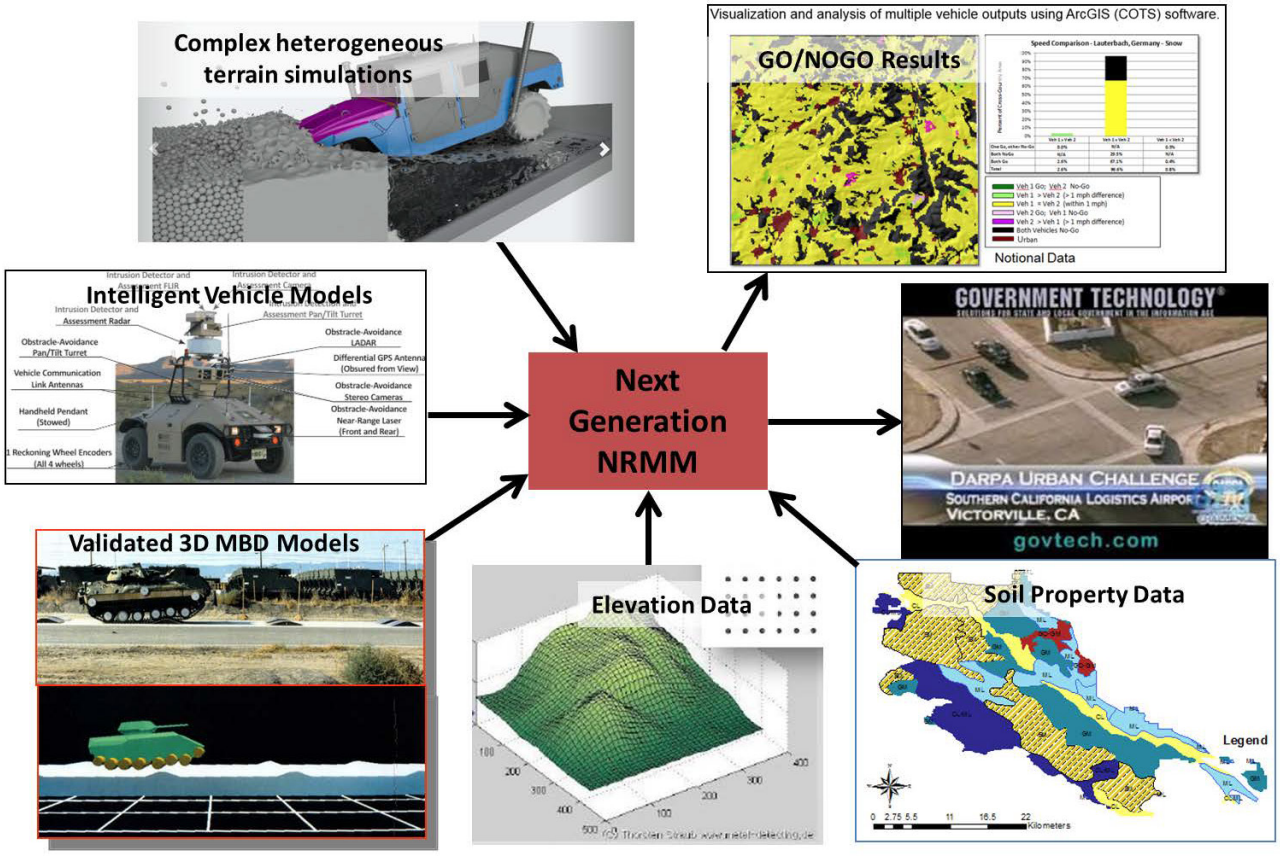


Figure 6-1: NG-NRMM Mobility Map Generation [1].

The current NRMM output is given in terms of a deterministic mobility map [2], [3]. This map shows the means of cross-country speed between two points in a given region for a given vehicle. As recommended by Refs. [4] and [5], a stochastic analysis should be carried out in terms of probability densities and reliabilities. However, previous attempts to convert NRMM from a deterministic framework to a stochastic one have failed in the origin of uncertainties. No formal mathematical reasoning about the uncertainty types that need to be introduced in the simulations was given in Refs. [4], [5], [6]. Also, the current NRMM does not support autonomous mobility (this issue was pointed out in Ref. [7]. While this capability is highly desirable in the NG-NRMM because current and future defence forces include autonomous systems, it was not considered by Thrust Area 5.

The stochastic approach for mobility predictions over large regions should be integrated into NG-NRMM, where both the terrain profile and vehicle-terrain interaction play a key role. The following recommendations are made in Ref. [8].

- Any extension of NRMM in terms of stochastic mobility prediction should allow for consideration of uncertainty in elevation as well as in soil physical properties. This is addressed in this study.
- Computation time constitutes a key factor that must be considered in the development of the new NRMM. In this sense, any new proposal should focus on efficient algorithms. This is addressed in this study.
- It is desirable from a stochastics perspective to base vehicle-terrain interaction on the Bekker-Wong model [9], [10], as these models are compatible with numerous multibody dynamic simulation codes. This is addressed in this study for a Simple Terramechanics model.

In developing reliability-based stochastic mobility maps, as described in Section 6.5.1 in detail, there are two types of uncertainties: irreducible uncertainty (variability) and reducible uncertainty (imperfection). Irreducible uncertainty refers to the inherent variability of data such as in terrain elevation and soil property variables. It is often expressed through statistical metrics such as variance, standard deviation, and interquartile ranges that reflect the variability of the data. Variability cannot be reduced, but it can be better characterized (i.e., better distribution model). Reducible uncertainty refers to imperfections in mechanical simulation models or distribution models. The term imperfection in mechanical simulation models is biasness of the terramechanics simulation model. The term imperfection in input distribution models is the uncertainty caused by the inability to correctly predict the input distribution and its parameters from limited data – it does not refer to variability. The variability in the NG-NRMM exist in terrain property variables (e.g., elevation, soil composition, bulk density, temperature, moisture content, etc.) or in terramechanics input parameters (e.g., slope, soil cohesive strength, soil friction coefficient and bulk density; or Bekker-Wong parameters, etc.). When evaluating reliability, only variabilities should be considered as the input since the reliability is not a function of reducible uncertainty. In this study, only terrain property variabilities are considered for development of the reliability-based stochastic mobility map. To deal with reducible uncertainty, a confidence measure needs to be developed. In addition, existence of reducible uncertainty calls for employment of Verification and Validation (V&V) procedure to ensure the effectiveness of the terramechanics models.

Two objectives to achieve the goals of Thrust Area 5 are developments and demonstrations of:

Objective 1) Framework for Terrain Modeling: Develop advanced Kriging models of terrain variables for high resolution estimation; and input distribution models for terramechanics input parameter variabilities.

Objective 2) Framework for Propagation of Variability: Calculate propagation of variabilities from elevation and soil property measurements into mobility, such as Speed-Made-Good and GO/NOGO decisions, using terramechanics models for generation of reliability-based stochastic mobility maps, across the given geographic area.

This study is mainly focused on Objective 2) development of a Framework for Propagation of Variability. In this report, we describe a framework that is developed for a stochastic approach for vehicle mobility prediction over a region of interest [11]. In this framework, an input model of the terrain is created using geostatistical methods. The performance of a vehicle is then evaluated while considering the terrain profile and the vehicle-terrain interaction. In order to account for terrain property variability, Monte Carlo simulations are carried out, leading to a statistical analysis.

Specifically, this framework involves methods for using ArcGIS/ENVI data [12] from Thrust Area 1 and Simple or Complex Terramechanics models from Thrust Areas 2 and 3, respectively, to generate reliability-based stochastic mobility prediction maps. It is noted that the developed framework will allow continuous future improvements, which can be repeated when a) the input distribution models are refined with better data and b) the terramechanics models used are revised, improved or changed as long as the terramechanics models accept the same input format from the ArcGIS/ENVI database [12] and generate appropriate speed outputs.

6.3 FRAMEWORK/METHODOLOGY

This section describes the framework and methodology for Objective 2), namely, the prediction of stochastic vehicle mobility over large regions and generation of reliability-based stochastic mobility maps, such as Speed-Made-Good and GO/NOGO decisions associated with specified target reliabilities.

6.3.1 Elevation and Soil Property Data Including Variability

While the terrain elevation data can come from various sources and take on various formats, in our study, the elevation data typically is provided in a raster format. Common resolutions for the elevation data are 30 m and 90 m. The variability information for the elevation data is required to take into account the uncertainty of the elevation data measurement. This variability information should ideally come in the form of a plus-minus tolerance with an associated confidence interval with, e.g., ± 12 m with 90% confidence. This can then be used to construct a normal (i.e., Gaussian) distribution that represents the variability of the elevation measurements. For the prototype demonstration presented in this study, the Monterey, California, data is used. The elevation data for this location was provided by the Shuttle Radar Topography Mission (SRTM) database [13]. The website for SRTM provides the variability information and states that for the 30x30 m data the accuracy is ±16 m with accuracy being at the 90% confidence level. Figure 6-2 shows how the elevation variability information is used to construct a distribution for the elevation for a cell of the raster.

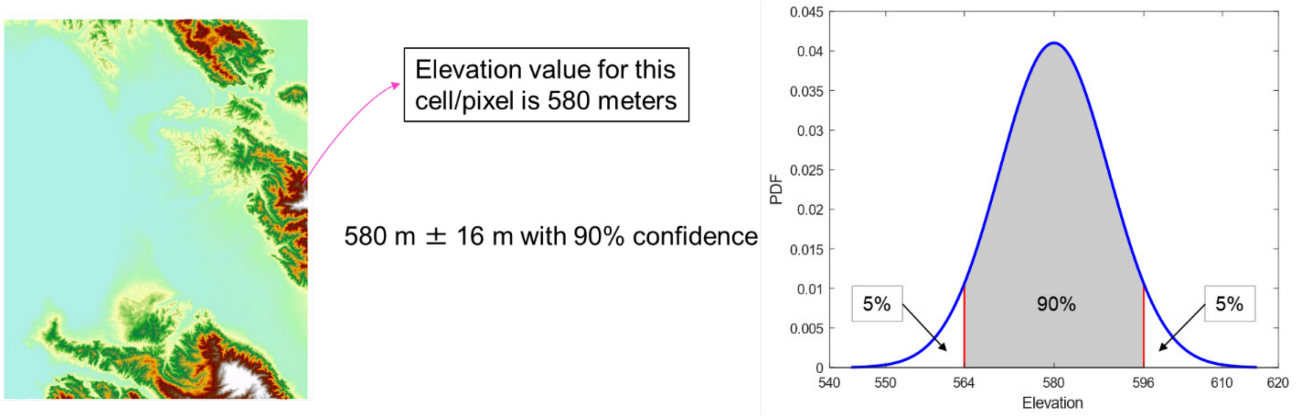


Figure 6-2: Elevation Variability and Distribution.

The slope is calculated by ArcGIS using the elevation raster. Thus, to obtain the variability of the slope, the variability of the elevation is needed so it can be propagated through the slope calculation. A simple toolbox was created in ArcGIS that calculates the slope for an elevation raster as shown in Figure 6-3. The toolbox loops over all the elevation rasters provided in a directory and calculates the slope for each raster. To generate the

distribution of the slope at given point, realizations of the elevation raster have to be generated using the normal distribution. Once the elevation raster realizations are generated, the slope realizations can be generated using the toolbox in ArcGIS. This then provides the variability of the slope.

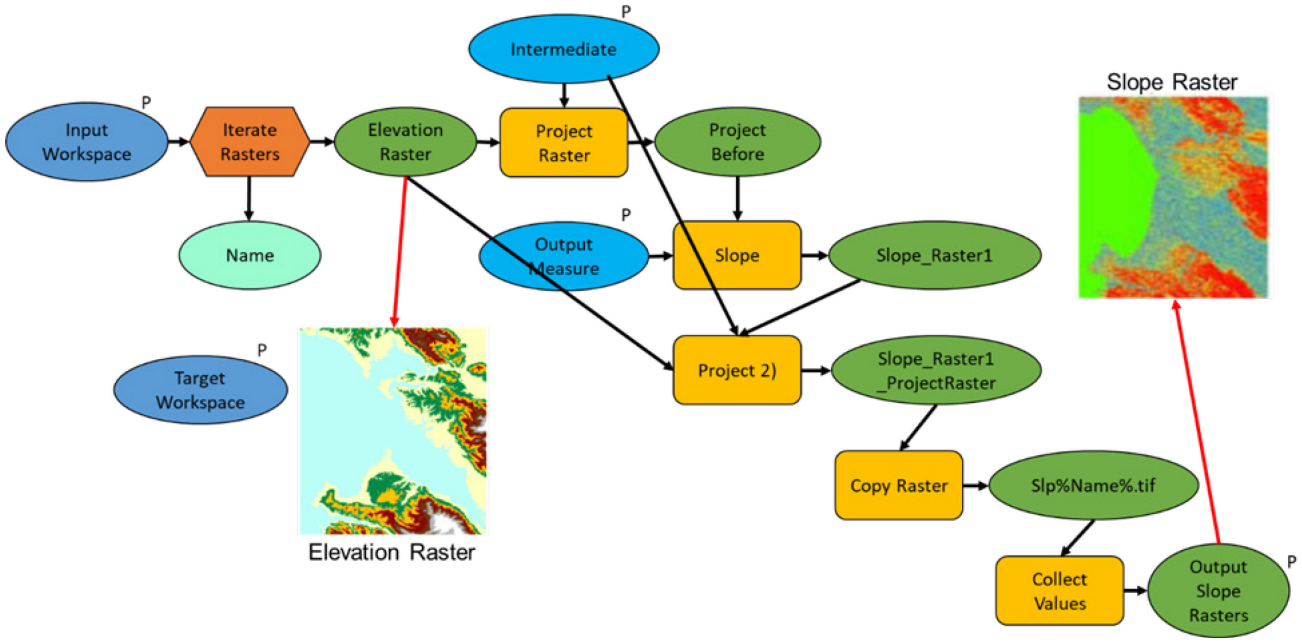


Figure 6-3: ArcGIS Slope Calculation Toolbox.

Currently there is very little information available on the variability of the soil properties. The only information currently found was from the Geotechnical Parameters site [14]. This site provided two tables, one for soil cohesion values and the other for friction angle values. These two tables provided very minimal variability, which is all that is currently available. For some of the soil types, the min. and max. values of the soil property were provided. For some other soil types, a specific value was provided without min. and max. values. Using the min. and max. values the distribution type was assumed to be a normal distribution with a 99% confidence on the min. and max. value range. Using these two assumptions, the distributions for the soil parameters for each of the different soil types were constructed. For the soil types that did not have min. and max. values provided, an assumption was made on the min. and max. values based on the specific value and other soil types that were similar. It is acknowledged that this may not be accurate but was the best information available at the time. For the peat soil type, the Geotechnical Parameters site [14] did not provide a range or a specific value. For peat, Ref. [15] provided a min. and max. value for the cohesion of undistributed and reconstituted peat. Since there was no other variability information provided, these min. and max. values were used with the same assumptions as the other soil types to construct the distribution.

For the bulk density, a USDA SSURGO Web Soil Survey database [16] containing bulk density measurements was available. There were only a few measurements available for each soil type in the database. Thus, there was not enough data available for fitting a distribution. Therefore, these measurements were used to determine the min. and max. values of the bulk density for the different soil types. These min. and max. values were used with the same assumptions to construct the distribution for the bulk density for different soil types. With all of the soil variability information gathered, each soil type has its own distribution for each of the soil properties, cohesion,

friction, and bulk density. Figure 6-4 shows a representation of this variability information: for a given soil classification, there is a distribution for the cohesion, friction, and bulk density. It is acknowledged that more data on the soil properties are required in order to construct accurate distributions for each soil type and parameter.

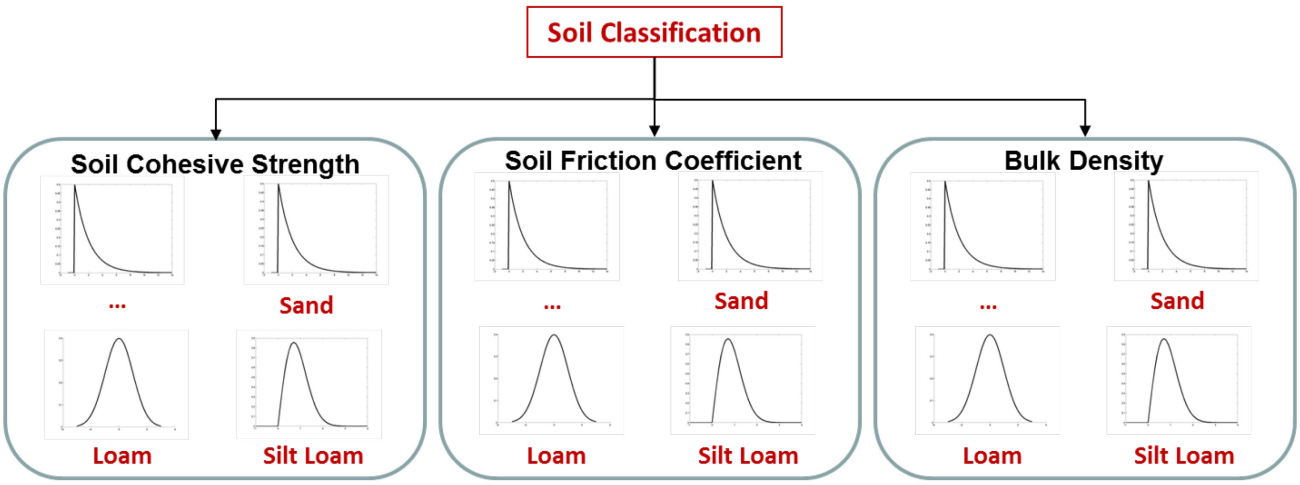


Figure 6-4: Variability of Soil Properties.

6.3.2 Advanced Kriging for Terrain Modeling

The previous NG-NRMM uncertainty treatment efforts for Theme 3 in ET-148, led by the MIT Robotic Mobility Group, used simple Kriging (i.e., conventional ordinary Kriging) to fit elevation data via the ArcGIS Geostatistical extension – Chapter 8 in Ref. [8]. This was used to generate a sample of random elevation realizations. They generated a mobility map accounting for two sources of uncertainty, namely measurement errors (Root Mean Square Error (RMSE) of a digital elevation model) and interpolation error (Kriging method), without considering variability of the soil properties. However, as described in Section 6.2, the interpolation error is reducible uncertainty and should not be included in the generation of stochastic mobility prediction. The slopes from each realization were used to make a stochastic mobility prediction. This was overlaid with a soil type map and all points with silty soil were declared off limits. The resulting GO/NOGO maps were used for an optimal route planning demonstration using ArcGIS functions.

In conventional universal Kriging, the responses at Design Of Experiment (DOE) points $\mathbf{x}_i$, $i = 1,\ldots, n$, are represented by:

$$\mathbf{y} = \mathbf{F}\boldsymbol{\beta} + \mathbf{Z}, \qquad \mathbf{F}=[f_k(\mathbf{x}_i),\ k = 1,...,K,\ i = 1,...,n\,]_{n\times K} \tag{6-1}$$

where $\boldsymbol{\beta}_{K\times 1}$ are regression coefficients, $f_k(\mathbf{x}_i)$ are polynomial basis functions, and $\mathbf{Z}_{n\times 1} = \left[Z(\mathbf{x}_1),...,Z(\mathbf{x}_n)\right]^T$ are realizations of Gaussian random process $Z(\mathbf{x})$ with zero mean and covariance $Cov\left(Z(\mathbf{x}_i), Z(\mathbf{x}_j)\right) = \sigma^2 R(\boldsymbol{\theta}, \mathbf{x}_i, \mathbf{x}_j)$. Here $R(\boldsymbol{\theta}, \mathbf{x}_i, \mathbf{x}_j)$ is the correlation function of the stochastic process, σ^2 is the process variance and $\boldsymbol{\theta}$ is the process correlation parameter vector.

For the two objectives described in the beginning of Section 6.2, the features identified from literature that are desirable to be included in the advanced Kriging method to deal with the non-stationary and non-Gaussian geostatistical data are listed below:

- The first one is a subregion-based Kriging model to deal with the common issue of non-stationary variogram models [11], [17], [18], [19], [20], as within the smaller subregion the variogram can be considered stationary. In addition, the subregion method will allow parallel processing in the generation of the Kriging models and thus achieve faster computational time. Furthermore, this will yield a smaller dimension of the correlation matrices that need to be inverted.
- The second method to deal with the non-stationary issue is using the universal Kriging with higher order polynomials [17], [21] instead of the ordinary Kriging (simple Kriging) that uses 0^{th} order polynomial for the trend function. Combined with the subregion-based Kriging model, up to the second order polynomial would be sufficient for the trend function. However, using one second order polynomial as the default trend function for all subregions would not provide accurate results. Thus, a method to select the best polynomial order of the trend function for each subregion is desirable for an accurate Kriging model.
- Kriging produces an interpolation function based on a covariance (i.e., variogram) model derived from the data rather than an a priori model of the interpolating function. For this, the Gaussian correlation model is widely used. To improve accuracy for the non-stationary and non-Gaussian data, a standard approach is finding some non-linear transformation that enables the use of Gaussian models [18]. However, as the models grow more complex, for example by introducing non-stationary covariance functions; spatially varying measurement errors; or covariates for the mean, the effects of the transformation methods become less transparent and more stale [22]. In these situations, one would like to use latent non-Gaussian models without resorting to transformations. Seven correlation functions (exponential, general exponential, Gaussian, linear, spherical, cubic, spline) could be used to model the covariance. Like the trend function, the best correlation function needs to be selected for each subregion depending on the data in the subregion.
- A method for selection of a combination from three trend functions and seven correlation functions for each subregion to yield the best accuracy of the Kriging model would be desirable.
- It is necessary to find the global optimal correlation parameters $\boldsymbol{\theta}$ of the covariance function that maximizes the likelihood function based on all observations. It is desirable that the method provides the global optimal correlation parameter $\boldsymbol{\theta}$.
- It is desirable to have a sub-sampling method for reduced order representation of the DEM points for the Kriging model that minimizes the Kriging variance (and thus reduces uncertainty). Also, the sub-sampling method would help in reducing the computational time as well as inverting the correlation matrix in the Kriging model by avoiding close data points (i.e., singularity) when inverting.

In this study, the Dynamic Kriging (DKG) method developed in RAMDO is used as the advanced Kriging for terrain modeling. The uniqueness of the DKG method includes:

- Select best trend function from 0^{th}, 1^{st}, and 2^{nd} order polynomials using Cross Validation (CV) error.
- Select best correlation function $R(\boldsymbol{\theta}, \mathbf{x}_i, \mathbf{x}_j)$ from seven candidates using Maximum Likelihood Estimation (MLE).
- Automatically select best DKG model from $7 \times 3 = 21$ different options for surrogate models.

- Search global optimal correlation parameter θ using MLE and the Global Pattern Search (GPS) algorithm [23].
- Adaptive sequential DOE points to minimize the variance of the Kriging results in between DOE sample points.

The DKG method [20], [24], [25] is identified as one of the most accurate surrogate modeling methods in Ref. [26].

6.3.3 Propagation of Uncertainty for Reliability Assessment of Mobility

For Objective 2), the capability that needs to be developed is Uncertainty Quantification (UQ) and reliability assessment for Speed-Made-Good and GO/NOGO decisions based on the input distribution models of the terrain elevation and soil property parameters. For this, the DKG surrogate model of the vehicle Speed-Made-Good with respect to four parameters for Complex Terramechanics (slope, bulk density, soil adhesive strength and soil friction coefficient) or Bekker-Wong parameters for Simple Terramechanics needs to be generated using the Complex or Simple Terramechanics model (i.e., the vehicle) runs, respectively, at the DOE points as shown in Figure 6-5. Using the DKG surrogate model of the Speed-Made-Good; input distribution models of the four parameters or Bekker-Wong parameters; and the ArcGIS/ENVI data of the region of interest; inverse reliability analysis is carried out to obtain reliability-based stochastic mobility map for the Speed-Made-Good and GO/NOGO decision.

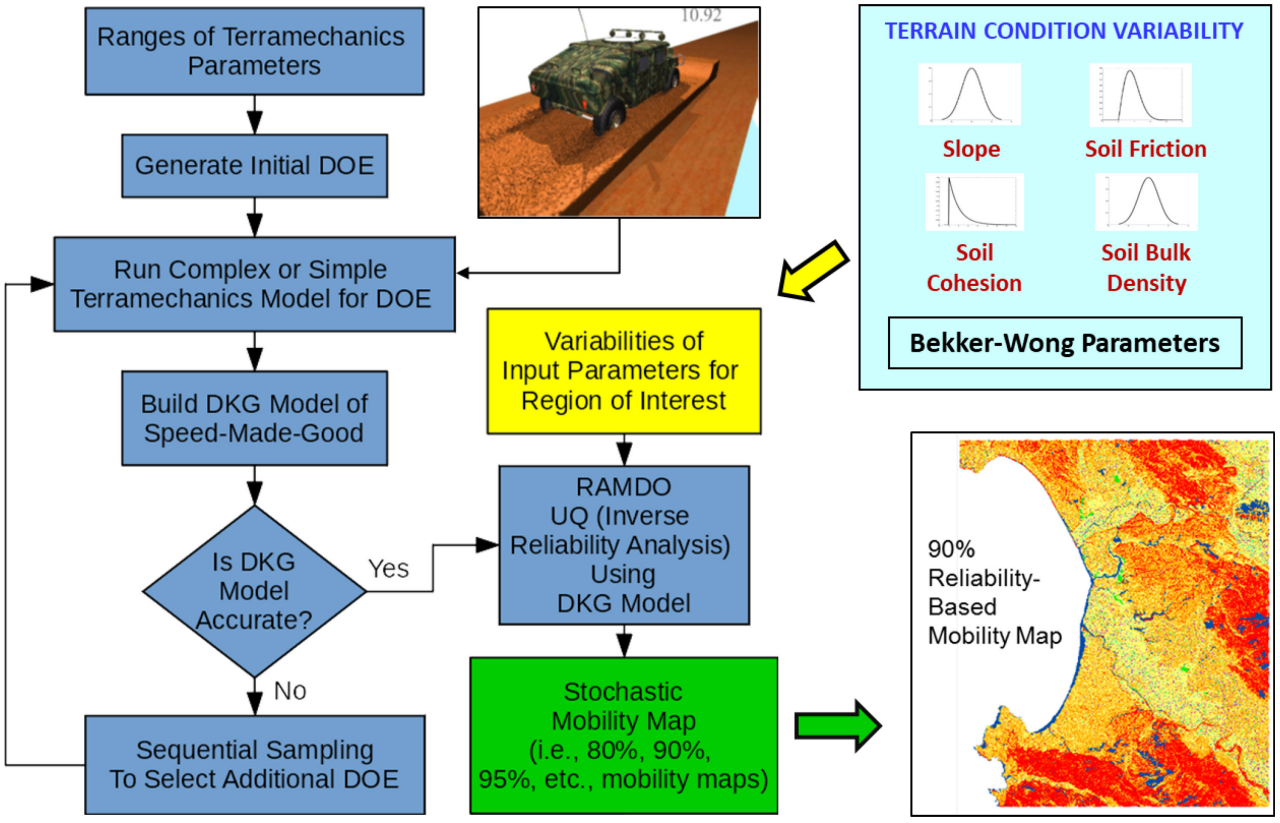


Figure 6-5: Generation of Reliability-Based Stochastic Mobility Map.

The developed framework for Propagation of Uncertainty in Objective 2) is the following (see Figure 6-5):

Step 1. Identify Ranges of Terramechanics Input Parameters That Will Cover the Regions of Interest:

Use the ranges (lower and upper bounds) of terramechanics input parameters over the regions of interest to construct a Dynamic Kriging (DKG) surrogate model of the Speed-Made-Good using the Complex or Simple Terramechanics model.

Step 2. DOE Samples of Speed-Made-Good for DKG:

a) Generate the initial Design of Experiment (DOE) points within the lower and upper bounds of terramechanics input parameters using a modified Transformations Gibbs Sampling (TGS) algorithm.

b) Evaluate Speed-Made-Good (i.e., steady-state speed) at the selected DOE points by running the Complex or Simple Terramechanics model on a High Performance Computing (HPC) system.

c) Add additional multiple DOE points using an adaptive sequential DOE sampling method at locations where the DKG surrogate model has the largest amount of the Kriging (DKG) variances.

d) The sequential sampling process is iterative and continues until the accuracy tolerance of the convergence Mean Square Error (MSE) of the DKG surrogate model is achieved.

Step 3. DKG Surrogate Model of Speed-Made-Good:

Generate the DKG surrogate of the Speed-Made-Good as a function of the terramechanics input parameters. Steps 2 and 3 are the most compute intensive processes. However, the surrogate model can be reused for other regions of interest to generate the reliability-based stochastic mobility map, which is the map for the same terramechanics model (i.e., the same vehicle).

Step 4. Input Distribution Models:

Obtain input distribution models for the terramechanics input parameters (slope, soil cohesive strength, soil friction coefficient and bulk density as described in Section 6.3.1; or Bekker-Wong parameters) for the region of interest.

Step 5. Inverse Reliability Analysis of Speed-Made-Good:

Carry out inverse reliability analysis to predict the Speed-Made-Good for reliability-based stochastic mobility map of the region of interest. A number of Monte Carlo Simulation (MCS) samples at each location of pixels was used to generate the reliability-based stochastic mobility map. Using the DKG surrogate of the Speed-Made-Good previously generated, this process can be carried out efficiently. This will allow quicker generation of the stochastic mobility map without requiring the use of an HPC. If necessary, then repeat Steps 4 and 5 to generate a new stochastic mobility map for another region of interest.

The simulation-based uncertainty quantification of the mobility map is accurate assuming:

1) Accurate input distribution models;

2) Accurate terramechanics simulation models; and

3) Accurate surrogate model.

However, in reality, as we have seen in this study, only limited numbers of input data for terramechanics parameters are available for modeling input distributions. Thus, the estimated input distribution models are uncertain. Also, the terramechanics simulation model could possibly be biased due to assumptions and idealizations used in the modeling process. In addition, the surrogate model could be inaccurate. For validation of the Speed-Made-Good prediction, only a limited number of physical vehicle driving test data can be obtained in practical applications. As a result, target output distributions for the vehicle speed, against which the terramechanics simulation model can be validated are uncertain and the corresponding reliability becomes uncertain as well. To assess the conservative reliability of the vehicle speed properly under these reducible uncertainties due to limited numbers of both input and output test data and a biased terramechanics simulation model, a confidence-based reliability assessment method [27] would be desirable to be developed in the future.

6.4 PROTOTYPE DEMONSTRATION

To better describe the process, a prototype demonstration will be shown for two cases: the Complex Terramechanics case using the soil parameters of bulk density, soil adhesive strength and soil friction coefficient as described in Chapter 5; and for Simple Terramechanics using Bekker-Wong parameters for the different types of soil as described in Chapter 3.

6.4.1 Complex Terramechanics Prototype

This section presents the prototype demonstration of generation of the reliability-based stochastic mobility maps. For the prototype demonstration, Monterey, California is selected as the region of interest. First, for the Complex Terramechanics model, the NATC Wheeled Vehicle Platform shown in Figure 6-6 is used. The Complex Terramechanics model was developed by Advanced Science and Automation Corporation and is described in Chapter 5 [28], [29].

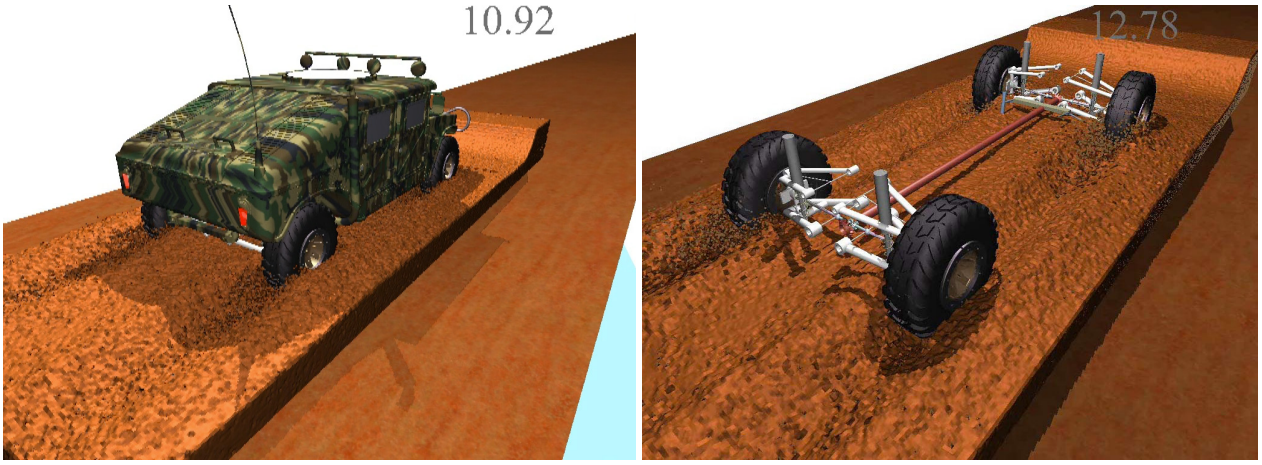


Figure 6-6: Complex Terramechanics Model of NATC Wheeled Vehicle Platform.

Figure 6-7 shows the concept of how the variability of terrain and soil properties are used with a UQ tool [30] together with the terramechanics simulation model to generate the reliability-based stochastic mobility maps. The deterministic soil type data is provided as a GeoTIFF as shown in Figure 6-7. The provided soil type is assumed to be correct, i.e., no variability in the soil type (e.g., sand, clay, etc.) is assumed. Variability in the soil comes from the variability in the soil parameters.

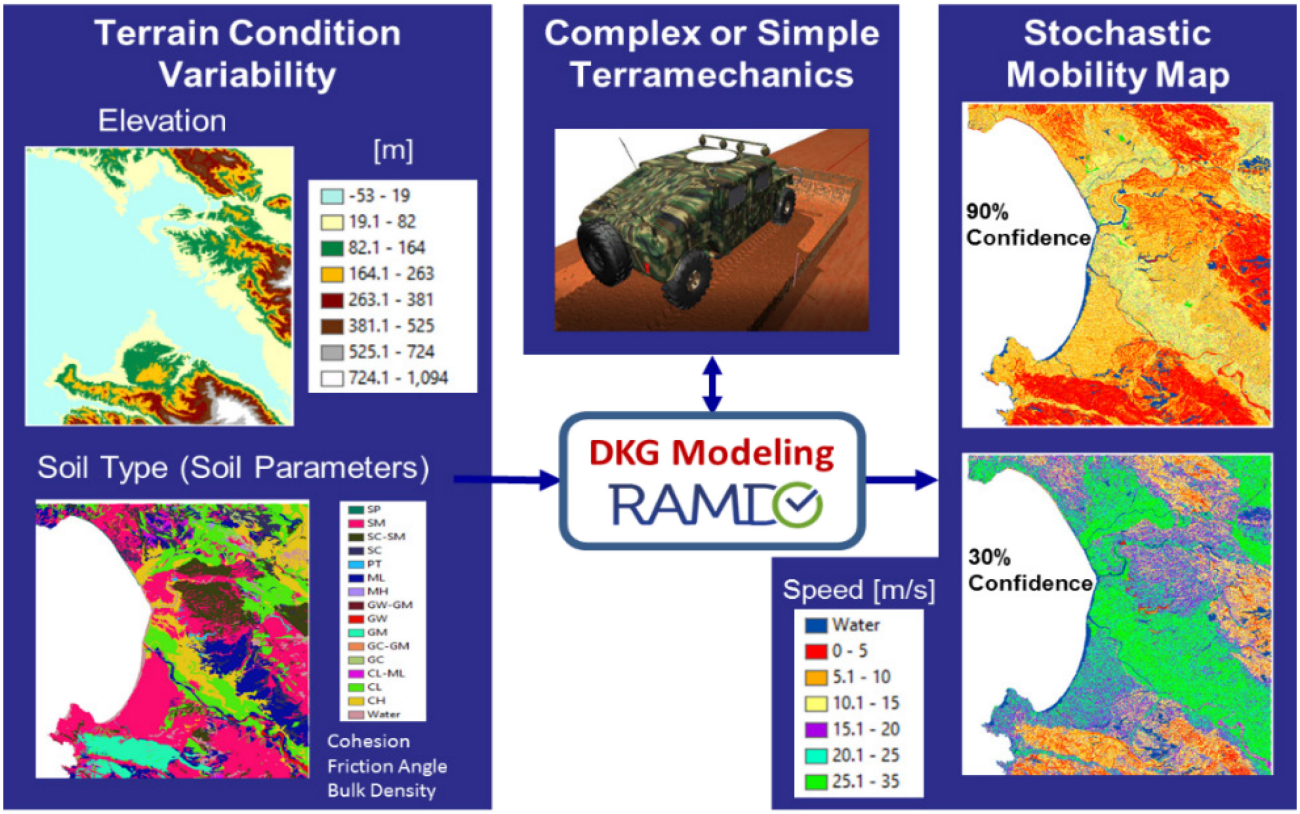


Figure 6-7: Propagation of Variability to Generate Reliability-Based Stochastic Mobility Maps for Terramechanics.

RAMDO [30] is used to create the DKG model of the Complex Terramechanics simulation model (i.e., the vehicle) of the NATC Wheeled Vehicle Platform. To create the DKG model 32 DOE points were created for the four-dimensional problem. The four variables used were slope, cohesion, friction angle, and bulk density of the soil. The 32 Complex Terramechanics simulation models were created. The 32 runs were carried out using 32 cores for each job and running all 32 jobs in parallel. Each run took between 5-7 days to complete. The response of interest from the simulation was the Speed-Made-Good. Once the DKG model is created, it is used together with the UQ tool for the variability propagation by carrying out inverse reliability analysis to predict the Speed-Made-Good for reliability-based stochastic mobility map of the region of interest. For the inverse reliability analysis, we need more than 1,000 Monte Carlo Simulation (MCS) samples at each location of $3{,}601^2 = 12{,}967{,}201$ pixels for Monterey, California to generate the reliability-based stochastic mobility map. However, using the DKG surrogate of the Speed-Made-Good previously generated, this process can be carried out efficiently. This will allow quicker generation of the stochastic mobility map without requiring the use of an HPC. Using the UQ tool the distribution of the Speed-Made-Good at each cell of the raster is obtained as shown in Figure 6-8. These distributions can then be used to create the reliability-based stochastic mobility maps as shown in Figure 6-9. The 90% Speed-Made-Good map means that there is a 90% probability that the maximum obtainable speed is greater than or equal to the value shown on the map in Figure 6-8. If speed is mission critical, e.g., delivering supplies urgently needed, then using a higher probability map would be desirable. If speed is not mission critical, then using a lower probability map could be acceptable.

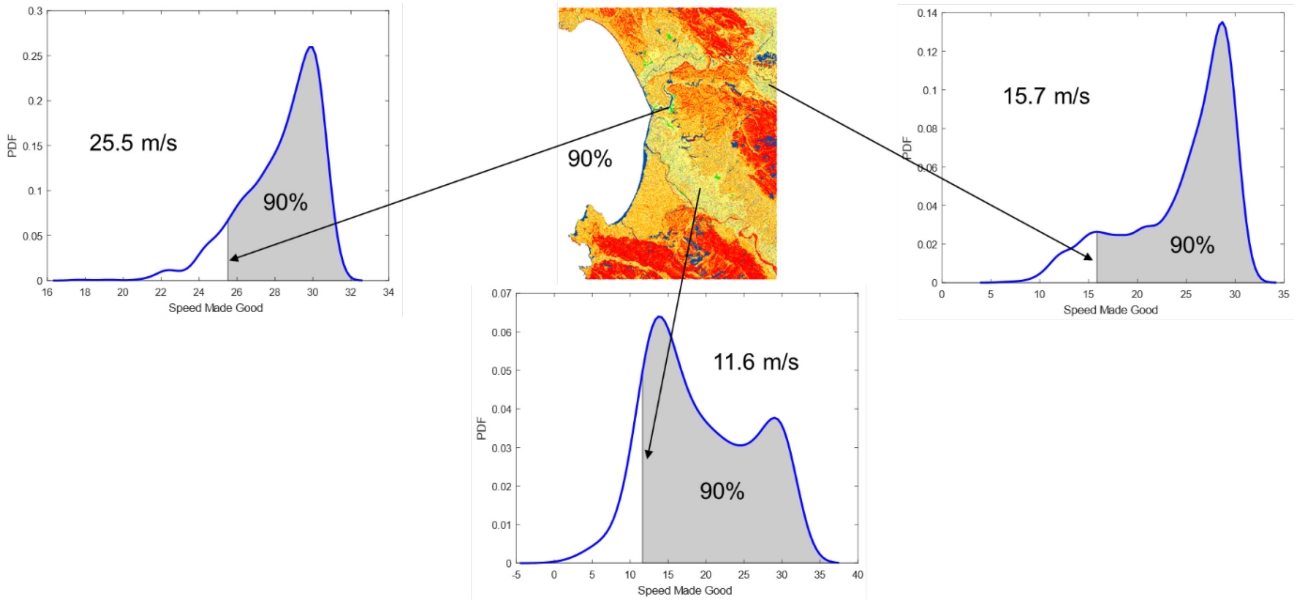


Figure 6-8: Distribution of Speed-Made-Good for Each Cell of Raster for Complex Terramechanics.

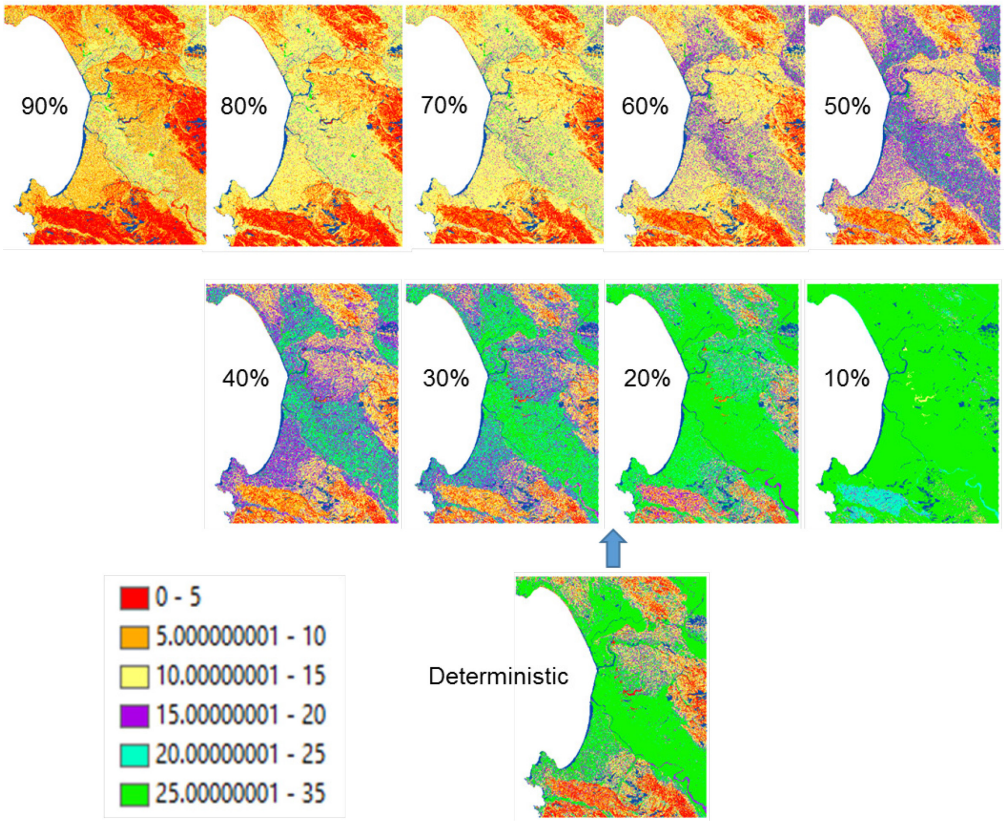


Figure 6-9: Reliability-Based Stochastic and Deterministic Speed-Made-Good Mobility Maps for Complex Terramechanics.

The propagation of the variability of the terrain and soil properties was successfully demonstrated in creating the reliability-based stochastic mobility maps shown in Figure 6-9 for Monterey, California. If variability is not taken into consideration when generating the Speed-Made-Good maps, then a deterministic map is generated as shown in the last figure in Figure 6-9. In this map, the color-coded speed is meters/sec. (To convert these speeds to miles/hour, we need to multiply these numbers by 2.24). For Monterey, California used in this study, it is seen that the deterministic map appears to be somewhere between the 20% and 30% reliability maps, meaning the deterministic map only has a probability of approximately 25% to achieve the indicated speed just from visual comparison. To estimate reliability of the deterministic Speed-Made-Good map at each location, Figure 6-10 is obtained where the color legend indicates reliability. It can be seen from the figure that the maximum reliability of the deterministic Speed-Made-Good map is less than 72%. This demonstrates the need for taking into account the variability so that accurate Speed-Made-Good maps can be generated and have a given reliability or confidence attached to them, in order to provide more information to the decision maker.

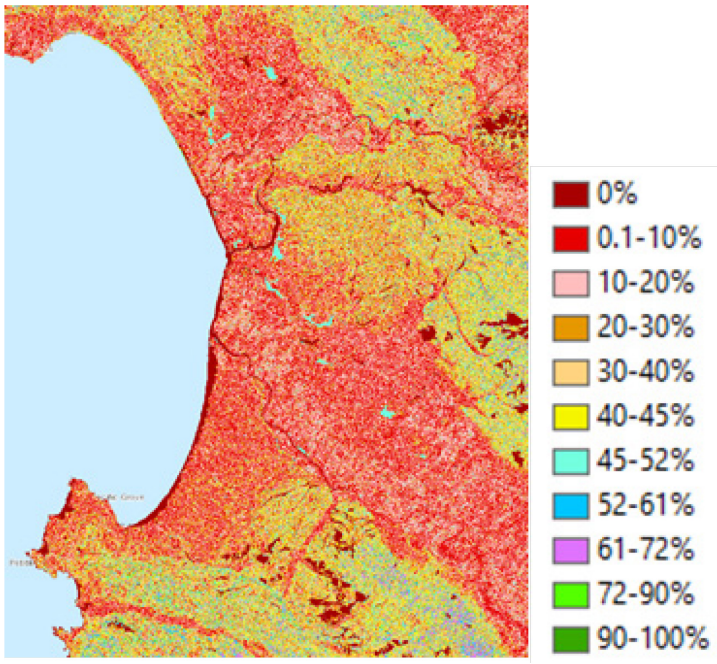


Figure 6-10: Reliability of Deterministic Speed-Made-Good Mobility Maps for Complex Terramechanics.

It is interesting to note that these reliability-based stochastic mobility maps are like “FEMA Flood Maps”. For example, the 100-year flood map is referred to as the 1% annual exceedance probability of flood, since it is a flood that has a 1% chance of being equaled or exceeded in any single year (i.e., 99% reliability).

The same DKG model of the Complex Terramechanics simulation model (i.e., the vehicle) in Figure 6-7 is used for the variability propagation by carrying out inverse reliability analysis to predict the GO/NOGO region. The UQ tool that is used to obtain reliability-based Speed-Made-Good at each cell of the raster shown in Figure 6-8 is used to create the reliability-based GO/NOGO maps for Monterey, California as shown in Figure 6-11. For GO/NOGO maps, the cut-off speed used is 5 miles/hour. In this map, the green color means GO, the red color means NOGO and the blue color means water. Thus, the green color in the 90% GO/NOGO map means that there is a 90% probability that the vehicle can move with a speed of at least 5 miles/hour. If interested,

GO/NOGO maps for different cut-off speeds can be generated. Note that for up to 40% reliability, the NOGO region does not seem to significantly show on the map. However, starting at 50% reliability, the NOGO region is beginning to show up clearly. It is seen that the deterministic map appears to be like the 60% reliability map.

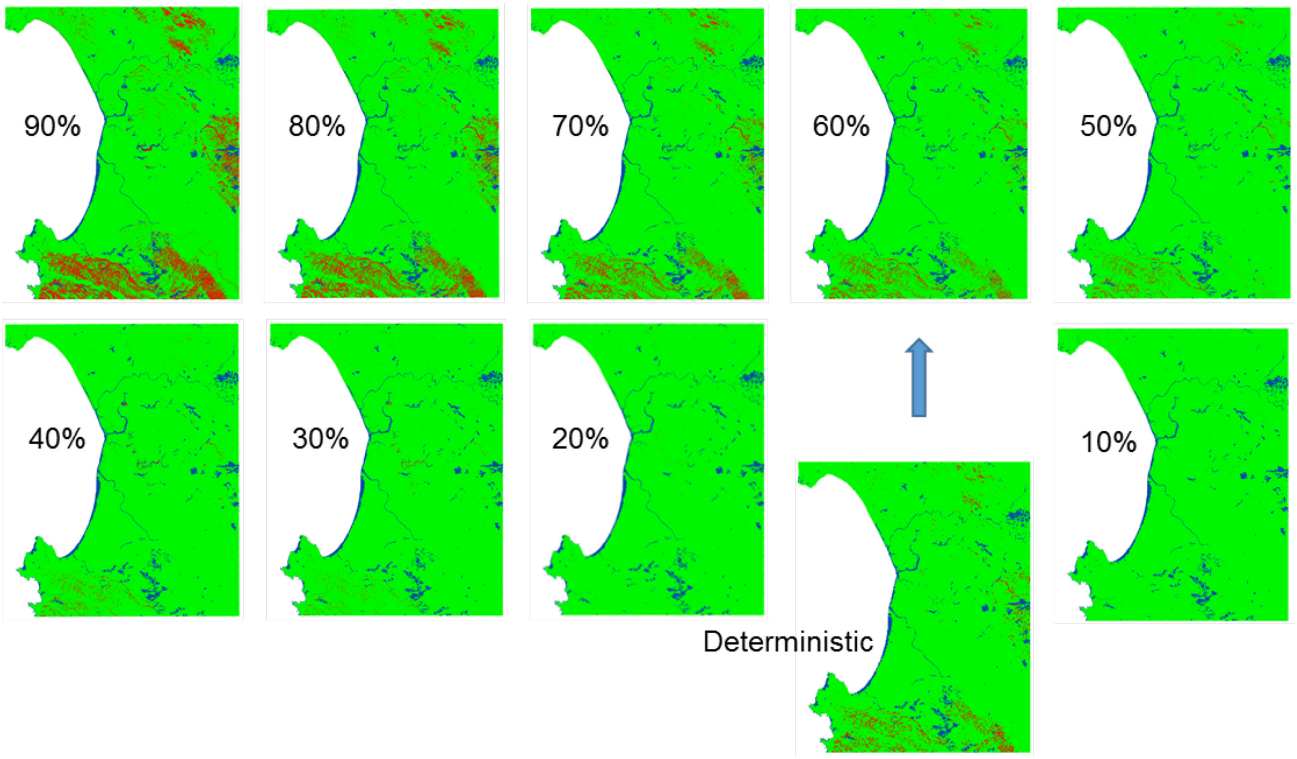


Figure 6-11: Reliability-Based GO/NOGO Mobility Maps for Complex Terramechanics.

To find the effect of moisture on mobility, the same DKG model of the Complex Terramechanics simulation model (i.e., the vehicle) in Figure 6-7 is used for the variability propagation by carrying out the inverse reliability analysis to predict the Speed-Made-Good. For input, the deterministic data for bulk density that is provided by a USDA SSURGO Web Soil Survey database [16] and the deterministic data for slope that is provided by the Shuttle Radar Topography Mission (SRTM) database [13] are used as described in Section 6.3.1. On the other hand, the deterministic data for friction angle in degrees for Monterey, California is provided by the Colorado State University (CSU) team [31] as a GeoTIFF and shown in Figure 6-12. As the moisture affects the cohesion, the variability of seasonal moisture is used by the CSU team [31] to obtain the variability of cohesion for the dry and wet seasons, respectively. The CSU team provided the realizations of the cohesion for the variability. They provided 1000 GeoTIFFs for both dry and wet seasons containing the cohesion realizations. The variability of the cohesion for both the dry and wet dates is shown below in Figure 6-13 and Figure 6-14. In these figures the probability value shown is the probability of the cohesion being less than or equal to the value shown in the map. With these input data and variability, the inverse reliability analyses are carried out using the same DKG model of the Complex Terramechanics simulation model (i.e., the vehicle) in Figure 6-7 to obtain reliability-based Speed-Made-Good for the dry season and wet seasons, as shown in Figure 6-15 and Figure 6-16 below, respectively. From these figures, we can clearly see the effect of moisture on mobility with the reliability-based Speed-Made-Good is lower during the wet season. In addition, the Speed-Made-Good is lower as the reliability requirements are increased.

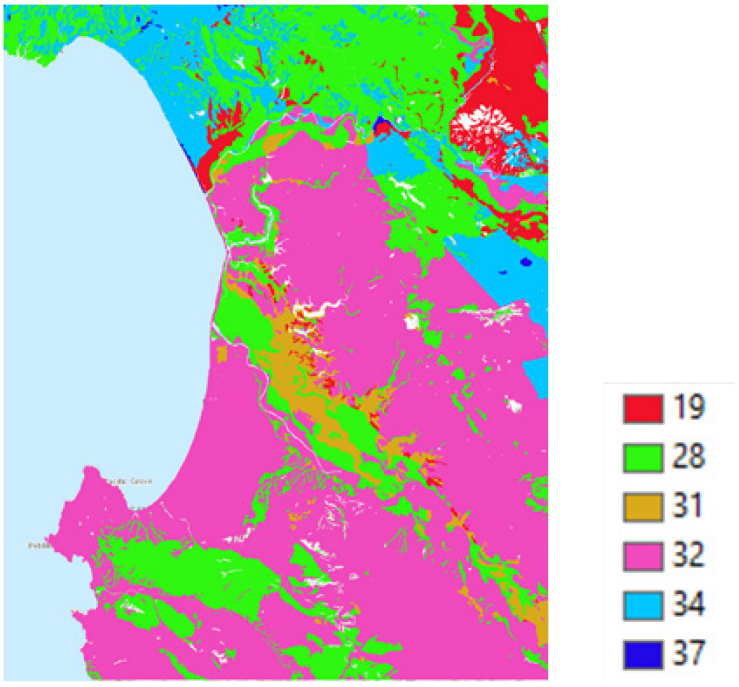


Figure 6-12: Deterministic Friction Angle in Degrees.

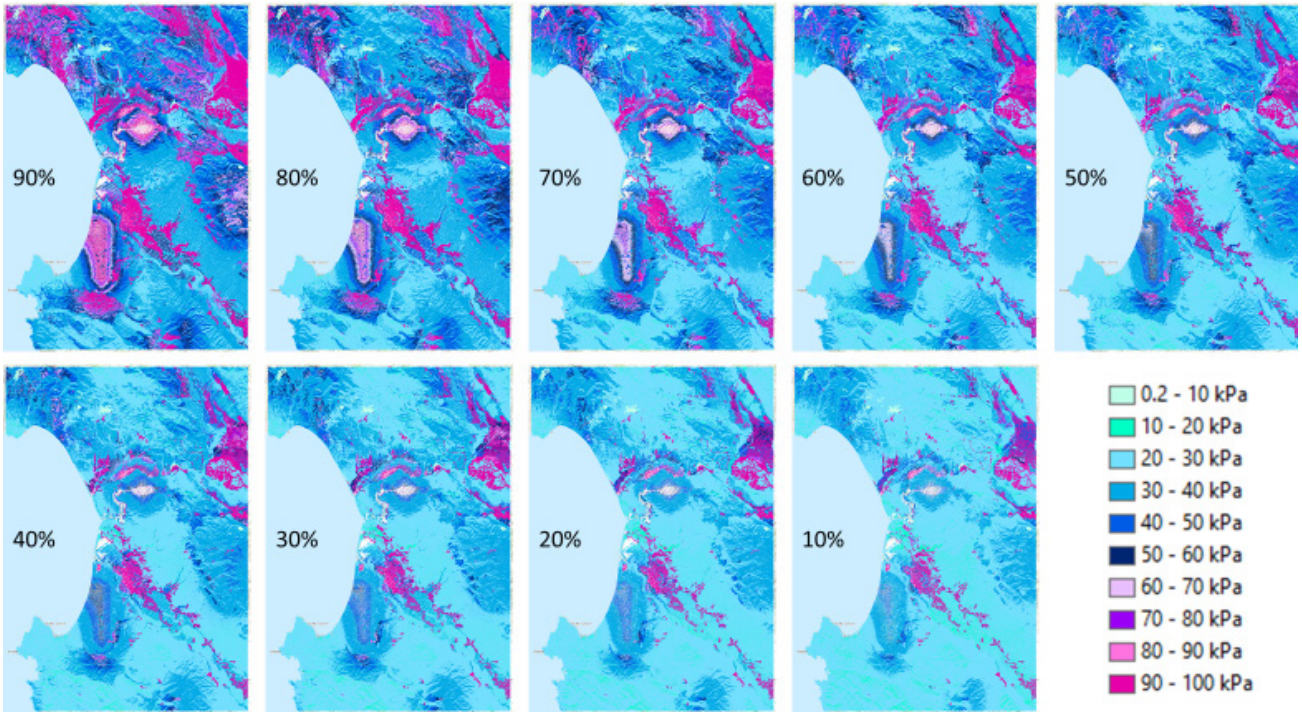


Figure 6-13: Cohesion Maps in Dry Season.

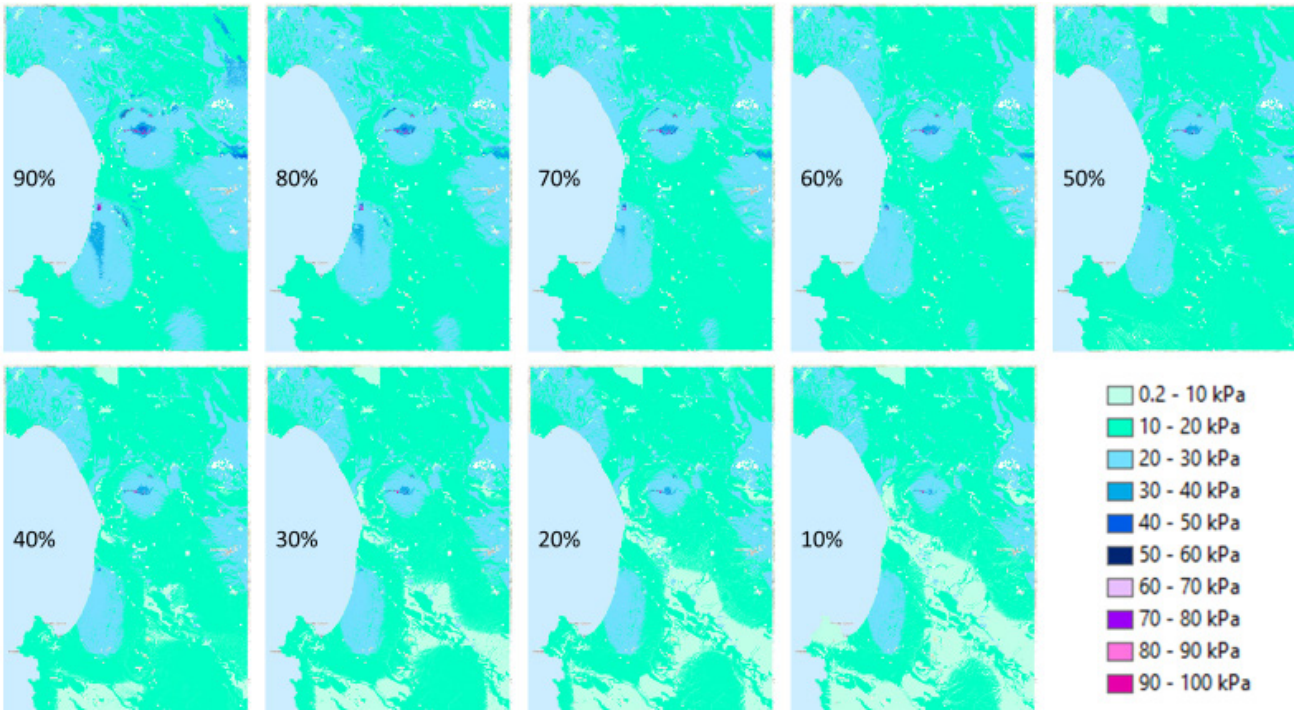


Figure 6-14: Cohesion Maps in Wet Season.

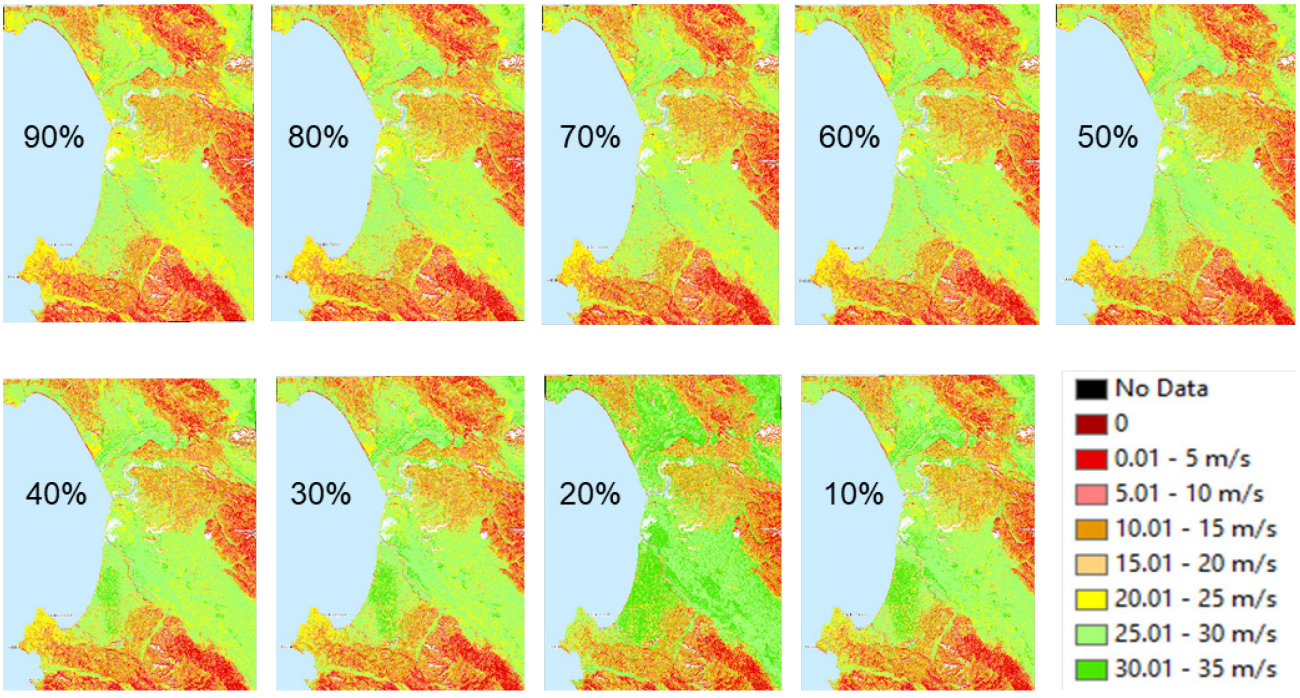


Figure 6-15: Reliability-Based Stochastic Speed-Made-Good Mobility Maps in Dry Season.

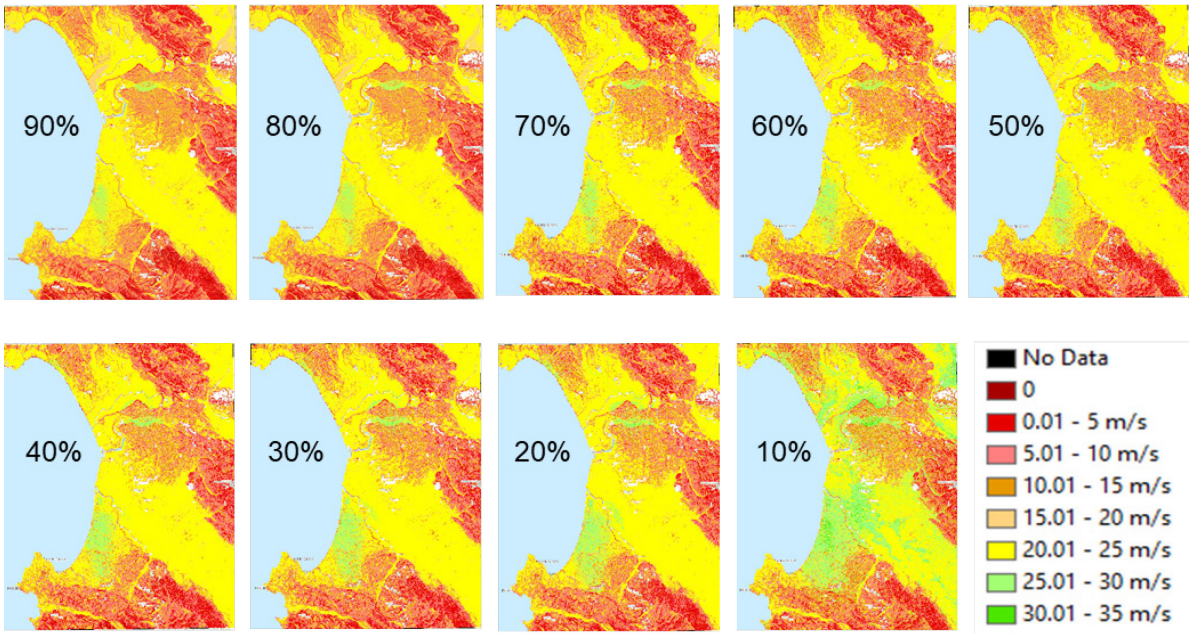


Figure 6-16: Reliability-Based Stochastic Speed-Made-Good Mobility Maps in Wet Season.

6.4.2 Simple Terramechanics Prototype

Second, for the Simple Terramechanics model, the same framework is applied to generate the reliability-based stochastic mobility map of Monterey, California. For the Simple Terramechanics model, the M113 tracked vehicle is used. The tracked vehicle and Simple Terramechanics simulations were conducted with the Chrono open source multi-physics package [32], [33]. A description of the M113 vehicle model is provided in Chapter 8, while the Simple Terramechanics formulation is discussed in Chapter 4. For simulation of the Simple Terramechanics model, six of eight Bekker-Wong-Janosi (BWJ) parameters [34] shown in Table 6-1 are used, while two parameters k_0 and A_u are not used. Thus, a total of eight parameters: six BWJ parameters plus soil type and slope are used for simulation of the Simple Terramechanics model. The six BWJ parameters in Table 6-1 are dependent and fully characterized by only 2 quantities: soil type and saturation level (moisture). Thus, there are three independent parameters: soil type, saturation and slope. The soil type is a discrete variable (nine unique classes of soil are shown in Table 6-2) and saturation and slope (shown in Table 6-3) are continuous variables. Since surrogate models cannot be accurately constructed for the discrete variable, instead of one surrogate model of three independent parameters, nine DKG surrogate models of two parameters are developed. RAMDO [30] is used to create the DKG model of the Simple Terramechanics simulation model (i.e., the vehicle) of the M113 tracked vehicle. Thus, a total of nine two-dimensional DKG surrogate models are generated. The total number of DOE samples for nine surrogates was 513 as described below:

- 1st DOE set: 17 DOEs for each surrogate – 153 DOEs (9 surrogates × 17 = 153).
- 2nd DOE set: 15 DOEs added for each surrogate – 135 DOEs (9 surrogates × 15 = 135).
- 3rd DOE set: 15 DOEs added for each surrogate – 135 DOEs (9 surrogates × 15 = 135). Three surrogates converged at this stage of DOE sampling.
- 4th DOE set: 15 DOE added for each surrogate, 90 DOEs (6 surrogates × 15 = 90).
- Total number of DOEs = 513 = 153 + 135 + 135 + 90.

Table 6-1: Eight Bekker-Wong-Janosi Parameters.

Types of Parameters	Symbols of Parameters	# Parameters
Pressure-Sinkage	k_c, k_ϕ, n	3
Repetitive Loading	k_o, A_u	2
Terrain Internal Shearing	c, ϕ, K	3
	Total	**8**

Table 6-2: Nine Unique Soil Type List.

Number	Soil Types
1	GW, GW-GM, GM
2	GC-GM
3	GC
4	SP
5	SM
6	SC-SM
7	SC
8	ML, CL-ML, CL, CH
9	MH

Table 6-3: Two Parameters for the DKG Surrogate Models.

Parameters used for DKG Modeling
Saturation
Slope

The conversion from saturation to the BWJ parameters for each soil type was carried out by TA2 and described in Chapter 4. Like the Complex Terramechanics, the response of interest from the Simple Terramechanics simulation is the Speed-Made-Good. Once the DKG models are created, it is used together with the UQ tool for the variability propagation by carrying out inverse reliability analysis to predict the Speed-Made-Good for reliability-based stochastic mobility map of the region of interest as shown in Figure 6-17. As described in the Complex Terramechanics case, the 90% Speed-Made-Good map means that there is a 90% probability that the maximum obtainable speed is greater than or equal to the value shown on the map in Figure 6-17 It is interesting that, unlike the NATC Wheeled Vehicle Platform, the deterministic map for the M113 tracked vehicle appears to be like the 20% reliability map for some region of the Monterey map, while it is like the 50% reliability map for some other region based on visual comparison.

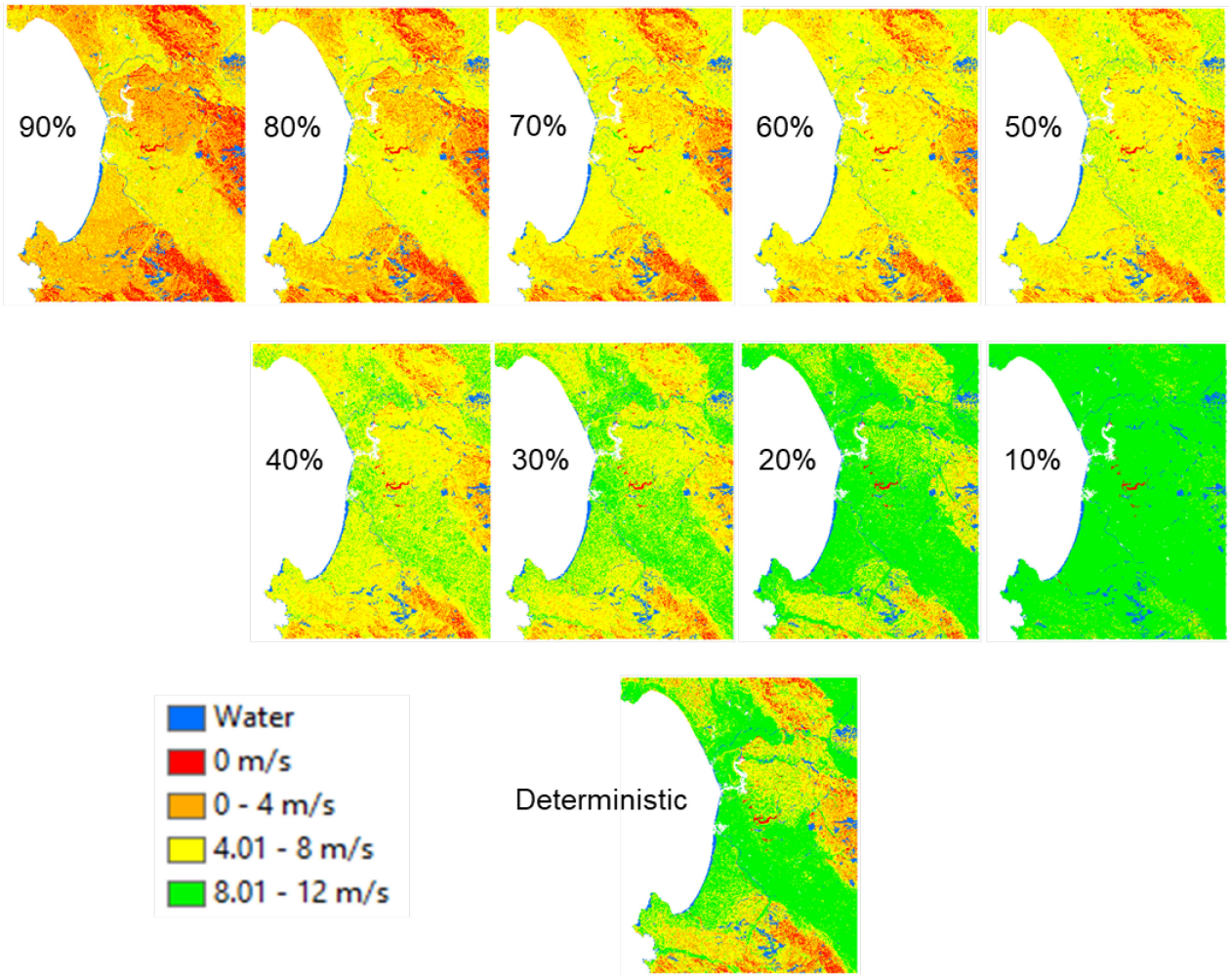


Figure 6-17: Reliability-Based Stochastic and Deterministic Speed-Made-Good Mobility Maps for Simple Terramechanics.

The same DKG model of the Simple Terramechanics simulation model (i.e., the vehicle) in Figure 6-7 is used for the variability propagation by carrying out inverse reliability analysis to predict the reliability-based GO/NOGO maps for Monterey, California as shown in Figure 6-18. For GO/NOGO maps, the cut-off speed used is 5 miles/hour. Like the Complex Terramechanics map, in this map, the green color means GO, the red color means NOGO and the blue color means water. Thus, the green color in the 90% GO/NOGO map means that there is a 90% probability that the vehicle can move with a speed of at least 5 miles/hour. It is seen that the deterministic map appears to be like the 50% reliability map. By developing reliability-based mobility maps for different vehicles (like NATC Wheeled Vehicle Platform and M113 tracked vehicle), the decision maker can select capable vehicles for the required mission in the Monterey, California.

6.5 STANDARD

This section describes uncertainty treatment, as it will be incorporated into a NATO standard.

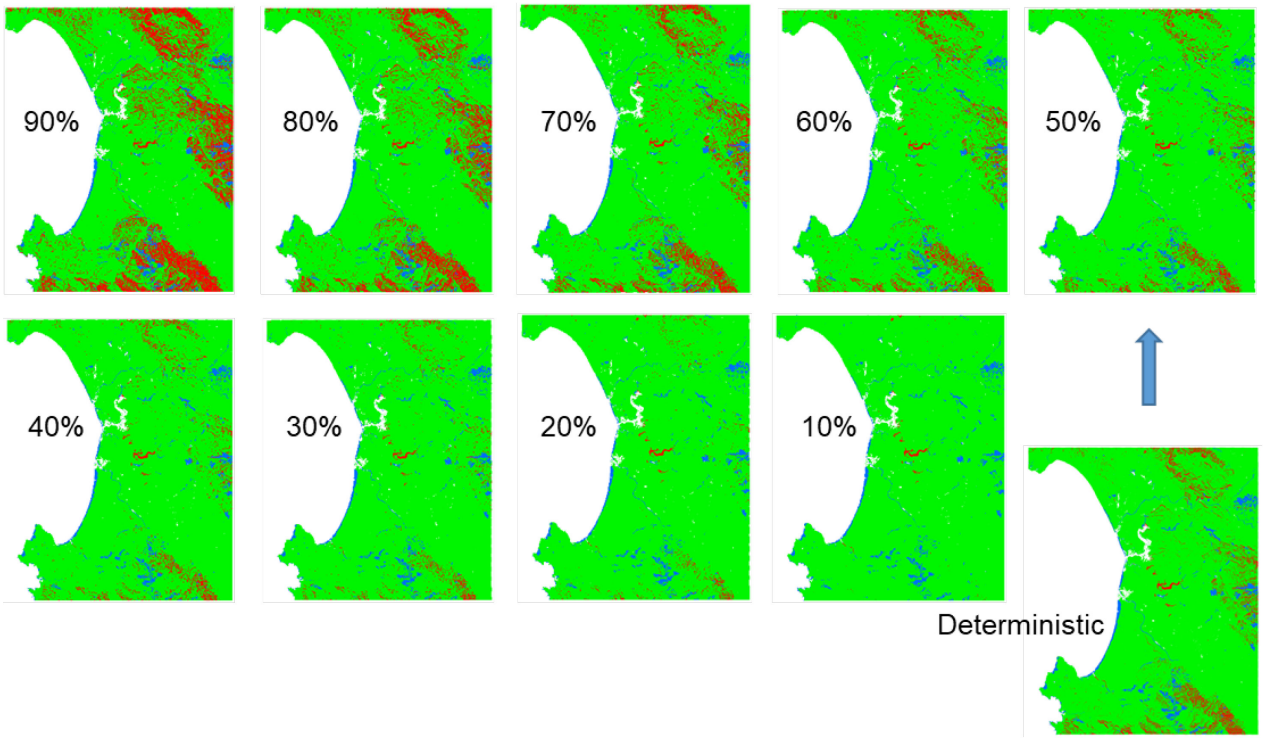


Figure 6-18: Reliability-Based GO/NOGO Mobility Maps for Simple Terramechanics.

6.5.1 Variability Versus Uncertainty in NG-NRMM

In developing reliability-based stochastic mobility maps, it is necessary to use correct definitions of input uncertainties as they affect the reliability-based stochastic mobility map results. There are two types of uncertainties: irreducible uncertainty and reducible uncertainty. Irreducible uncertainty, which is also called variability or aleatory uncertainty, refers to the inherent heterogeneity or diversity of data in an assessment. It is "a quantitative description of the range or spread of a set of values" [35], and is often expressed through statistical metrics such as variance, standard deviation, and interquartile ranges that reflect the variability of the data. Variability cannot be reduced, but it can be better characterized (i.e., modeled). Reducible uncertainty refers to imperfections in mechanical simulation models or distribution models. The term imperfection in mechanical simulation models is biasness of the terramechanics simulation model. The term imperfections in input distribution models is the uncertainty caused by the inability to correctly predict the input distribution and its parameters from limited data – it does not refer to variability. Reducible uncertainty can be either qualitative or quantitative [35]; and can be eliminated or reduced with better simulation models and more or better data.

Based on these definitions, the variability and uncertainty in NG-NRMM are as follows:

- Irreducible uncertainty:
  - Terrain property variables (e.g., elevation, soil composition, bulk density, temperature, moisture content, etc.), including known measurement errors.
  - Terramechanics input parameters (e.g., slope, soil cohesive strength, soil friction coefficient and bulk density; or Bekker-Wong parameters, etc.).

- Reducible uncertainty:
  - Input distribution models obtained using limited number of terrain data.
  - The terramechanics simulation models are abstractions of the physical system (i.e., vehicle) and it is possible that these models may not depict the actual physical event correctly. Uncertainty about the model's structure, i.e., uncertainty about the cause-and-effect relationships, is often very difficult to quantify. If so, it should be treated as reducible uncertainty.
  - Another situation is, when generating response surfaces using Design Of Experiment (DOE) samples, if the response surface includes error, then we have reducible uncertainty. Thus, the Kriging variance (estimation error) should not be treated as irreducible uncertainty but as reducible uncertainty.

When evaluating reliability, only irreducible uncertainty (i.e., variability) needs be considered as the input. Reliability is not a function of reducible uncertainty. If uncertainty exists due to:

1) Lack of information in input terrain data for input distribution modeling,
2) Terramechanics simulation models that do not depict the actual physical event correctly, or
3) Kriging surrogate model variances that are not ignorable;

then attempts should be made to reduce imperfections in mechanical simulation models and/or input distribution models instead of using these reducible uncertainties as input variabilities.

If we believe there exists reducible uncertainty in development of reliability-based stochastic mobility maps, then it is desirable to perform Verification and Validation (V&V) to have confidence in the reliability-based stochastic mobility map.

6.5.2 GIS Data and Higher Resolution of Terrain Variables

The framework of natural terrain modeling starts with a set of sparse measurements obtained using a remote sensor for a terrain region of interest. In Part 1 of Figure 6-19, the GIS data layers can include satellite data, manual observations, soil type and geological maps, as well as estimated or known measurement errors. The GIS data include elevation, slope, soil composition, soil cohesive strength, soil friction coefficient, bulk density, temperature, moisture content, etc. Currently, the GIS data are available only in lower resolution, which may not be sufficient to meet the modeling and simulation needs. For development of an NG-NRMM reliability-based stochastic mobility map with higher resolution, surrogate modeling methods [36] such as the advanced Kriging method need to be used to obtain higher resolution models of terrain variables as shown in Figure 6-18. Collecting higher resolution data (e.g., less than 1 m) using satellite data and/or manual observations is very costly and requires very large datasets to manage. Thus, it is desirable to develop and store surrogate models of terrain variables instead of obtaining and storing higher resolution data for each region of interest. That is, the surrogate models can be used to compute higher resolution data whenever needed. It is important that the surrogate modeling method should be able to handle non-stationary and non-Gaussian geostatistical data.

6.5.3 Variability Models of Terrain Variables

In addition to the high resolution of terrain variables (e.g., elevation, slope, soil composition, soil cohesive strength, soil friction coefficient, bulk density, temperature, moisture content, etc.), their variabilities need to be modeled for the development of a reliability-based stochastic mobility map. Variabilities should be modeled using statistical distribution types and parameters such as mean and standard deviation. Typical statistical

distribution types are: Normal, Lognormal, Weibull, Gumbel, Gamma, Extreme and Extreme type-II distributions. If any of those terrain variables are correlated, then copula can be used to model the correlation [37]. Typical copula types are: Independent, Clayton, Frank, FGM, Gaussian, AMH, Gumbel, A12 and A14 copulas [37]. In addition to the physical variability, GIS data may also include other variabilities such as known measurement error, estimated variation based on measurement type, terrain, etc.

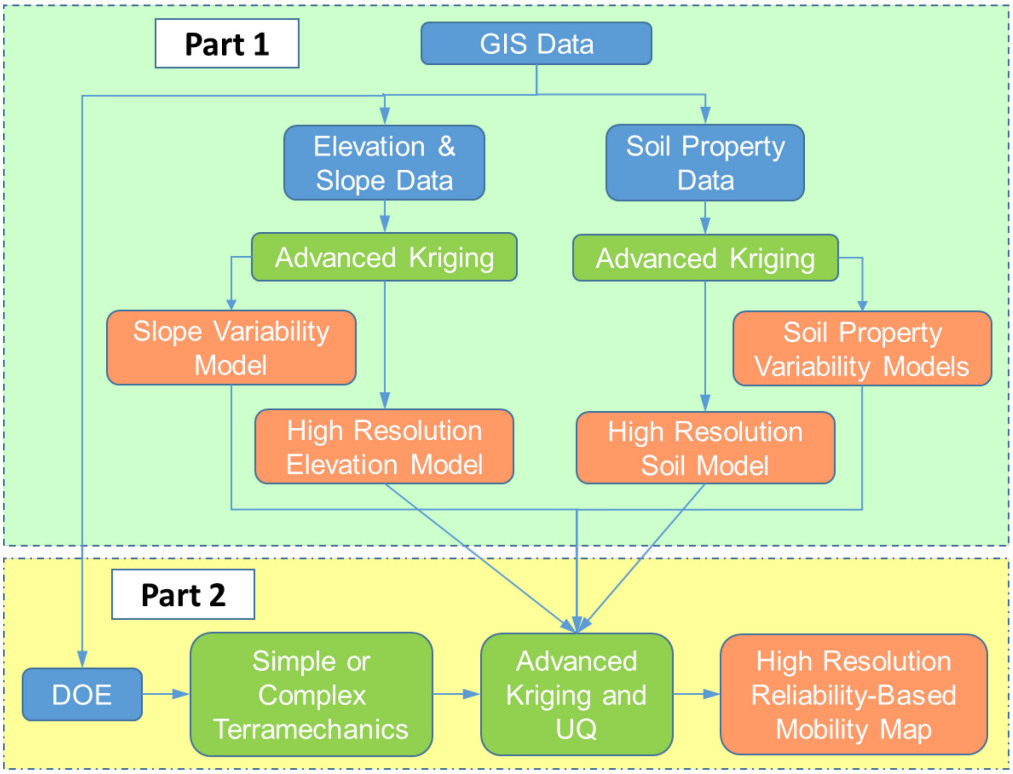


Figure 6-19: Framework for Developing Reliability-Based Stochastic Mobility Map.

6.5.4 Propagation of Uncertainty

For Part 2 of Figure 6-19, it is necessary to estimate propagation of variabilities of terramechanics input parameters to mobility, such as Speed-Made-Good and GO/NOGO, for generation of a reliability-based stochastic mobility map. As a typical reliability analysis requires MCS with a large number of terramechanics analyses, which could take a very long computational time even using an HPC, it is expected to utilize surrogate models. The DOE samples need to be determined for either Simple or Complex Terramechanics analysis results.

Using a surrogate modeling method integrated with the DOE samples, uncertainty quantification and reliability analyses can be carried out for the Speed-Made-Good and GO/NOGO. For uncertainty quantification, no less than 1,000 MCS samples at each pixel location may be required to generate high resolution mobility maps with a high level of reliability (e.g., higher than 90%). For generation of the high resolution reliability-based stochastic mobility map, it is desirable to store the surrogate models of the Speed-Made-Good as a function of terramechanics parameters instead of generating a huge amount of Speed-Made-Good and GO/NOGO data for each region of interest and store them.

6.5.5 Output Mobility Map

There are three key outputs in TA5:

1) High resolution advanced Kriging model of elevation,
2) Advanced Kriging model of vehicle Speed-Made-Good as a function of terramechanics parameters, and
3) High resolution reliability-based stochastic mobility map for three Speed-Made-Good data fields (upslope, downslope, across slope) and GO/NOGO (1 = GO, 0 = NOGO) for each region of interest.

6.6 RESULTS

The propagation of the variability of the terrain and soil properties was successfully demonstrated in creating the reliability-based stochastic mobility maps shown in Figure 6-9, Figure 6-10, Figure 6-16, Figure 6-17. It was also shown that for the Monterey, California site used in this study, the deterministic Speed-Made-Good map for the Complex Terramechanics provided a reliability of only 25%, i.e., there is only a 25% probability of the maximum obtainable speed being greater than or equal to that shown in the deterministic map. On the other hand, for Simple Terramechanics, the deterministic Speed-Made-Good map provided reliability in the 20~50% range. It was also noted that there is very little variability information available for the soil properties and that more information is required in order to generate accurate reliability-based stochastic mobility maps.

6.7 GAPS AND PATH FORWARD

This section breaks down the gaps that need to be filled for continuous future improvement of the framework for a stochastic approach for vehicle mobility prediction over large regions and generation of accurate reliability-based stochastic mobility maps for Speed-Made-Good and GO/NOGO decisions.

6.7.1 Raster Data

For the area of interest all the raster data should be the same size. This is because the uncertainty propagation is done cell-by-cell in the raster. Converting the data to the same raster size may introduce additional approximations or errors. A standard method for how to handle this should be developed in the future.

6.7.2 Terramechanics Simulation Model

There are several features needed for the terramechanics simulation model to be robust and fully automated for effective and seamless development of DKG surrogate models and integration with UQ Tools for a non-terramechanics expert to be able to use it. First, the model should have an auto-steering capability to keep the vehicle on the track during the simulation. It is very desirable that the model input be the raw soil parameter data as variabilities of these raw soil parameter data will be used for input distributions for the reliability-based stochastic mobility map. The terramechanics simulation model should take these raw soil parameter data values and convert them to the input values needed/used in the terramechanics simulation. A time step determination and adjustment capability should be available so that models will run successfully or will need to be rerun with a different time step if they fail due to an incorrect time step. An automatic result extraction capability is needed so that the responses can be easily extracted. Currently it is carried out by a manual process of looking at the history file and averaging the time-history results. A method to automatically determine if steady-state speed has been reached is needed. This is so that terramechanics simulations do not continue to run if steady-state is reached.

6.7.3 Soil Parameter Data

As mentioned throughout the report there is little to no soil parameter data available and little to no variability information on the soil parameters. This data is required for each soil type in order to generate accurate reliability-based stochastic mobility maps. The ideal data would be data on the soil parameters for the area of interest. However, this may not be possible, thus, a general database for different soil types should be put together so that it can be used for a given area of interest. This may result in some inaccuracies as the variability and parameter values for a given soil type might be different from the actual properties in the area of interest; however, it is probably the best obtainable result.

6.8 SUMMARY

A framework for propagation of the variability of the terrain and soil properties was successfully demonstrated in creating the reliability-based stochastic off-road mobility maps for Speed-Made-Good and GO/NOGO decisions to support the NG-NRMM using full stochastic knowledge of terrain properties and modern terramechanics modeling and simulation capabilities. To generate the distribution of the slope at a given point, realizations of the elevation raster are generated using the normal distribution.

For the soil property parameters, such as cohesion, friction and bulk density, the min. and max. values obtained from geotechnical databases for each of the soil types are used to generate the normal distribution with a 99% confidence value range. In the framework, the ranges of terramechanics input parameters (i.e., slope, cohesion, friction and bulk density; or Bekker-Wong parameters) that will cover the regions of interest are first identified. Within these ranges of terramechanics input parameters, Dynamic Kriging (DKG) surrogate models of the Speed-Made-Good are generated using Complex or Simple Terramechanics model runs at the design of experiment points. This is the most compute intensive process in the framework that may require an HPC.

Once the DKG surrogate model is generated for the selected ground vehicle, then inverse reliability analyses using Monte Carlo Simulation are carried out to generate the reliability-based stochastic Speed-Made-Good and GO/NOGO maps of the region of interest. Using the generated DKG surrogate of the Speed-Made-Good, this process can be carried out efficiently. This will allow quicker generation of the stochastic mobility map without requiring the use of an HPC. For a prototype demonstration of the developed framework, Monterey, California was selected as the region of interest. For the Complex Terramechanics model, the NATC Wheeled Vehicle Platform is used. It is found that the deterministic map appeared to have a probability of approximately only 25% to achieve the indicated speed. For the Simple Terramechanics model, the M113 tracked vehicle is used. It is found that the deterministic map appeared to have a probability of approximately only 20% for some regions, while 50% for other regions, to achieve the indicated speed. This demonstrates the need for taking into account the variability so that accurate Speed-Made-Good maps can be generated and have a given reliability or confidence associated with them, in order to provide reliable information to the decision maker.

The variability information of the terrain and soil parameters was discussed and it was found that currently there is a gap in the available information for the soil parameters. It was also noted how there is little to no variability information available for the soil properties and that more information is required in order to generate accurate reliability-based stochastic mobility maps. This is one of the bigger gaps that needs to be addressed in the near future. There are additional gaps with the raster data and terramechanics simulation models that were discussed as well.

6.9 REFERENCES

[1] McCullough, M., Jayakumar, P., Dasch, J. and Gorsich, D. 2016. Developing the Next-Generation NATO Reference Mobility Model. 2016 Ground Vehicle Systems Engineering and Technology Symposium (GVSETS), Novi, MI.

[2] Rula, A.A. and Nuttall, C.J. 1971. An Analysis of Ground Mobility Models (ANAMOB). Tech. Report M-71-4. US Army WES, Vicksburg, Mississippi.

[3] Haley, P.W., Jurkat, M.P. and Brady, P.M. 1979. NATO Reference Mobility Model, Edition I. Tech. Report 12503. US Army TARDEC, Warren, Michigan.

[4] Lessem, A., Ahlvin, R., Mason, G. and Mlakar, P. 1992. Stochastic Vehicle Mobility Forecasts Using the NATO Reference Mobility Model – Report I: Basic Concepts and Procedures. Technical Report GL-92-11. US Army TARDEC, Warren, Michigan.

[5] Lessem, A., Ahlvin, R., Mlakar, P. and Stough, W. 1993. Stochastic Vehicle Mobility Forecasts Using the NATO Reference Mobility Model – Report II: Extension of Procedures and Application to Historic Studies. Technical Report GL-93-15. US Army TARDEC, Warren, Michigan.

[6] Lessem, A., Mason, G. and Ahlvin, R. 1996. Stochastic Vehicle Mobility Forecasts Using the NRMM. Journal of Terramechanics, 33(6):273-280.

[7] Vong, T., Haas, G. and Henry, C. 1999. NATO Reference Mobility Model (NRMM) Modeling of the DEMO III Experimental Unmanned Ground Vehicle (XUV). ARL-MR-435, Army Research Laboratory, Aberdeen Proving Ground, Maryland.

[8] Iagnemma, K., and Gonzalez, R. 2016. Chapter 9 – Theme 3: Stochastics. In Dasch, J. and Jayakumar, P. (Eds.) Next-Generation NATO Reference Mobility Model (NG-NRMM), ET-148 Final Report.

[9] Bekker, M. 1969. Introduction to Terrain-Vehicle Systems. University of Michigan Press.

[10] Wong, J.Y. 2008. Theory of Ground Vehicles (Fourth Edition). John Wiley & Sons, Inc., USA.

[11] Gonzalez, R., Jayakumar, P. and Iagnemma, K. 2016. An Efficient Method for Increasing the Accuracy of Mobility Maps for Ground Vehicles. Journal of Terramechanics, 68:23-35. Available from: https://doi.org/10.1016/j.jterra.2016.09.002.

[12] ArcGIS 2018. ArcGIS/ENVI. Available from: ARC https://www.arcgis.com/features/index.html.

[13] Jet Propulsion Laboratory 2018. Shuttle Radar Topography Mission (SRTM). Available at: http://www2.jpl.nasa.gov/srtm/statistics.html.

[14] Geotechdata. Geotechnical Parameters 2018. Available from: http://www.geotechdata.info/parameter/parameter.html.

[15] Azhar, A.T.S., Norhaliza, W., Ismail, B., Abdullah, M.E. and Zakaria, M.N. 2016. Comparison of Shear Strength Properties for Undisturbed and Reconstituted Parit Nipah Peat, Johor. IOP Conference Series: Materials Science and Engineering, 160, 12058.

[16] United States Department of Agriculture 2018. USDA SSURGO Web Soil Survey. Available from: https://websoilsurvey.sc.egov.usda.gov/App/HomePage.htm.

[17] Cressie, N. 1986. Kriging Nonstationary Data. Journal of the American Statistical Association, 81(395):625-634.

[18] Zhang, J., Atkinson, P.M. and Goodchild, M.F. 2014. Scale in Spatial Information and Analysis. CRC Press, Inc., USA.

[19] Zhao, L., Choi, K.K. and Lee, I. 2011. Metamodeling Method Using Dynamic Kriging for Design Optimization. AIAA Journal, 49(9):2034-2046.

[20] Atkinson, P.M. and Lloyd, C.D. 2007. Non-stationary Variogram Models for Geostatistical Sampling Optimisation: An Empirical Investigation using Elevation Data. Computers & Geosciences, 33(10):1285-1300.

[21] Chen, C. and Li, Y. 2012. An Adaptive Method of Non-stationary Variogram Modeling for DEM Error Surface Simulation. Transactions in GIS, 16(6):885-899.

[22] Wallin, J. and Bolin, D. 2015. Geostatistical Modeling Using Non-Gaussian Matérn Fields. Scandinavian Journal of Statistics. DOI: 10.1111/sjos.12141.

[23] Lewis, R.M. and Torczon, V. 1999. Pattern Search Algorithms for Bound Constrained Minimization. SIAM Journal on Optimization, 9(4):1082-1099.

[24] Zhao, L., Choi, K.K., Lee, I. and Gorsich, D. 2013. Conservative Surrogate Model using Weighted Kriging Variance for Sampling-based RBDO. Journal of Mechanical Design, 135:1-10.

[25] Song, H., Choi, K.K., and Lamb, D. 2013. A Study on Improving the Accuracy of Kriging Models by Using Correlation model/Mean Structure Selection and Penalized Log-Likelihood Function. 10th World Congress on Structural and Multidisciplinary Optimization, Florida, Orlando.

[26] Sen, O., Davis, S., Jacobs, G. and Udaykumar, H.S. 2015. Evaluation of Convergence Behavior of Metamodeling Techniques for Bridging Scales in Multi-Scale Multimaterial Simulation. Journal of Computational Physics, 294:585-604.

[27] Moon, M., Cho, H., Choi, K.K., Gaul, N., Lamb, D. and Gorsich, D. 2018. Confidence-Based Reliability Assessment with Limited Numbers of Input and Output Test Data. Structural and Multidisciplinary Optimization. DOI: 10.1007/s00158-018-1900-z.

[28] Wasfy, T.M., Jayakumar, P., Mechergui, D. and Sanikommu, S. 2016. Prediction of Vehicle Mobility on Large-Scale Soft-Soil Terrain Maps Using Physics-Based Simulation. 2016 NDIA Ground Vehicle Systems Engineering and Technology Symposium, Modeling and Simulation, Testing and Validation (MSTV) Technical Session, Novi, MI.

[29] Wasfy, T.M., Wasfy, H.M. and Peters, J.M. 2015. High-Fidelity Multibody Dynamics Vehicle Model Coupled with a Cohesive Soil Discrete Element Model for predicting Vehicle Mobility. 11th ASME International Conference on Multibody Systems, Nonlinear Dynamics, and Control (MSNDC), DETC2015-47134, Boston, MA.

[30] RAMDO. 2018. RAMDO Solutions, LLC, Iowa City, IA, https://www.ramdosolutions.com.

[31] NAVFAC. 1982. Design Manual 7.02, Foundations and Earth Structures. Naval Facilities Engineering Command.

[32] Tasora, A., Serban, R., Mazhar, H., Pazouki, A., Melanz, D., J. Fleischmann, J., Taylor, M., Sugiyama, H. and Negrut. D. 2016. Chrono: An Open Source Multi-Physics Dynamics Engine. T. Kozubek (Ed.), High Performance Computing in Science and Engineering – Lecture Notes. Springer, Computer Science, pp. 19-49.

[33] Serban, R., Taylor, M., Negrut, D. and Tasora, A. 2018. Chrono: Vehicle – Template-Based Ground Vehicle Modeling and Simulation. Intl. J. of Vehicle Performance.

[34] Janosi, Z. and Hanamoto, B. 1961. The Analytical Determination Of Drawbar Pull as a Function of Slip for Tracked Vehicles in Deformable Soils. Proceedings of the 1st Intl Conf Mech Soil-Vehicle Systems, Turin, Italy.

[35] US EPA 2011. Exposure Factors Handbook, 2011 Edition. Chapter 2. Variability and Uncertainty. US Environmental Protection Agency: EPA/600/R-090/052F, Washington DC.

[36] Detweiler, Z.R. and Ferris, J.B. 2010. Interpolation Methods for High-Fidelity Three-dimensional Terrain Surfaces. Journal of Terramechanics, 47(4):209-217.

[37] Nelsen R.B. 1999. An Introduction to Copulas. Springer, New York.



Chapter 7 – TA4: INTELLIGENT VEHICLES

Abhinandan Jain
Jet Propulsion Laboratory
UNITED STATES

Paramsothy Jayakumar
US Army CCDC Ground Vehicle Systems Center
UNITED STATES

7.1 INTRODUCTION

The NG-NRMM effort for performance modeling of manned vehicles involves several areas of effort: integration of GIS-based terrain data into simulation software; development of vehicle-terrain interaction models; measurement tools for identifying terrain parameters; integration of terramechanics models into simulation software; tailoring of outputs of the simulation to yield useful mobility predictions; and the development of more efficient algorithms in order to maximize the effect of onboard computation. Developing a similar performance modeling capability for Intelligent Vehicles, where human interaction may be remote and limited, involves a number of additional development strategies and is the focus of a NG-NRMM for Intelligent Vehicles, or an NG-NRMM(I).

7.1.1 Intelligent Vehicles

Intelligent mobility is made up of components such as shown in Figure 7-1. A key characteristic of intelligent vehicles is the presence of an onboard sensor suite and use of onboard software and algorithms for:

- Sensor fusion, localization, state estimation, handling of noise and signal dropouts, obstacle detection, situational awareness, map building;
- Locomotion, obstacle avoidance, slippage detection, model predictive motion-control algorithms;
- Balance control, foot placement, gaits, manipulation, etc. for legged vehicles;
- Executive for real-time coordination and control, shared control; and
- Planning and executive layer for deliberative long-term motion and path/trajectory planning, vehicle fault diagnosis and recovery.

Operation of an intelligent vehicle typically involves a combination of offline planning and online execution. Off-line planning may be used to plan high level routes for the vehicle based on the mission scenario, available maps of the region and performance models of the vehicle. The role of the onboard autonomy is to execute the mobility plan in real-time, while negotiating obstacles and maintaining situational awareness during the traverse. The performance of an intelligent vehicle can be inferior (from less sophisticated sensing and control), as well as superior (no fatigue or distractions), when compared with manned vehicle.

7.1.2 Mobility

Intelligent Mobility can involve several different classes and sizes of unmanned vehicles traversing a variety of environments. Being unmanned, intelligent vehicles are not constrained in size, stability, or acceleration to a regime that keeps a human comfortable (or even alive). Without such encumbrances, a vehicle can be small and can handle acceleration and ride roughness that a human could not sustain.

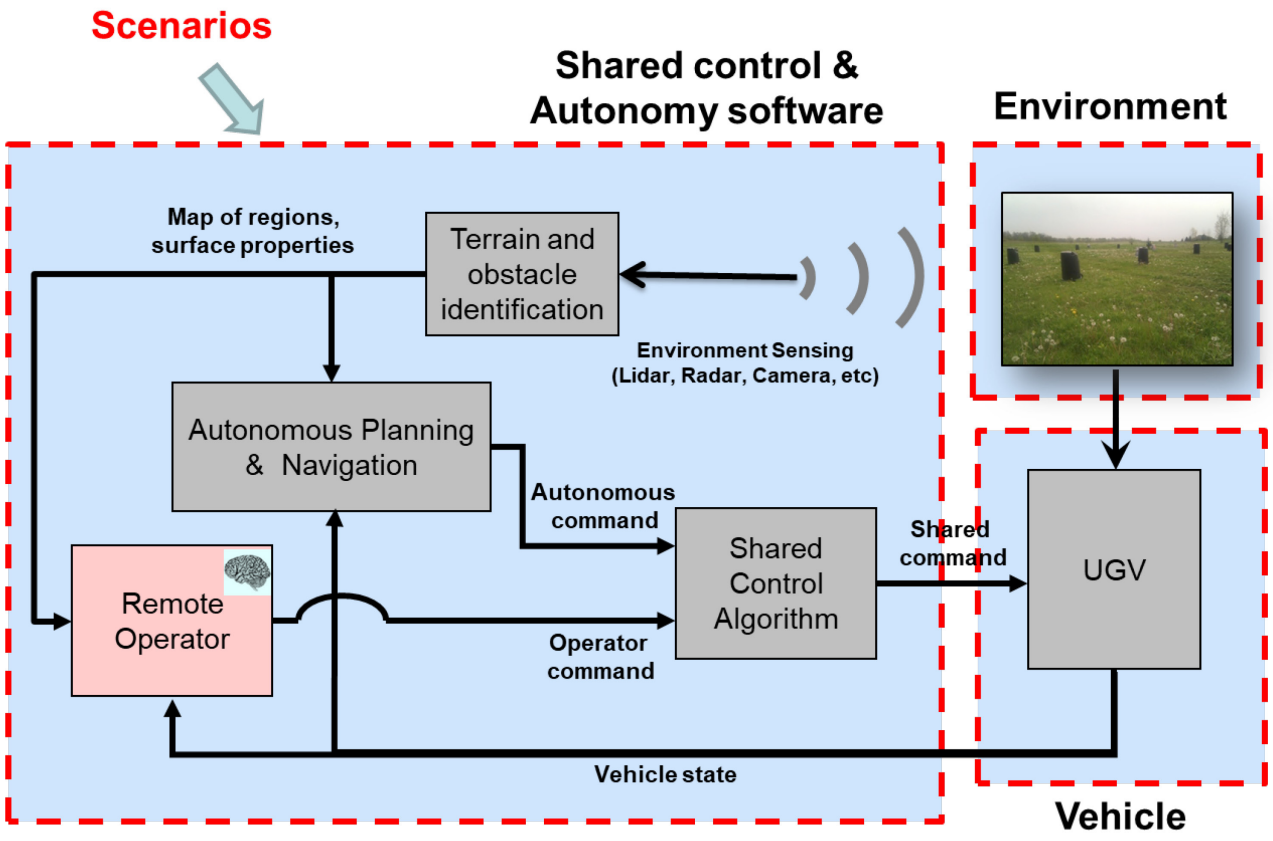


Figure 7-1: Closed-Loop Interaction Between the Onboard Intelligent Control and Autonomy Software, the Environment, and the Vehicle.

Traditional NRMM has focused on large wheeled and tracked vehicles with human drivers. The family of intelligent vehicles is broader and includes:

- Large wheeled/tracked vehicles: These are unmanned versions of the traditional large wheeled/tracked vehicles. These may be operated individually or be part of a convoy of manned and unmanned vehicles.
- Small robots: A number of portable, small wheeled/tracked vehicles, e.g., Talons, Pacbots, are already in active use in operational settings and are emerging as an important new class of vehicles.
- Legged robots: While wheeled and tracked vehicles are the dominant class of mobile vehicles, they can only operate in smooth or moderately rough terrains. Legged vehicles (e.g., Big Dog) are being developed for scenarios involving rough terrains.
- Bipedal Humanoids: Humanoid robots (e.g., Petman, Atlas) are another area of development where limbs can be used as support legs as well as for manipulation tasks.
- Emerging technologies: There are ongoing technological developments involving non-traditional platforms such as climbing/insect robots, as well as ones involving coordinated mobility and manipulation. Moreover, vehicles can be operated as cooperating vehicles and robots, loosely coupled swarms, and more.

7.1.3 Operational Environments

The following are potential environments for intelligent vehicle mobility:

- On-road, urban: Operation on roads, following traffic rules (i.e., lane-following, lane change, traffic signals, speed limits, etc.). Maneuvering in the presence of other traffic as well as pedestrians. Present day automobiles already include autonomy features used on city streets. We expect to see such vehicle autonomy to keep rapidly improving over time. Such autonomy capabilities rely on road markings and well-developed maps and traffic rules to guide both human and autonomous drivers.
- Off-road: Operation in off-road areas over a variety of terrain types and vegetation. Such environments are unstructured with significant uncertainty in terrain properties and conditions. The terrain environment can include hazards and impassable areas for the vehicle. Vehicle autonomy capabilities are relatively immature for off-road operation.
- Building interiors: Operation within building interiors, navigating doors, stairs, hallways, railings, etc.

7.1.4 Intelligent Vehicle Operation

Some key issues important for the operation of intelligent vehicles are discussed here.

Coupling between Dynamics and Vehicle Intelligence: Complex vehicle dynamics present particular challenges to intelligent mobility. While the effect of ride roughness and vibration on drivers does not matter for Unmanned Ground Vehicles (UGVs) (except for durability of vehicle components), it can degrade sensor performance, leading to dropouts and increased error. Degraded sensor performance directly impacts detection of obstacles, as well as of traffic and road cues. Vehicle speed also directly affects the performance and update rates of sensors, as well as time windows available for onboard algorithms. Vehicle slippage degrades accuracy of knowledge of the vehicle's state and controllability. Vehicle stability and rollover limits can affect obstacle avoidance and path planning. And time delays in control action can impact vehicle performance. Thus vehicle dynamics is clearly an important factor in the performance of intelligent vehicles. The introduction of vehicle intelligence requires the expanded characterization and modeling of the vehicle's suite of advanced sensors, simulated environment, and intelligent control software (see Figure 7-1) along with the system level, closed-loop dynamics of the vehicles. An overarching challenge is the limited interaction between the respective communities studying vehicle dynamics and autonomous vehicles.

Autonomy Levels: Vehicle intelligence is not an all or nothing capability. Typical of any complex system, intelligent vehicles are designed with multiple levels and modes of autonomous operation. While more advanced modes may offer superior or more autonomous performance, this may come at the price of additional computational and sensing resources and potentially reduced vehicle speed. Operation of an intelligent vehicle requires the judicious selection and tradeoffs among autonomy modes while accounting for the associated performance/risks and costs. For example, a UGV may have the following intelligent mobility modes (aka autonomy "knobs") in order of increasing level of autonomy:

- Teleoperation: vehicle is directly controlled via teleoperation by a remote operator.
- Blind drive: vehicle runs in open loop, executing operator defined commands that control vehicle speed and direction.
- Reactive control: vehicle uses sensors to detect obstacles and autonomously alters its trajectory to avoid them.

- Simultaneous Localization And Mapping (SLAM): uses sensor-detected features to significantly improve the accuracy of the vehicle's onboard state and situational awareness.

The blind drive option maximizes speed, but can only be used when the terrain is benign and the mobility risks are low. While computationally expensive, SLAM is essential in regions of high slippage, where one must trade speed for safety. Reactive control is an intermediate option that is suitable for moderate terrains. Vehicles may even support and resort to teleoperation mode for difficult or anomalous situations where the remote operator takes full control of the vehicle.

Supervised Autonomy: Even as full autonomy remains the eventual goal, the high cost and mission criticality of military vehicle assets implies that the operation of UGVs for some time to come will involve some level of supervised autonomy with remote operators in the loop. Essential to the reliable operation of a UGV in the field to successfully carry out a mission is the ability to predict its mobility performance and risk over the specified region. Such predictive capability is needed to effectively monitor and guide the UGV to keep the vehicle safe while meeting mission constraints (e.g., no-go areas, communication limitations, lighting) and maximizing performance metrics (e.g., time, speed, fuel consumption). The quantum jump in complexity arising from the onboard intelligence makes performance prediction daunting even for the UGV developers intimately familiar with the vehicle, let alone for operators in the field. The viable use of UGVs depends on the development of predictive models and data products that can guide the operator on safe and effective operation in the field.

Manned and Intelligent NG-NRMM: While it may be tempting to assume that manned vehicles will perform better than autonomy software, it is easy to identify situations (e.g., no fatigue, large sensor coverage, low-light conditions) where intelligent vehicles have advantages. Thus NG-NRMM data products for manned vehicles may not be directly usable for intelligent vehicles and we may need to pursue an independent path for intelligent vehicles as illustrated on the right of Figure 7-2. However, it would be desirable to leverage the large body of work done on NG-NRMM for manned vehicles, and even more so given the large analysis effort in generating these data products. So a question to be addressed as to how can NG-NRMM(I) benefit from the manned NG-NRMM performance prediction and analysis capabilities.

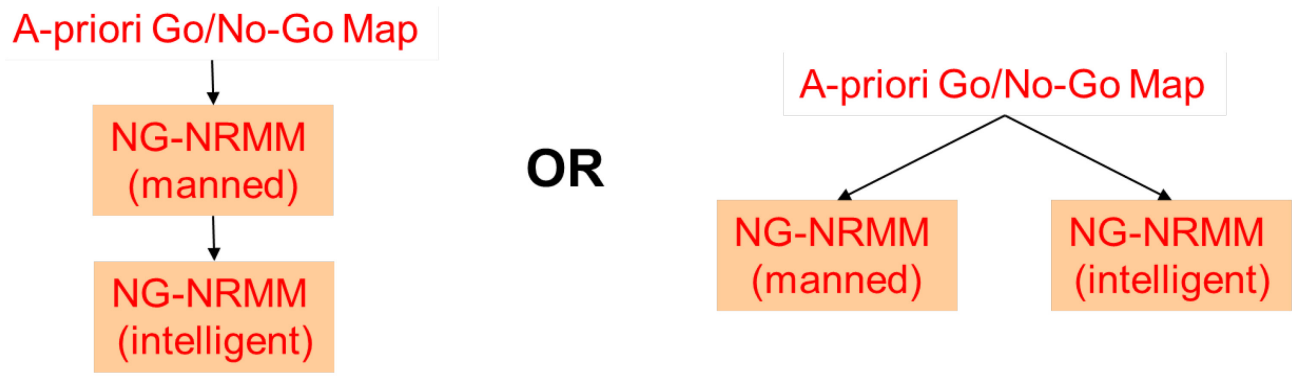


Figure 7-2: Building NG-NRMM(I) Off Of, or In Parallel with, NG-NRMM.

Challenges: Vehicle intelligence remains an amorphous concept spanning multiple intelligence architectures and capabilities. At this point there are few quantitative performance metrics for autonomous systems, especially so from the high-dimensional state space and unstructured/uncertain nature of operational environments. Moreover vehicle intelligence is a rapidly evolving area and any

NG-NRMM(I) framework needs to be able to evolve to meet emerging intelligent vehicle capabilities. The challenge of NG-NRMM(I) is to characterize the performance of the provided intelligent vehicle as is – rather than to improve the vehicle's intelligence or mobility.

7.2 PROCESS AND METHODOLOGY

The objective of NG-NRMM(I) is to generate models and data products for predicting vehicle performance that can be used to execute desired mission scenarios over specified regions. Beyond operational use, these capabilities can guide UGV development, as well as the UGV acquisition process. NG-NRMM(I) is a new capability. It lacks the extensive experience, maturity and community base existing for manned NRMM, its development involves rapidly evolving technologies, and the approaches, challenges, and scope for NG-NRMM(I) is also continuing to evolve.

Broadly speaking, an intelligent system consists of a collection of behaviors that can be called upon individually and in combination to meet goals and handle contingencies for a range of scenarios. Thus intelligence is like a toolbox with a set of tools used in combination and sequentially to execute desired scenarios. The degree of intelligence is defined by the breadth and depth of the toolbox, and the degree to which the behaviors are chosen autonomously.

7.2.1 Autonomy Levels

Methods of control of autonomous vehicles range from being partially controlled by a remote human operator, to shared control, to full autonomy. Closed-loop control can be impacted by bandwidth and latency limitations over the communication link.

Running with full autonomy 'on' all the time is not a practical option. Each autonomy level places demands on available resources which can include computational power, memory, communication bandwidth and latency, sensor availability, visibility, etc. Moreover, some autonomy levels may impose constraints on the vehicle mobility, such as the maximum speed possible for reliable sensor performance or computational time required for the execution of the associated autonomy algorithms. Thus turning on all autonomy levels may not be practical or might even degrade mobility performance. Teleoperation level, where the remote human operator takes command, may be an available option, though it may place large demands on communication with the remote supervisor. Figure 7-3 shows an example of a region with varying terrain characteristics and obstacles that require different autonomous mobility levels across the region during a traverse. Operation of intelligent vehicles requires the management of the available autonomy levels in order to meet multiple conflicting objectives, such as speed vs. safety. Architecturally, each **autonomy level** represents a unique combination of **autonomy mode** settings where an autonomy mode denotes autonomy component level choices (e.g., onboard or off-board obstacle detection, onboard obstacle avoidance vs operator assisted, low/medium/high vehicle speed, enabling/disabling onboard map building). It is important to keep in mind that while autonomy modes often represent distinct methods, some of these modes can belong to a continuum such as maximum speed, or obstacle detection threshold, etc. Such continuous modes can also be binned to convert them into discrete mode options.

7.2.2 Autonomy Map

Mission execution requires meeting multiple objectives, some of which conflict with one another, such as average speed, rollover stability, or fuel efficiency. To be deemed a success, the vehicle must exceed a minimum threshold

for each performance metric across the traverse. An area is considered a no-go area when the vehicle is unable to meet the minimum level for the specified performance thresholds. While avoiding no-go areas, a mobility plan that maximizes performance is desired for intelligent vehicles. A combined metric, such as derived using weights, is needed to compare performance. Path planning techniques for designing vehicle paths that simply avoid no-go areas by themselves are not adequate. Even for manned vehicles, additional Speed-Made-Good maps that specify the maximum speed that the driver is permitted to use are needed to guide vehicle operation. For intelligent vehicles, in addition to a path a specification, a plan that specifies the best autonomy level to utilize along the path is needed for operating the vehicle. Accompanying such a plan, should be predictions on the expected vehicle performance for each of the specified metrics.

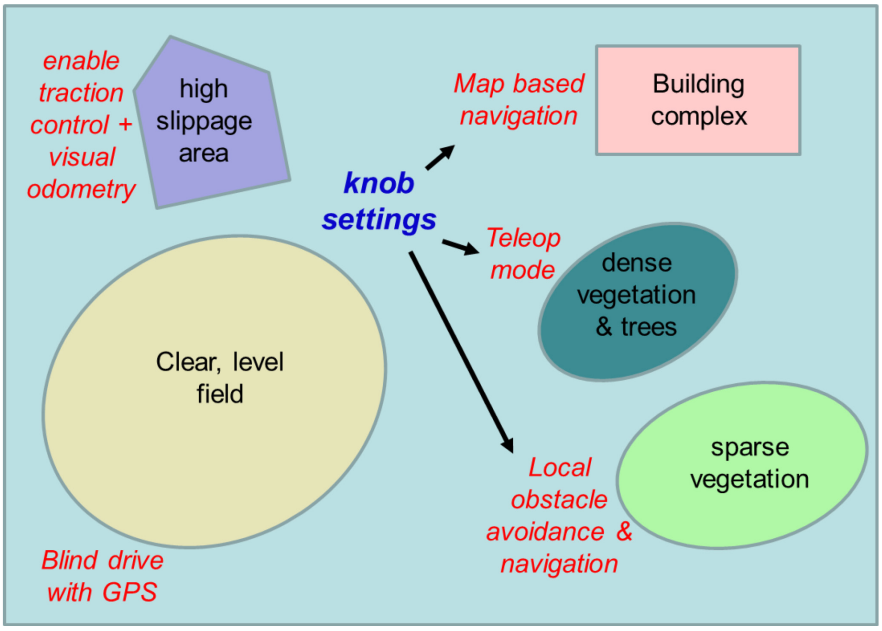


Figure 7-3: Different Autonomous Mobility Level Knob Settings are Required for Different Terrains and Scenarios.

Designing such a mobility plan for an intelligent vehicle is the responsibility of the remote supervisor. Since this is a challenging task for an operator in the field, we propose the development of an **autonomy map** data product to assist the operator in developing a mobility plan for an intelligent vehicle. An autonomy map may be viewed as a generalization of Speed-Made-Good maps for manned vehicles. Instead of simply specifying the maximum speed across a region, an autonomy map will also specify the recommended autonomy mode (or combinations thereof) across the region. Indeed, development of a process and approach for generating such autonomy maps is the current focus of NG-NRMM(I). As illustrated in Figure 7-4, NG-NRMM(I) will take as inputs the vehicle, the environment region for a traverse, and the desired scenario and metrics and generate an autonomy map that identifies the best autonomy modes to use across the region. Changing any of the inputs, e.g., the vehicle, the terrain environment or the metrics, may require the regeneration of the autonomy map and a new plan.

The knob settings recommendations from the autonomy map provide guidance for the proper operation of an intelligent vehicle across a region; the generation of this map is the primary responsibility of NG-NRMM(I) across different cells and autonomy levels. A successful autonomy map would provide guidance of the optimal autonomy level across the region.

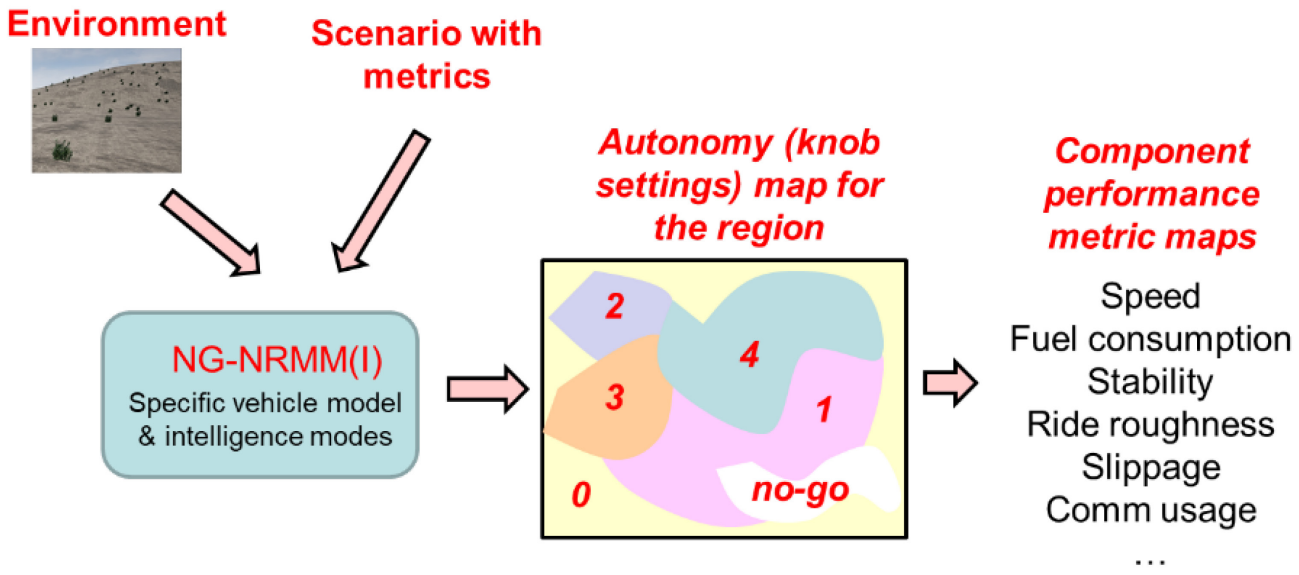


Figure 7-4: Inputs to and Outputs from a Sample Autonomy Map.

Note: To summarize, operationally the **autonomy map** is a data product for designing best tactical plans for executing the scenario at hand. Given a tactical plan, simulations can be used to predict performance.

7.2.3 Intelligent Vehicle Performance Modeling

Performance of autonomous vehicles can be predicted using simulation models. For intelligent vehicles, such simulations close the loop with autonomy control software and models of autonomy sensors such as cameras, LIDARs, etc. However, such simulations can be complex and computationally demanding. Furthermore, determining vehicle performance can be even more expensive because of the high-dimensional state space of intelligence software and unstructured/uncertain environments. A range of reduced order models that are computationally less expensive are needed to make performance modeling computationally tractable. Figure 7-5 shows a process for generating such reduced order models by using a combination of high-fidelity models and experimental data.

7.3 PROTOTYPE DEMONSTRATION

A pilot project has been carried out to flesh out the process for generating NG-NRMM(I) autonomy and performance maps. It explores techniques that can be used for intelligent mobility and output products needed for NG-NRMM(I). The pilot project provided an avenue for testing out intelligent vehicle scenarios and approaches. Its purpose is to stimulate discussion on the feasibility of approaches, identify challenges, gaps and opportunities and provide a testbed to evaluate new methods.

A pilot project was necessary because NG-NRMM(I) is a new capability, and practical evaluation of the ideas is needed. NG-NRMM(I) lacks manned NRMM's extensive experience, maturity, and community base, and involves rapidly evolving technologies. In addition, the approaches, challenges and scope and process for NG-NRMM(I) are not yet well defined or understood.

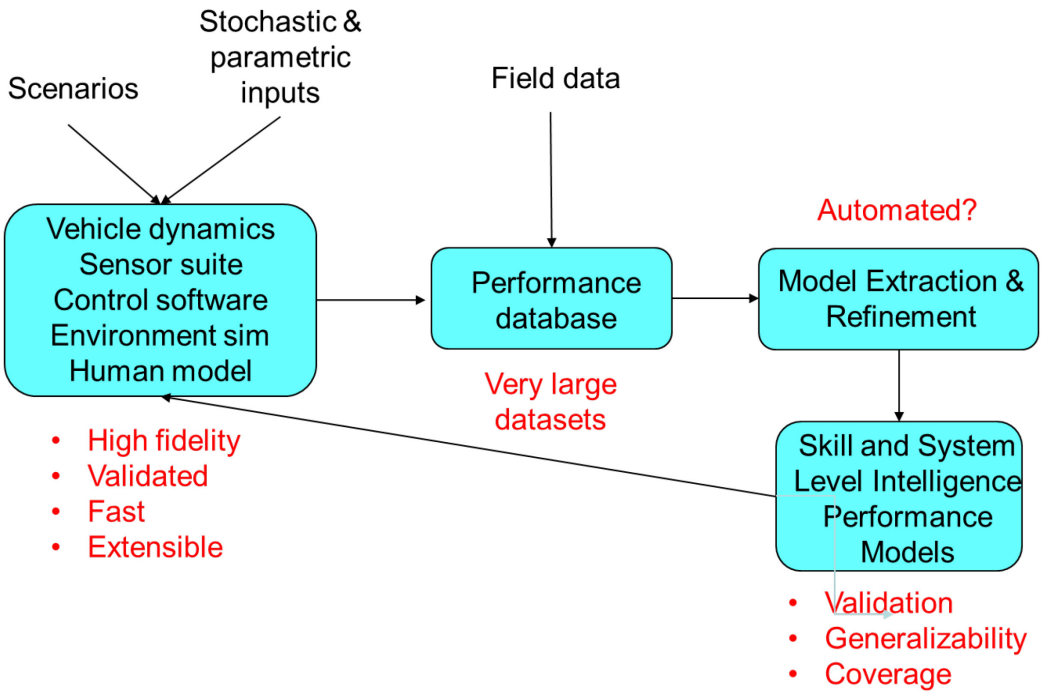


Figure 7-5: Model for Developing Performance Metrics and Autonomy Levels from Available Data; Currently Lacks Established Capability Across All of the Pipeline Elements.

7.3.1 Pilot Project

The pilot project helped to flesh out a process for generating NG-NRMM(I) autonomy and performance maps. It investigated the question of how to adapt the techniques for manned NG-NRMM to intelligent mobility. Furthermore, it clarified what output products are needed for NG-NRMM(I).

7.3.2 Pilot Project Approach

The emphasis of this pilot project was on breadth to explore end-to-end issues, with increase in depth to come in follow-up stages. The pilot project selected a reference problem to evaluate the NG-NRMM(I) process. It built upon methods used for manned NG-NRMM and used a representative intelligent vehicle, environment, and scenarios, to explore methods to generate NG-NRMM(I) GO/NOGO and other output products. The pilot project explored multiple autonomy levels and generated autonomy map and performance map outputs. The results guided the evolution of the pilot project.

7.3.2.1 NG-NRMM via M&S

Modeling and Simulation (M&S) tools were used to evaluate vehicle performance for the pilot project. While the project focused on a reference wheeled UGV, the approach can be applied to wide variety of platforms (wheels, tracks, legs) and multi-vehicle simulations. Simulations permit the use of various autonomy sensors including cameras. Simulations also allow the exploration of scenarios over a wide variety of terrains and soil types. The major advantage of using M&S is that it is much less expensive than carrying out experimental performance evaluation in the field.

7.3.2.2 Sampling Approach

Legacy NRMM uses an empirical data-based procedure that is applied to cells in a grid over the region to generate performance predicts. This makes it fast and relatively simple, and provides complete coverage over the grid. NG-NRMM proposes converting from empirical to physics-based M&S methods to generate performance predictions that are more accurate and easier to adapt to new problems. These M&S based studies are typically carried out off-line since they can be computationally expensive and complex with adequate coverage over the grid requiring sampling via a sufficiently large number of traverse simulations.

The goal of the sampling approach is to assess mobility performance over the whole region. In the pilot project, the approach used Monte Carlo Simulation consisting of multiple traverses with randomized initial and goal positions for evaluating mobility performance.

7.3.2.3 ROAMS UGV Mobility Simulator

The Rover Analysis, Modeling and Simulator (ROAMS) simulation engine developed at the Jet Propulsion Laboratory (JPL) was used for the pilot project [1]. The ROAMS physics-based simulator was originally developed to support the design, development and test of planetary surface rovers such as the Mars Exploration Rovers (MER), aka Spirit and Opportunity, and the Mars Science Lab (MSL), aka Curiosity. ROAMS has evolved to support the modeling of terrestrial UGVs. ROAMS uses a range of inputs:

- **Vehicle Platforms**: Single and multi-vehicle simulations; parameterized model classes; Dynamics Algorithms for Real-Time Simulation (DARTS) recursive dynamics.
- **Motion**: Vehicle mobility, arm models, wheel/soil dynamics, Bekker/Wong soft soil terramechanics, and Fiala/Pacejka 2002 tire models.
- **Hardware Models**: Kinematics, dynamics, motors, encoders, Inertial Measurement Unit (IMU), inertial sensors, LIDAR, GPS.
- **Mobility Algorithms**: Representative path planning, waypoint following, drive to goal, obstacle detection and avoidance, and locomotion autonomous mobility algorithms.
- **Camera Sensors**: Image synthesis for cameras with non-idealities, rover and terrain shadows.
- **Environment**: SimScape synthetic, empirical and analytic terrains, ephemerides interface for sun position.

ROAMS provides closed-loop visualization, such as dSPACE 3D graphics (CAD / auto-generated vehicle models), and data logging. It can be installed on a workstation or in an embedded system, with a C++ and Python interface for configuring and closing the loop with mobility software. It also includes Monte Carlo Simulation capability.

7.3.3 Pilot Project Reference Problem

The pilot project included representative implementations of each of the key components for intelligent mobility to exercise intelligent mobility scenarios end-to-end:

- Intelligent Mobility Scenario, featuring a vehicle platform, onboard intelligence, terrain environment, and various scenarios.
- Methodology and process included intelligent mobility testbed capabilities, M&S based sampling, and Monte Carlo capability.
- Preliminary outputs included GO/NOGO maps, autonomy maps, and performance maps.

Though available, some of the simulation features were deliberately not exercised (e.g., variable soil types) in this initial effort.

7.3.3.1 Prototype Intelligent Vehicle

The High Mobility Multipurpose Wheeled Vehicle (HMMWV) vehicle model available within the ROAMS simulator was used as the reference vehicle for the pilot project [2]. The vehicle model included component models for Vehicle-Terrain Interaction (VTI), autonomy sensors, cameras, LIDAR, GPS, IMU, etc. In addition, representative autonomous mobility algorithms available within ROAMS were used to create an intelligent HMMWV vehicle.

For the pilot project, vehicle intelligence was established by adapting existing autonomous drive to goal with obstacle avoidance algorithms available within ROAMS. In the future, we can close the loop with externally developed autonomy and shared control software for the HMMWV as well as for other vehicles.

7.3.3.2 Autonomy Modes

The pilot project included obstacle avoidance and motion planning algorithms as illustrated in Figure 7-6.

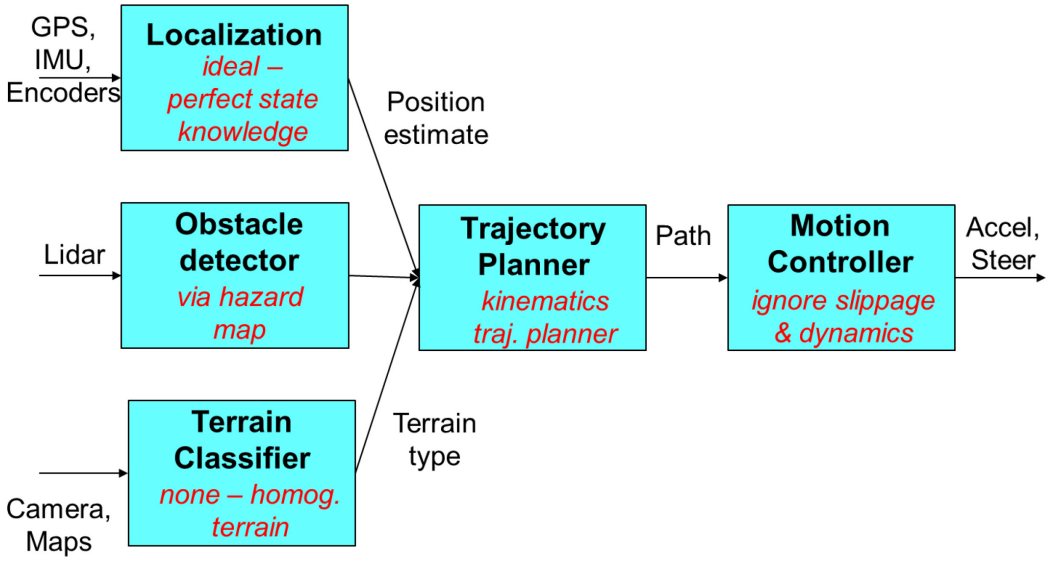


Figure 7-6: Simplified Approach to Obstacle Avoidance and Motion Planning.

Figure 7-7 shows the simplest situation, zero obstacles, where the vehicle simply goes from point A to point B.

The obstacle avoidance approach is driven by obstacle sensors on the front of the vehicle, with set parameters for sensing depth and field of view. The obstacle detector looks in left, right, and center bins, and uses turn-to-avoid logic for obstacle avoidance, restricted to local and current sensed obstacle data, as illustrated in Figure 7-8.

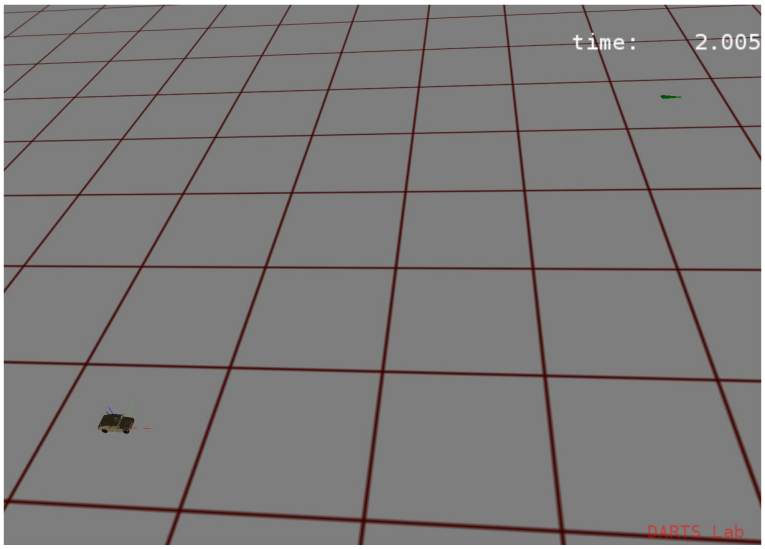


Figure 7-7: HMMWV Autonomous Drive to Goal (No Obstacles).

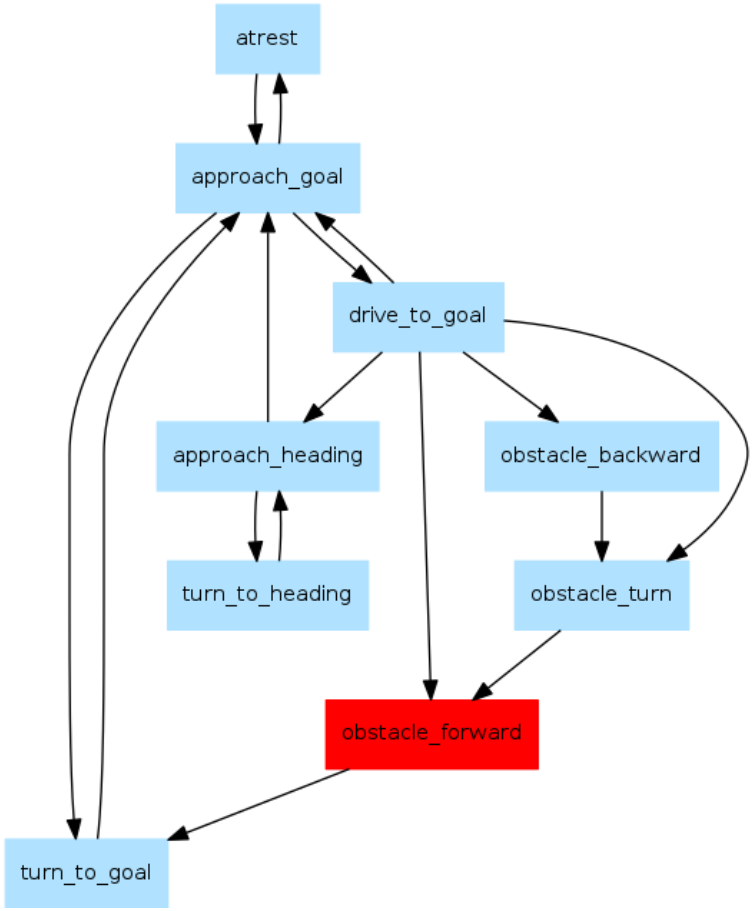


Figure 7-8: Autonomous Obstacle Avoidance Algorithm in ROAMS.

A waypoint mode is available in ROAMS for getting around extended obstacles (Figure 7-9).



Figure 7-9: Autonomous Waypoint Following in ROAMS.

Autonomy modes selected for the pilot project HMMWV vehicle included autonomousr obstacle avoidance, and autonomy mode knobs for maximum speed, sensor depth and Field Of View (FOV), and reactivity:

- Max. speed: 5 m/s, 10 m/s, or 15 m/s;
- Obstacle detection modes;
- Depth of view: 10 m vs. 30 m;
- Field of view: $\pi/4$ vs. $\pi/2$; and
- Drive blind: disable obstacle detection and avoidance.

The various combination of mode settings represent 13 available autonomy levels. The slope threshold, i.e., the maximum slope that is safe for the vehicle to handle, was set at 22° for the first set of experiments.

7.3.3.3 Prototype Terrain Environment

The terrain region in the initial pilot was 1 km flat square with hazards. Later versions used GIS terrain topography over a two square kilometer region. The grid cells for map generation are 20 square meters, with each traverse distance at least 400 m.

The topography data was generated with the open source qgis tool to import California Geographic Information Systems (GIS) data. The data set contains multiple tiles of topography data, with each tile being about 11 km square at 3 m resolution for a region in California (Figure 7-10). It also has several associated dataset layers (such as imagery, land cover, etc.). The GeoTiff topography was imported into the SimScape terrain toolkit for use with ROAMS simulation of HMMWV mobility dynamics (Figure 7-11). Other GIS layers, such as landcover, were not used.



Figure 7-10: (Left) California GIS Data Imported into Simscape; (Right) Topography Tiles in Simscape.



Figure 7-11: ROAMS HMMWV on the GIS Terrain.

Using the embedded projections and georeferencing information, importing the topography data into the SimScape terrain module was mostly straightforward, but there were certain issues [3]. Among them, the resolution and number of samples varied from tile to tile, and the tiles did not align at the edges. A 2 km square region within one tile that was the least mountainous was chosen (Figure 7-12) for the prototype mobility simulation experiments.

7.3.4 Obstacles and Hazards

Once the terrain topography was available, additional hazard features were overlaid on the terrain to serve as obstacles for the vehicle to negotiate and avoid during its traverses. Such hazards included extended ones (representing buildings and lakes) that spanned tens of meters, to sparse and dense clusters of trees. The varied

set of obstacles allowed evaluation of the performance of the different autonomy modes under different difficult terrain conditions. Figure 7-13 shows typical traverse paths requiring obstacle avoidance maneuvers.

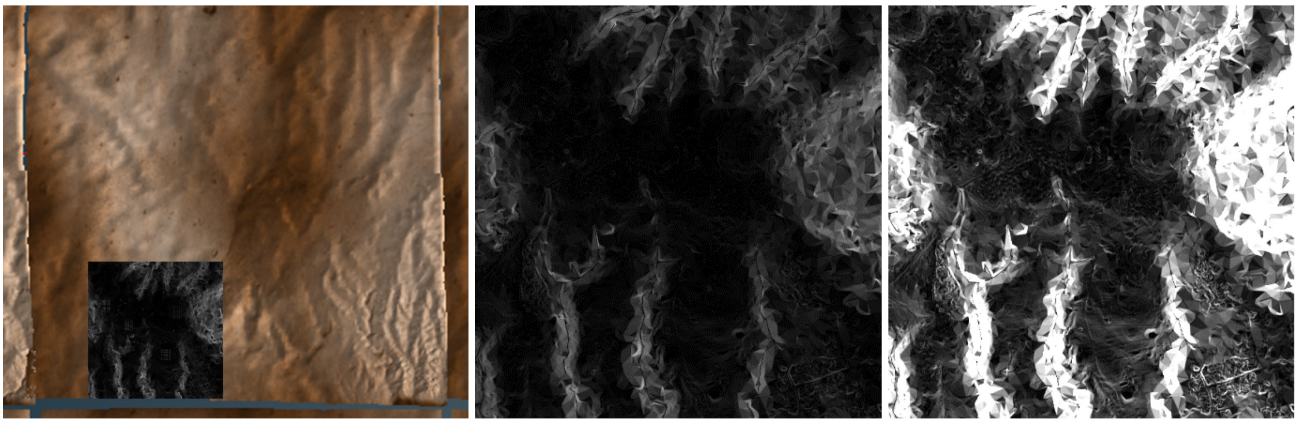


Figure 7-12: (Left) Selected 2 Km Square Region; (Middle) Slope Map for Chosen Region; (Right) Accentuated Slope Map with 22.5° Slope Threshold.

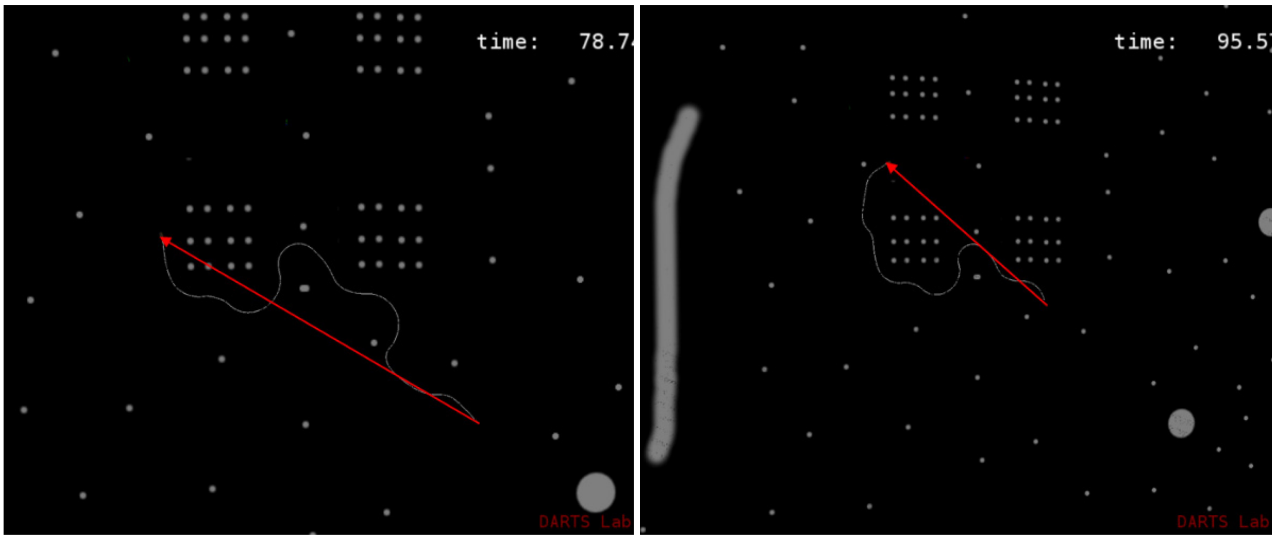


Figure 7-13: Traverse Paths in the Presence of Obstacles.

7.3.5 Simulation Experiments

Several experiments were conducted in the pilot project. The experiments varied scenarios, autonomy level options, performance metrics, sampling, and the environment to generate autonomy maps. Figure 7-14 shows the variants used. Data from traverses that did not complete (e.g., colliding with an obstacle) or timed out were not included in the analysis.

Extended traverses spanning multiple cells were used because intelligent mobility performance is intrinsically coupled across grid cells due to the use of long distance sensors, maps and global path planners.

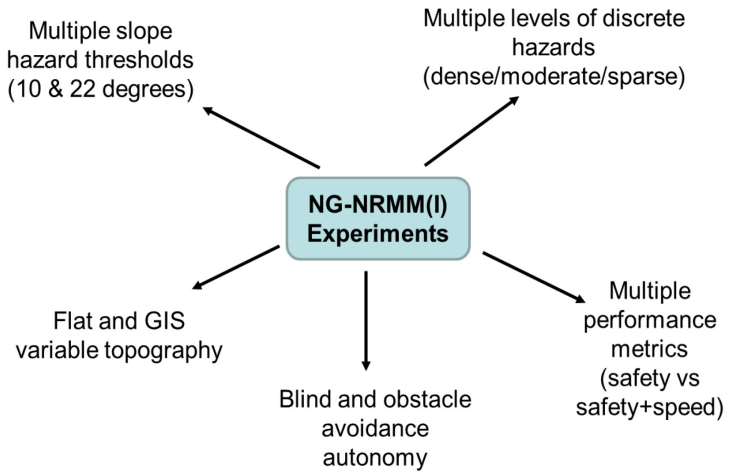


Figure 7-14: Multiple Prototype Experiment.

The simulation setup is diagrammed in Figure 7-15. ROAMS was set up to run individual traverses with different initial vehicle states, different autonomy modes enabled, and a specified destination goal. Detailed trajectory data along each such traverse was logged to an HDF5 data file. An outer Monte Carlo layer on an HPC platform exercised this single traverse module multiple times with randomized initial vehicle state and destination goal values. The selected autonomy level was not changed through the course of each individual traverse. A number of such traverses were carried out for each autonomy level (with each level representing a specific combination of autonomy modes).

As mentioned earlier, the simulation experiments generated traverse data for the 13 selected autonomy levels:

- No obstacle avoidance (blind drive);
- Obstacle detection depth (small/large);
- Obstacle detection Field Of View (FOV) (small/large); and
- Maximum speed (slow/medium/fast).

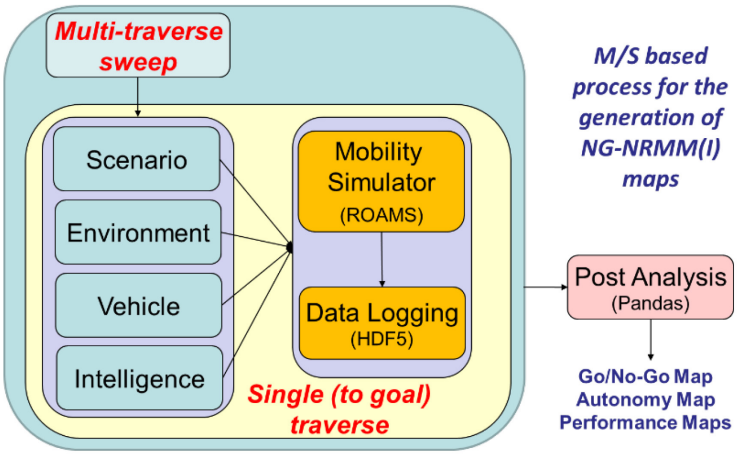


Figure 7-15: Simulation Setup.

Each such simulation study generated large amounts of traverse data spanning the several thousand Monte Carlo runs across the different autonomy levels. This logged data was stored in HDF5 data files for post-analysis. A data analysis pipeline as shown in Figure 7-16 was developed to analyze the data and extract performance results.

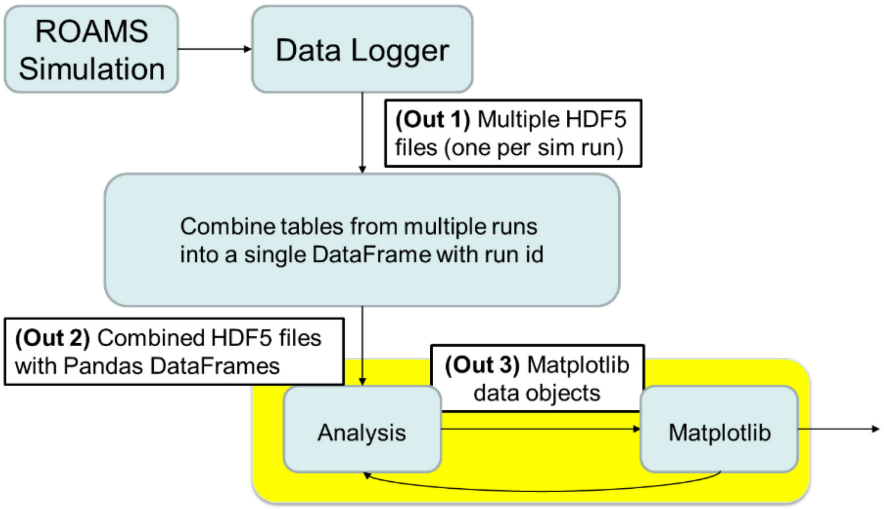


Figure 7-16: Data Analysis Pipeline.

The data analysis used the autonomy level with the best score for each region cell to select the best autonomy level for the cell. A map with the best autonomy level for each cell represents the autonomy map. This process ignored costs and risks associated with the different autonomy levels and the impact on other performance metrics which should be included in future work. This scoring allowed us to designate the best autonomy level for each cell.

7.4 RESULTS

This section discusses the results from the prototyping effort. Runs were deemed failures if they timed out, entered hazard area, or had vehicle rollover. A large number of traverses were simulated to get sufficient coverage (Figure 7-17).

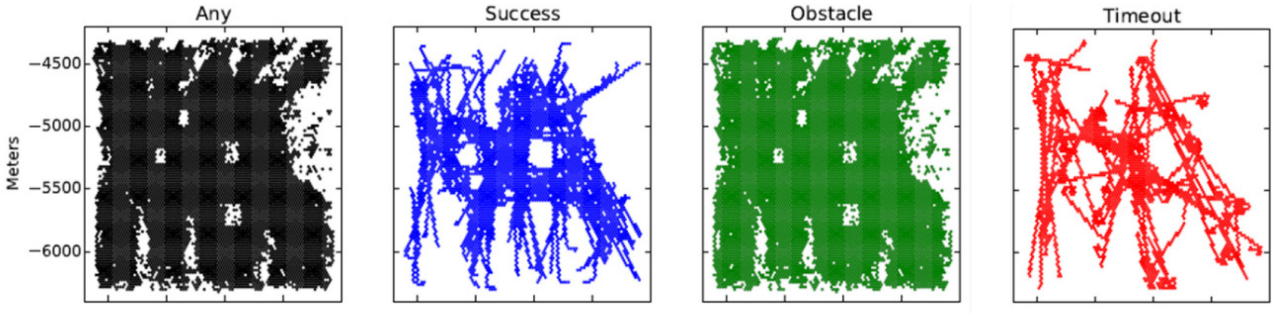


Figure 7-17: Sampling Coverage.

While we observed a 50% success rate for traverses through sparse hazards, the initial experiments yielded successful traverse rates of only 5 to 10 % in the vicinity of extended obstacles (Figure 7-18). Subsequent experiments included a global path planner for generating waypoints to get around extended hazards to significantly improve the number of successful traverses.

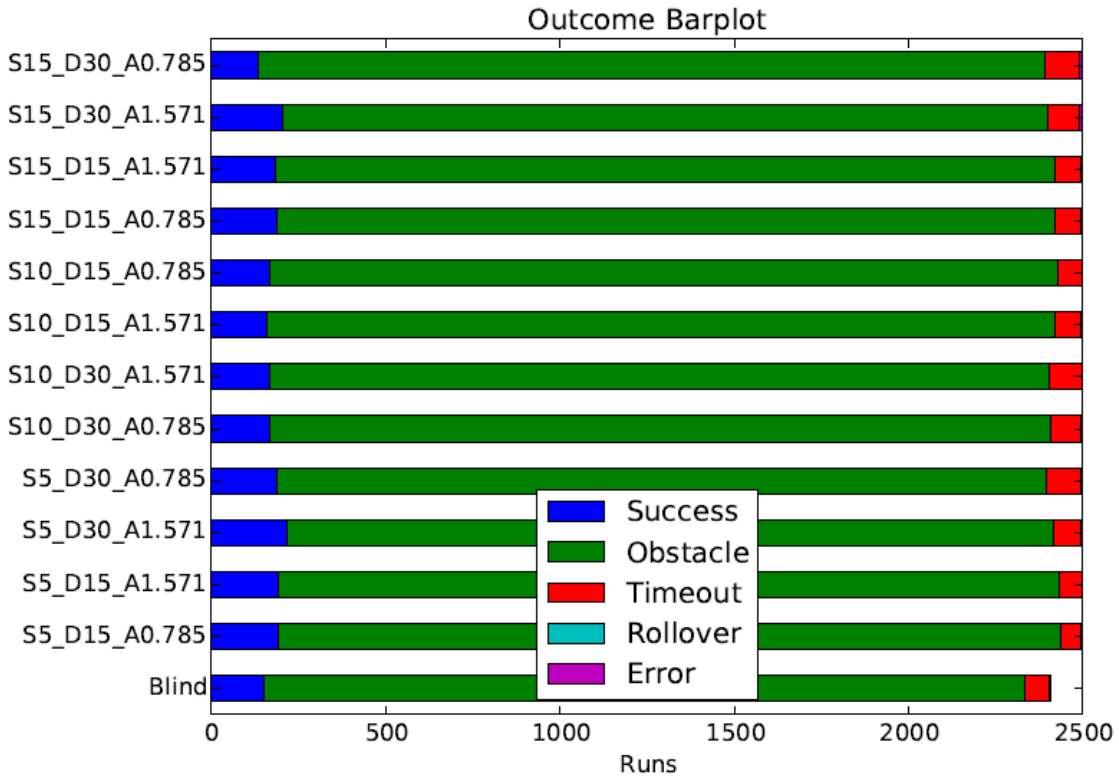


Figure 7-18: Traverse Success and Failure Rates.

7.4.1 Traverse Performance Results

Figure 7-19 contains the color-coded performance maps for traverses for each of 12 autonomy levels defined by the combinations of the following autonomy modes:

- Max. speed: 5, 10, or 15 m/s;
- Cam. depth: 10 or 30 m; and,
- Cam. FOV: 0.78 or 1.57 radians.

We can see the variability of the traverse maps depending on max. speed, cam. depth and cam. FOV. The white areas denote regions with no data points from any of the vehicle traverses. These regions can be interpreted as no-go areas for the specific autonomy level. With obstacle detection and avoidance disabled, the blind drive results are shown in Figure 7-20. Notice that the no-go areas are significantly larger for this “no-autonomy” mode.

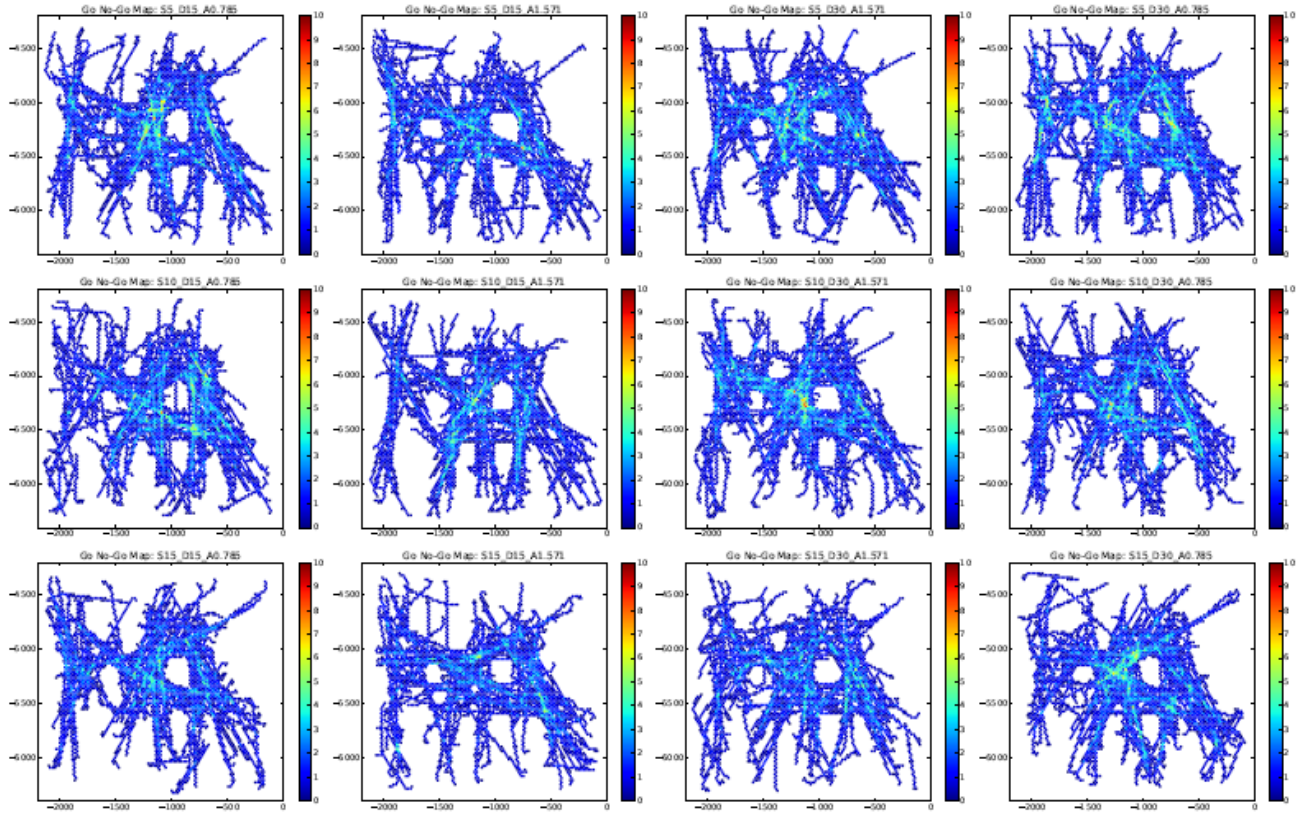


Figure 7-19: Top Row is for Low Maximum Speed; Bottom Row is for High Maximum Speed.

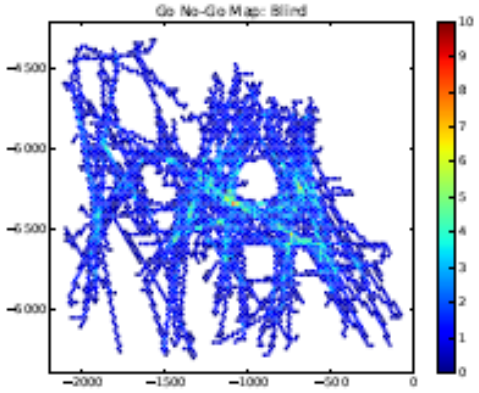


Figure 7-20: Blind Drives with Obstacle Detection and Avoidance Disabled.

7.4.1.1 Performance with Decreased Slope Threshold for Obstacles

With a smaller slope threshold of 10° rather than 22°, the vehicle can drive more aggressively and enter areas of higher slope. The performance maps change to those shown in Figure 7-21.

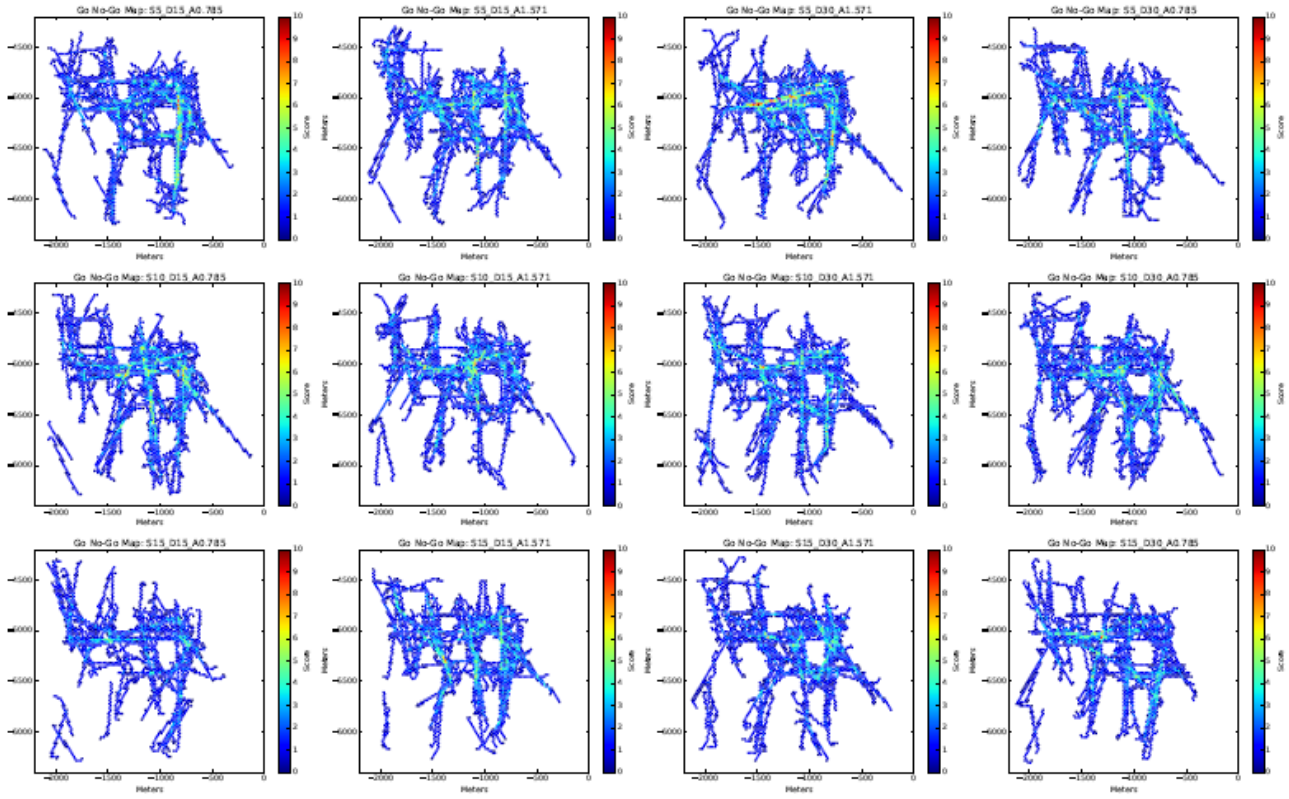


Figure 7-21: Occupancy Maps with a Lower Slope Threshold.

With obstacle detection and avoidance disabled, the blind drives in this situation are shown in Figure 7-22.

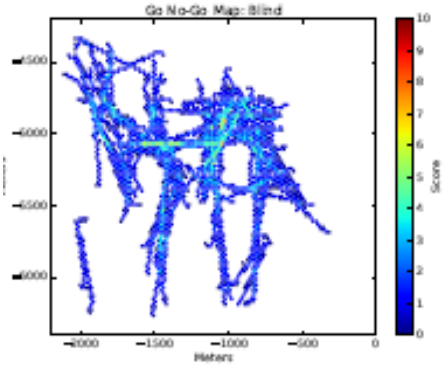


Figure 7-22: Blind Drives with Obstacle Detection and Avoidance Disabled.

7.4.2 Qualitative Validation

One of the initial analysis goals was to qualitatively validate that the simulation results reflected expected behavior to identify any problems in the methodology used. The following sections describe the side by side comparisons of results where we compared the effect on performance of changing just one of the autonomy modes.

7.4.2.1 Effect of Changing Obstacle Detection Field of View

Figure 7-23 shows the performance maps from changing the obstacle detector's field of view. The effect of decreasing FOV is to reduce the ability of the vehicle to detect an obstacle. The increase in the no-go areas confirms that the vehicle performance drops with reduced field of view.

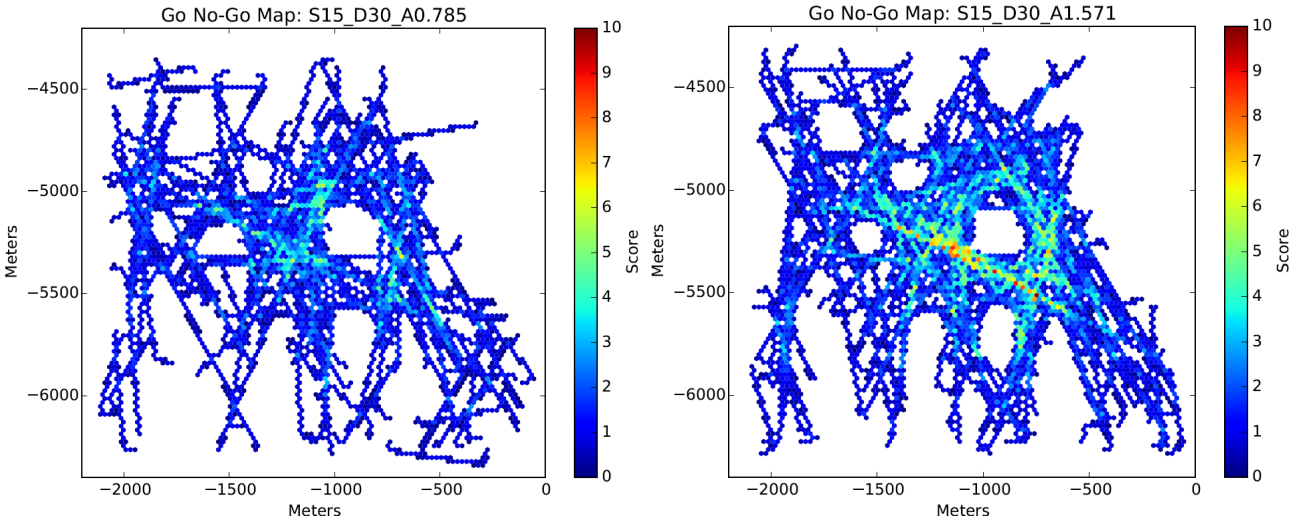


Figure 7-23: (Left) Small Camera FOV; (Right) Large Camera FOV.

7.4.2.2 Effect of Changing Camera Depth

Figure 7-24 compares the performance from reducing the depth at which the obstacle detection camera can detect an obstacle. This can be a result of changing sensors on the vehicle. We can observe that decreasing camera depth drops scores because the vehicle sees hazards too late to avoid.

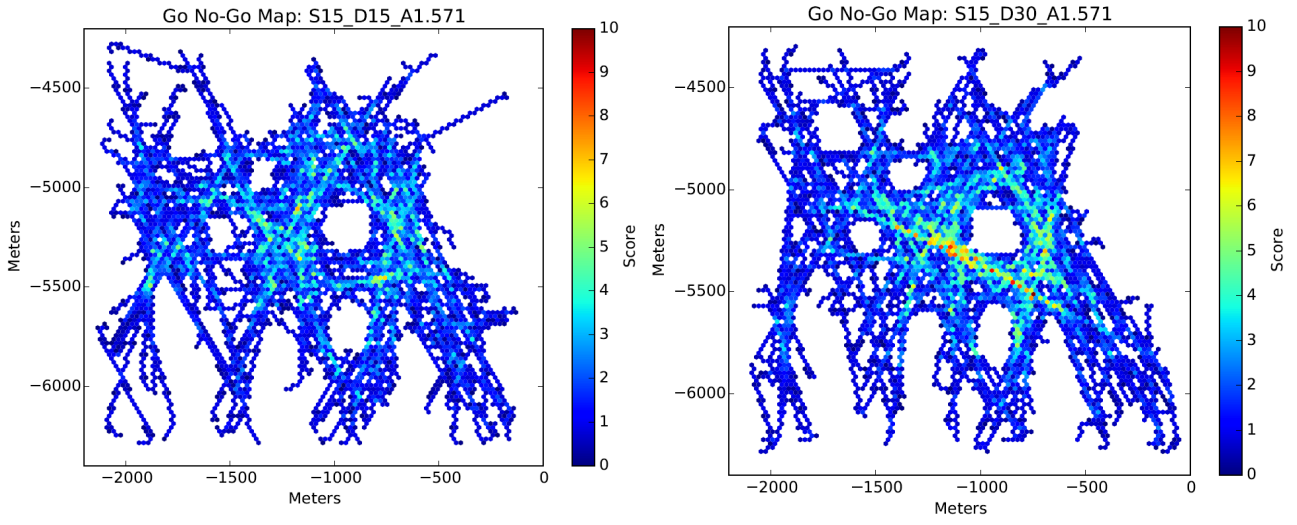


Figure 7-24: (Left) Small Camera Depth; (Right) Large Camera Depth.

7.4.2.3 Effect of Low vs. High Speed Limits

Figure 7-25 compares the effect changing the allowed maximum drive speed within the autonomy algorithms. As we can observe in the plots, increasing vehicle speed drops scores because there is more risk at higher speeds.

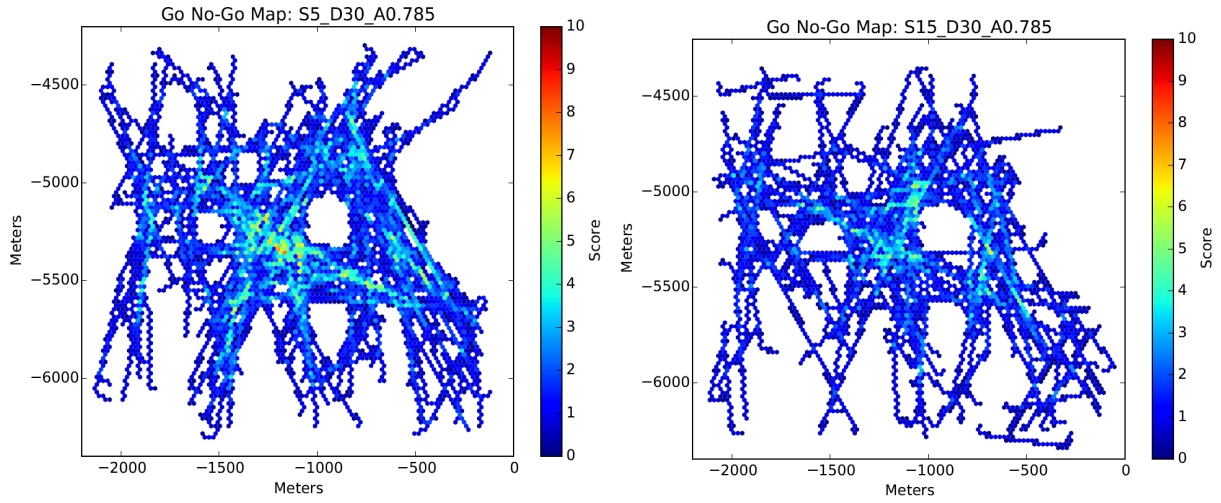


Figure 7-25: (Left) Low Maximum Speed; (Right) High Maximum Speed.

7.4.3 Autonomy Maps

Using the performance score maps for each of the autonomy levels, it is now possible to compare the vehicle performance across all of the levels for each cell in the region. The level with the highest score is assigned to the cell as the optimum autonomy level. The autonomy map on the left of Figure 7-26 shows a color code map of the autonomy level assigned to each cell, and is the autonomy map for the region. When designing traverses, this map can be used to select the autonomy level to use along the chosen path. The map on the right of Figure 7-26 shows the performance of one of the metrics – vehicle speed – across the cells in the region. It can be interpreted as an analog of the Speed-Made-Good maps for manned vehicles.

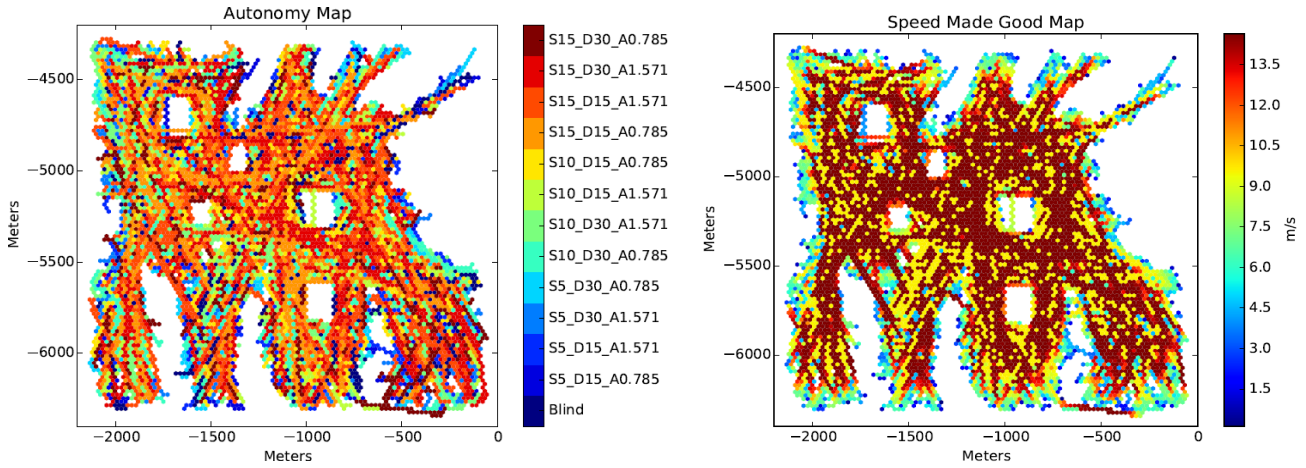


Figure 7-26: Autonomy and Speed Maps Over the 2 Km Area.

The performance metrics were then changed to alter the balance of safety versus speed plus safety to yield the new autonomy maps in Figure 7-27. Note that rewarding speed tends to bias the autonomy levels to the higher speed options. The charts on the right of Figure 7-27 show the autonomy maps and Speed-Made-Good maps when the metric is changed from just speed to safety plus speed performance metric.

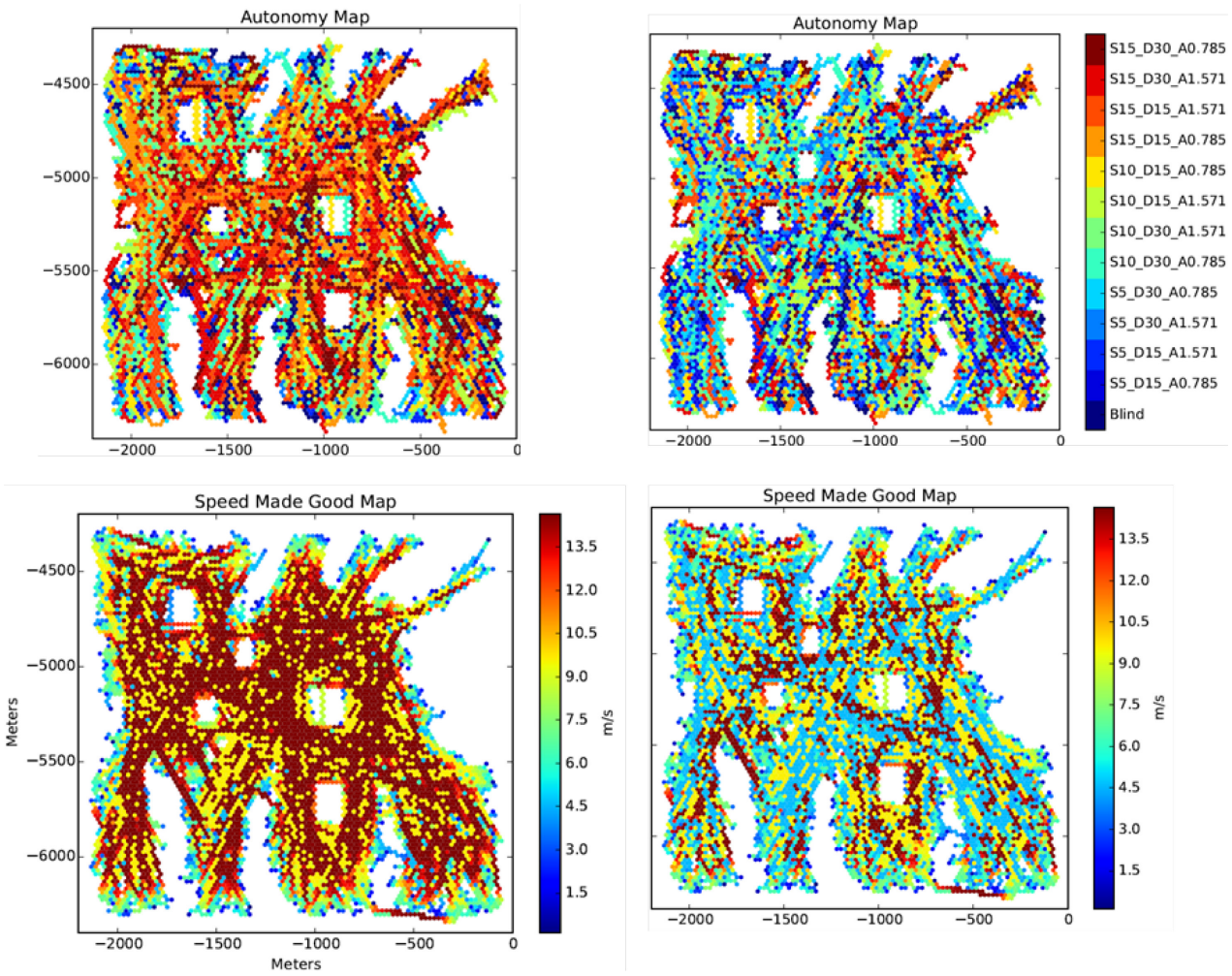


Figure 7-27: Balancing Criteria: (Left) Safety and Speed; (Right) Safety Only.

In Figure 7-28, we see the dramatic effect on the autonomy maps of an aggressive versus a conservative slope hazard threshold. A conservative slope threshold for hazardous areas decreases go areas but increases speeds.

7.5 STANDARDS

Developing standards for NG-NRMM(I) is premature because vehicle intelligence remains an amorphous and rapidly evolving area. At this stage we can best focus on defining input/output product requirements and the process. We list here items that can help guide the scope, requirements and development of an NG-NRMMM(I) capability:

- NG-NRMM(I) toolkit needs for intelligent vehicles;identify current capabilities and gaps.
- What types of autonomy are to be considered?
- Define intelligent vehicle classes and mobility types to be considered, eg. urban and off-road scenarios, wheeled/tracked/legged vehicles.
- Define range of operational environments to be considered.
- What NG-NRMM(I) output products are expected for intelligent vehicles?
- What mobility performance metrics and constraints are to be considered?

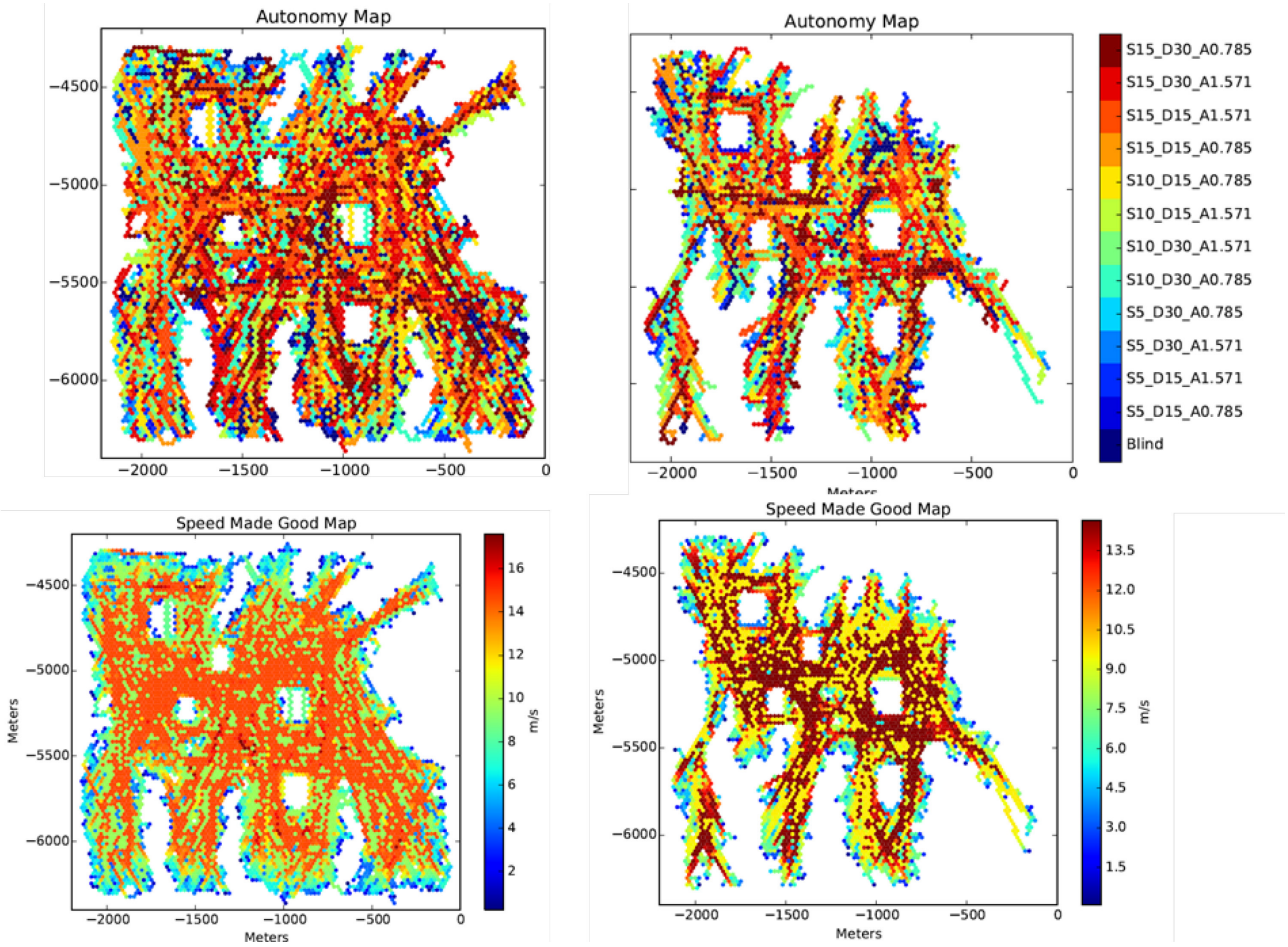


Figure 7-28: Balancing Criteria; (Left) Aggressive Slope Threshold Of 22°; (Right) Conservative Slope Threshold of 10°.

7.5.1 NG-NRMM(I) Challenges

Challenges to developing standards for NG-NRMM(I) include:

- Vehicle intelligence is an amorphous concept; there are a variety of intelligence architectures and capabilities.

- There is a lack of performance metrics for autonomous systems, and quantitative techniques are essential for NRMM.
- Vehicle intelligence is a rapidly evolving area, and needs a framework that can continue to evolve NRMM to meet emerging intelligent vehicle capabilities.
- Vehicle intelligence is not all or nothing; NRMM needs to provide guidance for sliding autonomy options.
- Performance evaluation is significantly more complex, because of the high-dimensional state space and unstructured/uncertain environments.
- Coupling between vehicle dynamics and intelligence is poorly understood, due to there being little interaction between two communities.
- Leveraging classical NG-NRMM for human driven vehicles is desirable; there is extensive parallel assessment capability that should be built upon.
- Will have off-line as well as in-the-field NG-NRMM(I) usage needs; use during operations requires speedy turnaround times.

7.5.2 NG-NRMM(I) Inputs

The use of NG-NRMM(I) requires certain inputs defining the vehicle, operational environment, mobility constraints and performance metrics. The following lists items that may be required:

Environment Inputs

- Terrain region:
  - Large regions – synthetic or real data from GIS source.
  - Variable topography.
  - Variable roughness.
  - Variable soil properties.
  - Cliff, ridge, etc. features.
- Stationary obstacles (e.g., buildings, bodies of water, vegetation) and moving obstacles (e.g., other vehicles, humans, animals).
- Lighting conditions for sensor models.
- Rain, snow, fog, vegetation, etc.

Vehicle Inputs

- Usual wheeled/tracked vehicle dynamics model (as for manned case):
  - Terramechanics models.
  - Detailed power/drive train models.
  - Suspensions, bushings, flex bodies.
- Intelligent mobility sensors (e.g., LIDAR, cameras, GPS, IMU, etc.) and their models:
  - Sensor hardware details – depth, coverage area, errors (false positives, failures). resource costs (power, latency, bandwidth).

- Sensor performance as a function of lighting, speed, vibrations, texture variation, rain, fog, occlusions.
- Sensor operational regime and limitations.
- Smart sensors – performance characteristics of embedded software.
- Sensing and actuation latencies.

Scenario and Performance Metrics Inputs

- Single vehicle or multiple vehicle convoys.
- Static and moving obstacles.
- Traverse constraints for scenario.
- Desired hard and soft metrics for scenarios, for example:
  - Time: to move, for algorithms to do their computations, to communicate with operator.
  - Energy consumption.
  - Bandwidth use.
  - Distance traveled.
  - Accuracy of traverse.
  - Ride roughness (for sensors, vehicle wear and tear).
  - Exposure.
  - Rollover margins, spin out, loss of control.
  - Risk.
- Hazard sources – structures, soil type, topography, from GIS data, comm, sensors.

Intelligence Inputs

- Available intelligent mobility capabilities:
  - System-level functions (e.g., single vs convoy operations, drive to goal).
  - Component functions (e.g., terrain classification, slam, obstacle avoidance, path planning, state estimation).
  - Their performance (e.g., as a function of vehicle speed, lighting, compute time/latencies).
  - Resource needs (e.g., memory/cpu, comm, power).
  - Selectable intelligence modes and settings to tailor vehicle behavior (e.g., enable/disable slam, tune hazard thresolds).
  - Limitations (e.g., max. Vehicle speed, vehicle vibration, rain/fog).
- Shared control needs:
  - Man/machine interface between operator and vehicle intelligence.
  - Onboard versus remote functions (i.e., what is done remotely and what is onboard).

    - Remote monitoring of vehicle behavior (i.e., telemetry available to operator).
    - Time delay latencies and bandwidth requirements (e.g., latencies in operator/vehicle interactions).
- Hardware resources:
    - Computational (e.g., CPUs, memory, etc.).
    - Sensing and actuation hardware.
    - Comm availability and characteristics.

7.5.3 NG-NRMM(I) Outputs

- Generate an autonomy map tailored to the scenario, environment and metrics for operating the vehicle for operating the intelligent vehicle:
    - This is a generalization of the Speed-Made-Good data product for manned vehicles.
- Go/NoGo maps.
- Expected performance of the intelligent vehicle for all the desired metrics (speed, stability, comm bandwidth).
- Surrogate models that allow trading off fidelity for faster performance.
- Sensitivity of predictions to changes in intelligent mobility parameters and component modules.

7.5.4 NG-NRMM(I) Process

- Strategy to build on manned vehicle NG-NRMM capabilities.
- How does NG-NRMM(I) accommodate updates to a vehicle's intelligence hardware/software?
- Operational requirements – time constraints on NG-NRMM-I execution, accuracy.
- Physics-based models with dynamics, vehicle intelligence and remote human operator interactions models in the loop.
- Sampling methodology used for evaluating performance for scenario and metrics at hand:
    - Brute force Monte Carlo sampling.
    - Design of experiments and uncertainty quantification for smart sampling.
    - Primitive maneuvers tailored to vehicle, intelligence, environment and scenario (similar to double lane change maneuvers for NG-NRMM).
- Performance metrics defined by the user and the minimum acceptable performance thresholds.
- Generation and refinement of models from empirical performance data.
- Running on workstations to HPC platforms.

7.6 GAPS AND PATH FORWARD

This section discusses near and longer term gaps in existing capabilities that need to be addressed for the development of a NG-NRMM(I) capability.

7.6.1 Extending the Prototype Demonstration

While Section 4 describes a valuable initial prototype demonstration, there are several new areas for broadening its scope:

- Urban scenarios with controller for on-road mobility.
- Remote operator-in-the-loop, shared control, cognition models in the loop.
- Communication latencies and bandwidth.
- Sensing non-idealities.
- Terrain uncertainty.
- Variable soil properties.
- More varied terrain topography.
- Use manned NG-NRMM GO/NOGO maps as input hazard maps.
- Extend to other mobility M&S tools and models.
- Use intelligence modules from third-party sources.
- Smarter sampling techniques.
- Advanced performance model extraction.
- Broader HPC platform usage.
- Larger class of mobility performance metrics with performance/risk thresholds.
- Performance/risk outputs.

The following sections describe additional areas for improving the pilot project.

7.6.1.1 Vehicle Platform

The vehicle platform used in the current prototype is the HMMWV. The range of vehicles or other devices with mobility can be widened to different wheeled or tracked vehicles, as well as multiple vehicles or swarms to simulate a convoy.

Other vehicles may require different terramechanics models with different detailed power/drive train models including bushings and flexible bodies. The vehicles may have multiple sensors such as LIDAR, cameras, GPS, and IMU. The new sensors will have different abilities and limitations such as depth, coverage area, errors (false positives, failures), as well as different resource costs (power, latency, bandwidth). Sensor performance should be affected by lighting, speed, vibrations, texture variation, rain, fog, occlusions, etc.

New vehicle platforms will have new and different communication features for remote operators.

7.6.1.2 Intelligent Mobility

Future NG-NRMM(I) prototype development can reduce dependence on maps prepared by human operators and rely on vehicle-borne obstacle detection, with possibly a remote operator or sensor based algorithms that take into account noise, failures and false positives. The vehicle may build its own hazard map, including near and far obstacles, and be able to handle static and moving obstacles. Mobility modes can include full teleoperation mode with terrain classifiers, global path planning and model predictive control (trajectory) in the loop. The vehicle intelligence may include state estimators; sensor fusion; and advanced state machines, and be able to share control with a remote operator. Models of vehicle communication systems may account for variable bandwidth with latencies and dropouts. Advanced versions may include the ability of the vehicle to work in convoys and interact with dismounted soldiers.

7.6.1.3 Terrain Environment

Future developments should include more varieties of terrain. This will entail:

- Large regions – synthetic or real data from GIS source;
- Variable soil properties; and
- Cliffs and ridge features.

In addition to the range of environments, future efforts may include moving obstacles; using variable lighting in sensor models; and modeling rain, fog, and other atmospheric phenomena.

7.6.1.4 M&S Process

Efforts to go beyond the current brute force Monte Carlo sampling may include:

- Far more traverse simulations to increase coverage.
- Explore design of experiments methods for more efficient sample coverage.
- Smart sampling via test maneuvers tailored to vehicle, intelligence, environment and scenario (like double lane change maneuvers for NG-NRMM).
- Broader HPC platform usage.

7.6.1.5 GO/NOGO Map Generation

Users should be able to define their own performance metrics and minimum acceptable performance thresholds. Traverses falling below any of the performance thresholds would be designated as failures. Each cell could have "go" desirability computed and confidence measurements assigned, using a weighted combination of performance metrics.

7.6.1.6 Autonomy Map Generation

Autonomy maps will need to support more autonomy level options. Choosing the best autonomy level may take into account criteria such as resource costs and penalties associated with the autonomy levels; confidence levels from GO/NOGO data; and impact on other import performance metrics. Extensions are needed to allow assignment of confidence levels to cells in output maps that are generated.

7.6.2 Longer Term Challenges

There are a number of fundamental gaps and issues that will need to be resolved in the longer term:

- How to handle small changes to autonomy (parameters, sensors) without having to repeat the expensive NG-NRMM(I) characterization process.
- Expand output maps such as Speed-Made-Good maps for intelligent vehicles. Speed is just one among a larger class of performance metrics.
- Use of multiple granularity simulations to reduce model complexity and computational costs.
- Explore ways to derive simpler surrogate models that can be used instead.
- Use levels of abstraction such as hazard maps? Others?
- Definition of intelligent vehicle scope, platforms, scenarios, etc., to help prioritize and shape next iterations.
- Capturing uncertainty; predicting confidence levels.
- Scale up to sample across larger autonomy parameter space and automating reduced order performance model extraction.
- Decomposition strategies for reducing sampling combinatorics (e.g., skills-based).
- Include human-in-the-loop impact on performance.
- Defining multiple levels of abstraction like the hazard cost maps, kinematics mode.
- Increasing range of performance metrics.
- More complex autonomy modules.
- More detailed sensor models.
- More complex scenarios.
- Working with real sites and GIS source data.
- Urban scenarios.
- Other autonomy scenarios such as convoy ops, dismounted soldier and autonomous vehicle, moving obstacles, other vehicles, etc.
- Large-scale runs on High Performance Computing (HPC) clouds.

7.6.2.1 Open Issues with M&S Based Sampling

The regime of modeling and simulation-based sampling requires significant new capabilities:

- The ability to handle increased modeling complexity, and the significant increase in computational cost.
- How can we reduce the number of M&S runs needed for adequate sampling?
- What is the modeling fidelity that is adequate? What are the multi-resolution models needed – for what level of speed/fidelity gains?
- Are there other data products (besides GO/NOGO, etc. maps) that should be generated given the added sophistication of the M&S capability?

- Are there ways to partition the sample space to reduce combinatorics?
- Taking into account traverse directionality, how can the vehicle state be communicated in M&S based sampling?

The use of highest fidelity models at all times is unlikely to scale for the large amount of simulation runs needed for NG-NRMM(I). The use of multi-resolution models and simulations as illustrated in Figure 7-29 is one possible strategy. The challenge is in defining the model coarsening strategies and their application domain.

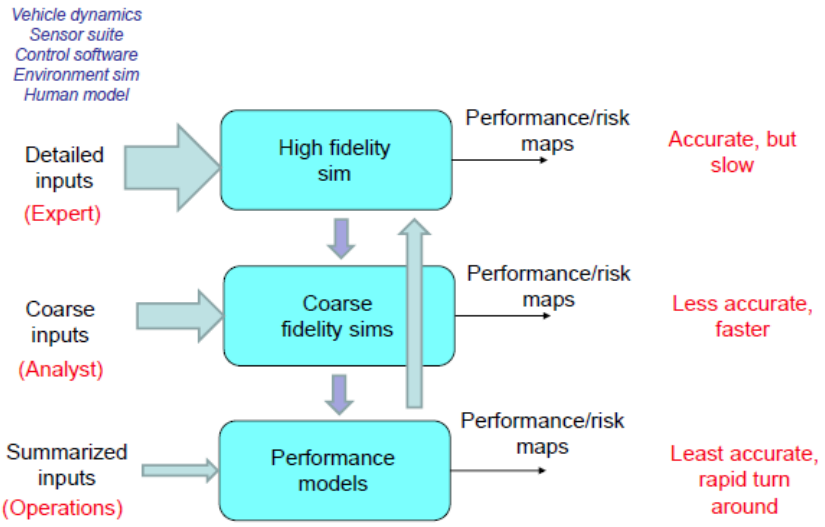


Figure 7-29: Multi-Resolution Modeling Strategy.

Figure 7-30 shows examples of multiple resolution models in sub-areas to support multi-resolution modeling at the system level.

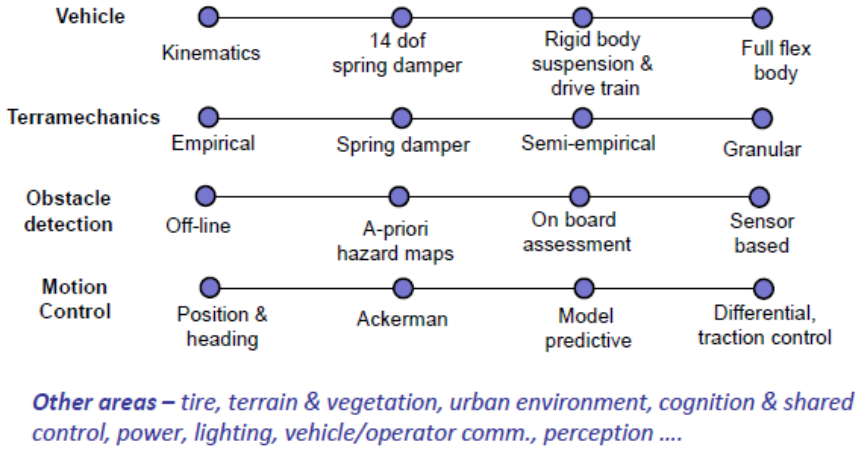


Figure 7-30: Examples of Multi-Resolution Models in Specific Areas.

7.7 ACKNOWLEDGEMENTS

This research was carried out in part at the Jet Propulsion Laboratory, California Institute of Technology, under a contract with the National Aeronautics and Space Administration. Government sponsorship is acknowledged. We would like to thank Aaron Gaut and Sharat Chandra for setting up and running the pilot project, and for generating the analysis data products discussed here.

7.8 REFERENCES

[1] Cameron, J.M., Myint, S., Kuo, C., Jain, A., Grip, H., Jayakumar, P. and Overholt, J. 2013. Real-Time and High-Fidelity Simulation Environment for Autonomous Ground Vehicle Dynamics. 2013 NDIA Ground Vehicle Systems Engineering and Technology Symposium, Troy, Michigan.

[2] Jain, A., Kuo, C., Jayakumar, P. and Cameron, J. 2016. Constraint Embedding for Vehicle Suspension Dynamics. Archive of Mechanical Engineering, 63(2): 193-213.

[3] Jain, A., Cameron, J., Lim, C. and Guineau, J. 2006. SimScape Terrain Modeling Toolkit. Second International Conference on Space Mission Challenges for Information Technology (SMC-IT 2006), Pasadena, CA.



Chapter 8A – TA6: TRACKED VEHICLE VERIFICATION AND VALIDATION

Ole Balling
Aarhus University
DENMARK

Michael McCullough
BAE Systems Inc.
UNITED STATES

8A.1 GOALS AND TEAM MEMBERS

The objective of the Verification and Validation (V&V) Thrust Area is to describe a framework for benchmarking the ability of modeling and simulation software solutions to predict mobility performance and validate against available test data. It is an open-ended V&V effort since additional vehicle descriptive data and benchmarking tests can be added as they become available. In particular, the objectives for the AVT-248 benchmarking effort has been to demonstrate this process for a tracked and a wheeled vehicle. A number of software developers were invited to participate in the benchmarks on a volunteer basis. No funding was offered. This chapter describes the effort undertaken in the tracked vehicle part of this work.

The team members of the AVT-248 V&V Thrust Area for the tracked vehicle benchmarking are listed below by country in alphabetical order:

- **Ole Balling, Leader**; Denmark;
- Tom von Sturm zu Vehlingen, Germany;
- Ozgen Akalin, Turkey;
- Henry Hodges, USA;
- Paramsothy Jayakumar, USA;
- Michael Letherwood, USA;
- Michael McCullough, USA.

8A.2 INTRODUCTION

It is the goal of the V&V effort to establish a reliable and comprehensive analysis process of the simulation predictive capabilities of off-road vehicle simulation models. This goal can be achieved by establishing a recommendation for software capability by means of modeling and simulation in connection with calibration, verification and validation with existing tests. In order to provide confidence in such models, well-known hard surface vehicle dynamic performance events are performed at first followed by low coefficient of friction events as well as soft soil mobility events. The categories of events are listed in Table 8A-1.

8A.3 PROCESS/METHODOLOGY

The intent of the V&V benchmarks is to begin codifying the expected capabilities of the NG-NRMM and describe a process for evaluation of the Modeling and Simulation capability of mobility capable software.

To establish a scale of achievement, the team has adopted and modified a Modeling and Simulation Maturity Scale used as depicted in Table 8A-2. The scale is modified from a NAFEMS presentation on simulation governance as a strategic management of simulation as a corporate competence [1].

Table 8A-1: Tracked Vehicle Events Categories.

Event Group Name	Event Group Details
1) Steering Performance (hard surface)	• Vehicle steering performance. Low as well as limit speed steering performance.
2) Side Slope Stability (hard + deformable surface)	• Ability to maintain directional control on a side slope.
3) Grade Climbing (hard + deformable surface)	• Determine maneuverability up and down slope as well as grade climbing to max steerable up slope.
4) Ride Quality (hard surface)	• Random terrain 6 watt limiting speeds on provided RMS profiles. Half round obstacles, 2.5G limiting speed.
5) Obstacle Crossing (hard surface)	• Step climb height limit, gap crossing limits, trapezoidal fixed barrier limits, trapezoidal ditch crossings. MOUT limits (N/A in this phase).
6) Off-road Trafficability	• Single pass soil strength limit, Max GVW, Multi-pass soil strength limit (Max GVW for 50 passes), drawbar pull vs slip performance, motion resistance.
7) Fuel Economy	• On-road and off-road 3D path loop determine net motion resistance coefficient.
8) Amphibious Operations	• Fording depth, speed in calm water, sea state limit, speed in waves (N/A in this phase).
9) Intelligent Vehicle	• Look ahead speed limit, speed through an offset corridor, soft soil limit sensing (N/A in this phase).

Table 8A-2: NG-NRMM Benchmark Modeling and Simulation Predictive Capability Maturity Levels.

1)	**DEMONSTRATION**: Demonstration of a correct implementation of a theoretically and conceptually consistent model.
2)	**PARAMETER SENSITIVITY DEMONSTRATION:** Verification that performance change with a change in system parameter such as Gross Vehicle Weight (GVW) or terrain deformability is consistent with theory and physics principles.
3)	**INDEPENDENT USER VERIFICATION:** Independent user demonstration and correlation to vendor results.
4)	**CROSS CODE VERIFICATION:** Cross verification with another accepted mobility simulation code.
5)	**CALIBRATION:** Calibration to a real vehicle test data set.

6)	**VALIDATION:** Blind correlation to a real vehicle test data set.
7)	**PARAMETER VARIATION VALIDATION:** Blind correlation to a real vehicle test data set with a change in system parameter(s).

8A.4 TRACKED VEHICLE BENCHMARK EVENTS

Nine groups of tracked vehicle benchmark events were defined based on the V&V team's judgement and experience in capturing the mobility prediction capability from software simulations. Where possible, the intent is to use current NRMM definitions, Allied Vehicle Testing Publications (AVTPs), International Organization for Standardization (ISO), and Society of Automotive Engineers (SAE) standards and recommendations. Mobility metrics have been provided where none currently exist. It is also thought that new events that capture particular vehicle designs, mobility metrics can be added. It is hoped that corresponding test results be made available for calibration and V&V.

The test descriptions for the event categories are explained in detail in the following subsections except for Amphibious Operations, as this test was not included in the Benchmark. Descriptions denoted by * indicate that test results are available.

8A.4.1 Steering Performance

a) Wall-To-Wall turn radius (WTW) in accordance with AVTP 03-30 [2] (Neutral axis spin maneuver): slow speed, maximum steer input (drive right reverse and left tracks in forward direction to achieve a clockwise vehicle spin), compute the maximum diameter of a plan view trace of vehicle chassis outer most points that will impinge upon a wall of any height and thus prevent the turn maneuver, spinning at least 360 degrees. Repeat in the counterclockwise direction.

b) Steady-State Cornering (SSC): per SAE J266 [3], asphalt skid pad (coefficient of friction mu = 0.8), 100 feet turn radius, starting at 5 mph increase velocity at constant acceleration rate to achieve approximate expected max speed in 100 seconds. Continue acceleration until loss of traction or unable to maintain turn radius. Plot turn angle and vehicle roll angle vs lateral acceleration. Repeat to get both right and left turns.

c) Double Lane Change (DLC) paved: Determine max attainable speed per AVTP 03-160W [4], hard surface, mu = 0.8.

d) Double Lane Change (DLC) gravel: Determine max attainable speed per AVTP 03-160W [4], hard surface, mu = 0.5.

8A.4.2 Side Slope Stability (SSS)

a) Paved (mu = 0.8) surface serpentine steerable slope speed limit: Determine maximum 30% side slope speed maneuverability. This is defined as the maximum speed on a 30% side slope for which the vehicle can traverse across a 30% side slope, first in a straight path line for 20 meters, then execute a downhill obstacle avoidance maneuver in less than 30 meters of traverse path length, around a 3 meter wide obstacle while recovering to the original straight line path and elevation on the slope. TOP 2-2-610 [5] serves as a guideline for the side slope stability event.

b) Deformable terrain serpentine steerable 20% slope speed limit. Determine maximum speed for obstacle avoidance (same description as for paved) on a 20% side slope on sand defined by LETE sand from Ref. [6]. TOP 2-2-610 [5] serves as a guideline for the side slope stability event.

8A.4.3 Grade Climbing

a) Max steerable/breakable up slope and down slope. For paved (mu = 0.8) surface determine max up slope and down slopes for which a 3 meter wide obstacle avoidance maneuver can be executed in 30 meters of path length while recovering original path line. The event is conducted with TOP 2-2-610 [5] as a guideline.

b) Speeds on grades in accordance with TOP 2-2-610 [5]. Determine maximum speed on grades up to maximum steerable up slope.

c) Deformable terrain grade limits and speeds (initial benchmark on dry sand). For LETE sand from Ref. [6] determine maximum steerable up slope and down slopes and maximum speed on grades up to the maximum up slope. TOP 2-2-610 [5] serves as a guideline for the event.

8A.4.4 Ride Quality

All terrain assumed equivalent to non-deformable hard terrain:

a) *Random terrain ride limiting speeds: Determine 6 watt ride limiting speeds due to vertical driver accelerations on standard 2D profiles provided defined by ISO 8608 3737 [7]. TOP 1-1-014 [8] outlines the guideline for the random terrain event.

b) *Half round obstacle ride limiting speeds outlined by TOP 1-1-014 [8]: Determine 2.5G ride limiting speeds due to vertical driver accelerations on standard half round profiles from 4” to 12”.

8A.4.5 Obstacle Crossing

Assume all hard ground surfaces with mu = 0.8.

a) Step climb height limit: determine maximum traversable height in forward direction. TOP 2-2-611 [9] is used as a general guideline for the event.

b) Gap crossing limits: determine maximum gap traversable in forward direction in accordance with TOP 2-2-611 [9].

c) Trapezoidal fixed barrier limits: determine traversability limits for obstacles parameterized by trapezoidal slope angle, barrier height, and barrier top surface width. Assume 12 different obstacles generated by the combinations resulting from the following obstacle parameter values: height (30 inches), top/bottom widths: 6”, 30”, 140”; up angles: 16 deg, 26 deg, 38 deg, 68 deg. AVTP 03-170 [10] serves as a guideline.

d) Trapezoidal ditch crossing limits: determine traversability limits parameterized by trapezoidal slope angle, ditch depth, and ditch bottom surface width. Assume 12 different ditch obstacles generated by the combinations resulting from the following obstacle parameter values: depth (30 inches), top/bottom widths: 6”, 30”, 140”; down angles (for ditch obstacles): 16 deg, 26 deg, 38 deg, 68 deg. AVTP 03-170 [10] serves as a guideline.

e) MOUT limits (rubble pile, crater). Not applicable this phase.

8A.4.6 Off-Road Trafficability

Assume LETE sand, snow, and muskeg [6].

a) Single pass soil strength limit. Determine maximum gross vehicle weight traversable in one pass including reversing back through the path per standard VCI measurement methods.

b) Multi-pass soil strength limit. Determine max GVW traversable for 50 passes (forward and reverse).

c) *Drawbar pull vs slip performance curve. For the LETE sand and standard M113 GVW, determine the drawbar pull at 2 mph and at stall, assuming drawbar is attached at rear hitch location [6]. The event is conducted after TOP 2-2-604 [11] as general guideline.

d) Motion Resistance (MR) (powered or towed). Determine powered and towed motion resistance coefficients in LETE sand. Powered motion resistance is defined to be MR at zero drawbar pull.

8A.4.7 Fuel Economy

A fuel economy course, partially in accordance with AVTP 03-10 [12], is designed as pictured in Figure 8A-1. The 90-degree turns must be executed within a 15 meter Wall-to-Wall corner.

a) On-road. For a given 3D path loop determine net terrain dependent motion resistance coefficient.

b) Off-road deformable terrain. For a given 3D path loop of LETE sand determine net terrain induced motion resistance coefficient.

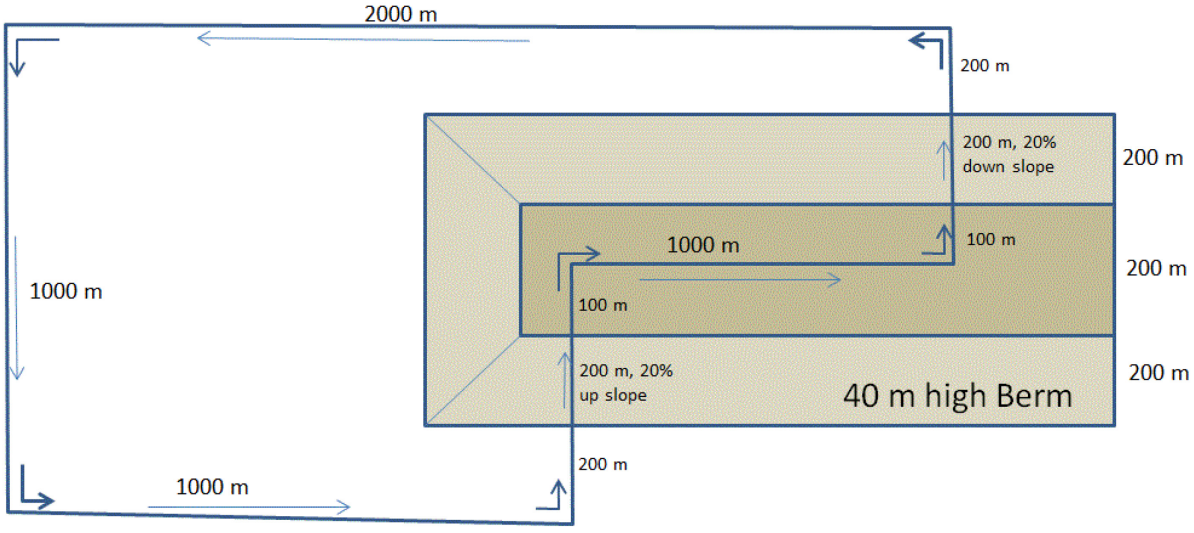


Figure 8A-1: Fuel Economy Loop Course.

8A.4.8 Amphibious Operations

The amphibious operation is not used in this benchmark, but it is included in the list of events for future expansion. Performance metrics related to fording depth, speed in calm water, sea state limit, etc. are thought of as areas for the definition of amphibious benchmark events.

8A.4.9 Intelligent Vehicle

The purpose of the Intelligent Vehicle testing is to address the capability of the particular level of intelligence. There can be several levels of intelligence in a vehicle system. With limited information about the intelligent system's inner workings, the real vehicle testing as well as the simulation thereof can be a matter of black box testing/simulation with vehicle states as input and vehicle control actuation as output, such as steering braking and acceleration. The black box would include the sensor suite for the particular system, hence if a particular sensor input from a comparable synthetic environment is needed, this has to be facilitated by providing such an environment. This is an area of research going forward and is not used in the tracked vehicle benchmark.

8A.5 BENCHMARK ENTRIES AND DATA SOURCES

The data sources for the tracked vehicle are listed in this section. This is limited to the parameters needed for mathematical modeling of the vehicle as well as the test data available to this benchmark. The intention of public releasable nature of such data limited the availability.

8A.5.1 Tracked Vehicle Data

Limited vehicle parameters and test data are available and published in Ref. [6] for the M113 tracked vehicle used in this benchmark. Additional performance metrics are available online through a military database of publicly available data [13]. The validity of this data is judged by the V&V team to be suitable for the benchmarking work.

8A.5.2 NRMM

The following sections give a brief introduction to the legacy NATO Reference Mobility Model (NRMM) used as a simulation entry in the benchmark. The NRMM simulations in the tracked vehicle benchmark are performed by GVSC using their latest version of VehDyn.

There are two types of vehicle models with NRMM, each serving a different purpose:

- Vehicle dynamics (VehDyn); and
- Mobility predictions.

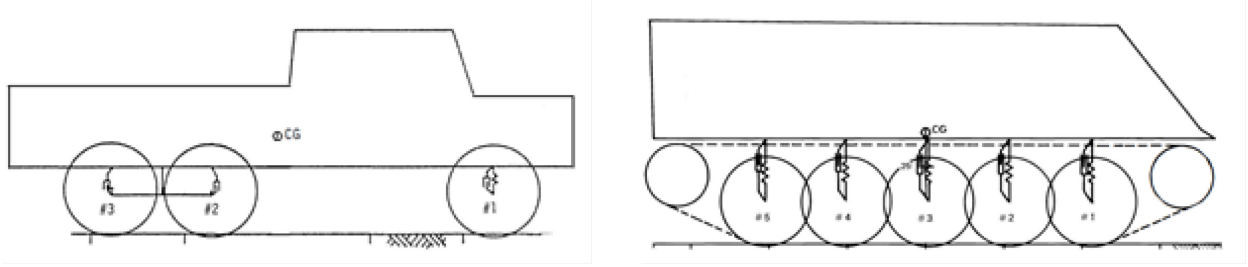
8A.5.2.1 VehDyn Model Overview

The vehicle dynamics model is a 2D pitch-plane model used to estimate ride quality, shock quality, obstacle crossing, and other performance metrics based on vehicle properties such as suspension rates and damping, wheel travel, axle loads, and others. The outputs from the vehicle dynamics module are a subset of the inputs required by the main NRMM module to predict off-road mobility performance. Other vehicle dynamics software may be used to generate the same outputs as VehDyn (Figure 8A-2).

Table 8A-3 contains a sample list of vehicle properties required to model the vehicle in VehDyn.

Table 8A-3: Sample List of Vehicle Properties Required to Model the Vehicle in VehDyn.

Mass	Inertia	Spring Rates	Damper Rates	Suspension Travel
Vehicle Dimensions	Axle/RW Loads	Tire Data	Track Data	Misc.



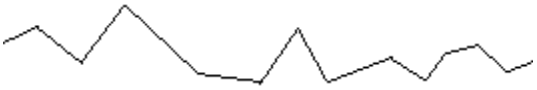
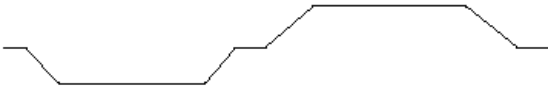
Example Wheeled Vehicle Model

Example Tracked Vehicle Model

Figure 8A-2: VehDyn Model Overview.

To generate the necessary inputs for the main NRMM prediction module, the VehDyn model was run on the following courses to test ride quality, shock quality, and its obstacle crossing ability (Table 8A-4).

Table 8A-4: Courses Used to Test Ride Quality, Shock Quality, and its Obstacle Crossing Ability.

	Description	Size Range	Road Profile Example
Ride quality	RMS profiles	3, 6, 9 cm	
Shock quality	Half round bumps	4 – 12 in radius	
Obstacle crossing	Mounds/ditches	72 sizes	

8A.5.2.2 Ride Quality

The ride quality data required by the main NRMM module from VehDyn is the 6W speed curve. This curve describes vehicle speed as a function of off-road terrain roughness while maintaining 6W absorbed power at the driver's seat. Terrain roughness is described by its RMS value. Using VehDyn, the dynamics model was run at increasing constant speeds along the RMS terrain profile up through the 6W limit speed. Combining results from a range of RMS profile simulations produces the 6W speed curve.

8A.5.2.3 Shock Quality

The shock quality data required by the main NRMM module from VehDyn is the 2.5G speed curve. This curve describes the speed of the vehicle as a function of half round bump radius while reaching 2.5G of vertical acceleration at the driver's seat. Using VehDyn, the dynamics model was run at increasing constant speeds over the bump up until the 2.5G limit was reached. Combining results from a range of half round bump simulations produces the 2.5G speed curve.

8A.5.2.4 Obstacle Crossing

The obstacle crossing data required by the main NRMM module from VehDyn contains underbelly clearance and force override information as a function of mound/ditch dimensions. To generate this data, a series of mounds and ditches of various heights and widths were defined in VehDyn. The vehicle was run over these obstacles at a slow, constant speed to determine the clearance between the vehicle and obstacle, as well as the force necessary to overcome each obstacle. The results are combined into a table which is used by the main NRMM prediction module for off-road mobility.

8A.5.2.5 NRMM Mobility Prediction Overview

The mobility prediction model is used by the main NRMM module to perform off-road mobility predictions of VCI, GO/NOGO, Speed-Made-Good, and other statistics over the terrain being considered. Contrary to the VehDyn model, there are no dynamics within this model. Instead, interpolation is used with lookup tables to generate the estimated mobility performance of the vehicle.

8A.5.3 NG-NRMM Benchmark Participants

In addition to NRMM, the benchmark participants for NG-NRMM tracked vehicle demonstration are listed in Table 8A-5 and followed by a description of the individual entrants capabilities. In the table, Simple Terramechanics solutions are indicated with the abbreviation ST and Complex Terramechanics solutions are identified with CT:

Table 8A-5: Tracked Vehicle Benchmark Participants Listed by Software Developer Organization.

Software Developer (Letter Identifier)	Country	Software
Advanced Science and Automation Corporation (A)	USA	IVRESS/DIS CT
FunctionBay (B)	ROK	RecurDyn ST
MSC Software (C)	USA	ADAMS ST
University of Wisconsin – Madison (D)	USA	Chrono ST
Vehicle Systems Development Corporation (E)	CAN	NTVPM/NWVPM ST

8A.5.3.1 Advanced Science and Automation Corporation

Advanced Science and Automation Corp. (ASA) was founded in 1998. ASA's mission is to provide advanced software solutions for physics-based modeling, simulation, visualization, and design optimization of mechanical systems. Industries that ASA serves include automotive, aerospace, ship building, manufacturing, mining, construction, and pharmaceutical industries.

8A.5.3.1.1 Software Capability: IVRESS/DIS

ASA's DIS (Dynamic Interactions Simulator) software is used to predict the motion, deformation and internal forces/stresses of mechanical systems as a function of time. This can be used to optimize those systems and ensure that they meet their design requirements. DIS seamlessly integrates into one solver the following computational techniques:

1) **Multibody Dynamics (MBD)** for modeling rigid bodies, joints, frictional contact between bodies, rotary/linear actuators, and control algorithms.
2) **Finite Element Method (FEM) f**or modeling flexible bodies using large rotation/deformation brick, shell, thin beam, and thick beam elements.
3) **Discrete Element Method (DEM)** for modeling granular non-cohesive soils (such as dry sand, gravel and rubble piles) and cohesive soils (such as wet sand/clay/silt or snow). The DEM soil material model includes the effects of soil elasticity, plasticity, cohesion, friction, viscosity, and damping. Figure 8A-3 show examples of DIS coupled MBD – DEM simulations for off-road vehicles. The model naturally accounts for traction due to tire tread blocks/track grousers, side rutting, bulldozing of soil in front of the tire/track, and multi-pass effects (front then rear wheels passing on the soil, or a vehicle driving along the tire imprint made by another vehicle).
4) **Smoothed Particle Hydrodynamics (SPH)** for modeling fluid interaction with rigid and flexible bodies for simulating vehicle fording, swimming, and driving on flooded roads with standing or running water. SPH can also be used to model liquid sloshing in tanks carried by the vehicle. DEM and SPH can be used simultaneously to model interactions of the tire with the soil and interactions of the tire and vehicle body with water during water fording.



Figure 8A-3: Snapshots of Typical DIS Soft Soil Vehicle Mobility Simulations of Wheeled and Tracked Vehicles With the Soil Modeled Using DEM.

ASA's IVRESS (Integrated Virtual Reality Environment for Synthesis and Simulation) software is a virtual reality engine that can be used for pre-processing and post-processing (scientific visualization) of the DIS simulations. Examples of mechanical systems that the IVRESS/DIS software has been used to simulate and visualize include cars, trucks, construction equipment, airplanes, ships, gear-boxes, belt-drives, chain-drives, conveyor belts, bio-dynamic systems, and satellites. Key features of IVRESS/DIS include:

1) Semi-explicit time-integration solution procedure with lumped mass and inertia tensor.
2) Distributed/shared memory parallel solver.
3) Penalty technique used for modeling joint and contact constraints.
4) Master/slave contact model where contact is detected between discrete points on a master contact surface and a polygonal slave contact surface.
5) General fast binary-tree hierarchical bounding box/sphere contact search algorithm.
6) Total-Lagrangian lumped parameters 3D large rotation and deformation finite elements including solid brick and thick beam elements.
7) Ability to simulate vehicle motion on arbitrarily long soft-soil rough complex topography terrains.
8) Hierarchical object-oriented framework which enables creating large complex models.
9) High-fidelity Finite Element (FE) tire model.
10) Ability to model tracked vehicles with single and double-pin segmented tracks, as well as continuous tracks.
11) Integrated JAVAscript and Python interpreters.
12) Model tree editor with on-screen editing.
13) Ray tracing for photo-realistic rendering.
14) Scientific visualization objects including colored/contoured model surfaces and iso-surfaces.

DIS/GroundVehicle is a specialized version of DIS that is used to predict the mobility of ground vehicles, including wheeled, tracked, and legged vehicles, while rolling/sledding/walking on complex topography soft soil or hard terrains. DIS/GroundVehicle seamlessly integrates IVRESS/DIS with a user-friendly spreadsheet template-based interface for creating the vehicle and the terrain models. DIS/GroundVehicle uses DEM to model the soil and SPH to model water for vehicle fording and swimming. Typical DIS vehicle simulations on hard terrains run in real-time to 10 times slower than real-time. Typical DIS vehicle simulations on soft soil terrains with about one million DEM/SPH particles run 1000 to 5000 times slower than real-time running in parallel across 4 to 8 HPC compute nodes with 32 to 40 cores per node.

8A.5.3.2 MotionPort

MotionPort was founded in 2004 and is the master distributor for the RecurDyn software in the Americas. The MotionPort headquarters is located in St. George, Utah, with a support office in Ann Arbor, Michigan. MotionPort serves clients from a wide variety of industries such as the US Army GVSC, John Deere, NASA, Xerox, and P&G. MotionPort has successfully conducted two Small Business Innovative Research (SBIR) projects for NASA.

8A.5.3.2.1 Software Capability: RecurDyn

The RecurDyn multibody dynamics software was first offered commercially in 1999 and initially offered a track assembly simulation toolkit. The capabilities and ease of use of RecurDyn have been expanded since then. The images below show the icons for:

1) The current set of specialty toolkits;
2) The capabilities of the track assembly toolkit for military vehicles; and
3) Some of the interfacing capabilities to control systems, hydraulics, FMI systems, and particle-based CFD.

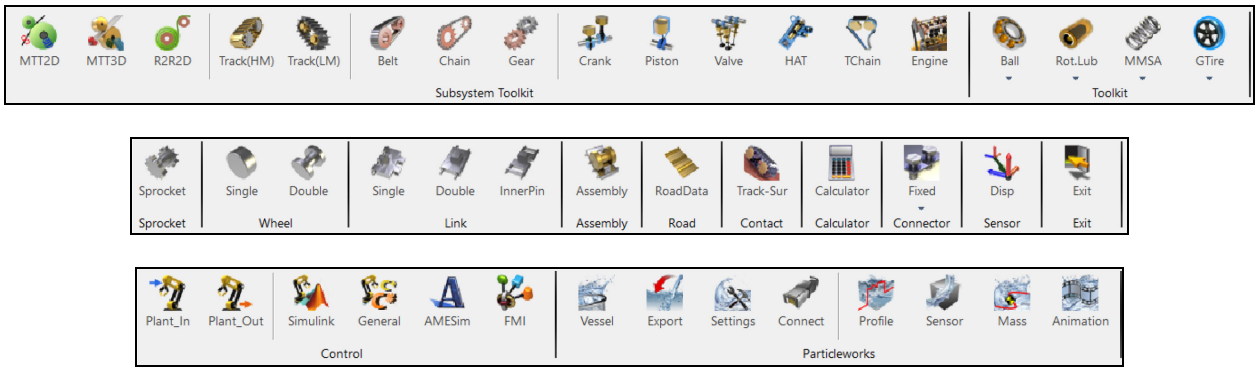


Figure 8A-4: RecurDyn Icons.

RecurDyn uses a recursive, multibody dynamics formulation for the basic kinematic calculations, a "linear" (or FEA-style) solver for the non-linear flexible bodies, and supports co-simulation with various other CAE software such as Simulink for control system models.

Tire modeling on hard surfaces can be done with the Fiala and the University of Arizona tire models, and all tires that support the Standard Tire Interface (STI). Custom tire models may be included through a user subroutine. Tire modeling on soft soils can be done with a co-simulation with the EDEM software. Track assembly modeling (Figure 8A-5) is well supported with a custom toolkit with regular contact for hard surfaces and Bekker equations for soft soils.

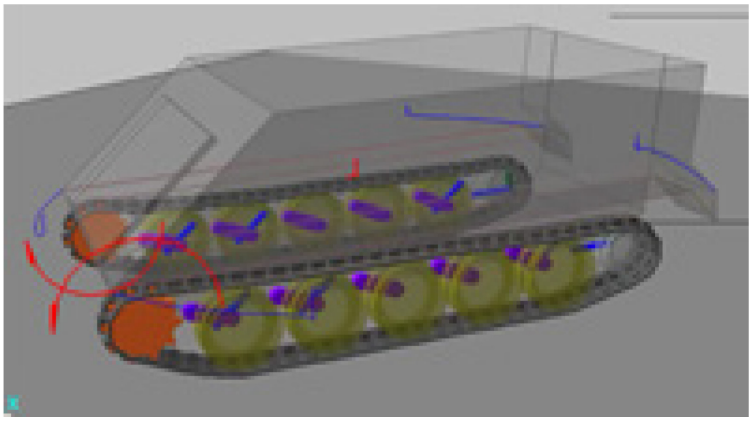


Figure 8A-5: Track Assembly Modeling.

The computational effort for a double lane change event on a hard surface (Figure 8A-6) was 84 seconds on a Dell laptop for a 10-second event. Soft soil runs that require co-simulation with EDEM typically take several days to run on a workstation.

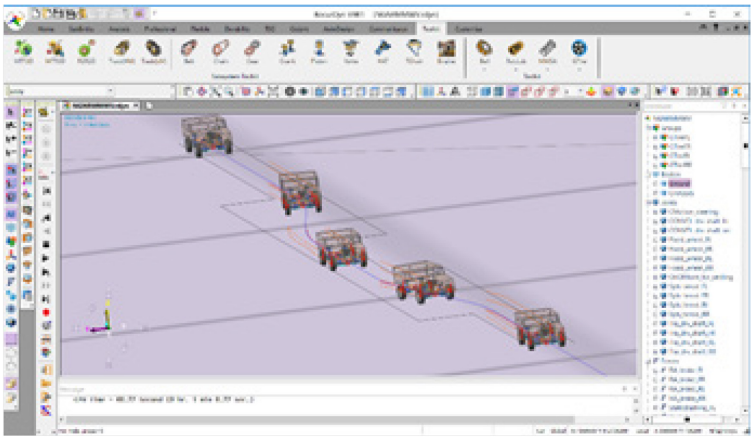


Figure 8A-6: Computational Effort for a Double Lane Change Event on a Hard Surface.

RecurDyn is open. Custom processes and user interfaces are readily defined through a supported link with Microsoft Visual Studio.

8A.5.3.3 MSC Software Corporation

MSC Software develops and distributes engineering software products that are used to simulate, among many other things, the behavior of vehicles in virtual test environments. These products are capable of simulating vehicle components, subsystems and full-vehicle systems, to predict both system response and component behaviors such as motion, deformation, stress, internal forces, fatigue and vibration.

As vehicle complexity grows to include new capabilities such as autonomous operation, and analysis requirements expand to include more and varied terrains, MSC has continued to anticipate these needs and enhance its simulation software accordingly.

Based in Newport Beach, California, MSC was established in 1963, and has expanded to over 1,000 employees worldwide. MSC is now a subsidiary of Hexagon AB, a publicly traded company in Sweden.

8A.5.3.3.1 Software Capability: MSC Adams

MSC Adams is the world's most widely used software for analysis and simulation of multibody dynamic systems. It provides a comprehensive modeling toolset that allows engineers to build, test, study and evaluate dynamic, multibody systems using virtual prototypes.

Adams provides a robust system dynamics equation solver. The software checks the user's model and automatically formulates and solves the non-linear differential equations of motion representing that model. The solver can perform static, quasi-static, kinematic or dynamic analysis. Adams models can incorporate numerous complex component behaviors, such as finite element-based linear and non-linear flexible bodies, contacts, bushings, gears, bearings, belts, hydraulic components and other common machine elements.

The Adams software is provided in modules, allowing the engineer to configure an analysis environment that meets their individual needs. For the NG-NRMM benchmark, we configured version 2017.2 of MSC Adams with both the Adams Car package and the Adams Tracked Vehicle (ATV) Toolkit.

Adams Car

Adams Car makes it easy to model many types of vehicles by providing a logically organized assembly topology oriented to vehicle systems as well as a library of pre-defined templates for common vehicle subsystem topologies. These templates can be used as is, or customized to represent new topologies and subsystem behaviors. This template approach facilitates the standardization and re-use of modeling strategies – improving both efficiency and consistency. Adams Car also includes both integrated driver control systems and capability for detailed user-defined control systems. Finally, a variety of road and tire modeling methodologies are available in Adams Car to accurately simulate the critical road-tire interface.

Adams Tire

Adams Tire is a module for incorporating tires into your mechanical model in order to simulate maneuvers such as braking, steering, acceleration, free-rolling, or skidding. Adams Tire models are typically used for vehicle handling, ride comfort, and durability analyses. The Adams Handling Tire offers six different tire model formulations: PAC2002, PAC-TIME, Pacejka '89 and '94, Fiala, UA-Tire, and 521-Tire. In addition, the following more specialized models are also available: Pacejka Motorcycle Tire, Soft Soil Tire, Aircraft Tire, and FTire.

Adams supports numerous methods for representing the road surface, depending on the available data and analysis requirements. Similarly, the tire interaction with this surface can be addressed at several different levels of fidelity. Through these options, Adams Tire is capable of capturing responses up to 15 Hz with the simpler methods, 80 Hz if belt dynamics are incorporated, and 125 Hz if FTire is used.

Adams Car Soft Soil Capability

The Adams Tire Soft Soil tire model offers a basic model to simulate the tire-soil interaction forces for any tire on terrain that can be characterized as either elastic-plastic or viscoelastic e.g., – sand, clay, loam and snow. Two tire-soil contact models are offered. The first is an elastic-plastic soil deformation model (see Refs. [14] [15] [16] [17] [18]) with optional "bulldozing" resistance [19] and optional multi-pass effect. The second is a viscoelastic soil deformation model [20] with an optional multi-pass effect that considers a transient relaxation time. Through more advanced co-simulation methods, it is also possible to represent a Discrete Element (DEM) soil bed interacting with a rigid tire.

Adams ATV Toolkit

The ATV Solution is an add-on "toolkit" for Adams developed in cooperation with end users. It leverages both the template-based Adams Car architecture and the broad Adams Solver capabilities to provide an environment for modeling and simulating tracked vehicles.

ATV is used for a wide range of applications such as dynamic mobility studies, turret and weapon control design, sprocket tooth design, high speed turning events, road wheel suspension design, track tension optimization, failure and panic event studies, and the generation of accurate loads for tracked vehicle stress and fatigue investigations.

The detailed track representation computes the forces acting on each individual track element as it interacts with the ground, neighboring track elements and the suspension wheels. The ground may be modeled as either rigid or deformable. The deformable model uses a Bekker-Wong pressure-sinkage relationship and Janosi/Hanamoto shear-slip relationships. A simplified string-track method is also available for preliminary analysis work.

ATV is suitable for simulation and analysis of tanks and other defence-related equipment, construction equipment, agricultural and forest equipment, mining and mining operations snowmobiles and off-road vehicles. As with Adams Car, model subsystem templates are provided to the user for getting started with typical model topologies.

Extensibility

The entire Adams infrastructure is user-extensible, allowing for differing levels of detail/refinement in the component and subsystem modeling and practically unlimited process customization in the form of custom user interfaces and pre- or post-processing automation (Table 8A-6).

For an application similar to the NG-NRMM assessment, this extensibility could manifest as added menu-driven events, pre-packaged roads and incorporated mobility-related metrics. This could be accomplished by users or in cooperation with MSC as a consulting effort. In addition, optimizations of some the underlying methods are possible that might yield substantial performance improvements especially for soft soil calculations. Script-driven sequences where limit handling or performance envelope data are being determined could also be accelerated through script-driven iteration or in conjunction with commercial Multi-Discipline Optimization (MDO) tools.

Table 8A-6: Computational Effort. All results on laptop workstations.

ATV, Hard Surface Double Lane Change	74 min
ATV, Soft Soil Drawbar Pull, 10 s	3000 min
Adams Car WVP, Hard Surface Double Lane Change	9 s
Adams Car WVP, Soft Soil Drawbar Pull, 10 s	61 s

8A.5.3.4 University of Wisconsin

Developed at the University of Wisconsin – Madison, USA, and at Universita di Parma, Italy, Chrono is an open source multi-physics software package, which is distributed under a permissive BSD-3 license.

The core functionality of Chrono provides support for the modeling, simulation, and visualization of rigid multibody systems, with additional capabilities offered through optional modules. These modules provide support for additional classes of problems (e.g., deformable multibody systems through finite element analysis and fluid-solid interaction), for modeling and simulation of specialized systems (such as ground vehicles and granular dynamics problems), or for providing specialized parallel computing algorithms (multi-core, GPU, and distributed) for large-scale simulations. For more details on Chrono capabilities, formulations, solvers, and applications, see the project website at http://projectchrono.org.

8A.5.3.4.1 Software Capability: Chrono::Vehicle

Chrono::Vehicle is a specialized Chrono module which provides a collection of templates (parameterized models) for various topologies of both wheeled and tracked vehicle subsystems, as well as support for modeling of rigid, flexible, and granular terrain, support for closed-loop and interactive driver models, and run-time and off-line visualization of simulation results. Chrono::Vehicle leverages and works in tandem with other Chrono modules, such as Chrono::FEA (for finite element support); Chrono::Granular (for granular dynamics support); Chrono::Irrlicht and Chrono::OpenGL (for run-time visualization) and Chrono::Parallel and Chrono::Distributed for parallel computing support.

Chrono::Vehicle provides a comprehensive set of vehicle subsystem templates (for tires, suspensions, steering mechanisms, drivelines, sprockets, track shoes, etc.), templates for external systems (for powertrains, drivers, terrain models), and additional utility classes and functions for vehicle visualization, monitoring, and collection of simulation results. As a middleware library, Chrono::Vehicle requires the user to provide C++ classes for a concrete instantiation of a particular template. An optional Chrono library provides complete sets of such concrete C++ classes for a few ground vehicles, both wheeled and tracked, which can serve as examples for other specific vehicle models. An alternative mechanism for defining concrete instantiation of vehicle system and subsystem templates is based on input specification files in the JSON format. For additional flexibility and to allow integration of third-party software, Chrono::Vehicle is designed to permit either monolithic simulations or co-simulation where the vehicle, powertrain, tires, driver, and terrain/soil can be simulated independently and simultaneously.

Chrono::Vehicle currently supports three different classes of tire models: rigid, semi-empirical, and finite element. Rigid tires can be modeled as cylindrical shapes or else as non-deformable triangular meshes. From the second class of tire models, Chrono::Vehicle provides templated implementations for Pacejka (89 and 2002), Fiala, Lugre, and TMeasy tire models, all suitable for maneuvers on rigid terrain. Finally, the third class of tire models offered are full finite element representations of the tire. While these models have the potential to be the most accurate due to their detailed physical model of the tire, they are also the most computationally expensive of the tire model currently available in Chrono::Vehicle. Using ANCF or Reissner shell elements, these FEA-based tire models can account for simultaneous deformation in tire and soil, for high-fidelity off-road simulations.

Tracked vehicles in Chrono::Vehicle are full multibody system models. Templates for both segmented and continuous-band tracks are available, the latter providing options for modeling using 6-DOF bushing elements or else FEA shell elements. Frictional contact interaction, both internal (between vehicle components) and with the terrain, relies on the underlying Chrono capabilities and supports both non-smooth (i.e., complementarity-based) and smooth (i.e., penalty-based) contact formulations.

Chrono::Vehicle provides several classes of terrain and soil models of different fidelity and computational complexity, ranging from rigid, to semi-empirical Bekker-Wong type models, to complex physics-based models based on either a granular or finite element-based soil representation. For simple terramechanics simulations, Chrono::Vehicle provides a customized implementation of the Soil Contact Model, based on Bekker theory, with extensions to allow non-structured triangular grids and adaptive mesh refinement. Second, Chrono provides an FEA continuum soil model based on multiplicative plasticity theory with Drucker-Prager failure criterion and a specialized 9-node brick element which alleviates locking issues with standard brick elements. Finally, leveraging the Chrono::Granular module and support for multi-core and distributed parallel computing in Chrono, off-road vehicle simulations can be conducted using fully-resolved, granular dynamics-based complex terramechanics, using a Discrete Element Method approach. Such simulations can use either of the two methods supported in Chrono, namely a penalty-based, compliant-body approach, or a complementarity-based, rigid-body approach.

Computational efficiency of Chrono::Vehicle simulations is difficult to quantify, as it depends on the complexity of the vehicle, tire, and soil models, on the contact formulation employed, on accuracy levels, and on available hardware. Typical mobility simulations on hard surface, such as double lane change, can be performed in close to real-time for wheeled vehicles (depending on choice of tire model) or in a few minutes for tracked vehicles. Off-road simulation execution times can range from a few hours (for example for a tracked vehicle on SCM soil) to several days (in the case of a wheeled vehicle with FEA-based flexible tires on million-body granular terrain).

Written almost entirely in C++, Chrono is middleware and therefore supports customized solutions that involve user code and potentially third-party software. The software is portable and can be built on different platforms,

under different operating systems, and using various compilers. Chrono is available for download (latest release is 3.0.0) from https://github.com/projectchrono/chrono. Full API documentation and additional tutorials are available at http://api.projectchrono.org. Animations generated through Chrono simulations are available at https://vimeo.com/uwsbel/videos.

8A.5.3.5 Vehicle Systems Development Corporation (VSDC), Toronto, Ontario, Canada

VSDC specializes in research, development, and consulting services in off-road vehicle mobility. VSDC has developed two models for simulating vehicle mobility on deformable terrain, one for tracked vehicles (NTVPM) and the other for off-road wheeled vehicles (NTWPM).

8A.5.3.5.1 Software Capability: Nepean Tracked Vehicle Performance Model (NTVPM)

Approach: It is physics-based and developed on the analysis of the mechanics of tracked vehicle-terrain interaction. It is for simulating the steady-state cross-country performance of single-unit or two-unit articulated tracked vehicles, with segmented metal tracks or rubber tracks.

Procedures: Predictions of the steady-state cross-country performance are based on solving a set of non-linear dynamic equilibrium equations of the tracked vehicle. This is significantly more efficient and effective than the time integration of a large set of equations of motion used in multibody vehicle dynamics models. The computation time for simulating vehicle drawbar performance over a series of slips using NTVPM is usually less than one minute on a PC.

Input Vehicle Parameters: All major design parameters that affect tracked vehicle cross-country performance are taken into account. These include initial track tension (indication of initial tightness of the track), track longitudinal stiffness (for evaluating track elongation under tension), road wheel suspension characteristics (for evaluating load distribution among road wheels), ground clearance, vehicle belly longitudinal profile and width (for evaluating the load supported by vehicle belly and associated belly drag, when track sinkage is greater than vehicle ground clearance), etc.

Input Terrain Parameters: These include pressure-sinkage parameters, terrain internal shear parameters, rubber-terrain shear parameters (for vehicles with rubber tracks or tracks with rubber pads), parameters characterizing terrain response to repetitive loading, and belly material-terrain shear parameters, measured using a bevameter.

Output Performance Metrics: These include vehicle sinkage, motion resistance, thrust, drawbar pull, and tractive efficiency as functions of slip. The normal pressure and shear stress distributions on the track-terrain interface are also part of the output. It is planned to include vehicle speed-made-good and fuel economy as part of output metrics in the next version.

Operations: Operations are via a Control Center shown on computer screen. All vehicle and terrain data are input using dialog (edit) box format. Output is in graphical/tabular format. Operating procedures are designed for user-friendliness.

Applications: NTVPM has been employed to assist military tracked vehicle manufacturers in the development of new products and governmental agencies in the evaluation of military tracked vehicle mobility in North America, Europe, and Asia. NTVPM has also been licensed to industry and governmental agencies in North America, Europe, and Asia.

8A.5.3.5.2. Nepean Wheeled Vehicle Performance Model (NWVPM)

Approach: It is physics-based and developed on the analysis of the mechanics of wheeled vehicle-terrain interaction.

Capability: It is for simulating the steady-state cross-country performance of multi-axle wheeled vehicles.

Procedures: The procedures are similar to those of NTVPM.

Input vehicle parameters: All major vehicle design parameters that affect wheeled vehicle cross-country performance are taken into account. These include the number of driven/non-driven axles, axle suspension stiffness, tire dimensions, inflation pressure and nominal ground contact area, ground clearance, etc.

Input terrain parameters: These are the same as those for NTVPM.

Output performance metrics: These are similar to those for NTVPM.

Operations: They are similar to that for NTVPM.

Applications: NWVPM has been employed to assist governmental agencies in Canada and the United States in the evaluation of military wheeled vehicle mobility. NWVPM has also been licensed to governmental agencies in North America and Asia.

8A.6 BENCHMARK RESULTS

This section summarizes the results obtained by the participating vendors, outlines the main difference between results and emphasizes differences in the methodology chosen by the vendors in each of the simulations. The vendors are scored on the Maturity Scale depicted in Table 8A-1. Calibration data is available for the wall-to-wall, step climb height, gap crossing and the drawbar pull events. For this benchmark effort the vendors did have a priori access to the test data, therefore Level 5 is possible for those events, where test data was available. Level 5 is given to vendors who have provided results that do not deviate more than 50% compared to the calibration data. For events where multiple vendors have provided data, but no test data is available, the maximum level obtainable is 4 based on the average result. If a vendor has provided results that deviates more than 50% compared to the average result the given Maturity Level is 2, otherwise it is 4.

8A.6.1 Wall-To-Wall Turn Radius

The wall-to-wall event is performed both Clockwise (CW) and Counterclockwise (CCW). All vendors, except Vendor E and NRMM, have simulated the event. Test data is available for the wall-to-wall event.

The wall-to-wall analyses show similar results for all vendors that have performed the event, for both clockwise and counterclockwise simulation as shown in Figure 8A-7. All participating vendors received a Maturity Level of 5 shown in Figure 8A-8 based on the calibration data.

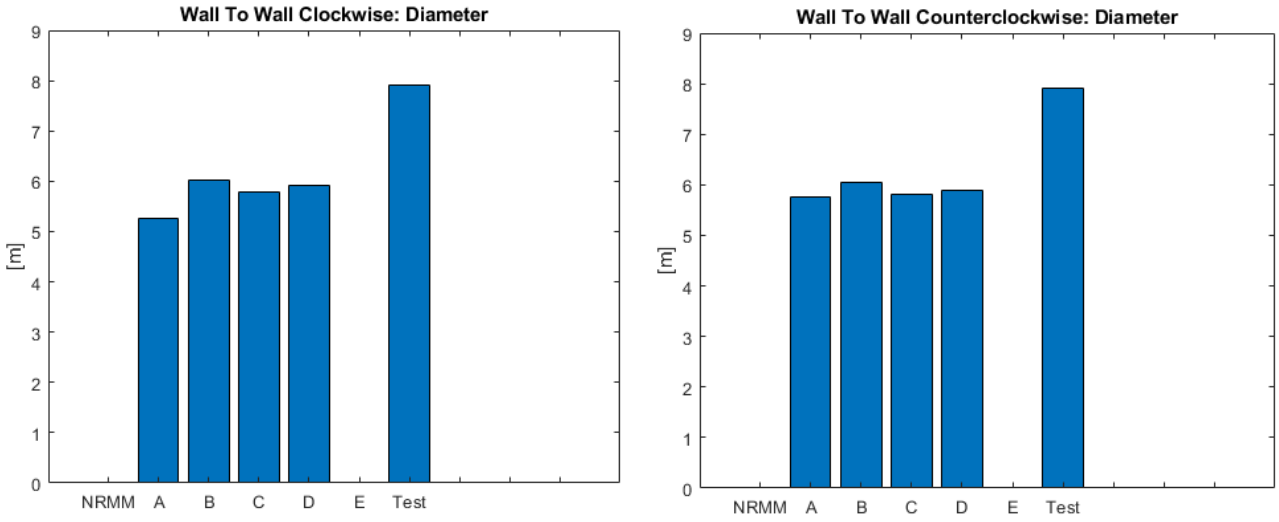


Figure 8A-7: Wall-To-Wall Clockwise (Left) and Counterclockwise (Right): Diameter.

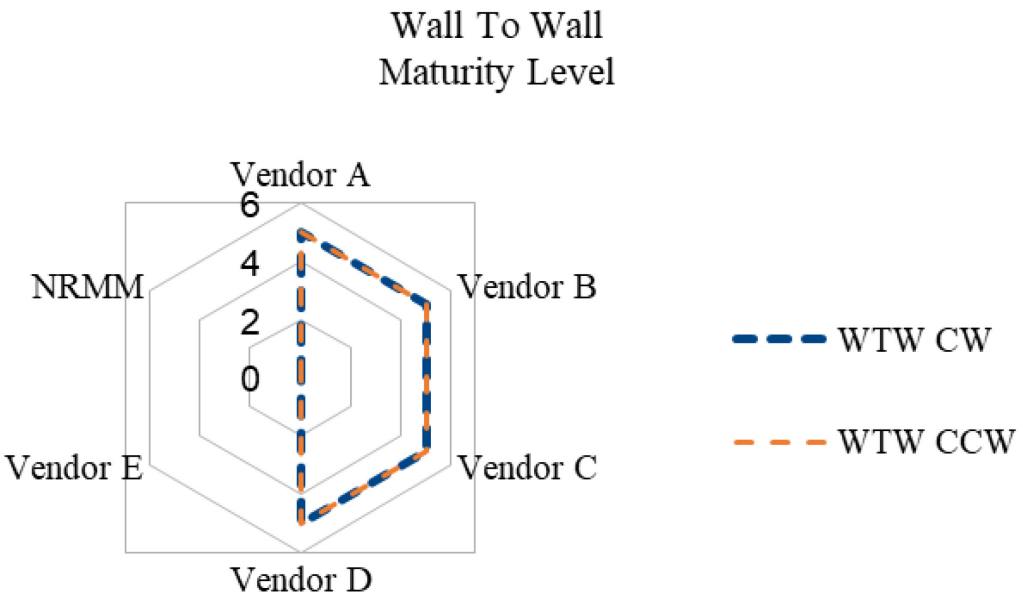


Figure 8A-8: Wall-To-Wall Maturity Level Achieved by Vendors.

8A.6.2 Steady-State Cornering

The steady-state cornering event is specified to be performed with limited and unlimited power, see Figure 8A-9 for results. Vendor C has conducted the unlimited power event, but not the limited power event.

For the unlimited power event the vendors have obtained comparable results, whereas the limited power results are scattered. Nonetheless, Vendors A, B, C and D achieved a Level of 4 as seen in Figure 8A-10. The scores are given based on the average result.

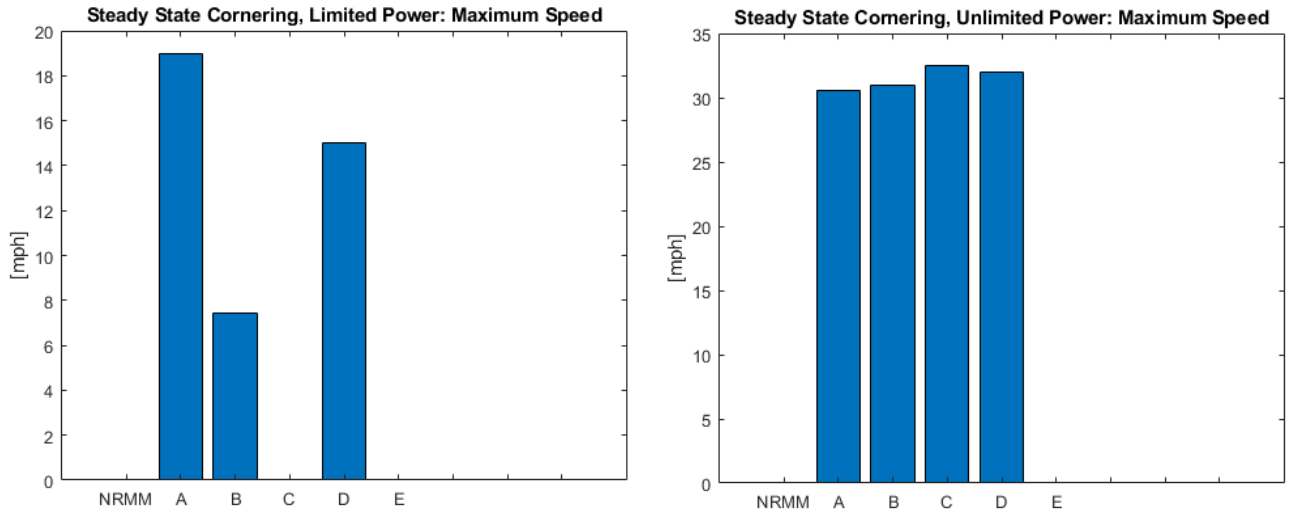


Figure 8A-9: Steady-State Cornering Limited Power (Left) and Unlimited Power (Right): Maximum Speed.

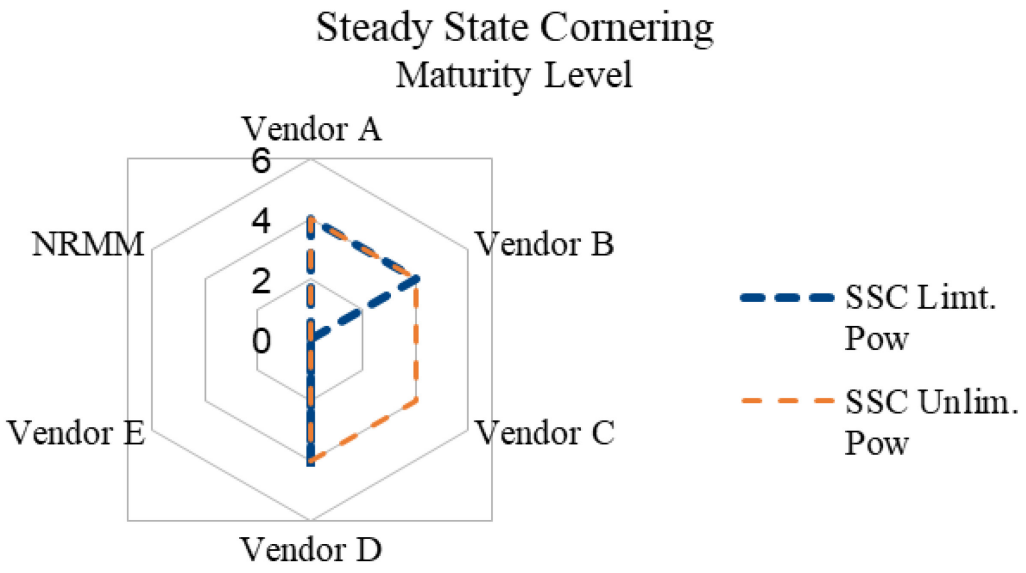


Figure 8A-10: Steady-State Cornering Maturity Level Achieved by Vendors.

8A.6.3 Double Lane Change

The double lane change event is performed on paved and gravel. Figure 8A-11 shows the results of the events.

Vendor B has performed the double lane change with limited power, whereas the remaining vendors have performed the analysis with unlimited power. Vendor D has obtained results for both unlimited and limited power; Figure 8A-12 shows the results of the unlimited study.

Each vendor was scored based on the average maximum speeds achieved during the double lane change maneuver resulting in Maturity Level 4 for Vendors A, C and D and Level 2 for Vendor B, since the result obtained by Vendor B deviates by more than 50% compared to the average result. It is possible that Vendor B could reach Level 4 if the event was simulated with unlimited power.

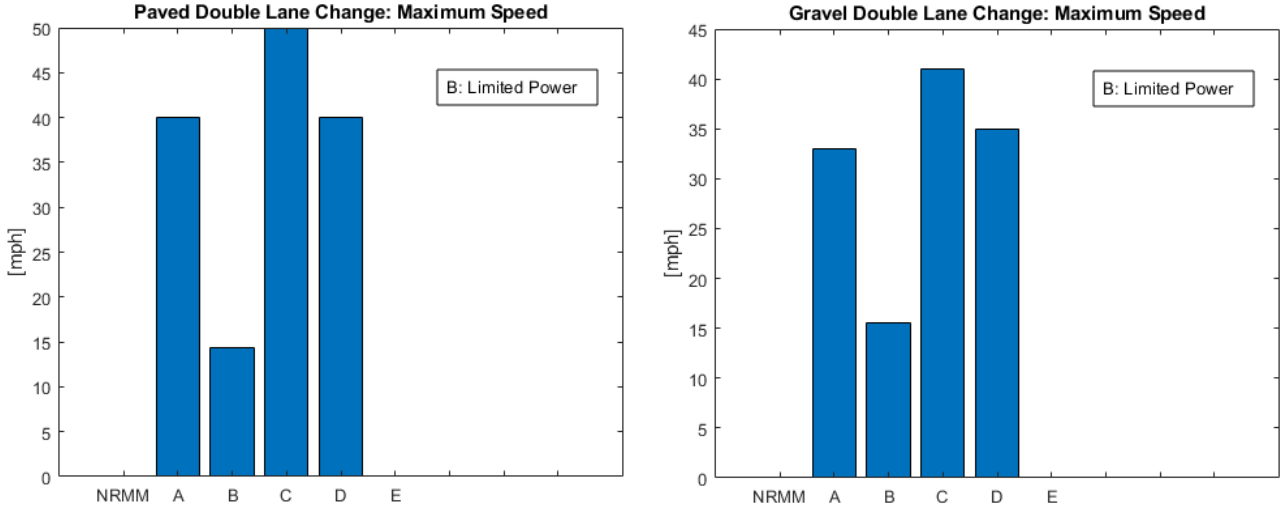


Figure 8A-11: Double Lane Change Paved (Left) and Gravel (Right): Maximum Speed.

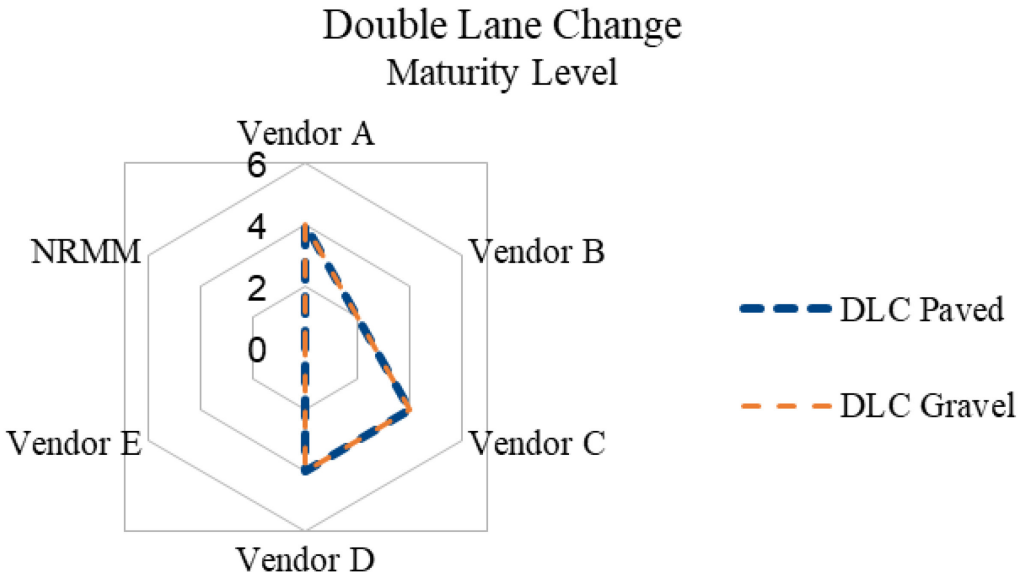


Figure 8A-12: Double Lane Change Maturity Level Achieved by Vendors.

8A.6.4 Side Slope Stability

The side slope stability analysis is implemented on paved and deformable terrain, as shown in Figure 8A-13.

The results obtained by the vendors agree for the deformable terrain, whereas ambiguous results were achieved for the paved event. This results in the Maturity Levels seen in Figure 8A-14. Comparing the paved results to the average result reveals that despite of the scattered paved results, no vendors have provided results that deviates more than 50% compared to the average result.

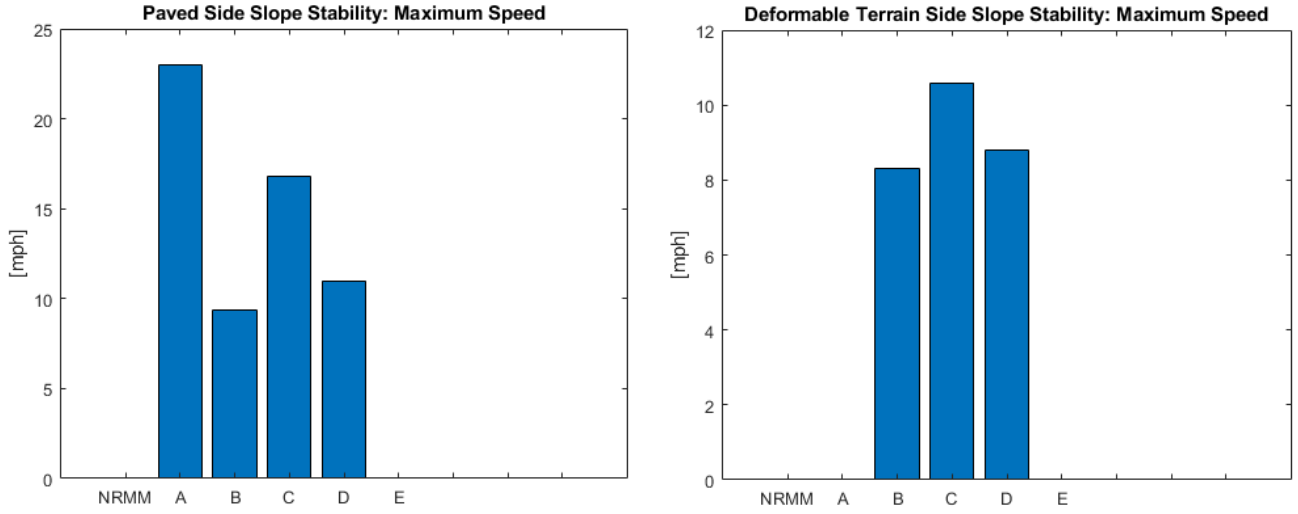


Figure 8A-13: Side Slope Stability Paved (Left) and Deformable Terrain (Right): Maximum Speed.

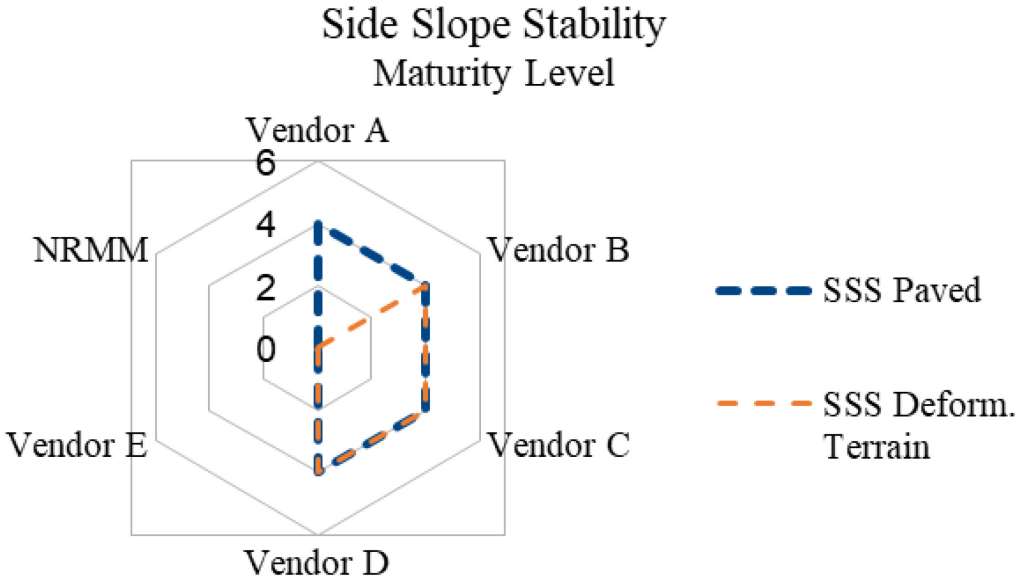


Figure 8A-14: Side Slope Stability Maturity Level Achieved by Vendors.

8A.6.5 Grade Climbing

The grade climbing analyses are specified to include maximum steerable up and down slope and a straight maximum speed on grades up to the maximum steerable slope uphill for both paved and deformable terrain. Vendors A and B have tested slopes up to 30% whereas Vendors C and D performed the analyses until failure.

Figure 8A-15 shows the highest obtained uphill slopes, where the vendors were able to maneuver the vehicle around an obstacle within 30 meters. Given that not all vendors have conducted the analyses on slopes until failure, there is a possibility of a higher true maximum slope for Vendors A and B. The resulting Maturity Levels are depicted in Figure 8A-16. The vendors have generally scored higher in the paved event, where all participating vendors have achieved Level 4.

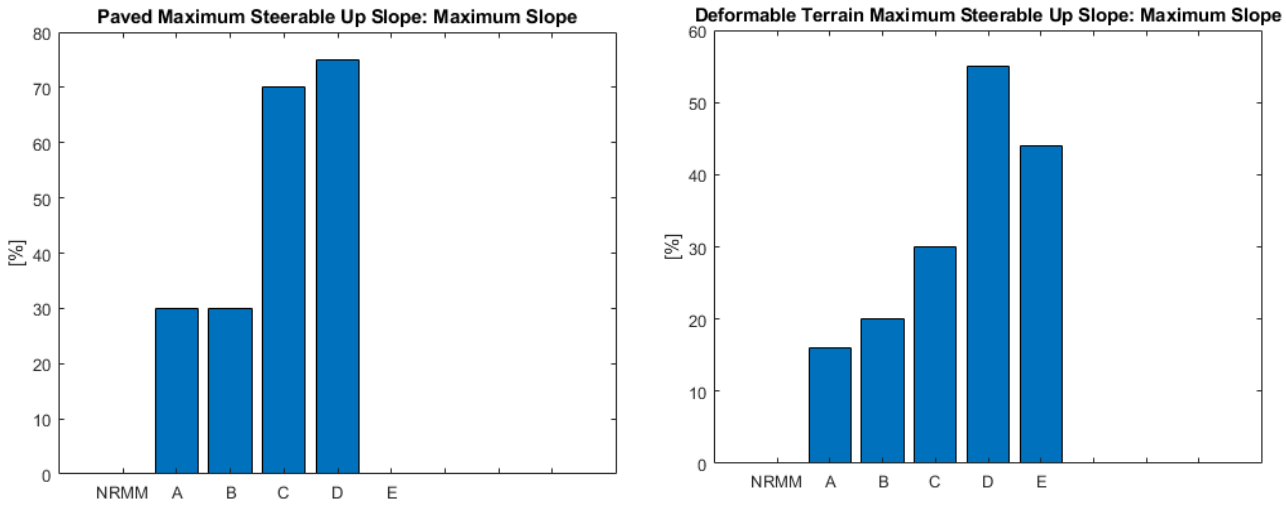


Figure 8A-15: Maximum Steerable Up Slope Paved (Right) and Deformable Terrain (Left): Maximum Slope.

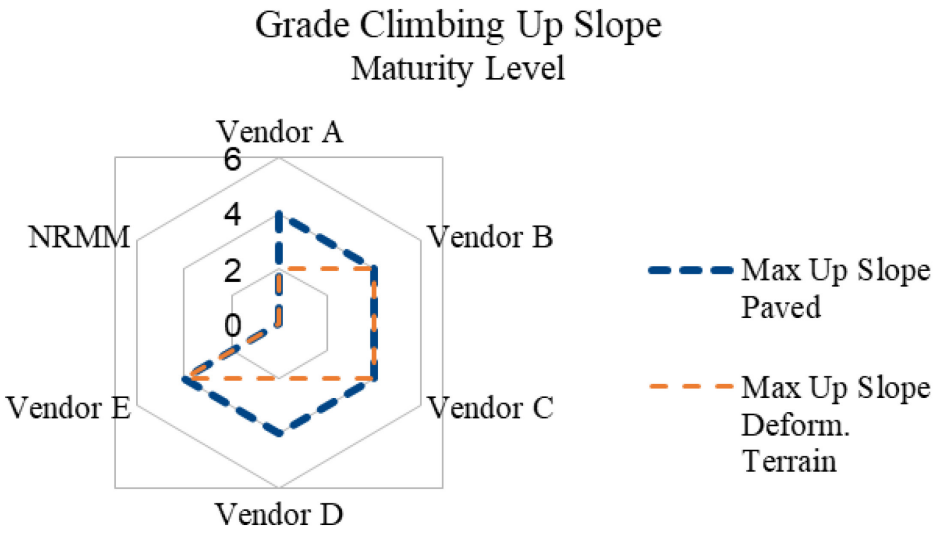


Figure 8A-16: Grade Climbing Up Slope Maturity Level Achieved by Vendors.

The down slope event on deformable terrain has been performed by fewer vendors as only Vendors B, C and D have provided results.

The grade climbing down slope results are shown in Figure 8A-17. Vendors D and C have performed the analysis on slopes up to failure. All vendors that have performed the down slope event have achieved the maximum Level of 4 as shown in Figure 8A-18.

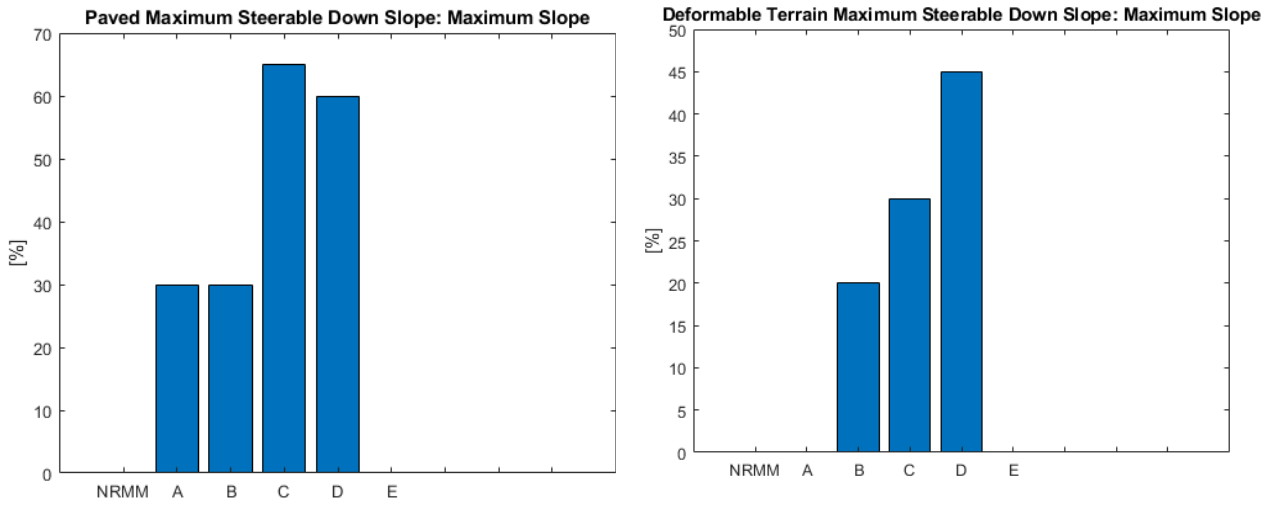


Figure 8A-17: Maximum Steerable Down Slope Paved (Left) and Deformable Terrain (Right): Maximum Slope.

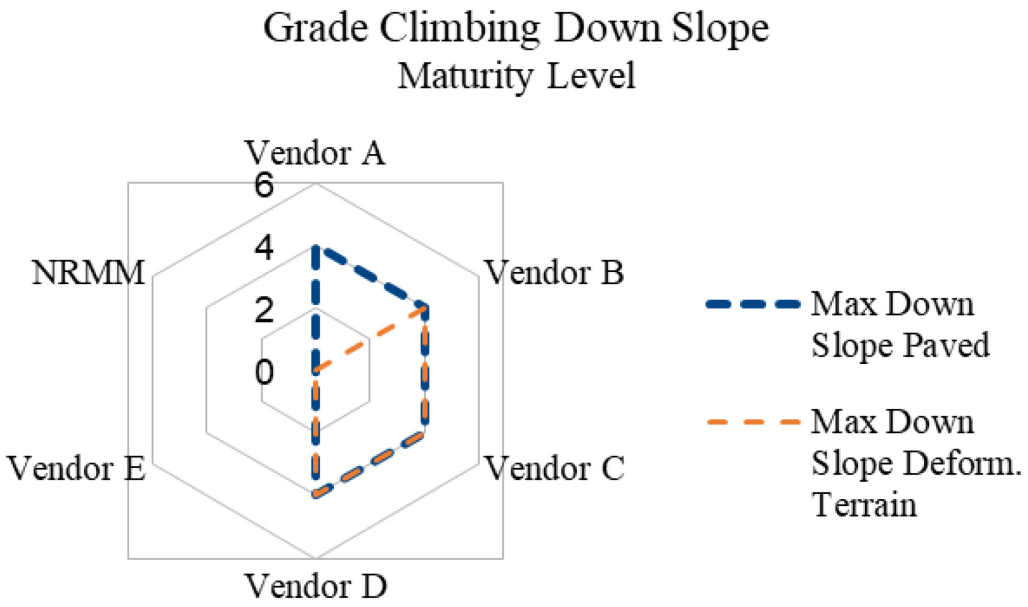


Figure 8A-18: Maximum Steerable Down Slope Paved (Left) and Deformable Terrain (Right): Maximum Slope.

Vendors A and D have performed a straight maximum speed analysis for increasing slopes. This event tests the maximum speed of the vehicle without negotiating an obstacle. Figure 8A-19 shows the maximum speed on the paved slope and Figure 8A-20 shows the maximum speed on the deformable terrain slope. Vendor B has delivered maximum steerable speeds for negotiating the obstacle, but not any maximum straight speeds.

Only Vendors A, C and D have performed the maximum speed on grade event, but all results are within the |50% limit of the average result, hence the three vendors reached Level 4. See Figure 8A-21.

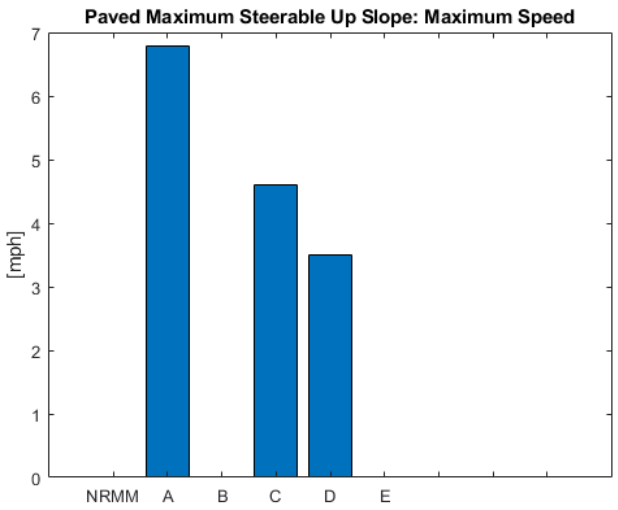


Figure 8A-19: Straight Maximum Speed from Up Slope Paved: Maximum Speed.

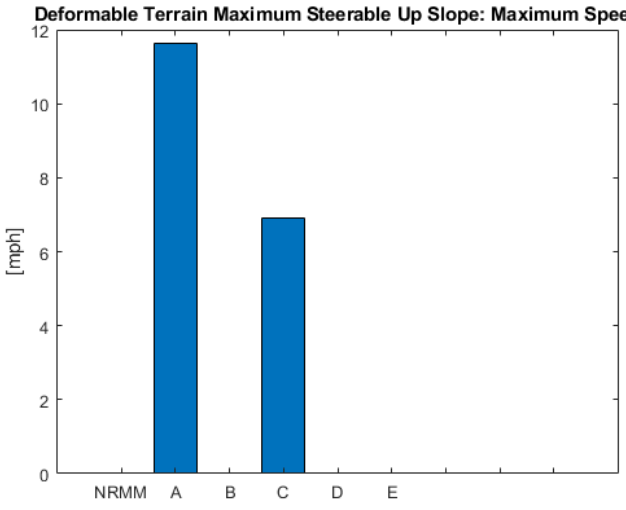


Figure 8A-20: Straight Maximum Speed from Up Slope Deformable Terrain: Maximum Speed.

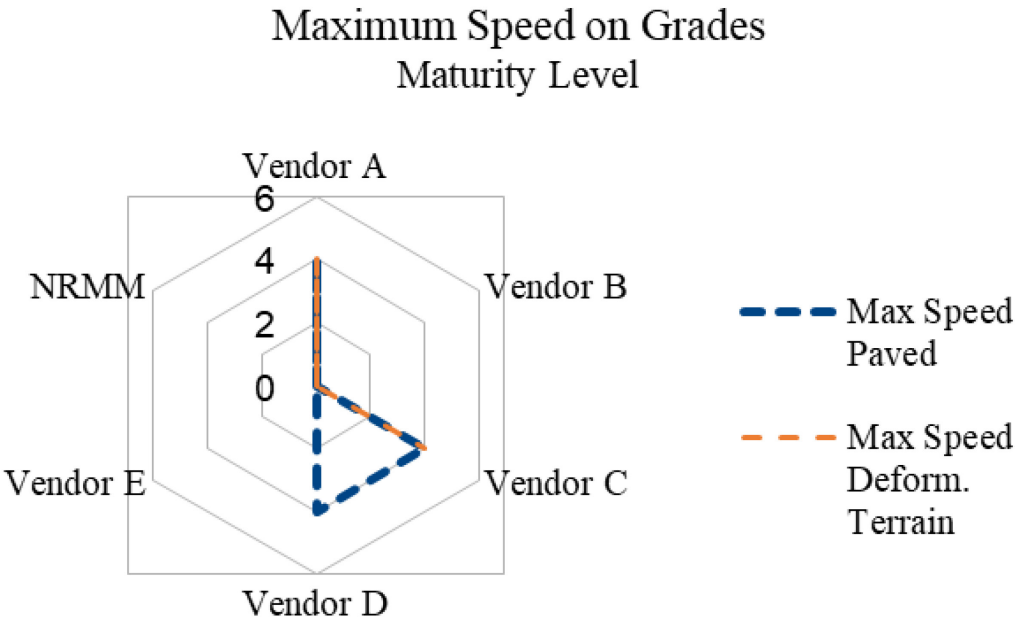


Figure 8A-21: Maximum Speed on Grades Maturity Level Achieved by Vendors.

8A.6.6 Random Terrain Ride

The ride quality event includes analyses of random terrain ride limiting speeds that are limited by 6 watt absorbed power at the driver seat location. The event is performed on varying terrain heights until the limiting factor is achieved.

Most vendors have conducted the random terrain height events; Figure 8A-22 and Figure 8A-23 show that the results agree well. Vendor C overestimated the limiting speed compared to the average result, while NRMM underestimated the limiting speed compared to the average. NRMM achieved a Maturity Level of 2, while the remaining vendors that provided a result achieved Level 4, as shown in Figure 8A-24.

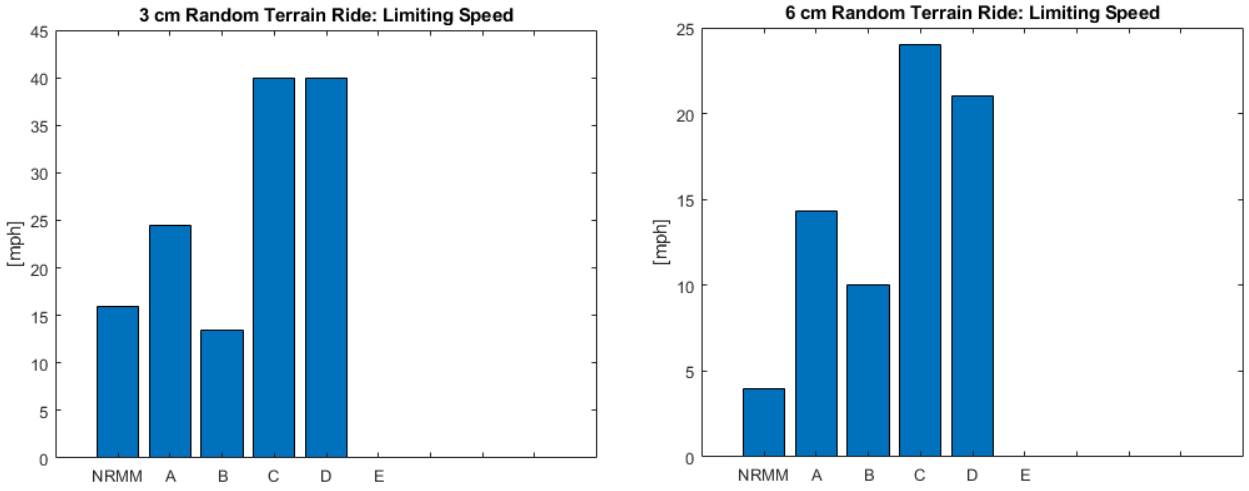


Figure 8A-22: Random Terrain Ride 3 cm RMS (Left) and 6 cm RMS (Right): Limiting Speed.

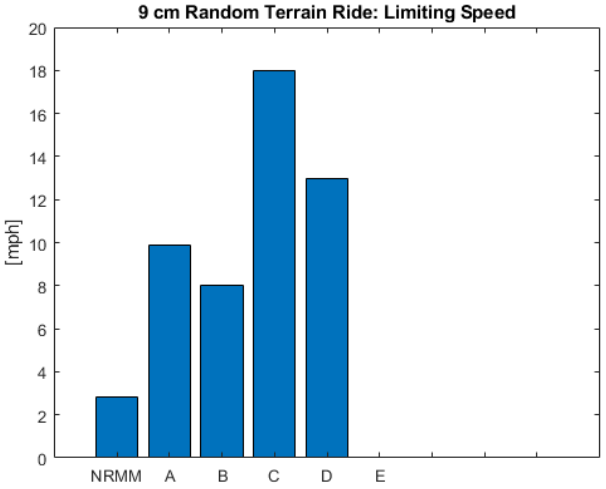


Figure 8A-23: Random Terrain 9 cm RMS: Limiting Speed.

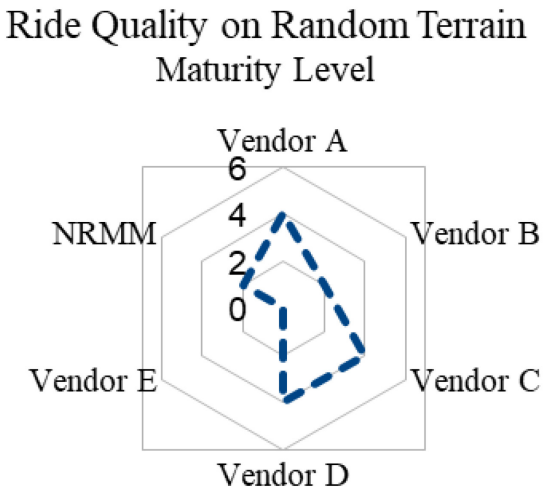


Figure 8A-24: Ride Quality on Random Terrain Maturity Level Achieved by Vendors.

8A.6.7 Half Round Obstacle

The half round obstacle rides are limited by a 2.5G acceleration at the driver seat location. The event is performed on varying terrain obstacles until the limiting factor is achieved. The half round obstacle events have been performed by most of the vendors. Vendor A, however, has only provided results for the 8 – 12 inch obstacles (Figure 8A-25, Figure 8A-26, Figure 8A-27).

Vendor A only provided results for the 8 – 12 inch half round and generally overestimated the limiting speeds when comparing to the other results. The remaining vendors have provided results that are more in agreement. The NRMM results are comparable to Vendors B, C and D. The Maturity Levels (Figure 8A-28) show that Vendor A has obtained Maturity Level 2, while Vendors B, C, D and NRMM have acquired Level 4 based on the average result.

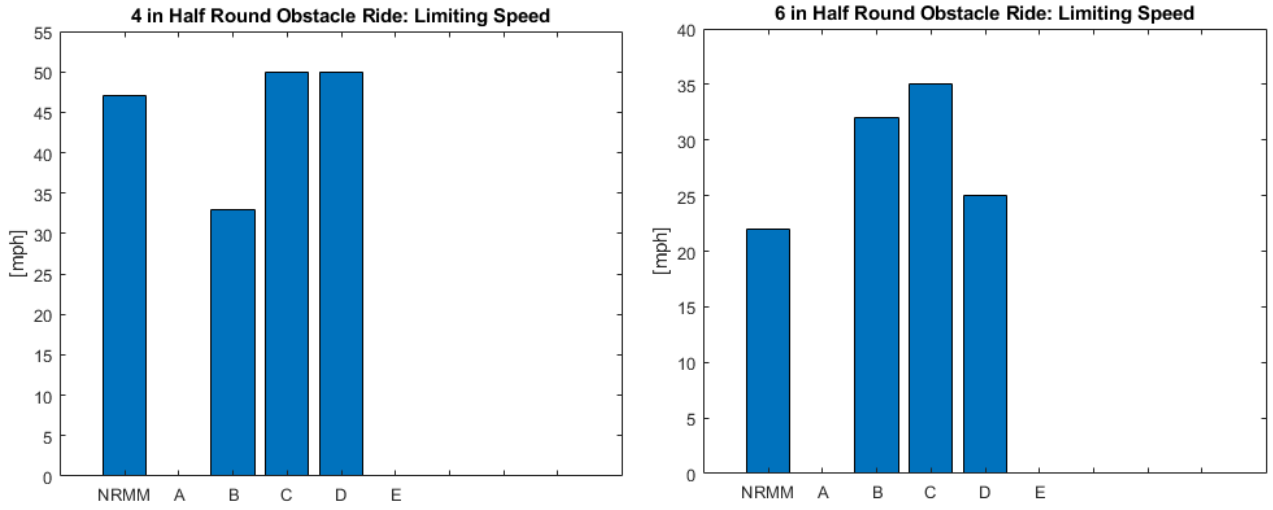


Figure 8A-25: Half Round Obstacle 4 Inch (Left) and 6 Inch (Right): Limiting Speed.

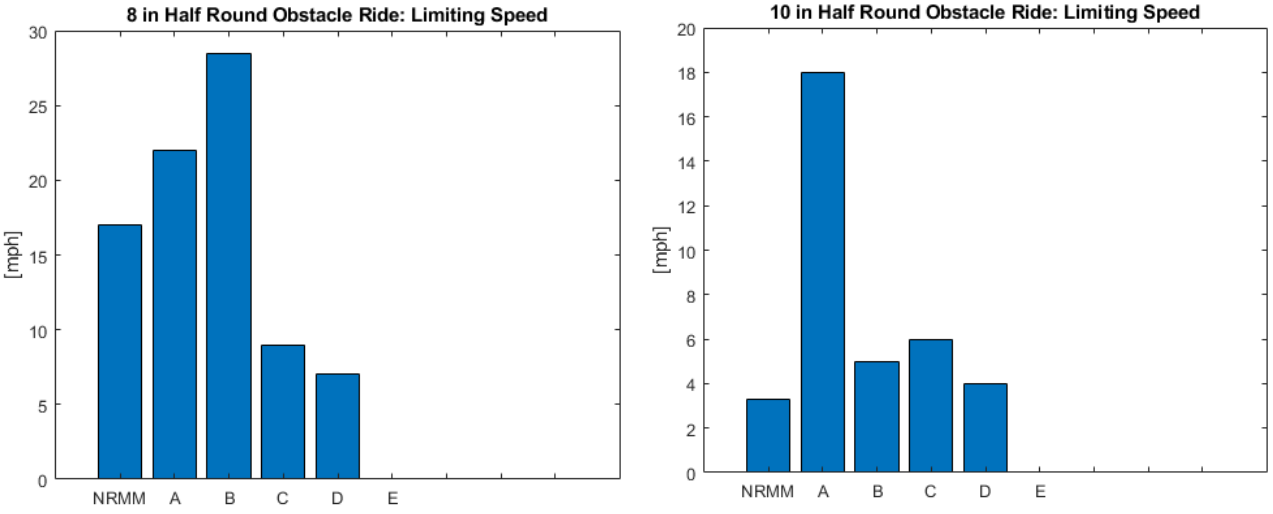


Figure 8A-26: Half Round Obstacle 8 Inch (Left) and 10 Inch (Right): Limiting Speed.

8A.6.8 Step and Gap Obstacle Negotiation

The step climb and the gap crossing events have been performed by all vendors, except Vendor E and NRMM. Test data is available for both the step climb and the gap crossing event.

Vendor D has performed both analyses with a power limited vehicle and Vendor B performed the gap crossing limits analysis with a traction limited vehicle, shown in Figure 8A-29. The remaining results are obtained with a power unlimited vehicle, but the result are comparable. This is also depicted in the Maturity Levels, Figure 8A-30, since all vendors, that have performed the event, have been given the maximum Maturity Level of 5.

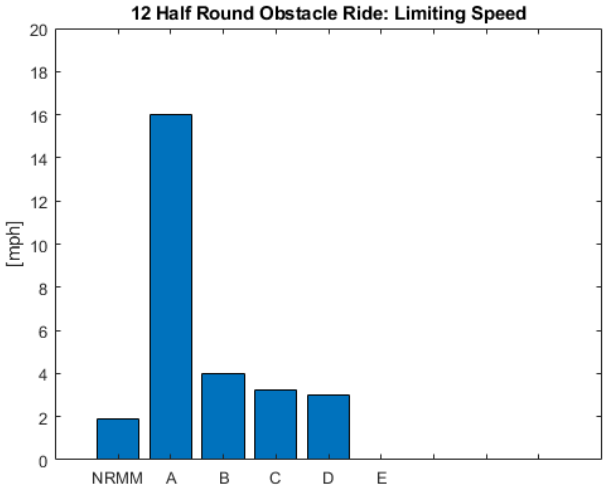


Figure 8A-27: Half Round Obstacle 12 Inch: Limiting Speed.

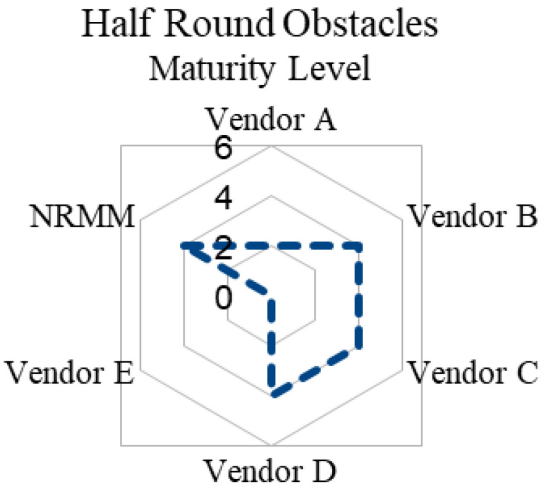


Figure 8A-28: Half Round Obstacles Maturity Level Achieved by Vendors.

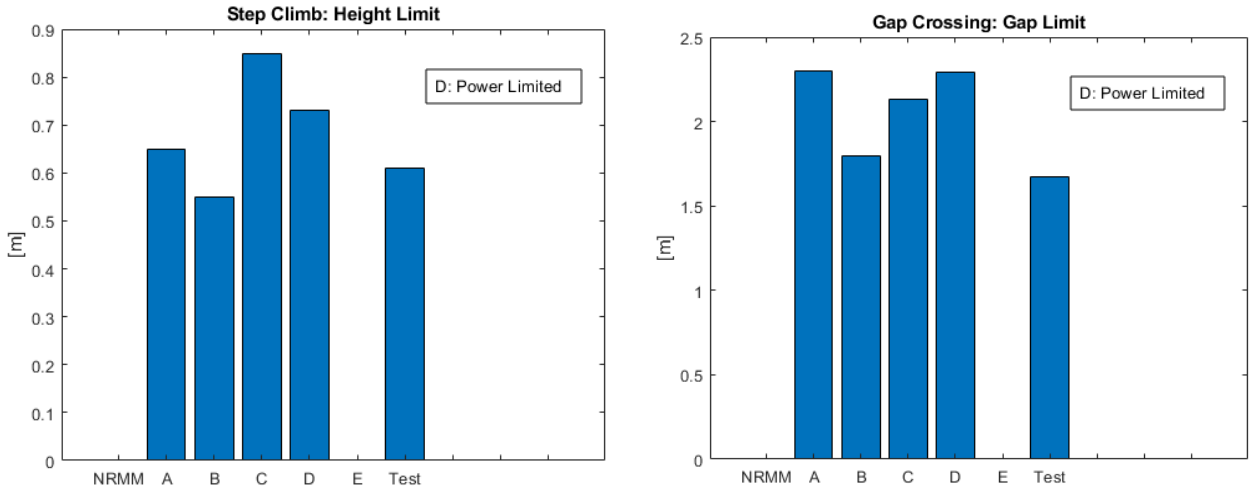


Figure 8A-29: Step Climb Height Limit (Left) and Gap Crossing Limits (Right): Height/Gap Limit.

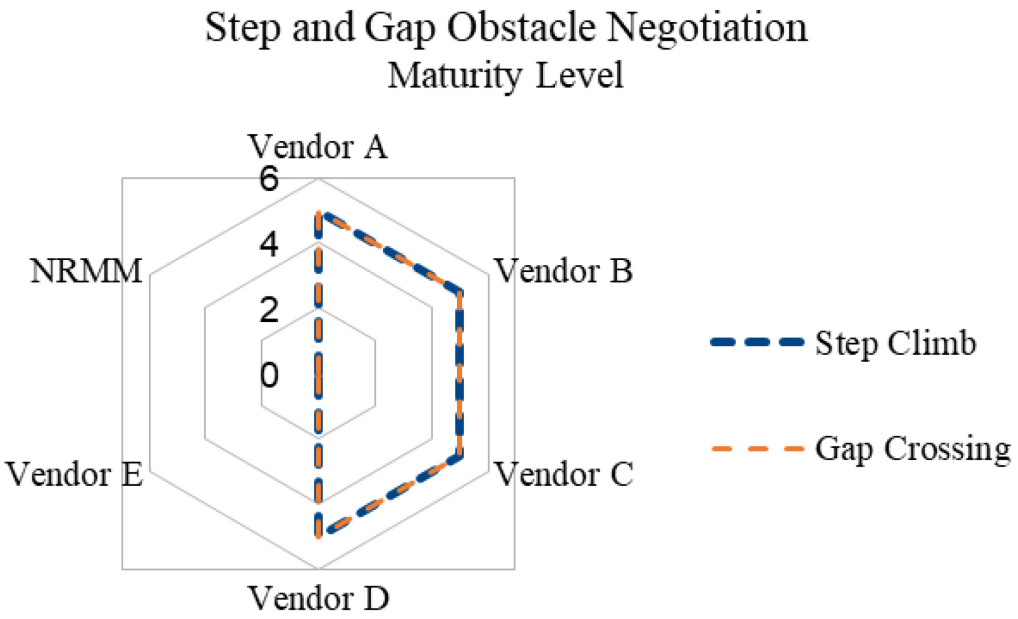


Figure 8A-30: Step and Gap Obstacle Negotiation Maturity Level Achieved by Vendors.

8A.6.9 Trapezoidal Obstacle Negotiation

The results of the trapezoidal fixed barrier limits and trapezoidal ditch crossing limits are depicted in Table 8A-7 and Table 8A-8.

Table 8A-7: Trapezoidal Fixed Barrier Limits. S = Successful, F = Failed, NR = No Results.

	1	2	3	4	5	6	7	8	9	10	11	12
NRMM	S	S	S	F	S	S	S	S	S	S	S	S
A	S	S	S	S	S	S	S	S	S	S	S	S
B	S	S	S	F	S	S	S	F	S	S	S	F
C	S	S	S	S	S	S	S	S	S	S	S	S
D	S	S	S	S	S	S	S	S	S	S	S	S
E	NR	NR	NR	NR	NR	NR	NR	NR	NR	NR	NR	NR

The trapezoidal fixed barrier limits and the trapezoidal ditch crossing limits both consist of 12 trapezoidal obstacles with varying slope angles (16 deg – 68 deg) and top/bottom widths (6 in – 140 in), that are either treated as a barrier or a ditch. If the vendor has succeeded, the table cell contains an S, and if the vendor has failed the analysis, the table cell contains an F. A table cell of NR means No Results. As can be seen in Table 8A-7 and in Table 8A-8, the vendors, including NRMM, have obtained results that agree. The Maturity Levels, Figure 8A-31 are based on the average result since no test data is available. The results agree, hence the vendors that have simulated the event have all obtained Level 4.

Table 8A-8: Trapezoidal Ditch Crossing Limits. S = Successful, F = Failed, NR = No Results.

	1	2	3	4	5	6	7	8	9	10	11	12
NRMM	S	S	S	S	S	S	S	S	S	S	S	F
A	S	S	S	S	S	S	S	S	S	S	S	S
B	S	S	S	S	S	S	S	S	S	S	S	S
C	S	S	S	S	S	S	S	S	S	S	S	F
D	S	S	S	S	S	S	S	S	S	S	S	F
E	NR	NR	NR	NR	NR	NR	NR	NR	NR	NR	NR	NR

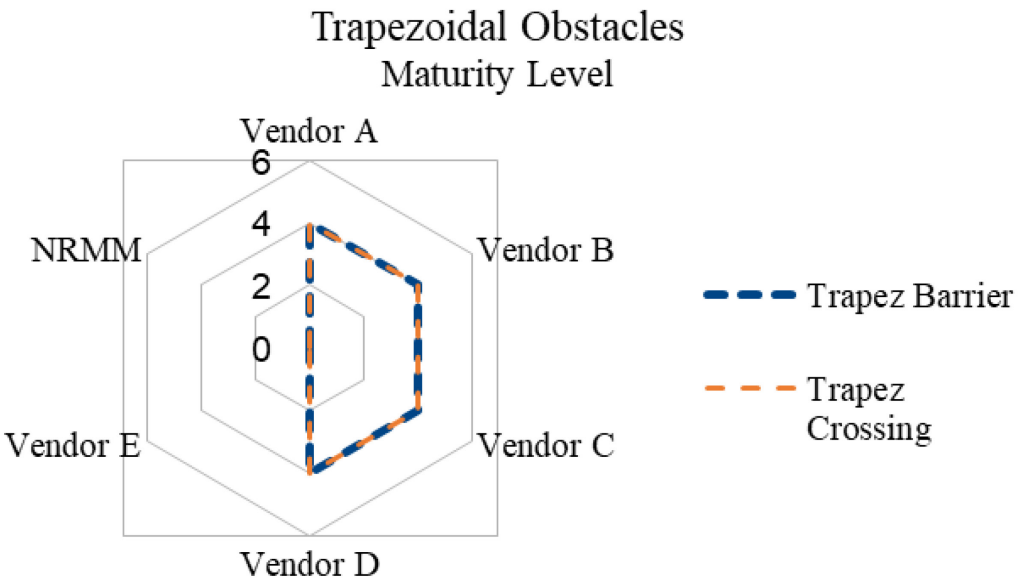


Figure 8A-31: Trapezoidal Obstacles Maturity Level Achieved by Vendors.

8A.6.10 Off-Road Trafficability

The results of the off-road single and multi-pass traverses are depicted in Figure 8A-32.

Vendor D has attempted both the single pass and the multi-pass traverse event but has not been able to obtain a soil limit in either event. Likewise, Vendor E has conducted the single pass event without achieving a limit but has not attempted the multi-pass event. This result in a sparse Maturity Level plot, Figure 8A-33, where the maximum achievable level is 2, since a cross code verification has not been possible.

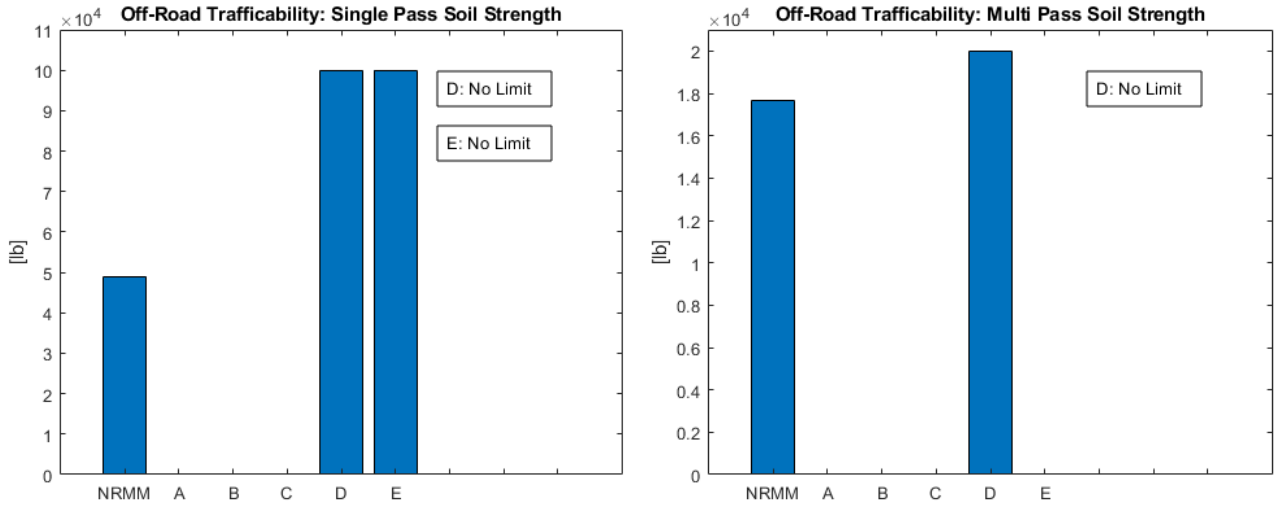


Figure 8A-32: Single (Left) and Multi (Right) Pass: Soil Strength Limit.

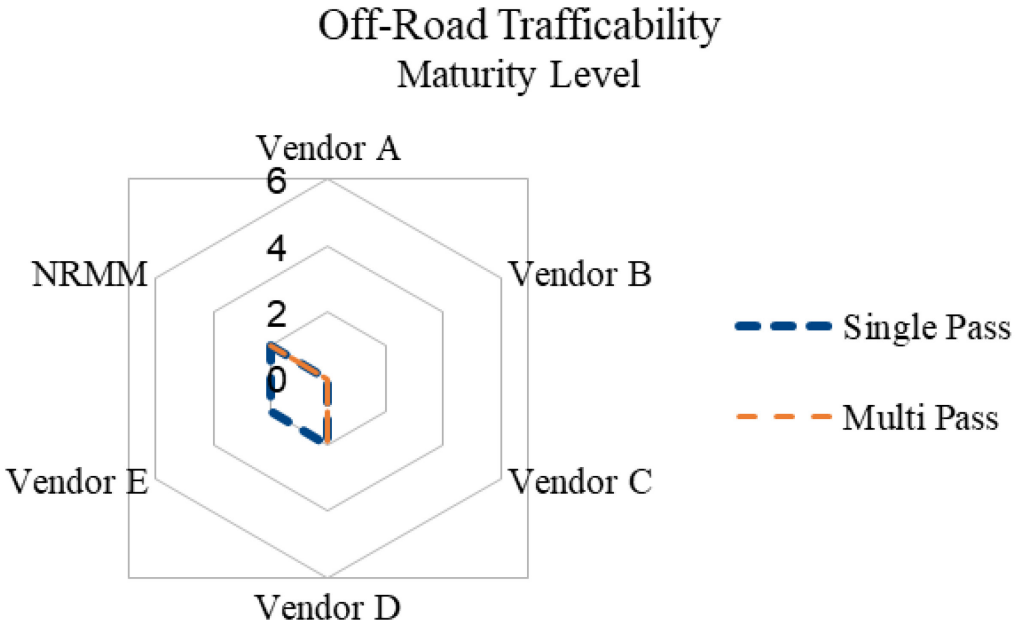


Figure 8A-33: Off-Road Trafficability Maturity Level Achieved by Vendors.

8A.6.11 Drawbar Pull

The drawbar pull event, Figure 8A-34, was analyzed by four vendors. Vendors D and E have comparable results as NRMM and have achieved Maturity Level 5 based on the calibration data (Figure 8A-35). The result provided by Vendor A is not close to the test data; however, the result is within the 50% limit, hence vendor A is also judged as Level 5.

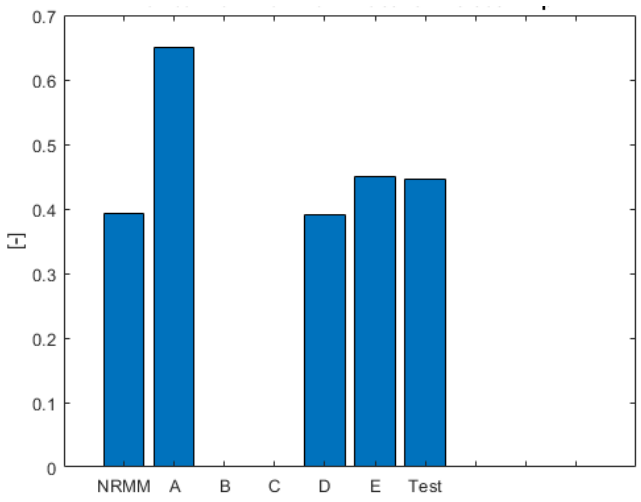


Figure 8A-34: Drawbar Pull 2 Mph: Drawbar Pull Coefficient.

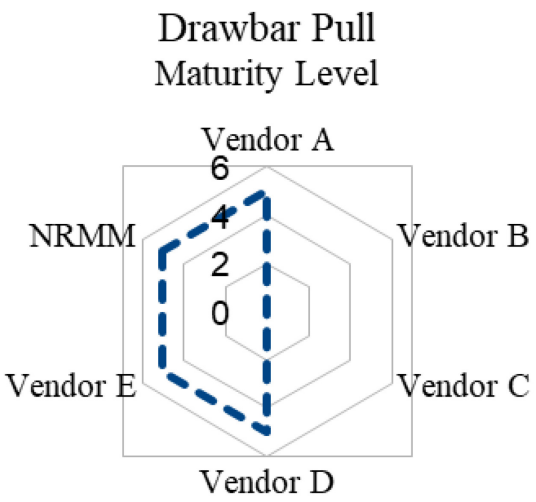


Figure 8A-35: Drawbar Pull Maturity Level Achieved by Vendors.

8A.6.12 Motion Resistance

The motion resistance events, Figure 8A-36, have been conducted by Vendors A, D and NRMM.

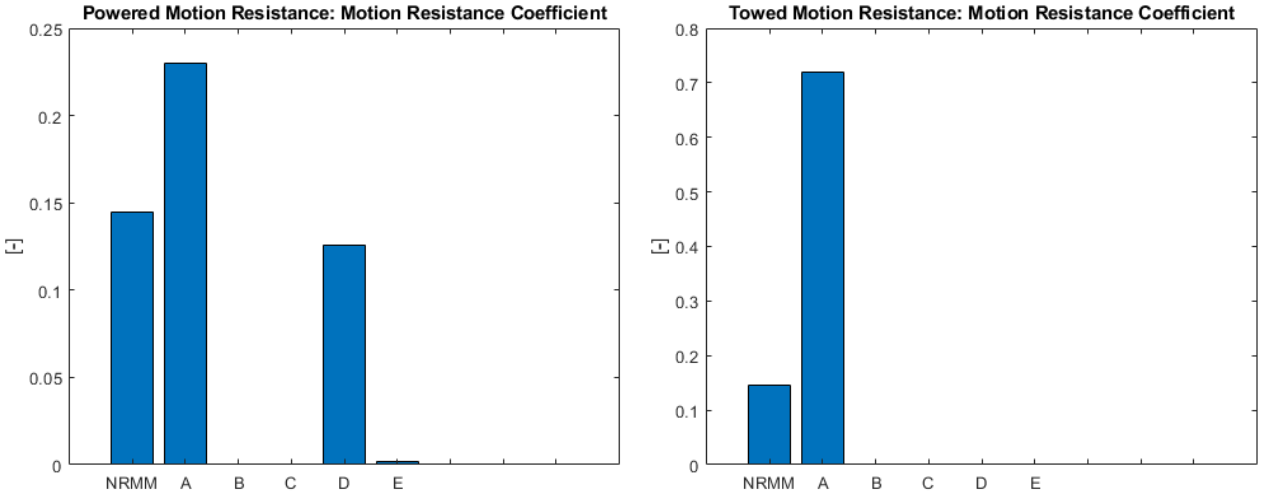


Figure 8A-36: Motion Resistance Powered (Left) and Towed (Right): Motion Resistance Coefficient.

The motion resistance analyses have resulted in ambiguous results. The result obtained by Vendor E in the powered analysis is very low compared to the remaining results. The analyses of the towed vehicle lead to two very different results. This is seen in the Maturity Levels, Figure 8A-37, that are varying between 2 and 4 based on the average result. For the towed result only two vendor results are available, allowing for a maximum Level of 4, but due to different results, the two vendors have both achieved Level 2. For the powered event, Vendor D and NRMM have both obtained Level 4, whereas Vendors A and E have reached Level 2 based on the average result.

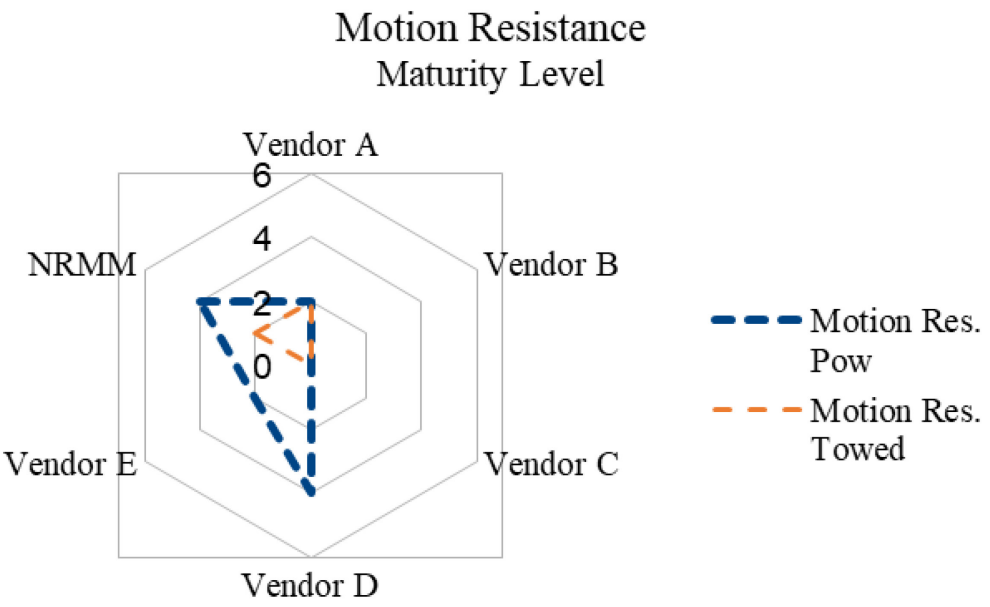


Figure 8A-37: Motion Resistance Maturity Level Achieved by Vendors.

8A.6.13 Closed-Loop Traverse/Fuel Economy

The fuel economy analyses include on-road and off-road studies. Vendors A and D provided the results seen in Figure 8A-38.

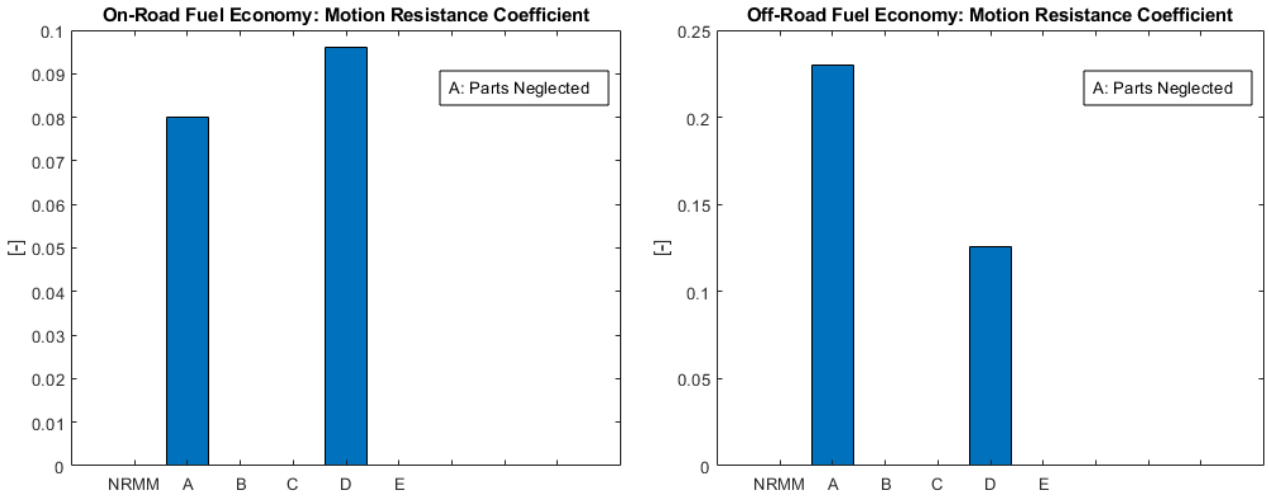


Figure 8A-38: Fuel Economy On-Road (Left) and Off-Road (Right): Motion Resistance Coefficient.

Vendor A has neglected turning effects as well as the acceleration and deceleration parts of the loop, affecting the results shown in Figure 8A-38. Figure 8A-39 show the Maturity Levels obtained by the vendors in the fuel economy event. Two vendors have provided a result, resulting in a maximum Maturity Level of 4, which the two vendors have achieved for both the on-road and off-road event. The scores are based on the average result.

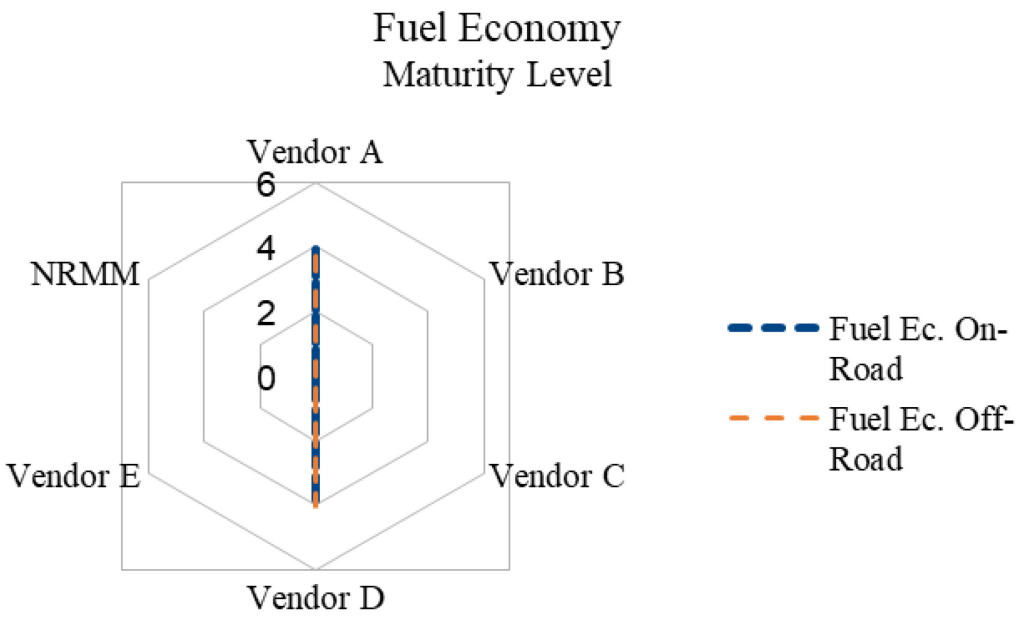


Figure 8A-39: Fuel Economy Maturity Level Achieved by Vendors.

8A.7 SUMMARY AND CONCLUSIONS

This section summarizes the main efforts of the tracked vehicle benchmark exercise. Based on the Maturity Scale definition in Table 8A-1 the tracked vehicle benchmark was performed. In Figure 8A-40, Figure 8A-41, Figure 8A-42, and Table 8A-9, the submitted benchmark results maturity were scored. The number of submissions were limited which has an impact on how the Maturity Scale can be applied. In an event where there was only one vendor providing a result, it forces the Maturity Level back to 2, except where test data is available (Level 6 possible). Where one vendor could be compared to at least one other, the Maturity Level achieved was 4. The percent on the score column is always with respect to the average of the results of all vendors submitting results, except where a result was identified as an outlier. When counting points for the score of events, a single hard surface test event yielded one point and a single soft soil test event yielded two points to emphasize the importance of the soft soil mobility aspect for the NG-NRMM effort.

	Max Possible Ranking Score	Max Achievable Maturity Level	Industry Achieved Maturity
Total score	88	4.11	3.89
Score Hard Surface	59	4.10	4.10
Score Soft Soil	29	4.14	3.29

	Participant/Vendor					
	NRMM	A	B	C	D	E
Total Score	44%	68%	59%	50%	90%	9%
Score Hard Surface	50%	81%	78%	71%	92%	0%
Score Soft Soil	31%	41%	21%	7%	86%	86%

Figure 8A-40: Scoring based on Maturity Scale. Note, the Score is Primarily Based on Submission, not Values.

A Maturity Level of 4 is achievable in most of the tracked vehicle results, where no test data is available. It is judged to have been achieved by the vendors who predicted comparable results to a known physical principle, or, in the absence of that, the mean of all submitted results. An industry wide Maturity Level is assigned based on the maximum achieved across all vendors. A high level summary of all results was provided in Figure 8A-40.

These results show that at least one vendor was able to demonstrate the maximum Maturity Level for each event, except for the single pass and multi-pass trafficability as well as motion resistance events. Thus the most significant challenge for most vendors was the soft soil events. Nevertheless, one vendor demonstrated an 85% score on soft soil events. A unit score point was possible for each individual event result on hard surfaces, two points per event for each soft soil result, and double points were awarded for events with test data (Levels 5 – 7).

The general conclusion is that the vehicle dynamics M&S software developers, as an industry, do have the mature capability to predict most of the required events identified by the NG-NRMM effort. Furthermore, by virtue of its 2D theoretical basis, the NRMM model falls short in events requiring 3D modeling for maneuvering. It is also noted that soft soil modeling for the 3D transient dynamics simulation is in need of tailored soil characterization data dedicated to this purpose, in order to rigorously demonstrate Maturity Level of 6 and above.

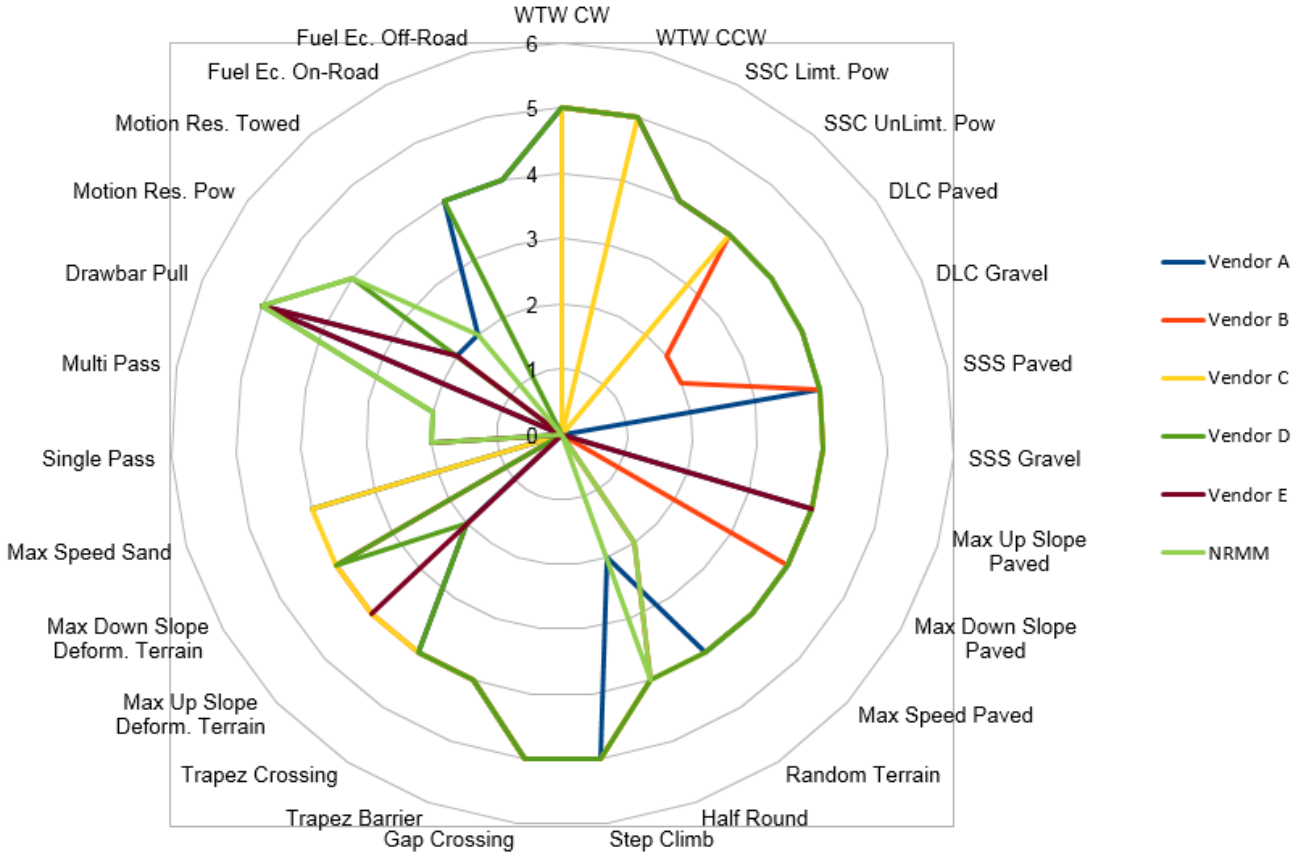


Figure 8A-41: Tracked Vehicle Maturity Level.

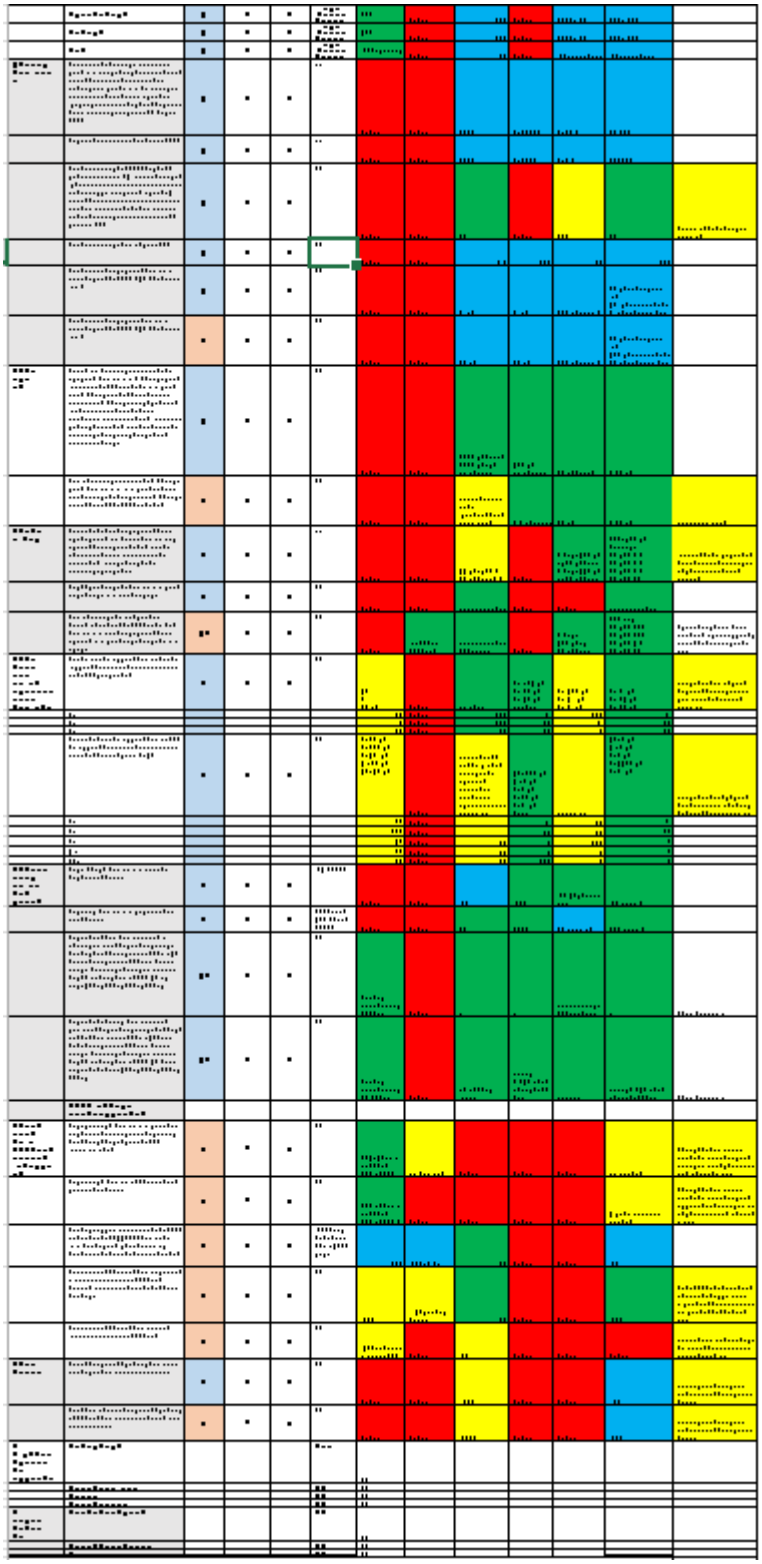


Figure 8A-42: Participant Simulation Maturity Level.

Table 8A-9: Tracked Vehicle Benchmark Maturity Levels.

SIMULATION		NRMM	A	B	C	D	E
Sprocket Height		4	4	4	-	4	-
Idler Height		4	4	4	-	4	-
Pitch		-	4	4	-	4	-
Wall-to-Wall Turn Radius	Clockwise	-	6	6	6	6	-
	Counterclockwise	-	6	6	6	6	-
Steady-State Turning Speed	Limited Power	-	4	4	-	4	-
	Unlimited Power	-	4	4	4	4	-
Double Lane Change Speed	Paved	-	4	2	4	4	-
	Gravel	-	4	2	4	4	-
Side Slope Stability Speed	Paved	-	4	4	4	4	-
	LETE Sand	-	-	4	4	4	-
Max Steerable Up Slope	Paved	-	4	4	4	4	4
	LETE Sand		2	4	4	2	4
Max Steerable Down Slope	Paved	-	4	4	4	4	-
	LETE Sand	-	-	4	4	4	-
Straight Max Speed	Paved	-	4	-	4	4	-
	LETE Sand	-	4	-	4	-	-
Random Terrain Ride Limiting Speed		2	4	2	4	4	-
Half Round Obstacle Limiting Speed		4	2	4	4	4	-
Step Climb Height Limit			6	6	6	6	-
Gap Crossing Limit		-	6	6	6	6	-
Trapezoidal Fixed Barrier Limits		-	4	4	4	4	-
Trapezoidal Ditch Crossing Limits		-	4	4	4	4	-
Single Pass Soil Strength Limit		2	-	-	-	2	2
Multi-Pass Soil Strength Limit		2	-	-	-	2	-
Drawbar Pull		6	6	-	-	6	6
Motion Resistance	Powered	4	2	-	-	4	2
	Towed	2	2	-	-	-	-
Fuel Economy	On-Road	-	4	-	-	4	-
	Off-Road	-	4	-	-	4	-

8A.8 REFERENCES

[1] Meintjes, K. 1995. Simulation Governance. NAFEMS Conference, Troy MI.

[2] AVTP 03-30. 1991. Steering and Maneuverability. September 1991.

[3] SAE J266. 1996. Steady-State Directional Control Test Procedures for Passenger Cars and Light Trucks. January 1996.

[4] AVTP 03-160W. 1991. Dynamic Stability. September 1991.

[5] TOP 2-2-610. 1980. Gradeability and Side Slope Performance. July 1980.

[6] Wong, J.Y., Garber, M. and Preston-Thomas, J. 1984. Theoretical Prediction and Experimental Substantiation of the Ground Pressure Distribution and Tractive Performance of Tracked Vehicles. Proceedings of the Institution of Mechanical Engineers, Part D, Transport Engineering, 198:265-285.

[7] ISO 8608:2016. Mechanical Vibration – Road Surface Profiles Reporting of Measured Data.

[8] TOP 1-1-014. 2007. Ride Dynamics. October 2007.

[9] TOP 2-2-611. 1980. Standard Obstacles. June 1980.

[10] AVTP 03-170. 1993. Suspension Performance. October 1993.

[11] TOP 2-2-604. 2007. Test Operation Procedure: Drawbar Pull. September 2007.

[12] AVTP 03-10. 1991. Fuel and Oil consumption.

[13] Conner, C. 2018. Armored Personnel Carrier. http://afvdb.50megs.com/usa/m113.html. Accessed November 2018.

[14] Bekker, M.G. 1960. Off-the-Road-Locomotion, Ann Arbor, The University of Michigan Press.

[15] Bekker, M.G. 1969. Introduction to Terrain-Vehicle Systems, Ann Arbor, The University of Michigan Press.

[16] Wong, J.Y., Reece, A. 1967. Prediction of Rigid Wheel Performance Based on the Analysis of Soil-Wheel Stresses Part I, Performance Driving Rigid Wheels, Journal of Terramechanics, 4, 81-98.

[17] Wong, J.Y. 1993. Theory of Ground Vehicles, Second Edition, John Wiley & Sons, Inc.

[18] Janosi, Z. Hanamoto, B. 1961. The Analytical Determination of Drawbar Pull as a Function of Slip for Tracked Vehicle in Deformable Soils, In Proceedings of the 1st Int. Conf. on Terrain-Vehicle Systems, Torino, Italy.

[19] Hegedus, E. 1960. A Simplified Method for the Determination of Bulldozing Resistance, Land Locomotion Research Laboratory, Army Tank Automotive Command Report, Vol. 61.

[20] Wanjii, S., Hiroma, T., Ota, Y., Kataoka, T. 1997. Prediction of Wheel Performance by Analysis of Normal and Tangential Stress Distributions under the Wheel-Soil Interface, Journal of Terramechanics, Vol. 34, No. 3, 165-186.

Chapter 8B – TA6: WHEELED VEHICLE PLATFORM VERIFICATION AND VALIDATION

Ole Balling
Aarhus University
DENMARK

Henry Hodges
Hodges Transportation, Inc.
UNITED STATES

Michael McCullough
BAE Systems Inc.
UNITED STATES

8B.1 GOALS AND TEAM MEMBERS

The objective of the Verification and Validation Thrust Area is to describe a framework for benchmarking the ability of software solutions to predict mobility performance and validate against available test data or perform cross code validation in case of lack of test data. It is intended as an open-ended Verification and Validation (V&V) effort as additional vehicles and benchmarking tests can be added as they become available.

The team members are listed below by country in alphabetical order:

- **Ole Balling, Leader**, Denmark;
- Tom von Sturm zu Vehlingen, Germany;
- Ozgen Akalin, Turkey;
- Henry Hodges, USA;
- Michael Letherwood, USA;
- Michael McCullough, USA; and
- Paramsothy Jayakumar, USA.

8B.2 INTRODUCTION

It is the goal of the V&V effort to establish a reliable and comprehensive analysis process of the mobility capabilities of off-road vehicles. This goal is achieved by means of modeling and computer simulation in connection with verification and validation with existing tests. In order to provide confidence in such models, well-known hard surface, high coefficient of friction vehicle dynamic performance events are performed at first, followed by low coefficient of friction events as well as soft soil mobility events. To the extent possible, these tests are rooted in existing test standards and technical operating procedures. A short description of these events is listed in Section 8B.4.

8B.3 PROCESS/METHODOLOGY

A challenge for the V&V team has been how to evaluate Modeling and Simulation capability of mobility capable software. To accomplish this task, the team has adopted and modified a Modeling and Simulation Maturity Scale as depicted in Table 8B-1 [1].

Table 8B-1: NG-NRMM Benchmark Modeling and Simulation Predictive Capability Maturity Levels.

1.	**DEMONSTRATION**: Demonstration of a correct implementation of a theoretically and conceptually consistent model.
2.	**PARAMETER SENSITIVITY DEMONSTRATION:** Verification that performance change with a change in system parameter such as GVW or terrain deformability is consistent with theory and physics principles.
3.	**INDEPENDENT USER VERIFICATION:** Independent user demonstration and correlation to vendor results.
4.	**CROSS CODE VERIFICATION:** Cross verification with another accepted mobility simulation code.
5.	**CALIBRATION:** Calibration to a real vehicle test data set.
6.	**VALIDATION:** Blind correlation to a real vehicle test data set.
7.	**PARAMETER VARIATION VALIDATION:** Blind correlation to a real vehicle test data set with a change in system parameter(s).

8B.4 WHEELED VEHICLE BENCHMARK EVENTS

The wheeled vehicle benchmark events are briefly described below. The differentials and transfer case are open for all tests unless otherwise specified.

8B.4.1 Paved Straight Line Acceleration (SLA)

The general guideline for the straight line acceleration event is outlined by TOP 2-2-602 [2]. The vehicle drives on a straight line path at full throttle starting in 1st gear. The path has a paved level surface with an allowed slope deviation of +/- 1% slope. The test is performed until maximum speed is attained.

8B.4.2 Wall-to-Wall Turn Radius (WTW)

The event is conducted in accordance with AVTP 03-30 [3]. At slow speed and maximum steer angle, the vehicle turns at least a full 360 degrees. The event traces the most overhanging points on the vehicle chassis or the tire, whichever is defining a vertical walled boundary, within which the vehicle can negotiate the turn.

8B.4.3 Steady-State Cornering (SSC)

SAE J2181 [4] serves as a general guideline for the steady-state cornering event. The vehicle drives on a paved circular path while slowly increasing speed in segments and attains steady-state in each segment. The path is a 200 ft constant radius circular path coinciding with the center of the front axle of the vehicle. The steering angle is adjusted to keep the vehicle on the constant radius path. The event is conducted in the clockwise and counterclockwise direction. The speed is increased until near loss of control of the vehicle.

8B.4.4 Paved Double Lane Change (DLC)

The event is performed as a double lane change following NATO test procedure AVTP 03-160 W [5] as a guide. The surface is paved, simulated as a friction coefficient of 0.8. The event is performed with constant

speed throughout the course and is repeated at increasing speeds. If the vehicle crosses the course boundaries, it has failed at the given speed. The event is conducted in two directions: Left Turn First (LTF) or Right Turn First (RTF).

8B.4.5 Gravel Double Lane Change (DLC)

The event is conducted as a double lane change following the Allied Vehicle Test Procedure AVTP 03-160 W [5] as a guide. The surface is gravel, with a coefficient of friction of 0.5. The event is performed with constant speed throughout the course and is repeated at increasing speeds. If the vehicle crosses the course boundaries, the event has failed at that given speed. The event is conducted in two directions: Left Turn First (LTF) or Right Turn First (RTF).

8B.4.6 Side Slope Stability (SSS)

The event is conducted with TOP 2-2-610 [6] as a guideline. The vehicle drives on a 30% side slope while performing a slalom maneuver. The event is repeated with increased speed until loss of control of the vehicle. The event is performed for both left and right side down slope.

8B.4.7 Sand Slope Gradeability (SSG)

The event is conducted with TOP 2-2-610 [6] as a guideline. The vehicle climbs an incline with a surface of dry sandy soft soil. The test continues until the vehicle obtains a steady-state speed. The test is repeated with increased slopes in increments of 5 degrees until a slope is tested at which the vehicle loses traction. The test is conducted with two different vehicle configurations: open and locked differentials.

8B.4.8 Ride Quality

The general guideline for the Ride Quality acceleration event is outlined by TOP-1-1-014 [7]. Four standardized Root Mean Square (RMS) ride quality courses are specified to simulate rough and uneven terrain. Each terrain is traveled by the vehicle at a constant speed. The test is repeated with increasing speeds until the absorbed power at the driver seat location exceeds 6 watts.

8B.4.9 Drawbar Pull

The general guideline for the drawbar pull event is outlined in TOP 2-2-604 [8]. The vehicle drives on a flat surface of dry sand soft soil with a towing force applied. The initial speed of the vehicle is 5 mph and the initial towing force is 0 N. The towing force is increased gradually until the vehicle loses traction, hence is immobilized. The test is conducted with two different vehicle configurations, open and locked differentials.

8B.5 BENCHMARK ENTRIES

8B.5.1 Vehicle and Test Data

The vehicle is a high mobility 4WD vehicle designed and built by the Nevada Automotive Test Center (NATC). The vehicle design data as well as the reference test data are provided by NATC and are presented in Annex H.

8B.5.2 NRMM

For the benchmark, a legacy NRMM reference model was generated representing the test vehicle. The NRMM model and description of the functionality of NRMM's modules are described in the Tracked Vehicle Benchmark chapter (Chapter 8A).

8B.5.3 Benchmark Participants

The benchmark participants are the same as for the tracked vehicle (Chapter 8A) with the addition of CM Labs, identified by G, described below.

8B.5.3.1 CM Labs Organization

CM Labs is an employee-owned private corporation that employs approximately 100 people, mostly engineers and software professionals, many with advanced technical degrees. The company is stable, profitable, and well-financed, and continues to grow. CM Labs provides expertise in advanced real-time simulation, 3D visualization, and integration with both hardware and software, with a focus on simulation for engineering, operator training and operations planning. CM Labs produces Vortex Studio, a unified simulation and visualization platform.

8B.5.3.1.1 Software Capability: Vortex Studio

Vortex Studio is built around a general-purpose multibody simulation engine based on an augmented Lagrangian formulation. It supports primitive and advanced constraint types, as well as collision detection between simple geometries and triangle mesh shapes. It is optimized for real-time performance, and can maintain stable, high-fidelity simulation of 60 Hz or higher for reasonably complex models, such as vehicles with fully simulated suspension.

Vehicles are considered multibody models, with the chassis, wheels, suspension and steering linkages, and drive shafts represented as rigid bodies. Relaxation can be added to constraints to represent compliance in bushings or flexibility in members. The engine is modeled as a simple torque source, and transmissions and differentials transfer force between shafts with a speed ratio. Springs and dampers can be non-linear, and logic or scripting can be added to modify the behavior of components to simulate advanced controls or behaviors.

Wheels and tracks (which are modeled as a combination of over-sized wheels and sliding plates) can collide accurately with any geometric primitives, triangle meshes or height fields that represent the terrain. Vortex Studio includes Composite Slip, Magic Formula (Pacejka) and Fiala contact models for tires on hard ground, and a Coulomb friction model for any general contacts. It also allows generic, custom contact models to be programmed. For soft ground, Vortex Studio supports the Bekker-Janosi-Wong soft soil model and has developed a custom soil model based on standard Cone Index measurements.

Vortex Studio is usually configured for 1/60th of a second (16.7 ms) simulation time steps and is synchronized with a graphical display of 60 frames per second to allow for human interaction. If human interaction is not needed and the frame rate limit is removed, it is capable of simulating a vehicle, including chassis, drive train components, suspension and steering linkages, and hard or soft tire model approximately 2 to 3 times faster than real time. When higher-frequency results are needed, such as for a ride quality analysis, the time step can be arbitrarily reduced, with a corresponding increase in time required to simulate.

8B.5.3.1.2 Ease of Use

Vortex Studio provides a graphical user interface that renders all models during creation and can instantly simulate the results in real time. It supports a content pipeline to develop simulation models from graphical 3D models or CAD models. The tools can be used to develop complex mechanisms and vehicles, as well as interactive environments in which to use the mechanisms and vehicles.

Vortex Studio has a library of vehicle templates that allow instant creation of a vehicle model for many different drivetrain topologies. Parameters can then be defined for the components (e.g., engine, torque converter, transmission). Suspensions can also be parameterized, or custom designed. The models developed for analysis can also be directly used in a real-time driving simulator, taking advantage of all of Vortex Studio's simulation and rendering capabilities.

8B.6 BENCHMARK RESULTS

This section summarizes the results obtained by the participants, outlines the main difference between results and emphasizes differences in the methodology chosen by the participants in each of the simulation events. The participants are scored on the Maturity Scale depicted in Table 8B-1. For this benchmark effort the participants did not have a priori access to the test data; Level 6 is possible for those events where test data was available. Level 6 is given to participants who have provided results that do not deviate by more than 50% compared to the test result. For events, where multiple participants have provided data, but no test data is available, the maximum level obtainable is 4 based on the average result. If a participant has provided results that deviate more than 50% compared to the average result the given Maturity Level is 2, otherwise it is 4.

8B.6.1 Paved Straight Line Acceleration

The speed vs time plot for all participants is shown in Figure 8B-1. The outlier curve is obtained by Vendor C and exhibits a general tendency of higher accelerations compared to the remaining participants.

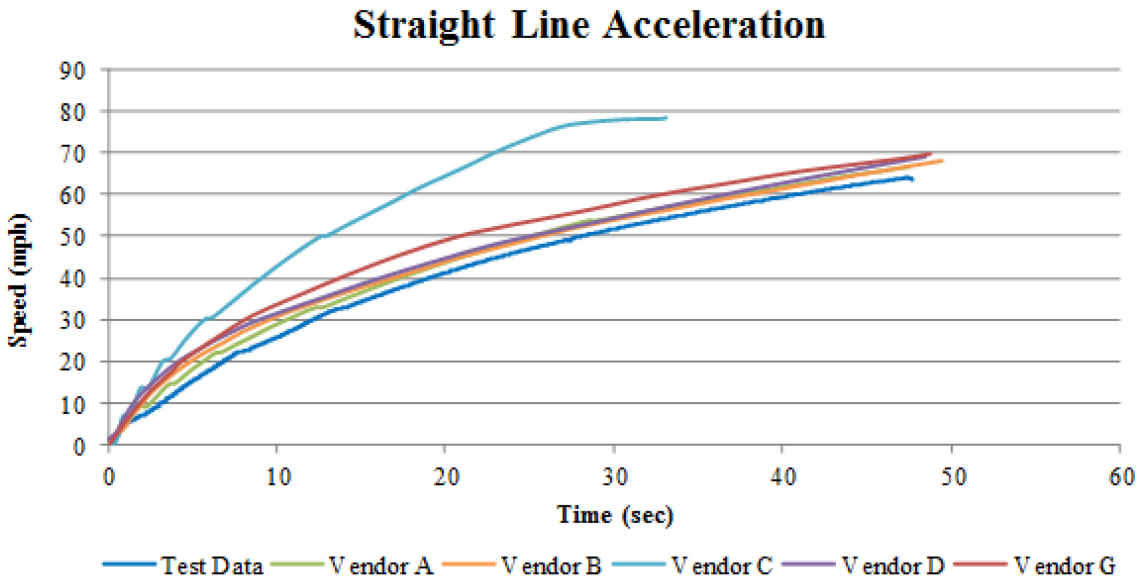


Figure 8B-1: Straight Line Acceleration Speed.

The maximum speeds achieved by the participants are plotted in Figure 8B-2. As can be seen, Vendor C has obtained the highest speed, but has only simulated the acceleration for 35 sec. All vendors that have performed the analysis have delivered results that are in high agreement with test data, both for maximum speed and acceleration.

The resulting Maturity Levels obtained by the vendors are depicted in Figure 8B-3. All participating vendors have achieved Level 6 based on the maximum speed and the speed vs time plot. Vendor C diverges the most compared to test data but does not exceed the test data by more than 50%, hence obtains Level 6.

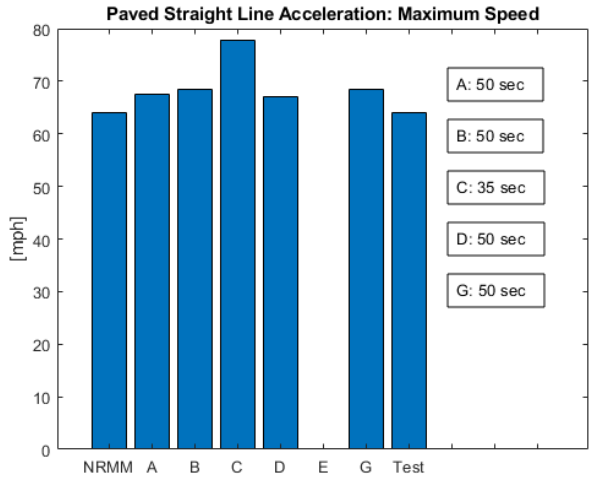


Figure 8B-2: Paved Straight Line Acceleration: Maximum Speed.

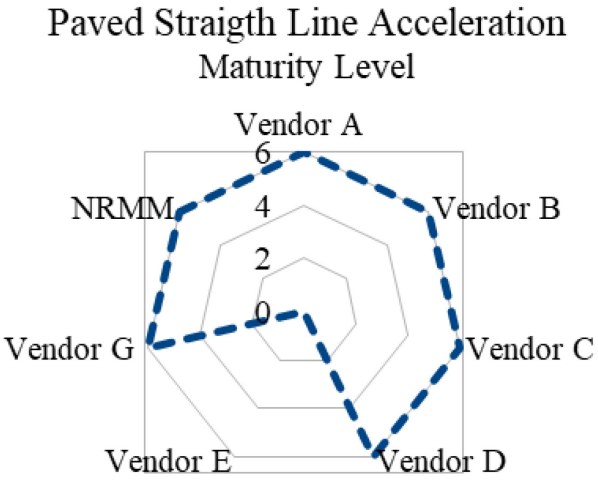


Figure 8B-3: Paved Straight Line Acceleration Maturity Level Achieved by Vendors.

8B.6.2 Wall-to-Wall Turn Radius

The wall-to-wall analysis is performed both in clockwise and in counterclockwise direction. The diameter obtained through the vendor analyses are depicted in Figure 8B-4. Vendor G has conducted the analysis using both a Coulomb and a Pacejka tire model. The results obtained through the Coulomb model are shown in Figure 8B-4.

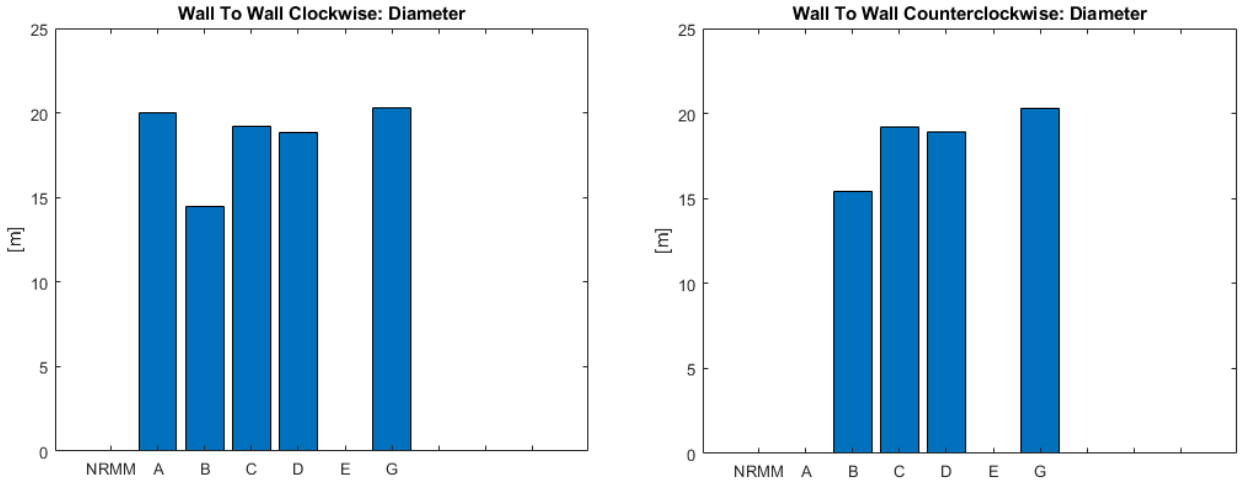


Figure 8B-4: Wall-To-Wall Clockwise (Left) and Counterclockwise (Right): Diameter.

The Maturity Level is given based on the diameter obtained in the wall-to-wall event. No test data is available; hence the maturity level assessment is based on the average vendor result. Since all vendors that contributed a result have achieved comparable diameters within 50% of the average, the maximum achievable Level of 4 is given to all participating vendors (Figure 8B-5).

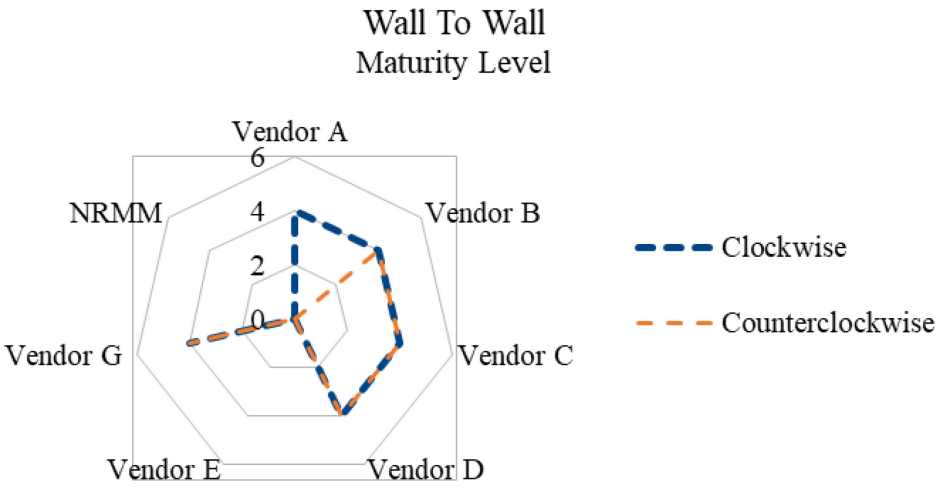


Figure 8B-5: Wall-To-Wall Maturity Level Achieved by Vendors.

8B.6.3 Steady-State Cornering 200 ft. Radius

The steering wheel angle versus lateral acceleration results of the steady-state cornering tests are shown in Figure 8B-6. The participating vendors have all obtained curves that resembles the limit understeer behavior as indicated by the test data. The curves are shifted vertically compared to the test data, which can be due to difficulty in measuring and/or modeling the steering gear compliance.

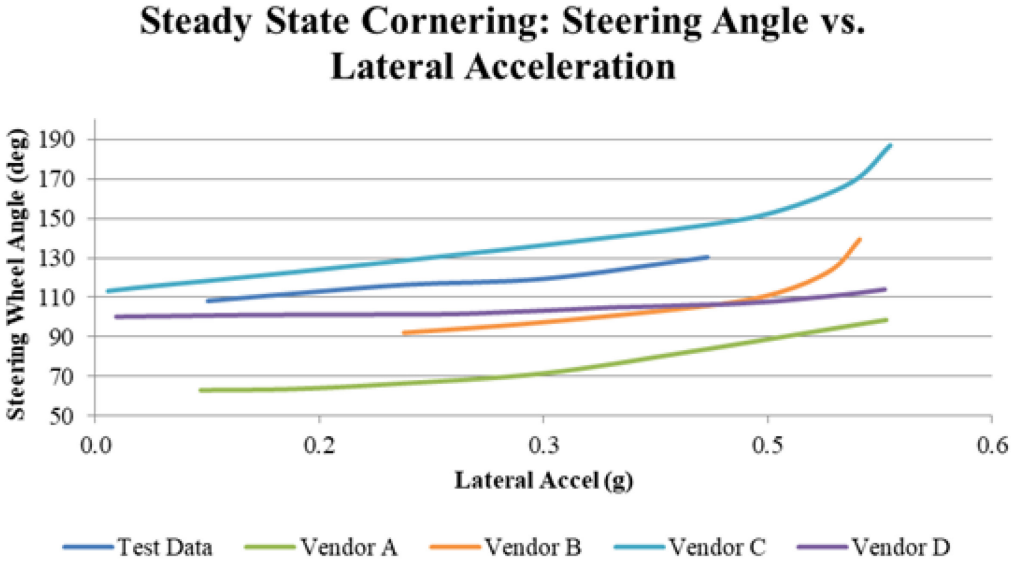


Figure 8B-6: Steady-State Cornering 200 ft. Radius: Steering Angle vs. Lateral Acceleration.

Figure 8B-7 through Figure 8B-8 show the maximum speed before loss of control and the maximum lateral acceleration.

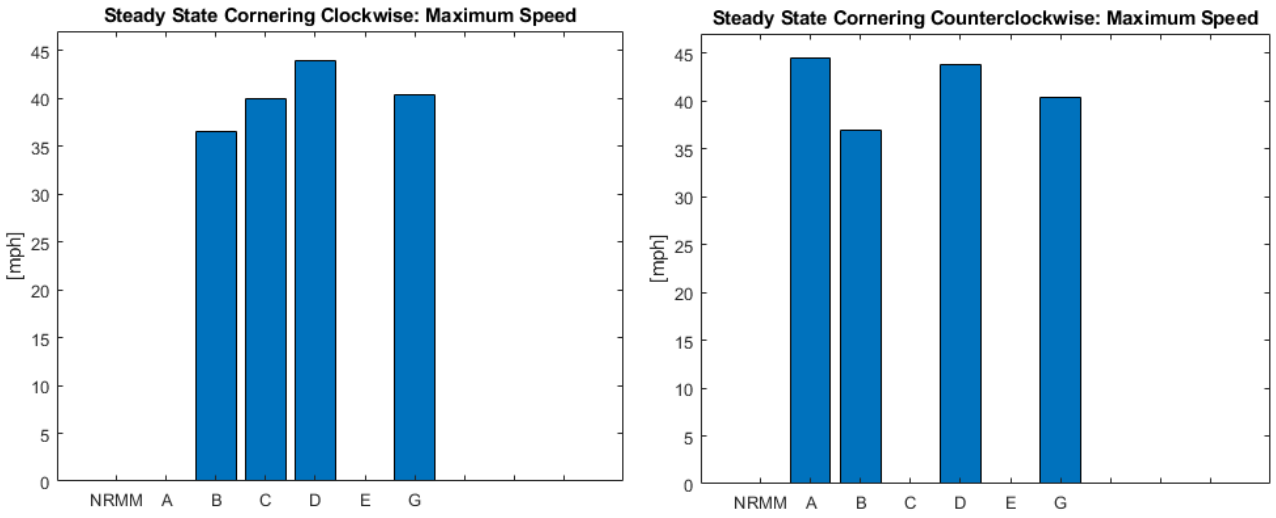


Figure 8B-7: Steady-State Cornering Clockwise (Left) and Counterclockwise (Right): Maximum Speed.

Based on the steering angle vs lateral acceleration plot, the maximum speed and the maximum lateral acceleration have been scored. Figure 8B-9 shows the Maturity Level for each vendor for both the clockwise and the counterclockwise events. The participating vendors have all been judged as Level 6.

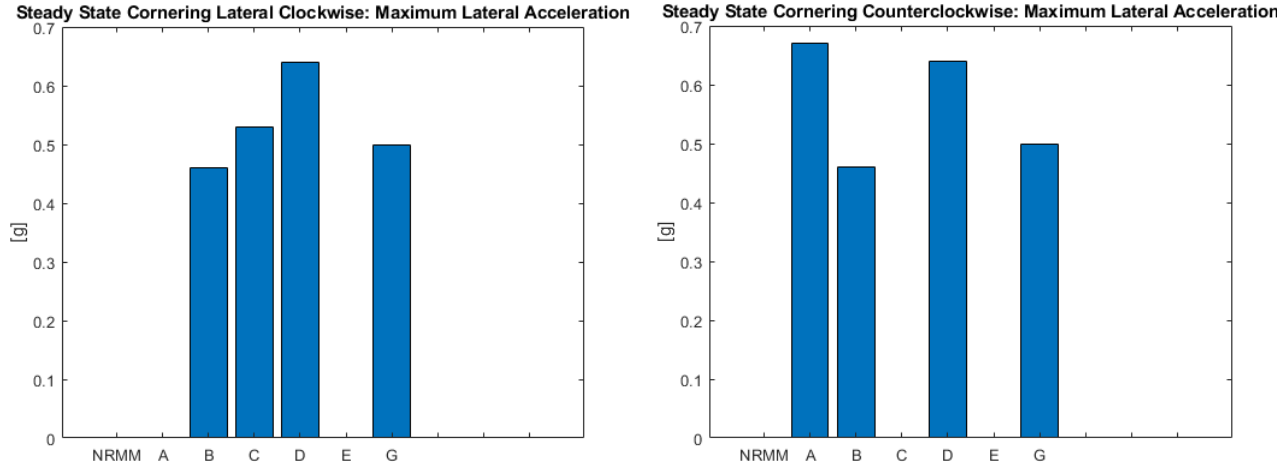


Figure 8B-8: Steady-State Cornering Clockwise (Left) and Counterclockwise (Right): Maximum Lateral Acceleration.

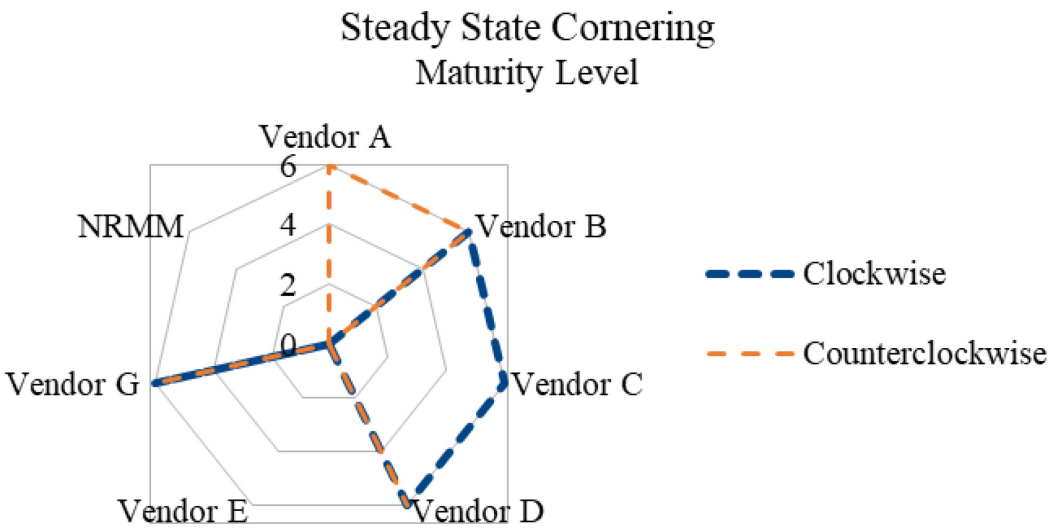


Figure 8B-9: Steady-State Cornering Maturity Level Achieved by Vendors.

8B.6.4 Paved Double Lane Change

The paved double lane change is specified to implement two different steering strategies, an open loop event using a prescribed steering input and a closed-loop event using a steering controller. The roll and yaw rate, lateral acceleration and steering angle are shown in Figure 8B-10, Figure 8B-11, Figure 8B-12 and Figure 8B-13. Figure 8B-13 shows the given steering input as well as individual vendor steering responses.

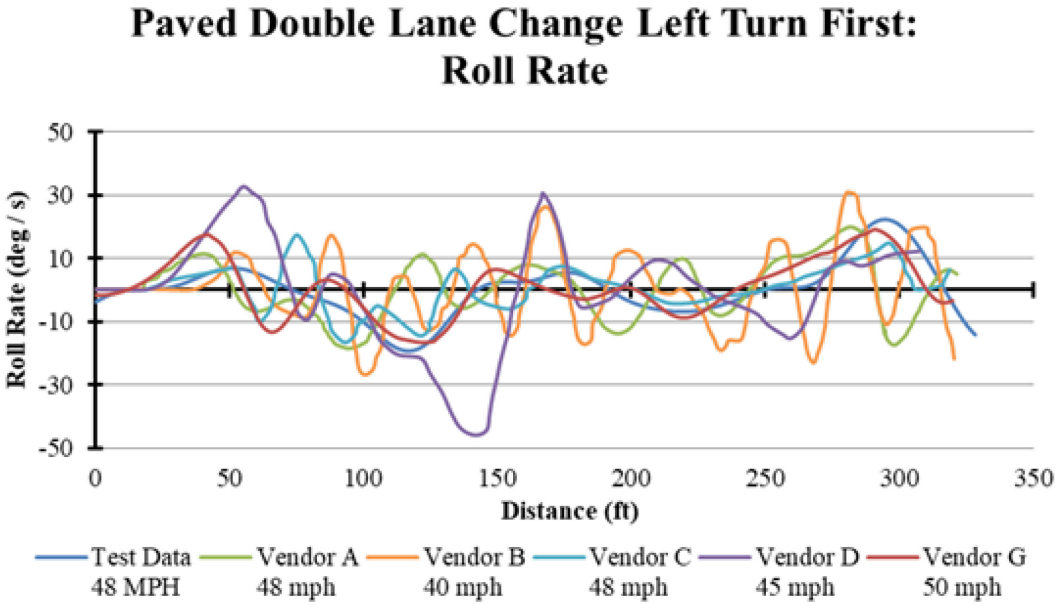


Figure 8B-10: Paved Double Lane Change LTF: Roll Rate.

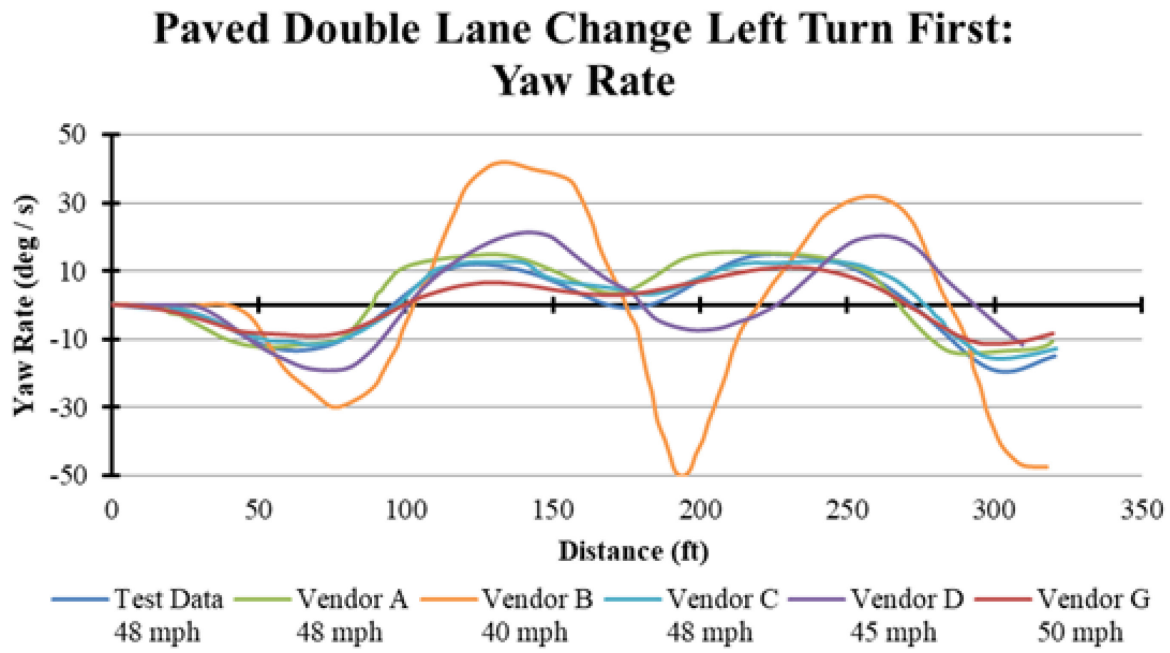


Figure 8B-11: Paved Double Lane Change LTF: Yaw Rate.

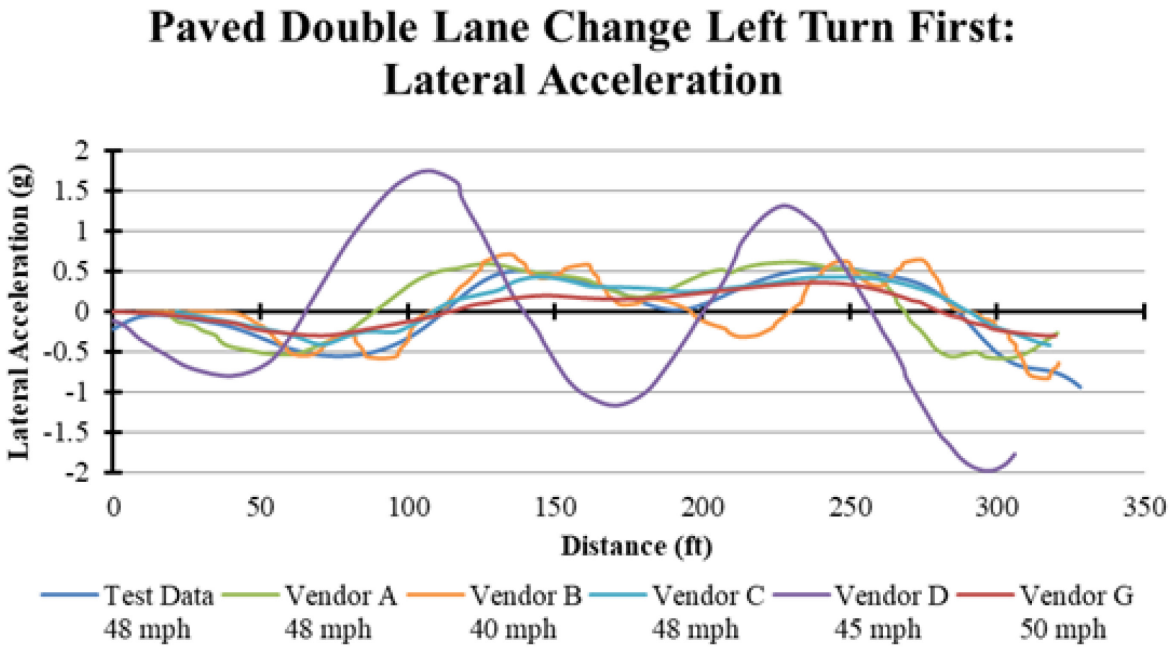


Figure 8B-12: Paved Double Lane Change LTF: Lateral Acceleration.

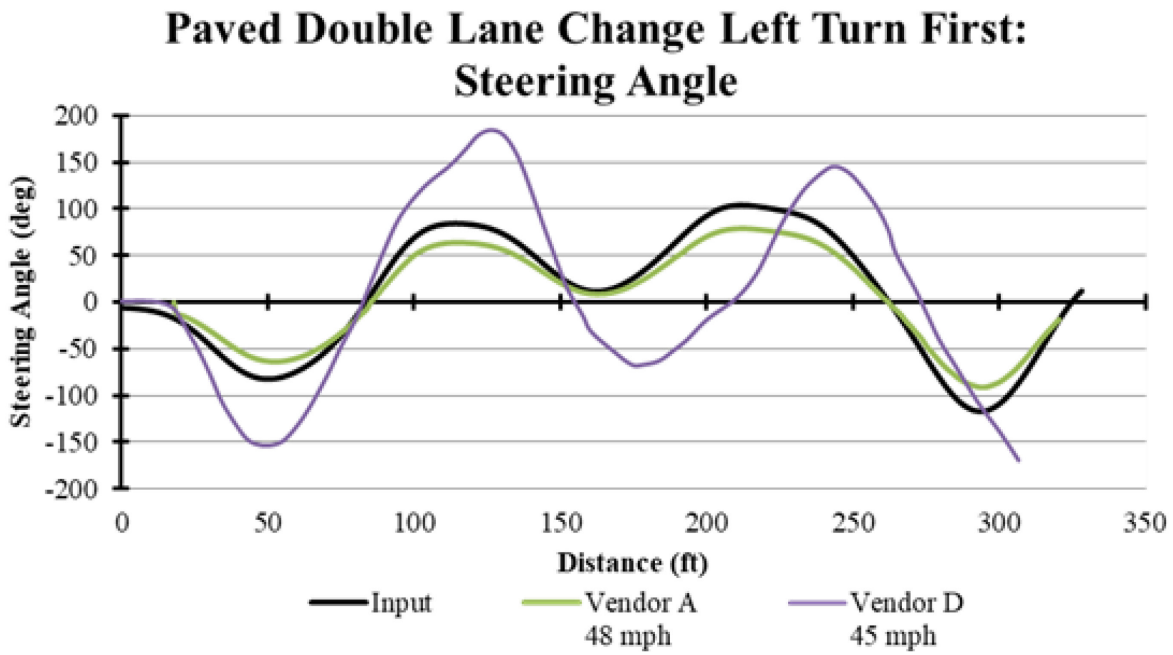


Figure 8B-13: Paved Double Lane Change LTF: Steering Angle.

The maximum speed obtained by each vendor is reproduced in Figure 8B-14 and Figure 8B-15 for all events. The vendors had difficulties staying inside the course boundaries using the prescribed steering input, as can be seen in Figure 8B-14 compared to Figure 8B-15. Vendor A, C, D and G performed the open loop event, but only Vendor G succeeded for the left turn first and only Vendor A succeeded for the right turn first. The two vendors did succeed in obtaining a result for the closed-loop event, where also Vendor B and NRMM have provided results.

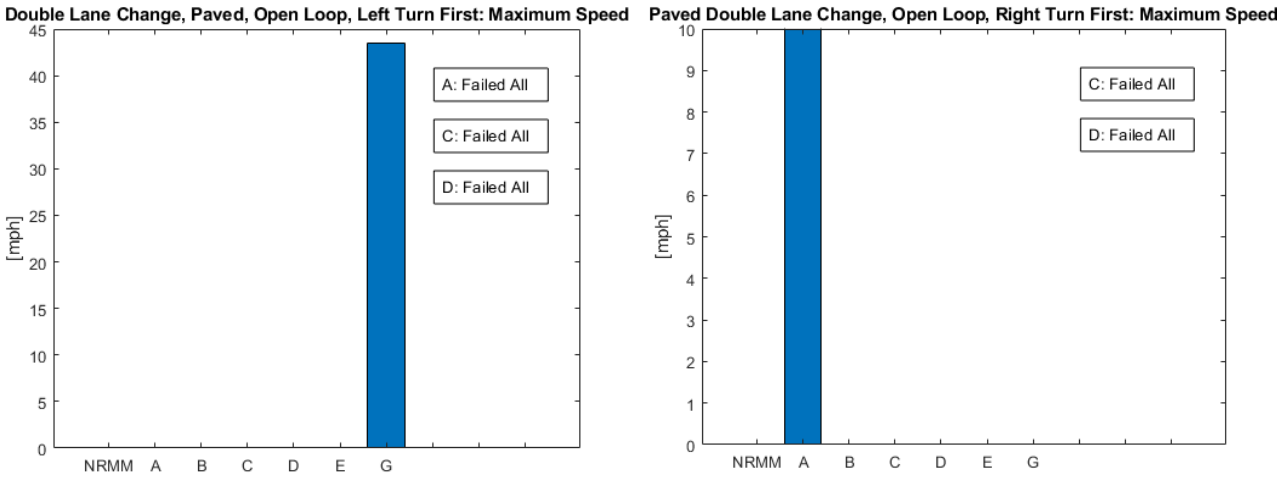


Figure 8B-14: Paved Double Lane Change Steering Open Loop, Left Turn First (Left) and Right Turn First (Right): Maximum Speed.

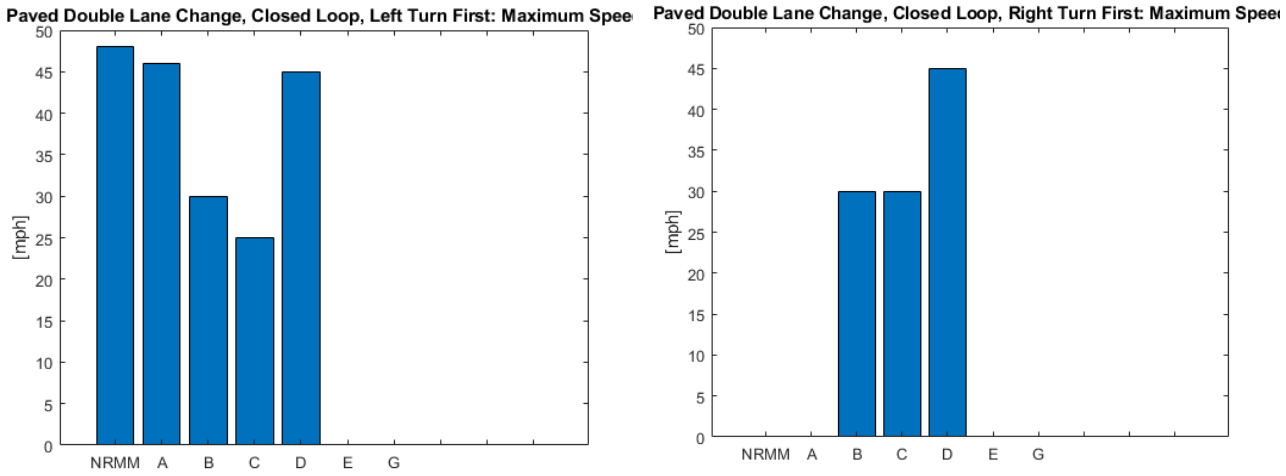


Figure 8B-15: Paved Double Lane Change Steering Closed Loop, Left Turn First (Left) and Right Turn First (Right): Maximum Speed.

8B.6.5 Gravel Double Lane Change

The gravel double lane change is specified as the paved event to be performed both as an open and a closed-loop event. The roll and yaw rate, lateral acceleration and steering angle are shown in Figure 8B-16, Figure 8B-17, Figure 8B-18 and Figure 8B-19 for the left side first event. Figure 8B-19 shows the prescribed steering input as well as individual vendor steering responses.

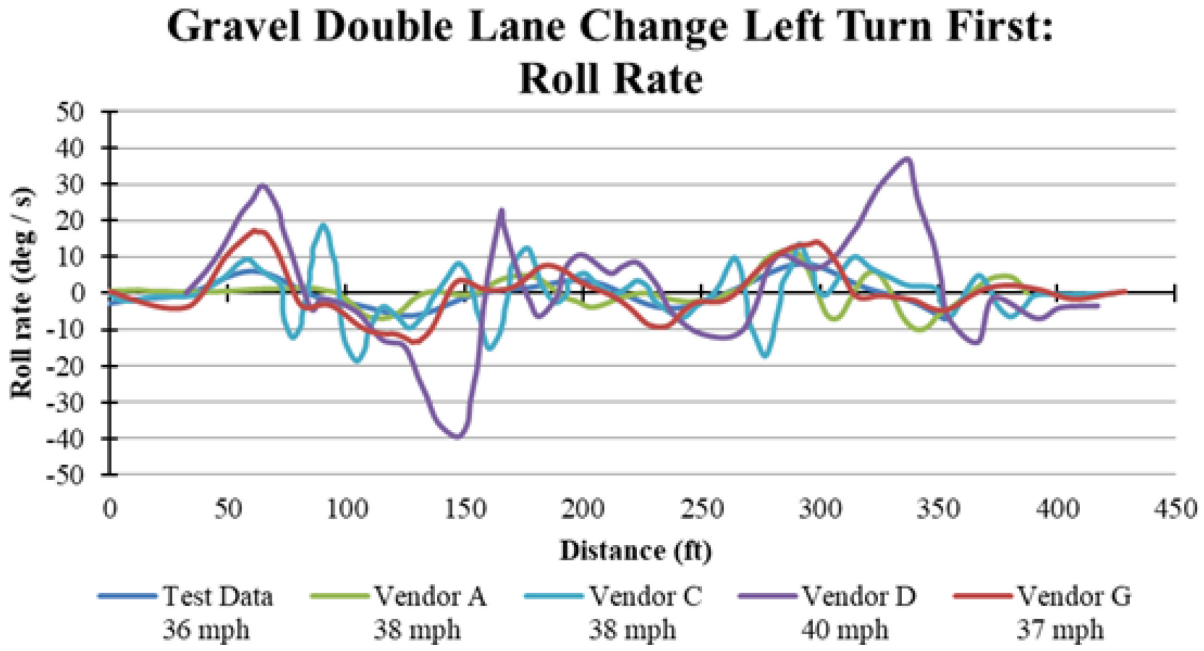


Figure 8B-16: Gravel Double Lane Change LTF: Roll Rate.

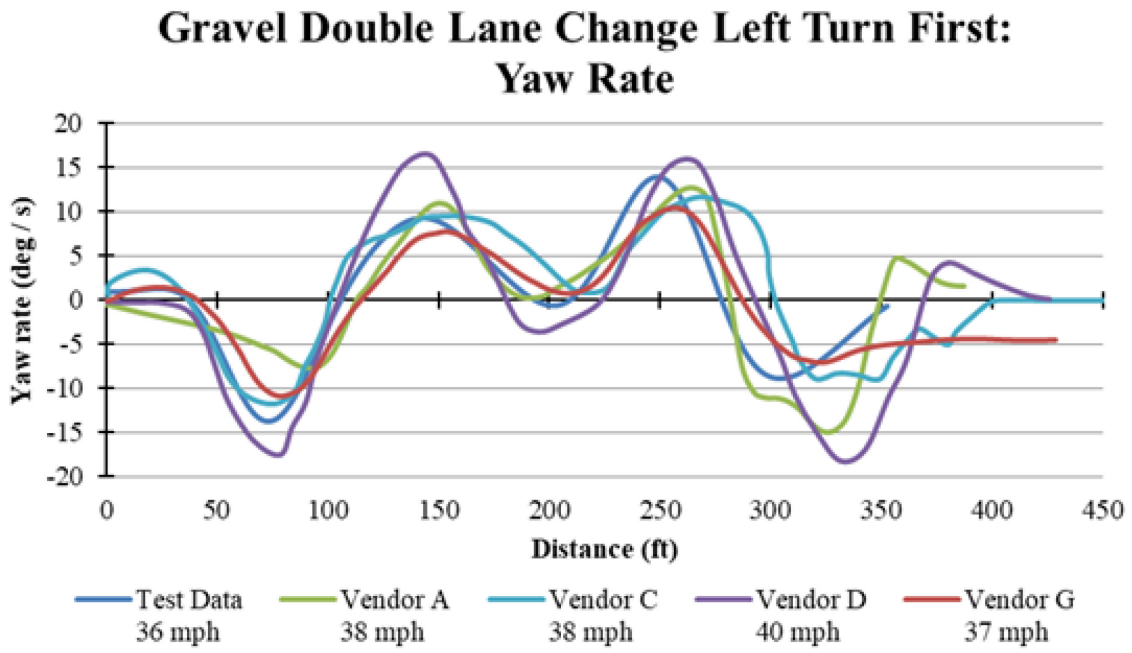


Figure 8B-17: Gravel Double Lane Change LTF: Yaw Rate.

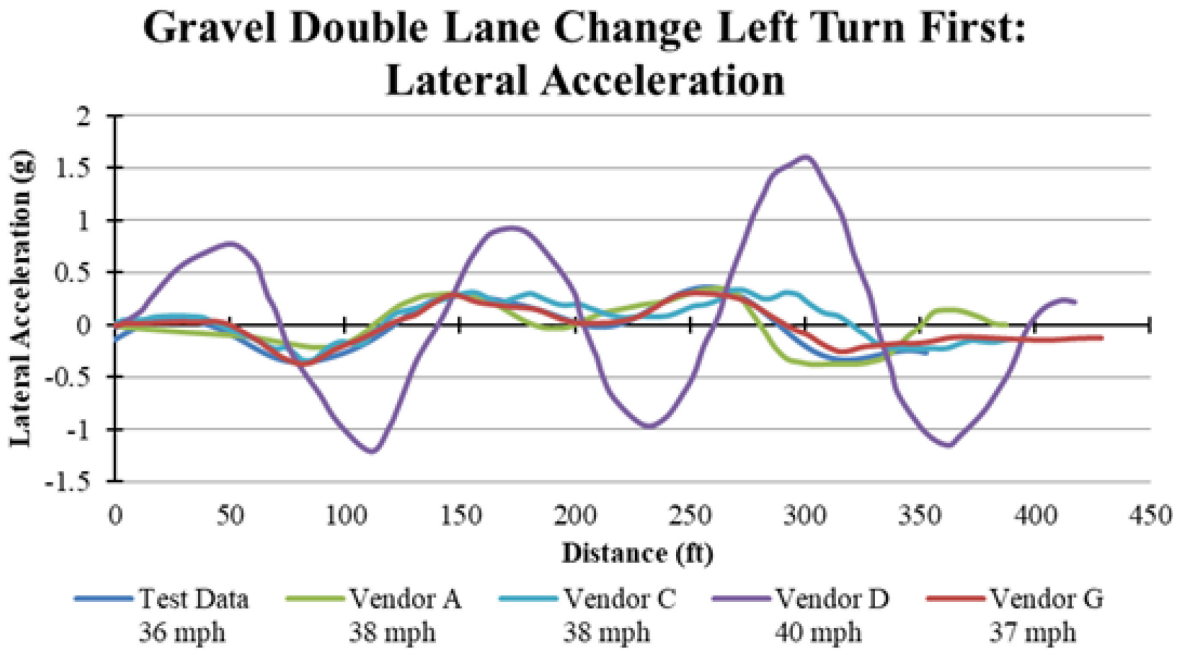


Figure 8B-18: Gravel Double Lane Change LTF: Lateral Acceleration.

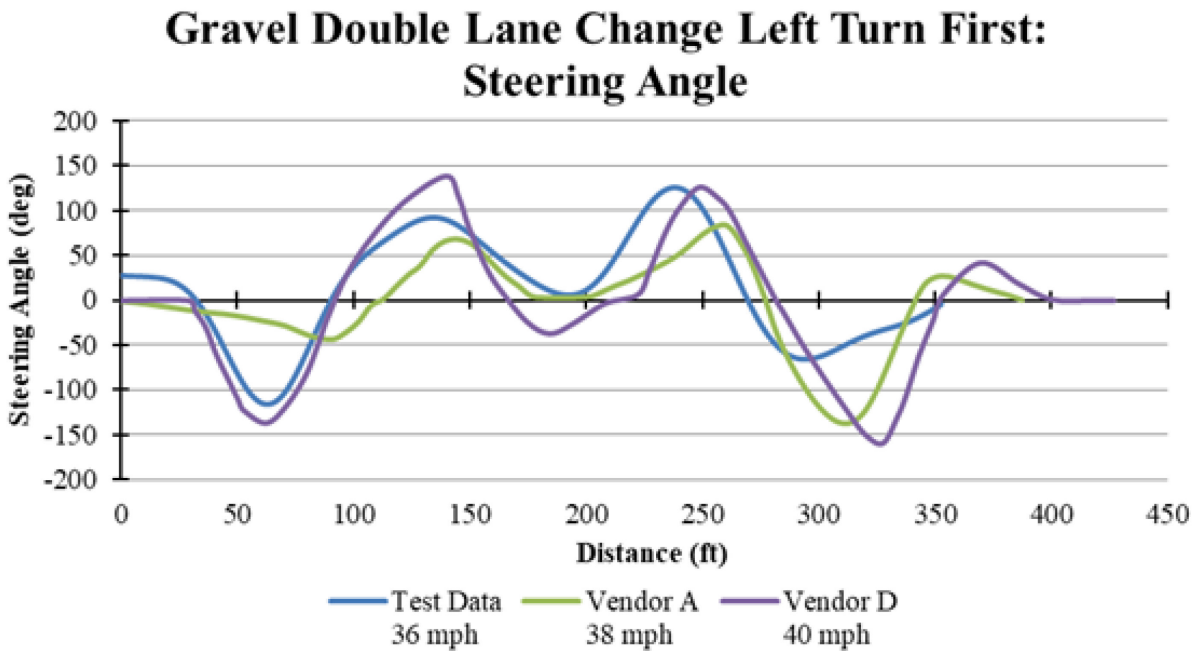


Figure 8B-19: Gravel Double Lane Change LTF: Steering Angle.

The maximum speed obtained by each vendor is depicted in Figure 8B-20 and Figure 8B-21 for all events. Like the paved event, the Vendor has likewise resubmitted a new result of the counterclockwise steady state cornering event, altering the maximum speed from 44.5 mph to 43 mph, not affecting the overall conclusion. Vendor C and D failed to perform the open loop event without exceeding the course boundaries but were able to produce results for the closed-loop event. Vendor A failed the left side first but did succeed in the right turn first open loop event.

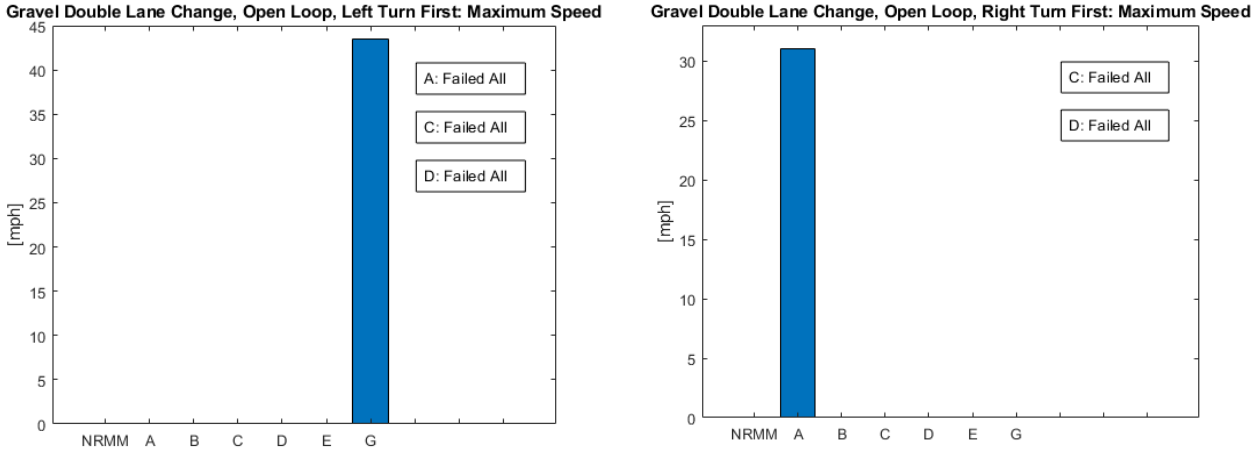


Figure 8B-20: Gravel Double Lane Change Steering Open Loop, Left Turn First (Left) and Right Turn First (Right): Maximum Speed.

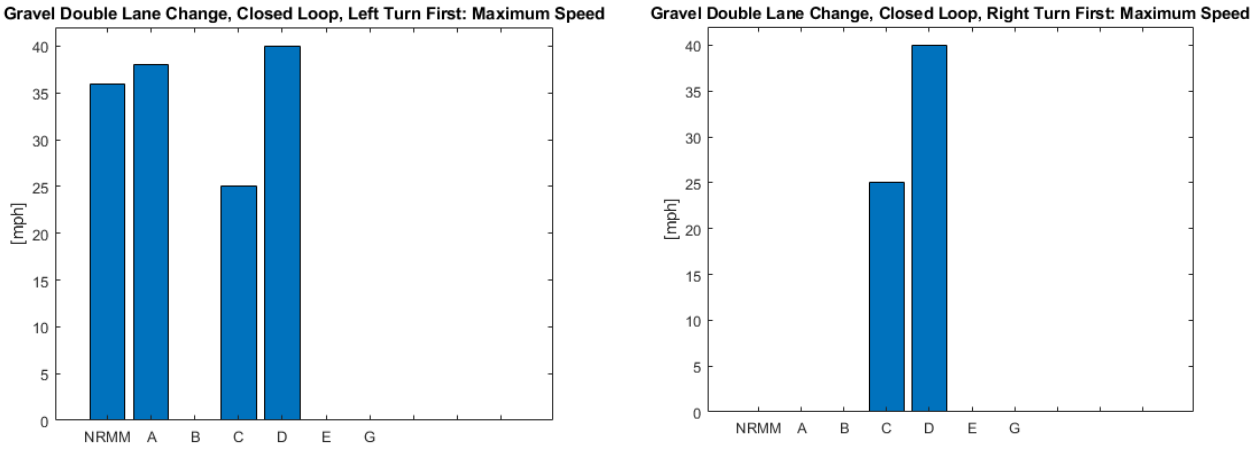


Figure 8B-21: Gravel Double Lane Change Steering Closed Loop, Left Turn First (Left) and Right Turn First (Right): Maximum Speed.

The vendor results have been assessed and scored based on speeds, peak roll, pitch and yaw angles and rates. The results illustrate that the vendors have had difficulties performing with the prescribed steer input. Figure 8B-22 and Figure 8B-23 show the obtained Maturity Levels for both paved and gravel double lane change events for the closed-loop simulations. Note that the tests have not been performed until failure. The vendor results are thus compared to test data by looking at yaw and roll rates and lateral acceleration through the course at speeds close to the test speed. When evaluating the maximum speed the average result of the vendors have been used.

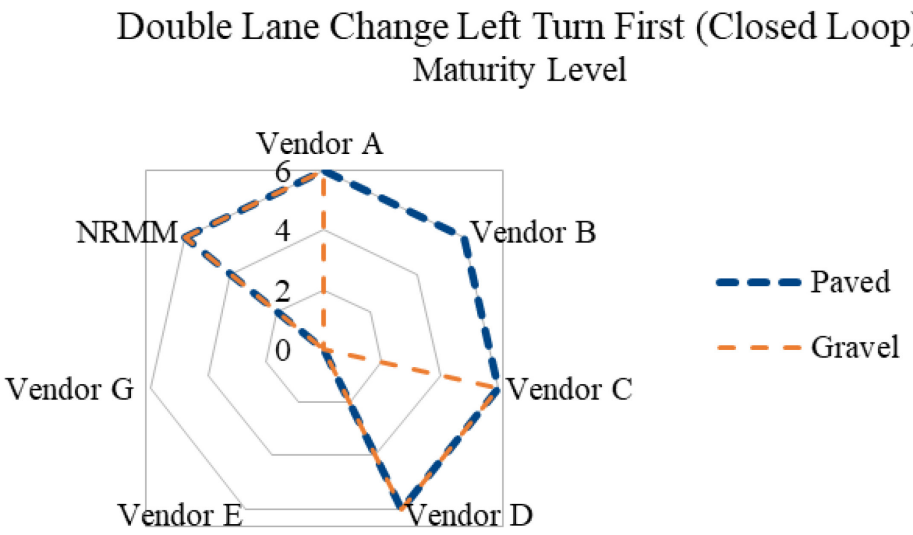


Figure 8B-22: Double Lane Change Left Turn First Maturity Level Achieved by Vendors.

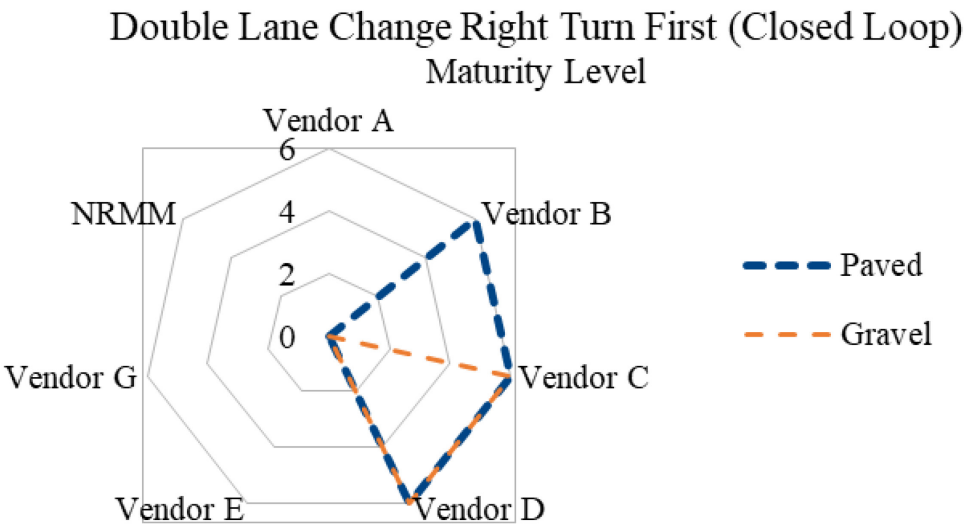


Figure 8B-23: Double Lane Change Right Turn First Maturity Level Achieved by Vendors.

8B.6.6 Side Slope Stability

The side slope event is specified to be conducted both as an open and a closed-loop event. In the open loop event, the vendors have been provided a steering input and for the closed-loop event, the vendors are expected to use own steering controller. The lateral acceleration, roll and yaw rate and steering angle obtained in the side slope stability event are shown in Figure 8B-24, Figure 8B-25, Figure 8B-26 and Figure 8B-27 for the right side down event. The test has not been repeated until failure; hence the vendor results are compared to the test data at a speed close to the test speed of 6.7 mph. Most vendors have succeeded in using the prescribed steering input and have therefore not conducted the closed-loop event.

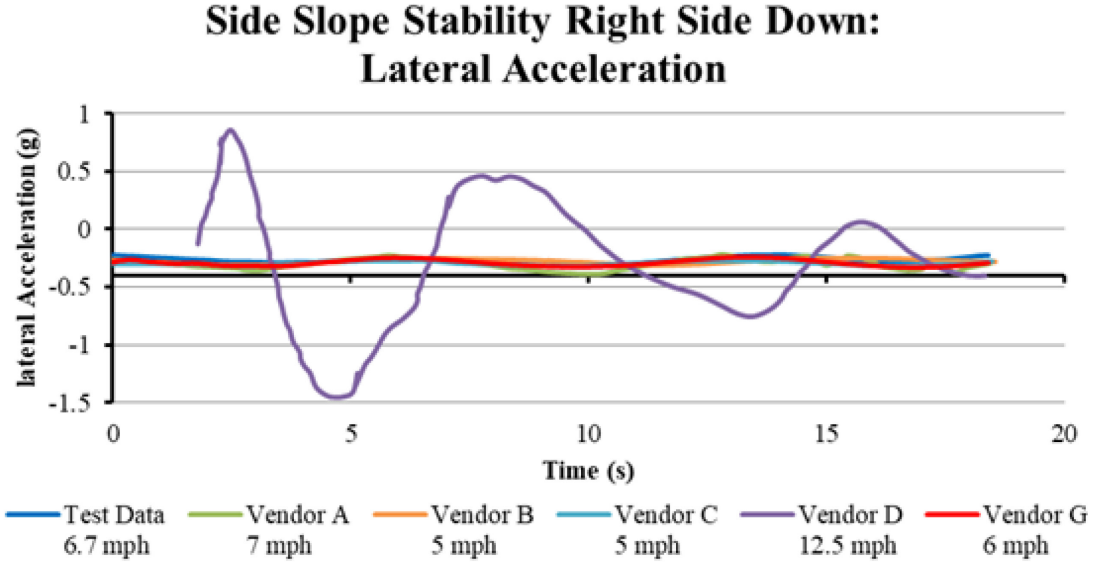


Figure 8B-24: Side Slope Stability: Lateral Acceleration.

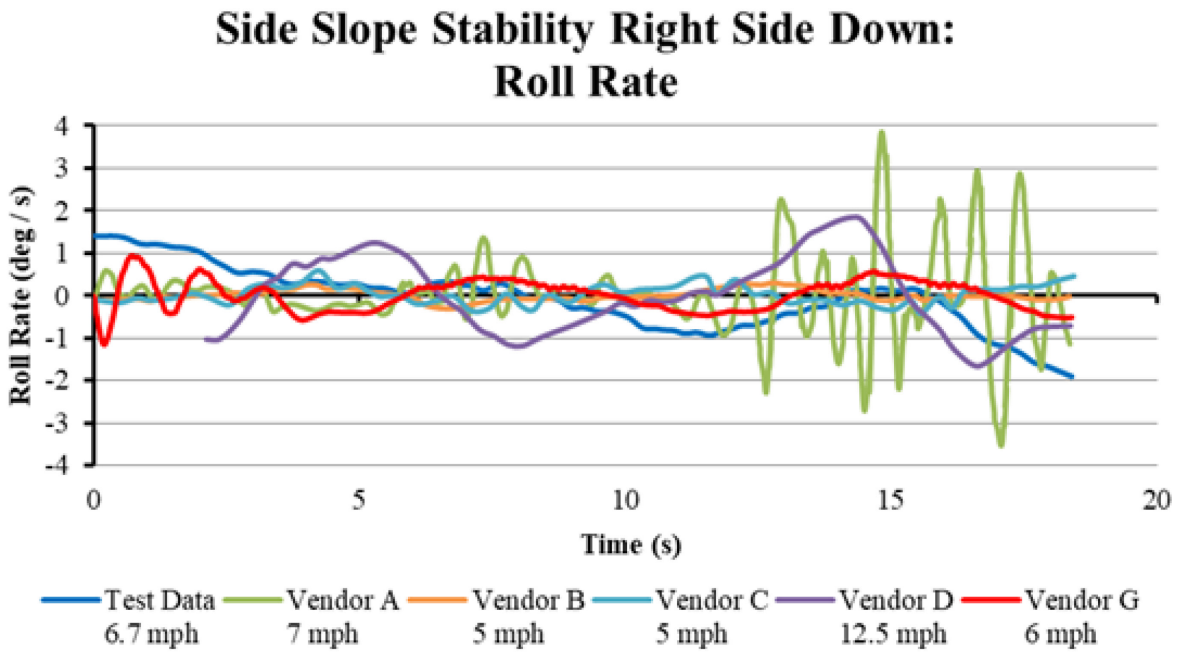


Figure 8B-25: Side Slope Stability: Roll Rate.

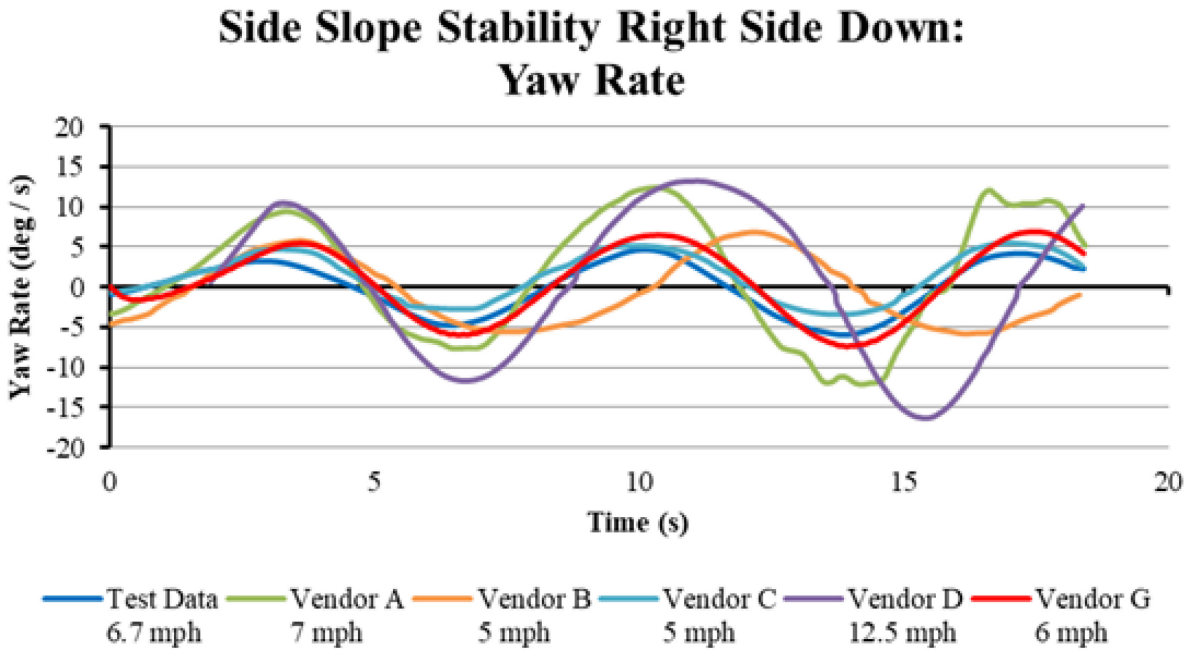


Figure 8B-26: Side Slope Stability: Yaw Rate.

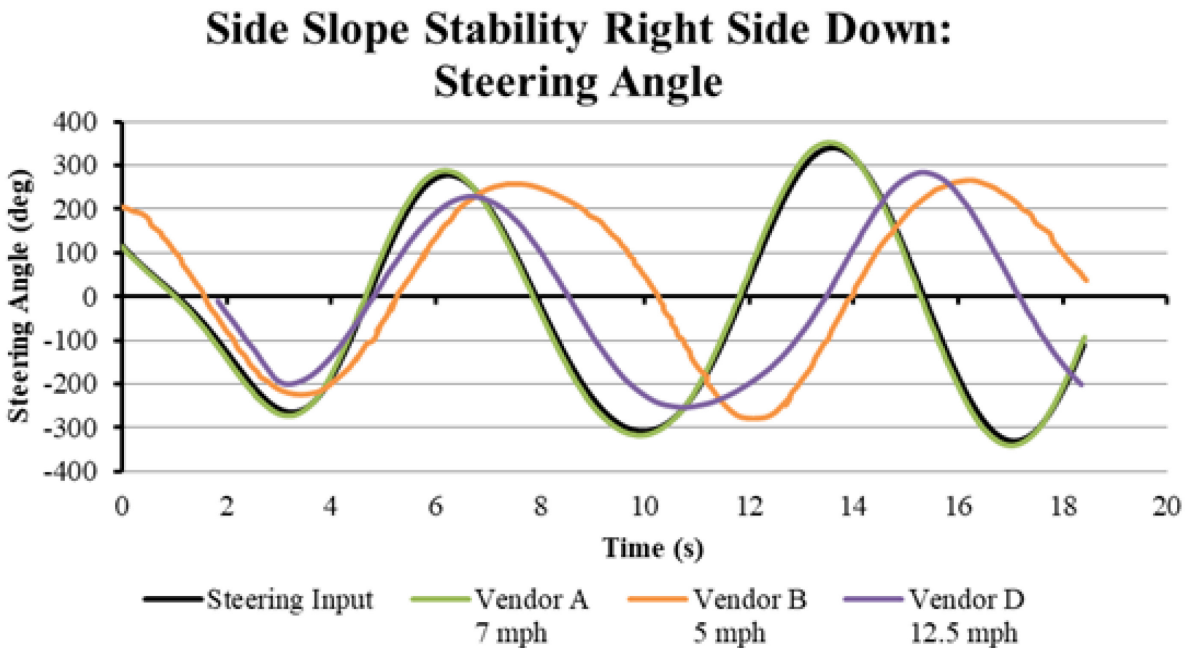


Figure 8B-27: Side Slope Stability: Steering Angle.

For the side slope stability analysis Vendor C was not able to find a limiting speed. This can be seen in Figure 8B-28.

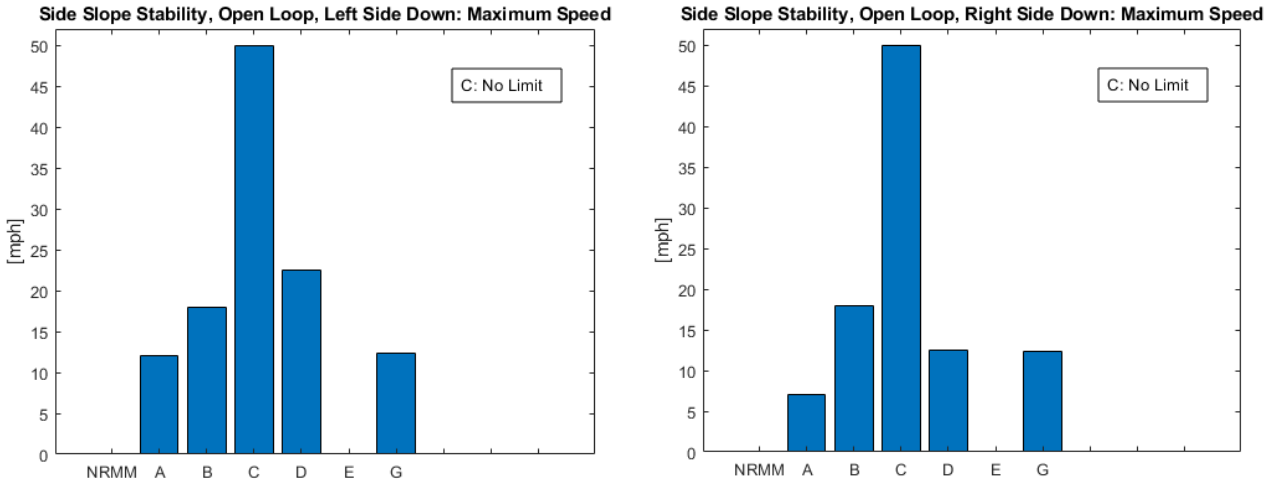


Figure 8B-28: Side Slope Stability Steering Open Loop, Left Side Down (Left) and Right Side Down (Right): Maximum Speed.

For the side slope stability events, the vendors have been successful in using the provided steering input for the simulation, hence Figure 8B-29 displays the Maturity Levels for the vendors using the steering input. As no test data is available for the Left Side Down (LSD), the maximum obtainable Level for this event is 4, which is acquired by all vendors that have provided a result. For the Right Side Down (RSD) test data is

available and all vendors, except for Vendor C that have performed the analysis, have achieved Level 6 based on peak yaw rate and maximum speed.

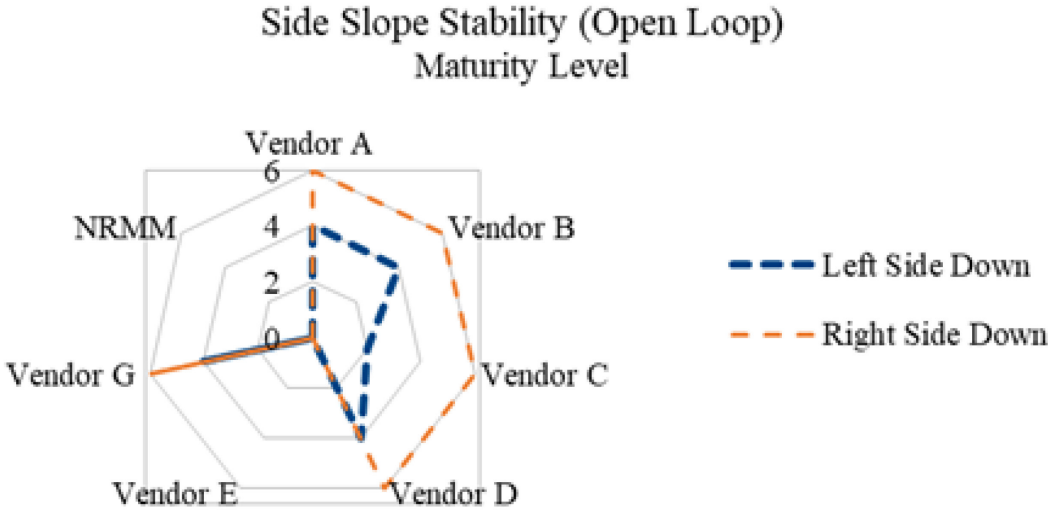


Figure 8B-29: Side Slope Stability Maturity Level Achieved by Vendors.

8B.6.7 Sand Slope Gradeability

Vendor results for engine RPM, engine torque, vehicle speed compared to sand slope gradeability test data can be seen in Figure 8B-30, Figure 8B-31 and Figure 8B-32.

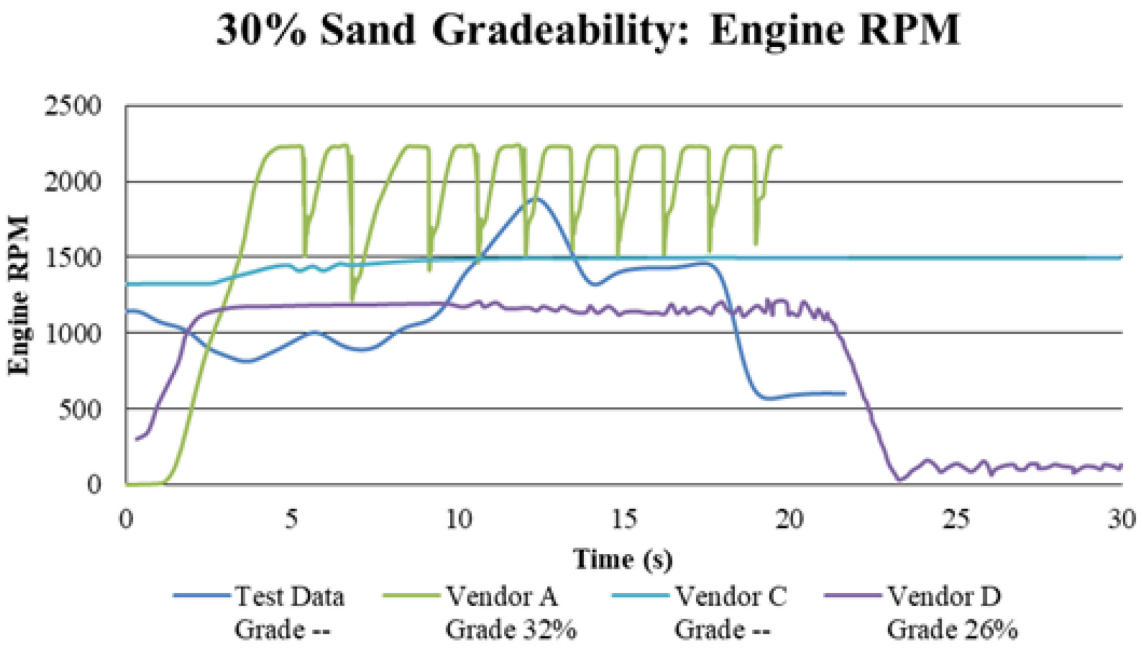


Figure 8B-30: 30% Sand Gradeability: Engine RPM.

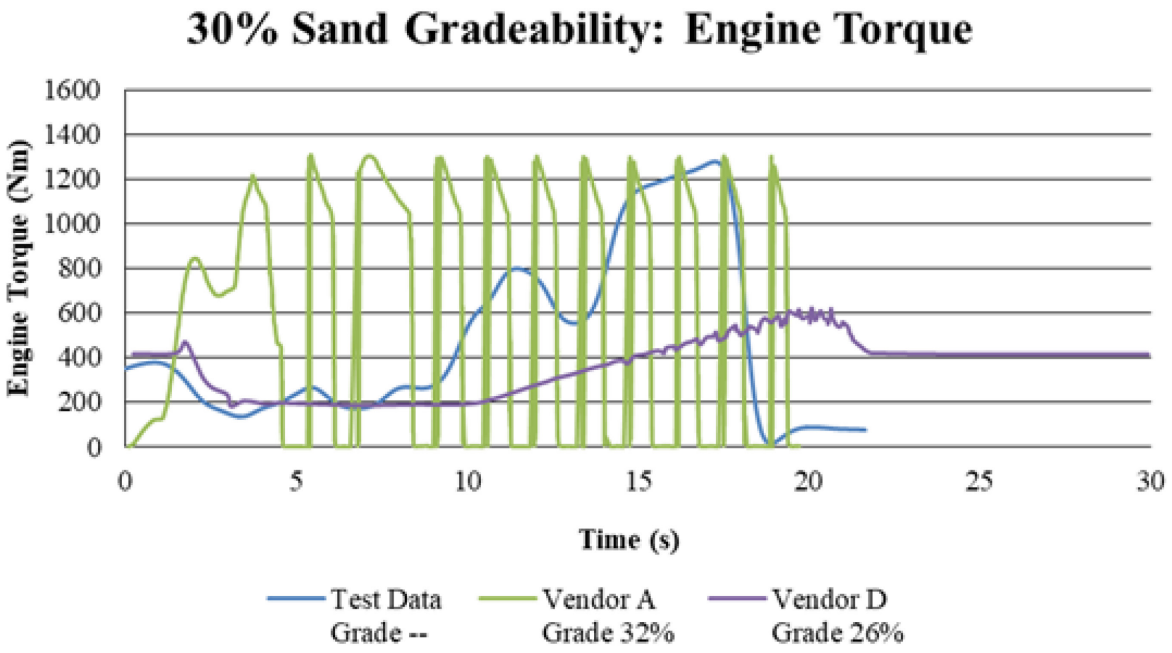


Figure 8B-31: 30% Sand Gradeability: Engine Torque.

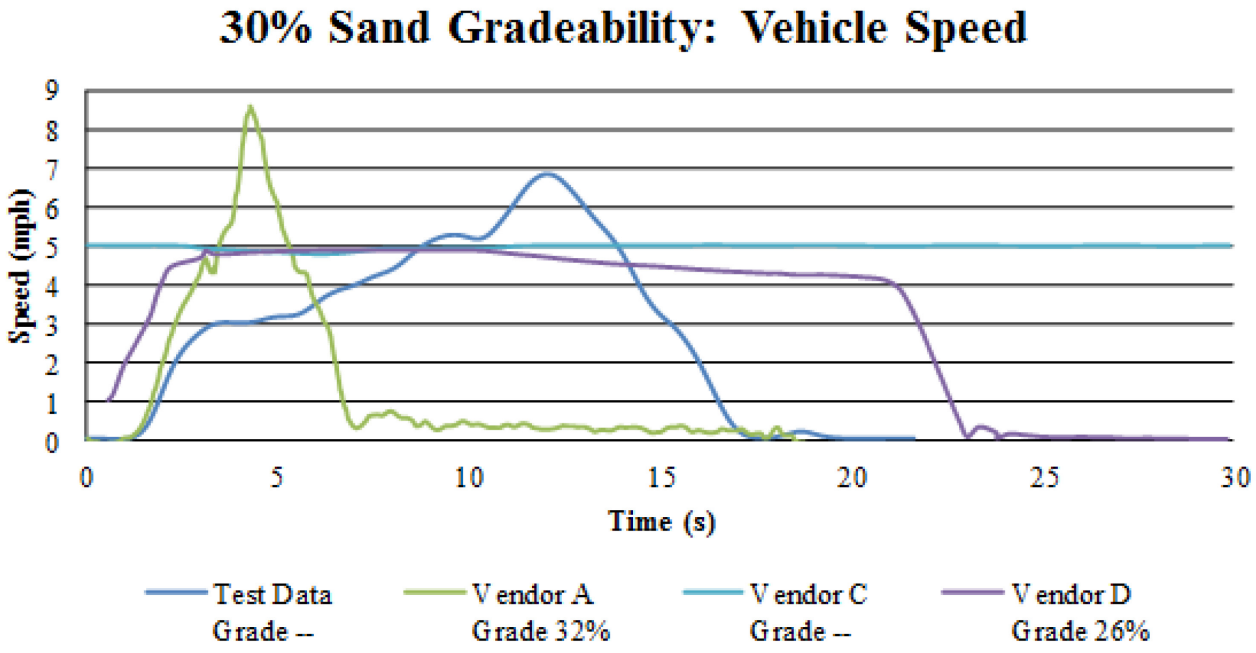


Figure 8B-32: 30% Sand Gradeability: Vehicle Speed.

The maximum speeds obtained by the participants are illustrated in Figure 8B-33 for both open differential and full locked driveline. Due to difficulties in interpreting the soil properties provided Vendor C and Vendor D have used LETE sand properties defined in Ref. [9].

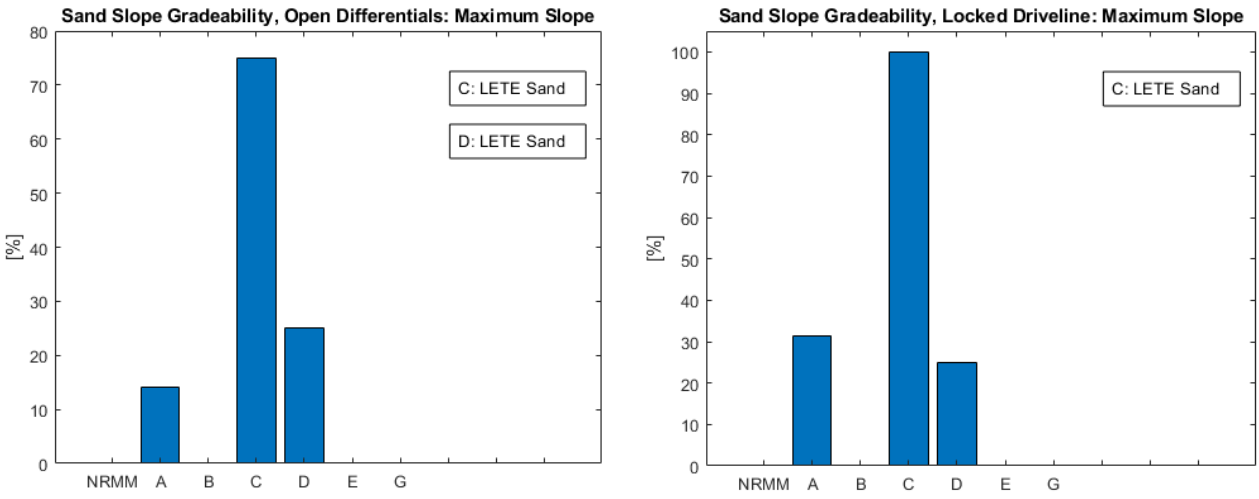


Figure 8B-33: Sand Slope Gradeability Open Differentials (Left) and Full Locked Driveline (Right): Maximum Slope.

Test data is available for the sand slope gradeability test, but due to the divergence between test data and vendors results in the engine RPM, engine torque and vehicle speed plots on a grade close to 30% Vendors A, C, D and G have all achieved a Level of 4 as can be seen in Figure 8B-34. The results are extremely divergent. Vendor C has been able to demonstrate driving on much steeper slopes compared to the other vendors, but displays engine plots, that are closer to test data and the vendor A. Vendors A and D have obtained comparable maximum speeds, but very different plots. Based on this ambiguity, an achieved Maturity Level of 2 for the participating vendors may be more appropriate.

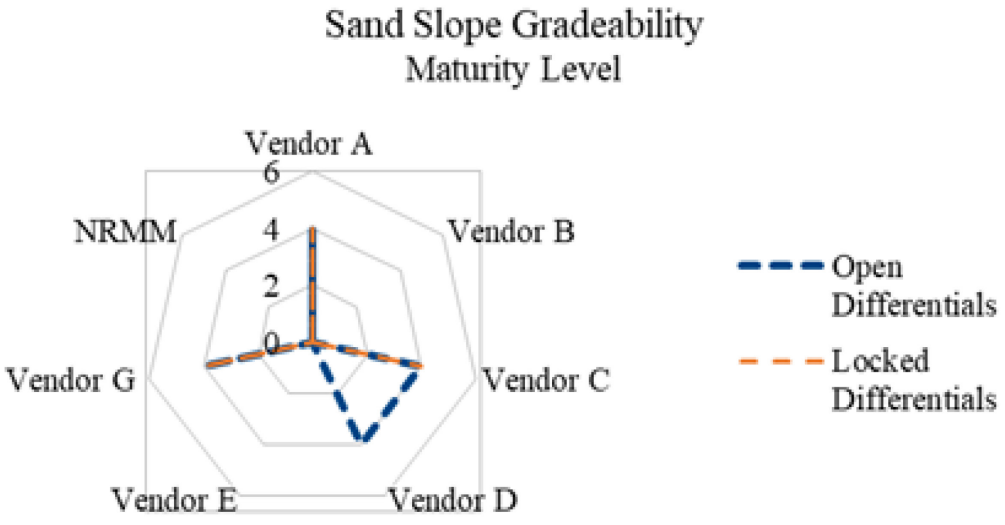


Figure 8B-34: Sand Slope Gradeability Maturity Level Achieved by Vendors.

8B.6.8 Ride Quality

The ride quality plots contains absorbed power curves for the four ride quality courses, 1.0 – 3.6 inches Figure 8B-35, Figure 8B-36, Figure 8B-37 and Figure 8B-38; and a 6-watt absorbed power curve, Figure 8B-39. All vendors, who have produced a 6-watt curve, have obtained results that resemble the test data.

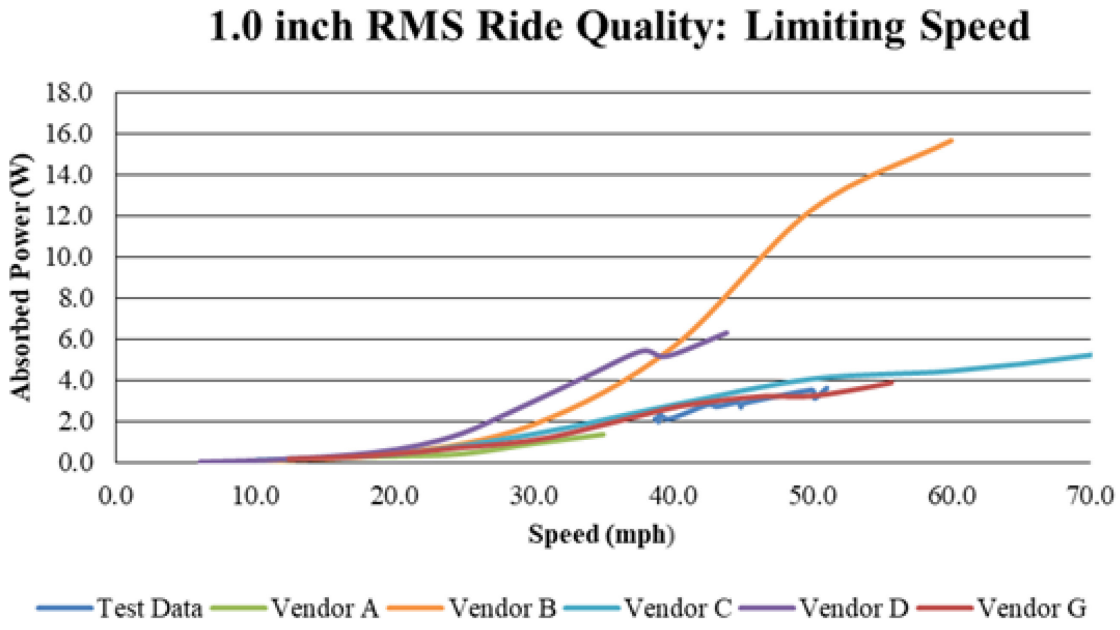


Figure 8B-35: Ride Quality: 1.0 RMS.

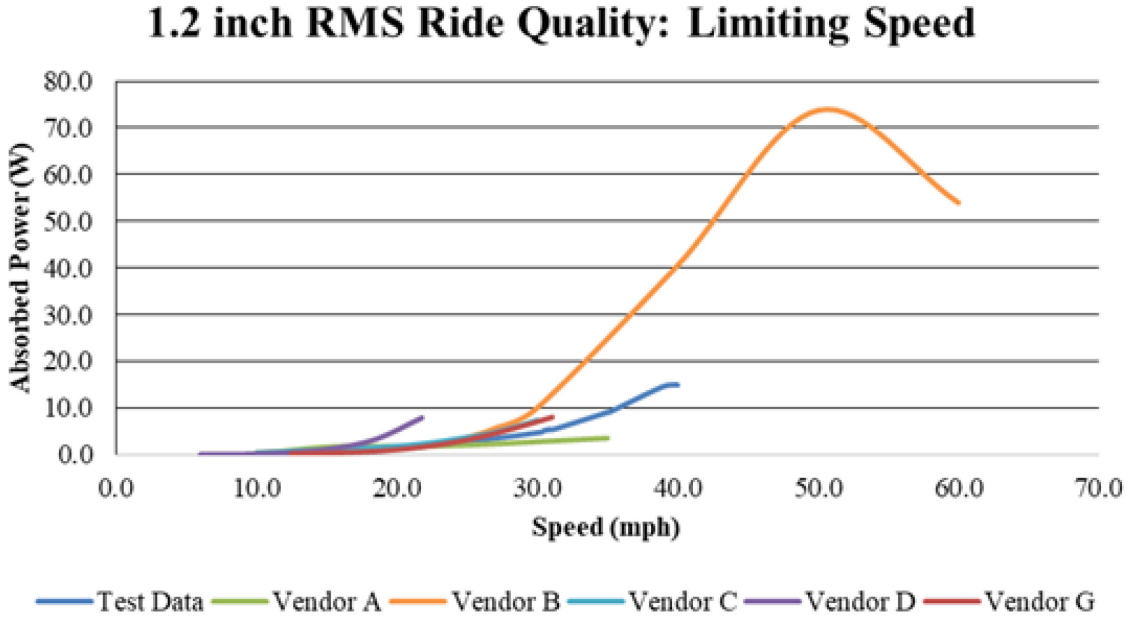


Figure 8B-36: Ride Quality: 1.2 RMS.

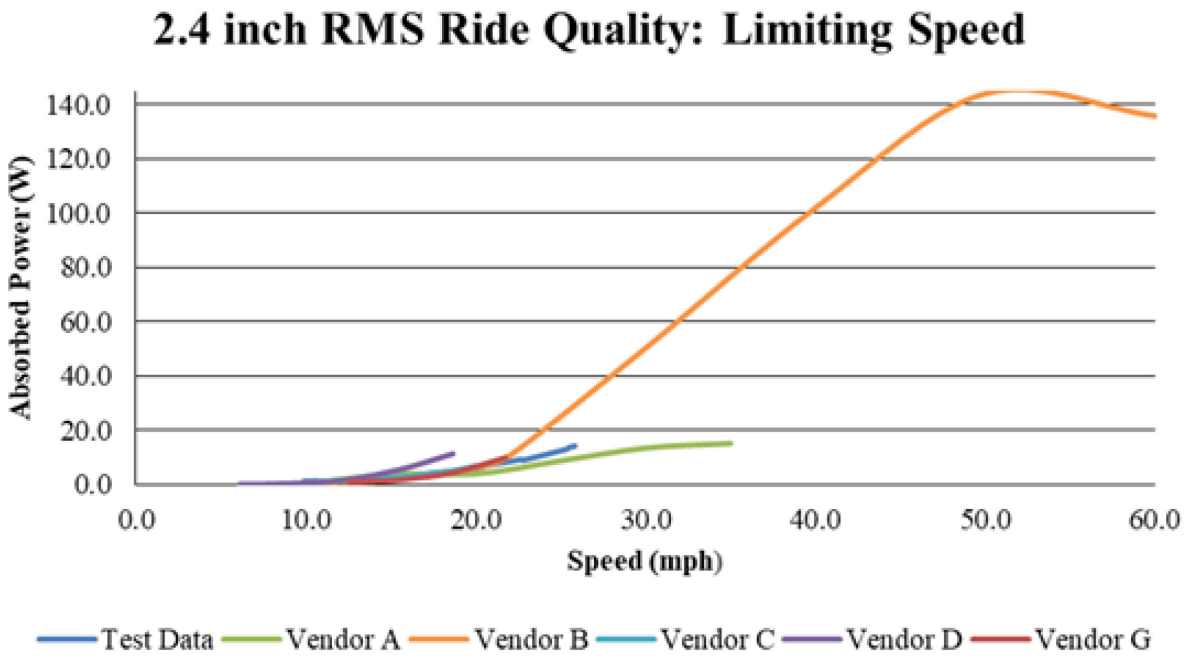


Figure 8B-37: Ride Quality: 2.4 RMS.

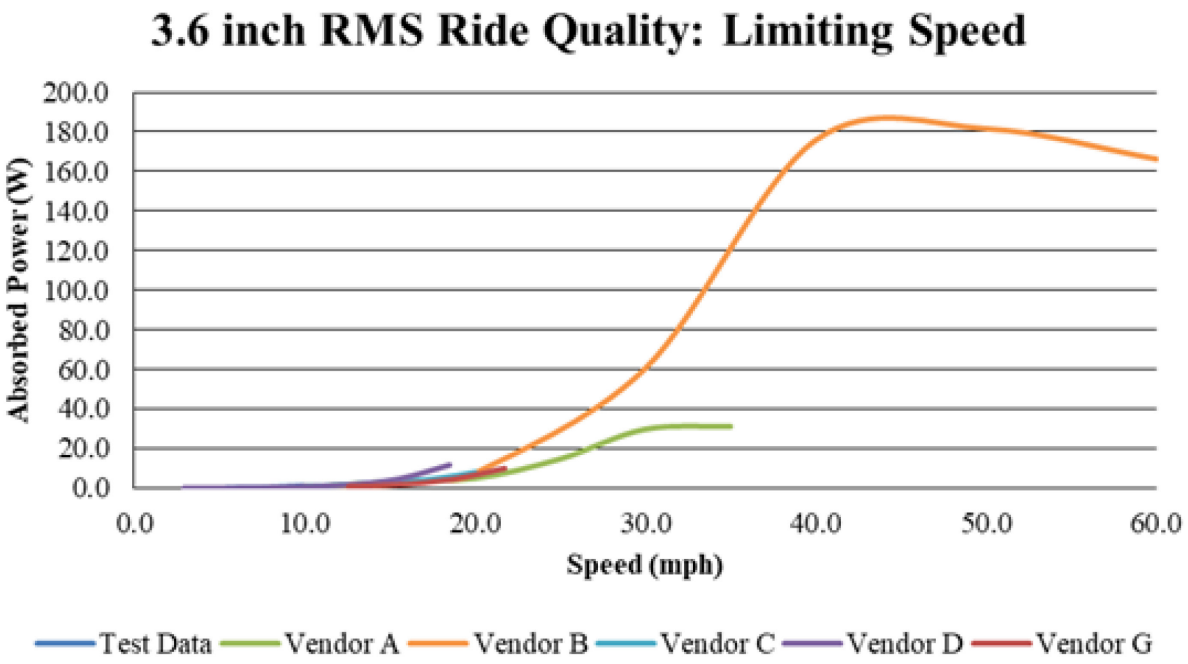


Figure 8B-38: Ride Quality: 3.6 RMS.

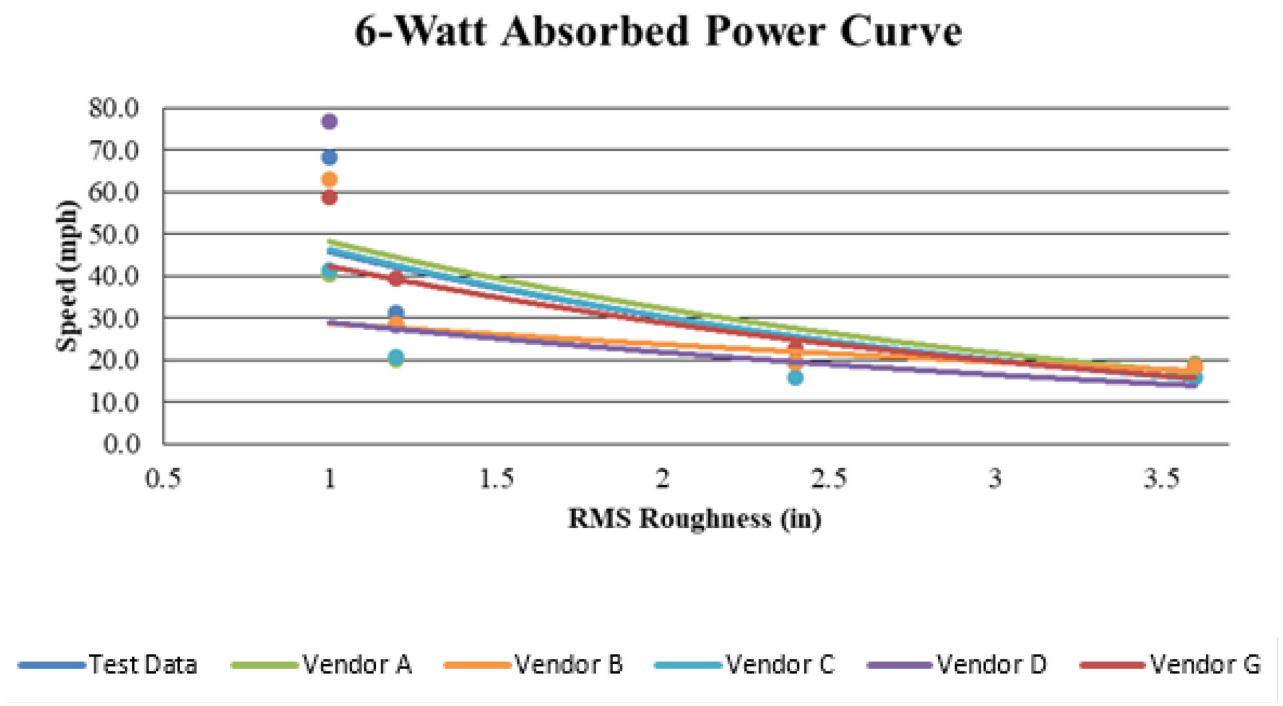


Figure 8B-39: Ride Quality: 6-Watt Absorbed Power Curve.

The limiting speeds of each vendor and each ride quality course are shown in Figure 8B-40 and in Figure 8B-41. The results obtained by Vendor D have been read from graphs, adding some uncertainty to the results. As shown, the vendors are capable of producing similar results.

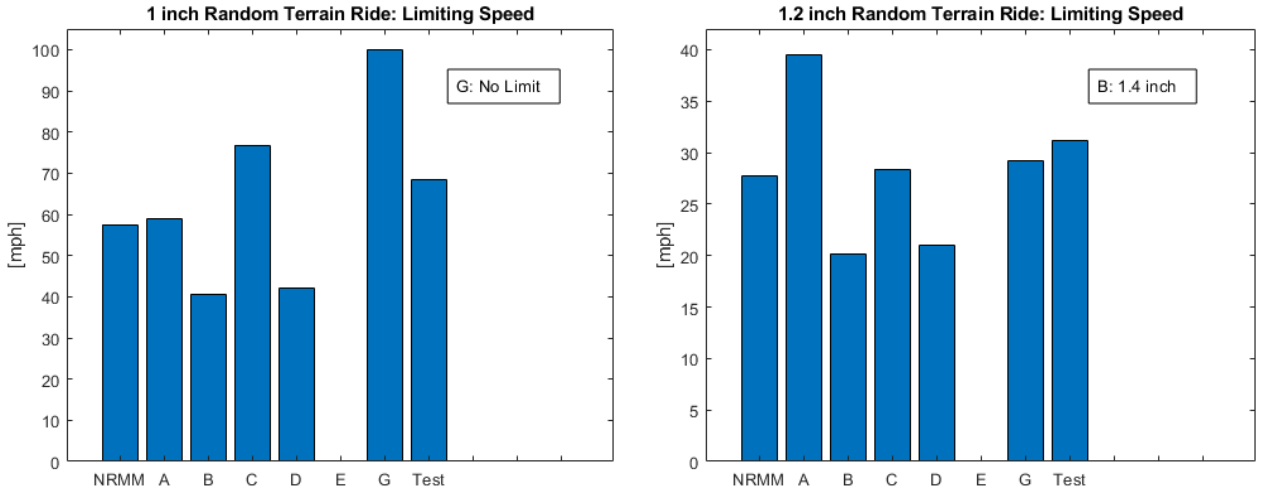


Figure 8B-40: Random Terrain Ride 1 Inch RMS (Left) and 1.2 Inch RMS (Right): Limiting Speed.

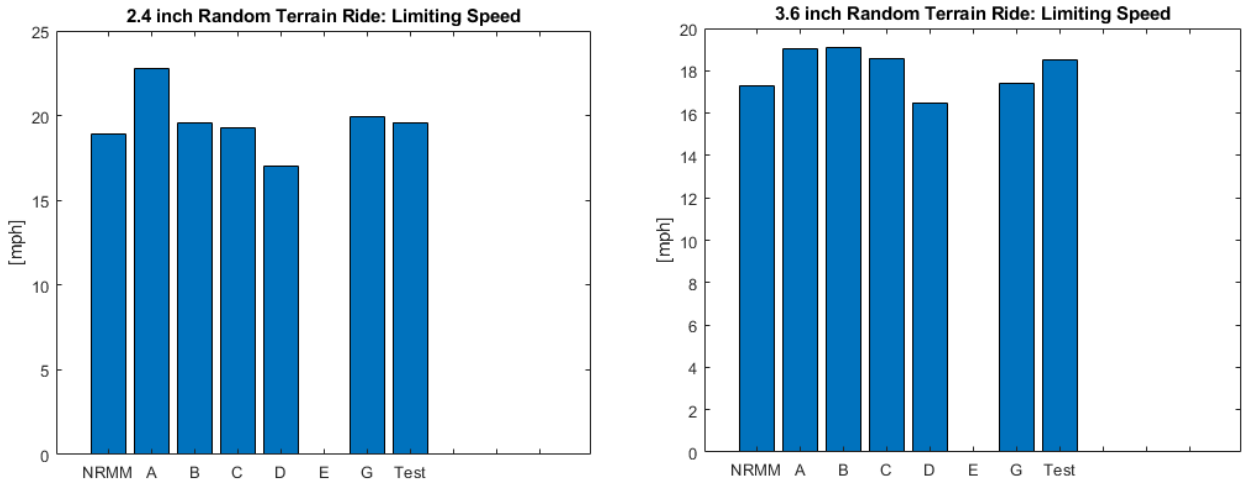


Figure 8B-41: Random Terrain Ride 2.4 Inch RMS (Left) and 3.6 Inch RMS (Right): Limiting Speed.

The Maturity Levels are based on the 6-watt curve obtained by the vendors compared to test data. All vendors, except for Vendor E, who did not perform the event, have achieved Level 6 as seen in Figure 8B-42.

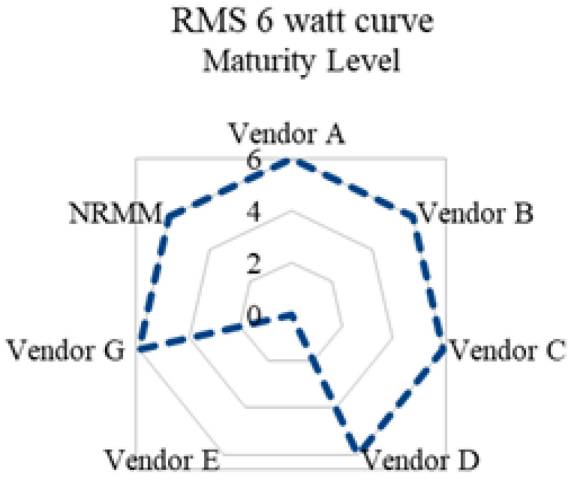


Figure 8B-42: RMS Maturity Level Achieved by Vendors.

8B.6.9 Drawbar Pull

Figure 8B-43 and Figure 8B-44 show the drawbar pull obtained by each vendor for both open and locked differentials at 20% slip and at peak slip. Vendor A has not provided data at 20% slip, but at 200% slip.

Due to difficulties in interpreting the soil properties provided Vendor C has used LETE sand properties defined in Ref. [9]. Furthermore, the results of speed and slip, obtained by Vendor C in Figure 8B-43 and Figure 8B-44 are read through graphs that were not particularly easy to read. Vendor D has provided results for some of the simulations, but due to an illegible graph, those results are not displayed in Figure 8B-43 or Figure 8B-44.

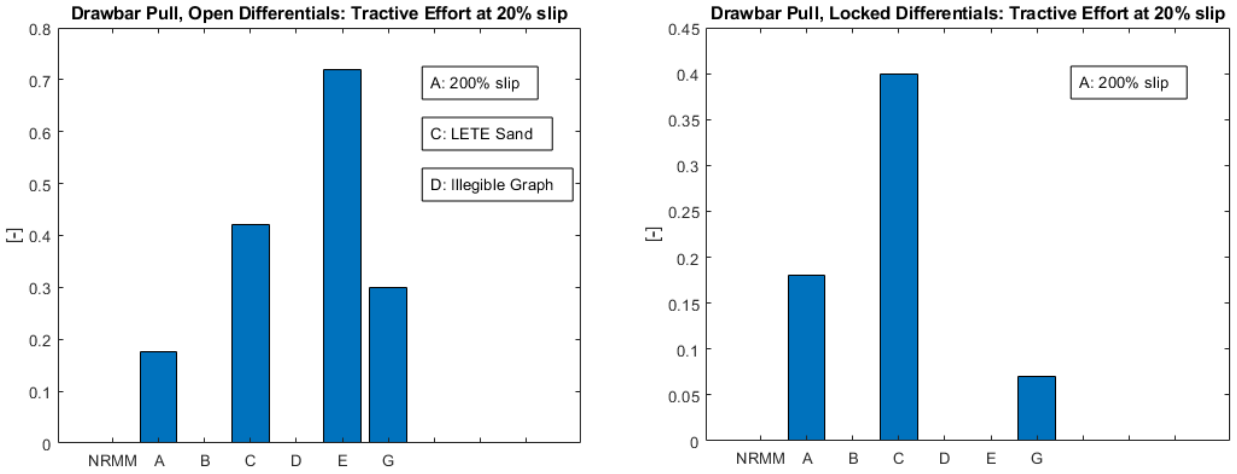


Figure 8B-43: Drawbar Pull Open Differential (Left) and Locked Differentials (Right): Drawbar Pull Coefficient at 20% Slip.

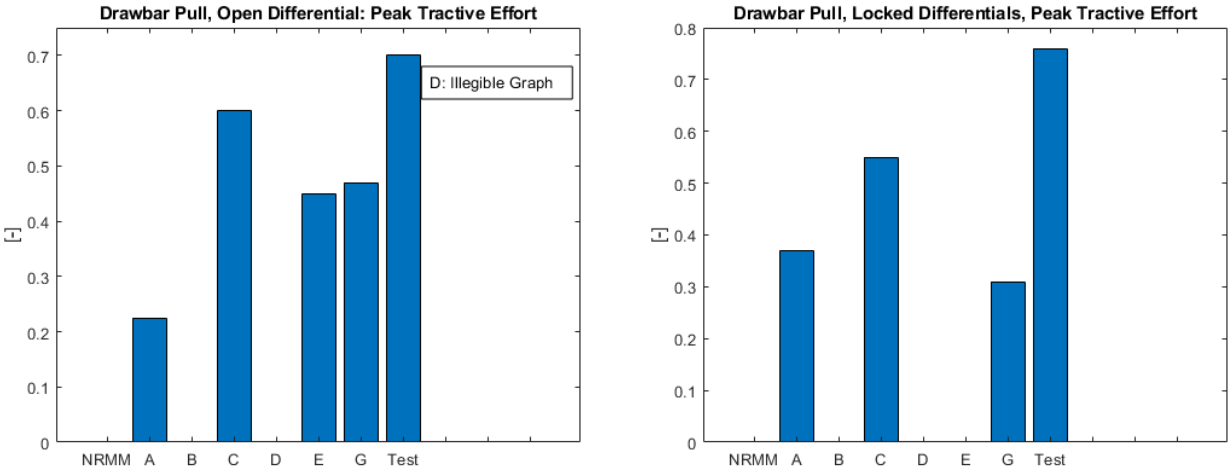


Figure 8B-44: Drawbar Open Differential (Left) and Locked Differentials (Right): Drawbar Pull Coefficient at Peak Slip.

Figure 8B-45 shows the Maturity Level achieved by the vendors for the drawbar pull event based on test results. Most vendors have achieved Level 6 in both the locked and the open differential event.

8B.7 BENCHMARK UPDATED RESULTS

Some of the vendors have provided new results after improvement of their respective vehicle model. The modified results are presented below.

8B.7.1 Wall-to-Wall Turn Radius

Vendor A has resubmitted the wall-to-wall result. The original diameter of 19.996 m has been altered to 19.64 m, not changing the general conclusion on the event.

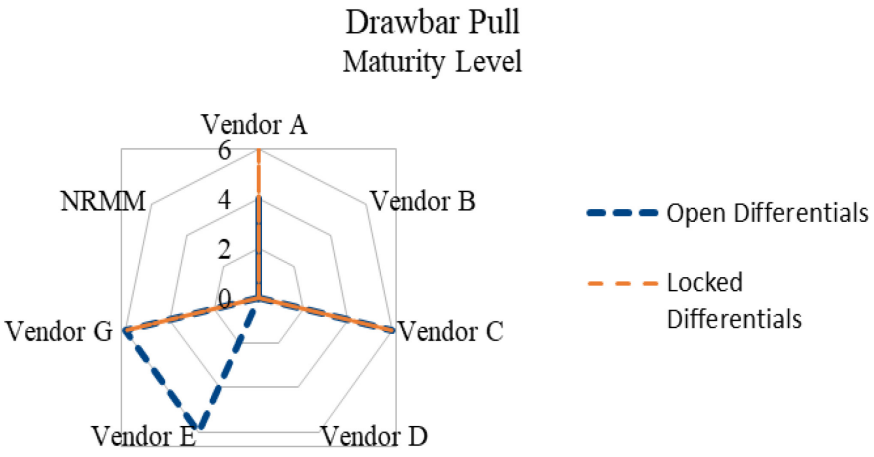


Figure 8B-45: Sand Traction Maturity Level Achieved by Vendors.

8B.7.2 Steady-State Cornering

The Vendor has likewise resubmitted a new result of the counterclockwise steady state cornering event, altering the maximum speed from 44.5 mph to 43 mph, not affecting the overall conclusion.

8B.7.3 Paved Double Lane Change

A new simulation of the double lane change left turn first without use of the steering input has been conducted by Vendor A. The maximum speed of 48 mph is only an increase of 2 mph compared to the first results obtained.

8B.7.4 Side Slope Stability

Vendor D later conducted the closed-loop side slope stability event as seem in Figure 8B-46. The result of Vendor D is within the same range as the speeds obtained in the open loop event in Figure 8B-28.

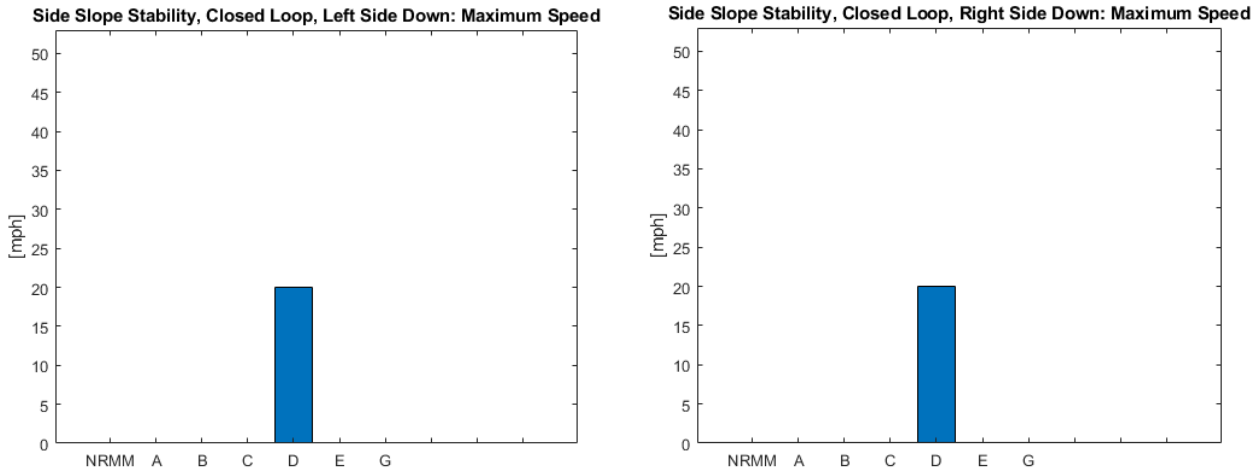


Figure 8B-46: Side Slope Stability Steering Closed Loop, Left Side Down (Left) and Right Side Down (Right): Maximum Speed.

8B.7.5 Sand Slope Gradeability

Vendor D has provided a new result of the maximum slope lowering the result from 25% to 23% with both open and locked differentials. This does not affect the overall conclusion on the vendor performance. The new results are seen in Figure 8B-47. Vendors A, D and G have obtained improved maximum slope results, resulting in Level 4.

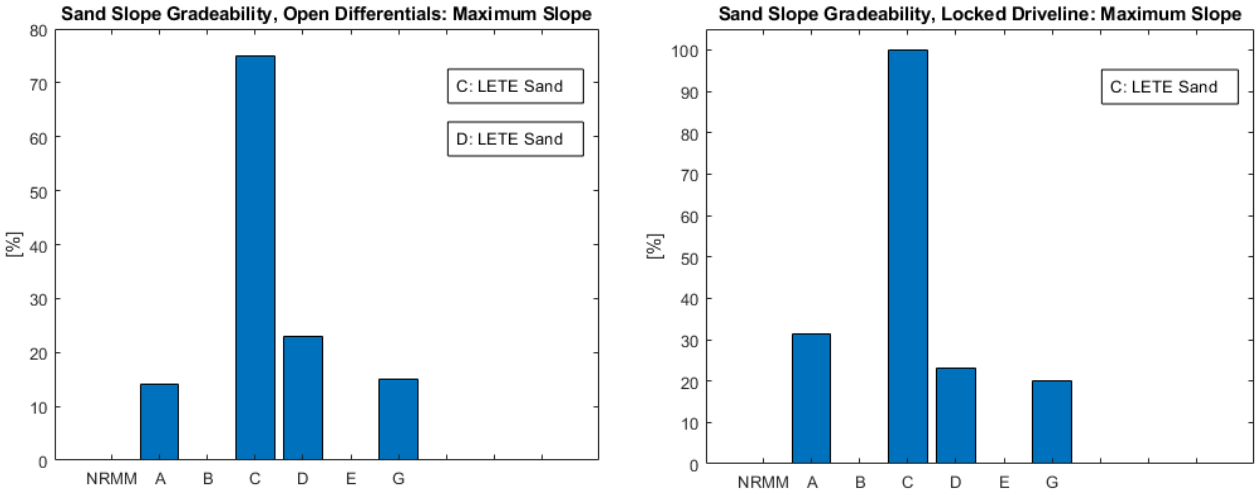


Figure 8B-47: Sand Slope Gradeability Open Differentials (Left) and Full Locked Driveline (Right): Maximum Slope.

8B.8 SUMMARY AND CONCLUSIONS

In Table 8B-2 and the corresponding spider chart in Figure 8B-48 the achieved wheeled vehicle benchmark Maturity Levels are summarized for the participating vendors. A Maturity Level of 6 is obtained by a vendor who has achieved blind correlation to test data. A Maturity Level of 4 is obtained when the results obtained by multiple vendors are comparable. A Maturity Level of 2 is the maximum possible where the test data were inadequate and only one vendor produced a simulation, or if a vendor was judged to be an outlier. An industry wide Maturity Level is assigned based on the maximum achieved across all vendors for the individual event. The composite industry maturity for the whole WVP benchmark is based on the average across the events. These results show that at least one vendor was able to demonstrate the maximum Maturity Level for each event, except for the locked differential drawbar pull event. Thus, the most significant challenge for most vendors was the soft soil events. Nevertheless, one vendor demonstrated an 87% score on soft soil events. However, it should be recalled that this WVP benchmark was for a limited subset of events, and counted hardpack gravelly conditions as “soft soil” and did not include soft soil trafficability or motion resistance (i.e., the unachieved events in the Tracked Benchmark).

Based on a review of the individual results:

1) Paved surface events were generally successful at Level 6 for events with reported test data.
2) Gravel surface turning and side slope events were also successful at Level 6.

3) Traction (drawbar pull) validations were partially successful at Level 6 demonstrating the need for further soft soil model development for simulation implementation. Nevertheless, good agreement among the vendors supported a strong Level 4 assessment, and though not explicitly demonstrated, Level 5 (model calibration) should also be very achievable.

4) Sand slope gradeability results demonstrated reasonable agreement at Level 4 but also highlighted this area as the most significant technical challenge for both consistent test procedures and repeatability as well as simulation and modeling.

The general conclusion is that the vehicle dynamics M&S vendors, as an industry, do have the mature capability to predict most of the required events identified by the NG-NRMM effort. Furthermore, by virtue of its 2D theoretical basis, the NRMM model falls short for all of the events requiring 3D modeling for maneuvering. It is also noted that soft soil modeling for the 3D transient dynamics simulation is in need of tailored soil characterization data dedicated to this purpose for the particular software implementations, in order to rigorously demonstrate Maturity Level of 6 and above.

Table 8B-2: Wheeled Vehicle Benchmark Maturity Levels.

SIMULATION		NRMM	A	B	C	D	E	G
CG Height		-	-	6	-	6	-	-
Straight Line Acceleration Max Speed	Paved	6	6	6	6	6	-	6
Wall-to-Wall Turn Radius	Clockwise	-	4	4	4	4	-	4
	Counterclockwise	-	-	4	4	4	-	4
Steady-State Turning Speed	Clockwise	-	-	6	6	6	-	6
	Counterclockwise	-	6	6	-	6	-	6
DLC Left Turn First Input Speed	Paved	-	2	-	2	2	-	6
	Gravel	-	2	-	2	2	-	6
DLC Left Turn First No Input Speed	Paved	6	6	6	6	6	-	-
	Gravel	6	6	-	6	6	-	-
DLC Right Turn First Input Speed	Paved	-	2	-	2	2	-	-
	Gravel	-	2	-	2	2	-	-
DLC Right Turn First No Input Speed	Paved	-	-	6	6	6	-	-
	Gravel	-	-	-	6	6	-	-
Side Slope Stability Input Speed	Left Side Down	-	4	4	2	4	-	4
	Right Side Down	-	6	6	6	6	-	6
Side Slope Stability	Left Side Down	-	-	-	-	2	-	-

SIMULATION		NRMM	A	B	C	D	E	G
No Input Speed	Right Side Down	-	-	-	-	2	-	-
Sand Slope Gradeability Speed	Open Differentials	-	4	-	4	4	-	-
	Locked Driveline	-	4	-	4	-	-	-
Ride Quality Speed	1 in	6	6	6	6	6	-	2
	1.2 in	6	6	6	6	6	-	6
	2.4 in	6	6	6	6	6	-	6
	3.6 in	6	6	6	6	6	-	6
	Avg.	6	6	6	6	6	-	6
Sand Tractive Effort	Open Differentials	-	4	-	6	-	6	6
	Locked Differentials	-	6	-	6	-	-	6

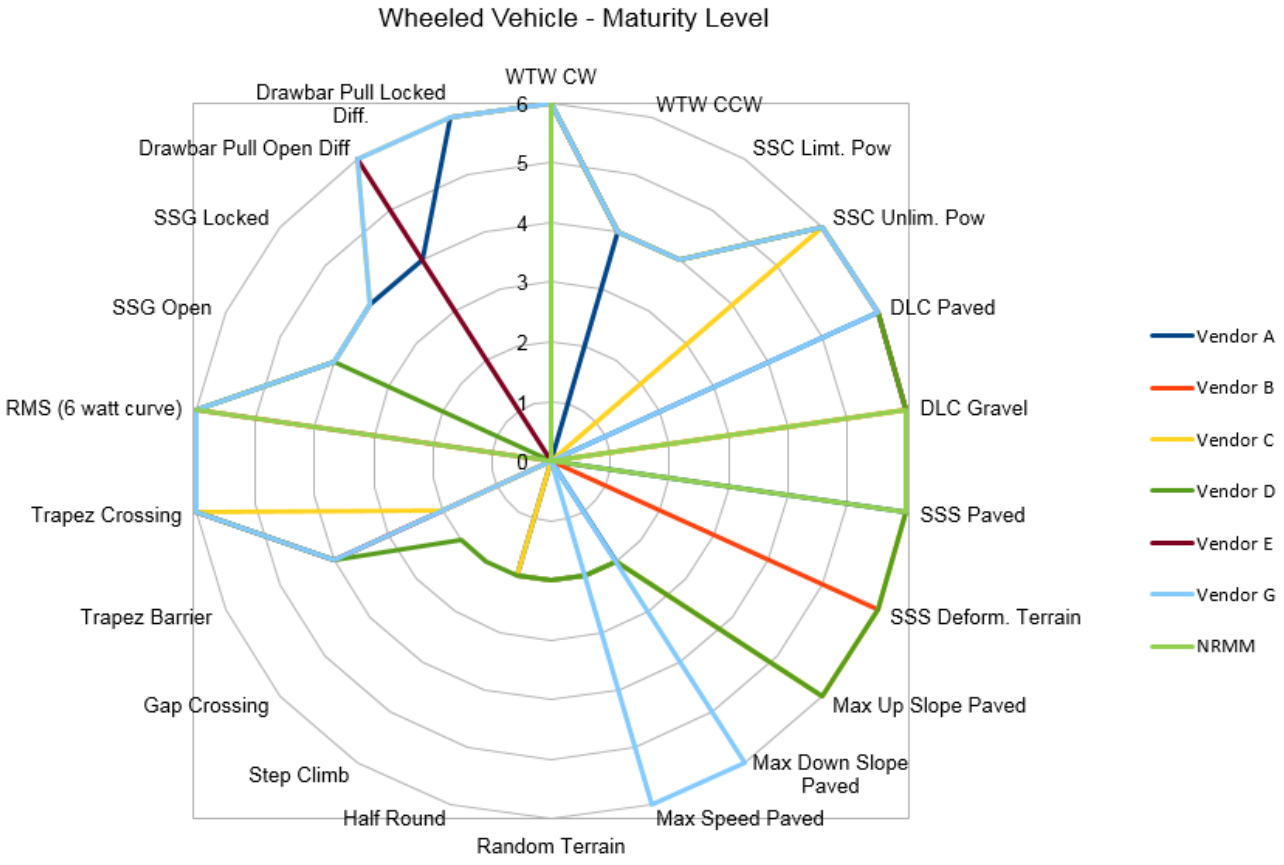


Figure 8B-48: Wheeled Vehicle Maturity Level.

8B.9 REFERENCES

[1] Meintjes, K. 2015. NAFEMS Americas Simulation 20/20. Webinar Presentation on Simulation Governance.

[2] TOP 2-2-602. 1981. Acceleration; Maximum and Minimum Speeds. January 1981.

[3] AVTP 03-30. 1991. Steering and Maneuverability. September 1991.

[4] SAE J2184. 2000. Vehicle Lift Points for Service Garage Lifting. February 2000.

[5] AVTP 03-160W. 1991. Dynamic Stability. September 1991.

[6] TOP 2-2-610. 1980. Gradeability and Side Slope Performance, July 1980.

[7] TOP 1-1-014. 2007. Ride Dynamics, October 2007.

[8] TOP-2-2-604. 2007. Test Operation Procedure: Drawbar Pull, September 2007.

[9] Wong, J.Y, Garber, M. and Preston-Thomas, J. 1984. Theoretical prediction and experimental substantiation of the ground pressure distribution and tractive performance of tracked vehicles. Proceedings of the Institution of Mechanical Engineers, Part D, Transport Engineering, 198:265-285.



Chapter 9 – TA7: DATA GAPS; OPERATIONAL READINESS

Mike Bradbury and Jonathan Bruce
Defence Science and Technology Laboratory (Dstl)
UNITED KINGDOM

9.1 GOALS AND TEAM MEMBERS

The aim of this Thrust Area was to identify gaps that will need to be addressed by future work in the pursuit of NG-NRMM, more specifically capability gaps and the challenges of implementing NG-NRMM.

Objectives:

1) Benchmark group views on how the emerging NG-NRMM will be used (to provide context to gaps and challenges identified).
2) Identify gaps and challenges in work to date against the ET-148 and STANREC requirements.
3) Make recommendations for NG-NRMM and the STANREC.

The team members are shown below:

- **Mike Bradbury, Leader**, UK;
- Jonathan Bruce, UK; and
- William Suttie, UK.

9.2 INTRODUCTION

Thrust Area 7 was originally proposed based on the observation that the increasing complexity of the terramechanics being considered in Thrust Areas 2 and 3 would make it more difficult to source appropriate terrain data to run the models. In turn, this may lead to a divergence between NG-NRMM capability and aspiration; e.g., the ability of a model with complex data requirements may not be practical for operational support.

To address this concern three questions were originally defined:

1) Has the group benchmarked the feasibility of data provision across domestic use, pre-deployment and operations for Simple versus Complex NG-NRMM?
2) For AVT-248 to be successful does this have to be demonstrated?
3) For AVT-248 to be successful does a roadmap of how gaps may be closed need to be considered?

From this a small scoping study was proposed approaching the problem in three steps and utilizing a group questionnaire to collect information. The task to:

1) Refine requirements:
    a) E.g., Model type versus exploitation path; how do members envisage NG-NRMM being used?
        i) Model: Legacy NRMM, Simple NG-NRMM, Complex NG-NRMM; and
        ii) Exploitation: Research, Procurement, Support to Operations.

2) Benchmark current feasibility of obtaining terrain data, by exploitation path, to generate priorities for intervention.
    a) E.g. do members generate new terrain files?
    b) If so, for what reasons, e.g., research versus support to operations?
    c) What sources are utilized, e.g., domestic, proprietary, open source?
    d) Are inference models used?
    e) Is statistical data used? If so based on what?
    f) Is international collaboration used?
    g) What are the resulting strengths and weaknesses across the data set?
    h) How does ability vary by geographic region?
3) Consider how terrain generation could be improved (from a data source perspective not TA1 implementation).
    a) Blue skies thinking, how to close the capability gaps (or not).
        i) Surrogates: transposed data.
        ii) On the ground: covert action, modified vehicles.
        iii) In the air: UAV, overflight, satellite.
        iv) 3rd party: online, open source.

However as the work of AVT-248 proceeded the work in this Thrust Area broadened to capture capability gaps in the work to date and the challenges with achieving operational readiness, the defined objectives superseding the planned scoping study.

9.3 CAPABILITY GAPS METHODOLOGY

9.3.1 Introduction

AVT-248 has concluded that NG-NRMM should adopt a general methodology approach as outlined in the DRAFT STANREC. This can support a model of models methodology in a similar way to the legacy NRMM2 implementation. (See Figure 9-1, cross-country example). Alternatively NG-NRMM can be implemented to assess a range contributing factors at the same time; for example combining soil interaction with obstacle crossing using dynamic modeling. The STANREC needs to recognize this is a decision for the methodology approach adopted for the implementation of NG-NRMM; NG-NRMM should be considered the Next-Generation NATO Reference Mobility **Methodology** and not **Model** to reflect the potential for a combination of tools and methods.

What initially appears as a trivial nuance is important in considering the gaps and challenges with achieving NG-NRMM operational readiness. In recognizing the implementation methodology is not prescribed and is a variable, it must be accepted that subsequently the capability gaps and challenges therein are also variable. Not all capability gaps and challenges will apply to all instances of NG-NRMM, those that do may vary in implications.

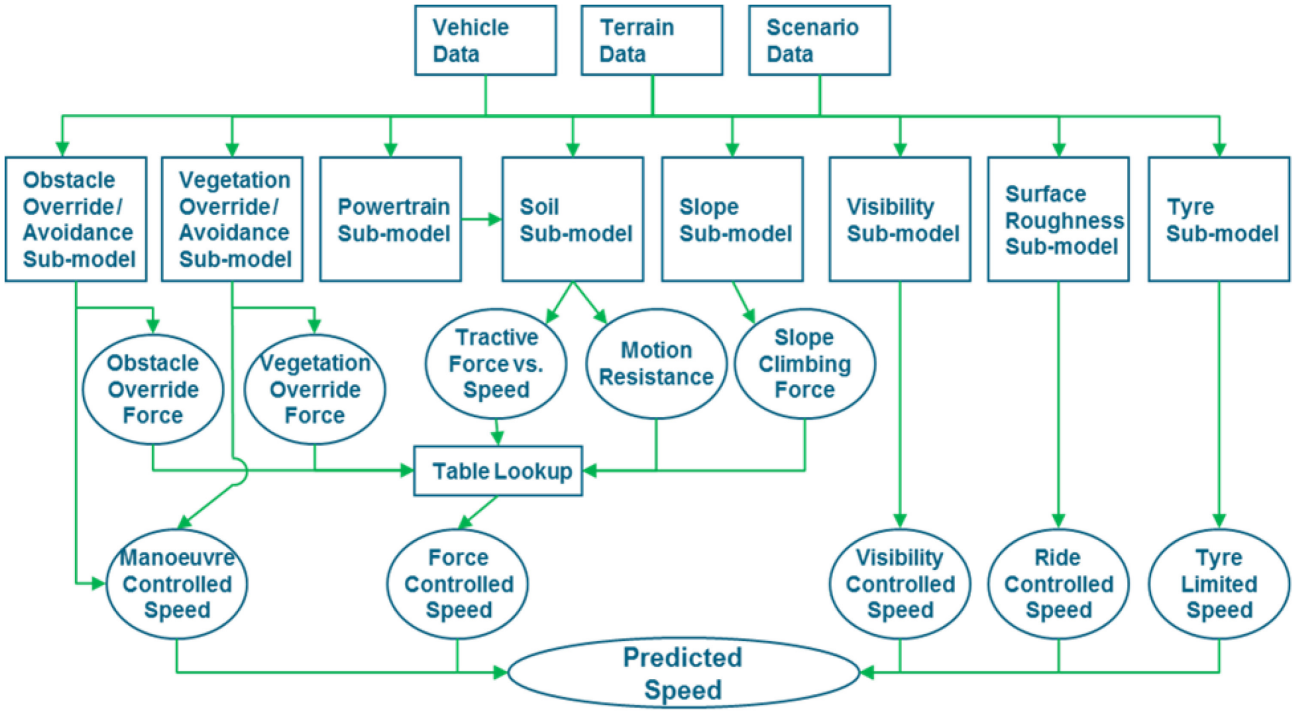


Figure 9-1: Legacy NRMM2 Cross-Country Methodology.

9.3.2 Methodology

Using the NRMM2 cross-country methodology as a comparator, an initial assessment was made (Figure 9-2) of which areas the group has addressed (no mark), partially addressed (question marks) and not addressed (circle strikeout). The overview given in Figure 9-2 is not intended to highlight any shortfall in the activities of AVT-248 but is a reflection of the following:

1) The terramechanics are the heart of the problem, the change driver and the most significant consideration. Typically any methodology or process diagram will not be representative of this. Improving terramechanics modeling is at the center of the group's aims and activity.

2) The areas not covered can be addressed by some of the tools used in the prototypes and testing, other means or collectively by common tools (this having a reduced development or procurement cost).

From this it was decided a generic definition of NG-NRMM was required so that the process could be considered independent of the implementation for the purposes of discussing capability gaps and challenges. This is defined in the next section (as it is linked to the proposals therein).

As part of the process the original requirements from ET-148 would need to be referenced. (See Figure 9-3, the key identifies areas that became the focus of AVT-248 Thrust Areas.)

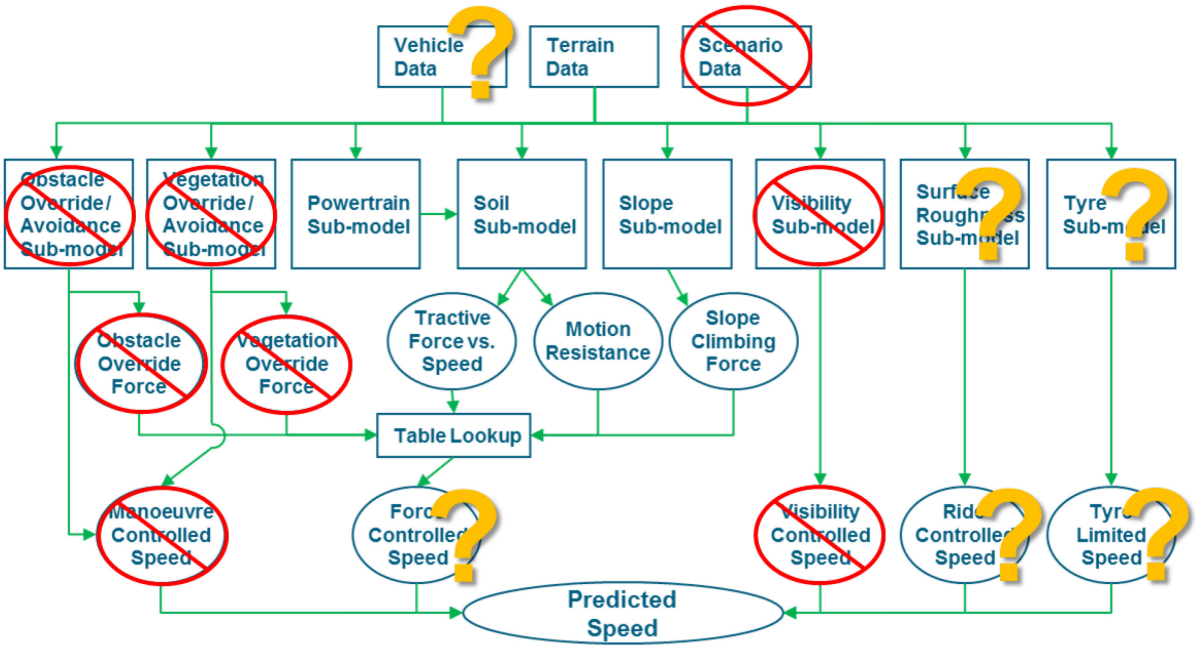


Figure 9-2: Assessment of Areas Addressed in NG-NRMM Compared to Legacy NRMM2 Cross-Country Methodology. Areas the group has addressed (no mark); partially addressed (question marks); and not addressed (circle strikeout).

Category	Sub- Category	Near-Term Priorities for NGN Threshold	Near-Term Priorities for NGN Objective
New System Capabilities	Vehicle Type	Wheeled Tracked	Legged
		Autonomous (simple)	Autonomous (complex)
	Vehicle Scale	Conventional manned vehicles	Lighter, smaller vehicles
	Terrain Scale	Regional, varied resolutions	Global, varied resolutions
New Modelling Capabilities	Suspension Types	Passive Semi-active Active	Active
	Control Types	Driver ABS, TCS, ESC, ABM CTIS	
		Autonomy (simple)	Autonomy (complex)
	Sub-systems	Steering, Powertrain	Human Cognition
		Autonomy (simple)	Autonomy (complex)
	Model Features	Terrain models (e.g. Bekker-Wong)	Terrain models (e.g. DEM, FEM)
		3D Physics based models	Stochastic models
		Multibody dynamic vehicle models	
		Flexible body models	
		Detailed tire and track models	
New Analysis Capabilities	Environment Types	On-road, off-road	
		Urban	Urban
		Soil	
		Snow/ICE	
	Powertrain performance	Grading Turning Fuel-efficiency	Cooling
	Amphibious Operations	Fording Swimming	
	Computations	Efficiency-fidelity trade-off	High fidelity
			High performance
New Output Capabilities	Assessment Types	Performance in operational context	
	Metric Considerations	Verifiable mobility metrics	

Key: Gap areas in:
- Mobility Mapping
- Environmental Modelling
- Intelligent Vehicles
- Stochastics
- Computational Performance
- Verification & Validation

Figure 9-3: Key New Requirements as Determined by ET-148.

With this in mind, the following approach was adopted for considering the capability gaps and challenges in achieving operational readiness:

1) **Identification**. How do you identify the capability of any given instance of NG-NRMM? If you cannot do this you cannot consider the gaps in capability.
2) **Use and Users**. Who will use NG-NRMM and what for? This insight provides context for the capability gaps and challenges.
3) **Capability Gaps and Challenges**. What are the perceived capability gaps and challenges?

9.4 IDENTIFICATION

9.4.1 Introduction

Gaps can be considered from two perspectives. Firstly from the perspective of what the Thrust Areas have been able to achieve and gaps against the original requirement, the aspirational NG-NRMM. Some of these gaps are driven by the art of what is currently possible; some of these simply reflect the priorities of the group's effort in generating and testing prototypes. Secondly, it has to be recognized that different users have different priorities and requirements; for example operating in sandy conditions versus snow. Given this:

- It should not be assumed that all implementations of NG-NRMM have the same aspirational end state.
- A system is required such that a given methodology's capability and configuration can be identified, managed and controlled with reference to the STANREC aspirational NG-NRMM.

This is essential for several reasons:

1) **Validation and verification**. For example the validation process is a function of tool fidelity, required level of confidence and risk tolerance. A subjective method might have different validation requirements to that of a dynamic model.
2) **Context**. When using evidence (i.e., model output) understanding the methodology behind the results is key to accurate analysis and interpretation. For example a model may show a vehicle slowing on road bends, it could be concluded this was due to vehicle stability. However without knowing if the model accounted for dynamic effects or not this conclusion could not be made.
3) **Comparing**. Assuming multiple tools are adopted and/or developed against the STANREC it will be important to understand how their output can be compared; e.g., evidence generated by multiple tools could be provided by suppliers in a procurement context.

By considering this problem and how to define a variable NG-NRMM we can build a construct to identify gaps against. The proposal for consideration by future work and the STANREC is to use a system of defined Layers (see Section 9.4.2) and Levels (Section 9.4.3).

9.4.2 Layers

The Esri Support GIS Dictionary (https://support.esri.com/en/other-resources/gis-dictionary/search/) describes a GIS layer as a data structure: "*The visual representation of a geographic dataset in any digital map environment. Conceptually, a layer is a slice or stratum of the geographic reality in a particular area, and is more or less equivalent to a legend item on a paper map.*"

For the purposes of the STANREC, it is proposed that this is taken in context of the building blocks of the mobility analysis methodology. To put that in context, the STANREC Layers for the cross-country methodology for the legacy NRMM2 (Figure 9-4) would be Obstacle Crossing, Vegetation Override, Soil, Slope, Visibility, Surface Roughness and Tire.

The initial proposed definition of a Next-Generation NRMM Layer is:

- *"A discrete factor of the mobility of a ground vehicle whose influence can be independently assessed for its impact on terrain accessibility and Speed-Made-Good, and whose significance is worthy of doing so."*

Note "can be independently assessed" not "must" or "will".

Based on this principle the proposed Layers for NG-NRMM are:

1) **Terramechanics**: The ground interaction being a combination of soil and surface material (or ground level vegetation), as pursued by Thrust Areas 2 and 3.
2) **Roads**: While certain roads and cross-country types will have common data (e.g., legacy NRMM2 cross-country and trails/tracks road terrain both consider terramechanics) they are sufficiently distinct from the perspective of performance metrics and potentially how they are implemented.
3) **Water**: It is suggested this is separated out for the reason that a methodology capable of simple terramechanics may still need to consider fording, wading and/or swimming. Further some nations may have an emphasis on this type of terrain over others. In contrast many vehicles have no requirement at all for swimming.
4) **Urban**: This is something the legacy NRMM2 does not model. Performance here is typically (but not exclusively) about physical dimensions, turning radii and non-terramechanics factors.
5) **Features**: Legacy NRMM2 considers obstacles and trees separately. It is proposed NG-NRMM simply considers features, something that can be broken down and implemented as a hierarchical data model and implemented as per user requirements.
6) **Ride**: Driver prudence and tolerance will remain a platform performance constraint and will need to be considered. Further there are occasions where such analysis would be of use outside of the context of NG-NRMM predictions.
7) **Control**: Legacy NRMM2 includes visibility and braking distance, speed limits and the ability to constrain performance. NG-NRMM must consider this more widely, for example the constraints of unmanned vehicles as well as manned. This is potentially where TA4 Intelligent Vehicles is addressed.

For the STANREC it is proposed obstacles and (above surface) vegetation (e.g., trees as implemented separately in the legacy NRMM2) can be considered as a collective ability, that to defeat or overcome "features". (This is discussed further in Annex I.)

With these Layers defined, the following generic definition of NG-NRMM (Figure 9-4), as suggested in the previous section) was drafted.

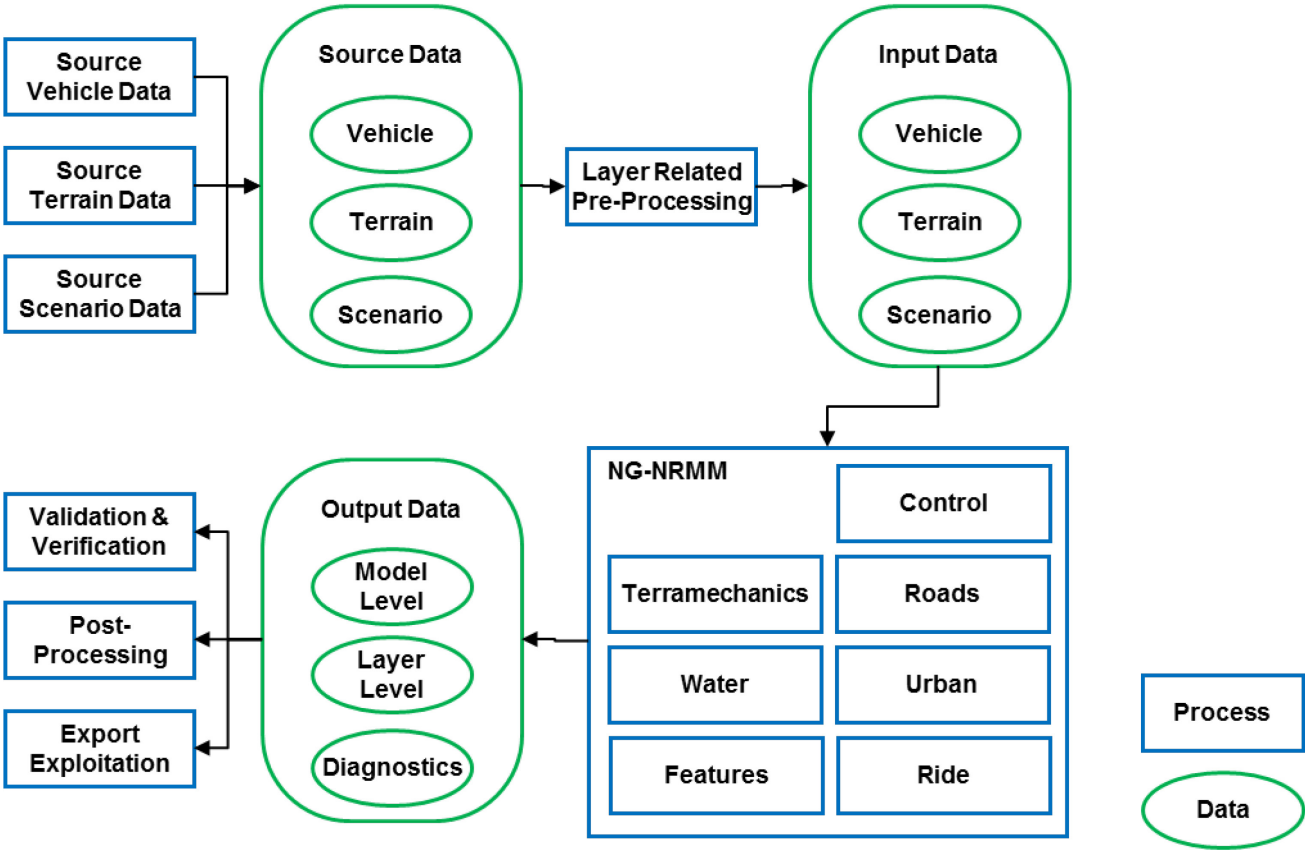


Figure 9-4: Generic NG-NRMM Methodology.

The process:

- All NG-NRMM implementations will need data. By its very nature terrain, vehicle and scenario will come from different sources.
    - Those processes will result in raw data stored in a database of some form but a key point to note is that raw data is unlikely to be sourced in the correct format and form for direct input to NG-NRMM. In addition the type and format of data is likely to vary with different NG-NRMM implementations. This data may be stored centrally or distributed by source type.
- The data will need to be pre-processed or exported into a format suitable for NG-NRMM to use, including for different NG-NRMM implementations.
    - Again the resulting data may be stored centrally or distributed. This is exemplified by the work TA1 has undertaken.
- The NG-NRMM implementation methodology may be anything from a single tool to a collection of tools and methods. Executing NG-NRMM will result in data, likely across three areas:
    - Model level output would be comparable to the current predictions and statistics files, or it could be the data to support a geographical information system interface.

- Layer level output will come from the methodology components, whether a combined system or separate tools. Analysts will want to be able to interrogate these underlying contributing factors.
- Diagnostic output is a useful tool to enable model and analysis verification.

- As with the legacy NRMM2, the NG-NRMM output will have wider exploitation beyond providing stakeholders research, procurement and operational decision support.
  - It will be used to support validation and verification, maintenance and improvements.
  - Output will be post-processed for made-to-order applications.
  - Output will be exported and exploited to provide the inputs to other systems such as operational analysis/research combat effectiveness models.
  - All forms of output can be used to support incremental development of the tools.

9.4.3 Levels

It is not enough to know whether a methodology covers a certain aspect, e.g., urban or obstacles, it is important to understand to what extent it addresses it, its strengths and weaknesses. For example a tool could be better appreciated if its terramechanics layer was qualified as utilizing a simple or complex method. It is proposed that setting Levels within Layers enables this.

The initial proposed definition of a NG-NRMM Level is:

- *"A measure of Layer complexity and capability in Next-Generation NRMM implementation."*

It is recognized that tools will not fit perfectly to any defined Levels but Levels need to be kept relatively coarse to reflect step changes in capability. At this time no mechanism is proposed to acknowledge tools that sit between Levels.

The STANREC has a decision to make if it adopts this approach:

1) Use the same fixed scale of Levels for each Layer.
   a) The benefit is that the Layers and Levels would be predictable and easier to follow. For example: Level 0 represents no capability; Level 2 is equivalent to the legacy NRMM2; Level 4 is the long-term NG-NRMM aspiration; Levels 1 and 3 are sensible partial solutions.
   b) The downside of this approach is some steps may be too course and not allow sufficient discrimination between capabilities with different levels of fidelity or validation. Equally some Levels may be redundant and undefinable.
2) Allow the number of Levels to vary by Layer in recognition of differing complexity and priority.
   a) The benefit is that this offers a scalable solution that can adapt as the STANREC develops.
   b) The downside of this approach is the configuration control burden of both the STANREC and legacy software that may have to be re-evaluated if the scheme changes its definitions. For example, in going from 3 Levels to 4, 4 may represent a new higher capability but equally 2 might be added between 1 and 3 to offer a previously unwarranted discrimination.

The following examples show how Layers and Levels would define a candidate NG-NRMM, based on Approach 1 (Figure 9-5, Figure 9-6). Approach 2 would be similar but with a varied length to each arm as opposed fixed at 4.

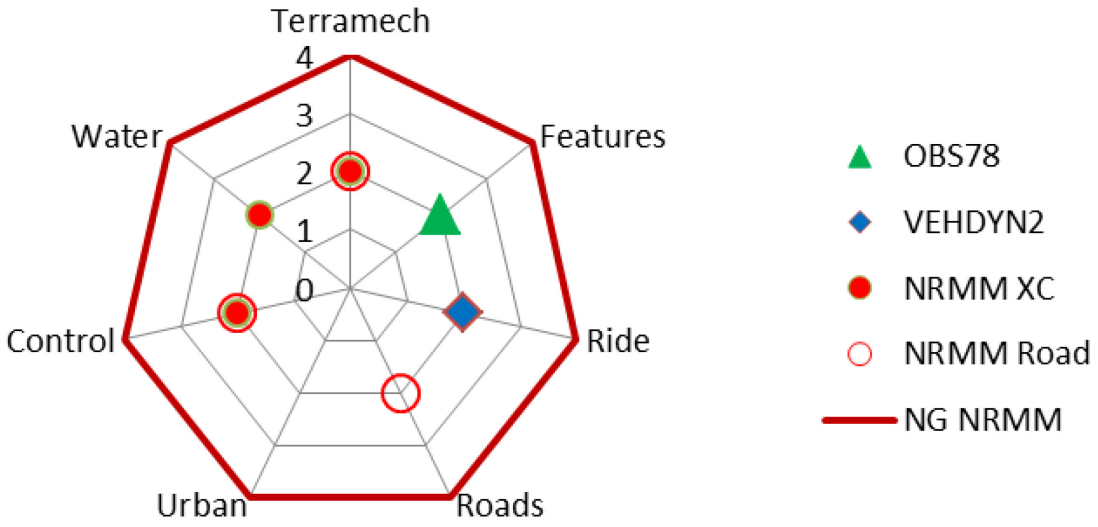


Figure 9-5: NRMM2 vs. Long-Term NG-NRMM Using Approach 1.

In this instance, starting at terramechanics and moving clockwise:

- NRMM2 would be identified as configuration 2-2-2-2-0-2-2, the 0 because NRMM2 does not model the urban environment.
- NG-NRMM (the aspirational end state) would be identified as configuration 4-4-4-4-4-4-4.

This allows the capability of these methodologies to be readily identifiable so if a new tool (e.g., "Tool X") was considered, its capability could be compared as in Figure 9-6.

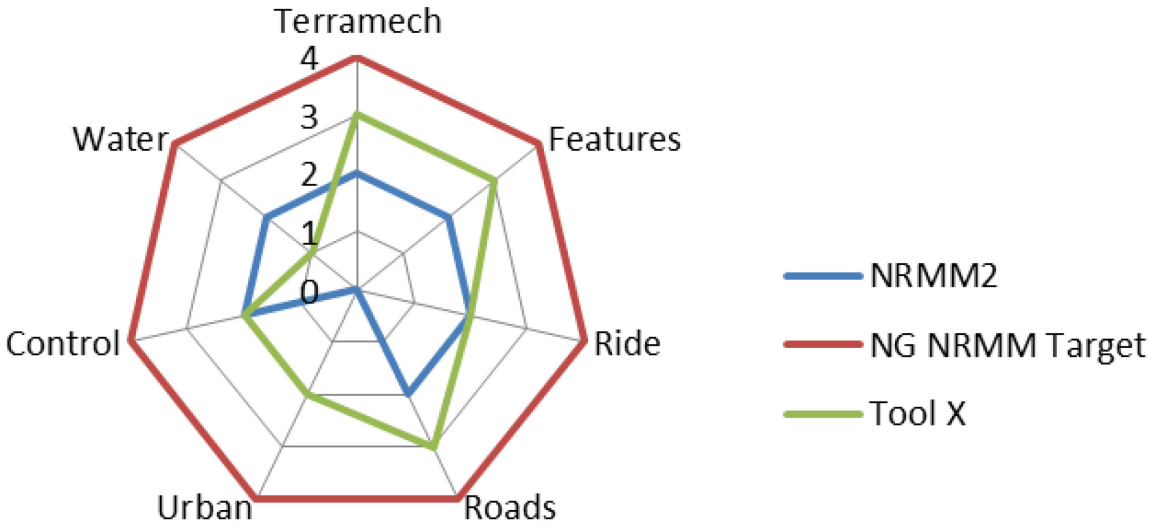


Figure 9-6: Example of Tool Comparisons Using Approach 1.

Table 9-1 shows how Levels for the Features Layer could be categorized, it shows the complexity increasing and the associated data requirements increasing but not correspondingly. For ease the complexity descriptions focus solely on the obstacles element.

Table 9-1: Levels Definition Example.

Level	Complexity	Data Implications
0	No obstacle crossing capability.	No data required.
1	Replicates legacy NRMM2 obstacle crossing capability.	Current trapezoidal data as found in legacy NRMM2.
2	Improved vehicle representation.	Potentially none if users have the data already for the Ride modeling – further the Ride model may service both needs for a relatively minimal overhead.
3	Improved vehicle and obstacle representation giving higher fidelity and confidence in results.	More data required and a new data model.

As part of an improved model the vehicle would by default be better represented even if using older definitions of the terrain. It should be remembered that the above table focuses on model functionality noting that in practice, for example, a level 2 model could be used instead of an available level 3 model in order to provide faster turnaround of multiple vehicle types and scenarios or to cope with lack of confirmed data.

9.4.4 Summary

A configuration control system of Layers and Levels has been proposed but the STANREC will still need to decide:

1) If this is the best way of achieving the goals of configuration control, verification and validation.
2) If adopted how this is to be implemented in the STANREC.
3) If this is sufficient to allow for comparison of output generated by different tools developed against the STANREC. For example it is highly plausible that in a procurement scenario different vendors may use different versions of NG-NRMM based on country of origin or other affiliations.

9.5 NG-NRMM USE/USER PROFILE

It is anticipated that the Complex NG-NRMM will require a greater skill set than the legacy NRMM2. With that in mind members were asked, “What do you consider the usage profile of the different NRMM options to be?” This was asked in context of the following potential users as defined by ET-148 [1] (Table 9-2).

Table 9-2: Definitions of User Types.

Supervised Practitioner	Someone who will require support and guidance; assistance with some aspects of data input, configuration, running the model, post-processing and/or presenting the resulting analysis to the Customer.
Practitioner	Someone that can interpret the Customers' needs, then define and execute analysis that provides appropriate decision support without supervision or guidance. Someone that can adapt how the software is used if needed but may require advice regarding the execution or validity of that adaptation.
Expert User	Somebody who not only is proficient in utilizing the software to provide decision support but understands the science behind it and the underlying functionality. This person is a recognized authority on the subject and can truly attest as to whether the software is being used in a viable and reliable manner.
Operational Planner[1]	This person has to operate independently, likely remotely from the core community, relying largely on re-using data (e.g., vehicle and/or terrain files) for typical, well understood analysis tasks, reaching back to core community practitioners as needed.

Note: The expert user could be required to undertake upgrades to the capability or to assess the validity of work by a practitioner. This was not included in the original definition.

Members were then asked how likely they might be to use NG-NRMM for research, procurement and support to operations. Support to operations was split into three categories of advice:

- **Pre-deployment**: Providing insights on likely performance factors prior to deployment based on limited prior knowledge.
- **General**: Provision of insights based on limited ground truth and coarse environmental data – used to inform at a higher operational level.
- **Specific**: Provision of insights based on variable ground truth and environmental data – used to inform tactical decisions.

For both of these two questions members were asked to rate as "Likely", "Occasional" and "Unlikely". Guidance was not provided as to how to interpret these ratings; it was left to the members to subjectively judge.

Lastly, the group was asked, "For 'Likely' and 'Occasional' use cases what level of confidence in the analysis and output is required?"

All three questions were asked as relating to legacy NRMM2, NG-NRMM Simple and NG-NRMM Complex – Simple and Complex as exemplified by Thrust Areas 2 and 3, respectively.

Figure 9-7 shows a summary of responses to questions 1 and 2. It shows the paired answers to both from 10 members of the group.

[1] It should be noted that operational planner could be an officer on a 2 – 3 year posting and hence with limited time to become familiar with the use and limitations of NG-NRMM.

Data Set		NRMM2 (current)	NG-NRMM Simple	NG-NRMM Complex
1	Supervised Practitioner	Likely	Likely	Occasional
	Practitioner	Likely	Likely	Likely
	Expert User	Likely	Likely	Likely
	Operational Planner	Unlikely	Unlikely	Likely
2	Supervised Practitioner	Likely	Unlikely	Unlikely
	Practitioner	Likely	Occasional	Unlikely
	Expert User	Likely	Occasional	Occasional
	Operational Planner	Likely	Likely	Occasional
3	Supervised Practitioner	Likely	Likely	Unlikely
	Practitioner	Likely	Likely	Unlikely
	Expert User	Likely	Likely	Unlikely
	Operational Planner	Unlikely	Unlikely	Unlikely
4	Supervised Practitioner	Likely	Likely	Unlikely
	Practitioner	Likely	Likely	Occasional
	Expert User	Likely	Likely	Likely
	Operational Planner	Occasional	Occasional	Unlikely
5	Supervised Practitioner	Likely	Likely	Unlikely
	Practitioner	Likely	Likely	Occasional
	Expert User	Likely	Likely	Unlikely
	Operational Planner	Unlikely	Unlikely	Unlikely
6	Supervised Practitioner	Occasional	Occasional	Unlikely
	Practitioner	Likely	Likely	Occasional
	Expert User	Likely	Likely	Likely
	Operational Planner	Unlikely	Unlikely	Unlikely
7	Supervised Practitioner	Likely	Occasional	Unlikely
	Practitioner	Likely	Occasional	Unlikely
	Expert User	Likely	Likely	Occasional
	Operational Planner	Unlikely	Unlikely	Unlikely
8	Supervised Practitioner	Likely	Likely	Unlikely
	Practitioner	Likely	Likely	Occasional
	Expert User	Likely	Likely	Likely
	Operational Planner	Unlikely	Unlikely	Unlikely
9	Supervised Practitioner	Likely	Likely	Unlikely
	Practitioner	Likely	Likely	Occasional
	Expert User	Likely	Likely	Likely
	Operational Planner	Unlikely	Unlikely	Unlikely
10	Supervised Practitioner	Unlikely	Unlikely	Unlikely
	Practitioner	Likely	Likely	Unlikely
	Expert User	Likely	Likely	Likely
	Operational Planner	Unlikely	Unlikely	Unlikely

	NRMM2 (current)	NG-NRMM Simple	NG-NRMM Complex
Research	Occasional	Likely	Likely
Procurement	Occasional	Likely	Likely
Pre-Deployment Advice	Likely	Likely	Likely
General Operational Advice	Likely	Likely	Likely
Specfic Operational Advice	Likely	Likely	Occasional
Research	Likely	Likely	Occasional
Procurement	Occasional	Likely	Likely
Pre-Deployment Advice	Likely	Unlikely	Unlikely
General Operational Advice	Likely	Occasional	Unlikely
Specfic Operational Advice	Likely	Occasional	Occasional
Research	Likely	Likely	Unlikely
Procurement	Likely	Likely	Unlikely
Pre-Deployment Advice	NA	NA	NA
General Operational Advice	NA	NA	NA
Specfic Operational Advice	NA	NA	NA
Research	Unlikely	Occasional	Likely
Procurement	Likely	Likely	Occasional
Pre-Deployment Advice	Occasional	Likely	Occasional
General Operational Advice	Occasional	Occasional	Unlikely
Specfic Operational Advice	Occasional	Occasional	Unlikely
Research	Likely	Likely	Occasional
Procurement	Likely	Likely	Unlikely
Pre-Deployment Advice	Occasional	Occasional	Occasional
General Operational Advice	Occasional	Occasional	Unlikely
Specfic Operational Advice	Unlikely	Unlikely	Unlikely
Research	Likely	Likely	Likely
Procurement	Likely	Likely	Likely
Pre-Deployment Advice	Likely	Occasional	Unlikely
General Operational Advice	Occasional	Occasional	Unlikely
Specfic Operational Advice	Unlikely	Unlikely	Unlikely
Research	Occasional	Occasional	Occasional
Procurement	Unlikely	Occasional	Unlikely
Pre-Deployment Advice	Unlikely	Unlikely	Unlikely
General Operational Advice	Unlikely	Unlikely	Unlikely
Specfic Operational Advice	Unlikely	Unlikely	Unlikely
Research	Occasional	Likely	Likely
Procurement	Unlikely	Occasional	Likely
Pre-Deployment Advice	Likely	Likely	Occasional
General Operational Advice	Likely	Likely	Occasional
Specfic Operational Advice	Likely	Likely	Unlikely
Research	Occasional	Likely	Likely
Procurement	Unlikely	Occasional	Likely
Pre-Deployment Advice	Likely	Likely	Occasional
General Operational Advice	Likely	Likely	Occasional
Specfic Operational Advice	Likely	Likely	Unlikely
Research	Unlikely	Likely	Likely
Procurement	Likely	Likely	Unlikely
Pre-Deployment Advice	Likely	Likely	Occasional
General Operational Advice	Likely	Likely	Occasional
Specfic Operational Advice	Unlikely	Likely	Likely

Figure 9-7: Questions 1 and 2 Paired Response Summary from Ten Respondents. Question 1: What do you consider the usage profile of the different NRMM options to be? Question 2: How likely would you be to use NG-NRMM for research, procurement and support to operations?

Question 1 members' (quoted) comments regarding who will use NG-NRMM:

- *"Data availability is a major hindrance for both the simple and complex NG-NRMM models."*
- *"We would see Simple NG-NRMM being used in the same way as NRMM2."*
- *"Rather than being a transition as the capability was established, NRMM2 would likely be kept in parallel."*
- *"The UK response for NG-NRMM Complex recognizes that, based on demand, we may not invest in or achieve Expert status internally – this will drive what modeling options are adopted and how they are deployed."*
- *"I would anticipate that the Complex Terramechanics form will only be used by Experts for design development and research. This is because:1) The highly complex nature of the input data and models, and 2) The high computing power needed / long processing times."*
- *"Both NG-NRMM and NRMM actually require two different skills sets to properly operate…. Note that under the model builders the set up and model verification can also be used for design loop simulations matching power train components, optimizing the suspension components, etc. which is of no use to the operational planner. However the output of the verified vehicle model is important to the acquisition engineer / operational planner."*

Question 1 observations:

1) Data availability has been identified and discussed across the Thrust Areas. While some techniques have been demonstrated, terrain data availability remains a significant constraint to utilizing NG-NRMM.
2) The scores seem to reflect the view that the skillsets are common across legacy NRMM2 and Simple NG-NRMM, or at least the training burden and resource requirements are comparable.
3) There was more variation in views for Complex NG-NRMM but the majority see it being limited to expert users, presumably due to the required skillsets and training burden.

Question 2 members' (quoted) comments regarding what NG-NRMM will be used for:

- *"We do not have good enough terrain data for any model to support specific operational advice."*
- *"We are often asked to provide pre-deployment and general operational advice in various locations on a seasonal basis."*
- *"Regarding the NGN Simple, the theory could be applied but it is difficult to apply in the field. For example, for the time being, it cannot be found a bevameter in Romania."*
- *"NGN Complex has a very long runtime (2 days!). Even together with RAMDO usability (for mobility map creation) usability will be a problem, I suppose. NGN Complex is more a research tool at the moment."*
- *"We would not adopt a Complex only based methodology due to 1) Resource constraints, user requirements, runtimes and technical expertise required; and 2) The nature of how our work is exploited. It is likely we would adopt the Simple terramechanics to achieve improvements in predictions."*
- *"If a sound tool is built and can be used with confidence, our DoD acquisition and operational planning environments WILL use those tools. (Operational planners spend as many hours working data as engineers, it is just not as precise)."*

- *"Note that NRMM has, what we understand, proved itself with scenario planning, decision making and operational support so has buy in by these users. As such it will continue to be used by these users as a) it is quick and b) trusted…. Complex requires a long runtime so its application will only be pertinent where there is time to model the various soils thus should be used for pre-deployment and general advice. If sufficient datasets are built up beforehand then it can be used operationally as it will simply access the performance archive to determine performance and thus should be just as fast as NRMM changing from occasional to Likely for specific Operational Advice".*

From the question 2 scores there are no clear trends. Observations:

1) It might be interpreted that members believe Simple NG-NRMM has the potential to be utilized more widely across the exploitation paths than the legacy NRMM2.
2) The group is split between whether Complex NG-NRMM is limited in use to just research and procurement or not, whether it has utility to support operations.

Figure 9-8 is a summary of responses for questions 2 and 3. It shows the paired answers to both from 10 respondents.

Question 3 members' observations regarding what level of confidence is required:

- *"Complex: Taking into consideration the resource constraints and technical expertise required, the level of confidence should be only 'High'."*
- *"Procurement is more likely to tolerate lower confidence for the understanding and setting of requirements than for assessing bids or making procurement decisions. This would be equally applicable for all tools. Driven by data availability and quality it was felt unreasonable to expect high confidence for operational support."*
- *"I don't see the accuracy of the model as changing with the application. It will change with the quality of the input data, however. Different applications may desire more accuracy – if so, then they need better input data."*
- *"It is understood that NRMM is fairly widely used both within research as well as procurement thus already has a medium / to high confidence in it therefore a high level of confidence is expected by these users. … within reportable use of NRMM that it is already widely accepted within the military user environment (Pre, General and Specific Operational) thus there is already a high degree of confidence in NRMM and this will continue to be required. NG Simple and Complex are unknown quantities thus will not be accepted by any of the users initially and will require verification and validation both against NRMM and operationally to derive the required high level of confidence in the outputs for all users. We believe that the speed of the simulation will be critical for all pre- and operational users thus this will be important for NG-NRMM to have a well modelled data set of tractive efforts prior o simulating the system performance for deployments. This feeds into acquisitions contracting not only requiring a NRMM / NG-NRMM modeling but that a verified (validated?) vehicle system model be delivered as part of the procurement."*

Data Set		NRMM2 (current)	NG-NRMM Simple	NG-NRMM Complex	NRMM2 (current)		NG-NRMM Simple		NG-NRMM Complex	
					From	To	From	To	From	To
1	Research	Occasional	Likely	Likely	Medium	High	Low	High	Low	High
	Procurement	Occasional	Likely	Likely	High	High	Low	High	Low	High
	Pre-Deployment Advice	Likely	Likely	Likely	High	High	Low	High	Low	High
	General Operational Advice	Likely	Likely	Likely	High	High	Low	High	Low	High
	Specfic Operational Advice	Likely	Likely	Occasional	High	High	Low	High	Low	High
2	Research	Likely	Likely	Occasional	High	High	High	Medium	Medium	Low
	Procurement	Occasional	Likely	Likely	High	Medium	High	Medium	Medium	Low
	Pre-Deployment Advice	Likely	Unlikely	Unlikely	Medium	Low	Medium	Low	Low	Low
	General Operational Advice	Likely	Occasional	Unlikely	High	Low	Low	Low	Low	Low
	Specfic Operational Advice	Likely	Occasional	Occasional	High	Medium	Low	Low	Low	Low
3	Research	Likely	Likely	Unlikely	Low	Low	High	High	NA	NA
	Procurement	Likely	Likely	Unlikely	Low	Low	High	High	NA	NA
	Pre-Deployment Advice	NA	NA	NA	NA	NA	NA	NA	NA	NA
	General Operational Advice	NA	NA	NA	NA	NA	NA	NA	NA	NA
	Specfic Operational Advice	NA	NA	NA	NA	NA	NA	NA	NA	NA
4	Research	Unlikely	Occasional	Likely	Low	Medium	Medium	High	Medium	High
	Procurement	Likely	Likely	Occasional	Low	Medium	Medium	High	Medium	High
	Pre-Deployment Advice	Occasional	Likely	Occasional	Low	Medium	Medium	High	Medium	High
	General Operational Advice	Occasional	Occasional	Unlikely	Low	Medium	Medium	High	Medium	High
	Specfic Operational Advice	Occasional	Occasional	Unlikely	Low	Medium	Medium	High	Medium	High
5	Research	Likely	Likely	Occasional	Medium	High	Medium	High	Medium	High
	Procurement	Likely	Likely	Unlikely	Medium	High	Medium	High		
	Pre-Deployment Advice	Occasional	Occasional	Occasional	Medium	Medium	Medium	Medium	Medium	Medium
	General Operational Advice	Occasional	Occasional	Unlikely	Medium	Medium	Medium	Medium		
	Specfic Operational Advice	Unlikely	Unlikely	Unlikely						
6	Research	Likely	Likely	Likely	Medium	High	Medium	High	Medium	High
	Procurement	Likely	Likely	Likely	Medium	High	Medium	High	Medium	High
	Pre-Deployment Advice	Likely	Occasional	Unlikely	Medium	High	Medium	High	NA	NA
	General Operational Advice	Occasional	Occasional	Unlikely	Low	High	Low	High	NA	NA
	Specfic Operational Advice	Unlikely	Unlikely	Unlikely	Medium	High	Medium	High	NA	NA
7	Research	Occasional	Occasional	Occasional	Medium	High	Medium	High	High	High
	Procurement	Unlikely	Occasional	Unlikely			Medium	High		
	Pre-Deployment Advice	Unlikely	Unlikely	Unlikely						
	General Operational Advice	Unlikely	Unlikely	Unlikely						
	Specfic Operational Advice	Unlikely	Unlikely	Unlikely						
8	Research	Occasional	Likely	Likely	Medium	High	Medium	High	High	High
	Procurement	Unlikely	Occasional	Likely	High	High	High	High	High	High
	Pre-Deployment Advice	Likely	Likely	Occasional	Medium	Medium	Medium	Medium	Low	Medium
	General Operational Advice	Likely	Likely	Occasional	Low	Medium	Medium	Medium	Low	Medium
	Specfic Operational Advice	Likely	Likely	Unlikely	Medium	High	Medium	High	Medium	High
9	Research	Occasional	Likely	Likely	Medium	High	Medium	High	High	High
	Procurement	Unlikely	Occasional	Likely	High	High	High	High	High	High
	Pre-Deployment Advice	Likely	Likely	Occasional	Medium	Medium	Medium	Medium	Low	Medium
	General Operational Advice	Likely	Likely	Occasional	Low	Medium	Medium	Medium	Low	Medium
	Specfic Operational Advice	Likely	Likely	Unlikely	Medium	High	Medium	High	Medium	High
10	Research	Unlikely	Likely	Likely	Low	Low	Medium	High	High	High
	Procurement	Likely	Likely	Unlikely	Low	Low	Medium	High	High	High
	Pre-Deployment Advice	Likely	Likely	Occasional	Low	Low	Medium	High	High	High
	General Operational Advice	Likely	Likely	Occasional	Low	Low	Medium	High	High	High
	Specfic Operational Advice	Unlikely	Likely	Likely	Low	Low	Medium	High	High	High

Figure 9-8: Questions 2 and 3 Paired Response Summary from Ten Respondents. Question 2: How likely would you be to use NG-NRMM for research, procurement and support to operations? Question 3: For 'Likely' and 'Occasional' use cases what level of confidence in the analysis and output is required?

Question 3 observations:

1) A subset of the members considered that NG-NRMM in any form would expect a higher level of confidence than existing NRMM despite the issues surrounding data availability.
2) A subset of the members considered the expected level of confidence would be consistent across research and procurement for the different versions.
3) Most variation in expectation was seen associated with the three types of operational support.

(The full set of comments can be found in Annex I.)

9.5.1 NG-NRMM Use/User Profile Observations

The following summary has been drawn and inferred from the questionnaire responses:

1) Firstly it would appear there is no common overall expectation in terms of who would use the different tools, what for and with what level of expectation but there are themes within the responses.
   - This is in part due to the different roles of the responders to the questionnaire, in part due to the organizations they belong to, and in part the stakeholders they support.
2) None of the options are seen as an operational planners' tool by the majority.
   - This is something the Thrust Areas have been working towards for NG-NRMM, e.g., the generation of terrain data for areas of interest.
3) Legacy NRMM2 is seen as likely being used by Supervised Practitioners, Practitioners and Experts alike by the majority.
   - This reflects the fact it is relatively simple to use and both the training and data burdens are relatively low. Also it is long established, successfully running at full operating capability.
4) Simple NG-NRMM is seen as comparable to legacy NRMM2 with respect to users.
   - Some differences acknowledge a learning and development curve to reach full operating capability for Simple NG-NRMM2.
5) Complex NG-NRMM is seen as only likely to be utilized by Expert Users.
   a) This has implications for the time analysts would have to devote to the capability, to both the tools and their own capability sustainment and development.
   b) This has implications for the time and cost of training mobility analysts.
   c) This has implications for the cost to organizations and projects.
6) Arguably it can be inferred Simple NG-NRMM is seen as the most exploitable of the options across the potential use cases.

For the STANREC and NG-NRMM implementation, the last point raises an interesting question: Is there an emerging requirement that:

1) Simple NG-NRMM should be a common tool; and
2) Complex NG-NRMM should be a framework that can accommodate multiple tools?

9.6 CAPABILITY GAPS AND CHALLENGES

The following sections use Figure 9-9 and the components therein to organize comments on capability gaps and challenges. As some gaps and/or challenges may be specific to how NG-NRMM is implemented, the discussions are based on the same three options as the other Thrust Areas where appropriate:

- Legacy NRMM2;
- Simple NG-NRMM; and
- Complex NG-NRMM.

It is recognized that a lot of the challenges raised cut across areas and that how distinct the subjects discussed actually are will be down to specific implementations. For the purposes of this section challenges are raised once in an appropriate section. A mapping of their applicability would likely not be too helpful at this stage.

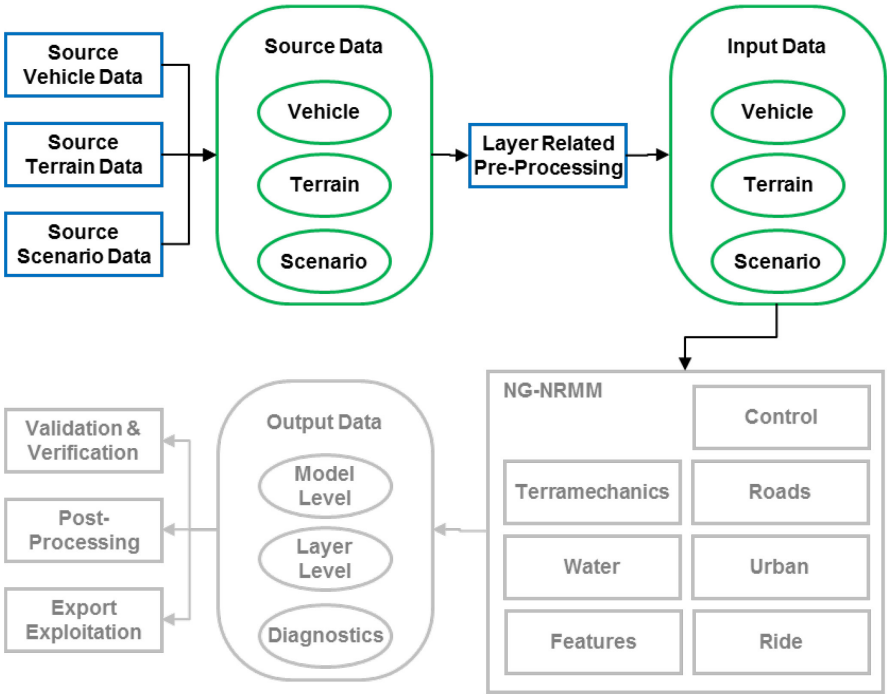


Figure 9-9: Scope of Section 'Input'.

9.6.1 NG-NRMM Input

This section covers gaps and challenges associated with input data.

The other Thrust Areas have identified specific gaps and challenges associated with their respective areas of focus that are applicable to NG-NRMM in general, for example:

- TA1: GIS Terrain and Mobility Mapping:
  - Resolution of data sources;
  - Data availability; and

    - Limitations of the MAPTBL format (one of the main restrictions identified being the ability to handle the volume of future data.).
- TA2: Simple Terramechanics:
    - A long-term configuration management approach to the database; and
    - Advancement of the vehicle-as-a-sensor method.
- TA5: Uncertainty Treatment:
    - Relative resolutions of data, specifically the introduction of uncertainty and error in converting to be the same (this being linked to challenges raised by TA1); and
    - Data availability – specifically soil parameter data.

The following subsection identifies additional challenges and gaps in work to date associated with NG-NRMM input data based on analysis in this Thrust Area.

Vehicle Input Data. Adopting more dynamic modeling and higher fidelity simulations requires that the vehicles will need to be better understood and represented, e.g., geometries of the moving parts:

- **Obtaining Data**. The impact and challenges of increased complexity (and volume) of data requirements will vary case by case. For example in a procurement activity the necessary data could be requested from suppliers, however, for research concepts new methods will be required to generate the information to enable virtual prototyping. The challenge of obtaining data is expected to be similar between legacy NRMM2 and Simple NG-NRMM, but significantly greater for Complex NG-NRMM.
- **Storing Data**. The current data structures in legacy NRMM2 are insufficient to store NG-NRMM vehicle data. For example legacy NRMM2 does not model explicitly electric drive or adaptive suspension. A more complex data model will be required; the choice of model will drive adaptability and interoperability.
- **Data Security**. For the legacy NRMM2 data security is not especially an issue for input data as engine performance and other components are often off-the-shelf and information is then available open source. Typically the level of information in legacy NRMM2 is commercially sensitive rather than a security concern. If the data for NG-NRMM is more complex this may have security implications. For example representations of enemy platforms in legacy NRMM2 are quite abstract and do not especially give away what you do or do not know about them (as arguably you can build a reasonable approximation from open source information). As the level of detail increases some aspects may become sensitive, not just the data values, but the collective data overall and/or the fact they are known. Equally information about how unmanned vehicles might perform and operate would be tactically useful to the enemy. In addition the detailed design information required for Complex NG-NRMM may have significant commercial sensitivities that need to be protected.

For NG-NRMM implementation, a data model will need to be chosen based on the scale of the implementation and interoperability (e.g., sharing with industry). It is likely that component and sub-assembly reference libraries will be required to facilitate concept work or bolster weak datasets where vehicles cannot be inspected. This implies an upfront investment or an increased effort in achieving full operating capability. (Noting some commercial software and data models may come with such libraries.)

For the STANREC, there will need to be a decision whether to prescribe a vehicle data model or leave it to individual implementations. The decision will have implications for interoperability and collaboration. For example, the ease of which one implementation of NG-NRMM can take another's data as input.

Terrain Input Data. The data requirement for Simple and Complex NG-NRMM is quite different but both require more than the legacy NRMM2. This has been addressed by ET-148 and Thrust Areas 1, 2, 3 and 5. There are further challenges to consider:

- **Legacy Cross-Country Data**. There is an existing library of legacy NRMM2 terrain files that an adopter of NG-NRMM would likely want to exploit; however, the data therein would be insufficient for Simple and Complex needs.
  - **Simple Soil Parameters**. A method would be required to generate the additional soil parameters Simple NG-NRMM requires beyond the Cone Index data in the legacy NRMM2 terrain files.
  - **Complex Soil Parameters**. A method would be required to generate the additional soil parameters Complex NG-NRMM requires beyond the Cone Index data in legacy NRMM2 terrain files.
  - **Slope**. NRMM2 slope data is non-directional, it is a representative angle. The other Thrust Areas have considered how to utilize DTED data and the uncertainty therein to generate this data.
  - **Surface Roughness**. Legacy NRMM2 uses a single RMS value for the main terrain units. This is potentially sufficient for NG-NRMM subject to a suitable underpinning method for ride modeling and analysis. The current PREVDYN/VEHDYN ride pre-processor for legacy NRMM2 has its own 2D terrain that uses these reference RMS values. The existing VEHDYN terrain could be used for 3D modeling by applying a track offset (subject to the form's suitability for the chosen metrics to be implemented).
  - **Obstacles**. Upgrading the representation of the obstacles present, as required for both simple and complex NG-NRMM, has two challenges:
    a) There is no way of knowing what the original obstacles were;
    b) Those obstacles may no longer exist (see Change Control) so a fresh survey or statistical data would be required.
  - **Trees**. Upgrading the representation of the trees present would face the same challenges as for the obstacles.
  - **Change Control**. It is unlikely the terrain as represented in the legacy NRMM2 terrain files is still representative of the real world. (e.g., de-forestation, urban spread.) All datasets would require a review and update as part of the upgrade to NG-NRMM compatibility if the terrain data were to be used for anything other than for abstract / comparative analysis.
- **Legacy Road Data**. There is an existing library of legacy NRMM2 terrain files that an adopter of NG-NRMM would likely want to exploit; however, the data therein would be insufficient for Simple and Complex needs. Similar challenges exist as for cross-country across the parameters. Areas which would need to be addressed for NG-NRMM include:
  - **Soil Parameters**. The tracks or trails road type is a non-man-made (i.e., soil) surface subject to the same terramechanics calculations as cross-country previously discussed; as such, the previous comments apply regarding Simple and Complex NG-NRMM.
  - **Bridges and Tunnels**. These are represented in the legacy NRMM2 however the data may be insufficient for all 3D dynamic modeling. For example tunnels have a defined width and height

but not profile. Upgrading their representation would require getting representative data of the original structures or using surrogates (which would in turn impact the potential use and exploitation of the data).

  - **Gaps**. The legacy NRMM2 road definitions do not include data such as central reservations or drainage ditches, all features NG-NRMM might need. For example a tracked vehicle and a logistics vehicle would have different levels of success if the carriageways were separated by a one meter high concrete wall.
  - **Change Control**. Road terrain is less likely to change than cross-country, recognizing that roads can be upgraded. It is more likely road networks change due to the addition of new roads or improvements (e.g., wider, additional lanes). Change control is something that potentially has more impact on operational support and validation than research where the emphasis is on comparative not absolute analysis.
- **Other Layers**. For the other Layers such as Urban, Features and Water there will need to be appropriate data models adopted, something the STANREC will have to address.
- **Obtaining Data**. The other Thrust Areas have highlighted and discussed the issues with obtaining terrain data.
- **Storing Data**. The other Thrust Areas have highlighted and discussed the issues with storing terrain data.
- **Data Security**. As for vehicle data, going from current to NG-NRMM, more complex terrain data may have security implications for how it is stored and handled.

In summary legacy NRMM2 terrain files provide a good starting point for NG-NRMM but:

- To utilize legacy NRMM2 terrain files a robust method is required to generate the additional soil parameters Simple or Complex NG-NRMM requires beyond Cone Index. The scale of effort required for this is considered to be comparable to a research project in itself.
- Utilizing legacy NRMM2 terrain files would likely benefit from a method for updating and/or enhancing the features (obstacles and trees) representation therein however at this time the benefit of enhanced feature representation has not been investigated or quantified with regards to predictions impact.

Scenario Input Data. The legacy NRMM2 scenario data is essentially a set of parameters that set input, output, runtime and analysis options, as well as providing some override or default values:

- **Legacy Scenario Data** is unlikely to be relevant to a NG-NRMM implementation as it is linked to the legacy NRMM2.
- **New Options** are likely to be required to deal with new functionality and intelligent (unmanned and autonomous) vehicles. This is discussed in the next section under model functionality.

Data Confidence. Some gaps and challenges are common across all input data, both vehicle and terrain, this is an example of such. In the same way that the DRAFT STANREC proposes a “Capability Maturity Scale” under verification and validation for the software, the input data models needs to be able to record metrics that will allow users to ensure they use the contents in an appropriate context; i.e., terrain data suitable for comparative research purposes may not be suitable for operational support. In the legacy NRMM2 this is left to the analyst to manually comment in the ASCII text files.

For the STANREC, there will need to be a discussion and decision as to whether it prescribes how data confidence should be addressed or whether it should be left to individual implementations. The decision may have implications for interoperability and collaboration.

For NG-NRMM implementation and the STANREC, it is recommended that NATO countries should consider the collaborative development of a soils / terrain database.

9.6.2 NG-NRMM Modeling

This section covers gaps and issues associated with the actual modeling of platform mobility (Figure 9-10).

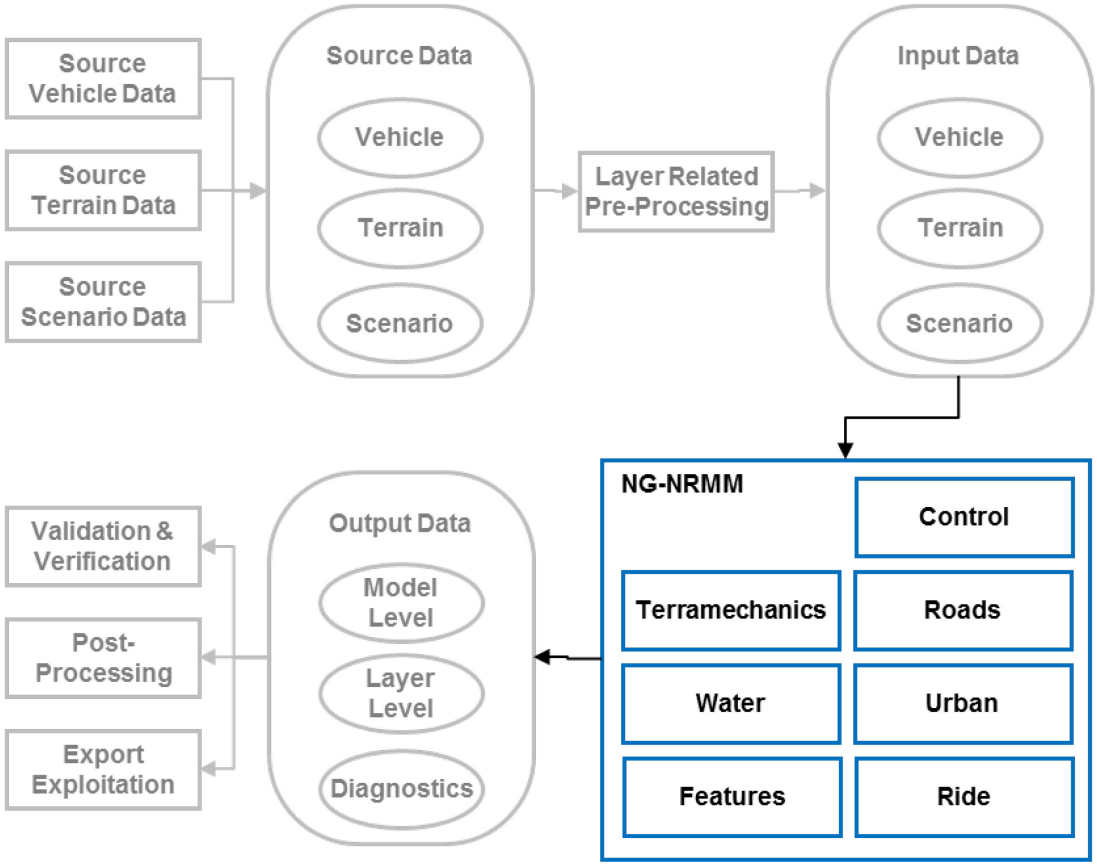


Figure 9-10: Scope of Section 'Modeling'.

The other Thrust Areas have identified specific gaps and challenges with their respective areas of focus with regards the modeling aspects of NG-NRMM, for example:

- TA2: Simple NG-NRMM terramechanics:[2]
  - A long-term configuration management approach to the STANREC;
  - Advancement of the vehicle-as-a-sensor method;

[2] While these are TA2 findings there is applicability to TA3, Complex NG-NRMM terramechanics.

    - M&S methods addressing the slope limitations;
    - M&S and parameter ID methods addressing slip-sinkage;
    - M&S methods addressing longitudinal bulldozing;
    - M&S methods addressing lateral bulldozing;
    - M&S along with experimental methods that address layer effects;
    - M&S along with experimental methods that address load rate effects;
    - Leverage Complex Terramechanics developments to extend the Simple Terramechanics database; and
    - Investigations correlating simpler closed form soil strength metrics, such as Terzaghi and Meyerhof methods, to first order vehicle trafficability prediction will facilitate real-time operational assessments of remotely sensed terrain, soil and moisture content data.
- TA5: Uncertainty Treatment:
    - Terramechanics simulation automations and efficiencies.

The following subsection outlines some additional challenges and gaps in work to date associated with the functionality of the modeling capability in context of the proposed layers that have been identified by this Thrust Area.

Terramechanics: This is covered in some detail by Thrust Areas 2 and 3. The following are observations regarding original requirements not explicitly addressed yet by the Thrust Areas and prototypes, and some associated challenges.

- **Legged Vehicles**. This was a specific ET-148 requirement given minimal consideration thus far. Complex NG-NRMM has considered legged vehicles' terramechanics but arguably it might be harder for Simple NG-NRMM to implement as military focused techniques have historically focused on wheeled or tracked vehicles.
    - Modeling legged vehicles is typically a specialized or specific niche area, e.g., Mars rovers and specific soils. This type of work does not directly translate to military applications due to platform scale, speed and breadth of potential operating environments.
    - Modeling legged vehicles on solid terrain or in the urban environment is a relatively simpler proposition and arguably a more likely requirement. (e.g., stair climbing.) The priority for this will vary by individual user, the group previously had it as an objective requirement.
- **Small Vehicles**. This was a specific ET-148 requirement not considered thus far. Small vehicles were considered to be any vehicle from a man-portable robot up to one/two man equivalent platform (e.g., a quad bike or load carriage). This poses challenges across all layers of the modeling from the relative weight of the platform impacting terramechanics to the relative size of features, e.g., rocks and debris.
    - The legacy NRMM2 is an empirical model based on trials and experimentation with known platforms, more specifically those representative of manned military vehicles of the time. The current equations, algorithms, legacy and historic data are unlikely to be suitable (without additional research) for smaller (e.g., unmanned) platforms. This is because unmanned vehicles tend to be different in size, weight and running gear configuration. For example you might find a wheeled platform equivalent to a small SUV with four wheels per side as

opposed two. In addition the small size of UGVs will mean that the level of detail in terrain and obstacle representation will need to be greater.

- **Vehicle Technologies**. A shortfall of the legacy NRMM2 is the breadth of technologies, and their associated performance impact, it can consider. Specifically the ET-148 requirements listed ABS, TCS, CTIS, and tire and track models. As the focus has been on implementing terramechanics in Simple and Complex NG-NRMM, these have not been explicitly addressed yet.
  - Some will be simpler to implement than others as some will be the controlled use of existing data (e.g., CTIS), whereas some will require specialized calculations.
  - For Simple NG-NRMM the challenge would likely be up front in developing the data, understanding and the algorithms. For Complex NG-NRMM the challenge would likely be more on the back-end developing the data and understanding to validate models. Albeit Simple and Complex NG-NRMM would face those same issues and similar trials may support both needs.
- **Snow and Ice**. This was a specific ET-148 requirement not considered thus far in detail. This is a discipline in itself, a capability gap for NG-NRMM and a serious challenge to anybody implementing it. A challenge that is compounded by the availability of, and access to, areas suitable for trialing and a lack of control over environmental conditions and resulting condition of snow and ice layers.
  - Not implementing a modeling solution for snow and ice will limit seasonal predictions for NATO areas of interest.
- **Fuel Efficiency**. Fuel efficiency was identified as an ET-148 requirement and there is a common benchmark event depicted in the DRAFT STANREC. The legacy NRMM2 predicts a steady-state top speed given set conditions; it does not consider driving across the map. Taking the extreme example of a chess board type predictions map (e.g., white cells 50 mph, black cells 5 mph) how would NG-NRMM account for the acceleration/deceleration, the ability to reach that steady-state via the adjacent terrain units? This challenge is not limited to fuel efficiency and the impact will vary by vehicle type. For example hybrid electric vehicles considering regenerative braking.
- **Soil Methods**. Simple NG-NRMM will rely on implementing one or more of the accepted terramechanics methods, e.g., Cone Index or Bekker-Wong. The challenge will be deciding 1) to what extend these methods are suitable to the breadth of vehicles, terrain and environments in scope; and 2) what to do where they are not applicable or have limitations. For example if available Cone Index data is not suitable and an implementer of NG-NRMM has no bevameter data for their vehicles they will have to generate it, if the research to date has not considered soil types appropriate to their areas of interest they will have to expand on the research. (Noting there is risk therein regarding a successful outcome.)
- **Tire Models**. Tread pattern and other tire properties are known to influence cross-country mobility performance, sometimes significantly. For the legacy NRMM2 a full tire model is a capability gap, for Simple NG-NRMM it is an ET-148 requirement and a challenge not addressed yet. Tire models do exist but integrating them in a computationally efficient way will be a challenge.

The growing focus on the use of robotic and unmanned systems, as reflected in NATO priorities, means that research will be required in this area. This will lead to new methods, new data and new validation requirements.

The challenges in generating a legged platform terramechanics model for NG-NRMM will not be trivial. Implementing a terramechanics model will involve significant investment in trials and development for a relatively niche exploitation path. Therefore development of a generic NG-NRMM model for legged vehicles may not be viable, hence development may be limited to supporting specific platforms.

The challenge of modeling small vehicles will be the exploitation of research done for (potentially) slower, lighter (not necessarily smaller) vehicles in less diverse environments. The opportunity however is that this could be relatively simpler than developing models for larger, manned vehicles as trials will be cheaper and easier to design and implement; e.g., test environments will be easier to control, concepts and prototypes will be cheaper to develop. Developing such a model via trials and experimentation could be laboratory as opposed to field-based work.

For the STANREC, the challenge will be to decide if legged and small vehicles should be subject to the same level of expectation as more traditional manned vehicles.

For NG-NRMM implementation and the STANREC, there is still a challenge to be addressed of how to take the individual discrete predictions and turn them into a representative and realistic map level analysis output in the requirements. Further there is a question as to how far the STANREC must prescribe this.

Roads. Platform performance on roads is a relatively simpler problem than cross-country mobility (assuming man-made surfaces) and it well within the capability of modern software solutions. To that end challenges are limited to areas already discussed:

- Data model;
- Data availability; and
- How to aggregate performance data to map level predictions and analysis.

Water. The mobility of vehicles in water was an ET-148 requirement (fording, swimming), and remains a gap in the work to date and a significant, relevant challenge for NG-NRMM given future predictions about populations, urban areas and littoral operations. Large bodies of water are present in legacy NRMM2 terrain files but not assessed in the modeling from the perspective of entering, negotiating, exiting, snorkelling or swimming.

- **Flooding**. Not all uses of NG-NRMM will be in support of combat operations, the military is often deployed for humanitarian courses, e.g., disaster relief. The conditions for such operations will often differ to combat operations and represent an atypical terrain/environment worst case (e.g., debris, flooding). Users of NG-NRMM will likely have a requirement and associated challenges to represent a temporary water layer above the soil layers, with some associated impact thereon.
- **Ingress/Egress**. Negotiating banks, getting in and out of water bodies is a real-world challenge and often more of a challenge than crossing a body of water. Banks could be highly deformable and vehicles will not achieve steady-state operating driving across them. For Complex NG-NRMM this is a matter of modeling (albeit non-trivial), for Simple NG-NRMM the challenge is method, how to represent a short-term, dynamic event.
- **Fording**. The challenges in representing fording include traction, buoyancy and water resistance adding multiple dimensions to the terramechanics problem.
- **Swimming**. Boat models are commercially available if the problem is considered independently of ingress/egress. It is possible some could adapt to the different shapes of military vehicles (shapes and weights) and account for their auxiliary propulsion (e.g., propellers if present) but there is a question over the impact of running gear and whether their ability to best represent it would impact results. A challenge is that a customized tool could be required, one independent of the other gaps and challenges being addressed.

- **Conditions**. Whether a lake, river, sea or ocean there are other factors to consider regarding modeling vehicles in water. For example tide or current, waves and wind which may or may not be moving in the same direction. A basic model should aspire to consider these as it matures.
- **Multi-pass at water entry and exit points**. A major challenge for terramechanics is the problem of multi-pass, the fact that any vehicle changes the properties of the terrain for the subsequent platforms. It is one thing to compare vehicles side by side, it is another set of challenges to consider the impact of, for example, 10 wheeled vehicles following 10 tracks over a given terrain. This same problem will apply to water feature terrain in terms of bank and bottom integrity and the impact on trafficability.

Modeling water terrain may be a natural progression in some regards from the terramechanics but there are unique challenges that will need to be overcome. For the STANREC, there are challenges regarding how to include the capability to model terrain involving water interaction from the requirements through to the testing. The majority of gaps and challenges associated with terramechanics data provision will be applicable and compounded.

Urban. The legacy NRMM2 does not consider urban terrain however some members of AVT-248 have developed complementary tools looking at urban mobility. At its simplest the urban problem is different from the cross-country, rather than terramechanics and traction performance it is a function of physical size, turning circles and other factors. However, complex urban environments can include features such as those below, that raise unique challenges for autonomous vehicles:

1) Features that will require overcoming such as vehicles and debris;
2) Alternative road surfaces requiring terramechanics; and
3) Bodies of water, e.g., canals, rivers and lakes.

In other words all the Layers that could be considered for off-road mobility performance could equally apply to some urban environments, the capability gaps and challenges therein therefore being applicable.

For NG-NRMM implementation, there will be a challenge in striking a balance between how many of the Layers are considered (and to what Level) versus the requirements of the users' exploitation paths (e.g., research versus support to operations).

For the STANREC, as previously raised under terrain input data, there will need to be appropriate data models characterized and/or adopted.

Features. In the legacy NRMM2 obstacles are defined as 3D non-deformable shapes to be avoided, straddled or traversed, whereas vegetation (trees) are seen as something to avoid or defeat by override (e.g., snap, deform). This is discussed further in Annex I. There are capability gaps in the legacy NRMM2 not covered in the work to date and hence challenges with implementing NG-NRMM. For example:

- Tree stem size versus ability to defeat is not a constant relationship, e.g., hard versus soft woods.
- Tree method of defeat is not a given, e.g., snap, uproot, bend.
- Tree roots will potentially have different properties depending on type, climate, environment, soil type and moisture content.
- Tree canopy types and impact thereof are not considered.
- Some obstacles are deformable, e.g., fallen trees, vehicles.

For the STANREC, as previously raised in the Layers definitions, it is proposed obstacles and (above surface) vegetation (e.g., trees) as implemented in the legacy NRMM2 can be considered as a collective ability, that to defeat or overcome Features. This is because the features of complex terrain should not be considered in isolation. For example from the perspective of avoidance one rock, one tree and one burned vehicle in the same terrain unit are actually three objects to be driven around. If you assessed driving around each independently you would get a very different answer.

For the STANREC it is proposed the vegetation "carpet layer" is included in the terramechanics. The rationale for this is complex terramechanics needs to include it as an integral factor. As the approach moves back towards simple terramechanics, these factors are still a consideration but in a less integrated way.

For NG-NRMM implementation, the Features Layer will have independent utility, for example assessing gap crossing or aircraft loading. Improving this capability will improve the utility of the Layer for independent exploitation. What is unknown (compared to the legacy NRMM2) is:

1) Whether improving methods will significantly reverse GO/NOGO predictions with regards overcoming features?
2) If not, will improved methods change the predicted speed at which features may be overcome?
3) To what extent the answers to these questions might impact map or aggregated (e.g., cumulative speed curve) outputs.

For NG-NRMM implementation there will however be methods and outputs that will be sensitive to individual predictions where obstacle crossing may be a discriminator; e.g., route following where each patch or cell is critical to mission success. Again however there is no work to date that demonstrates how well features need to be represented and the resulting impact on the sensitivity of results.

The STANREC and NG-NRMM implementation will require enhanced terrain definition if the Features Layer is to be included and improved.

Metrics for testing and evaluating Features and how they can be subsequently represented and validated in models will need to be addressed in the STANREC.

Vehicle design, specifically the steering performance, is not considered assessing the ability to avoid obstacles in the legacy NRMM2. A more complex representation may be required to offer discrimination between different systems, e.g., benefit of skid steer or not. Three-D dynamic modeling as in the original requirements has the potential to address this so from the perspective of gaps this falls into the "have not" as opposed "could not" category.

Ride. The legacy NRMM2 uses a pre-processor called VEHDYN to assess platform ride quality and driver tolerance / constraints. Specifically the vehicles are assessed (typically) against 2.5g vertical acceleration on obstacle impact and 6 watts absorbed power for ride tolerance (both as per the benchmark events in the DRAFT STANREC). This is in recognition of occupants potentially being a factor in limiting a vehicle's performance. ET-148 identified three main areas for improvement:

- 3D not 2D dynamic modeling.
- The requirement to consider deformable terrain.
- The need to model more complex suspension types, e.g., semi-active and active.

In considering the Ride Layer and the STANREC, a range of questions were initially raised, examples as follows:

- **Method**. Should the pre-processor implementation route, i.e., a discretely implemented Layer, be advised or mandated?
- **Metrics**. Are the current VEHDYN metrics still appropriate?
  - Is there a need to align to other metrics associated with noise, vibration, legislation?
- **Terrain**. Does the STANREC need to specify standard reference routes?
  - Do those routes need to exist in the real world for modeling validation?
  - Should each NG-NRMM user/developer identify and maintain reference routes that can be used for trials, experimentation, validation and verification?
- **Implementation**. Does the STANREC need to specify requirements or methodologies for both defining and assessing routes?
  - Does the answer to this question change depending on whether Ride was a Layer, a separate tool / pre-processor, or both.

Work to address these questions will be required to support STANREC development.

Control. In the legacy NRMM2 there is a scenario input that can be used to set high and low level runtime options, force defaults and direct the desired output. Part of this allows for driver prudence or constraints to override performance predictions or constrain them.

- **Intelligent Vehicles**. The concept of modeling unmanned vehicles in a directly comparable way to manned vehicles using NG-NRMM has been considered by Thrust Area 4: Intelligent Vehicles. Underlying platform performance is the same whether manned or unmanned however the constraints on how they are operated will be different due to sensor types, feedback, doctrine and tactics. It may be laws or rules governing the use of autonomous vehicles need to be considered. One potential approach could be to account for different levels of risk tolerance between operating manned and unmanned platforms; e.g., the balance between likelihood and impact of tipping will differ between manned and unmanned vehicles (i.e., if no people are present to self-recover).

For the implementation of NG-NRMM, the challenge will be in deciding if allowing for alternate control strategies (e.g., autonomy) need to be:

1) Part of the predictions calculations;
2) An input pre-processor (e.g., a filter using criteria to limit which terrain units are assessed);
3) An output post-processor (e.g., capping all predictions given terrain unit criteria); or
4) A combination of the above.

General. There are some gaps and challenges that are not specific to any of the layers but apply across the implementation of NG-NRMM:

- **Computational Efficiency**. How the terramechanics is implemented in the methodology will drive computational efficiency, runtimes and subsequently how timely NG-NRMM is to use. (Not just the individual predictions but how they are combined into map level predictions.)

- When Simple NG-NRMM achieves full operating capability it will likely be a capability broadly comparable to the legacy NRMM2, recognizing there will be some time penalty for the enhanced calculations. It will likely run on standard personal computers, desktops or laptops.
- When Complex NG-NRMM achieves full operating capability there will be a reliance on high power computing and analysis will be less timely.
- Rather than present a single view on the impact this will have for exploitation of the different NG-NRMM options, the reader is referred back to the questionnaire at the start of this section.

- **Analysis Time**. The speed of setting up, running and presenting coherent results will vary by user, requirement and implementation. The ability to generate timely advice is a key challenge in the utility of NRMM. If assessments using Complex NG-NRMM take many months the utility will be diminished.

For the implementation of NG-NRMM, the challenge for users and developers will be in striking a balance between how timely they want the analysis traded against the complexity and fidelity of it.

9.6.3 NG-NRMM Output

This section covers gaps and challenges associated with the actual output of the modeling process (Figure 9-11).

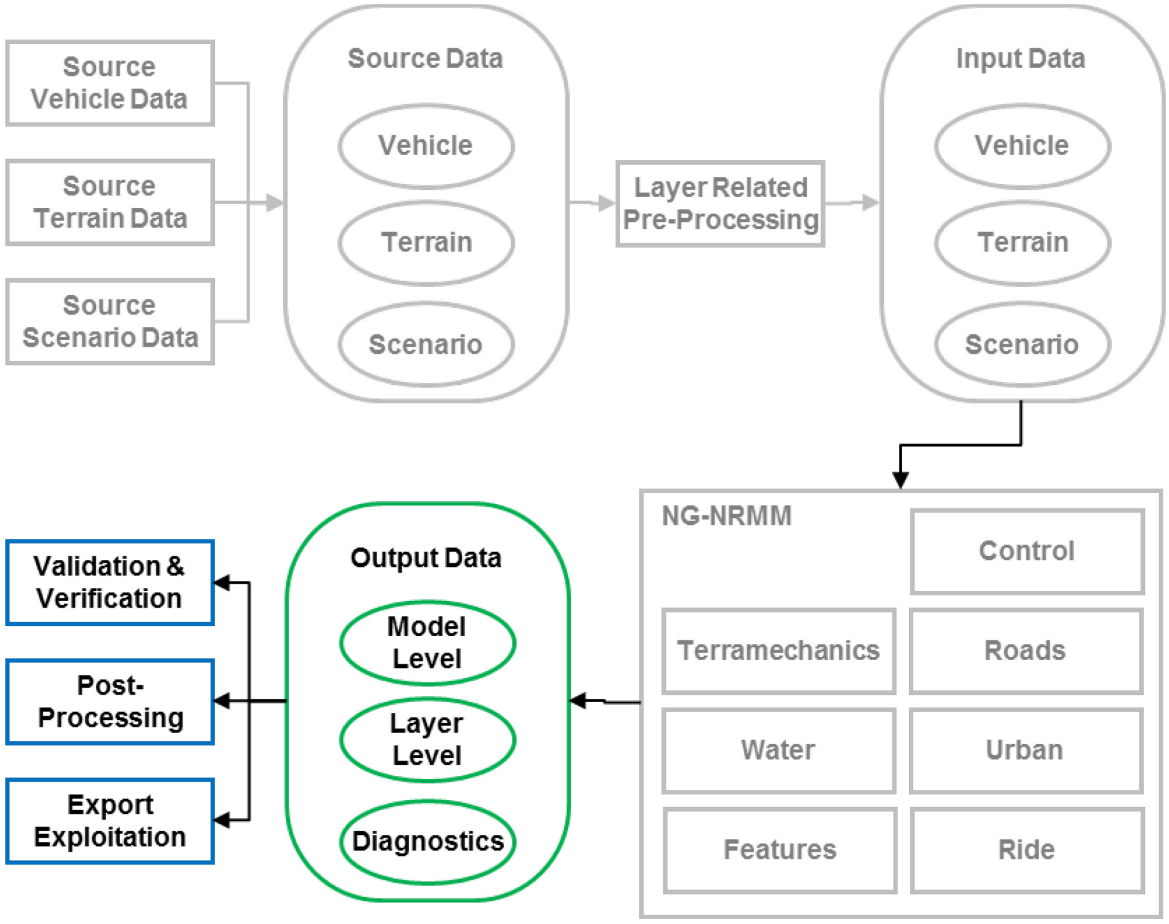


Figure 9-11: Scope of Section 'Output'.

The other Thrust Areas have identified gaps and challenges, for example:

- TA2: Simple Terramechanics.
  - Specific V&V efforts for whole-vehicle predictions for more rigorous benchmarks.

The following subsection identifies some additional challenges and gaps in work to date associated with NG-NRMM output based on analysis in this Thrust Area.

Output Data. As previously highlighted, NG-NRMM should have different levels of output with different exploitation paths, e.g., model level, layer level and diagnostic.

- **Model Level**. The model level outputs have been defined previously by this group and include the legacy NRMM2 terrain unit by unit predictions, associated statistics and aggregated forms, i.e., cumulative speed curves and maps. The challenges for implementing NG-NRMM will be taking individual terramechanics predictions and applying them to a map context.
- **Layer Level**. There will be a requirement to utilize the layers independently. Subsequently there will be a corresponding data output requirement. For example, if ride dynamics or obstacle crossing are modeled either as pre-processors (as in the legacy NRMM2 for computational efficiency) or to assess performance in their own right.
  - **Reason Codes**. The legacy NRMM2 uses reason codes to indicate which of the layers was predicted to be the limiting factor. For example, tipping on side slope, ride or obstacles. It will be a challenge for NG-NRMM to implement a standard set of limiting reason codes as they are linked to how the calculations are made. The legacy NRMM2 implementation is modular and considers the contributing factors separately so it can report them as such. If NG-NRMM combines elements at runtime it might not be feasible to separate which is the limiting factor.
- **Diagnostics**. Given users may not have access to run a given NG-NRMM implementation in debug or developer mode the tool(s) and method(s) must be able to be interrogated in a suitable way, beyond the typical output, as to understand how they are arriving at their predictions, aid in problem solving, debugging and verification.

For the STANREC, the challenge is to define suitable metrics for all layers without being too prescriptive as to force the methodology implementation. Associated with this there will need to be a discussion and decision on whether to prescribe limiting factor reason codes, and if so the definitions of. This is not straight forward as it has the potential to drive the implementation.

For the STANREC, the challenge will be to define the level of diagnostics required without overly influencing the implementation methodology.

Validation and Verification. This has been covered by other Thrust Areas and the STANREC, the following comments link to others raised in this section.

- **Legacy Data**. Similar challenges that exist for making legacy NRMM2 data fit for NG-NRMM will apply to its use in model validation and verification.
- **Empirical Evidence**. If new methods are adopted and need developing there will be an increased requirement for empirical evidence and methods. This will be a significant challenge as discussed by the other Thrust Areas – a challenge requiring both funding and time to implement. Trials take time to prepare and have dependencies (e.g., weather, environment, kit availability) that will drive

schedule feasibility. From that perspective it could take years to achieve limited operating capability with good levels of validation.

Post-Processing. There will be non-standard output requirements relevant to individual stakeholders that may impact the requirements for specific implementations, but it is not possible to identify specific, associated gaps and challenges.

Export Exploitation. The data and insights generated by the legacy NRMM2 are not limited to reporting platform performance as predicted. NG-NRMM is, and will continue to be, exploited for other purposes such as underpinning simulations, wargames and other operational analysis/research tools.

- **Evolution vs. Revolution**. Adopting or upgrading to NG-NRMM will provide a step-change in mobility performance analysis capability. Often combat models and simulations have simpler representations of mobility due to data aggregation and operational efficiency requirements, e.g., based on average speeds for map areas. One challenge will be how to take forward the mobility predictions improvements to revolutionize these tools to the same degree the mobility predictions have improved, specifically how to ensure the improved discrimination offered by NG-NRMM is factored into the exploiting tools" trade-space. Equally as historic constraints on the construction of combat models and simulations ease, e.g., improved computing power, there is a challenge to understand how their needs can drive the evolution of NG-NRMM output.
- **Data Model**. The wider interoperability and exploitation of data to support other capabilities re-enforces the need for a robust data model for NG-NRMM output.

9.7 SUMMARY

The aim of Thrust Area 7 was to identify gaps that will need to be addressed by future work in the pursuit of NG-NRMM, more specifically capability gaps and the challenges of implementing NG-NRMM. This was refined as three objectives (to benchmark views, identify gaps and challenges, and make recommendations for NG-NRMM and the STANREC) and implemented as a three step method:

1) **Identification**. How do you identify the capability of any given instance of NG-NRMM?
2) **Use and Users**. Who will use NG-NRMM and for what?
3) **Capability Gaps and Challenges**. What are the perceived capability gaps and challenges?

Identification. Firstly it was recognized that not all implementations of NG-NRMM will have the same aspirational end state. Understanding the configuration and status of any implementation is critical for appreciating the context of any output, comparing NG-NRMM instances/tools, validation and verification. As a result, an example method has been proposed for STANREC consideration and refinement.

Use and Users. Secondly, the group was asked who would use NG-NRMM, in what form, for what reason, and with what expectation regarding confidence in the findings. The reason behind this was to provide some context to the capability gaps and challenges identified, and to assist anybody considering implementing NG-NRMM. Observations from the groups' responses were:

1) It would appear there is no common overall expectation in terms of who would use the different tools, what for and with what level of expectation but there are themes within the responses reinforcing the view that there will be different aspirational end states for NG-NRMM.

2) None of the options are seen as an operational planner's tool by the majority.
3) Legacy NRMM2 is seen as likely being used by Supervised Practitioners, Practitioners and Experts alike by the majority.
4) Simple NG-NRMM is seen as comparable to legacy NRMM2 with respect to users.
5) Complex NG-NRMM is seen as likely to be utilized only by Expert Users.
6) Arguably it can be inferred Simple NG-NRMM is seen as the most exploitable of the options across the potential use cases.

Capability Gaps and Challenges. Thirdly, capability gaps and challenges were considered for NG-NRMM and work to date by the group. To do this a generic NG-NRMM methodology was generated (Figure 9-4) and each section was discussed in turn. Beyond what the other Thrust Areas identified, Thrust Area 7 discussed the following:

- Input Considered: Obtaining, storing and the security of vehicle data; the use of legacy NRMM2 terrain; scenario data; and data confidence.
- Modeling Considered: Terramechanics (legged vehicles, small vehicles, vehicle technologies, snow/ice, fuel efficiency, soil methods, tire models); Road, Water (flooding, ingress/egress, fording, swimming, conditions, multi-pass); Urban; Features (obstacles, vegetation, other); Ride; Control (e.g., intelligent vehicles); and general (computational efficiency and analysis time).
- Output Considered: Output data (model level, Layer level, reason codes, and diagnostics); validation and verification (legacy data, empirical evidence); post-processing; and export exploitation.

The capability gaps and challenges identified are not prioritized at this time. The STANREC will have to consider the points herein, whereas the priorities for NG-NRMM implementation will vary depending on the methodology and desired end state of the developer.

To summarize, the aim and objectives have been met. Anybody implementing NG-NRMM will have to carefully consider and assess which methods meet their current and potential future needs balanced against the ability to resolve any challenges therein. Ultimately further development of the NG-NRMM STANREC will require the points herein to be considered collectively and on balance for their applicability and utility.

9.8 REFERENCES

[1] Dasch, J. and Jayakumar, P. (Eds). 2016. Final Report ET-148 Next-Generation NATO Reference Mobility Model (NRMM). NATO-AVT, 2016.



Chapter 10 – SUMMARY AND CONCLUSIONS

Jean Dasch
Alion Science and Technology
UNITED STATES

The NATO Research Task Group (AVT-248) was formed as a follow-on effort to Exploratory Team (ET-148) with the goal of Developing a Next-Generation NATO Reference Mobility Model (NG-NRMM). The legacy NRMM is a simulation tool developed in the 1970s by the U.S. Army to predict the capability of a vehicle to move over a specified terrain. Due to limitations of NRMM as well as advances in simulation capabilities, the goal of AVT-248 was to explore methodologies and technologies required for an NG-NRMM. The Technical Activity Proposal (TAP) And Terms Of Reference (TOR) are included in Annex A. To enable the goals of NG-NRMM, seven Thrust Areas (TAs) were stood up, as shown below:

- Thrust Area 1: GIS Terrain and Mobility Map — Matt Funk, Brian Wojtysiak.
- Thrust Area 2: Simple Terramechanics — Mike McCullough.
- Thrust Area 3: Complex Terramechanics — Tamer Wasfy.
- Thrust Area 4: Intelligent Vehicle — Abhi Jain.
- Thrust Area 5: Uncertainty Treatment — K.K. Choi, Nick Gaul.
- Thrust Area 6: Verification and Validation — Ole Balling.
- Thrust Area 7: Data Gaps; Operational Readiness — Mike Bradbury, Jonathan Bruce.

AVT-248 conducted a full examination of improvements to NRMM through the Thrust Areas. An end-to-end prototype demonstration was conducted using the Monterey Basin as a test site. A new RTG was approved (AVT-327) to formulate a STANREC to formalize the requirements of an NG-NRMM. The first draft of the STANREC has already been submitted. A three-day Cooperative Demonstration of Technology (AVT-308) was held in September 2018 at the Keweenaw Research Center in Houghton, Michigan, USA to demonstrate the technology and to conduct a V&V exercise comparing software to actual vehicle tests. The CDT results will be described in a separate report. The remainder of this chapter will capture the goals and conclusions from each Thrust Area. Each chapter also included information for incorporation into a STANREC for that area.

10.1 TA1 GIS TERRAIN AND MOBILITY MAP

The goal of TA1 was to:

1) Develop improved, standardized methodologies to transform high resolution satellite imagery / remotely sensed GIS data into accurate NRMM terrain representations; and
2) Develop an example suite of geospatial terrain construction tools to demonstrate capabilities required by NG-NRMM.

An example suite of geospatial terrain construction tools was developed to demonstrate the capabilities required by NG-NRMM. Geoprocessing tools were used to ingest terrain data from various sources and resolutions and create a “standard” terrain file that could be utilized within NG-NRMM. A geospatial dataset was created for a

four-county area in Monterey, CA. The GIS data for each terrain parameter was collected and manipulated to produce NG-NRMM compliant terrain data that were then used by all Thrust Areas to demonstrate the "end-to-end" process to generate mobility results.

Three Annexes associated with TA1 explored associated areas. Annex B described a process to export data from the File Geodatabase to an NG-NRMM "interchange" terrain file format. Annex C described a method to estimate fine resolution soil moisture and Annex D provided an overview of methods to estimate soil strength.

10.2 TA2 SIMPLE TERRAMECHANICS (ST)

The goals of TA2 were to:

1) Define the input and output parameters required for ST models;
2) Identify and promote prototype demonstrations of GIS-based end-to-end ST models and simulations; and
3) Establish an NG-NRMM ST database of valid ST parameter data sets.

The equations used in ST calculations were described in detail. ST models have been hampered in the past by the lack of good terrain data. The methods required to collect terrain data required for a ST model were described in this chapter, including bevameters and vehicle-mounted sensors. In addition, a database was started that compiles existing terrain data and derived parameters needed for ST models. A snapshot of the initial dataset is included in Annex E and will be housed within the STANREC. The dataset will be continuously updated as additional data sources are located or new measurements made.

10.3 TA3 COMPLEX TERRAMECHANICS (CT)

NG-NRMM Complex Terramechanics models are those that utilize full three-dimensional (3D) soil models capable of accounting for the 3D flow/deformation of the soil, including both elastic and plastic (permanent) deformation under any 3D loading condition of a vehicle running gear/surface.

The chapter lays out the different approaches possible for a CT model and chooses a macro-scale model as the best compromise between high-fidelity and a reasonable computation time. Based on this choice, 14 requirements or needed capabilities for CT physics-based software tools were described. Examples of the 14 requirements are the ability to predict terrain deformation/damage or the ability to predict the response seen in laboratory terramechanics experiments.

The next part of the CT chapter (Chapter 8B) uses the software tool, DIS/Ground Vehicle from Advanced Science and Automation Corp, to show how it meets the above 14 requirements and areas where more research is needed. The final section (Chapter 8C) describes other CT software packages.

Annex F on the measurement and analysis of geotechnical properties is relevant to the chapters on both simple and complex terramechanics.

10.4 TA5 UNCERTAINTY TREATMENT

The goal of TA5 was to develop a stochastic framework for vehicle mobility prediction over large regions based on a stochastic knowledge of terrain properties and modern terramechanics Modeling and Simulation (M&S) capabilities and to demonstrate the generation of reliability-based stochastic mobility maps.

The framework was successfully demonstrated by creating reliability-based stochastic off-road mobility maps for Speed-Made-Good and GO/NOGO decisions for the Monterey Bay area. Stochastic maps were constructed for simple terramechanics, complex terramechanics, and for a wet vs. dry season. In each case, maps were constructed for 10%, 20%…90% reliability. Selecting a 90% reliability level will result in a much lower speed than a 10% reliability level, but a much higher confidence level. Stochastics were not considered by legacy NRMM, so this represents a major improvement in NG-NRMM.

10.5 TA6 INTELLIGENT VEHICLES

Intelligent vehicles represent another area not covered by NRMM and, in fact, represent a new capability that lacks the maturity and community base that exists for NRMM. The goal was to generate models and data products for predicting vehicle performance that could be used to execute desired mission scenarios over specified regions. These capabilities can help guide UGV development, as well as the UGV acquisition process.

Intelligent vehicles can span a large range from teleoperation to full autonomy and different situations will require different levels of autonomy. A prototype demonstration was carried out, again in the Monterey Bay area, to test out various intelligent vehicle scenarios, challenges, gaps and opportunities. The chapter concludes by calling out the many gap areas that exist in this arena, which became the basis for a proposed project on Mobility Assessment Methods and Tools for Autonomous Military Ground Systems (approved as ET-194).

10.6 TA6 VEHICLE VERIFICATION AND VALIDATION

The goal of TA6 was to describe a framework for benchmarking the ability of existing M&S software solutions to predict mobility performance and to validate those solutions against test data. The exercise took more than a year and was carried out for both a tracked and a wheeled vehicle.

In each case, five or six software developers simulated mobility over a series of events such as grade climbing or side slope stability on paved surfaces and on off-road soft surfaces. Test data was available to compare against the simulations. Comparisons were made and each event from each participant was assigned a “Maturity Level.” Through this method, the state of available software solutions could be assessed, and the software developers were able to improve areas of their software that were lacking.

The tracked vehicle V&V is described in Chapter 8A and the wheeled vehicle V&V is described in Chapter 8B. Two Annexes support this chapter with more detailed test data, Annex G for the tracked vehicle and Annex H for the wheeled vehicle. Those contain additional information on the vehicle, the terrain, and the field test data.

10.7 TA7 DATA GAPS AND OPERATIONAL READINESS

The goal of TA7 was to identify capability gaps to be addressed by future work in the pursuit of NG-NRMM and the challenges of implementing NG-NRMM. A questionnaire was created for the group members to obtain a benchmark on how the NG-NRMM would be used in the future and by whom. Next the gaps identified by the other six Thrust Areas were compiled. Finally, recommendations were made for future development of NG-NRMM.

It’s important to note that legacy NRMM is a code that anyone can use with the proper access. NG-NRMM is a guideline for making physics-based mobility predictions that account for the complexity of the vehicle-terrain

interface. Some areas that are dealt with in NRMM, such as the effect of visibility, have not been considered in NG-NRMM as it stands today. Rather a prototype methodology has been developed and described and will continue to be improved through the STANREC process.

Chapter 11 – ADDITIONAL REFERENCES

[1] Bekker, M.G. 1969. Introduction to Terrain-Vehicle Systems. University of Michigan Press, Ann Arbor, MI, USA.

[2] Birkel, P. 2003. Terrain Trafficability in Modeling and Simulation. SEDRIS Technical Paper 2003-1.

[3] Contreras, U., Recuero, A.M., Jayakumar, P., Foster, C D., Letherwood, M.D., Gorsich, D.J. and Shabana, A. 2017. Integration of ANCF Continuum-Based Soil Plasticity for Off-Road Vehicle Mobility in Multibody System Dynamics. Int. Journal of Vehicle Performance, Paper No. IJVP-133773, 3(1):36-70. DOI:10.1504/IJVP.2017.081267.

[4] Fleischmann, J., Serban, R., Negrut, D. and Jayakumar, P. 2016. On the Importance of Displacement History in Soft-Body Contact Models. Journal of Computational and Nonlinear Dynamics, ASME, Paper No. CND-15-1164, 11(4). DOI: 10.1115/1.4031197.

[5] Gonzalez, R., Jayakumar, P. and Iagnemma, K. 2017. Generation of Stochastic Mobility Maps for Large-Scale Route Planning of Ground Vehicles: A Case Study. Journal of Terramechanics, Paper No. JTERRA-D-16-00036, 69:1-11. DOI: 10.1016/j.jterra.2016.10.001.

[6] Gonzalez, R., Jayakumar, P. and Iagnemma, K. 2016. Stochastic Mobility Prediction of Ground Vehicles over Large Spatial Regions: A Geostatistical Approach. Autonomous Robots, Paper No. AURO-D-15-00104, 40(2). DOI:10.1007/s10514-015-9527-z.

[7] Janosi, Z. 1966. Land Locomotion Lab Research Report No. 6. TACOM Report 9560, DTIC Number AD651726.

[8] Jayakumar, P., Mechergui, D. and Wasfy, T. 2017. 1018 Understanding the Effects of Soil Characteristics on Mobility. Proceedings of ASME 58202; Volume 6. 13th International Conference on Multibody Systems, Nonlinear Dynamics, and Control, V006T10A035.

[9] Jayakumar, P., Melanz, D., MacLennan, J., Gorsich, D., Senatore, C. and Iagnemma, K. 2014. Scalability of Classical Terramechanics Models for Lightweight Vehicle Applications Incorporating Stochastic Modeling and Uncertainty Propagation. Journal of Terramechanics, Paper No. JTERRA-D-13-00075, 54:37-57. DOI:10.1016/j.jterra.2014.04.004.

[10] Jones, R.A. 1992. Validation Study of Two Rigid Body Dynamic Computer Models. Technical Report GL-92-17.

[11] Karafiath, L. and Nowatski, E. 1978. Soil Mechanics for Off-Road Vehicle Engineering. TransTech Publications.

[12] Lamb, D., Reid, A., Truong, N. and Weller, J. 2003. Terrain Validation and Enhancements for a Virtual Proving Ground. Presented at the Driving Simulation Conference-North America, October 8-10, 2003.

[13] Melanz, D., Jayakumar, P. and Negrut, D. 2016. Experimental Validation of a Differential Variational Inequality-based Approach for Handling Friction and Contact in Vehicle/Granular-Terrain Interaction. Journal of Terramechanics, Paper No. JTERRA-D-15-00099, 65:1-13. DOI:10.1016/j.jterra.2016.01.004.

[14] Parker, M.W., Shoop, S.A, Coutermarsh, B.A., Wesson, K.D., Stanley, J.M., 2009. Verification and Validation of a Winter Driving Simulator. J. Terramechanics 46. 127-139.

[15] Pazouki, A., Kwarta, M., Williams, K., Likos, W., Serban, R., Jayakumar, P. and Negrut, D. 2017. Compliant Contact Versus Rigid Contact: A Comparison in the Context of Granular Dynamics. Physical Review E, Paper No. ED11592, 96(4). DOI: https://doi.org/10.1103/PhysRevE.96.042905.

[16] Petrick, E.N., Janosi, Z.J. and Haley, P.W. 1981. The Use of the NATO Reference Mobility Model in Military Vehicle Procurement, SAE Paper 810373.

[17] Raymond, J.B. and Jayakumar, P. 2015. The Shearing Edge of Tracked Vehicle – Soil Interactions in Path Clearing Applications Utilizing Multi-Body Dynamics Modeling and Simulation. Journal of Terramechanics, Paper No. JTERRA-D-14-00006, 58:39-50. DOI: 10.1016/j.jterra.2014.12.003.

[18] Recuero, A., Serban, R., Peterson, B., Sugiyama, H., Jayakumar, P., Negrut, D. August 2017. A High-Fidelity Approach for Vehicle Mobility Simulation: Nonlinear Finite Element Tires Operating on Granular Material. Journal of Terramechanics, Paper No. JTERRA_2016_31, Vol. 72, pp. 39-54, doi: 10.1016/j.jterra. 2017.04.002.

[19] Reid, A.A., Shoop, S., Jones, R. and Nunez, P. 2007. High-Fidelity Ground Platform and Terrain Mechanics Modeling for Military Applications Involving Vehicle Dynamics and Mobility Analysis. Proceedings of the Joint North America, Asia-Pacific ISTVS Conference and Annual Meeting of Japanese Society for Terramechanics, Fairbanks, AK, USA.

[20] Richmond, P.W., Jones, R. A., Creighton, D.C. and Ahlvin, R.B. 2004. Estimating Off-Road Ground Contact Forces for a Real Time Motion Simulator, SAE 2004-01-2643.

[21] Richmond, P.W., Blais, C.L., Nagle, J.A., Goerger, N.C., Gates, B.Q., Burk, R.K., Willis, J. and Keeter, R. 2007. Standards for the Mobility Common Operational Picture (M-COP): Elements of Ground Vehicle Maneuver. U. S. Army Engineer Research and Development Center, Vicksburg, MS, USA. ERDC TR-07-4.

[22] Richmond, P.W, Reid, A.A., Shoop, S.A. and Mason, G.L. 2006. Terrain Surface Codes for an All-Season, Off-Road Ride Motion Simulator. The MSIAC online Journal. Available from: http://www.msiac.dmso.mil/journal/.

[23] Rohani, B. and Baladi, G.Y. 1981. Correlation of Mobility Cone Index with Fundamental Engineering Properties of Soil. AD A101409.

[24] Romano, R. and Schultz, S. 2004. Validation of Real-Time Multi-Body Vehicle Dynamics Models for Use in Product Design and Acquisition. SAE 2004-01-1582.

[25] Schafer, G. and Andre, S. 1997. PROSPER: A Useful Tool for Off-Road Vehicle Design. 7th European Conference of ISTVS.

[26] Schmid, I.C., Ruff, K. and Jakobs, R. 1997. Virtual Off Road Vehicle Testing with ORIS. 7th European ISRVS Conference, Ferrara, Italy.

[27] Schreiner, B.G. and Willoughby, W.E. 1976. Validation of the AMC-71 Mobility Model, Technical Report AD-A023 609. US Army Engineer Waterways Experiment Station, Vicksburg, MS.

[28] Serban, R., Negrut, D., Recuero, A. and Jayakumar, P. 2017. An Integrated Framework for High-Performance, High Fidelity Simulation of Ground Vehicle-Tire-Terrain Interaction. Int. Journal of Vehicle Performance, Special Issue on Vehicle Simulation with the Project Chrono Open Source Platform, Paper No. 185999.

[29] Shoop, S., Kestler, K. and Haehnel, R.L. 2006. Finite Element Modeling of Tires on Snow. Tire Science and Technology 34, Jan-Mar:2-37.

[30] Shoop S.A. 1993. Terrain Characterization for Trafficability. CRREL Report 93-6.

[31] Tasora, A., Mangoni, D., Negrut, D., Serban, R. and Jayakumar, P. 2017. Deformable Soil with Adaptive Level of Detail for Tracked and Wheeled Vehicles. Int. Journal of Vehicle Performance, Special Issue on Vehicle Simulation with the Project Chrono Open Source Platform, Paper No. IJVP-187299.

[32] Wasfy, T.M., Jayakumar, P., Mechergui, D. and Sanikommu, S. 2018. Prediction of Vehicle Mobility on Large-Scale Soft-Soil Terrain Maps Using Physics-Based Simulation. Int. Journal of Vehicle Performance, Paper No. IJVP-160689, 4(3).

[33] Wong, J.Y. 1988. NEPEAN Tracked Vehicle Performance Model (NTVPM-85), Contract Report 17/88. Prepared for Defence Research Establishment Suffield, Dept. of National Defence, Great Britain.

[34] Wong, J.Y., Jayakumar, P., Toma, E. and Preston-Thomas, J. 2017. Comparison of Simulation Models NRMM And NTVPM for Assessing Military Tracked Vehicle Cross-Country Performance. Journal of Terramechanics, Paper No. JTERRA_2017_31.

[35] Wong, J. Y., Senatore, C., Jayakumar, P. and Iagnemma, K. 2015. Predicting Mobility Performance of a Small, Lightweight Track System Using the Computer-Aided Method NTVPM. Journal of Terramechanics, Paper No. JTERRA-D-15-00020, 61:23-32. DOI: 10.1016/j.jterra.2015.07.002.

[36] Wong, J.Y., Jayakumar, P. and Preston-Thomas, J. 2019. Evaluation of the Computer Simulation Model NTVPM for Assessing Military Tracked Vehicle Cross-Country Mobility. Journal of Automobile Engineering, Proceedings of the Institution of Mechanical Engineers, Part D, Paper No. JAUTO-17-0038.

[37] Yamashita, H., Jayakumar, P., Alsaleh, M. and Sugiyama, H. 2018. Physics-Based Deformable Tire-Soil Interaction Model for Off-Road Mobility Simulation and Experimental Validation. Journal of Computational and Nonlinear Dynamics, ASME, Paper No. CND-17-1144, 13(2). DOI: 10.1115/ 1.4037994.



Annex A – TECHNICAL ACTIVITY PROPOSAL (TAP) AND TERMS OF REFERENCE (TOR)

A.1 TECHNICAL ACTIVITY PROPOSAL (TAP)

<table>
<tr><td rowspan="2">Activity reference number</td><td rowspan="2">AVT-248</td><td rowspan="3">Activity Title
Next-Generation NATO Reference Mobility Model (NRMM) Development</td><td>Approval
TBA</td></tr>
<tr><td rowspan="2">Start
January 2016</td></tr>
<tr><td>Type and serial number</td><td>RTG-085</td></tr>
<tr><td colspan="2">Location(s) and Dates</td><td>In conjunction with AVT PBW’s Planning year
20 – 24 April 2015, Rzeszow, Poland
12 – 16 October 2015, Prague, Czech Rep.
April 2016, Tallin Estonia
October 2016 Spain</td><td>End
December 2018</td></tr>
<tr><td colspan="2">Coordination with other bodies</td><td colspan="2">NAAG, MSG, LCG-LE</td></tr>
<tr><td colspan="2">NATO Classification of activity</td><td>NU</td><td>Non-NATO Invited
Yes</td></tr>
<tr><td colspan="2">Publication Data</td><td>TR</td><td>NU</td></tr>
<tr><td colspan="2">Keywords</td><td colspan="2">Mobility, Ground Vehicle, NRMM, Next-Generation, Physics-Based</td></tr>
</table>

I. Background and Justification (Relevance to NATO)

The NATO Reference Mobility Model (NRMM) is a simulation tool aimed at predicting the capability of a vehicle to move over specified terrain conditions. NRMM can be used for on-road and cross-country scenarios, it can account for several parameters such as terrain type, moisture content, terrain roughness, vehicle geometry, driver capabilities, etc.

NRMM was developed and validated by the U.S. Army Tank Automotive Research, Development, and Engineering Center (TARDEC) and Engineer Research and Development Center (ERDC) over several decades, and has been revised and updated throughout the years, resulting in the most recent version, NRMM II (arising partly out of AVT-107). NRMM is traditionally used to facilitate comparison between vehicle design candidates and to assess the mobility of existing vehicles under specific scenarios.

Although NRMM has proven to be of great practical utility to the NATO forces, when compared to modern modeling tools it exhibits several inherent limitations:

- It is based on empirical observations, and therefore extrapolation outside of test conditions is difficult or impossible.

- It is heavily dependent on in-situ soil measurements.
- Only one-dimensional analysis is possible; lateral vehicle dynamics are not considered.
- It does not account for vehicle dynamic effects, but instead only considers steady-state condition.
- It is specific to wheeled/tracked vehicles.
- It is not easily implementable within modern vehicle dynamics simulations.
- It exhibits poor (or poorly understood) interoperability and inter-scalability with other terramechanics and soil mechanics models.
- It is only suitable for mobility analysis, and does not provide auxiliary outputs (e.g., power efficiency analysis).

The proposed capability development is vital to NATOs mission. It promises to enable new capabilities in the design, modeling, and simulation of a broad class of vehicles. These modeling capabilities are of high importance to current and future NATO missions because they have the potential to significantly reduce costs and improve performance. The new tool will be applicable to various running gear morphologies, including conventional wheels and tracks, and more novel bioinspired limb designs. This could yield a new paradigm for ground vehicle mobility, which surpasses traditional analysis based on NRMMs go/no-go basis. An important aspect of modern simulations is the possibility to model complex vehicle maneuvering in high fidelity. Relying on High Performance Computing (HPC), it will be possible to utilize statistical representations of terrain profile and properties and to exploit very large-scale Monte Carlo simulations to yield rich outputs over a broad parameter space.

II. Objective(s)

The scope is to investigate an efficient simulation-based Next-Generation NRMM. Specifically, the proposed activity will focus on the following fundamental scientific objectives:

- Identify scale-invariant terrain descriptions for representing topographic map data (obtained at various scales) within a suitable multibody dynamic simulator. This will enable automated analysis of regions of interest, given heterogeneous map data products as inputs.
- Develop efficient, automated, parallelizable experimental design methods (i.e., sampling methods) for extracting metrics of interest from Monte Carlo simulations of the multibody dynamic simulator, including mobility-related metrics and auxiliary metrics. This will yield rich statistical mobility-related outputs in a computationally efficient manner, which will allow use of modern HPC resources.
- Explore the use of compact representations of vehicle dynamics (i.e., response surface methods or other approximation methods) within the multibody dynamic simulator, with a goal of further reducing computational cost.
- Establish compact, user-friendly representations of output metrics that capture important dependencies. This will yield an update to classical Speed-Made-Good or GO/NOGO maps.

III. Topics to be Covered

Modernizing the NRMM involves several areas of effort:

- Identification of vehicle – terrain interaction models, i.e., terramechanics models that balance fidelity with computational efficiency. These models may be semi-empirical, or fully analytical based on discrete elements.

- Development of in situ and online measurement tools to identify required terrain parameters.
- Identification of the type and form of desired responses, to yield rich mobility predictions and (ideally) useful auxiliary outputs.
- Integration of terramechanics models into modern dynamic simulation software, and develop efficient, automated computation tools, which will ideally enable the use of high performance computation techniques.
- Since the Next-Generation NRMM is expected to be extremely computationally intensive, there exists a need to investigate numerical methods to improve algorithmic efficiency and automate NRMM output generation, such as Monte Carlo sampling techniques and stochastic response surfaces.

IV. Deliverables (e.g., S/W Engage Model, Database, etc.) and/or End Product (e.g., Final Report)

Technical Report, other deliverable(s): In Jun – Aug 2015, ET-148 will prepare a report of findings and recommendations on the benefits and value of the Next-Generation NATO Reference Mobility Model for enhanced vehicle design and mobility performance. The report will also detail the various resources required and committed by the various member nations to develop this model. This summary report will detail the current state-of-the-art and provide recommendations for the Next-Generation NRMM that will be more predictive, more general, and more scalable than the current NRMM. This ET has had 4 monthly telephone conferences for a total of 6 hours ahead of the Brussels meetings, and in Brussels the team of 20 will be meeting during 5 slots for more than 8 hours. The ET includes 4 former members of the prior RTG activity (AVT-107) which also considered this problem earlier under TC-PSF, who provide unique perspectives and lessons learned from the prior activity. Specifically, the ET-148 team feels that the following considerations need to be taken into account regarding the two activities, both seemingly focused on the same topic, yet quite different in many ways.

V. Technical Team Leader and Lead Nation

Co-Chair: Dr. Michael HOENLINGER Germany.

Co-Chair: Dr. Paramsothy JAYAKUMAR United States.

Lead Nation: United States.

VI. Nations Willing/Invited to Participate

NATO Nations and Bodies: Canada, Czech Republic, Estonia, Germany, Italy, Poland, Romania, Slovakia, Turkey, United Kingdom, United States.

PfP Nations: Belarus.

MD Nations: None.

ICI Nations: None.

Global Partners: Australia, Japan, Republic of Korea.

Contact / Other Nations: South Africa.

VII. National and/or NATO Resources Needed (Physical and Non-physical Assets)

The RTG Team will need meeting space during AVT Panel Business Meeting Weeks. Standard support for an RTO Technology Group (RTG).

This will include:

National support for the RTG;

Funding for Technical Evaluator for the RTG meetings;

Distribution of electronic data via the STO/AVT Sharepoint; and

Publication of the Proceedings of the meetings and Reports on the RTO Website Publication of the RTG Report.

VIII. STO/CSO Resources Needed

Standard Support for an RTG.

It is possible that the RTG may approach NATO and the CSO for funds to be provided to nations to fulfil some of their responsibilities that have been given to them by the RTG. Given that this activity is likely to result in a long-lasting methodology and/or tool similar to the current NRMM tool which is used for free in military acquisitions by NATO member nations, such funding will be a valuable investment for the future.

A.2 TERMS OF REFERENCE (TOR)

Terms of Reference (TOR)

AVT-248, RTG-085 on

Next-Generation NATO Reference Mobility Model (NRMM) Development

I. Origin

A. Background

The NATO Reference Mobility Model (NRMM) is a simulation tool aimed at predicting the capability of a vehicle to move over specified terrain conditions. NRMM can be used for on-road and cross-country scenarios, it can account for several parameters such as terrain type, moisture content, terrain roughness, vehicle geometry, driver capabilities, etc.

NRMM was developed and validated by the U.S. Army Tank Automotive Research, Development, and Engineering Center (TARDEC) and Engineer Research and Development Center (ERDC) over several decades, and has been revised and updated throughout the years, resulting in the most recent version, NRMM II (arising partly out of AVT-107). NRMM is traditionally used to facilitate comparison between vehicle design candidates and to assess the mobility of existing vehicles under specific scenarios.

Although NRMM has proven to be of great practical utility to the NATO forces, when compared to modern modeling tools it exhibits several inherent limitations:

- It is based on empirical observations, and therefore extrapolation outside of test conditions is difficult or impossible.
- It is heavily dependent on in-situ soil measurements.
- Only one-dimensional analysis is possible; lateral vehicle dynamics are not considered.
- It does not account for vehicle dynamic effects, but instead only considers steady-state condition.
- It is specific to wheeled/tracked vehicles.
- It is not easily implementable within modern vehicle dynamics simulations.
- It exhibits poor (or poorly understood) interoperability and interscalability with other terramechanics and soil mechanics models.
- It is only suitable for mobility analysis, and does not provide auxiliary outputs (e.g., power efficiency analysis).

B. Justification (Relevance for NATO)

The proposed capability development is vital to NATOs mission. It promises to enable new capabilities in the design, modeling, and simulation of a broad class of vehicles. These modeling capabilities are of high importance to current and future NATO missions because they have the potential to significantly reduce costs and improve performance. The new tool will be applicable to various running gear morphologies, including conventional wheels and tracks, and more novel bioinspired limb designs. This could yield a new paradigm for ground vehicle mobility, which surpasses traditional analysis based on NRMMs go/no-go basis. An important aspect of modern simulations is the possibility to model complex vehicle maneuvering in high fidelity. Relying on High Performance Computing (HPC), it will be possible to utilize statistical representations of terrain profile and properties and to exploit very large-scale Monte Carlo simulations to yield rich outputs over a broad parameter space.

Current NRMM tools limitations were eventually not addressed by the past AVT-107 activity, the outcome of which has been that the NRMM tool is less effectively used by the NATO nations. One significant concern is that if the current tool is not enhanced with higher fidelity and efficiency, it will leave the NATO nations with a subpar mobility tool that is neither capable of accurately differentiating competing designs nor capable of accurately predicting mobility performance of a specific design in various operational scenarios.

Given that this activity is likely to result in a long-lasting methodology and/or tool similar to the current NRMM tool which is widely used in military acquisitions by NATO member nations, such funding will be a valuable investment for the future.

II. Objectives

1) This RTG will bring together Experts in the mobility field from all NATO and supporting nations in implementing the ET-148 recommendations in order to develop the Next-Generation NRMM model, and create an architecture of a back-bone for the new methodology. The focus will be on the development of a modular back-bone that will address various shortcomings in the current NRMM tool. The goal will be to keep the back-bone architecture tool-agnostic so that the best individual tools could be adapted to fit into this back-bone.

Four members of the prior AVT-107 team are also a part of the ET-148 team that will continue to form the proposed RTG, thereby ensuring continuity of expertise and lessons learned from the prior activity.

2) The proposed activity will also focus on the following fundamental scientific objectives:
   - Identify scale-invariant terrain descriptions for representing topographic map data (obtained at various scales) within a suitable multibody dynamic simulator. This will enable automated analysis of regions of interest, given heterogeneous map data products as inputs.
   - Develop efficient, automated, parallelizable experimental design methods (i.e., sampling methods) for extracting metrics of interest from Monte Carlo simulations of the multibody dynamic simulator, including mobility-related metrics and auxiliary metrics. This will yield rich statistical mobility-related outputs in a computationally efficient manner, which will allow use of modern HPC resources.
   - Explore the use of compact representations of vehicle dynamics (i.e., response surface methods or other approximation methods) within the multibody dynamic simulator, with a goal of further reducing computational cost.
   - Establish compact, user-friendly representations of output metrics that capture important dependencies. This will yield an update to classical Speed-Made-Good or GO/NOGO maps.
3) It is also the intent of this RTG to develop a prototype tool to demonstrate how different parts and tools could fit into the proposed back-bone making up the Next-Generation NATO Reference Mobility Model. This will demonstrate how a set of tools can be put together to fit the newly developed back-bone described above. The back-bone architecture will be modular, allowing the integration of individual mobility assessment modules that are the best state-of-the-art to form the Next-Generation NATO Mobility modeling methodology. The individual modules can be commercial, open source, or government developed.
4) A Final Report will be issued at the end of the 3-year period in 4Q2018 that will describe:
   a) The back-bone infrastructure for the NATO Mobility Model;
   b) The development of the prototype that demonstrates use of (a); and
   c) Lessons learned during the life of the RTG that could be of benefit to future NATO study groups.
5) The duration of this activity is not to exceed three years, including planning, execution and the Final Report. The proposed RTO Task Group (RTG) will work on this cooperative research and technology project in the 2015 – 2018 timeframe.

III. Resources

A. Membership

Co-Chair: Dr. Michael HOENLINGER Germany.

Co-Chair: Dr Paramsothy JAYAKUMAR United States.

Lead Nation: United States.

Nations Willing/Invited to Participate: Canada, Czech Republic, Estonia, Germany, Italy, Poland, Romania, Slovakia, Turkey, United Kingdom, United States.

B. National and/or NATO Resources Needed

The RTG Team will need meeting space during AVT Panel Business Meeting Weeks. Standard support for an RTO Technology Group (RTG). This will include:

National support for the RTG.

Funding for Technical Evaluator for the RTG meetings.

Distribution of electronic data via the STO/AVT Sharepoint.

Publication of the Proceedings of the meetings and Reports on the RTO Website Publication of the RTG Report.

C. STO/CSO Resources Needed

Standard Support for an RTG.

It is possible that the RTG may approach NATO and the CSO for funds to be provided to nations to fulfil some of their responsibilities that have been given to them by the RTG. Given that this activity is likely to result in a long-lasting methodology and/or tool similar to the current NRMM tool which is used for free in military acquisitions by NATO member nations, such funding will be a valuable investment for the future.

IV. Security Classification Level

The security level will be NATO Unclassified.

V. Participation by Partner Nations PfP Nations (Excluding Russia) Listed Above

Global Partners: Australia, Belarus, Japan, South Korea, South Africa.

PfP Nations: Belarus.

MD Nations: none.

ICI Nations: none.

Global Partners: Australia, Japan, Republic of Korea.

Contact / Other Nations: South Africa.

VI. Liaison

NATO-AVT-107.

ET-148.

NATO RTO.

US DoD.

US Army Corps of Engineers/ERDC.



Annex B – MODIFIED NRMM CODE 11 "MAPTBL" TERRAIN DATA INTERCHANGE FORMAT

Matthew Funk
Esri, Inc.
UNITED STATES

Brian Wojtysiak
U.S. Army Material Systems Analysis Activity (AMSAA)
UNITED STATES

B.1 *.ASC ASCII RASTER FORMAT

The ASCII Raster Format [1], [2], [3] is a raster-based thematic image of Numbered Terrain Units (NTUs) (see Figure B-1). These are identifiers of terrain units that are matched up to the NTU field in the associated *.TER file described in Section B.3 (Table B-1).

```
NCOLS xxx
NROWS xxx
XLLCENTER xxx | XLLCORNER xxx
YLLCENTER xxx | YLLCORNER xxx
CELLSIZE xxx
NODATA_VALUE xxx
row 1
row 2
...
row n
```

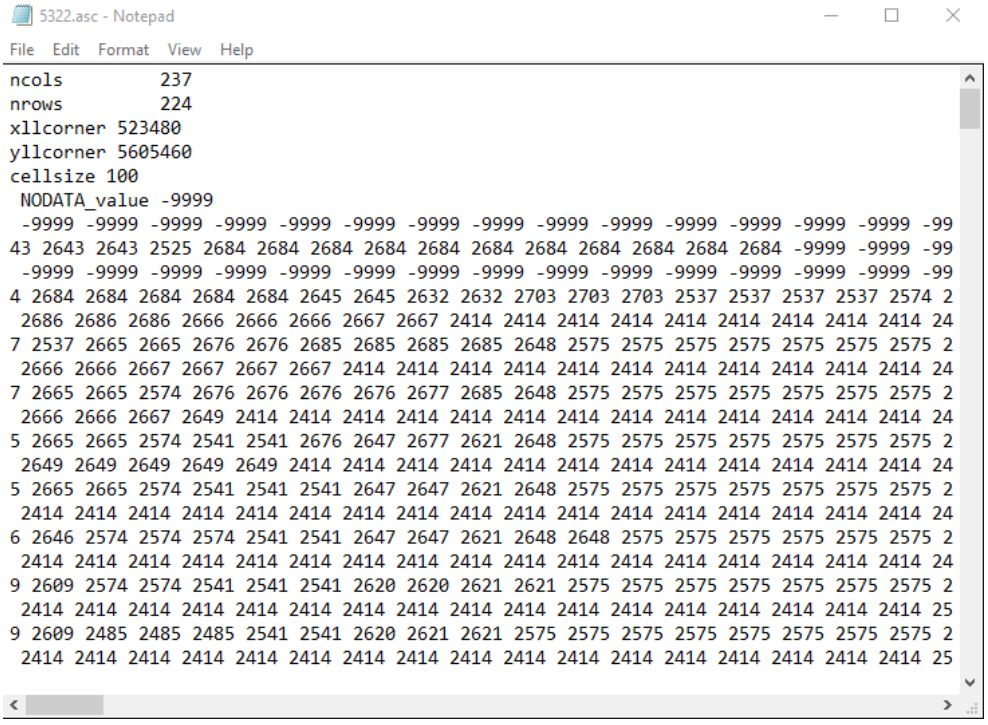


Figure B-1: Example *.ASC File.

Where:

Table B-1: ASCII Raster Format Identifiers.

Parameter	Description	Requirements
NCOLS	Number of cell columns.	Integer greater than 0.
NROWS	Number of cell rows.	Integer greater than 0.
XLLCENTER or XLLCORNER	X coordinate of the origin (by center or lower left corner of the cell).	Match with Y coordinate type.
YLLCENTER or YLLCORNER	Y coordinate of the origin (by center or lower left corner of the cell).	Match with X coordinate type.
CELLSIZE	Cell size.	Greater than 0.
NODATA_VALUE	The input values to be NoData in the output raster.	Optional. Default is -9999.

B.2 *.PRJ ASCII RASTER SPATIAL REFERENCE SUPPORT FILE

The *.PRJ support file stores the coordinate system information for the *.ASC raster [1], [2] file above. The format is a basic text file describing the basic coordinate system parameters. The coordinate systems and parameters are outlined in Map projections: Georeferencing spatial data. (1994). Redlands (Cal.): Environmental Systems Research Institute. ISBN 1-879102-28-5.

Example of Universal Transverse Mercator (UTM) PRJ:

```
Projection UTM
Zone 10
Datum WGS84
Spheroid WGS84
Units METERS
Zunits NO
Parameters
```

Example of Geographic WGS84 PRJ:

```
Projection GEOGRAPHIC
Datum WGS84
Spheroid WGS84
Units DD
Zunits NO
Parameters
```

The most common projection parameters are PROJECTION (Table B-2) and UNITS (Table B-3). The type of PROJECTION defines what other PARAMETERS (Table B-4) will be used [3].

Table B-2: PROJECTION Options

ALASKA_E	GALL_STEREOGRAPHIC	PERSPECTIVE
ALASKA_GRID	GEOCENTRIC	POLAR
ALBERS	GEOGRAPHIC	POLYCONIC
AZIMUTHAL	GREATBRITIAN_GRID	ROBINSON
BIPOLAR_OBLIQUE	GRINTEN	RSO
BONNE	HAMMER_AITOFF	SIMPLE_CONIC
CASSINI	LAMBERT	SINUSOIDAL
CHAMBERLIN	LAMBERT_AZIMUTH	SPACE_OBILIQUE_MERCATOR
CRASTER_PARABOLIC	LOCAL	STATEPLANE
CYLINDRICAL	MERCATOR	STEREOGRAPHIC
ECKERTIV	MILLER	TIMES
ECKERTVI	MOLLWEIDE	TRANSVERSE
EQUIDISTANT	NEWZEALAND_GRID	TWO_POINT_EQUIDISTANT
EQUIRECTANGULAR	OBLIQUE_MERCATOR	UPS
FLAT_POLAR_QUARTIC	ORTHOGRAPHIC	UTM

Table B-3: UNITS Options

DD (Decimal Degrees)
DM (Decimal Minutes)
DMS (Degrees Minutes Seconds)
DS (Decimal Seconds)
FEET
METERS
RADIANS
REAL NUMBER (Units \ Meter)

Other parameters depend on the PROJECTION used and will be noted in the PARAMETERS.

Table B-4: PARAMETERS.

Parameter	Units
1st standard parallel	DD MM SS
2nd standard parallel	DD MM SS
Central meridian	DD MM SS
Latitude of projection origin	DD MM SS
False easting (meters)	<decimal>
False northing (meters)	<decimal>
Longitude of central meridian	DD MM SS
Latitude of standard parallel	DD MM SS
Radius of sphere of reference	<decimal>, 0 = 6,370,997 meters
Longitude of center of projection	DD MM SS
Latitude of center of projection	DD MM SS
Longitude of point A	DD MM SS
Latitude of point A	DD MM SS
Longitude of point B	DD MM SS
Latitude of point B	DD MM SS
Longitude of point C	DD MM SS
Latitude of point C	DD MM SS
Longitude of 1st point	DD MM SS
Latitude of 1st point	DD MM SS
Longitude of 2nd point	DD MM SS
Latitude of 2nd point	DD MM SS
Scale factor	<decimal>
Azimuth	DD MMSS
Number of standard parallels	1, 2
Latitude of 1st standard parallel	DD MM SS
Latitude of 2nd standard parallel	DD MM SS
Quadrant	NE, NW, SE, SW
Landsat vehicle ID	1, 2, 3, 4, 5
Orbital path number	1 through 233

Parameter	Units
Zone	<coded number by projection type>
Pole	NORTHPOLE, SOUTHPOLE
View	EQUITORIAL, NORTHPOLE, SOUTHPOLE

B.3 *.TER TERRAIN FILE

A tabular format for terrain data input is devised as format code 11, "MAPTBL". This format provides the capability to enter the terrain data information in a space-delimited spreadsheet with the terrain data items being in fields (columns), and the terrain units as records (rows). The first row of the tabular input designates the specific terrain items. The remaining "header" are marked as comments, starting with a "!" and may include: date and time created, author, contact info, etc. After the general comments are the field header metadata, marked with "!#". These rows describe the field (columnar) data in the remaining table. The first row after the field header metadata are the field headers. They are in order (left to right) delimited by a space character. The remaining rows are the *.TER file's data section, and contain the actual data values in order noted in the field headers.

B.3.1 First Record

The first row of the file is the line with the number of data records in the file, the format type, and a description of the file (up to 60 characters in length). The first record is the "Standard" NRMM terrain file heading as follows:

<NTU> <KTYPE> <TERID>

Item	Format	Description
NTU	Integer	Number of terrain units (rows in *.TER file's Data Section)
KTYPE	Integer	Terrain file type and format code (must be 11 for this format)
TERID	Text (length = 60)	Alphanumeric title/description

Example: 53544233 11 Monterey California AOI-27JUN2015.

Where:

- NTU = 53544233.
- KTYPE = 11.
- TERID = Monterey California AOI-27JUN2015.

Other KTYPE formats were supported in earlier versions of NRMM, only code 11, MAPTBL, is supported in this description.

B.3.2 General Comments

The general comment rows start with a "!" character. The rest of the line is treated as text comment and are not processed.

B.3.3 Field Header Metadata

Information about each field included in the data table is included in the *.TER file's header. Each line is initialized with a "!" comment marker followed by a "#" character to identify a field metadata row.

The next string is the FIELD_NAME as it exists as the first line of the data values section of the file. This should contain any special characters or spaces. Separating the name from the metadata tags list is a colon ":".

Currently three metadata tags exist for the fields:

- FIELD_DESCRIPTION.
- DEFAULT_VALUE.
- DATA_SOURCE_TYPE.

The FIELD_DESCRIPTION is a single sentence describing the data field.

The DEFAULT_VALUE is the value that the row / field will receive in the absence of data. Note that a string "NULL" may be used in place of a number or other value as a "No Data" default flag. Earlier versions of NRMM did not support this flag and are forced to use a numeric value. Common values for earlier NRMM are 0 or -9999.

DATA_SOURCE_TYPE tag determines how the value was collected. This tag has five values:

- "MEASURED" the source was directly measured or calculated from a measured source.
- "INFERRED" the source was estimated or interpolated from single or multiple sources.
- "LEGACY" supporting source was built for previous versions of NRMM standard.
- "NOTIONAL" the data value is extrapolated or estimated from non-source data for fields that do not yet have a consistent data source available. This allows the modeling and simulation software to function with required data that does not yet exist.
- "UNKNOWN" a general flag for data that was captured or obtained without knowledge of origin.

The end user should have the option to scrub or deselect NOTIONAL data sources from processing for non-simulated exercises.

Format of each field line:

!# <FIELD_NAME>:[<FIELD_DESCRIPTION>, <DEFAULT_VALUE> , <DATA_SOURCE_TYPE>

Item	Description	Values
FIELD_NAME	Name of the field	Text
FIELD_DESCRIPTION	Description of the field	Text

Item	Description	Values
DEFAULT_VALUE	Default value used if no value exists	Various
DATA_SOURCE_TYPE	Source condition	Text "m" = "MEASURED" "i" = "INFERRED" "c" = "LEGACY" "n" = "NOTIONAL" "UNKNOWN"

Example: !# SHAPE_LENGTH:["boundary length","NULL","m"].

The following terrain data input items may be specified via this input method (Table B-5):

Table B-5: Terrain Data Input Items.

2.	Default Value	Units	Type	Item Description	Earliest NRMM Version[1]
ACTRMS	0	Inches	Double	Surface roughness	2.8.2
AREA	0	km^2	Double	Patch area	2.8.2
BRDGMLC(1) BRDGMLC(2) BRDGMLC(3) BRDGMLC(4)	0		Integer	Bridge MLC (1) – type 1, one-way, wheeled (2) – type 2, two-way, wheeled (3) – type 3, one-way, tracked (4) – type 4, two-way, tracked	2.8.2
CI(1) CI(2)	0	psi	real	Cone Index value Cone Index: (1) – 0 – 6 inches (2) – 6 – 12 inches	2.8.2
CLUTTER	0	Code	Integer	Road lane width restriction 0 – no effect 1 – reduced by 10% 2 – reduced by 6 ft	2.8.2

[1] The "Earliest NRMM Version" column lists the legacy NRMM software version, starting with 2.8.2, that the field is supported. So 2.8.2 is supported on 2.8.2 and possibly 3.0, while 3.0 is supported on 3.0, but not NG. NG is not supported on 2.8.2 or 3.0.

2.	Default Value	Units	Type	Item Description	Earliest NRMM Version[1]
CLUTTER (cont'd)	0	Code	Integer	3 – reduced by 8 ft 4 – greater of 8 ft reduction or 75% > 4 – minimum of all lane widths	2.8.2
CRVSPD	0.0	mph	Double	Curve speed limit	2.8.2
DBROCK	99.9	Inches	Double	Depth to bedrock	2.8.2
DFREEZ	0	Inches	Double	Depth of freezing	2.8.2
DIST	0	km	Double	Road terrain unit length	2.8.2
DSNOW	0	Inches	Double	Depth of surface snow	2.8.2
DTHAW	0	Inches	Double	Depth of thawing	2.8.2
EANG	0	Radians	Double	Super-elevation angle	2.8.2
ELEV	0.0	Meters	Double	Elevation at surface	2.8.2
GRADE	0.0	Percent	Double	Slope of surface [5]	2.8.2
IMTYPE (NOT USED)	0	Code	Integer	Material type 0 – not given 1 – soil 2 – concrete 3 – bituminous (asphalt) 4 – crushed rock 5 – gravel 6 – shale	2.8.2
IOST	1 (avoidable)	Code	Integer	Obstacle avoidability 1 – avoidable 2 – not avoidable	2.8.2
IROAD	0 (cross-country)	Code	Integer	Road type 0 – off-road 1 – super highway 2 – primary road 3 – secondary road 4 – trail	2.8.2

2.	Default Value	Units	Type	Item Description	Earliest NRMM Version[1]
ISCOND	0 (use scenario)	Code	Integer	Surface condition 0 – not given, use scenario value 1 – normal 2 – slippery 3 – flooded 4 – snow 5 – snow on ice	2.8.2
IST		Code	Integer	NRMM soil model code: 1 – fine grained 2 – coarse grained 3 – muck	2.8.2
ITURNLR	0	Code	Integer	Curve turn direction 0 – not given 1 – left -1, 2 – right	2.8.2
IURB	4	Code	Integer	Urban code 1 – village 2 – town 3 – city 4 – normal on/off-road 5 – canal 6 – river 7 – lake	2.8.2
KUSCS	5	Code	Integer	Soil type 1 – SW 2 – SP 3 – SM 4 – SC 5 – SMSC 6 – CL	2.8.2

2.	Default Value	Units	Type	Item Description	Earliest NRMM Version[1]
KUSCS (cont'd)	5	Code	Integer	7 – ML 8 – CLML 9 – CH 10 – MH 11 – OL 12 – OH 13 – water 14 – pavement 15 – rock 16 – GW 17 – GP 18 – GM 19 – GC 20 – Pt	2.8.2
KWI	3	Code	Integer	Wetness Index (SMSP) 0 – arid 1 – dry 2 – average 3 – wet 4 – saturated 5 – water logged	2.8.2
LOCHARD	.TRUE.	Logic	Boolean	Overhead clearance type	2.8.2
LTRAFFIC(NLANES)	MLANES*0	Code	Integer	Traffic flow direction 1 – forward 2 – reverse 3 – two-way	2.8.2
LUSE	0	Code	Integer	Land Use classification (various types)	2.8.2
NI	8	Number	Integer	No. vegetation classes Max = 9	2.8.2
NLANES	1	Number	Integer	No. traffic lanes	2.8.2
NTU	1	Number	Integer	Terrain unit number	2.8.2

2.	Default Value	Units	Type	Item Description	Earliest NRMM Version[1]
NUNITS	1	Number	Integer	Number of terrain units	2.8.2
OBAA	3.14159	Radians	Double	Obstacle approach angle	2.8.2
OBH	0.0	Inches	Double	Obstacle height	2.8.2
OBL	0.0	Inches	Double	Obstacle length	2.8.2
OBS	999.0	Inches	Double	Obstacle spacing	2.8.2
OBW	0.0	Inches	Double	Obstacle width	2.8.2
OHCLEAR	0.0	Inches	Double	Overhead clearance	2.8.2
RADC	5730.0	Inches	Double	Road curvature radius	2.8.2
RCIC(1,1) RCIC(1,2) RCIC(2,1) RCIC(2,2) RCIC(3,1) RCIC(3,2) RCIC(4,1) RCIC(4,2)	750.0	PSI	Double	Seasonal Soil Strength 1,1 – dry, 0" – 6" 1,2 – dry, 6" – 12" 2,1 – average, 0" – 6" 2,2 – average, 6" – 12" 3,1 – wet, 0" – 6" 3,2 – wet, 6" – 12" 4,1 – wet-wet, 0" – 6" 4,2 – wet-wet, 6" – 12"	2.8.2
RDA(1) RDA(2) RDA(3) RDA(4) RDA(5) RDA(6) RDA(7) RDA(8) RDA(9) RDA(10) RDA(11) RDA(12)	3600.0	Inches	Double	Recognition distance by month: 1 – January 2 – February 3 – March 4 – April 5 – May 6 – June 7 – July 8 – August 9 – September 10 – October 11 – November 12 – December	2.8.2

2.	Default Value	Units	Type	Item Description	Earliest NRMM Version[1]
RDBDANG(1) RDBDANG(2)	0.0	Radians	Double	Road embankment angle 1 – left side 2 – right side	2.8.2
RDBDHGT(1) RDBDHGT(2)	0.0	Inches	Double	Road embankment height 1 – left side 2 – right side	2.8.2
RDBDWID(1) RDBDWID(2)	0.0	Inches	Double	Road embankment width 1 – left side 2 – right side	2.8.2
RDSHWID(1) RDSHWID(2)	0.0	Inches	Double	Road shoulder width 1 – left side 2 – right side	2.8.2
RDSTRNGS(1,1,1) RDSTRNGS(1,1,2) RDSTRNGS(1,2,1) RDSTRNGS(1,2,2) RDSTRNGS(2,1,1) RDSTRNGS(2,1,2) RDSTRNGS(2,2,1) RDSTRNGS(2,2,2) RDSTRNGS(3,1,1) RDSTRNGS(3,1,2)	0.0	PSI	Double	Road soil strengths 1,1,1 – roadway, left side, 0" – 6" 1,1,2 – roadway, left side, 6" - 12" 1,2,1 – roadway, right side, 0" – 6" 1,2,2 – roadway, right side, 6" – 12" 2,1,1 – shoulder, left side, 0" – 6" 2,1,2 – shoulder, left side, 6" – 12" 2,2,1 – shoulder, right side, 0" – 6" 2,2,2 – shoulder, right side, 6" – 12" 3,1,1 – roadbed, left side, 0" – 6" 3,1,2 – roadbed, left side, 6" – 12"	2.8.2

2.	Default Value	Units	Type	Item Description	Earliest NRMM Version[1]
RDSTRNGS(3,2,1) RDSTRNGS(3,2,2)	0.0	PSI	Double	3,2,1 – roadbed, right side, 0" – 6" 3,2,2 – roadbed, right side, 6" – 12"	2.8.2
RDSTYPS(3,2)	0	Code	Integer	Road soil types 1 – left side 2 – right side	2.8.2
S(1) S(2) S(3) S(4) S(5) S(6) S(7) S(8) S(9)	3936.0	Inches	Double	Stem spacing, each class S(1) = 0.49 S(2) = 1.67 S(3) = 3.15 S(4) = 4.73 S(5) = 6.30 S(6) = 7.88S (7) = 9.25 S(8) = 12.42 S(9) = 99.0	2.8.2
SD(1) SD(2) SD(3) SD(4) SD(5) SD(6) SD(7) SD(8) SD(9)	0.49,1.67, 3.15,4.73, 6.30,7.88, 9.25,12.42, 99.0	Inches	Double	Stem average diameters SD(1) = 0.49 SD(2) = 1.67 SD(3) = 3.15 SD(4) = 4.73 SD(5) = 6.30 SD(6) = 7.88 SD(7) = 9.25 SD(8) = 12.42 SD(9) = 99.0	2.8.2
SDL(1) SDL(2) SDL(3) SDL(4)	0.98,2.36, 3.94,5.51	Inches	Double	Stem maximum diameters SDL(1) = 0.98 SDL(2) = 2.36 SDL(3) = 3.94 SDL(4) = 5.51	2.8.2

2.	Default Value	Units	Type	Item Description	Earliest NRMM Version[1]
SDL(5) SDL(6) SDL(7) SDL(8) SDL(9)	7.09,8.66, 9.84,15.0, 99.0	Inches	Double	SDL(5) = 7.09 SDL(6) = 8.66 SDL(7) = 9.84 SDL(8) = 15.0 SDL(9) = 99.0	2.8.2
SIGMA	0.1	g/cm^3	Double	Snow density	2.8.2
SNOMCH	.false.	Code	Boolean	Snow inferencing	2.8.2
TMOIST	0.0	Percent	Double	Thawing soil moisture content	2.8.2
TSPDMAX(1) TSPDMAX(2)	1760.0	In/sec	Double	Restricted clearance speeds 1 – bridge/tunnel/roadway speed limit 2 – VHGTMAX interference speed limit	2.8.2
TUID	BEST UNIT	Text		Terrain unit id.	2.8.2
TWIDMIN	0.0	Inches	Double	Roadway minimum width	2.8.2
WD	0.0	Inches	Double	Depth standing water	2.8.2
WLANES(NLANES)	0.0	Inches	Double	Road lane widths	2.8.2
ENG_C	0.0	psi	Double	Cohesion	3.0
ENG_G	0.0	psi	Double	Elastic shear modulus	3.0
ENG_GAMMA	0.0	lb/ft^3	Double	Total unit weight	3.0
ENG_PHI	0.0	Degrees	Double	Friction angle	3.0
EXTFRICT	0.0	Degrees	Double	External friction angle	3.0
CPRIS	0.0	psi	Double	Soil prism cohesion	3.0
DELTAPRIS	0.0	Degrees	Double	Soil prism external friction angle	3.0
GAMMAPRIS	0.0	lb/ft^3	Double	Soil prism unit weight	3.0
PHIPRIS	0.0	Degrees	Double	Soil prism friction angle	3.0
TEMP	295.4	Degrees (K)	Double	Soil temperature in degrees Kelvin	NG
ASPECT	-1 (flat surface)	Degrees	Double	Direction in degrees of surface normal vector -1.0 – 360.0.	NG

2.	Default Value	Units	Type	Item Description	Earliest NRMM Version[1]
SSL	0.0	Inches	Double	First significant strength layer depth	NG
SSL2	0.0	Inches	Double	Second significant strength layer depth	NG
KUSCS2	5	Code	Integer	KUSCS associated with SSL2	NG
TMOIST2	0.0	Percent	Double	TMOIST associated with SSL2	NG
TEMP2	295.4	Degrees (K)	Double	TEMP associated with SSL2	NG
BULKDNS	0	g/cm^3	Double	Values measuring soil bulk density.	NG

B.3.4 Field Header

The row after the File Header Metadata, which is the first row without a "!" starting character, is the file header row. This is a space-delimited list of the fields (columns) to follow in the data section. Each of the field names in the Field Header Metadata section is in this list. The order of the fields is the order of the data columns to follow:

<field_1> <field_2> <field_3> <field_4> <field_5> … <field_n>

Example:

NTU ASPECT BULKDNS CI(1) CI(2) DBROCK GRADE IOST IROAD ISCOND KUSCS KWI NLANES OBH OBL TMOIST USCS ELEV LUSE

B.3.5 Data Section

The subsequent rows in the file store the actual data values, separated by spaces. The number of data rows is the number of NTUs listed in the First Record. The order of the values is the same as the order of fields in the File Header.

Because of the nature of the delimiting character the data values will NEVER contain a space as this would cause a shift in field values and corrupt data values.

<row_1_field_1> <row_1_field_2> <row_1_field_3> <row_1_field_4> … <row_1_field_n>
<row_2_field_1> <row_2_field_2> <row_2_field_3> <row_2_field_4> … <row_2_field_n>
<row_3_field_1> <row_3_field_2> <row_3_field_3> <row_3_field_4> … <row_3_field_n>
<row_4_field_1> <row_4_field_2> <row_4_field_3> <row_4_field_4> … <row_4_field_n>
…
<row_m_field_1> <row_m_field_2> <row_m_field_3> <row_m_field_4> … <row_m_field_n>

Example:

1 0.0 0.1 0.0 0.0 201.0 9.0 0 0 1 20 2 0 0.0 0.0 12.0 PT 329.336222 0
2 0.0 0.1 0.0 0.0 201.0 12.0 0 0 1 20 2 0 0.0 0.0 12.0 PT 329.031422 0
3 0.0 0.1 0.0 0.0 201.0 12.0 0 0 1 20 2 0 0.0 0.0 12.0 PT 328.879022 0
4 360.0 0.1 0.0 0.0 201.0 12.0 0 0 1 20 2 0 0.0 0.0 12.0 PT 328.802822 0
5 0.0 0.1 0.0 0.0 201.0 12.0 0 0 1 20 2 0 0.0 0.0 12.0 PT 328.802822 0
6 360.0 0.1 0.0 0.0 201.0 9.0 0 0 1 20 2 0 0.0 0.0 12.0 PT 328.879022 0

B.4 REFERENCES

[1] How Aspect Works, Esri, Inc. (http://desktop.arcgis.com/en/arcmap/10.3/tools/spatial-analyst-toolbox/how-aspect-works.htm). Accessed 7/31/2017.

[2] Esri ASCII Raster Format, Esri, Inc. (http://resources.arcgis.com/en/help/main/10.1/index.html#/Esri_ASCII_raster_format/009t0000000z000000/). Accessed 6/6/2018.

[3] ASC ASCII Raster Format, Esri, Inc. (http://resources.esri.com/help/9.3/arcgisdesktop/com/gp_toolref/spatial_analyst_tools/esri_ascii_raster_format.htm). Accessed 12/19/2017.

[4] Environmental Systems Research Institute . 1994. Map projections: Georeferencing spatial data. Redlands, CA. ISBN 1-879102-28-5.

[5] How Slope Works, Esri, Inc. (http://desktop.arcgis.com/en/arcmap/10.3/tools/spatial-analyst-toolbox/how-slope-works.htm). Accessed 7/31/2017.

Annex C – FINE RESOLUTION SOIL MOISTURE ESTIMATION

Jeffrey D. Niemann
Colorado State University
UNITED STATES

Mark Cammarere
Technology Service Corporation
UNITED STATES

C.1 GOALS AND TEAM MEMBERS

C.1.1 Goal of Fine Resolution Soil Moisture Estimation

The objective is to develop fine resolution estimates of soil moisture of any Area Of Interest (AOI) that can be used in soil strength calculations and associated evaluations of uncertainty. To reach this objective, research has been conducted to generalize the Equilibrium Moisture from Topography, Vegetation, and Soil (EMT+VS) method for downscaling coarse resolution (5 – 40 km) soil moisture estimates from remote sensing and/or land-surface models to actionable fine resolutions (< 100 m pixels). Such fine resolution estimates are required for use as input to tactical tools including the Next-Generation NATO Reference Mobility Model (NG-NRMM).

Research has also included creating a prototype EMT+VS map-based application that can provide elevation, fine resolution soil moisture estimates, and fine resolution soil moisture uncertainty information for a user-designated AOI.

C.1.2 Team Members

The team members are:

- **Mark Cammarere, Leader**, USA;
- Keith Gemeinhart, USA;
- Andrew Jones, USA;
- **Jeffrey Niemann, Leader**, USA; and,
- Joseph Scalia, USA.

C.2 INTRODUCTION

A research team associated with AVT-248[1] has developed (and is continuing to develop) an EMT+VS model for application to NG-NRMM soil moisture estimation. This model downscales remotely sensed or modeled coarse resolution (5 – 40 km) soil moisture to tactical resolutions (< 100 meters) based primarily on topographic and vegetation cover information [1]. Coarse soil moisture and topographic (e.g., terrain elevation) information are required EMT+VS inputs while fine resolution vegetation (Soil Adjusted Vegetation Index – SAVI) and soil type information can also be input, if available. The original version of the EMT+VS model produces a single, deterministic soil moisture estimate in each fine resolution pixel.

[1] Drs. Jeffrey Niemann, Andrew Jones and Joseph Scalia of Colorado State University (CSU) along with Messrs. Mark Cammarere and Keith Gemeinhart of Technology Service Corp (TSC).

C.3 FINE RESOLUTION SOIL MOISTURE – MEAN

Unlike conventional hydrologic models, the EMT+VS model does not iterate through time, so it requires no initial or historical conditions and it can be applied rapidly to large regions (e.g., 150 km by 150 km regions in 3 – 4 minutes). It also can be applied to any selected date or even hypothetical moisture conditions. The parameters it requires can be estimated from global datasets, which means that it is applicable to data-limited environments. Yet it can accept additional data if such data are abundant.

The EMT+VS model calculates soil moisture using a mathematical structure that is similar to earlier approaches [2], [3] but the equations are built on conceptual descriptions of vadose zone[2] hydrology. The model estimates soil moisture by considering the water balance in the soil layer for the land area A that drains through the edge of a fine resolution grid cell. Four processes (see Figure C-1) can add or remove water from that layer: infiltration, deep drainage, lateral flow, and evapotranspiration or ET:

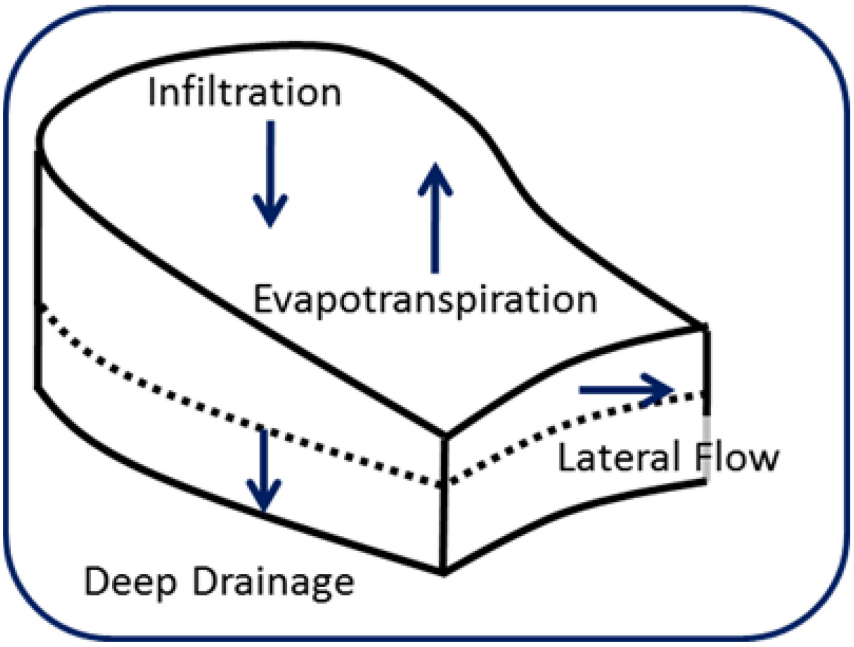


Figure C-1: Four Hydrologic Processes Considered in EMT+VS Model.

- **Infiltration *F*** is described using a simple approach that accounts for orographic effects on precipitation and interception of precipitated water by vegetation. Orographic precipitation is described using the elevation, slope, and topographic aspect when the topography is represented at intermediate (~7 km) resolution. This intermediate resolution has been shown to exhibit the strongest relationship between topographic attributes and precipitation patterns [4], [5].
- **Deep drainage *G*** describes the loss of water to deeper soil layers or groundwater. It is described using Darcy's Law under the assumption that gravity controls the vertical hydraulic gradient (i.e., using a percolation assumption). Unsaturated hydraulic conductivity is described using the Campbell equation [6].

[2] The **vadose** zone, also termed the **unsaturated** zone, is the part of Earth between the land surface and the top of the phreatic zone, the position at which the groundwater (the water in the soil's pores) is at atmospheric pressure.

- **Lateral flow *L*** describes the movement of water to lower locations on a hillslope. Lateral flow is also described using Darcy's Law under the assumption that the lateral hydraulic gradient is a function of the topographic slope. The thickness of the soil layer is modeled as a function of topographic curvature [7].
- **Evapotranspiration *ET*** model begins with a supplied spatial-average value or coarse grid of potential ET values. The local potential ET is then calculated by inferring spatial variations in temperature from the local elevation. This approach was compared to a full Penman-Monteith estimation method and found to produce very similar results [5]. The local potential ET is then partitioned into a potential evaporation and a potential transpiration using the fractional vegetation cover V. The fractional vegetation cover is also used to reduce soil evaporation in response to shading of the soil. The ET is then partitioned into a radiation ET term and an aerodynamic ET term using the Priestley-Taylor assumption [8]. Spatial variations in insolation are described using the Potential Solar Radiation Index (PRSI), which depends primarily on the topographic slope and aspect along with the latitude [9].

A summary of the model is provided below, but a detailed description and evaluation of the model are published in the scientific literature [10], [11], [12], [13], [14].

Using the equations for F, G, L and ET to describe the hydrologic processes, the soil moisture is determined using a novel solution strategy [10]. The strategy calculates the local (or fine resolution) soil moisture θ as a function of the spatial-average soil moisture $\bar{\theta}$. The spatial-average soil moisture $\bar{\theta}$ can be provided as a single value or a coarse resolution grid of values (e.g., from a land-surface model like Noah [15] or a remote sensing product like SMAP [16]). A series of exact analytical solutions are obtained for soil moisture under the assumption that each of the outflow terms in the water balance dominates. Once these analytical solutions are found, the final soil moisture is determined by a weighted average of the analytical solutions, where the weights are the magnitudes of the outflow terms in the water balance. The final soil moisture estimate is:

$$\theta = \frac{w_G\theta_G + w_L\theta_L + w_R\theta_R + w_A\theta_A}{w_G + w_L + w_R + w_A} \tag{C-1}$$

where θ_G, θ_L, θ_R, and θ_A are the analytical soil moisture estimates if deep drainage, lateral flow, radiation ET, and aerodynamic ET dominate, respectively. The weights w_G, w_L, w_R, and w_A control the importance of θ_G, θ_L, θ_R, and θ_A to the final estimate of θ.

The soil moisture when deep drainage dominates is:

$$\theta_G = \bar{\theta}\frac{\mathrm{DDI}}{\overline{\mathrm{DDI}}} \tag{C-2}$$

where DDI is the deep drainage index, and $\overline{\mathrm{DDI}}$ is the spatial-average of the DDI. The DDI is a spatial pattern that primarily depends on the fractional vegetation cover V. The DDI is one way that the model introduces fine resolution variations in the soil moisture pattern. The soil moisture when lateral flow dominates is:

$$\theta_L = \bar{\theta}\frac{\mathrm{LFI}}{\overline{\mathrm{LFI}}} \tag{C-3}$$

where LFI is the lateral flow index and $\overline{\mathrm{LFI}}$ is the spatial-average of the lateral flow index. The LFI is a spatial pattern that depends both on the fractional vegetation cover V and on topographic attributes (drainage area A,

slope S, and curvature κ). The LFI also can introduce fine resolution variations in soil moisture. The soil moisture when the radiation ET term dominates is:

$$\theta_R = \bar{\theta}\frac{\mathrm{REI}}{\overline{\mathrm{REI}}} \tag{C-4}$$

where REI is the radiation ET index and $\overline{\mathrm{REI}}$ is the spatial-average of the REI. The REI is a spatial pattern that depends primarily on the elevation Z, PSRI I_p, and vegetation cover V. The soil moisture when the aerodynamic ET term dominates is:

$$\theta_A = \bar{\theta}\frac{\mathrm{AEI}}{\overline{\mathrm{AEI}}} \tag{C-5}$$

where AEI the aerodynamic ET index and $\overline{\mathrm{AEI}}$ is the spatial-average of the AEI. The AEI is a final spatial pattern that depends primarily on the elevation Z and vegetation cover V. The contributions of θ_G, θ_L, θ_R, and θ_A to the weighted average are calculated from:

$$w_G = \left(\frac{\bar{\theta}}{\overline{\mathrm{DDI}}}\right)^{\gamma_v} \tag{C-6}$$

$$w_L = \left(\frac{\bar{\theta}}{\overline{\mathrm{LFI}}}\right)^{\gamma_h} \tag{C-7}$$

$$w_R = \left(\frac{\bar{\theta}}{\overline{\mathrm{REI}}}\right)^{\beta_r} \tag{C-8}$$

$$w_A = \left(\frac{\bar{\theta}}{\overline{\mathrm{AEI}}}\right)^{\beta_a} \tag{C-9}$$

These weights vary in time because $\bar{\theta}$ is expected to vary in time (see Figure C-2). As $\bar{\theta}$ changes, the weights emphasize different spatial patterns, which produces soil moisture patterns with different spatial structures. The ability of the EMT+VS model to produce temporally unstable patterns is important because some soil moisture patterns exhibit this behavior [17] but most estimation and downscaling methods do not. Figure C-3 shows a sample EMT+VS output for the Monterey Bay area in CA that was developed by the TA1 team for AVT-248. This sample result used a USGS 30 m Digital Elevation Model (DEM) with coarse soil moisture estimates from SMAP (~ 9 km resolution) and SAVI information derived from 30 m LandSat data. Fine resolution soil type information was not included as an EMT+VS input in this example.

In addition to the spatial-average soil moisture estimation model described above, the research team is also currently updating the model to produce estimates of soil moisture uncertainty.

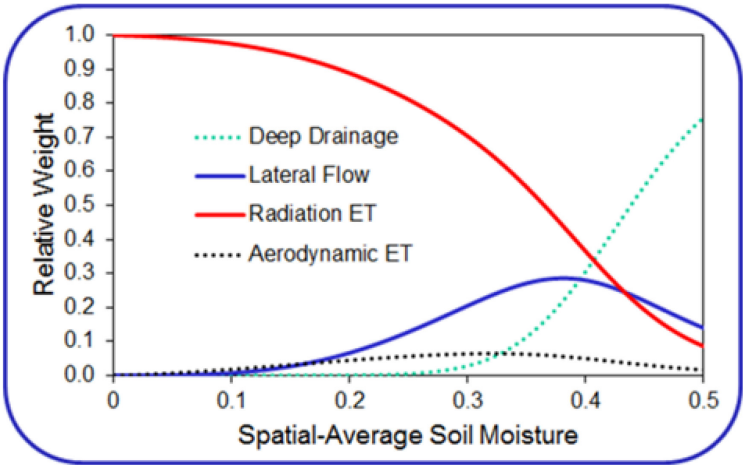


Figure C-2: Relative Importance of the Four Hydrologic Processes with Spatial-Average Soil Moisture.

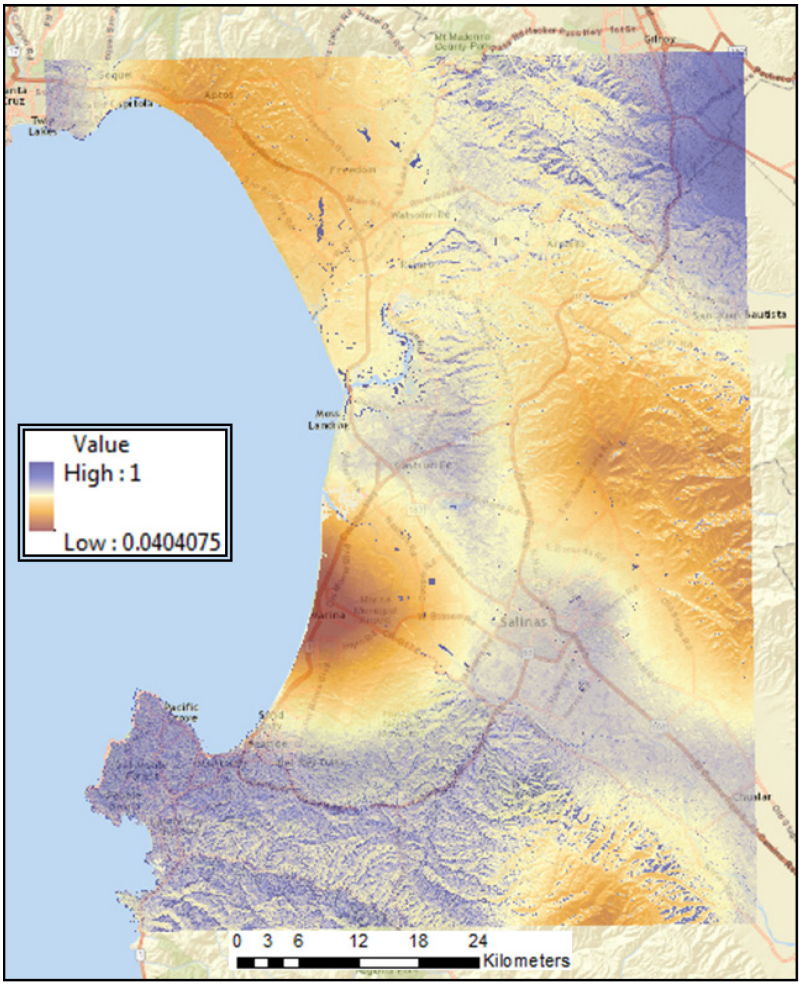


Figure C-3: Sample 30 m EMT+VS Output for Monterey Bay, CA Sample Area.

C.4 FINE RESOLUTION SOIL MOISTURE – STOCHASTIC VARIATIONS

Like any method, the original version of the EMT+VS model has some limitations. Specifically, a single deterministic estimate of the soil moisture in each pixel:

- May not reproduce the statistical properties of soil moisture patterns, and
- Does not provide confidence limits on the soil moisture estimates.

Therefore, preliminary research has been conducted to generalize the EMT+VS model to produce probabilistic results that allow:

1) Simulation of soil moisture patterns with realistic statistical properties, and
2) Generation of confidence limits for the soil moisture estimates.

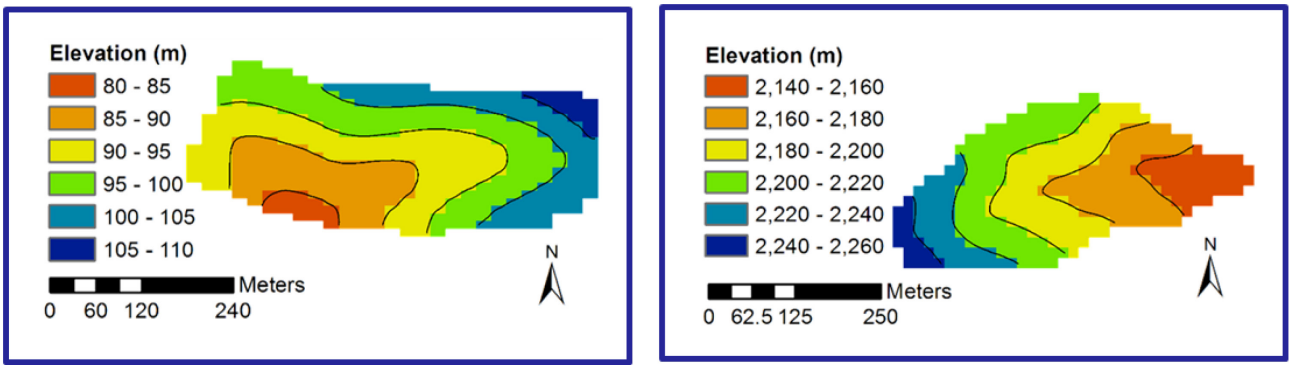
This research has been performed by first identifying stochastic features that should be reproduced by the model. Then, models were developed to introduce the required stochastic variations. Two model approaches were developed:

1) **Indirect Model** – Introduces stochastic variations through the regional characteristics that are supplied to the EMT+VS model.
2) **Direct Model** – Introduces stochastic variations directly in the fine resolution soil moisture estimates.

Development of these models was performed using two test catchments:

1) Tarrawarra in Southern Victoria Australia[3], and
2) Cache la Poudre near Rustic Colorado[4].

Elevation summaries of these catchments are shown in Figure C-4.



(a) Tarrawarra **(b) Cache la Poudre**

Figure C-4: Test Catchments for Soil Moisture Stochastic Variations Models.

[3] Sub-humid climate (820 mm precipitation per year); Total area = 10.5 Hectares (ha); 454 sample locations; 454 sample locations (30 cm TDR) on 13 dates (spanning 1 year).

[4] Semi-arid climate (400 mm precipitation per year); Total area = 8 ha; 350 sample locations (5 cm TDR) on 9 dates (spanning 2 months).

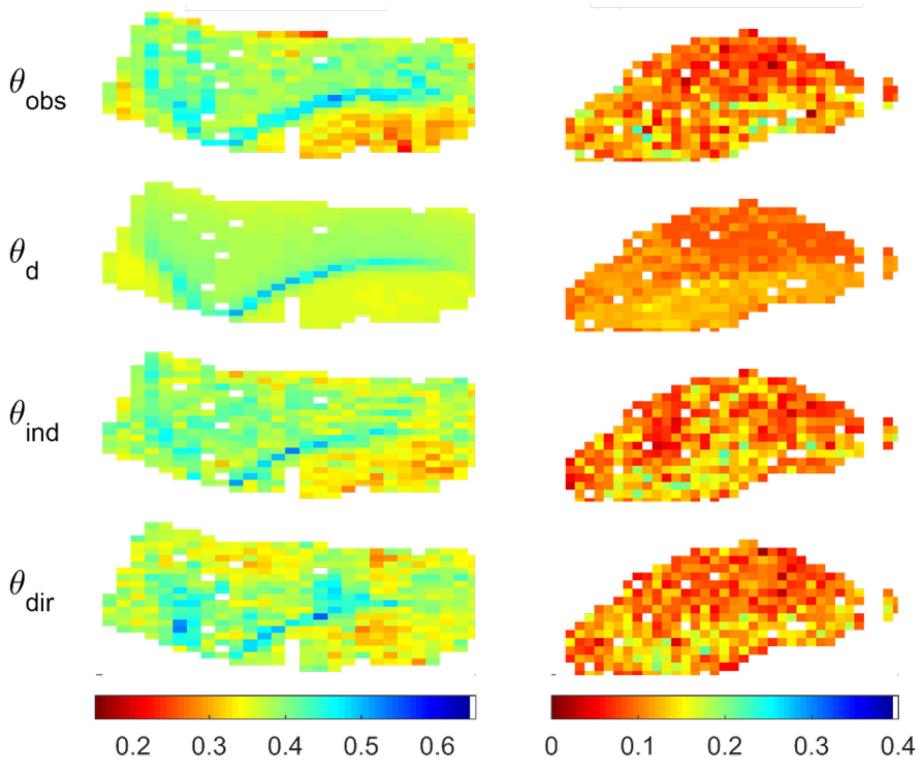
The indirect model introduces a stochastic soil moisture disequilibrium term (D), as well as stochastic variations in the porosity (ϕ) and precipitation (P). It also includes stochastic measurement errors (e) if desired. All these stochastic variations ultimately produce stochastic variations in the simulated soil moisture (θ_{ind}).

The *direct model* introduces the stochastic variations directly after the (deterministic) soil moisture estimates are generated. Unlike the indirect model (which includes temporally stable elements), the random fields in the direct model estimate (θ_{dir}) are temporally unstable, so the direct model does not attempt to reproduce any stable stochastic patterns. However, the direct model does capture the properties of the overall stochastic component (i.e., semivariogram nugget, range, and partial sill) and most of their dependencies on spatial-average soil moisture as observed at the Tarrawarra and Cache la Poudre catchments. The direct model is being included in the map-based EMT+VS application first.

Because the distribution shape of the direct model variations is normal, confidence intervals are computed directly from the standardized z-scores, z^*:

$$\text{Confidence Interval} = (\theta_d - z^* \cdot \sigma_{\pi \text{dir}}, (\theta_d + z^* \cdot \sigma_{\pi \text{dir}}). \quad \text{(C-10)}$$

Sample soil maps for the Tarrawarra and Cache la Poudre catchments are provided in Figure C-5. Inspection of the figure reveals that both models capture the speckle that is present in the observations at both sites. (Note: The gap at the east end of the Cache la Poudre maps is due to lack of measurement information in that area. Data are only presented for locations where measurement information is available.)



(a) Tarrawarra **(b) Cache la Poudre**

Figure C-5: Soil Moisture Maps (Top to Bottom: Observed Soil Moisture; Deterministic EMT+VS; Generalized EMT+VS, Indirect; and Generalized EMT+VS, Direct).

C.5 FINE RESOLUTION SOIL MOISTURE – MAP-BASED APPLICATION

While the members of the research team representing Colorado State University (CSU) have been developing the EMT+VS model itself, those members representing Technology Service Corporation (TSC) have been implementing the model processes in a combination of the C# and Python programming languages, and packaging them in a map-centric application. The EMT+VS model process chain is shown in Figure C-6, while Figure C-7 shows a screen shot of the map-centric tool interface. In Figure C-6, the blue italicized text indicates user-provided inputs to the EMT+VS process chain including AOI (an Area Of Interest rectangle).

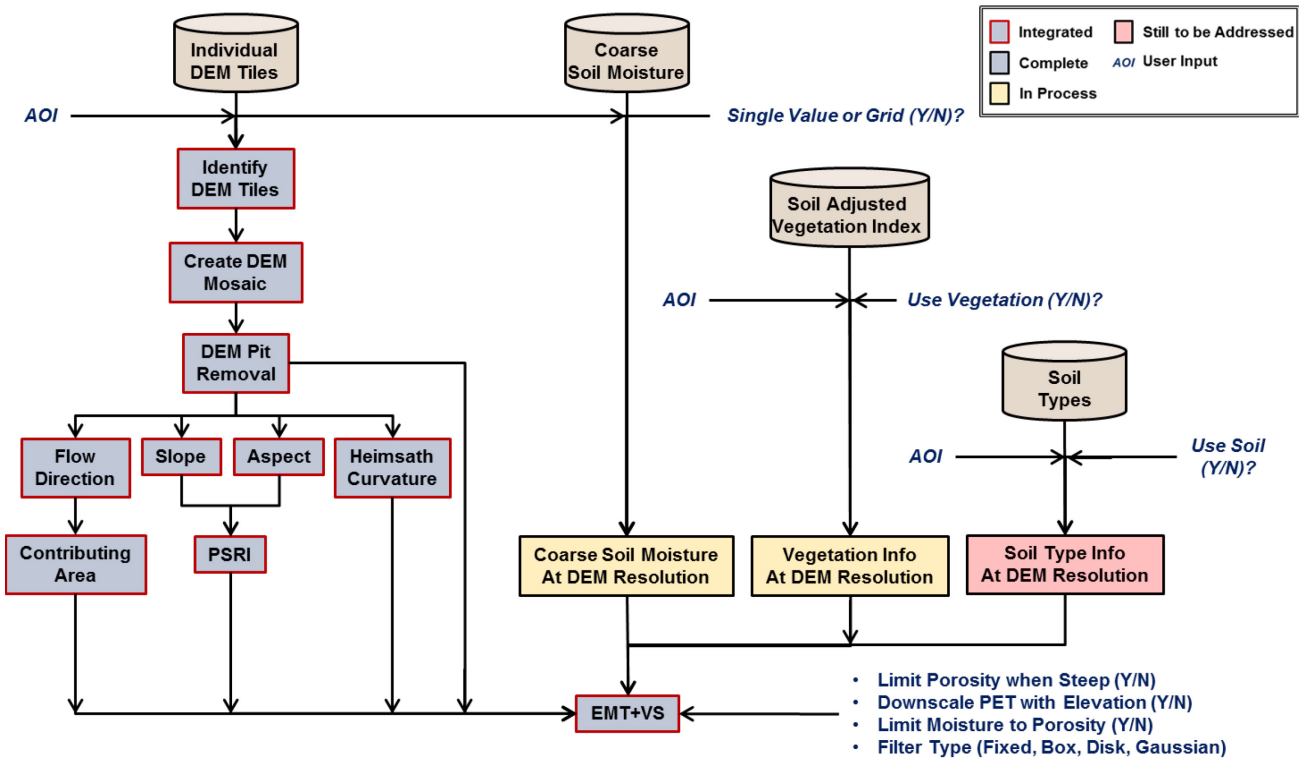


Figure C-6: EMT+VS Model Process Chain.

Sample intermediate EMT+VS results for the Fort Pickett U.S. Army National Guard installation near Blackstone, VA are shown in Figure C-8 – while final results (DEM mosaic and fine resolution soil moisture) are provided in Figure C-9. These sample results use a 30 m DEM constructed of Digital Terrain Elevation Data level 2 (DTED2) elevation tiles and a single value of input coarse soil moisture. All interim and final results are stored as single-band GeoTIFF files.

The work described in this Annex was performed under a U.S. Army Research Laboratory (ARL) Small Business Innovation Research (SBIR) contract for Dr. Paramsothy Jayakumar and Mr. Mike Letherwood of the US Army GVSC. Mr. Peter J. Grazaitis is the sponsor of the ARL SBIR effort.

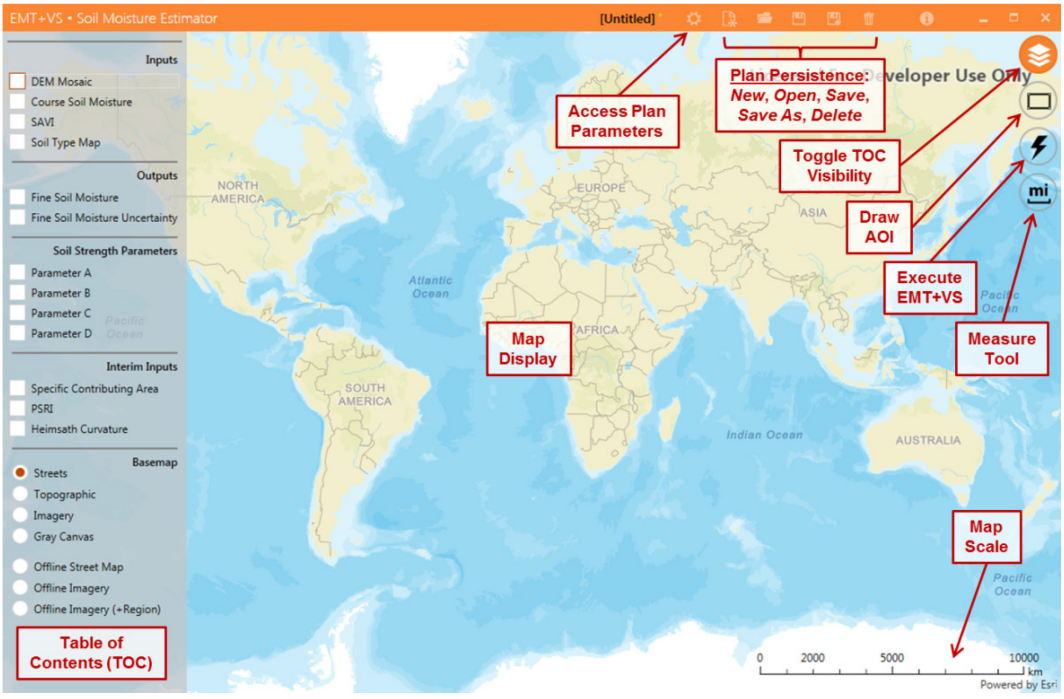


Figure C-7: EMT+VS Soil Moisture Estimator Map-Centric Application Interface.

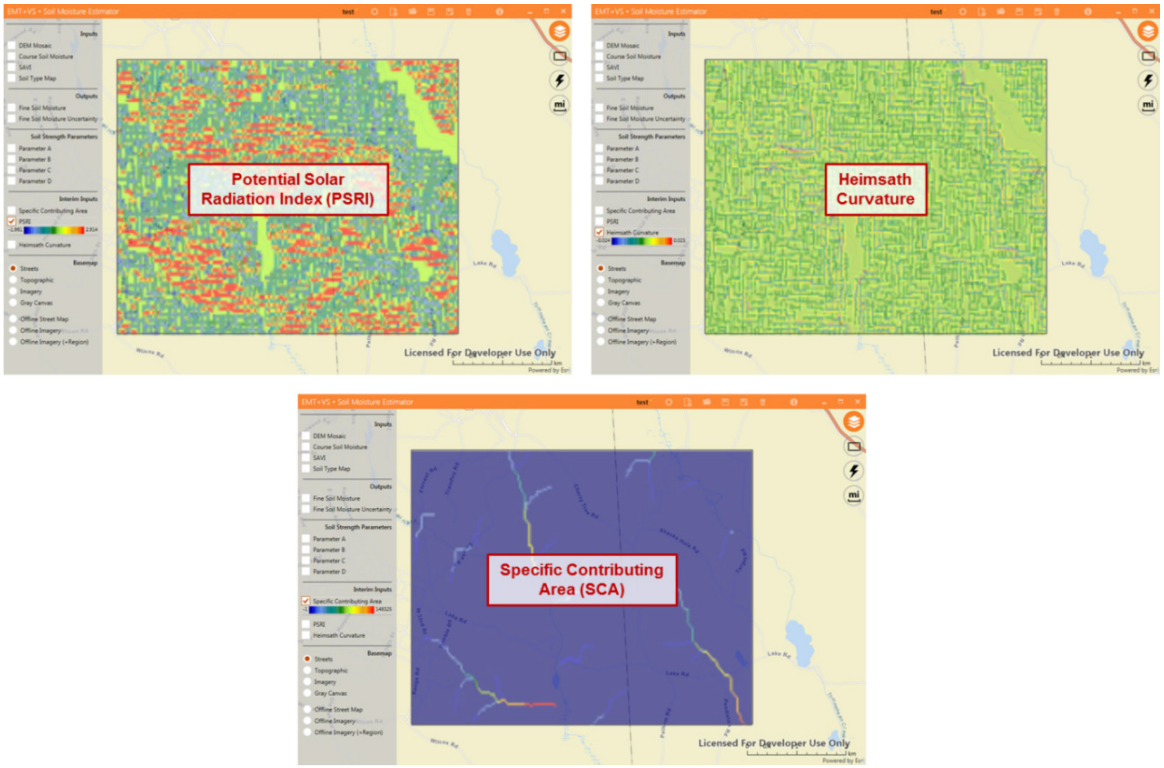


Figure C-8: Sample Intermediate EMT+VS Model Results for Fort Pickett.

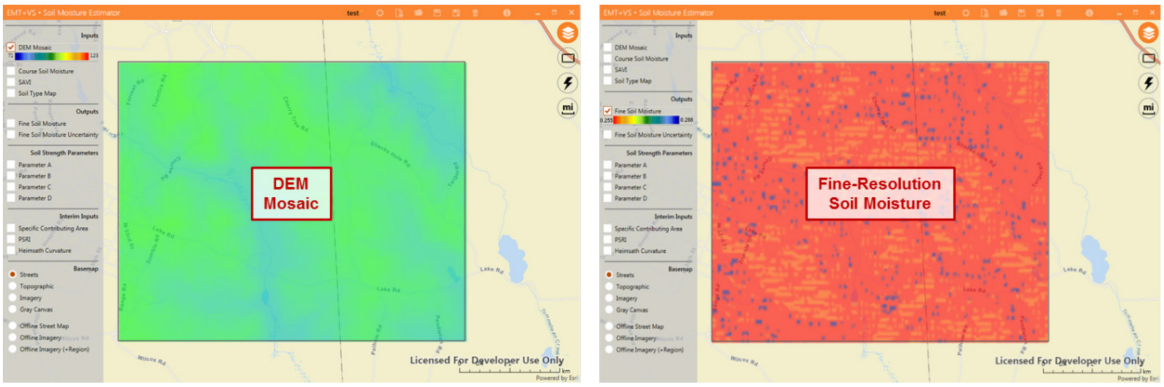


Figure C-9: Sample EMT+VS Model Outputs for Fort Pickett.

C.6 REFERENCES

[1] Ranney, K.J., Niemann, J.D., Lehman, B.M., Green, T.R. and Jones, A.S. 2015. A Method to Downscale Soil Moisture to Fine-Resolutions using Topographic, Vegetation, and Soil Data. Advances in Water Resources, 76: 81-96. DOI: 10.1016/j.advwatres.2014.12.003.

[2] Busch, F.A., Niemann, J.D. and Coleman, M.L. 2012. Evaluation of an EOF-Based Method to Downscale Soil Moisture Patterns Based on Topographical Attributes. Hydrologic Processes, 26:2696-2709. DOI: 10.1002/hyp. 8363.

[3] Werbylo, K.L. and Niemann, J.D. 2014. Evaluation of Sampling Techniques to Characterize Topographically-Dependent Variability for Soil Moisture Downscaling. Journal of Hydrology, 516:304-316. DOI: 10.1016/j.jhydrol.2014.01.030.

[4] Daly, C., Neilson, R.P. and Phillips, D.L. 1994. A Statistical-Topographic Model for Mapping Climatological Precipitation Over Mountainous Terrain. Journal of Applied Meteorology, 33:140-158.

[5] Cowley, G.S., Niemann, J.D., Green, T.R., Seyfried, M.S. and Jones, A.S. 2016. Downscaling Soil Moisture in Regions with Large Elevation Ranges. American Geophysical Union Hydrology Days, Fort Collins, Colorado.

[6] Campbell, G.S. 1974. Simple Method for Determining Unsaturated Conductivity from Moisture Retention Data. Soil Science, 117(6):311-314.

[7] Heimsath, A.M., Dietrich, W.E., Nishiizumi, K. and Finkel, R.C. 1999. Cosmogenic Nuclides, Topography, and the Spatial Variation of Soil Depth. Geomorphology, 27(1-2):151-172.

[8] Priestley, C.H.B., and Taylor, R.J. 1972. On the Assessment of Surface Heat Flux and Evaporation Using Large-Scale Parameters. Monthly Weather Review, 100(2):81-92.

[9] Dingman, S.L. 2002. Physical Hydrology (Second edition). Prentice Hall, Upper Saddle River, New Jersey. 646 pp.

[10] Coleman, M.L. and Niemann, J.D.,2013. Controls on Topographic Dependence and Time-Instability in Catchment-Scale Soil Moisture Patterns. Water Resources Research, 49:1-18. DOI:10.1002/wrcr.20159.

[11] Ranney, K.J., Niemann, J.D., Lehman, B.M., Green, T.R. and Jones, A.S. 2015. A Method to Downscale Soil Moisture to Fine-Resolutions using Topographic, Vegetation, and Soil Data. Advances in Water Resources, 76:81-96. DOI: 10.1016/j.advwatres.2014.12.003.

[12] Alburn, N.E., Niemann, J.D. and Elhaddad, A. 2015. Evaluation of a Surface Energy Balance Method Based on Optical and Thermal Satellite Imagery to Estimate Root-Zone Soil Moisture. Hydrological Processes, 29:5354-5368. DOI: 10.1002/hyp.10562.

[13] Cowley, G.S., Niemann, J.D., Green, T.R., Seyfried, M.S., Jones, A.S. and Grazaitis, P.J. 2017. Impacts of Precipitation and Potential Evapotranspiration Patterns on Downscaling Soil Moisture in Regions with Large Topographic Relief. Water Resources Research, 53:1553-1574. DOI: 10.1002/2016WRO19907.

[14] Hoehn, D.C., Niemann, J.D., Green, T.R., Jones, A.S. and Grazaitis, P.J. 2017. Downscaling Soil Moisture over Regions that Include Multiple Coarse-Resolution Grid Cells. Remote Sensing of Environment, Awaiting Release.

[15] Niu, G.-Y., Yang, Z.-L., Mitchell, K.E., Chen, F., Ek, M.B., Barlage, M., Kumar, A., Manning, K., Niyogi D., Rosero E., Tewari, M. and Xia, Y. 2011. The Community Noah Land Surface Model with Multiparameterization Options (Noah-MIP): 1. Model Description and Evaluation with Local-Scale Measurements. Journal of Geophysical Research, 116, D12109. DOI:10.1029/2010JD0151139.

[16] Entekhabi, D., Njoku E.G., O'Neill, P.E., Kellogg, K.H., Crow, W.T., Edelstein, W.N., Entin, J.K., Goodman, S.D., Jackson, T.J., Johnson, J., Kimball, J., Piepmeier, J.R., Koster, R.D., Martin, N., McDonald, K.C., Moghaddam, M., Moran, S., Reichle R., Shi, J.C., Spencer, M.W., Thurman, S.W., Tsang, L. and Van Zyl, J. 2010. The Soil Moisture Active Passive (SMAP) Mission. Proceedings of the IEEE, 98(5):704-716. DOI: 10.1109/jproc.2010.2043918.

[17] Western, A.W., Grayson, R.B., Bloschl, G., Willgoose, G.R. and McMahon, T.A. 1999. Observed Spatial Organization of Soil Moisture and Its Relation to Terrain Indices. Water Resources Research, 35(3):797-810.



Annex D – SOIL STRENGTH ESTIMATION OVERVIEW

Joseph Scalia
Colorado State University
UNITED STATES

Mark Cammarere
Technology Service Corporation
UNITED STATES

D.1 GOALS AND TEAM MEMBERS

D.1.1 Goal of Soil Strength Estimation

Primarily to advance the state-of-the-art in physics-based soil strength modeling by incorporating EMT+VS soil moisture downscaling model estimates (see TA1 Chapter, Annex C) as input to a soil strength estimation framework based on soil composition, pedotransfer functions, and unsaturated soil mechanics theory.

Secondarily to include soil strength estimates in a prototype EMT+VS map-based application that is being developed (see TA1 Chapter, Annex C).

D.1.2 Team Members

The team members are:

- **Mark Cammarere, Leader**, USA;
- Keith Gemeinhart, USA;
- Andrew Jones, USA;
- **Jeffrey Niemann, Leader**, USA; and
- Joseph Scalia, USA.

D.2 INTRODUCTION

At the time of this writing, a research team associated with AVT-248[1] was also developing a technique for estimating both the Effective Friction Angle (φ') and Effective Cohesion (c') components of soil strength as a function of soil composition (type), bulk density, and volumetric soil moisture content. The technique involves using binned parameters that relate the available soil types to moisture-independent soil strength and unsaturated soil parameters, and then to transform those parameters to soil moisture specific values using unsaturated soil strength theory. Ongoing improvements to this technique involve creating continuous functions to replace binned parameters.

The standard and widely used theory for soil strength is the Mohr-Coulomb shear strength theory where soil shear strength (τ) is given by:

$$\tau = c + \sigma \bullet \tan(\varphi), \qquad \text{(D-1)}$$

[1] Drs. Jeffrey Niemann, Andrew Jones and Joseph Scalia of Colorado State University (CSU) along with Messrs. Mark Cammarere and Keith Gemeinhart of Technology Service Corp (TSC).

where c is the cohesion (component of soil strength resulting primarily from electrostatic inter-particle forces, which is stress independent), σ is the total normal stress (on a plane in a soil mass) and φ is the friction angle (component of soil strength resulting from inter-particle friction, which is stress dependent). The total normal stress (σ) is given by:

$$\sigma = \sigma' + \mu, \tag{D-2}$$

where μ is the pore water pressure (water pressure in soil pores, which can be positive or negative) and σ' is the **effective stress** (stress felt by soil particles) – which is the item of interest here. Therefore, the relation for **effective stress-shear strength** (τ') is:

$$\tau' = c' + \sigma' \bullet \tan(\varphi'), \tag{D-3}$$

where c' is the cohesion independent of normal stress and φ' is the effective stress friction angle. The classic concept of effective stress (σ') can be applied to an unsaturated soil framework without violating existing shear strength theory by applying unsaturated soil parameters (suction stress in unsaturated soils, σ^s and effective stress in unsaturated soils, σ') as follows [1]:

$$\sigma^s = f(S_e, \alpha, \eta) \text{ and} \tag{D-4}$$

$$\sigma' = (\sigma - \mu_a) - \sigma^s, \tag{D-5}$$

where S_e is the effective saturation in soil (related to volumetric water content), η is the pore size spectrum number, α is the inverse of air entry pressure for water saturated soil, and μ_a is the pore air pressure in soil. The soil strength estimation framework being used to guide this effort is summarized in Figure D-1.

If the technique is effective, the following soil strength-related parameters will also be added to the prototype map-based application described in TA1 Chapter, Annex C:

1) Suction strength in unsaturated soil (σ^s), and
2) Effective friction angle (φ'), and effective cohesion (c').

The subsections below briefly describe the inputs to and sample outputs obtained from this framework.

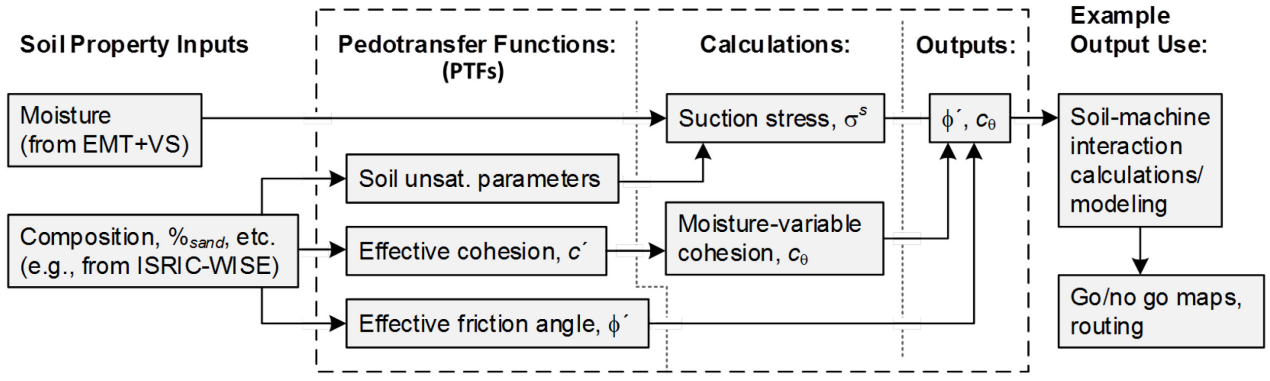
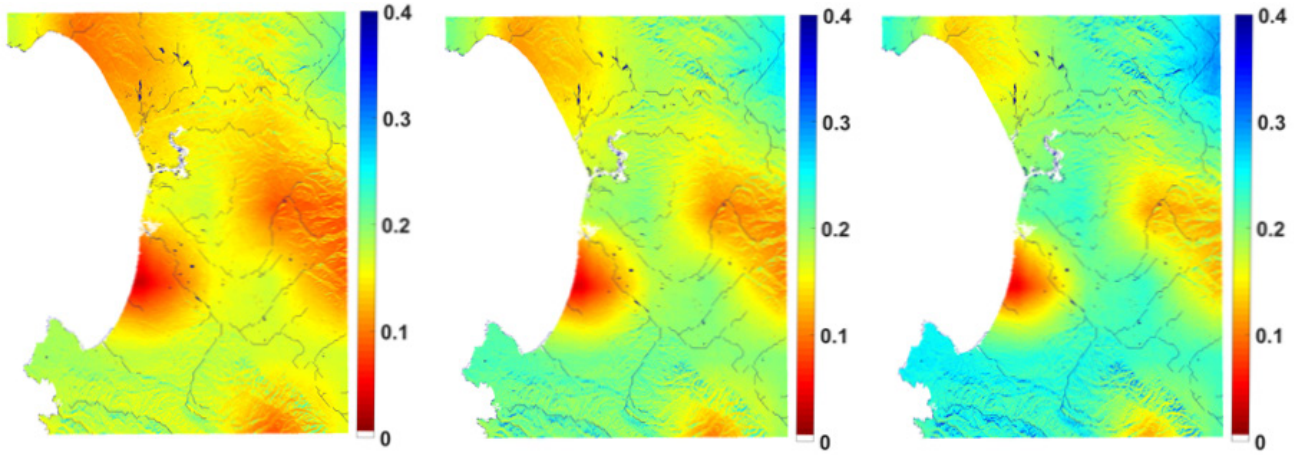


Figure D-1: Soil Strength Estimation Framework.

D.3 SOIL STRENGTH ESTIMATION FRAMEWORK – INPUTS

EMT+VS model fine-scale moisture estimates are from the direct-model generalized formulation (see discussion in TA1 Chapter, Annex C). The inputs include the average soil moisture estimates, along with a confidence interval meant to represent the soil moisture under best- and worst-case conditions. This is illustrated in Figure D-2, which shows the lower bound (10%; Figure D-2a), average (Figure D-2b), and upper bound (90%; Figure D-2c) moisture estimates for the Monterey Bay test area for November 2, 2015.



(a) Lower Bound (90%) **(b) Uncalibrated EMT+VS (50%)** **(c) Upper Bound (90%)**

Figure D-2: Generalized EMT+VS Soil Moisture Estimates for Monterey Bay (Nov 2015).

Given that the most consistent global data available are desired as input to the framework, Figure D-1 indicates that soil information will be obtained from the ISRIC-WISE Harmonized Global Soil Profile Dataset. ISRIC-WISE is a 30 arcsecond x 30 arcsecond (nominally 1 km x 1 km) resolution dataset of derived soil properties compiled for a vast range of environmental and agricultural applications. The useful data it contains includes: % composition sand, silt, and clay; soil bulk density; Cation Exchange Capacity (CEC); and available water capacity. Soil data from ISRIC-WISE was used in the EMT+VS model.

For the Monterey Bay site, United States Department of Agriculture (USDA) soil classifications from SSURGO database collected by the National Cooperative Soil Survey (USDA-NRCS) were used as soil property inputs for soil strength estimation. The SSURGO database describes soils at a scale of 1:12,000 over the area of interest (Monterey Bay). However, the USDA system differs from the Unified Soil Classification System (USCS) that is widely used for most geotechnical engineering applications. Existing class-average relationships exist based on USCS classifications, however attaining USCS classes from SSURGO data requires soil-class transcription (which are inherently poor often due to the inconsistencies in particle sizes assigned to the various soil names, see Table D-1). Nevertheless, usable transcriptions do exist and were employed to obtain the equivalent USCS soil classifications shown in Figure D-3.

Once USCS soil classifications have been obtained by transcription, binned estimates of unsaturated soil and soil strength parameters can be obtained from Refs. [2] and [3] and applied to the soil classes on a pixel-by-pixel basis. Binned unsaturated soil parameter estimates are summarized in Table D-2 [2], while Table D-3 [3] summarizes the soil strength parameter estimates.

Table D-1: Comparison of Particle Size Classifications.

Particle Diameter (mm)	0.002	0.05	0.0625	0.075	2.0	4.75	76.2
Unified Soil Classification System (USCS)	CLAY	SILT			SAND	Gravel	ROCK
United States Department of Agriculture (USDA)	CLAY	SILT	SAND		ROCK FRAGMENTS (Pebbles, Gravel, Cobbles)		Stones, Boulders
United Nations Food and Agriculture Organization (FAO)	CLAY	SILT	SAND		Coarse Fragments/Gravel		

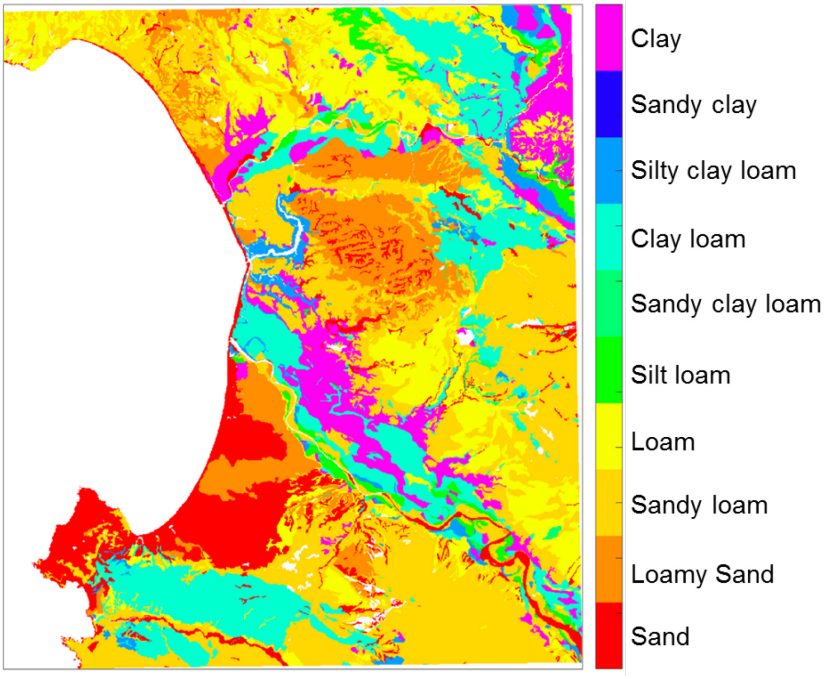


Figure D-3: USDA Soil Classes for the Monterey Bay Test Area.

Table D-2: Binned Unsaturated Soil Parameter Estimates [2].

Texture Class	N	-- θr -- cm3/cm3		-- θs -- cm3/cm3		-- log(α) -- log(1/cm)		-- log(n) -- log10	
Clay	84	0.098	(0.107)	0.459	(0.079)	-1.825	(0.68)	0.098	(0.07)
C loam	140	0.079	(0.076)	0.442	(0.079)	-1.801	(0.69)	0.151	(0.12)
Loam	242	0.061	(0.073)	0.399	(0.098)	-1.954	(0.73)	0.168	(0.13)
L Sand	201	0.049	(0.042)	0.390	(0.070)	-1.459	(0.47)	0.242	(0.16)
Sand	308	0.053	(0.029)	0.375	(0.055)	-1.453	(0.25)	0.502	(0.18)
S Clay	11	0.117	(0.114)	0.385	(0.046)	-1.476	(0.57)	0.082	(0.06)
S C L	87	0.063	(0.078)	0.384	(0.061)	-1.676	(0.71)	0.124	(0.12)
S loam	476	0.039	(0.054)	0.387	(0.085)	-1.574	(0.56)	0.161	(0.11)
Silt	6	0.050	(0.041)	0.489	(0.078)	-2.182	(0.30)	0.225	(0.13)
Si Clay	28	0.111	(0.119)	0.481	(0.080)	-1.790	(0.64)	0.121	(0.10)
Si C L	172	0.090	(0.082)	0.482	(0.086)	-2.076	(0.59)	0.182	(0.13)
Si Loam	330	0.065	(0.073)	0.439	(0.093)	-2.296	(0.57)	0.221	(0.14)

D.4 SOIL STRENGTH ESTIMATION FRAMEWORK – SAMPLE OUTPUTS

Based on the framework of Figure D-1 and the inputs described in the previous subsection, Figure D-4 shows the effective friction angle (ϕ') and effective cohesion (c', kPa) for the Monterey Bay test area. (No date is given because ϕ' and c' are moisture-independent parameters.) Figure D-5 shows the moisture-variable cohesion (c_θ, kPa) for the November 2, 2015 date. The moisture-variable cohesion (c_θ) represents the summation of two factors:

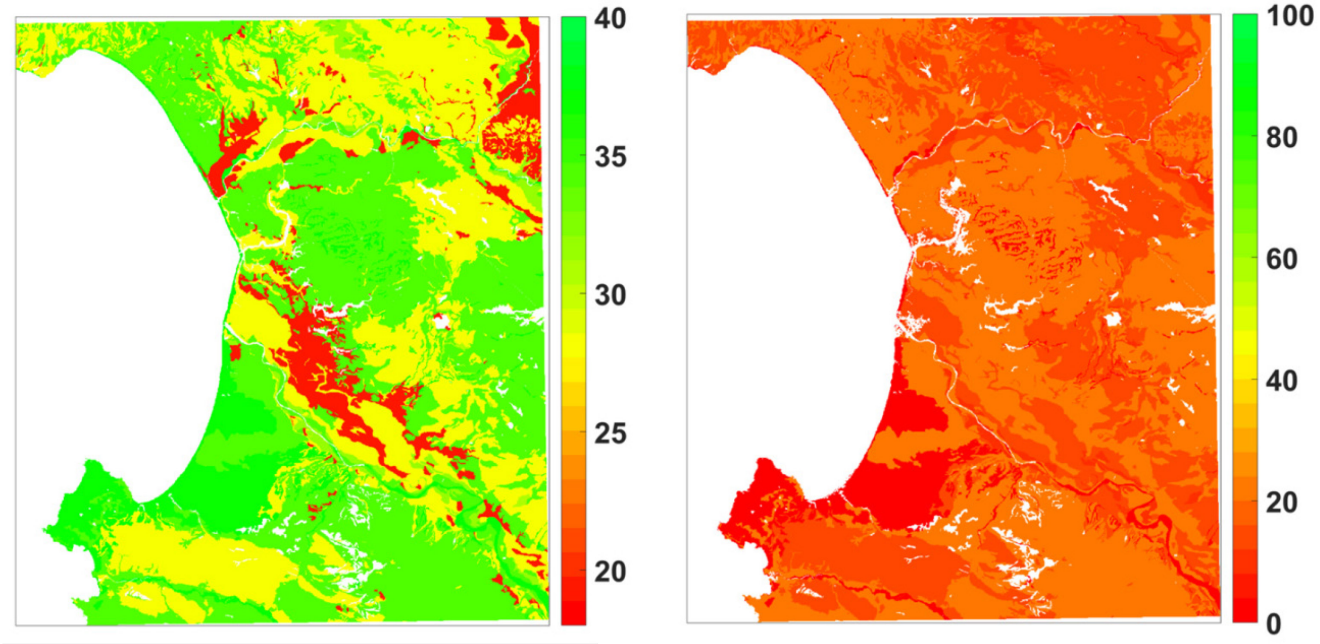
- **Effective Cohesion** – a material's inherent strength from inter-particle electrostatic forces (independent of applied stress).
- **Apparent Cohesion** – a shear stress resulting from the mobilization of suction stress by internal friction.

Table D-3: Binned Soil Strength Parameter Estimates [3].

Group Symbol	Soil Type	Range of Maximum Dry Unit Weight, pcf	Range of Optimum Moisture, Percent	Typical Value of Compression		Typical Strength Characteristics			
				At 1.4 tsf (20 psi)	At 3.6 tsf (50 psf)	Cohesion (as compacted) psf	Cohesion (saturated) psf	ϕ (Effective Stress Envelope Degrees)	Tan ϕ
				Percent of Original Height					
GW	Well graded clean gravels, gravel-sand mixtures.	125 - 135	11 - 8	0.3	0.6	0	0	>38	>0.79
GP	Poorly graded clean gravels, gravel-sand mix	115 - 125	14 - 11	0.4	0.9	0	0	>37	>0.74
GM	Silty gravels, poorly graded gravel-sand-silt.	120 - 135	12 - 8	0.5	1.1	.....	.....	>34	>0.67
GC	Clayey gravels, poorly graded gravel-sand-clay.	115 - 130	14 - 9	0.7	1.6	.....	.....	>31	>0.60
SW	Well graded clean sands, gravelly sands.	110 - 130	16 - 9	0.6	1.2	0	0	38	0.79
SP	Poorly graded clean sands, sand-gravel mix.	100 - 120	21 - 12	0.8	1.4	0	0	37	0.74
SM	Silty sands, poorly graded sand-silt mix.	110 - 125	16 - 11	0.8	1.6	1050	420	34	0.67
SM-SC	Sand-silt clay mix with slightly plastic fines.	110 - 130	15 - 11	0.8	1.4	1050	300	33	0.66
SC	Clayey sands, poorly graded sand-clay-mix.	105 - 125	19 - 11	1.1	2.2	1550	230	31	0.60
ML	Inorganic silts and clayey silts.	95 - 120	24 - 12	0.9	1.7	1400	190	32	0.62
ML-CL	Mixture of inorganic silt and clay.	100 - 120	22 - 12	1.0	2.2	1350	460	32	0.62
CL	Inorganic clays of low to medium plasticity.	95 - 120	24 - 12	1.3	2.5	1800	270	28	0.54
OL	Organic silts and silt-clays, low plasticity.	80 - 100	33 - 21	.....	.....	.....	.....	.....	.....
MH	Inorganic clayey silts, elastic silts.	70 - 95	40 - 24	2.0	3.8	1500	420	25	0.47
CH	Inorganic clays of high plasticity	75 - 105	36 - 19	2.6	3.9	2150	230	19	0.35
OH	Organic clays and silty clays	65 - 100	43 - 21	.....	.....	.....	.....	.....	.....

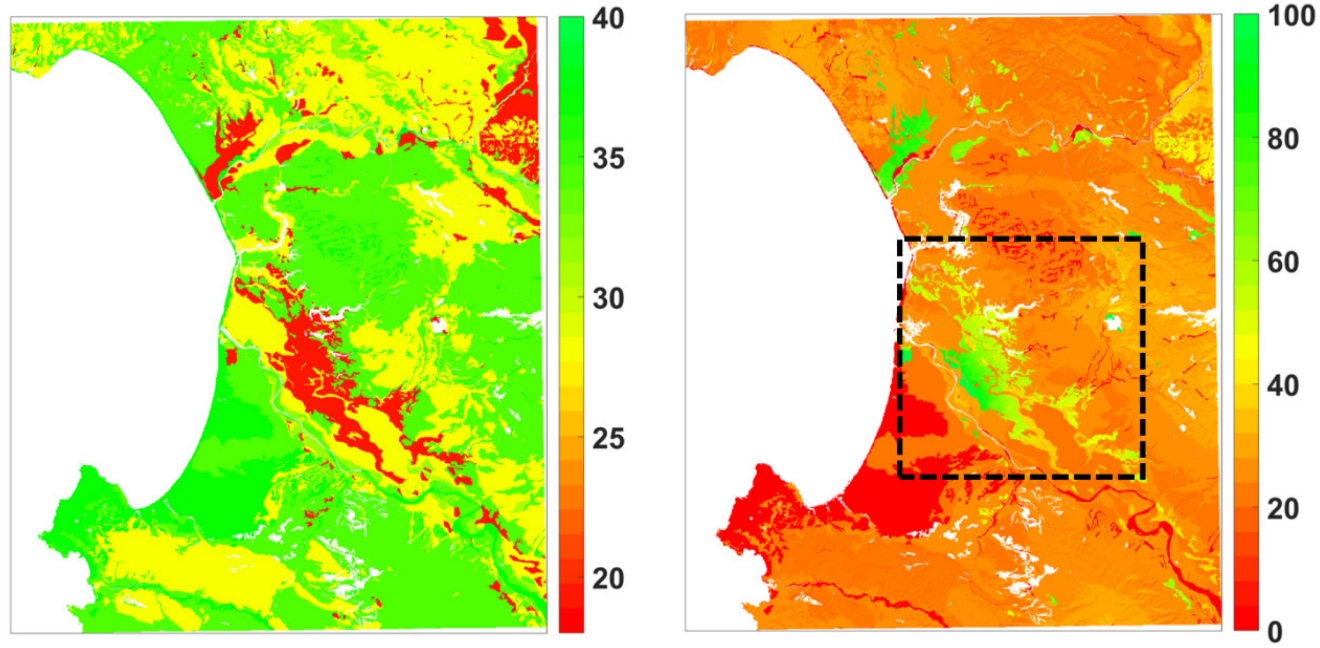
Figure D-6 summarizes the moisture-variable cohesion (c_θ) for the inset area of Figure D-5(b) for 10% confidence level (lower bound), average, and 90% confidence level (upper bound) EMT+VS soil moisture estimates. These sample results were posted to the Science Connect site in April 2018, and generation of soil strength estimates using the methodology described here is also planned for inclusion in the EMT+VS map-based application (see Chapter 3, Annex C).

The work described in this Annex was performed under a U.S. Army Research Laboratory (ARL) Small Business Innovation Research (SBIR) contract for Dr. Paramsothy Jayakumar and Mr. Mike Letherwood of the U.S. Army Ground Vehicle Systems Center (GVSC). Mr. Peter J. Grazaitis is the sponsor of the ARL SBIR effort.



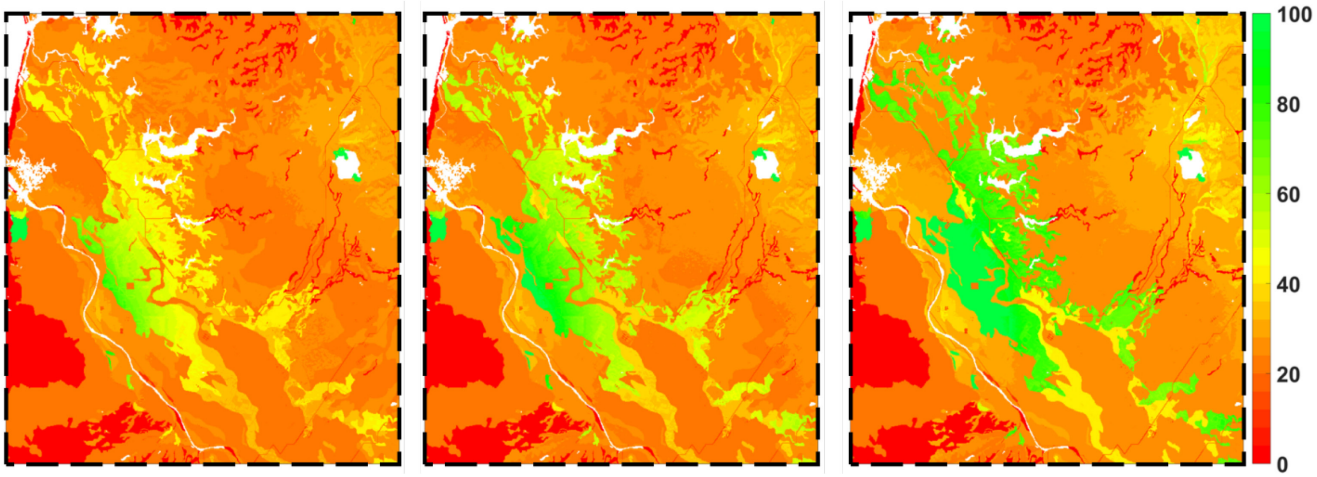
(a) Moisture Invariant Effective Friction (b) Moisture Invariant Effective Cohesion (kPa)

Figure D-4: Soil Strength Parameters for Monterey Bay Test Area.



(a) Moisture Invariant Effective Friction (b) Moisture Variable Cohesion (kPa)

Figure D-5: Soil Strength Parameters for Monterey Bay Test Area (Nov. 2015).



(a) 10% Confidence Lower Bound (b) Average (c) 90% Confidence Upper Bound

Figure D-6: Moisture-Variable Cohesion (kPa) for the Monterey Bay Test Area (Nov. 2015).

D.5 REFERENCES

[1] Lu, N., Godt, J. and Wu, D. 2010. A Closed-Form Equation for Effective Stress in Unsaturated Soil. Water Resources Research, 46.

[2] Schaap, M., Leij, F. and van Genuchten, M. 2001. ROSETTA: A Computer Program for Estimating Soil Hydraulic Parameters with Hierarchical Pedotransfer Functions. Journal of Hydrology, 251:163-176.

[3] NAVFAC. 1982. Design Manual 7.02, Foundations and Earth Structures. Naval Facilities Engineering Command. **NOTE:** USCS classifications based on conversion scheme by Garcia-Gaines, R. and Frankenstein, S. 2015. USCS and the USDA Soil Classification System, Development of a Mapping Scheme. ERDC/CRREL TR-15.4.

Annex E – TERRAMECHANICS DATABASE

Michael McCullough
BAE Systems Inc.
UNITED STATES

E.1 BACKGROUND

A difficulty in using Terramechanics has been finding the parameters needed for the models for different soil types. To that end, we have been collecting data from various sources and accumulating them into a database including the following sections:

- Bekker-Wong Model Parameters;
- Reece Model Parameters;
- Snow Model Parameters;
- Muskeg Model Parameters;
- References;
- Notional Inferred Dataset (same as Table 4-3);
- Porosities and Specific Gravity Values;
- USCS from Wikipedia; and
- Complex Terramechanics Model Parameters.

The Database will be part of the STANREC and will be a living document that evolves over time. As an example, a portion of the Bekker-Wong Model Parameters is shown in Figure E-1.

			Bekker-Wong Equation Bearing Model Parameters (SI units)										Shear Model									
			n		Kf		Kc		k0		Aunload		c (kPa)		f (deg)		k (cm)		Kr (brittle)		Kw (brittle)	
Terrain	Moisture Content (%)	pmax (kPa)	Mean	StdDev	Mean	StdDev	Mean	StdDev	Mean	StdDev	Mean	StdDev	Mean	StdDev	Mean	StdDev	Mean	StdDev	Mean	StdDev	Mean	StdDev
LETE Sand (internal)	dry	140	0.793	0.012	5301	775	102	54	0		503000		1.36	0.09	31.56	0.38	1.6	0.61				
rubber-soil interface	dry	140											0.65	0.23	27.51	0.05	1.14	0.34				
Upland sandy loam	51		1.1		2080		74.6						3.3		33.7							
Rubicon sandy loam	43		0.66		752		6.9						3.7		29.8							
North Gower clayey loam	46		0.73		2471		41.6						6.1		26.6							
Dry Sand (Land Locomotion Lab)	0		1.1		1528		1						1		28							
Sandy Loam(LLL)	15		0.7		1515		5.3						1.72		29							
Sandy Loam(LLL)	22		0.2		43		2.6						1.38		38							
Buchele (MI) Sandy Loam	11		0.9		1128		52.5						4.8		20							
Buchele (MI) Sandy Loam	23		0.4		809		11.4						9.7		35							
Hanamoto Sandy Loam	26		0.3		141		2.8						13.8		22							
Hanamoto Sandy Loam	32		0.5		52		0.8						5.2		11							
Clayey soil (Thailand)	38		0.5		692		13.2						4.1		13							
Clayey soil (Thailand)	55		0.7		1263		16						2.1		10							
Heavy Clay (Vicksburg MS)	25		0.13		1556		12.7						69		34							
Heavy Clay (Vicksburg MS)	40		0.11		103		1.84						20.7		6							
Lean Clay (Vicksburg MS)	22		0.2		1725		16.4						69		20							
Lean Clay (Vicksburg MS)	32		0.15		120		1.5						13.8		11							

Figure E-1: Current Bekker-Wong Model Parameter Sets.

Annex F – MEASUREMENT AND ANALYSIS OF GEOTECHNICAL PROPERTIES

Craig D. Foster
University of Illinois at Chicago
UNITED STATES

Elham Ramyar
Northwestern University
UNITED STATES

F.1 GOALS AND TEAM MEMBERS

F.1.1 Goal of Measurement and Analysis of Geotechnical Properties

The objective is to develop a procedure to determine soil properties and model parameters used in common soil models. A multitude of models have been developed for the mechanical behavior or soil and soil interaction with wheeled and tracked vehicles. All of the models have a set of material constants and/or initial values of state variables that must be determined. Because soils are highly variable materials with different constituents and states, testing either in the field or in the laboratory is almost always necessary to determine the soil properties and material parameters. While field testing disturbs the soil less, more controlled and sophisticated experiments can be conducted in the laboratory.

This annex examines some of the most common soil models, including semi-empirical models, continuum constitutive models, and discrete (sometimes called distinct) element models. For each model, the parameters are identified, the related soil properties are enumerated, and the relevant soil tests are determined.

F.1.2 Team Members

The team members are:

- **Craig Foster, Leader**, USA;
- Paramsothy Jayakumar, USA; and
- Elham Ramyar, USA.

F.2 INTRODUCTION

The effective movement of vehicles over terrain is an issue several millennia old and is a complex interaction of vehicle and soil parameters. For many centuries, the decision on when certain vehicles should attempt to pass a given terrain was based solely on judgement and experience. Starting in the twentieth century, the field of terramechanics arose to try to quantify under what conditions a given vehicle could pass safely. Initially, these models were empirical relationships between easy-to-obtain soil properties and vehicle characteristics. One of the earliest models used a cone penetrometer to measure stiffness of the soil [1]. Based on a Cone Index derived from the force needed to push the penetrometer into the soil, one could estimate the soil strength and stiffness. Decision-makers could then clear a vehicle to pass or not, or, in more sophisticated analyses, estimate the number of passes a vehicle could make over a soil.

Soil models have become progressively more sophisticated, including models based on the Boussinesq solution for a point load in an infinite half space, to semi-empirical models modified from the original work of

Bekker [2]. See Refs. [3], [4], [5], [6] for examples. More sophisticated models typically are unable to be solved by analytical means. The rise of computers allowed for the development of constitutive models and numerical techniques that could more accurately describe soil behavior. Most commonly soil plasticity of viscoplasticity models implemented in a finite element or mesh-free framework have been used. In recent years, the development of discrete element models, which model each particle individually, have started to become tractable. See Ref. [7] for a review of soil models used in terramechanics applications.

Soils are highly variable materials, made up of different minerals, organic matter, and varying amounts of water. Unlike some materials that have relatively well-known properties, each soil is unique and responds differently to loading. Soils must be tested to determine how it will behave. Every soil model above has some number of material parameters, related to the soil properties, which must be calibrated for a given soil.

The goal of this annex is to examine many of the commonly used models in terramechanics applications, and identify the related soil properties and testing procedures used by these models. To the extent possible, we identify standard soil mechanics tests that can be performed in most geotechnical labs. For some models, procedures using standard geotechnical tests have been developed to fit the model parameters. Instead, the models rely on specialized tests developed for the models. While this approach means that testing equipment is not always available, the tests usually more closely mimic field conditions, meaning that there is less extrapolation to actual vehicle testing.

Note that throughout this report we use continuum mechanics conventions for stress and strain. Importantly, mean stress is considered positive in tension and negative in compression, the opposite of the convention typically used in soil mechanics. However, this is the convention most often used by numerical modelers, and hence will be followed in this text.

The remainder of the annex is organized as follows:

1) Section F.3 discusses the parameter fitting for some of the more common continuum plasticity and viscoplasticity models.
2) Section F.4 discusses the semi-empirical models following the model of Bekker, Reece, Wong, and others.
3) Section F.5 does the same for discrete elements.

F.3 CONTINUUM SOIL MODELS

Continuum models treat the soil as a homogenized continuous material. Of course, on some level, soils are not continuous, but made of discrete particles. Nevertheless, this approximation is adequate for many applications. Grain size effect is not of great importance in terramechanics applications, except for gravels. Hence, in this report we will not discuss micromorphic, nonlocal, or gradient plasticity models that attempt to capture size effects and grain rotation in a continuum setting. Discrete elements can account for these effects, and will be discussed Section F.5.

Except for clean gravels and coarse sands, the permeability of most soils is small enough that there is no significant flow relative to the soil motion during vehicle loading. Hence, in this annex we do not discuss parameter fitting for multiphase models, and use the total stress in the soil to fit the material properties.

The differential equations arising from continuum constitutive models are usually not solvable by analytical means, and hence are implemented in finite element, mesh-free, and other numerical frameworks for solution.

F.3.1 Common Parameters and Properties

Most continuum soil models require elastic parameters and density. These can also be regarded as soil properties.

Elastic parameters can be fit from triaxial or unconfined compression tests. Though in theory these should produce similar results, in practice the results are often a little different. Triaxial tests are considered to be a little more accurate. For isotropic materials, there are two independent linear elastic parameters, but a variety of parameters have been used. From any two of the following, the others may be determined by simple algebraic relationships: Young's modulus E, shear modulus μ or G, bulk modulus K, Poisson's ratio v, and Lamé's first parameter λ. (Lamé's second parameter is the shear modulus.)

F.3.1.1 Common Tests

Density of the soil is usually measured using a standard density test, ASTM D2937.

Young's modulus can be derived from the linear initial part of the stress-strain response of the uniaxial or triaxial compression tests. Similarly, the bulk modulus can also be easily determined from the linear portion of the curve of the volumetric deformation, $K = \frac{\Delta p}{\epsilon_{vol}} = \frac{\Delta \sigma_{vert}}{3\epsilon_{vol}}$. It is important that the triaxial test be set up to measure changes in volumetric deformation. There do not appear to be standards on how to select the interval from which to fit the elastic parameters. Suggestions have included using the initial and the slope secant modulus from the start of the vertical loading phase to half the peak stress. This is illustrated in Figure F-1. Another approach derived from the rock mechanics literature is to take two points from the linear part of the stress-strain curve between about 20% and 70% of the peak stress [8]. This latter approach avoids any issues that might arise from inaccuracies at the beginning of loading where there may be imperfect contact between the specimen and apparatus. (This is more likely in uniaxial compression than triaxial). In any case, the engineer should use her or his judgement in obtaining the best modulus to fit the data. Figure F-1 shows the secant modulus fitting procedure.

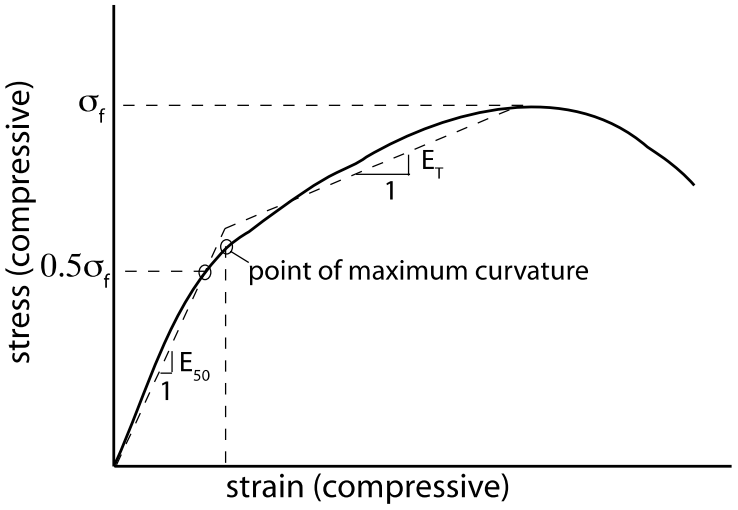


Figure F-1: Fitting the Secant Modulus E_{50} and Linear Hardening Tangent Modulus to a Uniaxial (or Shearing Phase of a Triaxial) Compression Test.

Some models use non-linear elasticity. In this case, a best-curve must be obtained for the elastic data. There is no exact procedure on how to do this, but parameters should be adjusted to best fit elastic loading and unloading curves.

The above discussion is for most continuum constitutive models. Below we discuss the parameters for some specific models. We have identified the following continuum plasticity models for study.

F.3.2 Mohr-Coulomb Model

F.3.2.1 Parameters

The elastic-perfectly plastic Mohr-Coulomb model is fit by three parameters: cohesion c, friction angle φ, and a dilation angle ψ. The yield surface f and plastic potential g can be written as:

$$f = |\tau| - c + \sigma \tan \varphi \tag{F-1}$$

$$g = |\tau| - c + \sigma \tan \psi \tag{F-2}$$

where τ is the shear stress and σ is the normal stress acting on a particular plane on the surface. To use this formulation, one must identify the plane on which the most critical normal and shear stress act. Alternately, they may be expressed in terms of principal stresses [9]:

$$f = \sigma_{max} - \sigma_{min} + (\sigma_{max} - \sigma_{min}) \sin\varphi - 2c \cos\varphi \tag{F-3}$$

$$g = \sigma_{max} - \sigma_{min} + (\sigma_{max} - \sigma_{min}) \sin\psi - 2c \cos\psi \tag{F-4}$$

where σ_{max} and σ_{min} are the maximum and minimum principal stresses.

In the associative case, following the principal of maximum plastic dissipation, the dilation angle is equal to the friction angle. However, this assumption leads to overprediction of soil dilation, and most modelers agree that breaking the principle of maximum plastic dissipation leads to more accurate models.

The cohesion c, friction angle φ, and a dilation angle ψ are considered properties, measured by standard geotechnical tests.

F.3.2.2 Tests

The above mentioned properties are best fit by the triaxial test. For most soils, the fluid does not much have time to drain during a vehicle pass, and hence undrained tests are most accurate. However, for clean coarse sands and gravels, drained tests may be used. The standards dictate that three tests should be run at different confining stresses, and a best fit line should be used to calculate the parameters. While a reasonable variation in confining stress should be used to obtain an accurate line, optimally tests should be given in the range of expected stresses. Tests over large ranges of confining stress show that the linear relationship between mean stress and shear strength is an approximation.

The standard governing consolidated drained triaxial tests is ASTM D7181-11, Standard Test Method for Consolidated Drained Triaxial Compression Test for Soils. This test may be used for sands. For cohesive soils, an unconsolidated-undrained test may be run, ASTM D2850-15, Standard Test Method for Unconsolidated-Undrained Triaxial Compression Test for Cohesive Soils.

The above standards are designed for saturated soils. In terramechanics applications, soils are typically partially saturated, though the saturated case is usually most critical. Undrained tests can easily be modified for the saturated case if total stress parameters are desired. Volume change can be measured by setting the apparatus to read the amount of water entering or leaving the cell, in the same manner in which the amount of water leaving the sample is measured in a drained saturated triaxial test.

Direct shear tests may also be used to fit these parameters. However, due to stress concentrations around the edges and other limitations, these tests are considered to be less accurate than triaxial tests. They are also typically done in drained or dry conditions, which will not accurately reproduce saturated soil behavior for vehicle loads. The standard for drained direct shear tests is ASTM D3080/D3080M-11, Standard Test Method for Direct Shear Test of Soils under Consolidated Drained Conditions. There are no standards for undrained tests, though some researchers have investigated this process, (e.g., Ref. [10]).

Finally, for clays, the friction and dilation angles are sometimes assumed to be zero, and the cohesion is fit to an unconfined compression test. The results of the unconfined compression test tend to differ somewhat from the triaxial test, and the triaxial test is again considered more accurate. The standard for that test is ASTM D2166/D2166M-13, Standard Test Method for Unconfined Compressive Strength of Cohesive Soil.

F.3.3 Approximations to the Mohr-Coulomb Model

Several models have been developed to approximate the Mohr-Coulomb model, either for algorithmic efficiency or for improved accuracy for different states of triaxiality. Because of the similarity of these models, the model parameters have been related directly to the Mohr-Coulomb parameters. We discuss three such models here: the Drucker-Prager model, the Lade-Duncan model, and the Matsuoka-Nakai model.

F.3.3.1 The Drucker-Prager Model

The Drucker-Prager model has yield surface defined by:

$$f = ||s|| - \alpha + \beta p \tag{F-5}$$

where ||s|| is the norm of the deviatoric stress, p is the mean stress, and α and β are material parameters. The plastic potential is similar:

$$g = ||s|| - \alpha + bp \tag{F-6}$$

Hence, there are three unknown parameters to fit: α, β, and b. These constants can be fit to Mohr-Coulomb parameters approximately using the relationships:

$$\alpha = \sqrt{\frac{2}{3}}\left(\frac{6c\cos\phi}{3 \pm \sin\phi}\right) \tag{F-7}$$

$$\beta = \sqrt{\frac{2}{3}}\left(\frac{6\sin\phi}{3 \pm \sin\phi}\right) \tag{F-8}$$

$$b = \sqrt{\frac{2}{3}}\left(\frac{6\sin\psi}{3 \pm \sin\psi}\right) \tag{F-9}$$

Here, the minus signs correspond to the triaxial compression corners of the Mohr-Coulomb yield surface, and the plus signs to the triaxial extension corners. See Figure F-2. The latter is more conservative and generally considered to be a better fit. It can be seen that for high friction angles, though, the Drucker-Prager cone is a poor approximation for the Mohr-Coulomb hexagonal pyramid.

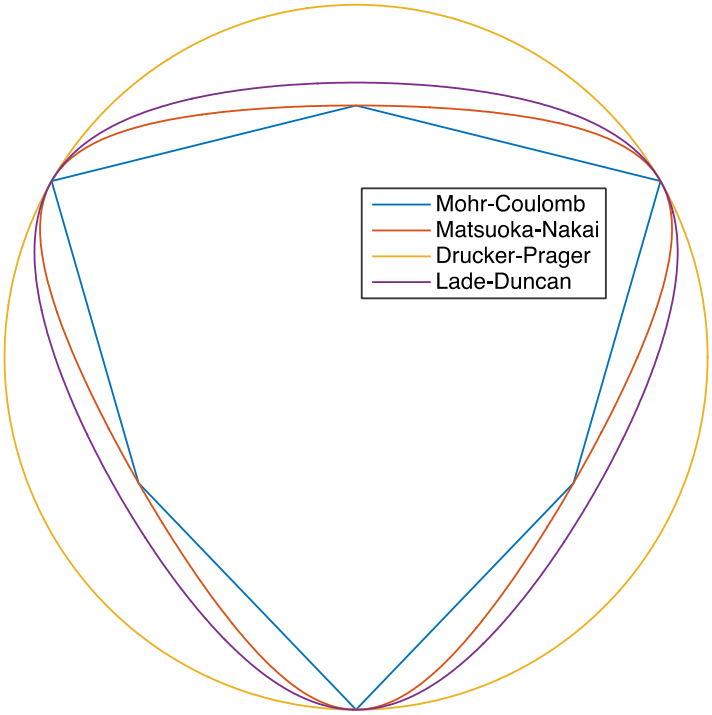


Figure F-2: Yield Surfaces for Mohr-Coulomb, Drucker-Prager, Lade-Duncan, and Matsuoka-Nakai Models Fit to the Triaxial Compression Corners.

Note: In practice, it is generally more accurate to fit to the triaxial extension corners. We fit to the compression corners here to give a clearer idea of relative shape.

F.3.3.2 The Lade-Duncan Model

The yield surface f and plastic potential g of the Lade-Duncan model may be written:

$$f = (\beta\, \bar{I}_3)^{\frac{1}{3}} - \bar{I}_1 \tag{F-10}$$

$$g = (b\, \bar{I}_3)^{\frac{1}{3}} - \bar{I}_1 \tag{F-11}$$

where $\bar{I}_1$ and $\bar{I}_3$ are the first and third invariants of the translated stress tensor $\bar{\boldsymbol{\sigma}} = \boldsymbol{\sigma} - \alpha \boldsymbol{1}$. Here, β, b, and α are material parameters. Like the Drucker-Prager model, the material parameters of the Lade-Duncan model can be fit to cohesion, friction angle, and dilation angle:

$$\beta = \frac{(3 \pm \sin\phi)^3}{1 \pm \sin\phi \mp \sin^2\phi - \sin^3\phi} \tag{F-12}$$

$$b = \frac{(3 \pm \sin\psi)^3}{1 \pm \sin\psi \mp \sin^2\psi - \sin^3\psi} \tag{F-13}$$

$$\alpha = c\cot\phi \tag{F-14}$$

with the top symbols indicating the triaxial extension corners and the bottom the triaxial compression corners. Again the triaxial extension corners are more conservative, and possibly a more accurate fit. In the pi-plane, the Lade-Duncan model does have a better fit to the Mohr-Coulomb hexagon.

F.3.3.3 The Matsuoka-Nakai Model

F.3.3.3.1 Parameters

The yield surface f and plastic potential g of the Matsuoka-Nakai model may be written:

$$f = (\beta\,\bar{I}_3)^{\frac{1}{3}} - (\bar{I}_1\bar{I}_2)^{\frac{1}{3}} \tag{F-15}$$

$$g = (b\,\bar{I}_3)^{\frac{1}{3}} - (\bar{I}_1\bar{I}_2)^{\frac{1}{3}} \tag{F-16}$$

where $\bar{I}_1$, $\bar{I}_2$, and $\bar{I}_3$ are the first, second, and third invariants of the translated stress tensor $\bar{\boldsymbol{\sigma}} = \boldsymbol{\sigma} - \alpha \boldsymbol{1}$. 123 Here, β, b, and α are material parameters.

Although we use the same notation, the parameters β and b do not share the same relationship with the cohesion and friction as in the Lade-Duncan model. To calculate the parameters for the Matsuoka-Nakai model:

$$\beta = \frac{9 - \sin^2\phi}{1 - \sin^2\phi} \tag{F-17}$$

$$b = \frac{9 - \sin^2\psi}{1 - \sin^2\psi} \tag{F-18}$$

$$\alpha = c\cot\phi \tag{F-19}$$

Here, the same parameters fit both the triaxial extension and compression corners. Hence, there is no choosing which corners of the Mohr-Coulomb hexagon to fit. This fact makes it easier to choose parameters, but does not necessarily make the model a better fit than the Lade-Duncan model.

F.3.4 Linear Hardening Models

Some versions of the above models allow for evolution, or hardening and softening, of the plastic parameters. A variety of evolution equations have been proposed, but we focus on linear hardening here. These models can be quite efficient and still account for change in the material parameters, though the complexity of the evolution is clearly limited.

To fit the linear hardening data, the engineer must make some judgement based on the stress-strain curve. After determining the elastic modulus, the yield point must be determined. This is different from perfectly plastic models, which are typically fit to the peak stress. We suggest here the abscissa of the point of maximum curvature of the transition from elastic to plastic state, which can be determined by eye. For linear hardening, a line may be drawn from here to the peak stress of the curve. See Figure F-1 for clarification. However, other data points may be used to better match the soil behavior in the region of interest.

The slope of the linear hardening curve may then be fit to the hardening modulus of the parameters. The Drucker-Prager model is the easiest to fit to the stress-strain curve in the triaxial test. It can be shown that, for a linear hardening model:

$$\dot{\alpha} = H\,\dot{\lambda} \tag{F-20}$$

The H can be found fitting the triaxial test data:

$$H = \frac{\Delta\sigma(\frac{\beta}{3} - \sqrt{\frac{2}{3}})}{\Delta\lambda} \tag{F-21}$$

where:

$$\Delta\lambda = \frac{\frac{\Delta\sigma}{E} - \Delta\epsilon}{\sqrt{2/3} - b/3} \tag{F-22}$$

Here, $\Delta\sigma$ and $\Delta\varepsilon$ are the change in uniaxial stress and strain between any two points on the plastic linear hardening model. Recall that they are negative according to the sign convention in this report.

It is worth noting that the above equations are valid for the formulations given in this report. For other formulations of the yield function (and there are several), the definitions will change.

From this model it is easy to fit the other models. For example, for the Mohr-Coulomb model, using the yield function [3] and plastic potential [4], we find that:

$$H_{MC} = \frac{(3 - \sin\phi)(3 - \sin\psi)}{12\cos\phi} H_{DP} \tag{F-23}$$

Again, it is important to emphasize that the definition of $\dot{\lambda}$, and hence H, depend on how the yield function and plastic potential are defined.

For non-linear hardening, the curves can be fit by a trial-and-error method to best match the data from the triaxial tests. A discussion for the non-linear hardening of the GeoModel is discussed below, and may give some guidance for the modeler.

F.3.5 Cam-Clay Model

The Cam-Clay model was originally developed for clay behavior in geotechnical applications. We discuss here the Modified Cam-Clay model [11], which has been applied much more extensively than the original. Traditionally, the model has been fit to consolidation data. This long-term behavior, however, is not applicable to terramechanics applications for most soils. The model does have some features that make it useful for terramechanics models, though the parameters will likely have different values than those used in consolidation. Unlike Mohr-Coulomb or related models, the model can predict both dilation and compaction at different mean stress values. Cap models can predict both dilation and compaction and have more flexibility but can be more complex.

F.3.5.1 Parameters

The yield surface and plastic potential are based on an elliptical relationship between the mean stress and deviatoric stress. The yield surface and plastic potential may be written:

$$f = \sqrt{||s|| - M^2 p(p_c - p)} \tag{F-24}$$

$$g = \sqrt{||s|| - M^2 (1 - a) p(p_c - p)} \tag{F-25}$$

Additionally, non-linear elasticity is typically applied with the Mohr-Coulomb yield surface, though this is not necessary. One proposed law is:

$$\boldsymbol{\sigma} = -p_0 \exp((\epsilon^e_{vol0} - \epsilon^e_{vol})/\tilde{\kappa})\mathbf{1} + 2\mu \boldsymbol{e} \tag{F-26}$$

where $\mathbf{1}$ is the second order identity tensor. Finally, pc evolves. A typical evolution law (9) is:

$$\dot{p}_c = -\tilde{\lambda} p_c / \dot{\epsilon}^p_{vol} \tag{F-27}$$

where $\tilde{\lambda}$ is a plastic compressibility index For a mean stress p more compressive than pc, the soil compresses with plastic deformation, otherwise it dilates.

There are four plastic parameters, the slope of the critical state line M, the initial value preconsolidation stress pc, a nonassociativity parameter a that helps prevent overprediction of volumetric strain, and the plastic compressibility constant $\tilde{\lambda}$.

In addition, there are four elastic parameters, here the elastic compressibility parameter $\tilde{\kappa}$, the reference point (p_0, ϵ^e_{vol0}), and the shear modulus μ.

F.3.5.2 Tests

Again, while the Cam-Clay test is traditionally fit to consolidation tests, the slow nature of the deformation in these tests does not match the conditions in vehicle loading. We recommend triaxial tests here.

The elastic parameters, p_c, and $\tilde{\lambda}$ can be determined from the log scale graph of mean stress versus volume change, see Figure F-3. This graph can be developed from a triaxial test. The shear modulus may be determined from the elastic part of the uniaxial curve, and comparing the equivalent elastic modulus around the stress magnitude of interest or from a direct shear test.

The slope M is related to the friction angle by:

$$M = \frac{6 \sin \phi}{3 - \sin \phi} \tag{F-28}$$

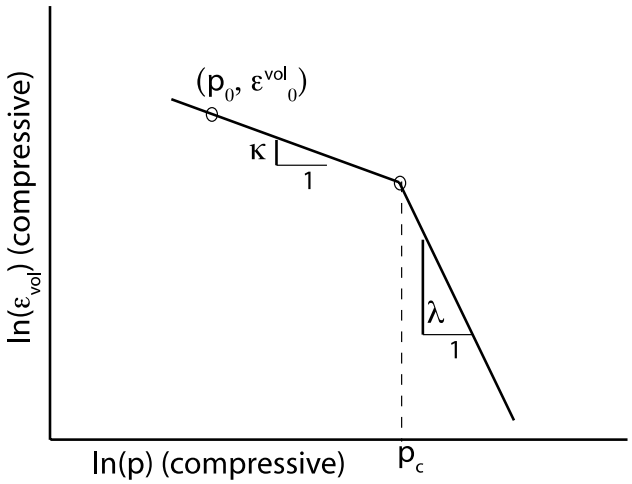


Figure F-3: Cam-Clay Volumetric Deformation.

F.3.6 The Sandia GeoModel

The Sandia GeoModel was originally developed by Arlo Fossum and Rebecca Brannon at Sandia National Laboratories [12]. It has since been extended at Sandia to the Kayenta Model [13]. Other extensions have developed the model in other ways [14], [15], [16]. We will follow the version of Ref. [14] for parameters.

The GeoModel is one in a family of cap plasticity models, and the procedure below should be able to be adapted to related models. Cap models not only model the typical shear-dilatant response at low confining stress, but also inelastic pore reduction and compaction at higher stresses. In vehicle interactions, compaction is sometimes observed, especially for loose soils, directly under the tire or tread, while shear induced dilation occurs to the sides. Mohr-Coulomb and related models are unable to capture both compaction and dilation.

F.3.6.1 Parameters

There are 17 material parameters for the version of the GeoModel described, coming from the elastic parameters, yield surface, plastic potential, and hardening laws.

There are two independent elastic parameters in the elastically isotropic case. We choose the elastic modulus E and the bulk modulus K, but equivalently shear modulus, Poisson's ratio, or Lamé parameters may be used.

The yield surface f and plastic potential g are:

$$f = (\Gamma^{\xi})^2 J_2^{\xi} - F_c(F_f - N)^2 \tag{F-29}$$

$$g = (\Gamma^{\xi})^2 J_2^{\xi} - F_c^g (F_f^g - N)^2 \tag{F-30}$$

where:

$$\Gamma(\beta) = \frac{1}{2}\left(1 + \sin 3\beta + \frac{1}{\psi}(1 - \sin 3\beta\ )\right) \tag{F-31}$$

$$= \frac{1}{2}\left(1 - \frac{3\sqrt{3}J_3}{2(J_2)^{\frac{3}{2}}} + \frac{1}{\psi}(1 + \frac{3\sqrt{3}J_3}{2(J_2)^{\frac{3}{2}}})\right) \tag{F-32}$$

$$F_c\ = 1 - H(\kappa - I_1)\left(\frac{I_1 - \kappa}{X - \kappa}\right)^2 \tag{F-33}$$

$$F_f\ = A - C\exp(BI_1) - \theta\ I_1 \tag{F-34}$$

$$F_c^g\ = 1 - H(\kappa - I_1)\left(\frac{I_1 - \kappa}{X^g - \kappa}\right)^2 \tag{F-35}$$

$$F_f^g\ = A - C\exp(LI_1) - \phi\ I_1 \tag{F-36}$$

Here I_1, J_2^{ξ}, and J_3^{ξ} are invariants of the relative stress tensor $\xi = \sigma - \alpha$. There is one scalar Internal State Variable (ISV) κ and one deviatoric tensor internal state variable α. The dependent parameters X(κ) and $X^g(\kappa)$ may be written:

$$X(\kappa) = \kappa - RF_f(\kappa) \tag{F-37}$$

$$X^g(\kappa) = \kappa - QF_f^g(\kappa) \tag{F-38}$$

This leaves 10 material parameters: A, B, C, and θ for the shear yield surface, the cap aspect ratio parameter R, the yield surface offset N, and the ratio of triaxial extension to compression strength ψ. The plastic potential parameters L, φ, and Q must be determined. Additionally, the initial value for the internal state variables must be known. The initial value of α is often chosen as 0, but κ must be fit to the data.

Finally, there are evolution equations for the ISVs. Those are:

$$\dot{\alpha} = c^{\alpha} G^{\alpha}\ \dot{\epsilon}^p \tag{F-39}$$

$$G^{\alpha} = 1 - \frac{\sqrt{J_2^{\alpha}}}{N} \tag{F-40}$$

$$J_2^{\alpha} = \frac{1}{2}\boldsymbol{\alpha}:\boldsymbol{\alpha} \tag{F-41}$$

and:

$$\dot{\kappa} = 3\dot{\gamma}\frac{\partial g}{\partial I_1} \Big/ \left(\frac{\partial \epsilon_{vol}^{p}}{\partial X}\frac{\partial X}{\partial \kappa}\right) \tag{F-42}$$

$$\epsilon_{vol}^{p} = W(\exp\{[D_1 - D_2(X(\kappa) - X_0)](X(\kappa) - X_0)\} - 1) \tag{F-43}$$

F.3.6.2 Tests and Fitting Procedure

The fitting procedure for the model is detailed in Appendix A of Ref. [12]. That procedure is summarized here. While many of the material parameters have a clear physical meaning and are easily derivable, others, in particular hardening parameters, are not so tangible.

F.3.6.2.1 Linear Elastic Parameters: Young's Modulus E and Bulk Modulus K

Young's modulus can be derived from the linear initial part of the stress-strain response of the uniaxial or triaxial compression tests, though triaxial compression tests are again seen as more accurate. Similarly, the bulk modulus can also be easily determined from the linear portion of the curve of the volumetric deformation, $K = \Delta p/\varepsilon_{vol} = \Delta\sigma_{vert}/3\varepsilon_{vol}$. It is important that the triaxial test be set up to measure changes in volumetric deformation.

F.3.6.2.2 Shear Failure Envelope Parameters

In order to derive the material parameters for the shear failure surface, a set of Triaxial Compression (TXC) tests are required. Figure F-4 shows the shear failure surface along with a series of triaxial loading tests depicted in meridional stress space ($\sqrt{J_2}$ versus I_1). The peak surface points are fit using a least squares fit to the data.

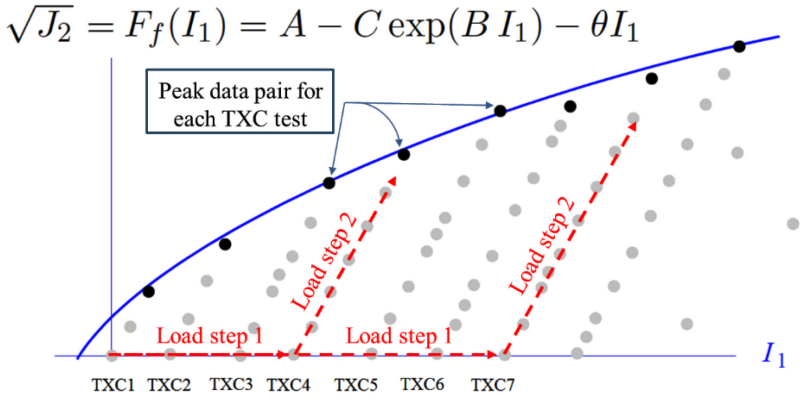


Figure F-4: Shear Failure Surface Plotted Using Series of Triaxial Compression (TXC) Tests Conducted to Failure [12].

F.3.6.2.3 Kinematic Hardening Parameters

Using the triaxial compression test affords us deriving two additional parameters incorporated in shearing-induced kinematic hardening of the model. The two parameters of interest are the yield failure

surface offset parameter, N, and the scalar decay parameter, c^{α}. N is the maximum kinematic translation that can occur before reaching the limit (failure) surface, while cα assigns the rate at which the initial yield surface translates to the failure envelope or surface.

Figure F-5 illustrates the effect of the offset parameter, N. The plot shows a simulated triaxial test. The initial elastic response can be seen. The offset parameter can be increased to allow for nearly instantaneous yielding which is often observed in soils.

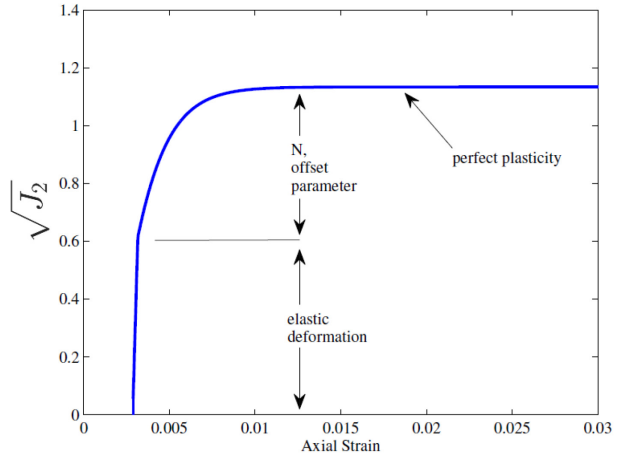


Figure F-5: Illustration of Offset Parameter, N [17].

Figure F-6 demonstrates the influence of the kinematic hardening parameter, c^{α}. Accordingly, as cα increases, the initial yield surface approaches the failure surface more rapidly [17]. Giving variety to c^{α} enables us to fit the non-linear yield response to the experimental data more accurately. As a result, for soils we used a trial-and-error method to capture acceptable values for these two parameters in accordance with triaxial data. These can be performed with a 1-element finite element simulation of the stress and strain in the triaxial test.

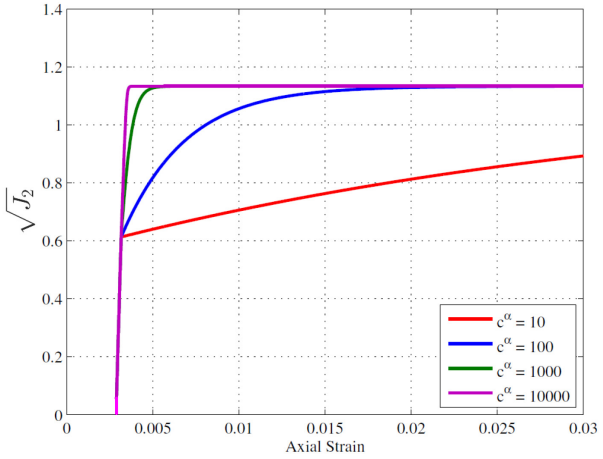


Figure F-6: Effect of Kinematic Hardening Parameter, cα [17].

F.3.6.2.4 Plastic Potential Parameters

The parameters L and φ are fit to the volumetric data of the triaxial tests. Again one element simulations are run to match the plastic volumetric strain. Reasonable initial guesses are half the values of B and θ.

F.3.6.2.5 Difference in Triaxial Extension and Compression Strength Ψ

To fit the difference in triaxial extension and compression strength, ψ, a triaxial extension test should be run, and the difference at the same mean stress compared. If this cannot be performed, a Mohr-Coulomb approximation may be derived using the formula:

$$\psi = \frac{1}{1 + \sqrt{3}(\theta + BC\exp(B\bar{I}_1))} \tag{F-44}$$

where $\bar{I}_1$ is the mean stress expected in the given simulations. Currently, ψ is treated as constant, but this formula assumes that it changes with varying mean stress. Hence, it is best to get an estimate in the range expected for a given application.

F.3.6.2.6 Cap Parameters and Volumetric Hardening Parameters

A hydrostatic compression test can be used to fit to cap parameters κ_0, R, and Q along with the cap hardening parameters. A trial-and-error approach is used to obtain reasonable values. Sandia Laboratories used to have a program for optimizing the values, but it is unknown whether this is still available. For some soils in an initially dense configuration, the cap may not be activated, and accurate fits of the parameters may not be necessary.

F.3.7 Viscoplasticity

Soil behavior is decidedly rate dependent for many vehicle applications. The two most common types of viscoplastic models are Perzyna and Duvaut-Lions.

We focus on the Duvaut-Lions model. This is a viscoplastic overlay that can be added to any plasticity with minimal additional work, unlike the Perzyna model which can have some issues in uniqueness for multisurface models [18]. The model also recovers the original elasto-plastic case for slow loading or vanishing viscosity.

F.3.7.1 Parameters

The viscoplastic model modifies a given plastic model by the formula:

$$\dot{\sigma} = \boldsymbol{c^e} : \dot{\boldsymbol{\epsilon}} - \frac{1}{\tau}(\boldsymbol{\sigma} - \overline{\boldsymbol{\sigma}}) \tag{F-45}$$

where $\overline{\boldsymbol{\sigma}}$ is the rate independent plastic solution and τ is the relaxation time. As τ approaches zero, the solution approaches the rate independent plastic solution. As τ approaches infinity, the elastic solution is recovered.

Hence, in addition to whatever parameters are needed for the given plasticity model that underlies the viscoplastic model, one additional parameter τ is necessary.

F.3.7.2 Tests

Reasonably fast loading is necessary to determine the fluidity parameter for terramechanics problems with accuracy. A cyclic triaxial test (ASTM D5311) is ideal. Most traditional triaxial or uniaxial apparati can be run at varying loading rates, but at much slower rates than are seen in vehicle loading. Hence, they are likely not very accurate in that range.

F.4 SEMI-EMPIRICAL TERRAMECHANICS MODELS

Semi-empirical were among the first developed for vehicle applications over terrain. Variations on the models developed over decades by Bekker, Reece, and Wong [3], and Janosi and Hanamoto [19] are in some sense less sophisticated than continuum models in that they do not explicitly model the soil geometry and material properties. However, their reliance on pressure-sinkage equations from tests that reasonably mimic vehicle passage make them a relatively reliable method for measuring whether a vehicle can pass safely over a given terrain. In addition, the methods are relatively simple, and do not need to be placed in a computation framework to run simulations to provide answers on passage.

F.4.1 Parameters

The semi-empirical method developed by Bekker, Reece, and Wong [3], among others, is based on a pressure-sinkage equation. Bekker proposed:

$$p = \left(\frac{k_c}{b} + k_\phi\right) z^n \tag{F-46}$$

where b is the smaller dimension of the contact patch, p is pressure (kPa), z is sinkage (m), n is a non-dimensional exponent; and k_c and k_φ are pressure-sinkage parameters with dimensions of kN/m^{n+1} and kN/m^{n+2}, respectively. Other researchers, including Janosi and Hanamoto [19] have taken this equation to represent the pressure-sinkage behavior of the soil, and hence use the same parameters.

Inspired by the Terzaghi bearing capacity theory in soil mechanics, Reece proposed another pressure – sinkage equation:

$$p = \left(ck_c' + \gamma b k_\phi'\right)\left(\frac{z}{b}\right)^n \tag{F-47}$$

where b, p, and z are defined in the same way as those in the previous; n, k_c', c and k_φ' are non-dimensional pressure-sinkage parameters; and γ is the unit weight of the soil, in kN/m^3. If we let $\gamma = \rho g$, where ρ is total density and g is acceleration due to gravity:

$$p = \left(ck_c' + \gamma b k_\phi'\right)\left(\frac{z}{b}\right)^n = \left(\frac{ck_c'}{b} + \frac{\rho g k_\phi'}{b^{n-1}}\right) z^n = \left(K_c + K_\phi g\right) z^n \tag{F-48}$$

where:

$$K_c = \frac{ck_c'}{b^n} = \frac{k_c}{b} \tag{F-49}$$

$$K_\phi = \frac{\rho k'_\phi}{b^{n-1}} = \frac{k_\phi}{g} \tag{F-50}$$

There are six independent parameters, then, for the Bekker-Reece-Wong model: the shear modulus of the soil μ, and the five parameters above. We will use k_c, k_φ, the exponent n, the cohesion c, friction angle φ, and the unit weight of the soil γ.

F.4.2 Tests

Cohesion, friction angle, and shear modulus may be determined from triaxial tests, as described earlier. The shear modulus is easily determined from Young's modulus and the bulk modulus. Unit weight can also be determined by a simple test for determining unit weight of soil (ASTM D2937-10).

The parameters k_c, k_φ, and n are usually fit using a bevameter. This is a pressure plate, ideally the width of the wheel or track being investigated, that is pushed into the soil, and pressure and sinkage are recorded. From the graph, the above parameters may be calculated.

To fit k_c and k_φ, the pressure-sinkage relationship is tested with two differently sized plates. In theory, Equation 46 is a linear relationship between pressure and sinkage in log-log scale. Rearranging Equation 46, we obtain:

$$a = \frac{\log p}{n \log z} = \frac{k_c}{b} + k_\phi \tag{F-51}$$

For a given plate size, the inverse of the slope of the log-log pressure-sinkage graph is n. See Figure F-7:

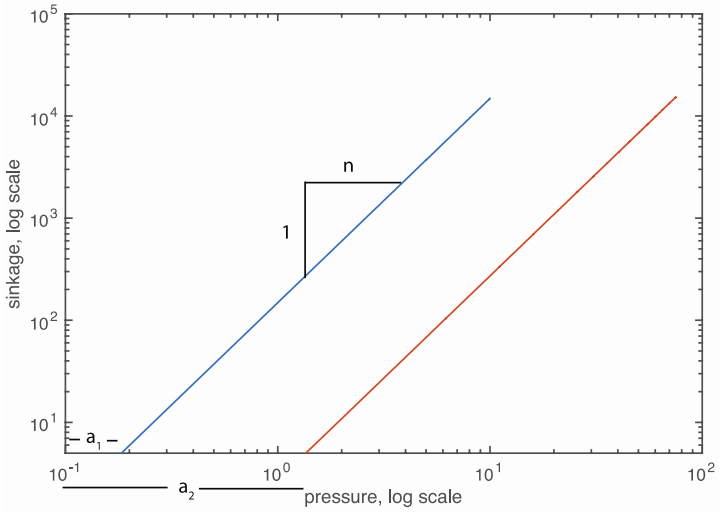


Figure F-7: Pressure-Sinkage Relationship and Parameters for Empirical Terramechanics Models.

For a given pressure p, the sinkage z_1 for plate diameter b_1 can be measured, and $a_1 = \log p/(n \log z_1)$ can be calculated. Similarly $a_2 = \log p/(n \log z_2)$ can be calculated for plate diameter b_2. From these calculations, the system of linear equations:

$$a_1 = \frac{k_c}{b_1} + k_\phi \tag{F-52}$$

$$a_2 = \frac{k_c}{b_2} + k_\phi \tag{F-53}$$

can be solved for k_c and k_φ. The resulting solution is:

$$k_c = \frac{a_2 - a_1}{b_2 - b_1} \tag{F-54}$$

$$k_\phi = a_2 - \frac{(a_2 - a_1)(b_2 - b_1)}{b_2} \tag{F-55}$$

There are more sophisticated statistical methods for fitting data from multiple bevameter tests. See Ref. [20] and Ref. [21] for examples of more advanced statistical techniques.

While bevameter tests are not always available, there appears to be little formal study in the literature of alternative methods for determining k_c, k_φ, and n. Since the test is similar in many ways to the California Bearing Ratio test, the results of this test could be correlated to bevameter results. However, more research needs to be performed to make a quantitative comparison.

F.5 DISCRETE ELEMENT MODELS

The Discrete Element Method (DEM), sometimes called the Distinct Element Method, is a numerical method that simulates the response of granular materials as the individual particles. This approach assumes the particles to be rigid and uses relatively simple models to simulate their interactions. DEM is used to simulate cohesionless soil and cemented sand/rock, but is less commonly used for clay. The particle size and shape, along with the complexity of the surface interaction forces and the particle geometry make clay particles more difficult to model individually. For granular materials, however, discrete elements overcome some limitations of more conventional continuum mechanics, such as heterogeneous force distribution throughout the sample, discontinuous motion, and particle rotation.

In DEM, each element ideally represents a single grain of soil, or may represent a group of soil particles moving together if necessary. One of the challenges of discrete elements is calibrating the parameters, which usually represent particle-scale behavior, to reproduce the bulk behavior of the soil. A quick survey of the literature reveals that DEM is computationally intensive relative to other methods, and that a great deal of simulation time is often spent calibrating the DEM model parameters to the desired characteristics of a given soil.

As with all simulation methods, the input parameters in a DEM simulation need to be calibrated to ensure that the material accurately demonstrates the physical characteristics important to the study. There have been two sets of approaches to this problem. The first is to actually try to understand the properties of the particles and the properties of their individual interaction with single other particles. While more physically motivated, typical approximations in particle geometry and simplified models of behavior mean that these properties may not best fit the bulk behavior of the soil. The second approach is to try to tune the micro-scale properties to quantitatively reproduce the bulk-scale behavior. While the particle-scale properties can often be related to bulk-scale properties approximately, some iteration on the properties is typically required to obtain good results. Each

iteration often requires many simulations to be computed. Although reasonable for quick-running simulations, this process can become time-consuming as simulation run times increase.

The challenge in discrete elements is to relate parameters such as friction coefficient, rolling resistance coefficient, restitution coefficient, normal contact stiffness, shear contact stiffness, porosity, rate of shear to macro-scale observed and measurable soil properties. In this report, we use software LIGGGHTS as an example for fitting DEM properties. We restrict ourselves to spherical particles and Hertzian contact. Each software and material model will require slightly different input, but it is hoped that the discussion here will be able to guide the modeler in creating a reasonable program for parameter identification.

F.5.1 Parameters

The first inputs needed for a simulation are the geometric parameters. LIGGGHTS focuses on spherical particles, so the distribution of particle radii is the only size parameter. Particle mass is also necessary, as well as the number of particles of each size and size of the domain to be modeled. One of the most important parts of the DEM algorithm is its handling of contact. Contact is the main mechanism of particle interaction and is heavily responsible for the behavior of the DEM material as a whole.

Commonly used normal contact models include linear elastic, Hertzian spring, Hookean spring, Johnson-Kendall-Roberts (JKR) model of elastic contact, Derjaguin-Muller-Toporov (DMT) model of elastic contact, linear damped linear spring, hysteretic linear spring, Damped (hysteretic), non-linear viscous damped Hertzian spring, elasto-plastic model and bilinear elastic model. Tangential contact models include the general tangential force model, simple Coulomb sliding, viscous damping and viscous damping with sliding friction. Some models couple normal and tangential contact, including Hertz-Mindlin contact (Hertz model with a tangential history without cohesion), Burger contact, Hertz-Mindlin contact in combination with JKR (Hertz model with tangential history with cohesion). There are also models which add rolling and twisting resistance.

For frictional-cohesive materials, a common issue is the storage and handling difficulties caused by cohesion. A number of cohesive models are available to simulate cohesive soil using DEM, the most commonly used being the Johnson-Kendall-Roberts (JKR) model [22]. The main feature of this model is the introduction of adhesion to the Hertz contact model. These adhesion forces deform the Hertz contact profile. The key of that method is the balance between the stored elastic energy and the loss in surface energy, and the model considers the effect of contact pressure and adhesion.

In this report, Hertz-Mindlin contact has been chosen as an example, as it is commonly used. This model uses a combination of normal force plus a tangential force without cohesion to simulate contact between particles and particles and between particles and container. This model is appropriate for cohesionless soils.

Mindlin and Deresiewicz [23] investigated the phenomena occurring at the contact surfaces of elastic spheres subjected to a variety of applied normal and tangential forces. Hertz considered only the forces normal to the contact surfaces. After Hertz, some investigators studied the effect of forces tangential to the contact surface and revealed the necessity of considering slippage for many applications. Voyiadjis, et al. [24] proposed a formulation for an anisotropic distortional yield model for granular media. The model applied the numerical solution for the Hertz-Mindlin problem of the contact of two rough, elastic spheres subjected to oblique compression. A series of hollow cylinder cyclic triaxial laboratory tests, in which both axial and torsional loads were applied to glass bead specimens was performed, and the results were confirmed using three-dimensional numerical simulations performed with the same loading.

The Hertz-Mindlin contact model is a granular model that uses the following formula for the frictional force between two granular particles, when the distance d between two particles of radii R_i and R_j is less than $r = R_i + R_j$. There is no force between the particles when $d > r$. The model is illustrated graphically in Figure F-8.

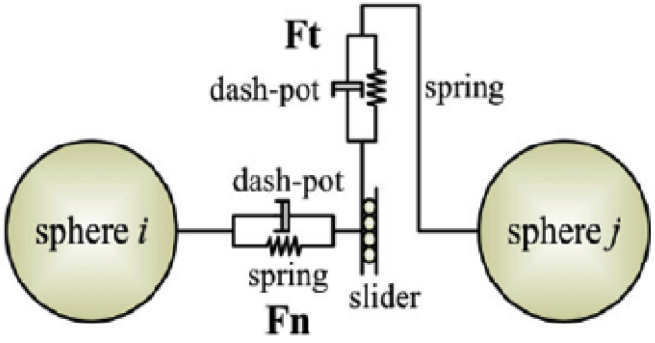


Figure F-8: Particle-To-Particle Contact Model for Hertz-Mindlin Contact.

The normal contact force F_n and tangential contact force F_t can be written:

$$F_n = k_n \delta_n - \gamma_n \dot{\delta}_n \tag{F-56}$$

$$F_t = k_t \delta_t - \gamma_t \dot{\delta}_t \tag{F-57}$$

where $\delta_n = d - r$, δ_t is the tangential displacement. The parameters k_n and k_t are the normal and shear inter-particle stiffnesses, while γ_n and γ_t are the normal and tangential damping coefficients, respectively. These four constants can be determined by the following equations:

$$k_n = \frac{4}{3} E^* \sqrt{R^* \delta_n} \tag{F-58}$$

$$\frac{1}{E^*} = \frac{1 - \nu_i^2}{E_i} + \frac{1 - \nu_j^2}{E_j} \tag{F-59}$$

$$\frac{1}{R^*} = \frac{1}{R_i} + \frac{1}{R_j} \tag{F-60}$$

$$\gamma_n = \langle -\sqrt{\frac{10}{3}} \beta \sqrt{S_n m^*} \rangle \tag{F-61}$$

$$\beta = \ln(e) / \sqrt{\ln^2(e) + \pi^2} \tag{F-62}$$

$$S_n = 2E^* \sqrt{R^* \delta_n} \tag{F-63}$$

$$\frac{1}{G^*} = \frac{2(2+\nu_i)(1-\nu_i)}{E_i} + \frac{2(2+\nu_j)(1-\nu_j)}{E_j} \tag{F-64}$$

$$\frac{1}{m^*} = \frac{1}{m_i} + \frac{1}{m_j} \tag{F-65}$$

$$\gamma_t = \langle -\sqrt{\frac{10}{3}}\beta\sqrt{S_t m^*}\rangle \tag{F-66}$$

$$S_t = 2G^*\sqrt{R^*\delta_n} \tag{F-67}$$

Here <·> are the McCauley brackets, ensuring that γ_n and γ_t are non-negative.

For this and many contact models, the particle Young's modulus and Poisson's ratio of the object must be determined. It is worth emphasizing that these are solid particle properties, different from the continuum properties used for the total soil assemblage, solid and void, discussed earlier for continuum and semi-empirical models. The friction coefficient between grains as well as between grains must also be determined. Again, these are particle-to-particle properties which are different from the continuum-scale frictional properties. The coefficient of restitution between particles and between particles and boundary objects must also be determined.

Hence, for each particle, we need five basic parameters thus far: the radius R_i, the mass m_i, Young's modulus E_i, Poisson's ratio $_{vi}$, and the coefficient of restitution e.

Additionally, the tangential force is capped by the frictional relationship $F_t \leq X_\mu F_n$, requiring an additional parameter X_μ.

Similarly, the interaction of the discrete elements with any continuum object, such as a tire tread or the wall of a testing container, should be known. This model is similar and shown in Figure F-9. The equations are nearly identical to those above, and hence we must know E, v, as well the coefficients of friction and restitution between the body and the particles. The radius R_i and mass m_i of the object may be considered infinite compared to the solid grains.

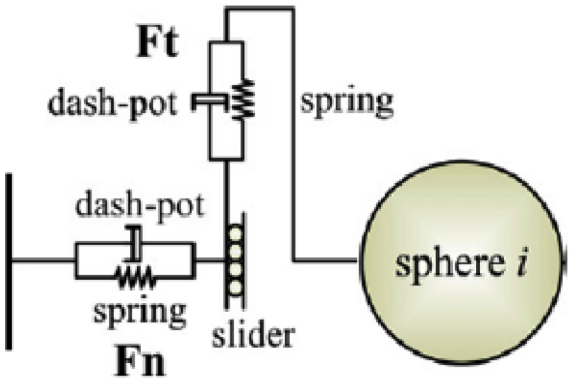


Figure F-9: Particle-to-Wall Contact Model for Hertz-Mindlin Contact.

F.5.2 Tests

One of the challenges of discrete elements is determining the particle-scale parameters that reproduce the given bulk behavior of soil. There are two general approaches for finding parameters: direct analysis of the particle-scale behavior, and fitting of lab-scale experimental data. Particle-scale analysis has been investigated by Lambe and Whitman [25] and Franco [26], among others. The model parameters can be determined using analytical assumptions. Cundall and Strack [27] and Taylor and Preece [28] used Hertzian contact theory and the Mindlin and Deresiewichs [23] approach to obtain the value of the parameters. Another method is based on the properties of the bulk material and the relations between the stress tensor that acts on a representative volume of particles and the forces between the particles in this volume [27], [29], [30], [31], [32] among others. While the direct approach is more physically motivated, a fitting approach may more accurately reproduce real soil behavior due to the simplifying assumptions of the particle interaction. In other words, using the actual material properties may not lead to the most realistic results. The elastic properties of quartz are well documented, for example, but because the particles are generally not the same shape in reality as in the simulation, using these properties for a quartz sand may not result in the best reproduction of bulk behavior.

Here we discuss both direct analysis and bulk fitting. We recommend the second approach, but direct analysis may yield decent to excellent initial guesses for some of the properties.

F.5.2.1 Particle-Scale Approach

The grain size distribution is a measurable soil property with standard tests. The equivalent particle diameter distribution is determined by a sieve analysis test, ASTM D422, followed by a hydrometer test, ASTM D7928, for fines. The equivalent diameter is measured through a sieve analysis and is approximate, but roughly equivalent to the actual size distribution. Ideally, these diameters would be used in the simulations' distribution. Up to a point, however, the soil behavior is reasonably self-similar, upscaling the grain size distribution may be permissible to improve simulation time. However, there is a limit to how far this can be done. In vehicle applications, when the particle size starts to become significant with respect to the tire or track width, a size effect may start to become apparent.

The particle mass is related to the solid density of each grain ρ_{si} by the formula:

$$m_i = \rho_{si} \frac{4}{3} \pi R_i^3 \tag{F-68}$$

Soil particle density ρ_s may be determined by pychnometer using ASTM D854, while total soil density ρ is determined by ASTM D 2937. This method assumes that all particles have the same density.

The total mass of the soil is then ρV, where V is the volume. The number of particles must be calibrated so that:

$$\sum_i m_i + \rho_w V_w = \rho V \tag{F-69}$$

where ρ_w and V_w are the density and volume of any fluid phase.

Note that because the particles are assumed to be spherical, when in reality they are not, it will not be possible to exact fit ρ_s, ρ and the porosity exactly. We fit the first two here, which will be more important to the contact law. The porosity should be close to the initial simulation.

The particle Young's modulus and Poisson's ratio may be known for some materials, such as quartz. While not quite a particle-scale approach, Liao and Chang [33] developed a method for determining the bounds of the spring constant between two particles. The upper bound is achieved using the Voigt hypothesis (uniform strain occurred in all the particles) and the lower bound is obtained using the Reuss hypothesis (uniform stress in all the particles).

The friction coefficient may also be known or can be tested for some materials, but this is a function of contact geometry as well as material, hence for soils the particle-to-particle friction coefficient should be considered a rough approximation.

The coefficient of restitution e may be considered a soil property, but is also related to the more common damping ratio β (see Equation (F-62)). Particle-scale testing for damping in soil can be challenging. The coefficient of restitution during particle-to-particle contact as well as particle-to-object contact is enforced by applying a fraction of the critical damping force [34]. This coefficient ranges from 0 to 1. The bigger the coefficient is, the more the energy is conserved until one can obtain a total energy conservation for a value of $e = 1$. It is difficult to measure with particle-scale experiments. In many cases, β can be determined from bulk-scale testing by using data from Resonant Column Test, Cyclic Triaxial Test or Cyclic Torsional Shear Test.

The coefficient of restitution between a granular material and a boundary (container) can be determined using a Drop Tester described in detail by [35].

In many applications, the coefficient of restitution between particle and particle and between particle and container have been considered to be a number between 0.5 and 0.9 such as 0.6 [36]. In many applications, simulation results are not overly affected by values in this range, especially for particle-to-object contact.

F.5.2.2 Bulk Fitting Approach

A second approach to parameter fitting is to fit the particle-scale properties to lab-scale tests. It is helpful in this case to obtain as accurately as possible a set of initial guesses to material parameters, as there are a number of parameters to be adjusted. Fitting simulations to bulk experimental data is also a time-consuming process, and hence a simple trial-and-error approach for all the parameters at once is not recommended. We outline one approach of many in the literature here. Researchers who have investigated this type of approach include Oida et al. [37], Tanaka et al. [38], and Asaf et al. [39]. Franco [26] suggested a method for calculating DEM parameters so that they represent the internal friction angle of a particular soil. Generally, the size distribution is not adjusted by bulk fitting, and test results from sieve and hydrometer analyses can be used as discussed in the previous section. Similarly, the density is not typically adjusted significantly.

Elastic constants and particle-to-particle friction coefficients can be fit to a series of tests such as direct shear or triaxial tests. Having a set of tests is ideal so that dilation can be calibrated at a variety of pressures. While we have noted that direct shear tests have issues maintaining uniform stress-strain conditions, the discrete element method simulates the same conditions, and as long as the DEM simulation can reproduce the experiments, any set of tests reasonably reproducing the behaviors of interest (e.g., elasticity, plasticity, shear and dilation) should be sufficient.

In theory, there is no frictional sliding during the elastic phase of the loading. Hence, the elastic parameters can be tuned to this phase of the test first, while ignoring the friction effects. In a triaxial test, the Young's modulus can roughly be tuned to the uniaxial stress-strain curve, while the bulk modulus is tuned to the volume change. There are some interaction effects, however.

Once the elastic parameters are fit, the particle-to-particle friction coefficient can be fit to the plastic part of the curve. Cohesion, rolling resistance, and other inelastic parameters can also be fit to the curves at this point. The larger the number of parameters, however, the more work is required trying to fit the parameters simultaneously.

For a more accurate solution, an inverse method may be applied from these initial parameters. Such methods rely on multiple runs of the solutions, analyzing the changes in the solution with the variation of each variable, until an optimum is reached. They rely on several simulations and can hence be quite time-consuming. There does not appear to be much research in the area of formal inverse modeling for DEM parameters.

Coefficient of restitution is related to the damping ratio β (sometimes ξ in the literature). This can be determined by higher strain-rate tests or fit with the other parameters, provided that there is a significant variation in strain rate. Again, special tests such as a cyclic triaxial test can be used.

A review of estimation of DEM parameters is given in Ref. [40].

F.6 SUMMARY

In this annex, we have reviewed some soil models used in terramechanics, including continuum plasticity and viscoplasticity models, semi-empirical models, and discrete element models. While it is impossible to detail every model, these models hold some promise for modeling in terramechanics applications.

Each soil will have its own strength and stiffness characteristics, and each model has its own parameters for approximating these characteristics. No model is perfect, but each of the models reviewed has a reasonable potential to adequately model soils for at least some terramechanics applications. For each model, we examine one or more methods for fitting the parameters of model. To the extent possible, we identify standard geotechnical tests. However, since those tests were developed primarily for geotechnical applications such as foundations, earth dams, and slope stability, some modification is necessary. In some cases, specialized tests for terramechanics applications such as the bevameter have been developed for fitting model parameters. While there certainly is value in using tests that more closely match actual vehicle characteristics, it may be possible to use standard geotechnical tests to fit the models adequately. Research in this area is ongoing.

In some cases, standard geotechnical tests may need to be modified somewhat to obtain data that is appropriate for terramechanics applications. This is particularly true for modeling the partially saturated soils found in vehicle-soil applications. Triaxial tests need to be modified to account for volume change in the undrained case. Alternately, estimates on Poisson's ratio exist in the literature and may be used. For the Cam-Clay model, we recommend replacing the standard consolidation testing with triaxial tests as well.

For discrete elements, two fitting approaches have been discussed. The model parameters may be fit using first principle particle-scale properties, which is attractive in that the model can be constructed from known material properties. However, simplifications in the model may mean that parameters are best adjusted from laboratory- or field-scale tests. The drawback of this approach is that some iteration, and hence significant computation time, is required to find good values of all the parameters.

Overall, parameter fitting will continue to evolve. Both testing procedures that better mimic actual applications will be developed, and more sophisticated soil models will be proposed that more effectively capture the important soil behaviors for soil-vehicle interaction.

F.7 REFERENCES

[1] Priddy, J.D. and Willoughby, W.E. 2006. Clarification of Vehicle Cone Index with Reference to Mean Maximum Pressure. Journal of Terramechanics, 43(2):85-96.

[2] Bekker, M.G. 1969. Introduction to Terrain-Vehicle Systems. The University of Michigan Press, Ann Arbor, MI, USA.

[3] Wong, J.Y. 2010. Terramechanics and Off-Road Vehicle Engineering. Elsevier: Amsterdam.

[4] Ryu, H.S., Huh, K.S., Bae, D.S. and Choi, J.H. 2003. Development of a Multibody Dynamics Simulation Tool for Tracked Vehicles – Part I, Efficient Contact and Non-Linear Dynamic Modeling. JSME International Journal Series C – Mechanical Systems Machine Elements and Manufacturing, 46(2):540-549. 1st Asian Conference on Multibody Dynamics, Iwaki Meisei Univ, Iwaki, Japan, July 31-August 2, 2002.

[5] Garber, M. and Wong, J.Y. 1981. Prediction of Ground Pressure Distribution Under Tracked Vehicles – An Analytical Method for Predicting Ground Pressure Distribution. Journal of Terramechanics, 18(1):1-23.

[6] Rubinstein, D. and Coppock, J.L. 2005. A Detailed Single-Link Track Model for Multi-Body Dynamic Simulation of Crawlers. Journal of Terramechanics, 44(5):355-364. 15th International Conference of the International-Society-of-Terrain-Vehicle-Systems, Hayama, Japan, September 2005.

[7] Contreras, U., Li, G., Foster, C.D., Shabana, A.A, Jayakumar, P. and Letherwood, M.D. 2013. Soil Models and Vehicle System Dynamics. Applied Mechanics Re- Views, 65(4).

[8] AlAwad, M.N.J. 2016. Triaxial Compression Testing. Technical Report, Kansas State University.

[9] Borja, R.I. 2013. Plasticity: Modeling and Computation. Springer: Heidelberg.

[10] Bro, A.D., Stewart, J.P. and Prandel, D. 2013. Estimating Undrained Strength of Clays from Direct Shear Testing at Fast Displacement Rates. In GeoCongress 2013.

[11] Roscoe, K.H. and Burland, J.B. 1968. On the Generalized Stress-Strain Behaviour of Wet Clay. In J. Heymann and F. A. Leckie, editors, Engineering Plasticity, pp. 535-609. Cambridge University Press, Cambridge, UK.

[12] Fossum, A.F. and Brannon, R.M. 2004. The Sandia GeoModel: Theory and Users Guide. SAND 2004-3226 uc-405, Sandia National Laboratories.

[13] Brannon, R.M., Fossum, A.F. and Strack, O.E. 2009. KAYENTA: Theory and Users Guide. SAND 2009- 2282, Sandia National Laboratories.

[14] Foster, C.D., Regueiro, R.A., Fossum, A.F. and Borja, R.I. 2005. Implicit Numerical Integration of a Three- Invariant, Isotropic/Kinematic Hardening Cap Plasticity Model for Geomaterials. Computer Methods in Applied Mechanics and Engineering, 194(50-52):5109-5138.

[15] Regueiro, R.A. and Foster, C.D. 2011. Bifurcation Analysis for a Rate-Sensitive, Non-Associative, Three- Invariant, Isotropic/Kinematic Hardening Cap Plasticity Model for Geomaterials: Part I Small Strain. International Journal for Numerical and Analytical Methods in Geome-Chanics, 35(2, SI):201-225.

[16] Motamedi, M.H. and Foster, C.D., An Improved Implicit Numerical Integration of a Non-Associated, Three-Invariant Cap Plasticity Model With Mixed Isotropic-Kinematic Hardening for Geomaterials. International Journal for Numerical and Analytical Methods in Geomechanics, 39(17):1853-1883, 2015.

[17] Sutley, G.H. 2009. Finite Element Analysis of Soil Under Explosive Loading. PhD thesis, University of Colorado at Boulder.

[18] Simo, J.C. and Hughes, T.J.R. 1998. Computational Inelasticity. Prentice Hall: New York.

[19] Janosi, Z. and Hanamoto, B. 1961. An Analysis of The Drawbar Pull vs Slip Relationship for Track Laying Vehicles. Technical report, Land Locomotion Laboratory.

[20] Apfelbeck, M., Kuss, S., Rebele, B. and Schaefer, B. 2011. A Systematic Approach to Reliably Characterize Soils Based on Bevameter Testing. Journal of Terramechanics, 48(5):360-371.

[21] Gallina, A., Krenn, R., Scharringhausen, M., Uhl, T. and Schaefer, B. 2014. Parameter Identification of a Planetary Rover Wheel–Soil Contact Model via a Bayesian Approach. Journal of Field Robotics, 31(1, SI):161-175.

[22] Johnson, K.L., Kendall, K. and Roberts, A. 197. Surface Energy and Contact of Elastic Solids. Proceedings of The Royal Society of London Series A – Mathematical and Physical Sciences, 324(1558).

[23] Deresiewicz, H. and Mindlin, R.D. 1952. Elastic Spheres in Contact under Varying Oblique Forces. Trans. ASME, J. Applied Mechanics, 20, 323-344.

[24] Voyiadjis, G., Thiagarajan, G. and Petrakis, E. 1995. Constitutive Modeling for Granular Media Using an Anisotropic Distortional Yield Model. Acta Me-Chanica, 110(1-4):151-171.

[25] Lambe, T. and Whitman, R.V. 1969. Soil Mechanics. John Wiley and Sons: New York.

[26] Franco, Y. 2009. Determination of Discrete Element Model Parameters for Soil Bulldozer Blade Interaction. Technical report, Agricultural Engineering, Technion-Israel Institute of Technology.

[27] Cundall, P.A. and Strack, O. 1979. Discrete Numerical-Model for Granular Assemblies. Geotechnique, 29(1):47-65.

[28] Taylor, L.E. and Preece, D.S. 1992. Simulation of Blasting Induced Rock Motion Using Spherical Element Model. Journal of Engineering Computations, 2:243-252.

[29] Chang, C.S. 1988. Micromechanical Modeling of Constitutive Relations for Granular Materials. In J.T. Jenkins and M. Satake, editors, Micromechanics of Granular Materials, pp. 271-278. Elsevier, Amsterdam.

[30] Rothenburg, L. and Bathurst, R. 1989. Analytical Study of Induced Anisotropy in Idealized Granular-Materials. Geotechnique, 39(4):601-614.

[31] Chang, C.S. and Gao, J. 1995. 2nd-Gradient Constitutive Theory for Granular Material with Random Packing Structure. International Journal of Solids and Structures, 32(16):2279-2293.

[32] Chang, C.S., Shi, Q. and Liao, C.L. 2003. Elastic Constants for Granular Materials Modeled as First Order Strain-Gradient Continua. International Journal of Solids and Structures, 40(21):5565-5582.

[33] Liao C.-L., Chang, T.-P., Young, D.-H. and Chang, S.C. 1997. Stress-Strain Relationship for Granular Materials Based on the Hypothesis of Best Fit. International Journal of Solids and Structures, 34(31):4087-4100.

[34] Kawaguchi, T., Tanaka, T. and Tsuji, Y. 1998. Numerical Simulation of Two-Dimensional Fluidized Beds Using the Discrete Element Method (Comparison Between the Two-and Three-Dimensional Models). Powder Technology, 96(2):129-138.

[35] Chung, Y.C. 2006. Discrete Element Modelling and Experimental Validation of a Granular Solid Subject to Different Loading Conditions. PhD thesis, University of Edinburgh.

[36] Das, B.M. and Luo, Z. 2016. Principles of Soil Dynamics. CL Learning.

[37] Oida, A., Schwanghart, H. and Ohakubo, S. 1999. Effect of Tire Lug Cross-Section on Tire Performance Simulated by Distinct Element Method. In Proceedings of the 13th International Conference of the ISTVS, Munich, pp. 345-352.

[38] Tanaka, H., Inooku, K., Nagasak, Y., Miyzaki, M., Sumikawa, O. and Oida, A. 2000. Simulation of Loosening at Subsurface Tillage Using a Vibrating Type Subsoiler by Means of the Distinct Element method. In Proceedings of the Eighth European ISTVS Conference, Umea, pp. 32-37.

[39] Asaf, Z., Rubinstein, D. and Shmulevich, I. 2006. Evaluation of Link-Track Performances Using DEM. Journal of Terramechanics, 43(2):141-161.

[40] Coetzee, C.J. 2016. Calibration of the Discrete Element Method and the Effect of Particle Shape. Powder Technology, 297:50-70.

Annex G – TA6: TRACKED VEHICLE TEST DATA

Ole Balling
Aarhus University
DENMARK

Michael McCullough
BAE Systems Inc.
UNITED STATES

G.1 INTRODUCTION

Annex G contains the vehicle data, terrain data, and test data for the tracked vehicle V&V. Nearly all the data was kindly provided by Dr. Joe Wong of Vehicle Systems Development Corporation of Toronto, Canada [1]. Since most of this material was published elsewhere, we are including the following disclaimer, suggested by Dr. Wong.

G1.1 Disclaimer

Disclaimer

The data contained in this document are from either papers published in scientific/technical journals or technical reports, which are listed as references at the end of this document. References [2]*, [4], and [5] and Part 1 – Tracked Vehicle Data of this document are copyrighted. It is the responsibility of the user of the data to comply with the copyright laws of appropriate jurisdictions.

While the data contained in this document were obtained with the best effort of the Authors of the publications and technical reports, no expressed or implied warranties of any kind on the data, including but not limited to their accuracy and completeness, are provided.

The Authors of the publications and technical reports shall not have any liability or responsibility to the user of the data for damages of any kind, including special, indirect or consequential damages, arising out of, or resulting from the use of the data.

The Authors of the publications and technical reports have not made and do not make any representations to the user that the data may be exploited without the possible infringement of proprietary rights of others.

*Numbers in Brackets designate references at the end of this document.

G.2 TRACKED VEHICLE DATA [1]

December 01, 2014

VEHICLE TYPE: APC (Test Vehicle)

VEHICLE PARAMETERS:

SPRUNG WEIGHT	78.57 kN
UNSPRUNG WEIGHT	10.14 kN
SPRUNG WEIGHT CENTRE OF GRAVITY X-COORDINATE	198.00 cm
SPRUNG WEIGHT CENTRE OF GRAVITY Y-COORDINATE	-48.10 cm
INITIAL TRACK TENSION	10.00 kN
DRAWBAR HITCH X-COORDINATE	427.50 cm
DRAWBAR HITCH Y-COORDINATE	-12.70 cm

FIXED WHEELS

WHEEL RADIUS (cm)	X-COORDINATE OF WHEEL CENTRE (cm)	Y-COORDINATE OF WHEEL CENTRE (cm)	NOTES
21.40	0.00	0.00	SPROCKET
21.90	402.30	15.10	

TORSION BAR SUSPENSION WHEELS

WHEEL RADIUS (cm)	TORSION ARM PIVOTS X-COORD. (+ IS TO THE REAR) (cm)	TORSION ARM PIVOTS Y-COORD. (+ IS DOWN) (cm)	TORSION BAR STIFFNESS (kN-m/deg)	TORSION ARM ANGLES (+ IS CW FROM HORIZONTAL) REBOUND LIMIT (deg)	FREE POSITION (deg)	JOUNCE LIMIT (deg)	TORSION ARM LENGTH (cm)	NOTES
30.50	39.69	8.73	0.1668	50.00	43.00	-4.59	31.75	T
30.50	106.36	8.73	0.1668	50.00	43.00	-4.59	31.75	T
30.50	173.04	8.73	0.1668	50.00	43.00	-4.59	31.75	T
30.50	239.71	8.73	0.1668	50.00	43.00	-4.59	31.75	T
30.50	306.39	8.73	0.1668	50.00	43.00	-4.59	31.75	T

NOTE: T = TRAILING ARM

NOTE: COORDINATE ORIGIN IS AT THE CENTRE OF THE SPROCKET. POSITIVE X- AND Y-COORDINATES ARE TO THE REAR AND DOWN, RESPECTIVELY.

*Source: [1].

APC (Test Vehicle) December 01, 2014 LETE Sand (ReN)

BELLY SHAPE	
WIDTH:	170.0 cm
COORDINATES (cm)	
X	Y
-21.4	-34.3
-4.1	14.3
417.0	14.3

TRACK LINK CONTACT AREA			
SINKAGE (cm)		INCREMENTAL AREA	PERCENTAGE CAUSING EXTERNAL SHEARING
FROM	TO	(cm^2)	
0.00	0.00	77.43	100.0
0.00	0.51	80.65	100.0
0.51	1.46	54.84	100.0
1.46	2.22	40.65	0.0
2.22	3.05	98.06	0.0
3.05	4.06	41.94	0.0
4.06	5.08	45.16	0.0
5.08	5.97	83.87	0.0

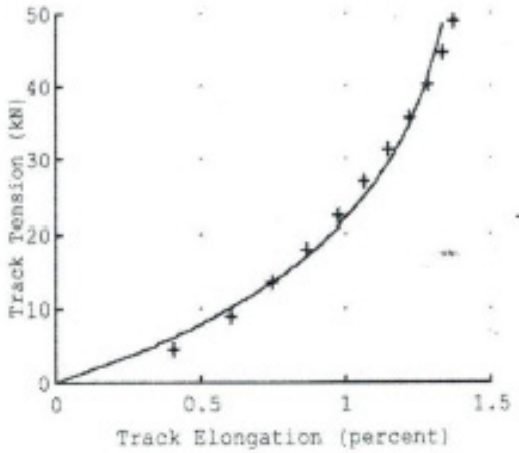
TRACK PARAMETERS:

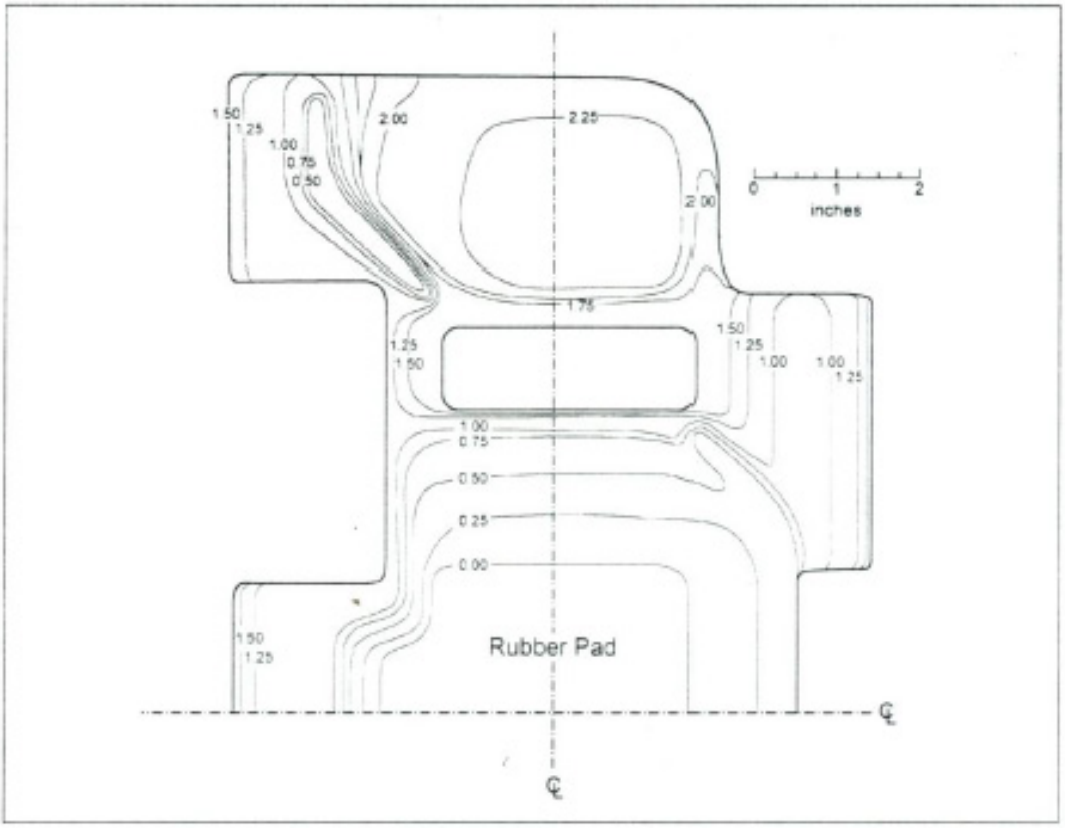
WEIGHT PER UNIT LENGTH	0.560	kN/m
WIDTH	38.0	cm
PITCH	15.0	cm
HEIGHT OF THE GROUSERS	4.7	cm
THICKNESS	6.7	cm
PERCENT EXTERNAL SHEAR AREA FOR COHESIVE SHEARING	41.0	%
LONGITUDINAL ELASTICITY CONST. Te (FROM T=-Te*ln(1-E/Emax))	18.208	kN
LONGITUDINAL ELASTICITY CONST. Emax (FROM T=-Te*ln(1-E/Emax))	1.434	%

TRACK ELASTICITY	
ELONGATION (%)	TENSION (kN)
0.000	0.00
0.408	4.45
0.605	8.90
0.745	13.34
0.867	17.79
0.975	22.24
1.063	26.69
1.151	31.14
1.219	35.59
1.282	40.03
1.334	44.48
1.373	48.93

NOTE: COORDINATE ORIGIN IS AT THE CENTRE OF THE SPROCKET. POSITIVE X- AND Y-COORDINATES ARE TO THE REAR AND DOWN, RESPECTIVELY.

APC (Test Vehicle) December 01, 2014 LETE Sand (ReN)





Contour map of the track link with 0.25 in. contour intervals.

G.3 SUPPLEMENTARY VEHICLE DATA [6]

NATO RTG-248 Tracked Vehicle Benchmark Simulations Supplementary Data Assumptions
1.0 Initial Release April 1, 2016

Vehicle Lateral Stance or Tread Width (in) 85 (center to center)

Assumed Suspension asymmetry	Left	Right
# Track Shoes	63	64
Road arm Offset	0	4 inches rearward (relative to Wong's plan view layout dimensions)

Power at Sprockets (Total) 200 hp
Stall Torque at one Sprockets 7021 ft-lbs
Max Speed 40 mph
Assume torque at low speed equals stall torque until power limited (~3.75mph)
Assume power at sprockets remains constant as a function of speed for speeds beyond the low speed range for stall torque applicability
Baseline run should assume nothing regarding the transmission and steering systems.
Parameter sensitivity runs on steering could assume more power and regenerative steering systems

Single Sprocket Power Curve

Speed	0	3,75	5	10	15	20	40
Torque	7021	7021	5266	2633	1755	1316	658

Lane Change
Vehicle corner points (inches)

	Front Left	*Front Right*	*Rear Left*	*Rear Right*
Vertical	0	0	5,9	5,9
Horizontal	-13,5	-13,5	178,2	178,2
Lateral	53	-53	53	-53

Obstacle Cross
Belly Corner Points (inches)

	Front Left	*Front Right*	*Rear Left*	*Rear Right*
Vertical	0	0	5,6	5,6
Horizontal	-12,9	-12,9	151,3	151,3
Lateral	33,5	-33,5	33,5	-33,5

Ride Dynamics	Aft	Up	
Driver Position (inches)	68,1	20	Aft and upward of sprocket center

Sprocket and Idler Radial Impact Stiffness 20.000 lb/in
Assumed linear governed by wheel rubber and track pad rubber in series deflects 1 inch under GVW

Roadwheel Jounce stop angle and Stiffness 30 degrees 20.000 lb/in
Radial at the roadwheel due to impact with hull sponson plate
Assumed linear governed by wheel rubber and track pad rubber in series deflects 1 inch under GVW

Dampers
Assume vertical linear dampers
attached at the road wheel center
on road wheels 1 and 5 , right and left
No actual data was found for damping.
These are fictional assumptions

Damper Force Curve			
velocity (in/s)	force (lbs)		
-50	-2000	jounce mode	
-10	-2000		
0	0		
10	500		
50	500	extension mode	

G.4 TRACKED VEHICLE-TERRAIN DATA

G.4.1 Terrain Parameters for LETE Sand

Pressure-sinkage relation:

Bekker's pressure-sinkage equation:

$$p = (k_c / b + k_\phi)\, z^n \tag{G-1}$$

where p is normal pressure; z is sinkage; k_c, k_ϕ and n are pressure-sinkage parameters of the terrain; b is the effective radius of the track link.

Pressure-sinkage relation during unloading or reloading:

$$p = p_u - k_u\,(z_u - z) \tag{G-2}$$

$$k_u = k_o + A_u\, z_u \tag{G-3}$$

where p is normal pressure; z is sinkage; pu is the normal pressure from which unloading begins; zu is the sinkage from which unloading begins; ko and Au are the unloading or reloading parameters of the terrain (Table G-1).

Table G-1: Pressure-Sinkage and Repetitive Loading Parameters for LETE Sand [2].

k_c kN/m^{n+1}		k_ϕ kN/m^{n+2}		n		k_o kN/m^3	A_u kN/m^4
Mean Value	**Standard Deviation**	**Mean Value**	**Standard Deviation**	**Mean Value**	**Standard Deviation**	**Mean Value**	**Mean Value**
102	54	5301	775	0.793	0.012	0	503,000

Shearing characteristics:

Janosi-Hanamoto's shear stress-shear displacement relation:

$$s / s_{max} = 1 - \exp(-j / K) \tag{G-4}$$

$$s_{max} = (c + p \tan \phi) \tag{G-5}$$

where s is shear stress; s_{max} is the maximum shear stress; p is normal pressure; c is the cohesion of the terrain (c_{ru} is the adhesion on the rubber-terrain interface); ϕ is the angle of internal shear resistance of the terrain (ϕ_{ru} is the angle of rubber-terrain shear resistance); j is shear displacement; K is shear deformation parameter of the terrain (K_{ru} is shear deformation parameter for rubber-terrain shearing). See Table G-2.

Table G-2: Parameters for Internal and Rubber-Terrain Shearing for LETE Sand [3].

Type of Shearing	Cohesion or Adhesion c *or* c_{ru} kPa		Angle of Shear Resistance ϕ or ϕ_{ru} degrees		Shear Deformation Parameter K or K_{ru} cm	
	Mean Value	Standard Deviation	Mean Value	Standard Deviation	Mean Value	Standard Deviation
Internal	1.36	0.09	31.56	0.38	1.60	0.61
Rubber-terrain	0.65	0.23	27.51	0.05	1.14	0.34

G.4.2 Terrain Parameters for Petawawa Muskeg B

Pressure-sinkage relation:

Muskeg pressure-sinkage equation:

$$p = k_m z \tag{G-6}$$

where p is normal pressure; z is sinkage; k_m is the muskeg pressure-sinkage parameter.

Pressure-sinkage relation during unloading or reloading:

$$p = p_u - k_u (z_u - z) \tag{G-7}$$

$$k_u = k_o + A_u z_u \tag{G-8}$$

where p is normal pressure; z is sinkage; p_u is the normal pressure from which unloading begins; z_u is the sinkage from which unloading begins; k_o and A_u are unloading or reloading parameters of the terrain (Table G-3).

Table G-3: Pressure-Sinkage Parameter Km for Petawawa Muskeg B, Obtained with the Surface Mat Being Cut [4].

Terrain	k_m kN/m^3		k_o kN/m^3	A_u kN/m^4
	Mean Value	Standard Deviation	Mean Value	Mean Value
Petawawa Muskeg B	555	105	147	29,700

Shearing characteristics:

Janosi-Hanamoto's shear stress-shear displacement relation:

$$s / s_{max} = 1 - \exp(-j / K) \quad \text{(G-9)}$$

$$s_{max} = (c + p \tan \phi) \quad \text{(G-10)}$$

where s is shear stress; s_{max} is the maximum shear stress; p is normal pressure; c is the cohesion of the terrain; ϕ is the angle of internal shear resistance of the terrain; j is shear displacement; K is shear deformation parameter of the terrain (Table G-4).

Table G-4: Shear Parameters for the Peat of Petawawa Muskeg B [3].

Terrain Type	Type of Shearing	Cohesion c kPa		Angle of Shear Resistance ϕ degrees		Shear Deformation Parameter K cm	
		Mean Value	Standard Deviation	Mean Value	Standard Deviation	Mean Value	Standard Deviation
Peat – Muskeg B	Internal	4.14	0.01	38.11	0.35	2.79	0.68

G.4.3 Terrain Parameters for Petawawa Snow A

Pressure-sinkage relation for each layer of a two-layer snow cover with a crust in between:

$$p = p_w [- \ln (1 - z / z_w)] \quad \text{(G-11)}$$

$$p_w = k_{p1} + b\, k_{p2} \quad \text{(G-12)}$$

$$z_w = k_{z1} + k_{z2} / b \quad \text{(G-13)}$$

where p is normal pressure; z is sinkage; k_{p1}, k_{p2}, k_{z1}, and k_{z2} are snow pressure-sinkage parameters; b is the effective radius of the track link.

Pressure-sinkage relation during unloading or reloading:

$$p = p_u - k_u (z_u - z) \quad \text{(G-14)}$$

$$k_u = k_o + A_u z_u \quad \text{(G-15)}$$

where p is normal pressure; z is sinkage; p_u is the normal pressure from which unloading begins; z_u is the sinkage from which unloading begins; k_o and A_u are unloading or reloading parameters of the terrain (Table G-5).

Table G-5: Pressure-Sinkage and Repetitive Loading Parameters for Petawawa Snow A [2], [5].

Terrain	Petawawa Snow A	
Parameters	**Before Failure of the Crust**	**After Failure of the Crust**
k_{p1}, kN/m^2	3.2	52.7
k_{p2}, kN/m^3	234	-48
k_{z1}, cm	0.9	14.2
k_{z2}, cm^2	39.7	67.3
L_{cr}, cm	16.7	
M_{cr}, kN	0.0402	
k_o, kN/m^3	0	
A_u, kN/m^4	109,600	

Note: L_{cr} and M_{cr} are strength parameters of the crust between the upper and lower layer of snow cover.

Internal shearing characteristics of snow:

$$s / s_{max} = K_r \{1+ [1/ (K_r (1\text{-}1/e)) – 1] \exp (1\text{-} j / K_w)\} [1 – \exp (\text{-} j / K_w)] \quad \text{(G-16)}$$

$$s_{max} = (c + p \tan \phi) \quad \text{(G-17)}$$

where s is shear stress; s_{max} is the maximum shear stress; c is the cohesion of the terrain; ϕ is the angle of internal shear resistance of the terrain; K_r is the ratio of the residual shear stress to the maximum shear stress; K_w represents the shear displacement where the maximum shear stress occurs; j is shear displacement (Table G-6).

Table G-6: Internal Shear Parameters for Petawawa Snow A [2].

Terrain Type	Cohesion c, kPa		Angle of Shear Resistance ϕ, degrees		Shear deformation Parameter K_w, cm		Shear deformation Parameter K_r	
	Mean Value	**Standard Deviation**	**Mean Value**	**Standard Deviation**	**Mean Value**	**Standard Deviation**	**Mean Value**	**Standard Deviation**
Petawawa Snow A	0.4	0.4	23.98	4.02	2.18	0.76	0.654	0.12

Rubber-snow shearing characteristics:

Janosi-Hanamoto's shear stress-shear displacement relation:

$$s / s_{max} = 1 - \exp(-j / K_{ru}) \quad \text{(G-18)}$$

$$s_{max} = (c_{ru} + p \tan \phi_{ru}) \quad \text{(G-19)}$$

where s is shear stress on the rubber-terrain interface; s_{max} is the maximum shear stress on the rubber-terrain interface; p is normal pressure on the rubber-terrain interface; c_{ru} is the adhesion on the rubber-terrain interface; ϕ_{ru} is the angle of rubber-terrain shear resistance; j is shear displacement; K_{ru} is shear deformation parameter of rubber-terrain shearing (Table G-7).

Table G-7: Parameters for Rubber-Snow Shearing for Petawawa Snow A [3].

Type of Shearing	Adhesion c_{ru}, kPa		Angle of Shear Resistance ϕ_{ru}, degrees		Shear Deformation Parameter K_{ru}, cm	
	Mean Value	Standard Deviation	Mean Value	Standard Deviation	Mean Value	Standard Deviation
Rubber-Snow A	0.14	0.14	17	1.80	0.61	0.33

G.5 TRACKED VEHICLE TEST DATA

G.5.1 Random Terrain Ride

Data can be found in STANREC [7].

3 cm course defined by ISO 8608 [8] with a length of 1000 m and 0.1 m uniform elevation spacing.

6 cm course defined by ISO 8608 [8] with a length of 1000 m and 0.1 m uniform elevation spacing.

9 cm course defined by ISO 8608 [8] with a length of 1000 m and 0.1 m uniform elevation spacing.

G.5.2 Half Round Obstacles

Ride Quality 2D Profiles
3D Terrain Profile

FLAT	PROFILE									
	2	0								
	0	0	100	0						
4INHR										
	4-INCH	HALF-ROUND	OBSTACLE							
	13	0								
	0	0	0,14	1,04	0,54	2	1,17	2,83	2	3,46
	2,96	3,86	4	4	5,04	3,86	6	3,46	6,83	2,83
	7,46	2	7,86	1,04	8	0				
6INHR										
	6-INCH	HALF-ROUND	OBSTACLE							
	13	0								
	0	0	0,2	1,55	0,8	3	1,76	4,24	3	5,2
	4,45	5,8	6	6	7,55	5,8	9	5,2	10,24	4,24
	11,2	3	11,8	1,55	12	0				

8INHR										
	8-INCH	HALF-ROUND	OBSTACLE							
	13	0								
	0	0	0,27	2,07	1,07	4	2,34	5,66	4	6,93
	5,93	7,73	8	8	10,07	7,73	12	6,93	13,66	5,66
	14,93	4	15,73	2,07	16	0				
10INHR										
	10-INCH	HALF-ROUND	OBSTACLE							
	13	0								
	0	0	0,34	2,59	1,34	5	2,93	7,07	5	8,66
	7,41	9,66	10	10	12,59	9,66	15	8,66	17,07	7,07
	18,66	5	19,66	2,59	20	0				
12INHR										
	12-INCH	HALF-ROUND	OBSTACLE							
	13	0								
	0	0	0,41	3,11	1,61	6	3,51	8,49	6	10,39
	8,89	11,59	12	12	15,11	11,59	18	10,39	20,49	8,49
	22,39	6	23,59	3,11	24	0				
14INHR										
	14-INCH	HALF-ROUND	OBSTACLE							
	13	0								
	0	0	0,48	3,62	1,88	7	4,1	9,9	7	12,12
	10,38	13,52	14	14	17,62	13,52	21	12,12	23,9	9,9
	26,12	7	27,52	3,62	28	0				
16INHR										
	16-INCH	HALF-ROUND	OBSTACLE							
	13	0								
	0	0	0,55	4,14	2,14	8	4,69	11,31	8	13,86
	11,86	15,45	16	16	20,14	15,45	24	13,86	27,31	11,31
	29,86	8	31,45	4,14	32	0				
18INHR										
	18-INCH	HALF-ROUND	OBSTACLE							
	13	0								
	0	0	0,61	4,66	2,41	9	5,27	12,73	9	15,59
	13,34	17,39	18	18	22,66	17,39	27	15,59	30,73	12,73
	33,59	9	35,39	4,66	36	0				

G.5.3 Trapezoidal Obstacles

The 72 trapezoidal obstacles are defined in NRMM v2.8.2, and associated documentation [9].

G.6 REFERENCES

[1] Vehicle Systems Development Corporation. 2016. NTVPM – Operator's Manual. Unpublished Report.

[2] Wong, J.Y., Garber, M. and Preston-Thomas, J. 1984. Theoretical Prediction and Experimental Substantiation of the Ground Pressure Distribution and Tractive Performance of Tracked Vehicles. Proceedings of the Institution of Mechanical Engineers, Part D. Transport Engineering, 198:265-285.

[3] Wong, J.Y. 2015. Evaluation of the Computer-Aided Method NTVPM for Assessing Tracked Vehicle Cross-Country Performance, Final Report – Part 1. Prepared by Vehicle Systems Development Corporation under Contract No. W911NF-11-D-0001, administered by Battelle Memorial Institute for U.S. Army RDECOM-TARDEC.

[4] Wong, J.Y., Radforth, J.R. and Preston-Thomas, J. 1982. Some Further Studies on the Mechanical Properties of Muskeg in Relation to Vehicle Mobility. Journal of Terramechanics, 19(2):107-127.

[5] Wong, J.Y. and Preston-Thomas, J. 1983. On the Characterization of the Pressure-Sinkage Relationship of Snow Cover Containing an Ice Layer. Journal of Terramechancs, 20(1):1-12.

[6] Conner, C. 2017. Armored Personnel Carrier. Available at: http://afvdb.50megs.com/usa/m113.html [updated February 25, 2017].

[7] AMSP-06 STANREC. 2018. Guidance for M&S Standards Applicable to the Development of Next Generation of NATO Reference Mobility Models (NG-NRMM). 1(1).

[8] ISO 8608. 2016. Mechanical Vibration – Road Surface Profiles – Reporting of Measured Data.

[9] Haley, P., et al. 1979. NATO Reference Mobility Model, Edition 1, Users Guide Volume II, Obstacle Module. US Army Tank-Automotive Research and Development Command, Technical Report 12503.

Annex H – TA6: WHEELED VEHICLE PLATFORM TEST DATA

Ole Balling
Aarhus University
DENMARK

Henry Hodges
Hodges Transportation, Inc.
UNITED STATES

Michael McCullough
BAE Systems Inc.
UNITED STATES

H.1 WVP VEHICLE DATA

Details of the wheeled vehicle platform are captured below (Figure H-1, Figure H-2, Figure H-3, Table H-1), but the full data set can be found in an Excel spread sheet available at the NATO Science Connect Server.



Figure H-1: Top View of Vehicle.

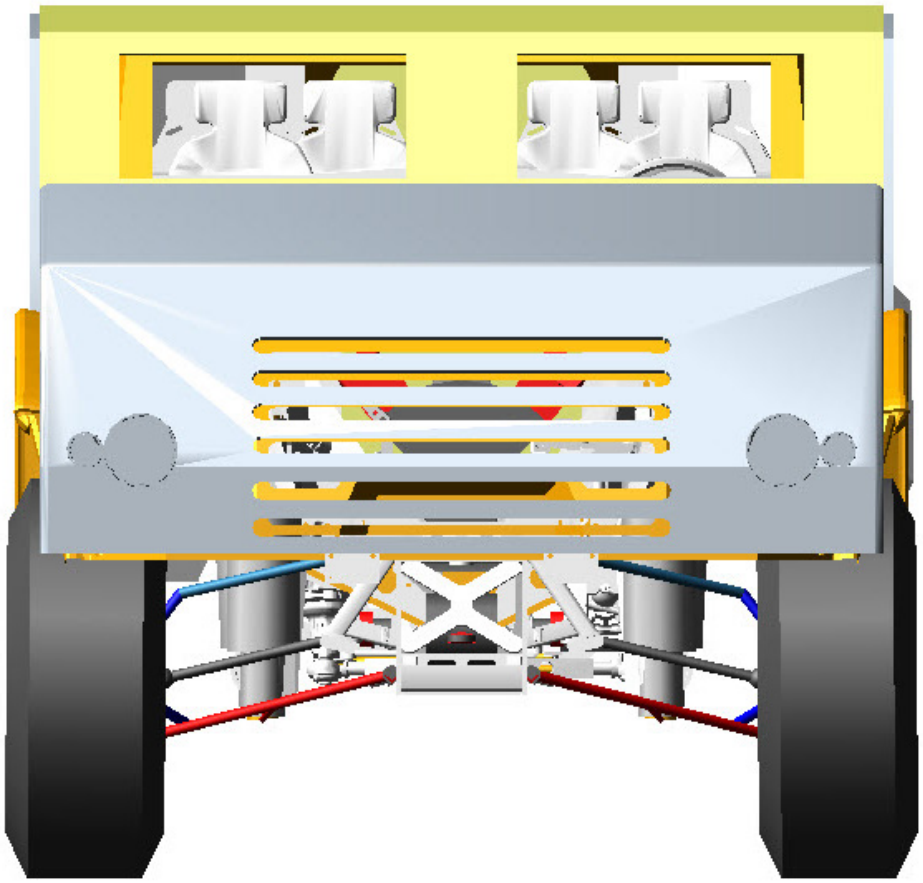


Figure H-2: Front View of Vehicle.

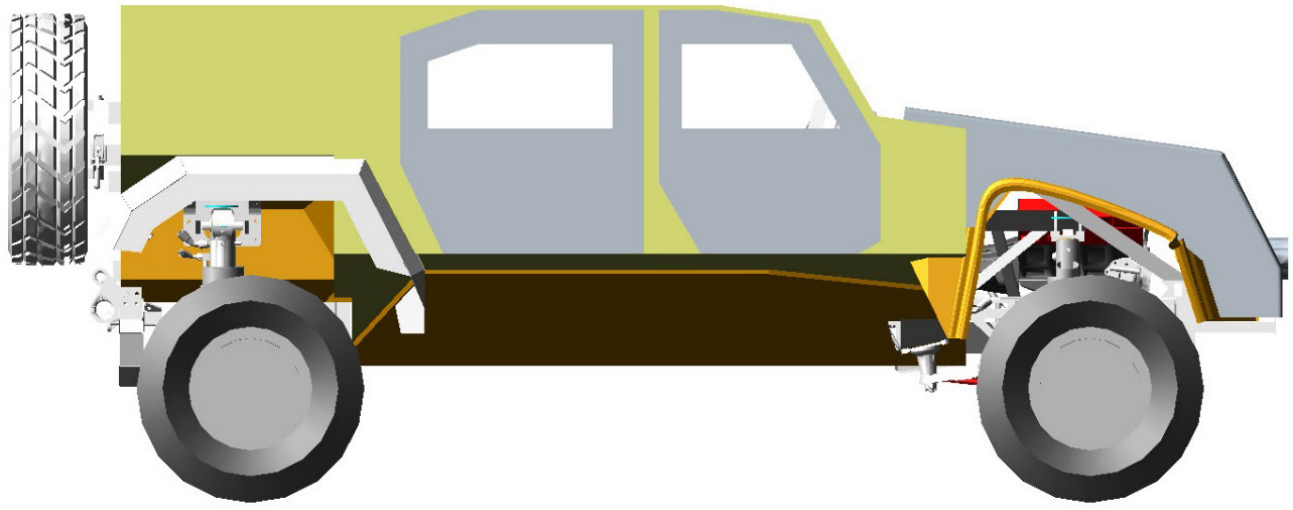


Figure H-3: Side View of Vehicle.

Table H-1: General Vehicle Data.

General Data		
wheel base	4039	mm
track width front axle	2066	mm
track width rear axle	2066	mm
total vehicle length	5588	mm
vehicle width	2449	mm
vehicle height incl. Cabin	2347	mm
hor. Distance Front to wheel center front	926	mm
hor. Distance Rear to wheel center rear	633	mm
vehicle approach angle	50	deg
vehicle departure angle	80	deg
fording depth	762	mm
payload	2727	kg
king pin inclination	8,9	deg
alignment data at static		
camber angle	-0,5	deg
toe	front = -0.9 deg	rear = +0.4 deg

Weight Distribution as Tested (fully payloaded)	Left (lb)	Right (lb)	Total (lb)
Front axle	5170	5100	10270
Rear Axle	4800	4630	9430
Total	9970	9730	19700

	X	Y	Z
Estimated CG at model design position (mm)	2070	-10	495
Estimated Inertia about CG			
Roll	6,7E+09	kg-mm^2	
Pitch	2,5E+10	kg-mm^2	
Yaw	2,8E+10	kg-mm^2	

H.2 SOFT SOIL DATA

Only one type of soft soil was used in the WVP testing. It was sand with the following properties:

Sand properties:

- Density: 1650 kg/m^3
- Moisture content: 1.1%
- Cohesion strength C: 1.10 E+03 n/m^2
- Friction angle: 32 degrees
- Janosi-Hanamoto shear modulus K:0.025 m

H.3 TEST DATA

Testing was done by Nevada Automotive Test Center. The data available for the benchmark are presented in the following figures:

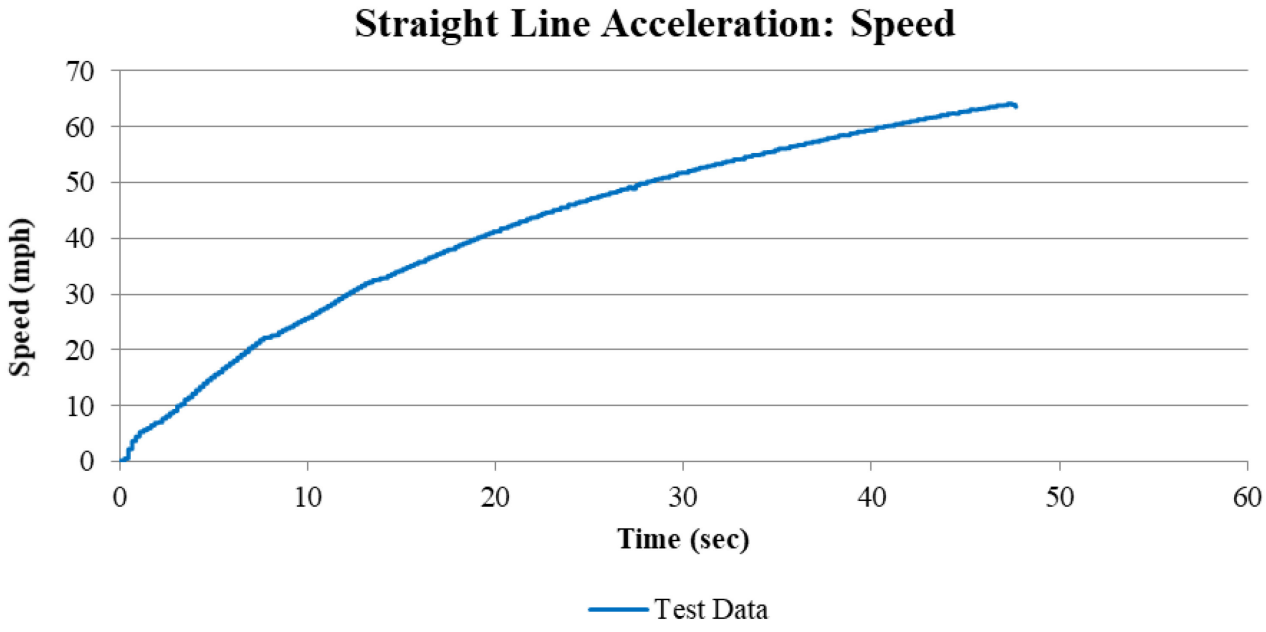


Figure H-4: Straight Line Acceleration.

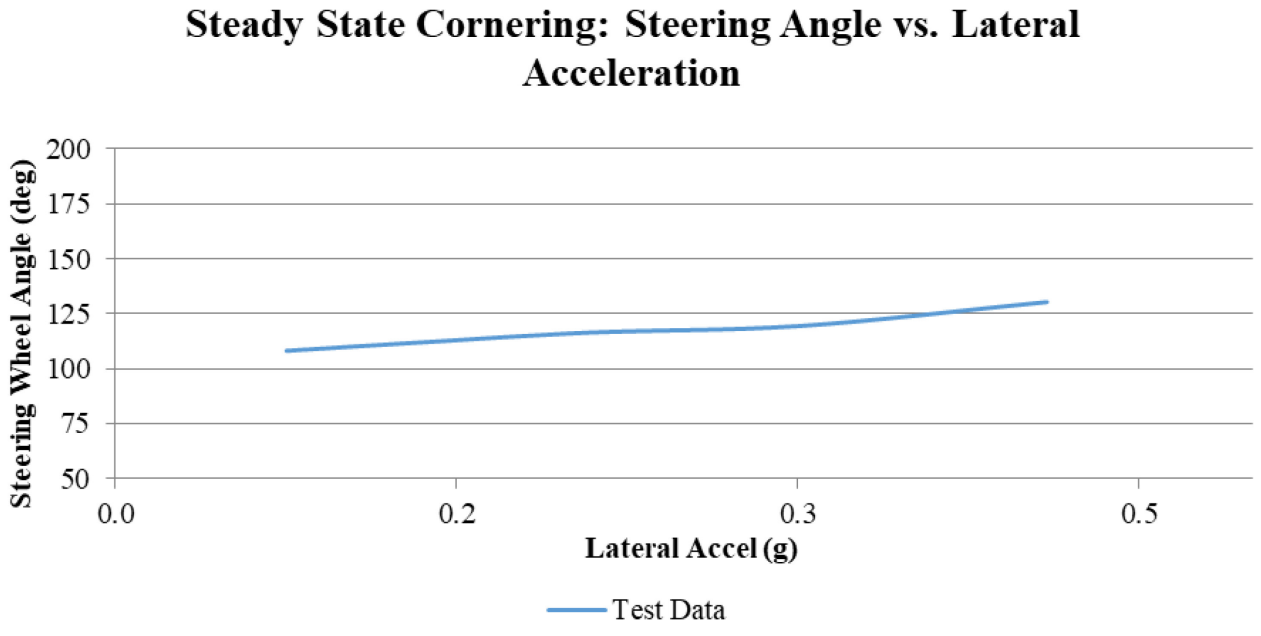


Figure H-5: Steady-State Cornering: Steering Angle vs. Lateral Acceleration.

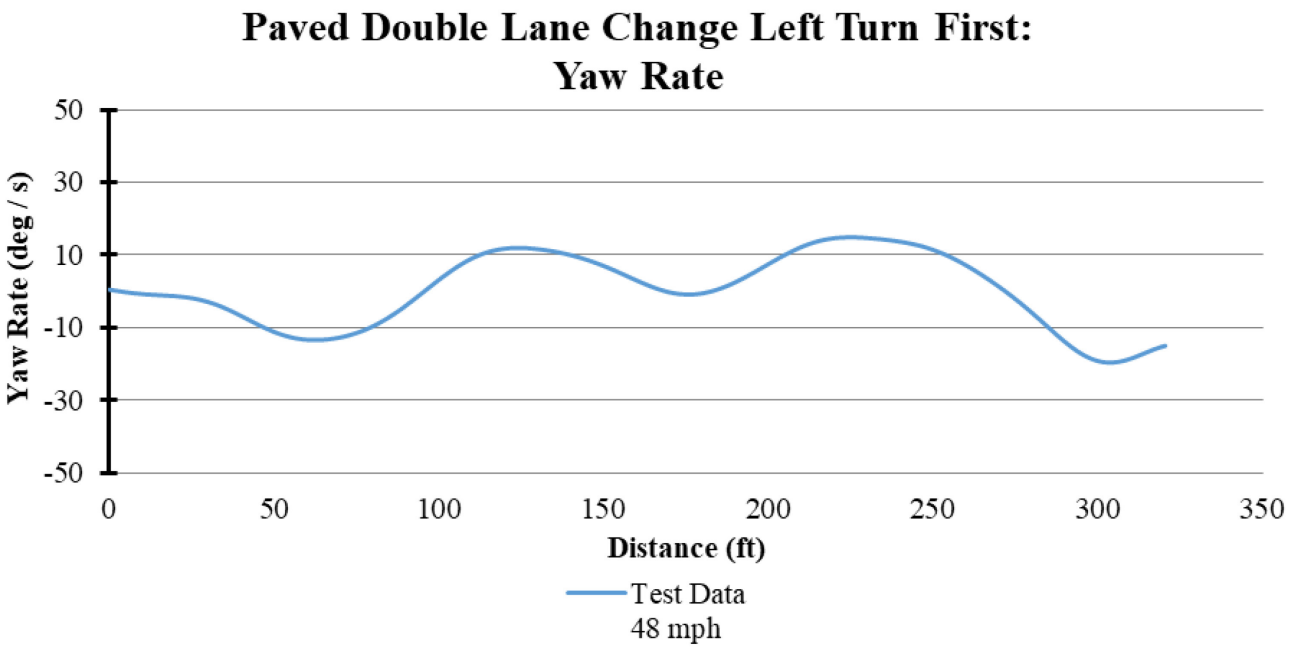


Figure H-6: Paved Double Lane Change Left Turn First: Yaw Rate.

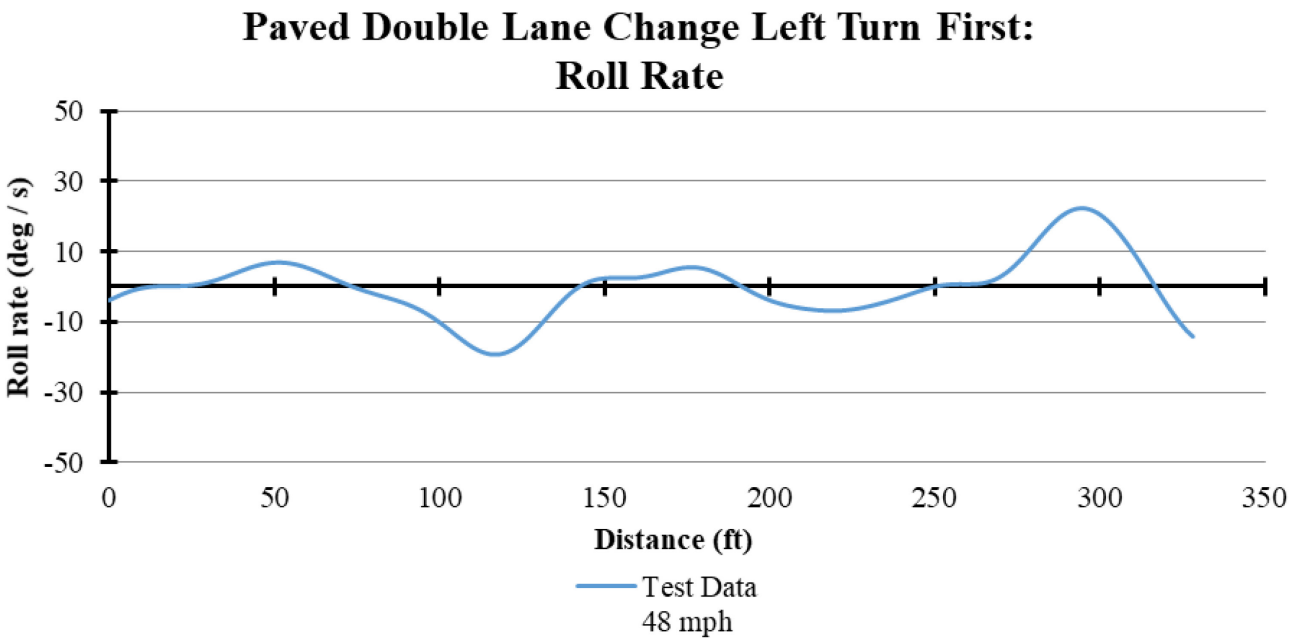


Figure H-7: Paved Double Lane Change Left Turn First: Roll Rate.

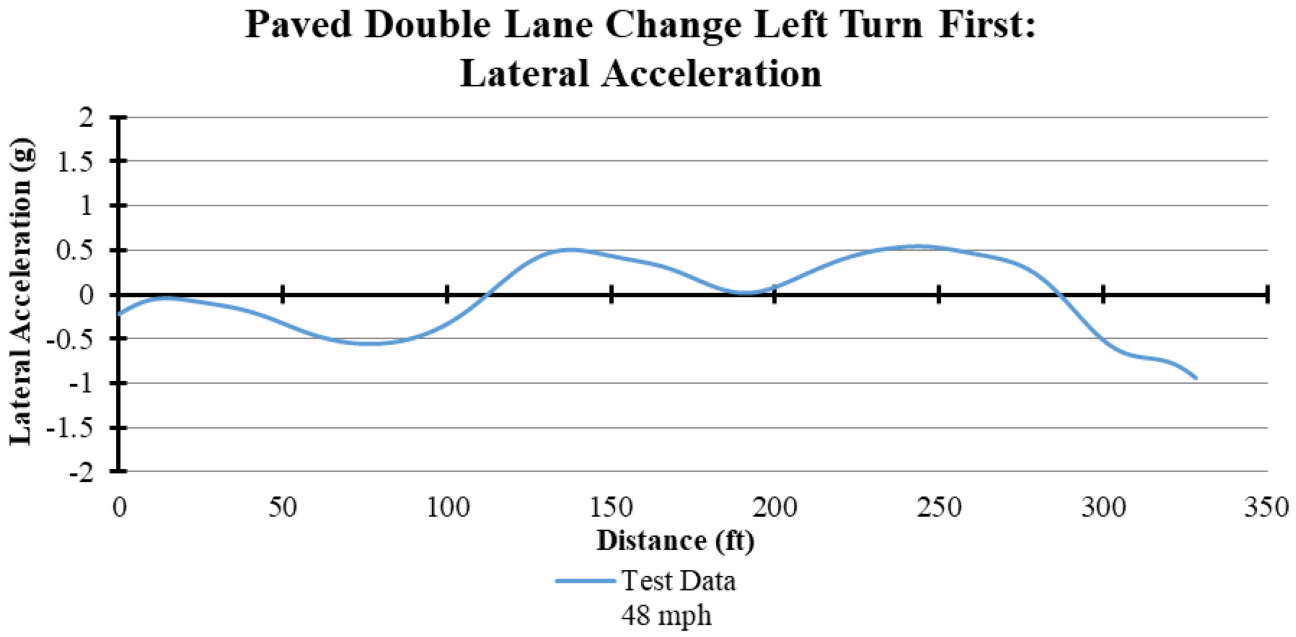


Figure H-8: Paved Double Lane Change Left Turn First: Lateral Acceleration.

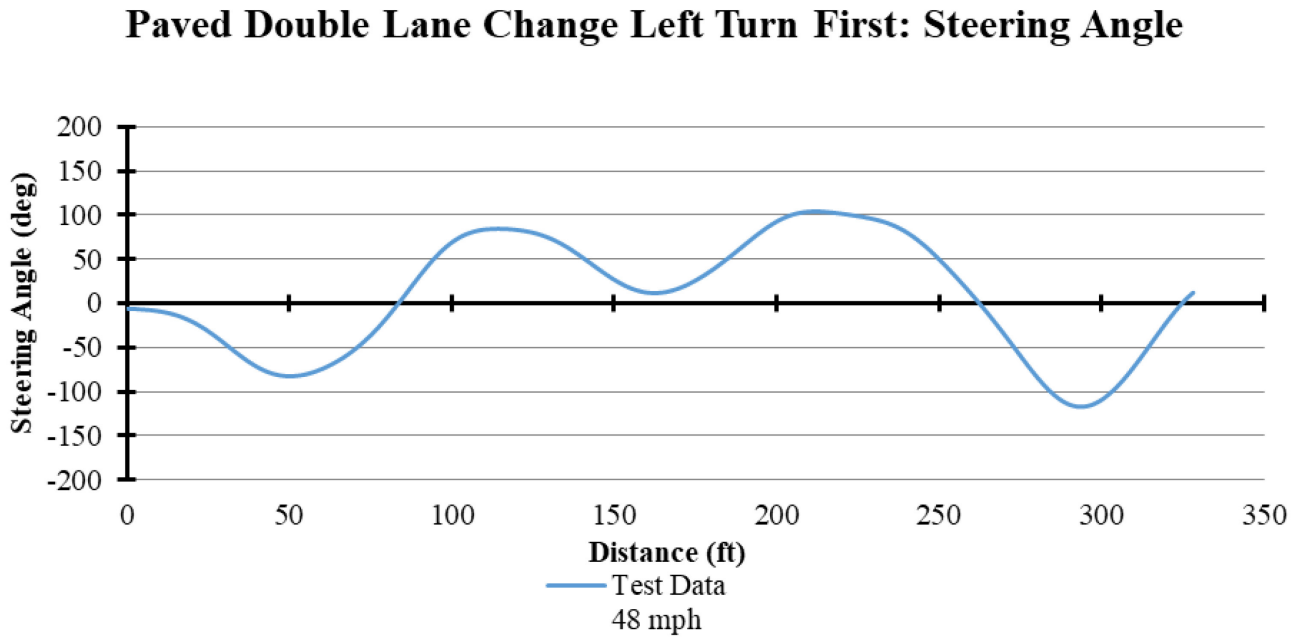


Figure H-9: Paved Double Lane Change Left Turn First: Steering Angle.

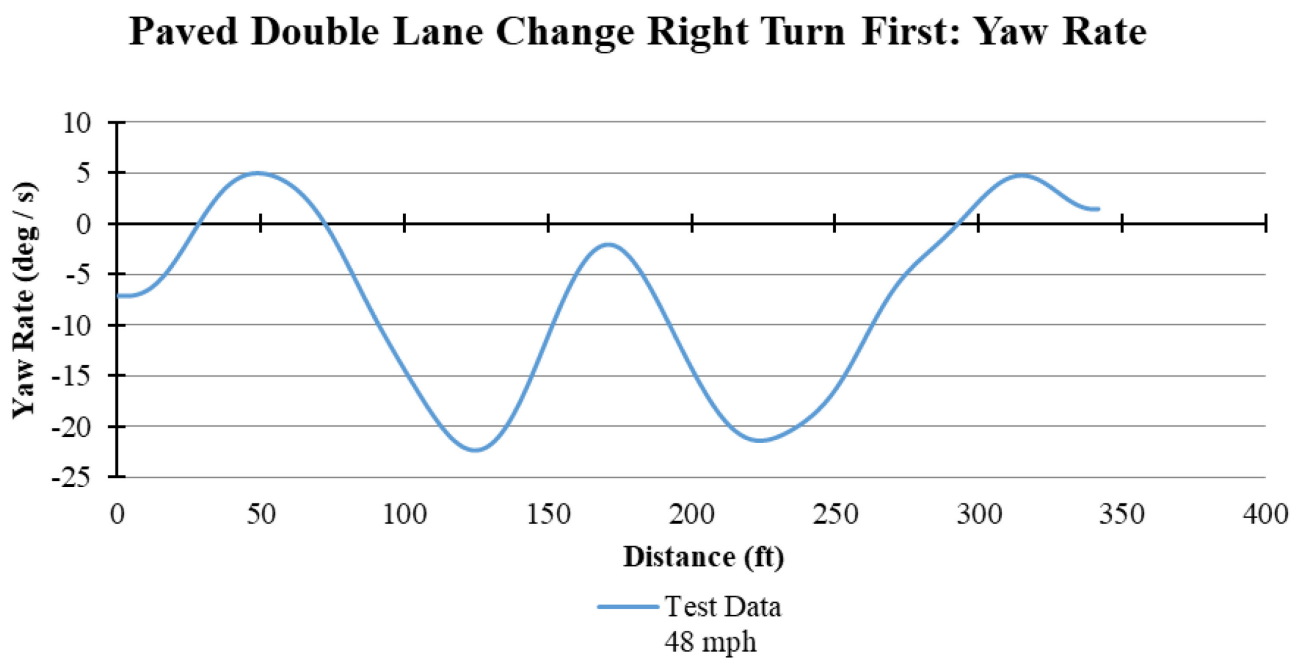


Figure H-10: Paved Double Lane Change Right Turn First: Yaw Rate.

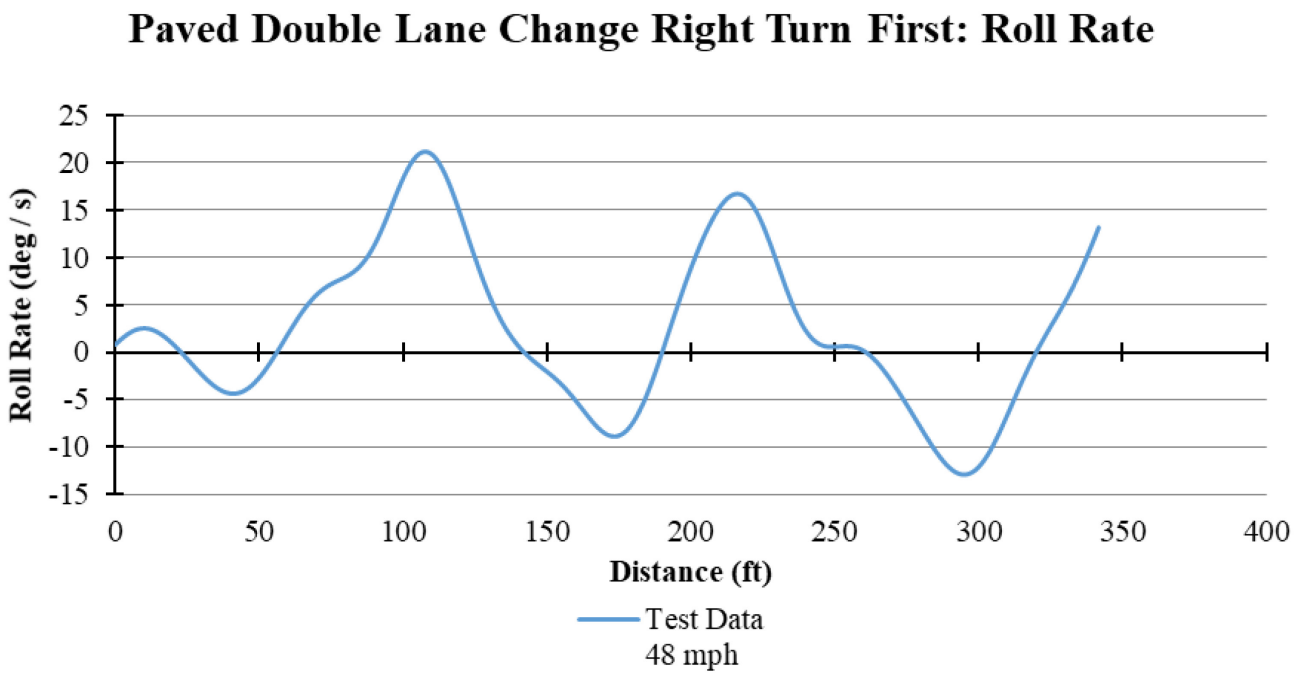


Figure H-11: Paved Double Lane Change Right Turn First: Roll Rate.

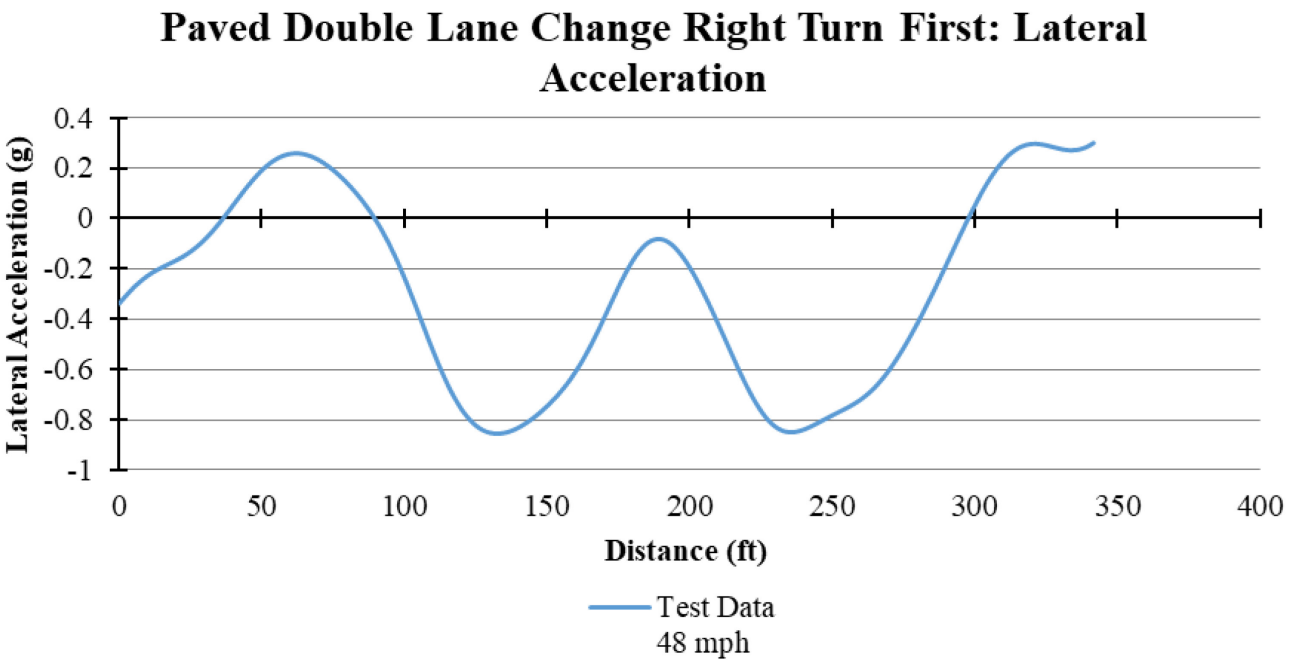


Figure H-12: Paved Double Lane Change Right Turn First: Lateral Acceleration.

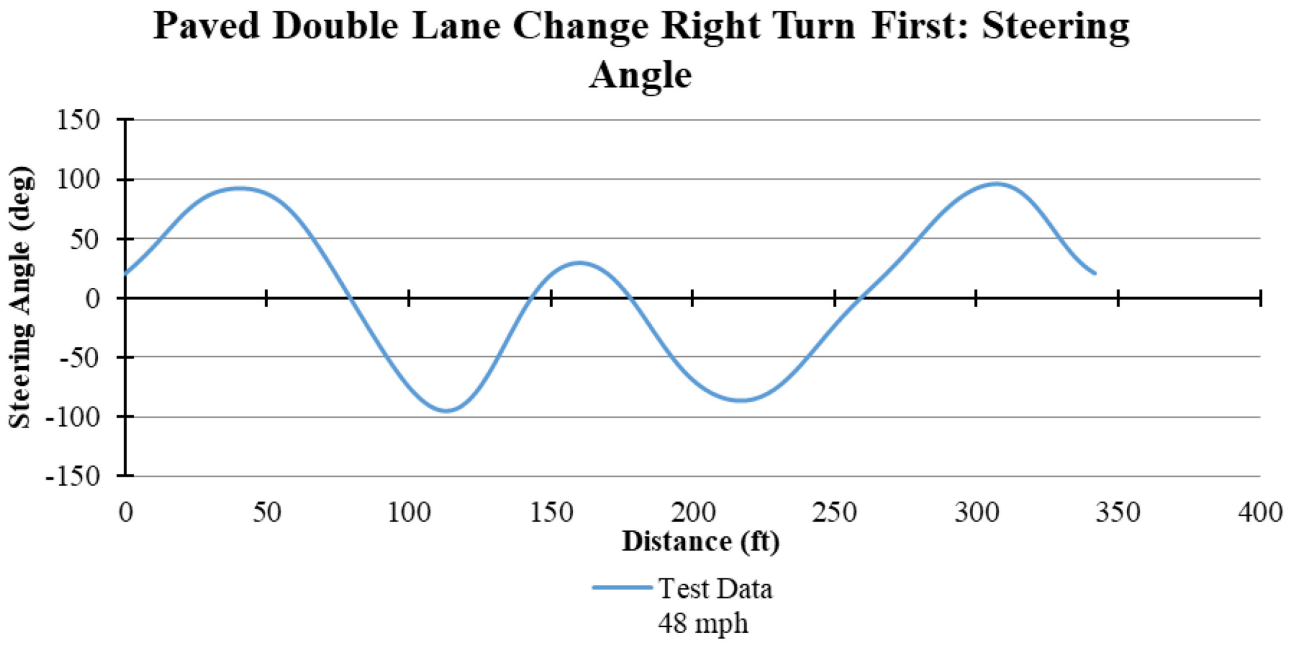


Figure H-13: Paved Double Lane Change Right Turn First: Steering Angle.

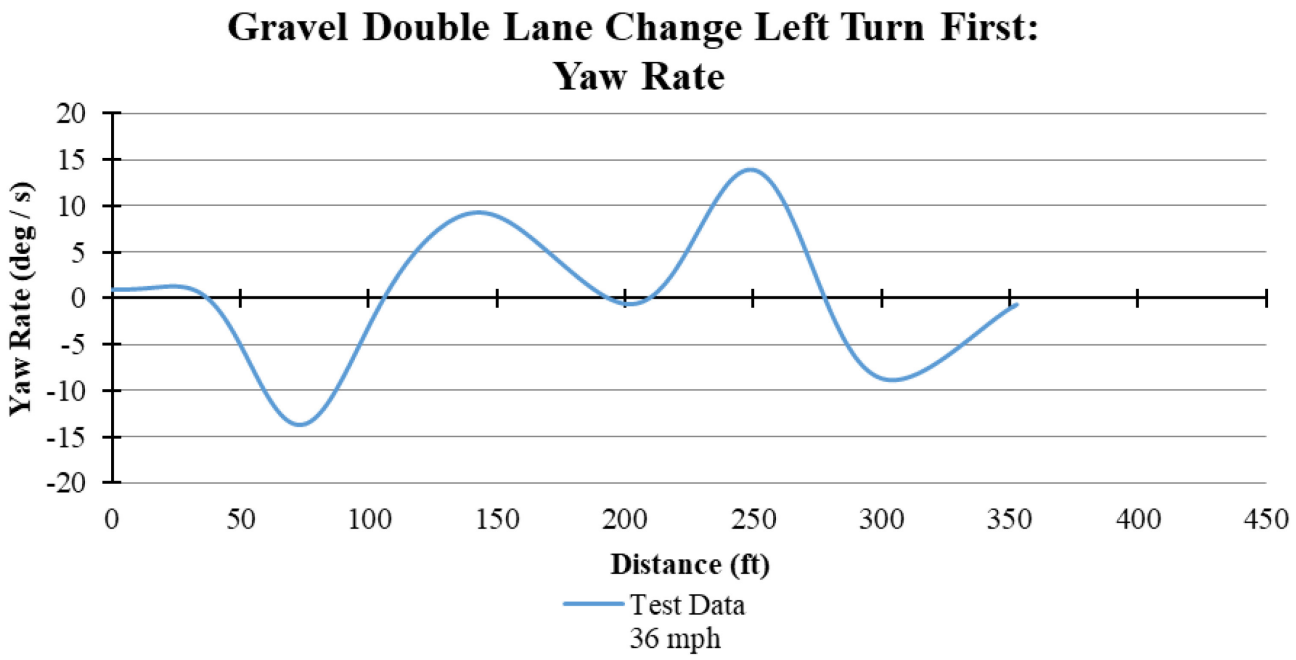


Figure H-14: Paved Double Lane Change Right Turn First: Yaw Rate.

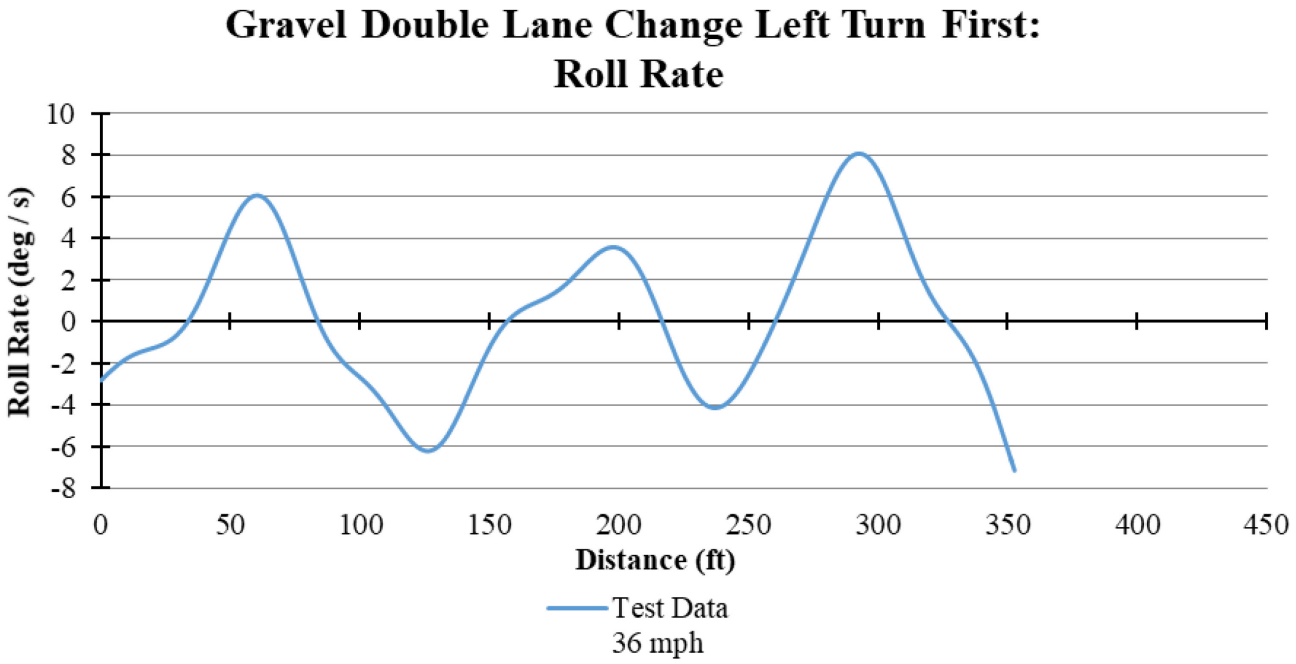


Figure H-15: Gravel Double Lane Change Left Turn First: Roll Rate.

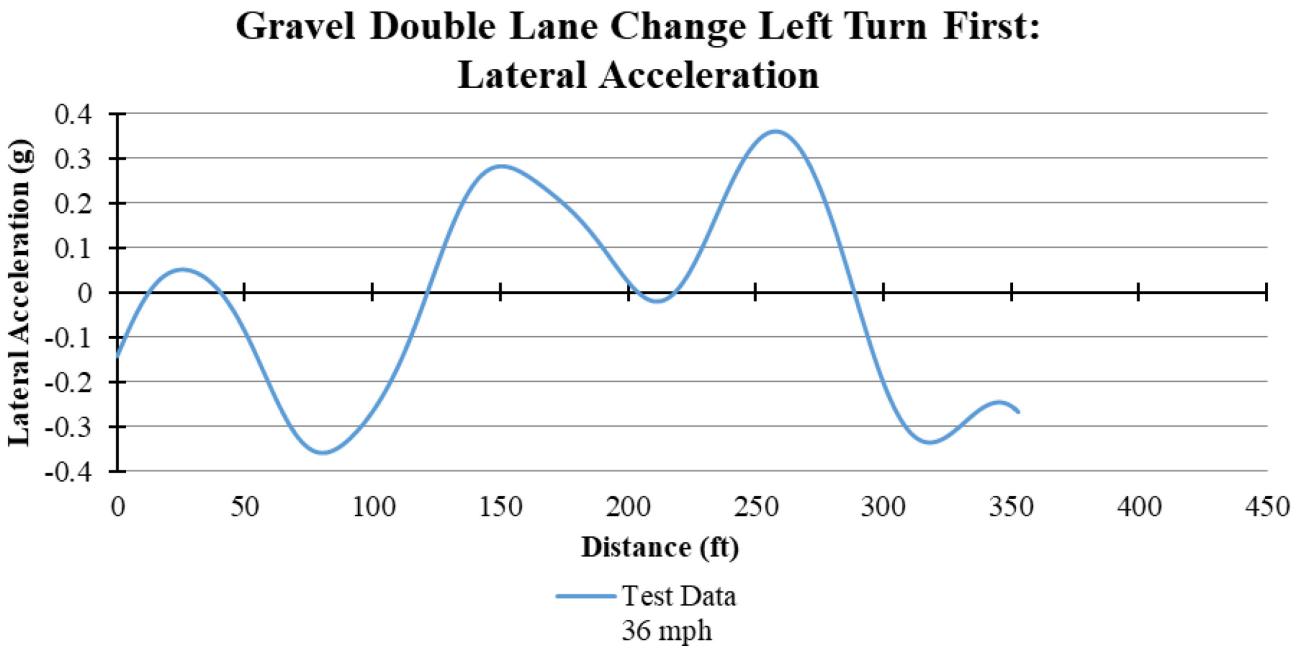


Figure H-16: Gravel Double Lane Change Left Turn First: Lateral Acceleration.

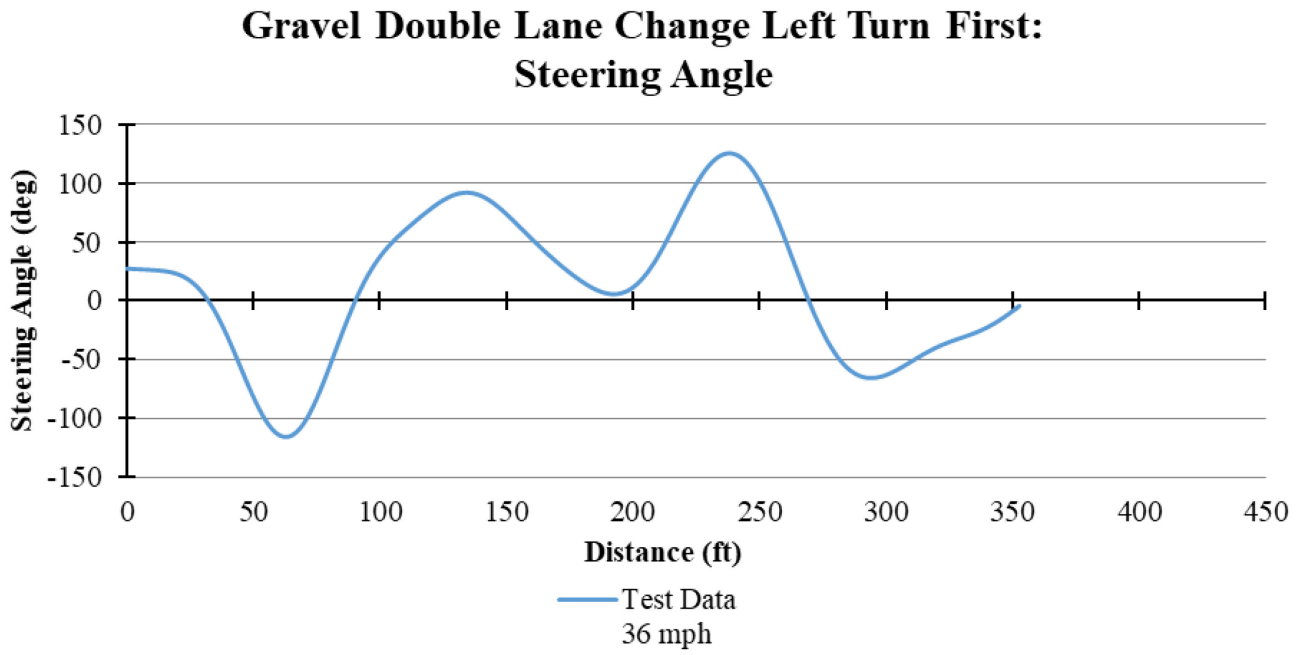


Figure H-17: Gravel Double Lane Change Left Turn First: Steering Angle.

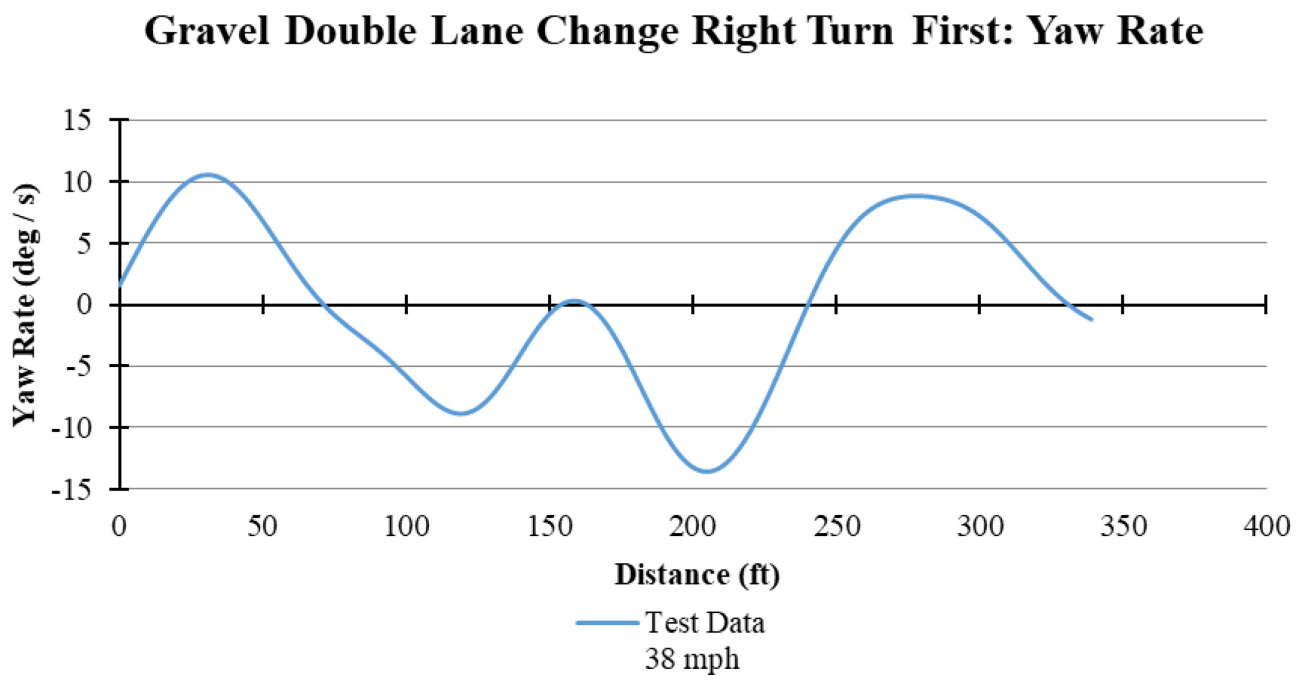


Figure H-18: Gravel Double Lane Change Right Turn First: Yaw Rate.

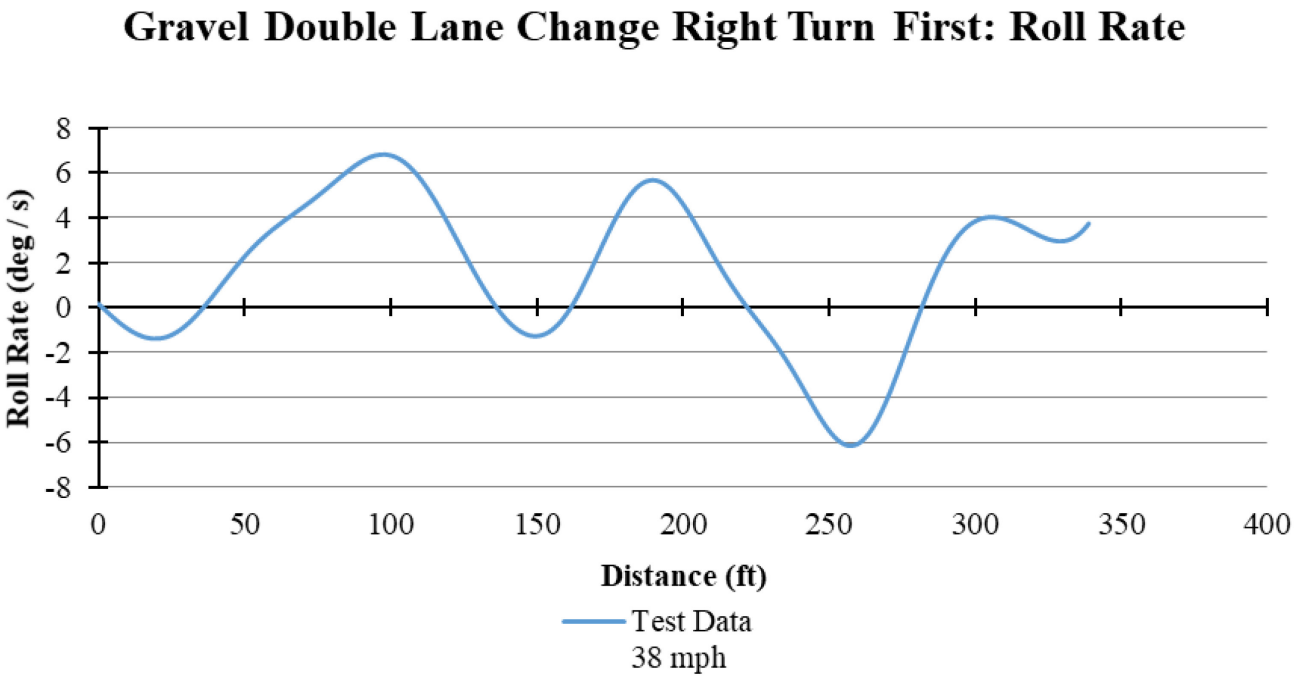


Figure H-19: Gravel Double Lane Change Right Turn First: Roll Rate.

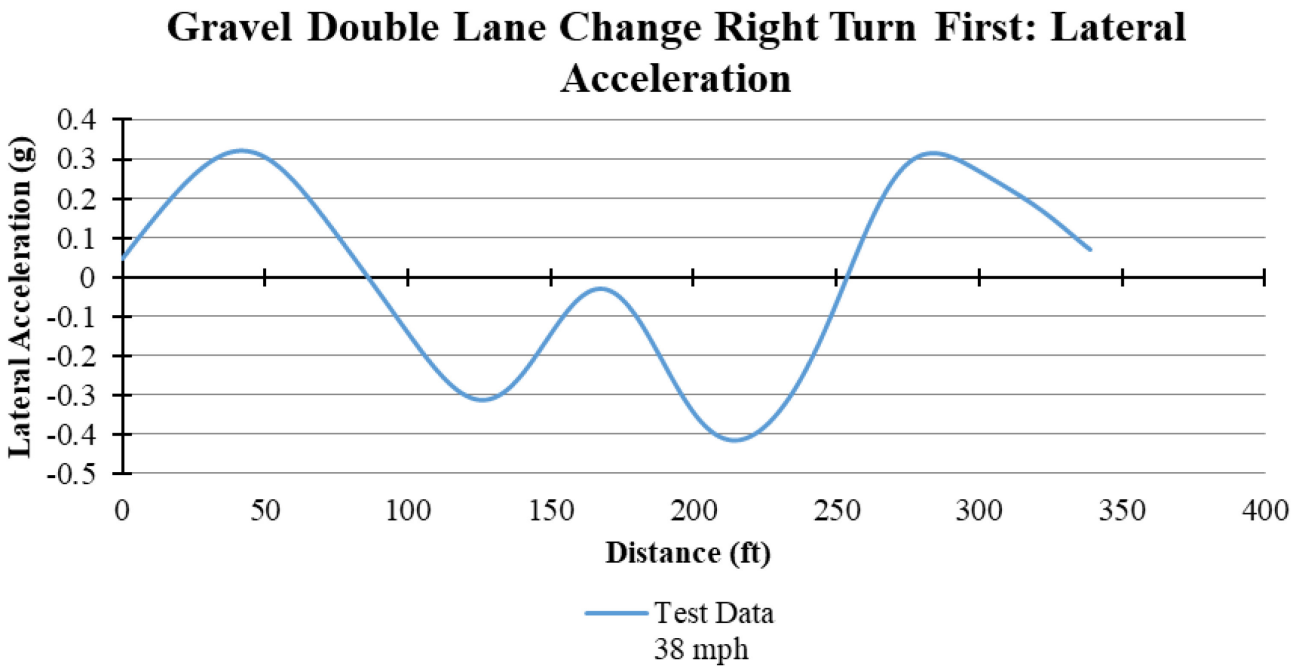


Figure H-20: Gravel Double Lane Change Right Turn First: Lateral Accleration.

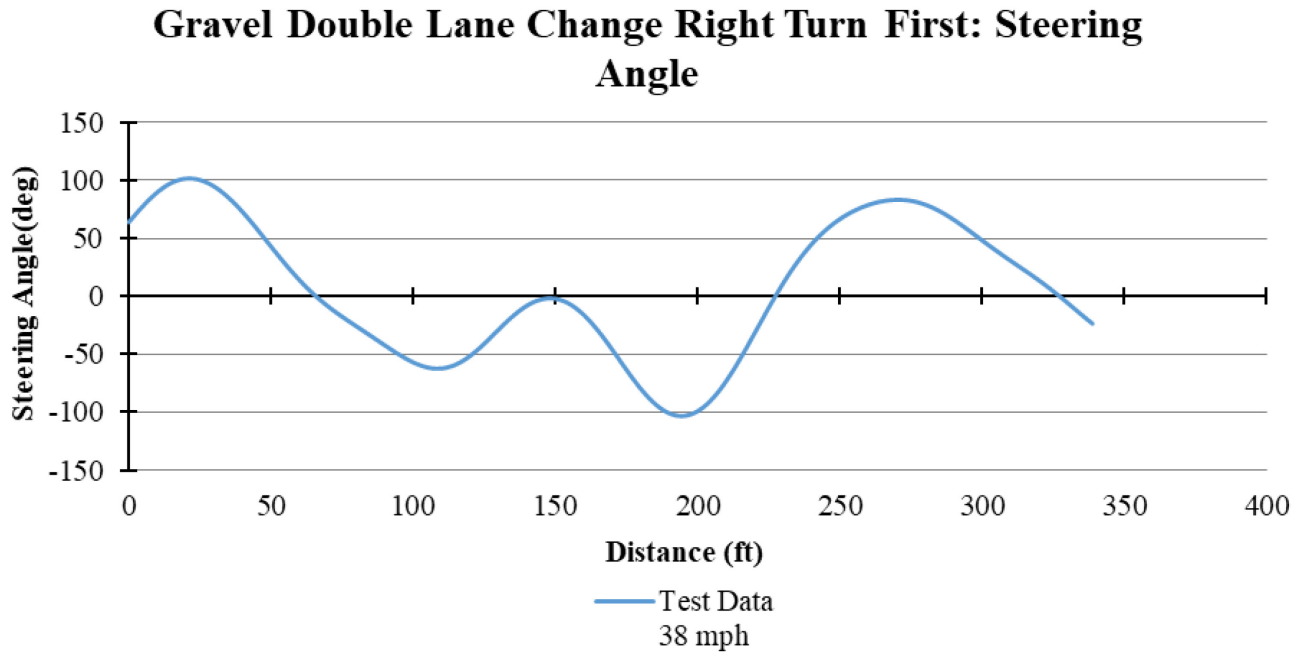


Figure H-21: Gravel Double Lane Change Right Turn First: Steering Angle.

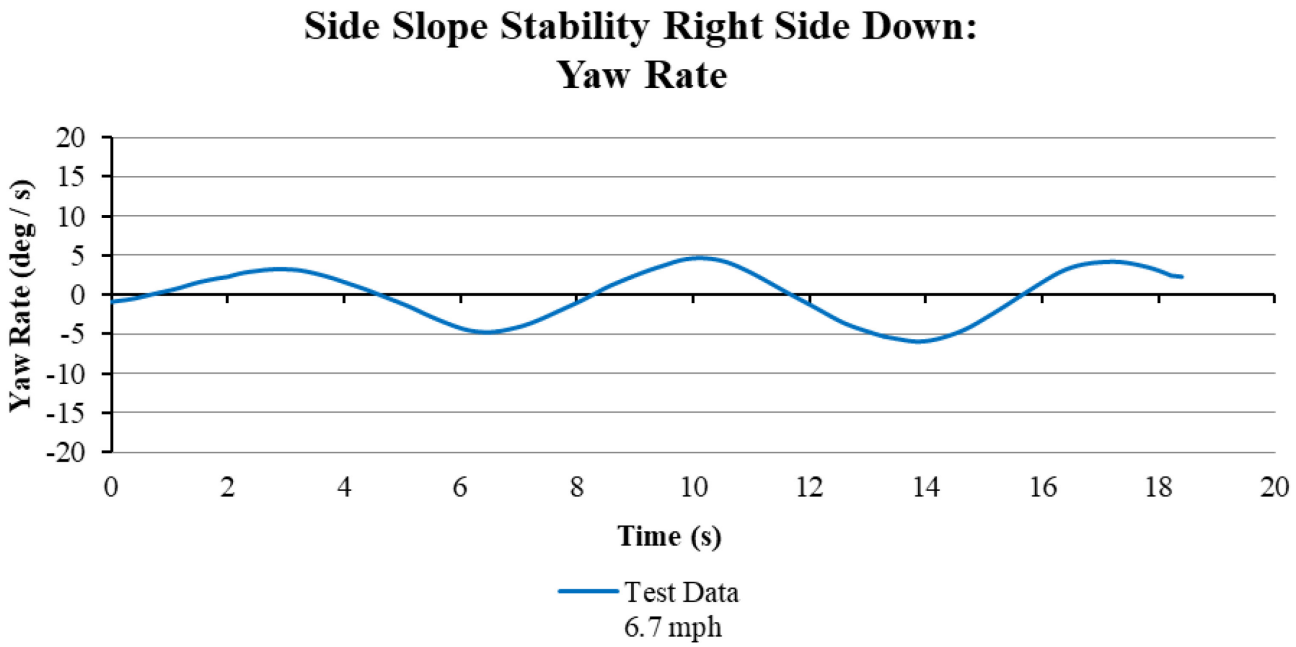


Figure H-22: Side Slope Stability Right Side Down: Yaw Rate.

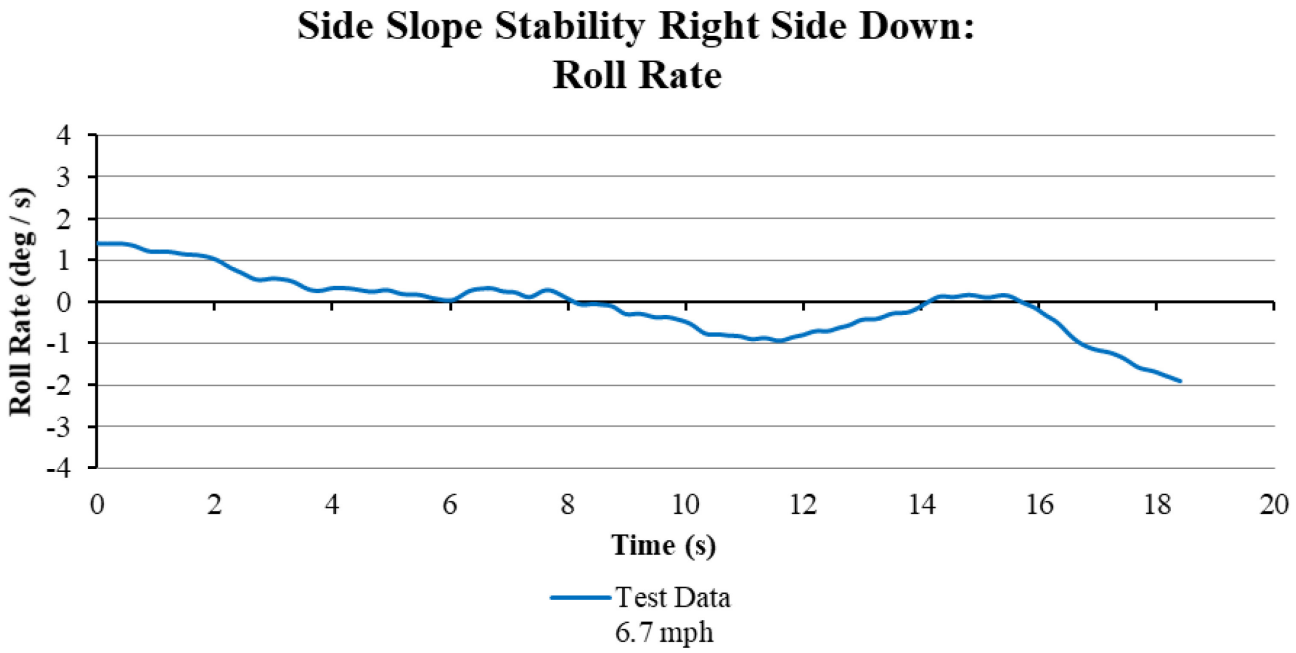


Figure H-23: Side Slope Stability Right Side Down: Roll Rate.

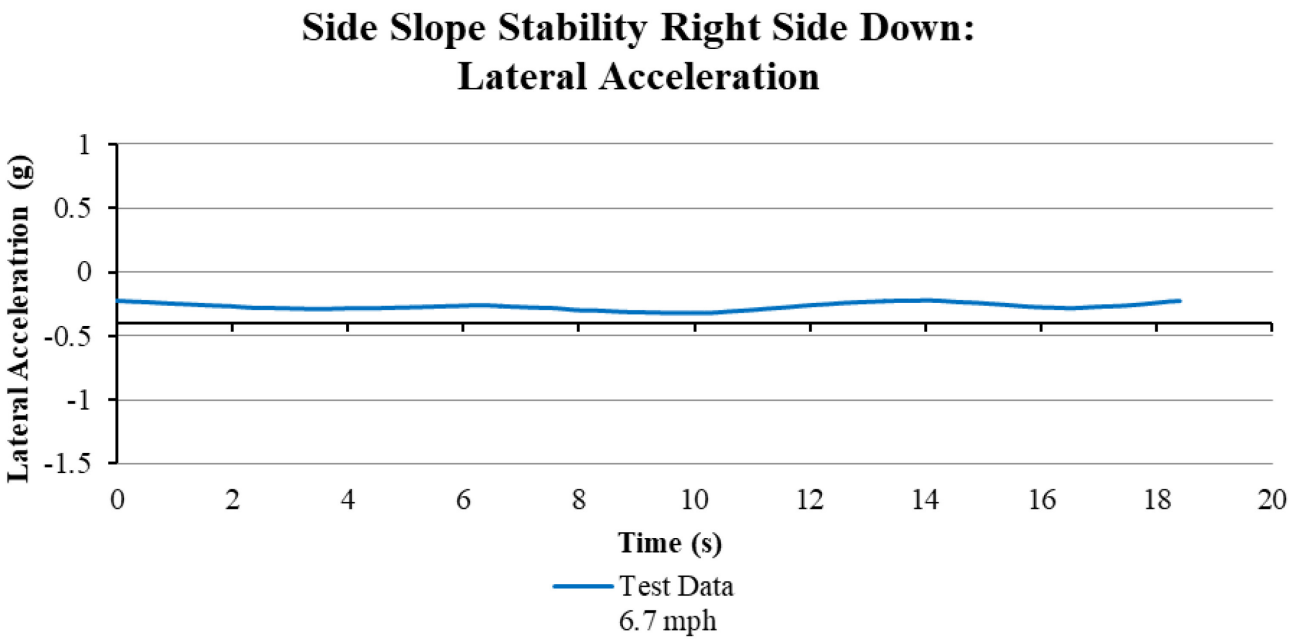


Figure H-24: Side Slope Stability Right Side Down: Lateral Acceleration.

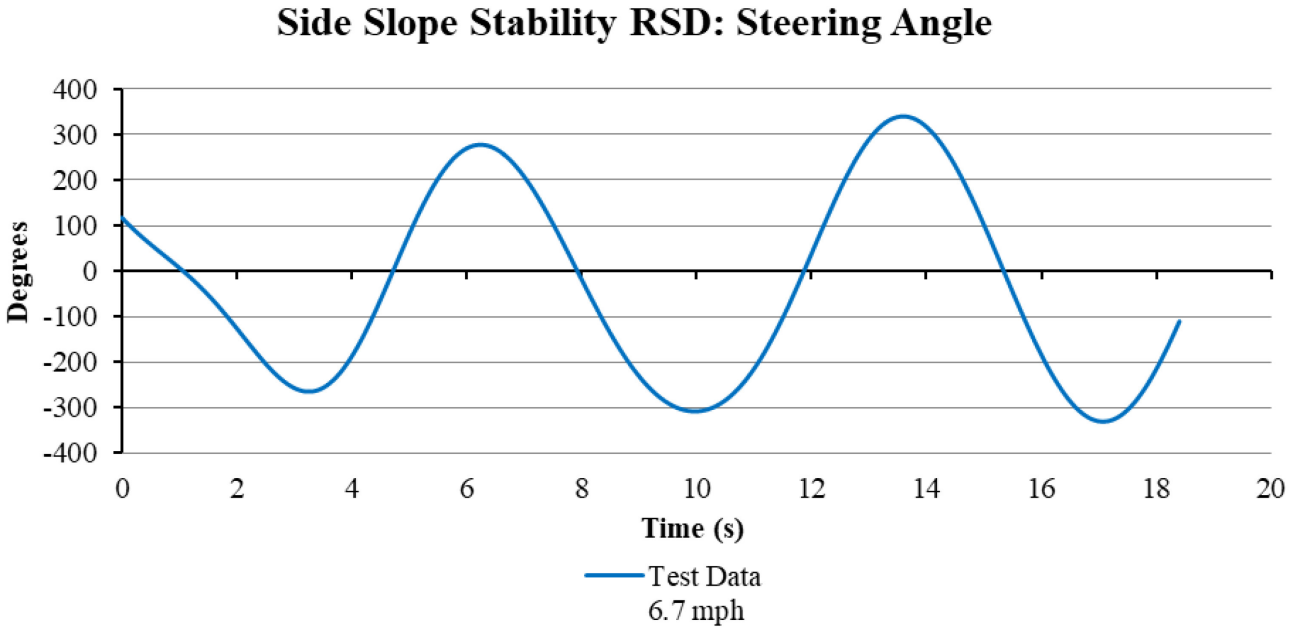


Figure H-25: Side Slope Stability Right Side Down: Steering Angle.

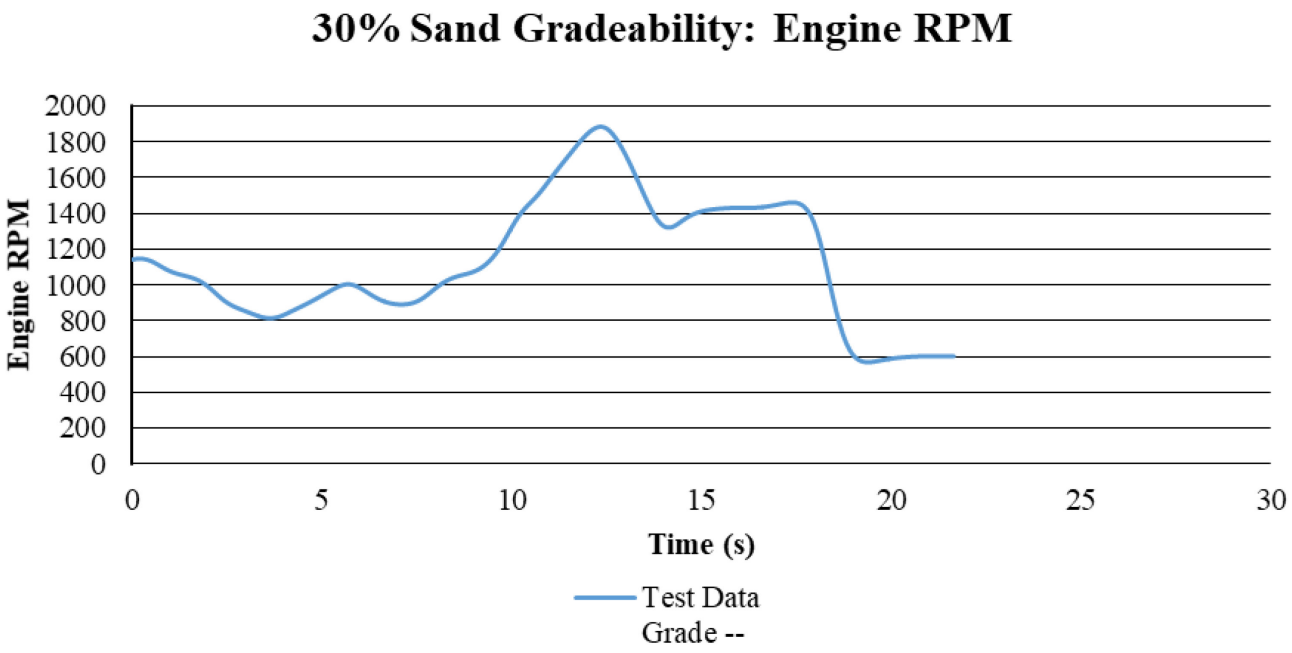


Figure H-26: 30% Sand Gradeability: Engine RPM.

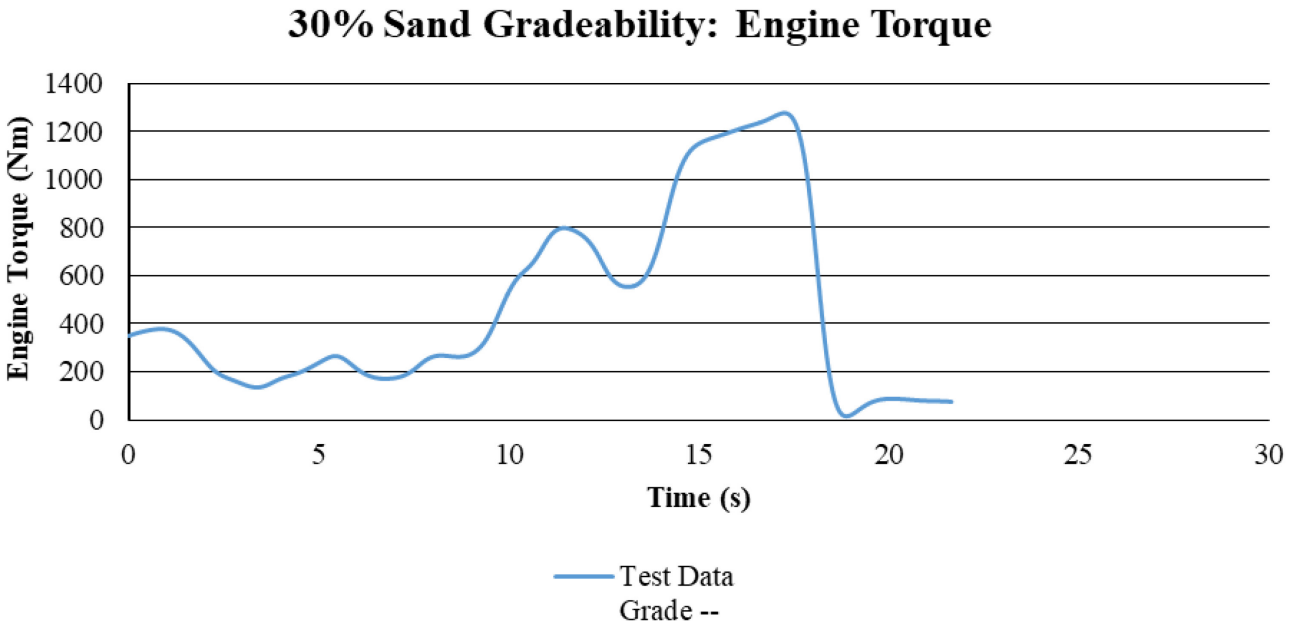


Figure H-27: 30% Sand Gradeability: Engine Torque.

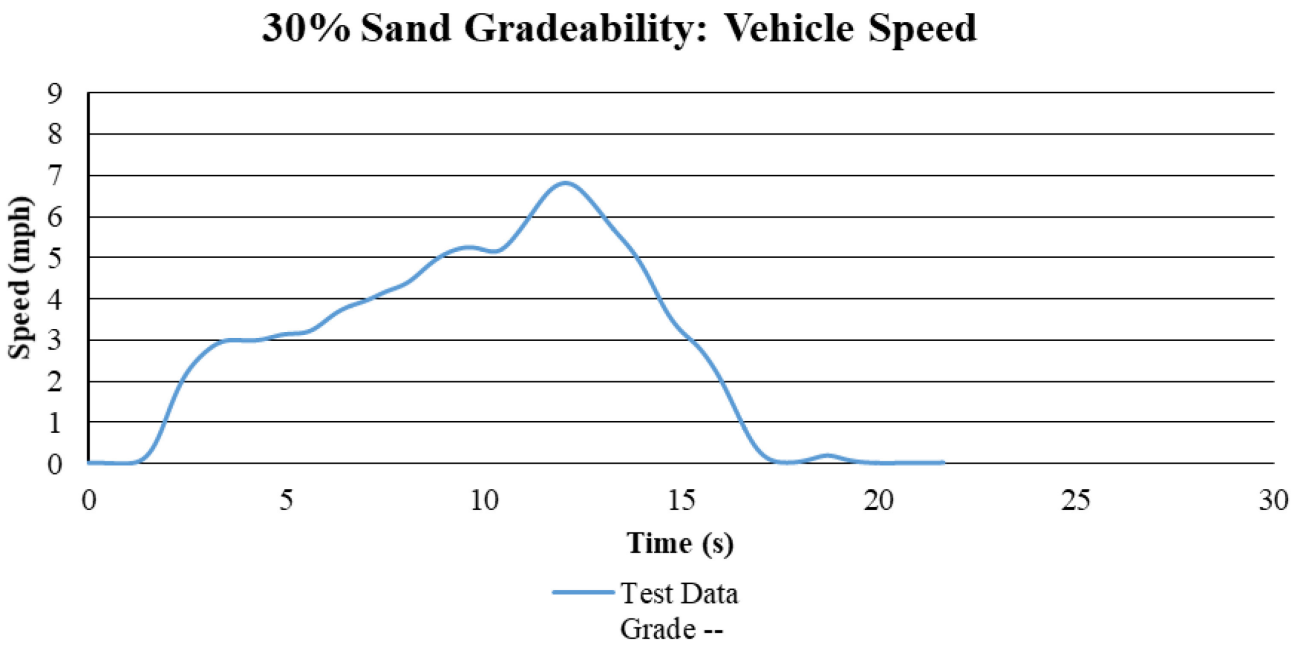


Figure H-28: 30% Sand Gradeability: Vehicle Speed.

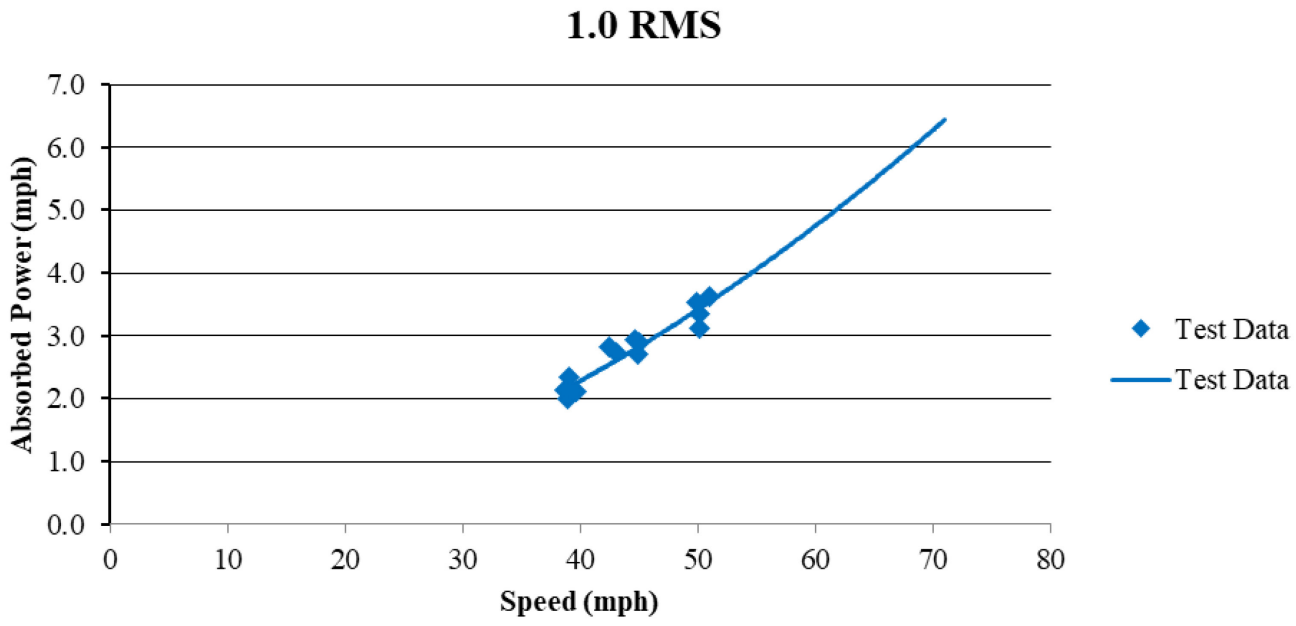


Figure H-29: 1.0 RMS.

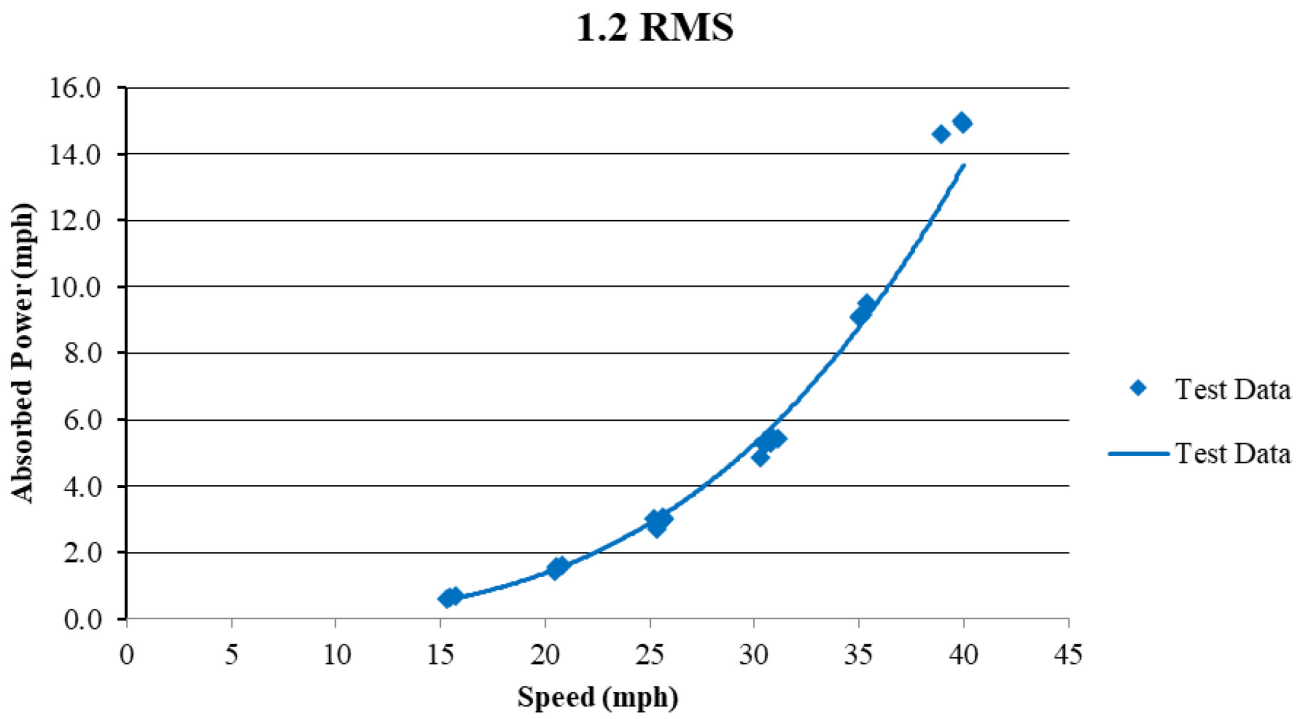


Figure H-30: 1.2 RMS.

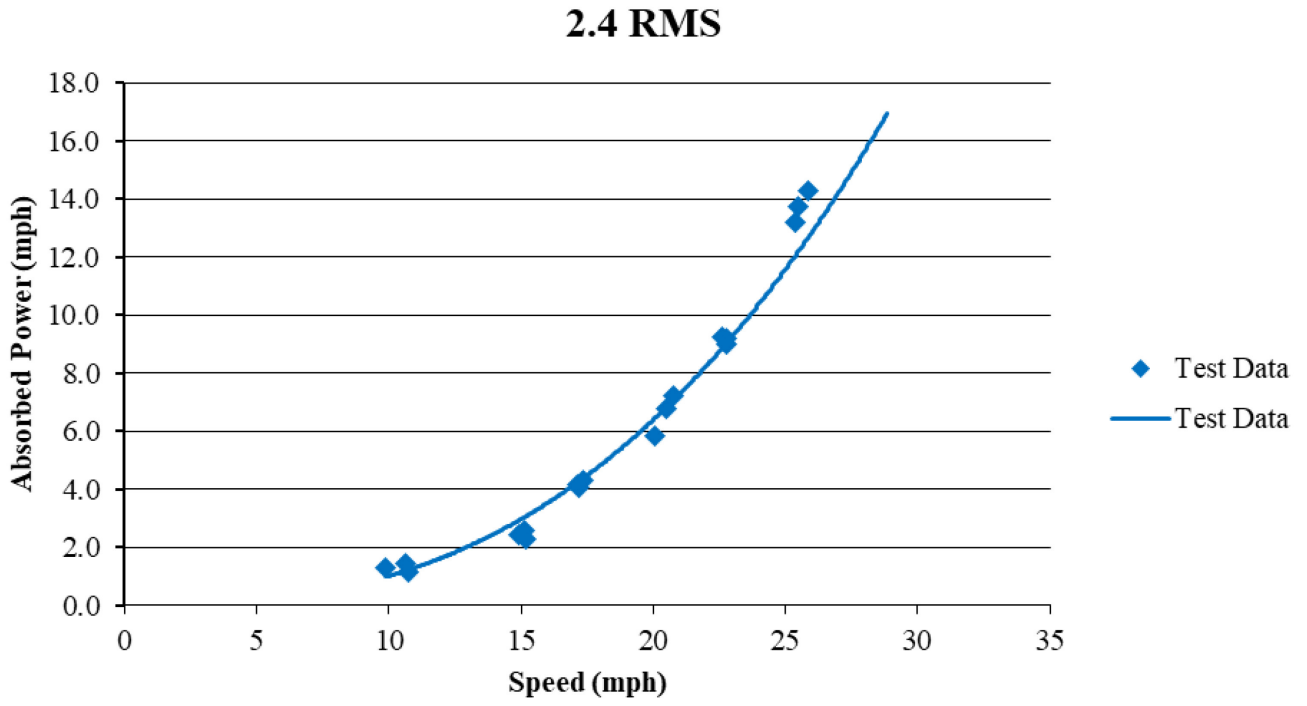


Figure H-31: 2.4 RMS.

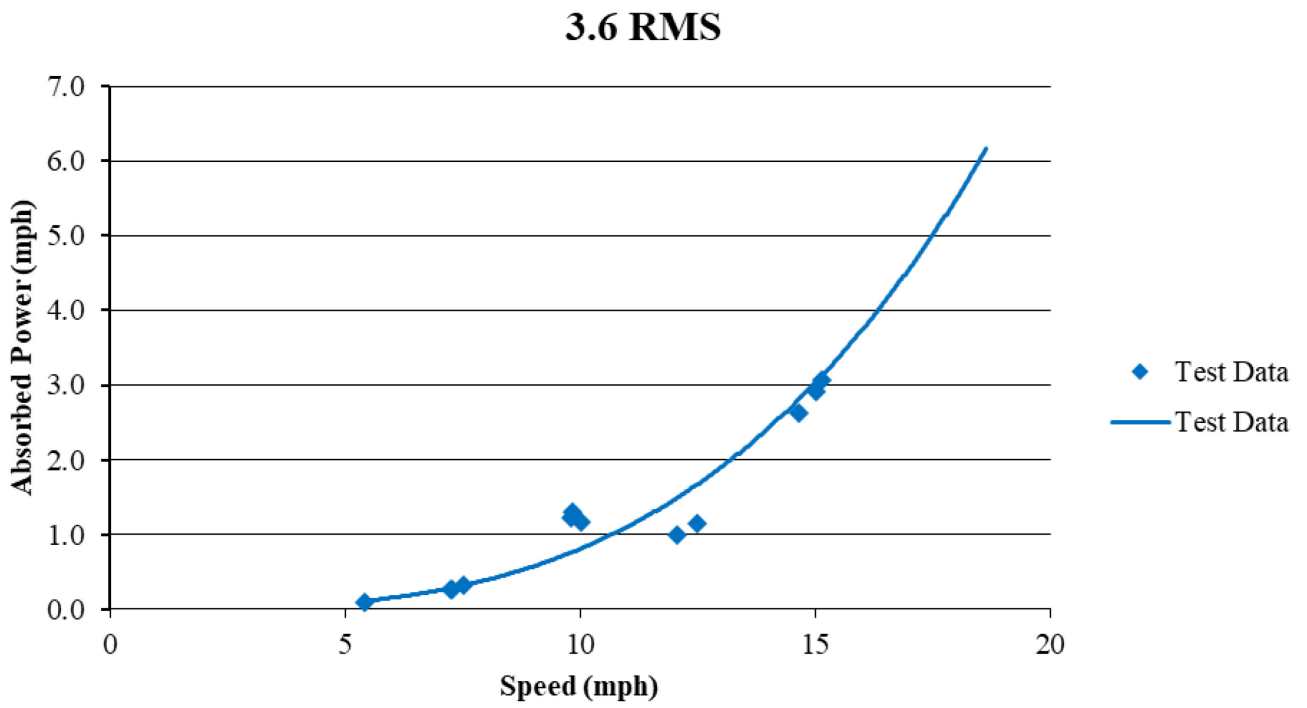


Figure H-32: 3.6 RMS.

Annex I – TA7: QUESTIONNAIRE COMMENTS AND OBSTACLE ANALYSIS

Mike Bradbury and Jonathan Bruce
Defence Science and Technology Laboratory (Dstl)
UNITED KINGDOM

I.1 QUESTIONNAIRE 1 COMMENTS

The following are the full comments from the questionnaire:

I.1.1 Question 1

Members were asked, "It is anticipated that the Complex NG-NRMM will require a stronger skill set than the legacy NRMM2. With that in mind what do you consider the usage profile of the different tools to be?" Comments received were:

"Both NG-NRMM and NRMM actually require two different skills sets to properly operate. One is an engineering skill set required to build and verify the vehicle model (performance curves, etc.) and then a GIS specialist to prepare and integrate the GIS data for the area of operations (this is seen as an Operational Planner but this may not be the case). Once these two steps are done then both NG-NRMM and NRMM can be run by any of the four operators as well as acquisition engineers, commanders, etc. These are deemed Supervised Practitioners. Note that under the model builders the set up and model verification can also be used for design loop simulations matching power train components, optimising the suspension components, etc. which is of no use to the operational planner. However the output of the verified vehicle model is important to the acquisition engineer / operational planner."

"I would anticipate that the Complex Terramechanics form will only be used by Experts for design development and research. This is because 1) the highly complex nature of the input data and models, and 2) the high computing power needed / long processing times."

"NRMM2: Operational Planner is seen as a deployed analyst as opposed a military officer in an HQ. Typically the UK deployed analysts have very specific tasks combined with reach-back to the UK for technical questions. This means mobility-related advice sought on operations would likely be provided from UK offices. NG-NRMM Simple: We would see Simple NG-NRMM being used in the same way as NRMM2. Rather than being a transition as the capability was established, NRMM2 would likely be kept in parallel. NG-NRMM Complex: The UK response for NG-NRMM Complex recognises that, based on demand, we may not invest in or achieve Expert status internally – this will drive what modeling options are adopted and how they are deployed."

"For the moment, even NRMM2 is not implemented. In Romania, there are few people (technical expert users) who know about it and try to completely understand it and to promote it between others."

"AMSAA has built a web-based GUI interface for the current NRMM that makes it very easy to use, especially if the vehicle and terrain files already exist. Much work has been done by TA1 and CRREL to document creating terrain files with GIS software. Much of the required input data is available from global sources. Data availability is a major hindrance for both the simple and complex NG-NRMM models."

I.1.2 Question 2

Members were asked, "How is the current NRMM used, and it is envisaged the Next-Generation NRMM would be used, in context of the following 6 exploitation paths: Research, Procurement, Pre-Deployment Advice, General Operational Advice, Specific Operational Advice, Other?" Comments received were:

"Note that this question is answered as if there was a successful NG-NRMM that introduces the complex and updated simple terramechanics to provide enhanced vehicle performance parameters over the range of terrain expected based on soil type (vegetation is the domain of the GIS and if one has the soil performance tractive effort then the vegetation / surface roughness / water / will be resolved in eth GIS mapping). These answers are based on how MOBSIM is planned for application in SA and not actual experience with NRMM. Note that NRMM has, what we understand, proved itself with scenario planning, decision making and operational support so has buy in by these users. As such it will continue to be used by these users as a) it is quick and b) trusted. Simple Terramechanics will also be used as it is quicker than complex although could be slower than CI. However, if the range of soils are covered it should be as quick as the performance mapping calculations are based on tractive effort and then GIS parameters of roughness, vegetation, etc. Complex requires a long runtime so its application will only be pertinent where there is time to model the various soils thus should be used for pre-deployment and general advice. If sufficient datasets are built up beforehand then it can be used operationally as it will simply access the performance archive to determine performance and thus should be just as fast as NRMM changing from Occasional to Likely for specific Operational Advice."

"I'm not sure if any one person can answer this question. Comment from former Marine / acquisition officer: If a sound tool is built and can be used with confidence, our DoD acquisition and operational planning environments WILL use those tools. (Operational planners spend as many hours working data as engineers, it is just not as precise)."

"Complex: Dstl's response to this is linked to the answers for the previous question. We would not adopt a Complex only based methodology due to: 1) Resource constraints, user requirements, runtimes and technical expertise required; and 2) The nature of how our work is exploited. Simple: It is likely we would adopt the Simple terramechanics to achieve improvements in predictions. Given those same constraints it is likely exploitation of Complex (if pursued) would be limited to tasks that were not time constrained."

"We do not use current NRMM. We use our own CCMod2 software with some formulars (RCI and CI) from NRMM. I think, NGN Simple will be a solution (together with RAMDO from Nick Gaul), people may use likely for a lot of purposes. NGN Complex has a very long runtime (2 days!). Even together with RAMDO usability (for mobility map creation) usability will be a problem, I suppose. NGN Complex is more a research tool at the moment."

"For the moment, even NRMM2 is not implemented. In Romania, there are few people (technical expert users) who know about it and try to completely understand it and to promote it between others. Regarding the NGN Simple, the theory could be applied but it is difficult to apply in the field. For example, for the time being, it cannot be found a bevameter in Romania."

"We do not have good enough terrain data for any model to support specific operational advice. We are often asked to provide pre-deployment and general operational advice in various locations on a seasonal basis. We use the current NRMM to do so. The current NRMM is also

being used to make procurement decisions. I foresee the latter being done with a simple and complex NG-NRMM once enough Bekker-Wong and soil physical property parameters have been measured."

I.1.3 Question 3

Members were asked, "For 'Likely' and 'Occasional' use cases what level of confidence in the analysis and output is typically expected or anticipated to be required?" Comments received were:

"It is understood that NRMM is fairly widely used both within research as well as procurement thus already has a medium / to high confidence in it therefore a high level of confidence is expected by these users. It is understood based on the NRMM application contracts received ... and within reportable use of NRMM that it is already widely accepted within the military user environment (Pre, General and Specific Operational) thus there is already a high degree of confidence in NRMM and this will continue to be required. NG Simple and Complex are unknown quantities thus will not be accepted by any of the users initially and will require verification and validation both against NRMM and operationally to derive the required high level of confidence in the outputs for all users. We believe that the speed of the simulation will be critical for all pre- and operational users thus this will be important for NG-NRMM to have a well modelled data set of tractive efforts prior o simulating the system performance for deployments. This feeds into acquisitions contracting not only requiring a NRMM / NG-NRMM modeling but that a verified (validated?) vehicle system model be delivered as part of the procurement."

"I don't see the accuracy of the model as changing with the application. It will change with the quality of the input data, however. Different applications may desire more accuracy – if so, then they need better input data."

"Dstl is unlikely to provide advice it has low confidence in, more likely if work was anticipated to generate low confidence the scope would be modified to mitigate the risk. Procurement is more likely to tolerate lower confidence for the understanding and setting of requirements than for assessing bids or making procurement decisions. This would be equally applicable for all tools. Driven by data availability and quality it was felt unreasonable to expect high confidence for operational support."

"Complex: Taken into consideration the resource constraints and technical expertise required, the level of confidence should be only 'High'."

I.2 OBSTACLE

Legacy NRMM2 terrain is made of many parameters, obstacle and vegetation definitions being two categories. As part of the methodology review the role of obstacles in the legacy NRMM2 was looked at. NRMM2 considers obstacles as things that can be straddled, driven over and/or driven around, either discrete or linear in nature. The methodology does this per terrain unit in a bottom-up approach. In considering alternatives the hypothesis was posed that:

- "For given geographical regions the impact to speed and accessibility of obstacles and vegetation can be assumed broadly consistent."

The rationale behind exploring this was to consider the feasibility of simplifying or omitting parts of the legacy NRMM2 methodology from NG-NRMM by using an alternate type of pre-processor, one that could pass predictions into the main module (if equated to NRMM2 methodology) as opposed to vehicle performance. (This does not negate the merit of an improved obstacle crossing as a standalone tool.)

It was not possible to conduct any level of geographical survey for this so existing NRMM2 terrain was used as a surrogate; specifically the maps known as All9 (a 3 x 3 grid of adjacent map areas in Germany, Europe) and 5322 (Lauterbach, Germany, Europe). Two analysis options were identified:

- **Plan A**: Compare 5322 to All9.
- **Plan B**: Compare each constituent map from All9 sequentially to the other eight as a whole.

Plan A was chosen as the most demanding of the hypothesis and the least effort to implement for a first pass. The terrain files were analyzed to understand the distributions of obstacle types therein, though this was complicated by the number of degrees of freedom in their definition[1]. The first parameter considered was obstacle height (Figure I-1). The chart shows **P**er inch and **C**umulative distributions, both showing visually similar trends (these not being tested for statistical significance).

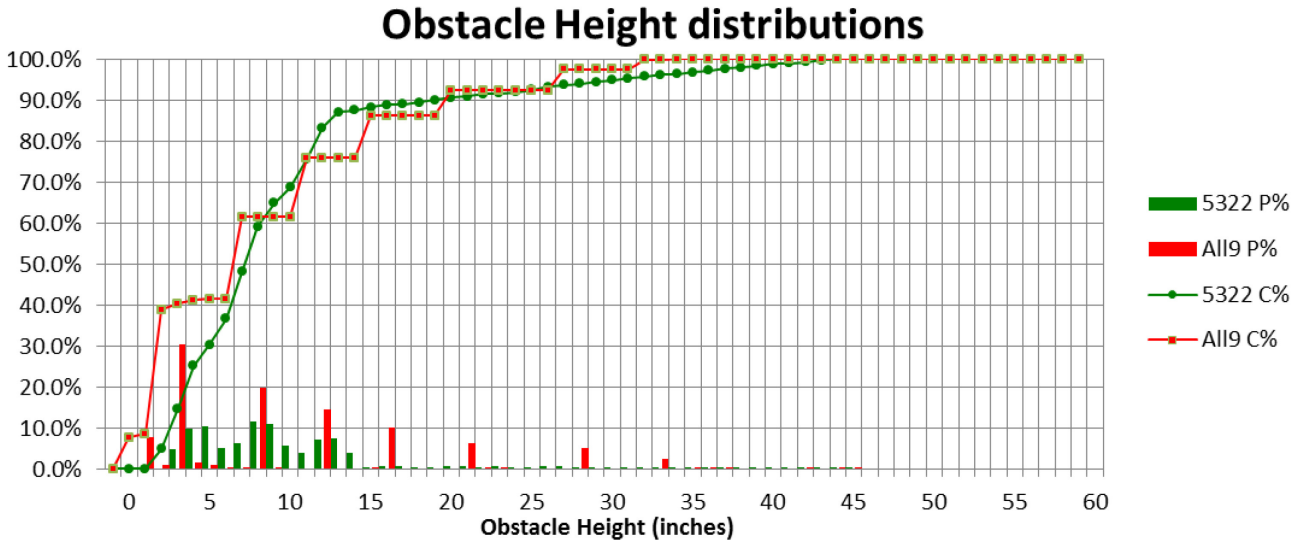


Figure I-1: Comparison of Obstacle Height Distribution in the Two Terrain Files.

Secondly, approach angle (Figure I-2 and Figure I-3) was considered to look for patterns in the types of mounds and ditches that might be encountered. For example if the ground was composed of a granular material the critical angle of repose might drive an observable pattern. Given this terrain is European, it might be that for trenches the prevailing slope, vegetation and rainfall drives erosion; for mounds it could be fallen trees of a similar nature or standing rocks based on geological features.

[1] In legacy NRMM2 obstacles are defined by their length, height/depth, width, approach angle and whether they are linear or not. A summary of the combination thereof cannot easily be visualised.

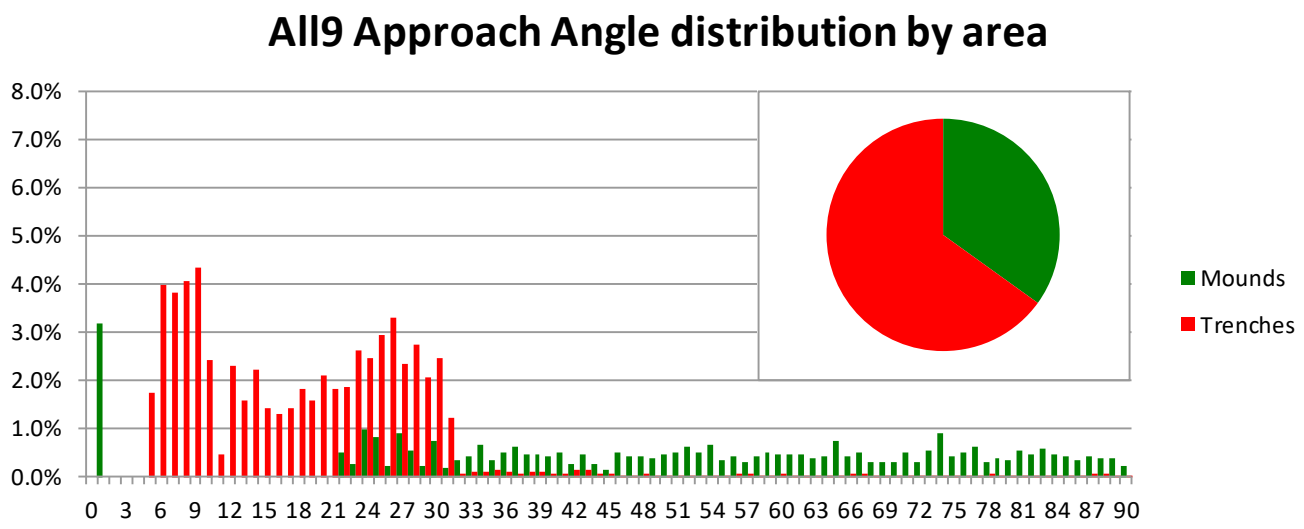


Figure I-2: Comparison of All9 Approach Angle Distribution in Terrain Files.

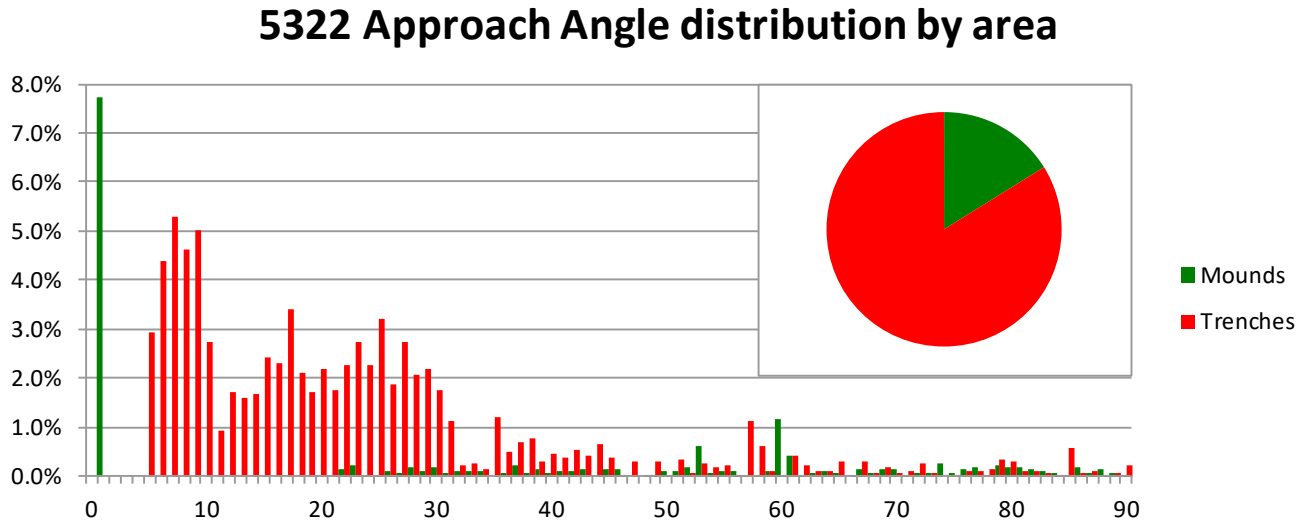


Figure I-3: Comparison of Approach Angle Distribution in Terrain Files.

In this instance the trenches show a potential similarity (up to ~ 30 degrees) but not in the mounds.

While these individual factors show some similarity in distribution when taken in isolation, the combined effect does not show this similarity (see Figure I-4).

To test if these observations carried through to NRMM2 predictions three generic vehicles (4 tonne wheeled 4 x 4, 30 tonne wheeled 8 x 8, 27t tonne tracked) and three variations of each terrain (no obstacles, no trees, neither obstacles nor trees) were created, the combinations modeled and the cumulative speed curves generated. The following (Figure I-5) shows a generic form followed by an explanation of how to interpret cumulative speed curves.

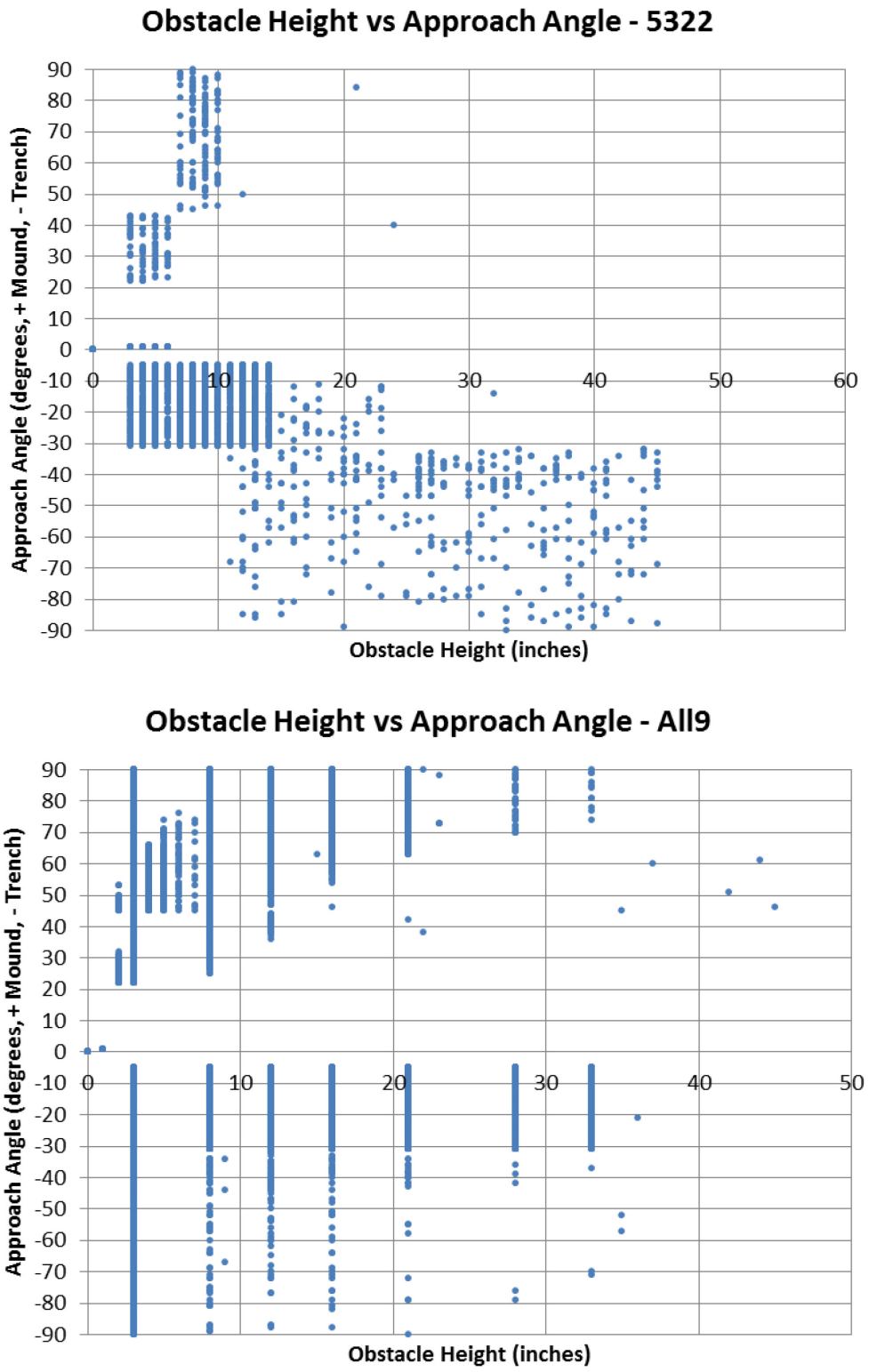


Figure I-4: Comparison of Obstacle Height vs Approach Angle for the Two Maps.

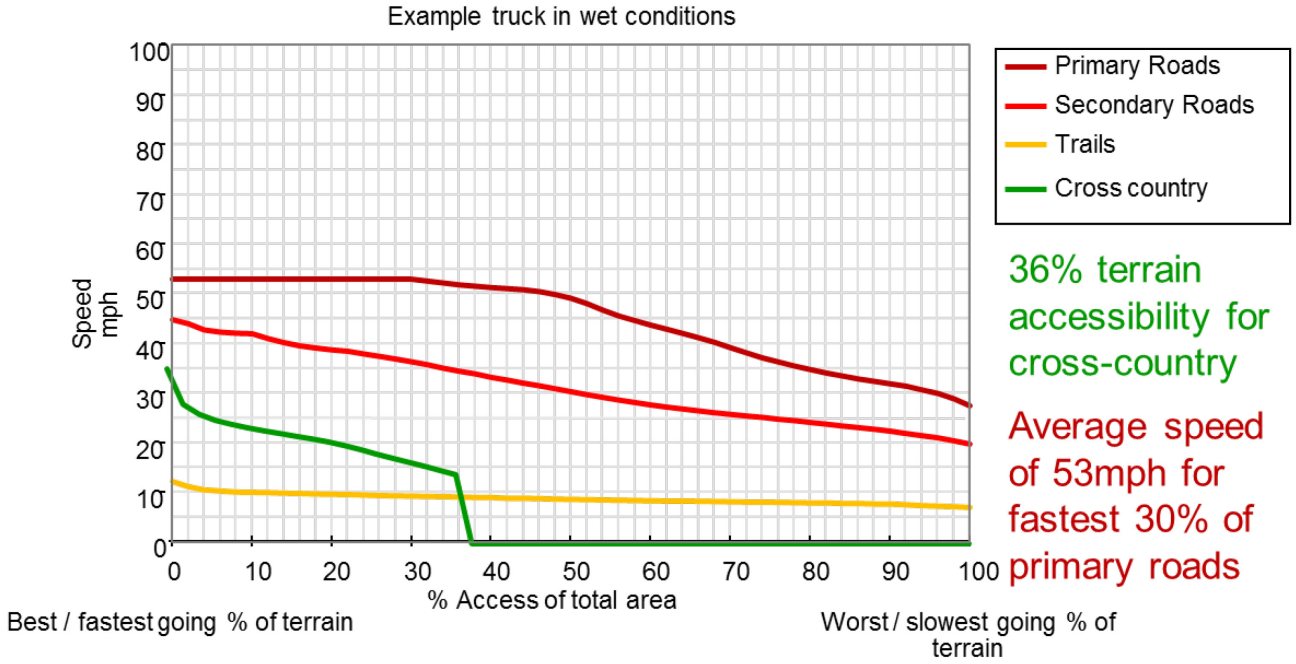


Figure I-5: Example Cumulative Speed Curve Chart.

Figure I-5 shows the several thousand individual predictions put into descending order by speed and presented in cumulative speed percentiles as calculated using a time based function. Any point (X, Y) on one of the curves plotted is read as the average speed (Y mph. y-axis) for the fastest given percentage (X%, x-axis) of the terrain in descending order. The two examples quoted on the chart are:

1) The cross-country curve shows an average speed of ~14 mph for the fastest 36% of the terrain. The zero speed thereafter shows that 62 - 64 % of the terrain is NOGO as you cannot calculate an average speed for terrain that cannot be traversed.

2) The primary roads curve shows a constant average speed of 53 mph up to 30% of the terrain. This type of result usually (as in this case) is the result of a constraint in the modeling, e.g., a road or tire speed limit. After 30% the performance of the vehicle drops below that constraint threshold and becomes dominant showing vehicle performance not artificially constrained.

The first results (Figure I-6) are for the model runs using a Dry/Normal scenario; Dry and Normal referring to the soil strength selection (one of four potential) in the terrain files.

There were some observations (but not conclusions) that could be made from the Dry/Normal results. The findings are limited because no patch by patch comparison of predictions and terrain units (i.e., paired data) was made. Observations, within the context of these specific legacy NRMM2 inputs and predictions, were:

1) Modifying the inclusion of obstacles and/or trees does not have a consistent impact across the terrain files.

   a) This implies that the assumption that the impact of obstacles and vegetation on speed and accessibility is broadly consistent for a given geographical region does not hold true.

   b) Therefore, applying a performance degradation based on geographic region would likely not be appropriate for NG-NRMM.

2) Modifying the inclusion of obstacles and/or trees does seem to have a consistent (albeit different level of) impact for all vehicle types on a given terrain.

   a) This implies that it may be possible to operate an obstacle and/or vegetation pre-processor based on the terrain as opposed to the vehicles.

   b) This is counterintuitive given different vehicles have different capabilities, but potentially warrants further investigation.

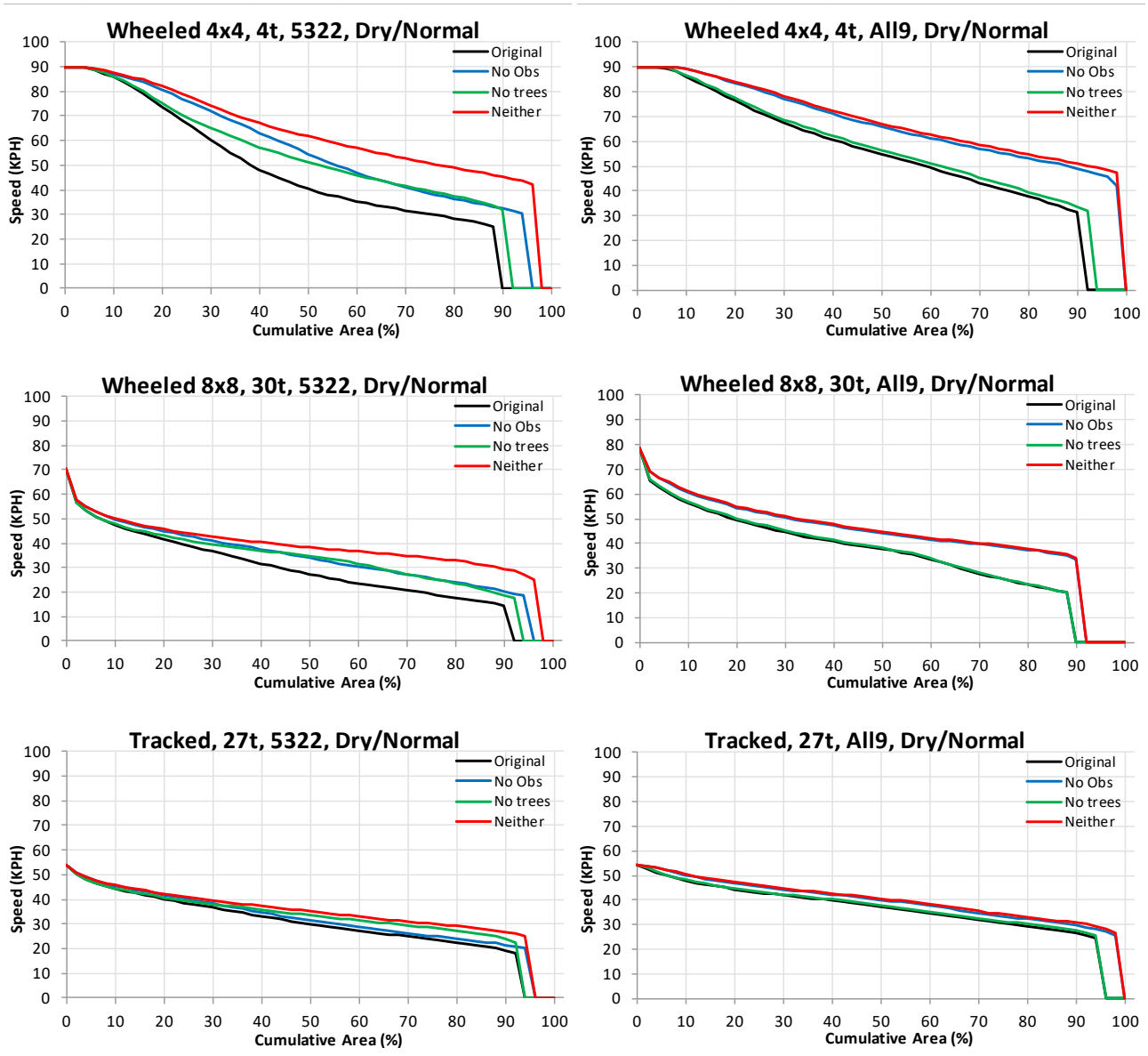


Figure I-6: Example NRMM2 Predictions for Three Generic Vehicles, Dry/Normal Scenario.

The following results are for the Wet/Slippery scenario (Figure I-7). The observations made for Dry/Normal do not translate directly. This is because the soft soil is becoming a more dominant factor in the predictions. The

main thing to take away from this is that it highlights that the relationships between the Layers are dynamic and the dominant factors (i.e., Layers) are therefore subject to change.

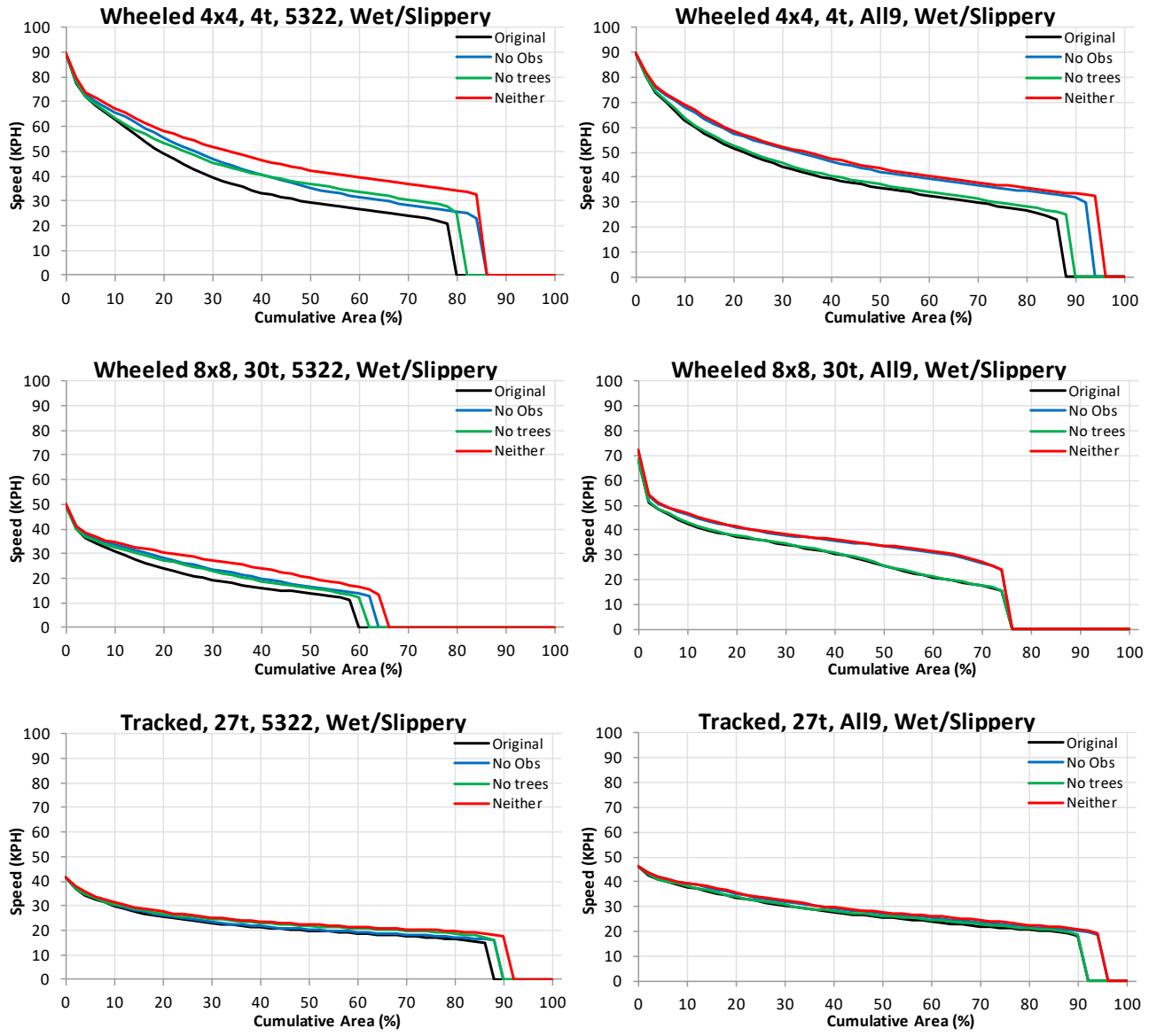


Figure I-7: Example NRMM2 Predictions for 3 Generic Vehicles, Wet/Slippery Scenario.

In parallel with this activity, the first attempts at drafting a questionnaire[2] tried to consider if and how the NG-NRMM should consider obstacles using legacy NRMM2 methodology as a comparator. Original questions included:

[2] A questionnaire was planned to engage with other members about potential NG-NRMM methodology components. This was superseded by the two questionnaires generated and the work on gaps.

- Does the STANREC need to include a standard approach to obstacle crossing modeling?
- Should the STANREC advocate a standard approach still using a lookup table pre-processor approach for areal type analysis?
- Does the STANREC need to specify a standard obstacle list?
- Should there be multiple standard obstacle lists that reflect vehicle type or class?
- Does the STANREC need to specify a methodology for defining obstacle lists?
- Does the STANREC need to specify a methodology for assessing obstacle lists?
- Does the STANREC need to define the metrics methodologies should use?

Methodology options for obstacle crossing were also considered:

1) Single representation of obstacles, e.g., trapezoidal as legacy NRMM2.
2) Multiple representations of obstacles, e.g., trapezoidal, half round and step.
3) Using military judgement to either limit accessibility or limit performance.
4) Take a practical as opposed to requirements driven approach, e.g., base obstacle representation on likely available data.

As this was discussed it became clear that arguably all of these questions start to cross the line between setting a standard requirement for what a model / methodology needs to be able to do versus how it should be implemented.

For NG-NRMM implementation, the Features Layer will have independent utility, for example assessing gap crossing or aircraft loading. Improving this capability will improve the utility of the Layer for independent exploitation. What is unknown (compared to the legacy NRMM2) is:

1) Whether improving methods will significantly reverse GO/NOGO predictions with regards overcoming features?
2) If not, will improved methods change the predicted speed at which features may be overcome?
3) To what extent the answers to these questions might impact map or aggregated (e.g., cumulative speed curve) outputs.

For NG-NRMM implementation there will, however, be methods and outputs that will be sensitive to individual predictions where obstacle crossing may be a discriminator; e.g., route following where each patch or cell is critical to mission success. Again, however, there is no work to date that demonstrates how well features need to be represented and the impact of sensitivity thereof.

Metrics for testing and evaluating Features and how they can be subsequently represented and validated in models will need to be addressed in the STANREC.

I.3 VEGETATION

In the legacy NRMM2 obstacles are defined as 3D non-deformable shapes to be avoided, straddled or traversed, whereas vegetation (trees) are seen as something to avoid or defeat by override (e.g., snap, deform). It is justifiable to consider the ability to traverse obstacles (singular or compound) independently of vegetation (e.g., trees) as the

defeat mechanisms vary. However it is not justifiable to consider avoiding obstacles and vegetation independently if they both impact the ability to maneuver by denying area on the same terrain unit.

The implementation of NG-NRMM could then potentially choose one of two approaches:

1) Keep obstacles and trees separate.
    a) The data may be simpler to represent, collate and assess.
    b) The data requirement better aligns to historic data sets.
2) Group obstacles and trees into a new category “features”.
    a) This may align better to commercial and open source data models and sources, and potentially any models or code built around them.

In either case it was considered that if there was to be better representation of these features, the data requirement should grow as for example:

- Canopy height and type is not a specific terrain input in NRMM2, this may affect maneuver.
- Root types is not a specific terrain input in NRMM2, this may impact ground interaction.
- Tree type is not an input in NRMM2, trees by species and region will defeat differently (e.g., bend, snap or uproot).

The other aspect of vegetation is the “carpet layer”, a surface layer that might affect traction. This would not fall into the Features category and methodology.

For the STANREC it is proposed:

1) Obstacles and (above surface) vegetation can be considered as a collective ability, that to defeat or overcome Features. (This is discussed in the main body under Layers.)
2) The vegetation “carpet layer” is included in the terramechanics. The rationale is that complex terramechanics needs to include it as an integral factor. As the approach moves back towards simple terramechanics, these factors are still a consideration but in a less integrated way.

From a NG-NRMM implementation perspective it is unclear if adopting a higher level of fidelity is required (from a results discrimination point of view) when considering vegetation or whether a simpler form is sufficient. Further analysis is required as suggested for obstacles.



REPORT DOCUMENTATION PAGE

1. Recipient's Reference	2. Originator's References	3. Further Reference	4. Security Classification of Document
	STO-TR-AVT-248 AC/323(AVT-248)TP/891	ISBN 978-92-837-2215-1	PUBLIC RELEASE

5. Originator

Science and Technology Organization
North Atlantic Treaty Organization
BP 25, F-92201 Neuilly-sur-Seine Cedex, France

6. Title

Next-Generation NATO Reference Mobility Model (NG-NRMM) Development

7. Presented at/Sponsored by

Final report of AVT-248.

8. Author(s)/Editor(s)	9. Date
Multiple	April 2020
10. Author's/Editor's Address	**11. Pages**
Multiple	520

12. Distribution Statement

There are no restrictions on the distribution of this document. Information about the availability of this and other STO unclassified publications is given on the back cover.

13. Keywords/Descriptors

Ground vehicles
Mobility
NATO Reference Mobility Model (NRMM)
Next-Generation NATO Reference Mobility Model (NG-NRMM)
Physics-based model
Terrain
Terramechanics
Vehicle dynamics

14. Abstract

The NATO Reference Mobility Model (NRMM) is a simulation tool used to compare vehicle design candidates and to assess the mobility of existing vehicles under specific conditions. NRMM was developed and validated in the 1970s and computer technology and models have advanced greatly since then. The AVT-248 team provided a basis to update and improve NRMM with physics-based models to replace the empirical data used in NRMM. The proposed result is the Next-Generation NRMM (NG-NRMM). The deliverables from AVT-248 include simple and complex terramechanics prototype demonstrations, a Verification and Validation benchmarking exercise, and the initial release of a STANREC documenting the requirements for an NG-NRMM. In addition, two complementary Research Task Groups were spun off as new activities: a Cooperative Demonstration of Technology (AVT-308); and an RTG to upgrade and manage the STANREC (AVT-327). NG-NRMM is vital to NATO's mission as it will add new capabilities in the design, modeling, and simulation of a broad class of vehicles, with the potential to reduce costs and improve performance. This could yield a new paradigm for ground vehicle mobility with the possibility to model complex vehicle maneuvers in high fidelity.



NORTH ATLANTIC TREATY ORGANIZATION

BP 25
F-92201 NEUILLY-SUR-SEINE CEDEX • FRANCE
Télécopie 0(1)55.61.22.99 • E-mail mailbox@cso.nato.int

SCIENCE AND TECHNOLOGY ORGANIZATION

DIFFUSION DES PUBLICATIONS
STO NON CLASSIFIEES

Les publications de l'AGARD, de la RTO et de la STO peuvent parfois être obtenues auprès des centres nationaux de distribution indiqués ci-dessous. Si vous souhaitez recevoir toutes les publications de la STO, ou simplement celles qui concernent certains Panels, vous pouvez demander d'être inclus soit à titre personnel, soit au nom de votre organisation, sur la liste d'envoi.

Les publications de la STO, de la RTO et de l'AGARD sont également en vente auprès des agences de vente indiquées ci-dessous.

Les demandes de documents STO, RTO ou AGARD doivent comporter la dénomination « STO », « RTO » ou « AGARD » selon le cas, suivi du numéro de série. Des informations analogues, telles que le titre est la date de publication sont souhaitables.

Si vous souhaitez recevoir une notification électronique de la disponibilité des rapports de la STO au fur et à mesure de leur publication, vous pouvez consulter notre site Web (http://www.sto.nato.int/) et vous abonner à ce service.

CENTRES DE DIFFUSION NATIONAUX

ALLEMAGNE
Streitkräfteamt / Abteilung III
Fachinformationszentrum der Bundeswehr (FIZBw)
Gorch-Fock-Straße 7, D-53229 Bonn

BELGIQUE
Royal High Institute for Defence – KHID/IRSD/RHID
Management of Scientific & Technological Research
for Defence, National STO Coordinator
Royal Military Academy – Campus Renaissance
Renaissancelaan 30, 1000 Bruxelles

BULGARIE
Ministry of Defence
Defence Institute "Prof. Tsvetan Lazarov"
"Tsvetan Lazarov" bul no.2
1592 Sofia

CANADA
DGSIST 2
Recherche et développement pour la défense Canada
60 Moodie Drive (7N-1-F20)
Ottawa, Ontario K1A 0K2

DANEMARK
Danish Acquisition and Logistics Organization
(DALO)
Lautrupbjerg 1-5
2750 Ballerup

ESPAGNE
Área de Cooperación Internacional en I+D
SDGPLATIN (DGAM)
C/ Arturo Soria 289
28033 Madrid

ESTONIE
Estonian National Defence College
Centre for Applied Research
Riia str 12
Tartu 51013

ETATS-UNIS
Defense Technical Information Center
8725 John J. Kingman Road
Fort Belvoir, VA 22060-6218

FRANCE
O.N.E.R.A. (ISP)
29, Avenue de la Division Leclerc
BP 72
92322 Châtillon Cedex

GRECE (Correspondant)
Defence Industry & Research General
Directorate, Research Directorate
Fakinos Base Camp, S.T.G. 1020
Holargos, Athens

HONGRIE
Hungarian Ministry of Defence
Development and Logistics Agency
P.O.B. 25
H-1885 Budapest

ITALIE
Ten Col Renato NARO
Capo servizio Gestione della Conoscenza
F. Baracca Military Airport "Comparto A"
Via di Centocelle, 301
00175, Rome

LUXEMBOURG
Voir Belgique

NORVEGE
Norwegian Defence Research
Establishment
Attn: Biblioteket
P.O. Box 25
NO-2007 Kjeller

PAYS-BAS
Royal Netherlands Military
Academy Library
P.O. Box 90.002
4800 PA Breda

POLOGNE
Centralna Biblioteka Wojskowa
ul. Ostrobramska 109
04-041 Warszawa

PORTUGAL
Estado Maior da Força Aérea
SDFA – Centro de Documentação
Alfragide
P-2720 Amadora

REPUBLIQUE TCHEQUE
Vojenský technický ústav s.p.
CZ Distribution Information Centre
Mladoboleslavská 944
PO Box 18
197 06 Praha 9

ROUMANIE
Romanian National Distribution
Centre
Armaments Department
9-11, Drumul Taberei Street
Sector 6
061353 Bucharest

ROYAUME-UNI
Dstl Records Centre
Rm G02, ISAT F, Building 5
Dstl Porton Down
Salisbury SP4 0JQ

SLOVAQUIE
Akadémia ozbrojených síl gen.
M.R. Štefánika, Distribučné a
informačné stredisko STO
Demänová 393
031 01 Liptovský Mikuláš 1

SLOVENIE
Ministry of Defence
Central Registry for EU & NATO
Vojkova 55
1000 Ljubljana

TURQUIE
Milli Savunma Bakanlığı (MSB)
ARGE ve Teknoloji Dairesi
Başkanlığı
06650 Bakanliklar – Ankara

AGENCES DE VENTE

The British Library Document
Supply Centre
Boston Spa, Wetherby
West Yorkshire LS23 7BQ
ROYAUME-UNI

Canada Institute for Scientific and
Technical Information (CISTI)
National Research Council Acquisitions
Montreal Road, Building M-55
Ottawa, Ontario K1A 0S2
CANADA

Les demandes de documents STO, RTO ou AGARD doivent comporter la dénomination « STO », « RTO » ou « AGARD » selon le cas, suivie du numéro de série (par exemple AGARD-AG-315). Des informations analogues, telles que le titre et la date de publication sont souhaitables. Des références bibliographiques complètes ainsi que des résumés des publications STO, RTO et AGARD figurent dans le « NTIS Publications Database » (http://www.ntis.gov).

NORTH ATLANTIC TREATY ORGANIZATION

BP 25
F-92201 NEUILLY-SUR-SEINE CEDEX • FRANCE
Télécopie 0(1)55.61.22.99 • E-mail mailbox@cso.nato.int

SCIENCE AND TECHNOLOGY ORGANIZATION

DISTRIBUTION OF UNCLASSIFIED STO PUBLICATIONS

AGARD, RTO & STO publications are sometimes available from the National Distribution Centres listed below. If you wish to receive all STO reports, or just those relating to one or more specific STO Panels, they may be willing to include you (or your Organisation) in their distribution.

STO, RTO and AGARD reports may also be purchased from the Sales Agencies listed below.

Requests for STO, RTO or AGARD documents should include the word 'STO', 'RTO' or 'AGARD', as appropriate, followed by the serial number. Collateral information such as title and publication date is desirable.

If you wish to receive electronic notification of STO reports as they are published, please visit our website (http://www.sto.nato.int/) from where you can register for this service.

NATIONAL DISTRIBUTION CENTRES

BELGIUM
Royal High Institute for Defence – KHID/IRSD/RHID
Management of Scientific & Technological Research for Defence, National STO Coordinator
Royal Military Academy – Campus Renaissance
Renaissancelaan 30
1000 Brussels

BULGARIA
Ministry of Defence
Defence Institute "Prof. Tsvetan Lazarov"
"Tsvetan Lazarov" bul no.2
1592 Sofia

CANADA
DSTKIM 2
Defence Research and Development Canada
60 Moodie Drive (7N-1-F20)
Ottawa, Ontario K1A 0K2

CZECH REPUBLIC
Vojenský technický ústav s.p.
CZ Distribution Information Centre
Mladoboleslavská 944
PO Box 18
197 06 Praha 9

DENMARK
Danish Acquisition and Logistics Organization (DALO)
Lautrupbjerg 1-5
2750 Ballerup

ESTONIA
Estonian National Defence College
Centre for Applied Research
Riia str 12
Tartu 51013

FRANCE
O.N.E.R.A. (ISP)
29, Avenue de la Division Leclerc – BP 72
92322 Châtillon Cedex

GERMANY
Streitkräfteamt / Abteilung III
Fachinformationszentrum der Bundeswehr (FIZBw)
Gorch-Fock-Straße 7
D-53229 Bonn

GREECE (Point of Contact)
Defence Industry & Research General Directorate, Research Directorate
Fakinos Base Camp, S.T.G. 1020
Holargos, Athens

HUNGARY
Hungarian Ministry of Defence
Development and Logistics Agency
P.O.B. 25
H-1885 Budapest

ITALY
Ten Col Renato NARO
Capo servizio Gestione della Conoscenza
F. Baracca Military Airport "Comparto A"
Via di Centocelle, 301
00175, Rome

LUXEMBOURG
See Belgium

NETHERLANDS
Royal Netherlands Military Academy Library
P.O. Box 90.002
4800 PA Breda

NORWAY
Norwegian Defence Research Establishment, Attn: Biblioteket
P.O. Box 25
NO-2007 Kjeller

POLAND
Centralna Biblioteka Wojskowa
ul. Ostrobramska 109
04-041 Warszawa

PORTUGAL
Estado Maior da Força Aérea
SDFA – Centro de Documentação
Alfragide
P-2720 Amadora

ROMANIA
Romanian National Distribution Centre
Armaments Department
9-11, Drumul Taberei Street
Sector 6
061353 Bucharest

SLOVAKIA
Akadémia ozbrojených síl gen M.R. Štefánika, Distribučné a informačné stredisko STO
Demänová 393
031 01 Liptovský Mikuláš 1

SLOVENIA
Ministry of Defence
Central Registry for EU & NATO
Vojkova 55
1000 Ljubljana

SPAIN
Área de Cooperación Internacional en I+D
SDGPLATIN (DGAM)
C/ Arturo Soria 289
28033 Madrid

TURKEY
Milli Savunma Bakanlığı (MSB)
ARGE ve Teknoloji Dairesi Başkanlığı
06650 Bakanliklar – Ankara

UNITED KINGDOM
Dstl Records Centre
Rm G02, ISAT F, Building 5
Dstl Porton Down, Salisbury SP4 0JQ

UNITED STATES
Defense Technical Information Center
8725 John J. Kingman Road
Fort Belvoir, VA 22060-6218

SALES AGENCIES

The British Library Document Supply Centre
Boston Spa, Wetherby
West Yorkshire LS23 7BQ
UNITED KINGDOM

Canada Institute for Scientific and Technical Information (CISTI)
National Research Council Acquisitions
Montreal Road, Building M-55
Ottawa, Ontario K1A 0S2
CANADA

Requests for STO, RTO or AGARD documents should include the word 'STO', 'RTO' or 'AGARD', as appropriate, followed by the serial number (for example AGARD-AG-315). Collateral information such as title and publication date is desirable. Full bibliographical references and abstracts of STO, RTO and AGARD publications are given in "NTIS Publications Database" (http://www.ntis.gov).

ISBN 978-92-837-2215-1